AIRFOILS AT LOW SPEEDS

AIRFOILS AT LOW SPEEDS

Michael S. Selig, John F. Donovan, and David B. Fraser

Soartech 8
H. A. Stokely, publisher

Airfoils at Low Speeds

H. A. Stokely, publisher
1504 North Horseshoe Circle
Virginia Beach, Virginia 23451
USA

FOREWORD AND ACKNOWLEDGEMENTS

The history of this experimental program on low-speed airfoils is extensive. In August 1986, work toward testing model sailplane airfoils in a wind tunnel at Princeton University began on an ambitious scale. The initial plan was to test 30 airfoils: 15 existing airfoils and 15 new airfoils to be designed concurrently with the tests. As news of the project caught the attention of radio control (RC) model soaring enthusiasts, the project grew far beyond the original goals and expectations, thanks to their generosity. When the experimental apparatus was finally dismantled in January 1989, almost two and a half years later, over 60 models were tested and over 130 airfoil polars were generated. It is our hope that the results of this work will be valuable to modelers and researchers for many years to come.

A word is in order to explain the role each of us played in this effort. The initial impetus for the project, its organization and day-to-day management, as well as the wind tunnel testing and data reduction were done by Selig and Donovan. They also designed all of the new airfoils except for the DF-series by Fraser.

The custom measurement apparatus was built jointly by Selig and Donovan at Princeton University and by Fraser at Fraser-Volpe Corporation. The digitizing of the models was done at Fraser-Volpe Corporation by Fraser, who also wrote the computer programs for reducing this part of the data. All three of us shared in the writing and editing of this book.

We would also like to mention that everything from the data collection to the writing of this book was done by computer. There is not a single number anywhere in any part of the data that was generated, computed, reduced, copied, averaged, printed, graphed, or manipulated by hand. Aside from the speed and convenience of this approach, the principal advantage is the complete elimination of several types of errors that may otherwise occur.

All of the airfoil polar data is available on $3\frac{1}{2}$ or $5\frac{1}{4}$ inch IBM compatible diskette from Fraser.

Sincere thanks go to Prof. Smits of the Princeton University Gas Dynamics Laboratory for his enduring support while this extracurricular project began to grow and consume seemingly endless hours of time away from the first two authors' regular thesis research. The gracious support of Prof. Lam and Prof. Curtiss of Princeton University, and the helpful discussions of Prof. Maughmer of The Pennsylvania State University are appreciated. Thanks also go to Lou Pizzarello who provided us with an air conditioner and new air intake filters for the tunnel.

We are indebted to Ray Olsen for his many contributions at times when we needed them most.

For monetary contributions which made possible the purchase of important elements essential to this work we thank Rolf Girsberger, H.A. Stokely, Jerry Jackson, Armin Saxer, Charles Griswald, C. Haverlan, H.J. Rogers, Preben Norholm, Brian Smith, Thomas Yamokoski, and Trey Wood.

The expertise of many skilled model builders made the lengthy set-up stage all worthwhile. In this respect we very deeply appreciate the work of Bob Champine, Ron Wagner, Stan Watson, Mark Allen, Michael Bame, Tony Beck, Woody Blanchard, Charles Fox, Peter Illick, Harley Michaelis, Forrest Miller, Ted Off, Mike Reed, Tyson Sawyer, Chuck Anderson, Norman Anderson, Jerry Arana, Bruce Baker, Ken Bates, David Batey Jr., Rich Border, John Boren, Mike Chiddick, Doug Dorton, Roger Egginton, Dale Folkening, Harlan Halsey, John Hohensee, Dave Jones, Stan Koch, Terry Luckenbach, Carl Mohs, Lee Murray, Mark Nankivil, R.J. Ostrander, Jef Raskin, Les Rogers, Joe Ruminski, and Karl Widiner.

Prof. Mark Drela of M.I.T. is gratefully acknowledged for making his ISES computer code available to aid in the analysis of the new airfoil designs. Finally, MKS Instruments, Inc. and Scientific Solutions, Inc. are acknowledged for their valuable contributions of instrumentation.

TABLE OF CONTENTS

LIST OF POLARS AND LIFT PLOTS

List of Symbols and Abbreviations

c	airfoil chord
C_l	lift coefficient, $l/\frac{1}{2}\rho V_\infty^2 c$
$C_{l_{max}}$	maximum lift coefficient
C_d	drag coefficient, $d/\frac{1}{2}\rho V_\infty^2 c$
$C_{m_{c/4}}$	pitching moment about the quarter-chord point
d	drag per unit span
h	trip height
l	lift per unit span
L/D	sailplane lift-to-drag ratio
$P_{d\infty}$	freestream dynamic pressure
ΔP_0	total pressure difference between freestream and wake
Rn	Reynolds number, $\rho V_\infty\, c/\mu$
u	streamwise velocity in wake
u'_{rms}	root-mean-square of the streamwise fluctuating velocity
V_∞	freestream velocity
V	inviscid local velocity on airfoil surface
w	trip width
x	distance along airfoil chord, or horizontal distance
y	vertical distance
α	angle of attack
μ	fluid viscosity
ρ	fluid density
u.s.	upper surface
u.s.t.	upper surface trip
l.s.	lower surface
l.s.t.	lower surface trip
PT	Princeton Tests

Chapter 1
Introduction

The primary goal of this work was to design a new group of high-performance airfoils for radio controlled model sailplanes. As can be imagined, this involved numerous preliminary steps from preparing and instrumenting the tunnel to arranging for the models to be built, establishing a design procedure and, of course, solving all the myriad problems that occur in a multi-year project of this size.

In order to establish baseline data, a number of existing airfoil designs were tested first. These were selected primarily by the modeling community and are representative of what is presently used. They ranged from very simple, flat-bottom types, as well as some of the older NACA sections and their close derivatives, to very modern FAI-contest airfoils. Aside from providing the baseline, testing these airfoils allowed us to compare our data with other facilities where the same sections had also been tested.

The flow behavior over an airfoil at high Reynolds numbers—greater, say, than 1–3 million—is well known. The boundary layer is laminar from the leading edge to a point typically near mid-chord where it makes a transition to turbulent flow. This transition, as well as the flow behind it, is generally well behaved. Unlike full-size airplanes, model sailplanes typically operate at chord Reynolds numbers between 50,000 and 500,000, often called the low Reynolds number regime. At these low Reynolds numbers the flow is fundamentally different and more complicated than at high Reynolds numbers. The transition process is neither abrupt nor does it usually take place while the boundary layer is attached to the airfoil. Instead the laminar boundary layer separates, that is, it physically detaches from the airfoil surface. The flow then becomes unstable while separated, and makes the transition to turbulent flow in "mid-air." Only then does the flow reattach to the airfoil. And sometimes, if the laminar separation point is sufficiently far aft or if the Reynolds number is very low, the flow entirely fails to return to the airfoil surface. In either case large energy losses are associated with this process. This laminar separation, transition to turbulence, and turbulent reattachment enclose a region of recirculating flow aptly called the "laminar separation bubble." It is this extended transition process that is the principal reason for the degradation in performance at low Reynolds numbers. Efforts towards drag reduction, therefore, largely concentrate on reducing the size and extent of the bubble.

In an effort to understand the flow phenomena at low Reynolds numbers in general (which includes RC sailplanes), there have been numerous theoretical and experimental investigations which have resulted in three major conferences in the past four years[1,2,3] and a special AGARD publication[4]. Because of the difficulty in mathematically modeling the bubble, computational efforts have not been entirely reliable in predicting this complex flow. Nonetheless, considerable progress has been made. In most studies and experiments, the primary emphasis has been on understanding the fundamental mechanisms that drive the bubble. Yet despite the high level of interest in this area, few systematic attempts have been made to apply the growing body of knowledge to the problem of airfoil design. This book discusses a major experimental program that was carried out to do just that, and to do it specifically for RC sailplane airfoils.

All the models were tested in the low-speed, low-turbulence, 3 × 4 ft smoke tunnel at Princeton University. The following is a list of the 54 different airfoils; several airfoils were duplicated in order to examine the effects of model variability, and these are indicated by an asterisk (*). The DF- and SD-airfoils are the new designs resulting from this work.

AQUILA	FX63-137	S3014	SD7037
CLARK-Y	HQ2/9	S3016	SD7043
DAE51	J5012	S3021*	SD7062
DF101	M06-13-128	S4061*	SD7080
DF102	MB253515	S4062	SD7084
DF103	NACA 0009	S4180	SD7090
E193	NACA 2.5411	S4233	SD8000
E193MOD	NACA 64A010	SD2030	SD8020
E205*	NACA 6409	SD2083	SD8040
E214*	RG15	SD5060	SPICA
E374*	S2048	SD6060	WB135/35
E387*	S2055	SD6080	WB140/35/FB
Flat Plate	S2091*	SD7003	
FX60-100	S3010	SD7032*	

In order to ensure the enthusiasm of the modeling community which built all of the test sections, we tested any airfoil that a builder wanted to supply. As a result of this policy, three things happened. First, a great variety of airfoils was tested spanning virtually the entire range of usefulness to RC sailplanes. Second, some airfoils previously unknown to us offered insights into the airfoil design process. And third, we were able to design new airfoils, have models of them built, and test them in the tunnel, thereby "closing" the design loop. As far as we know, this last step has not been done before on this scale for model aircraft applications.

This book has two major parts: (1) the documentation of the facility and the quality of the data; (2) the results of the tests on over 60 wind tunnel models. The first part is covered in Chapter 2 and extensively documents the experimental methods we used in this work. This part is intended primarily for those active in low Reynolds number airfoil research and may be skipped without loss of continuity by those more interested in the data. To help the non-specialist, the terminology we use is explained in Chapter 3. Chapter 4 briefly covers some of the ideas behind the new airfoil designs. Hopefully, a more comprehensive report will come at a later time. The second major part begins with Chapter 5, which discusses the airfoil polars at length. Airfoil polars and lift plots, tabulated data, coordinates, and other supporting data are given in Chapters 7 through 13. And finally, for those who may wish to contact the authors or obtain additional copies of this book, the addresses are listed in Chapter 14.

Chapter 2
Experimental Facility and Measurement Technique

The tests were performed in the Princeton University 3 × 4 ft smoke tunnel. A sketch of the tunnel is shown in Fig. 2.1 and also on the back cover. It consists of an inlet and stilling chamber 9 ft high by 12 ft wide containing screens and flow straighteners. The flow straighteners are 3 in square and 12 in long. This section is followed by a 9:1 contraction leading to the test section which is 3 ft high by 4 ft wide. Downstream of the test section the flow is turned 90° and exits through a 50 HP fan. The tunnel speed in the test section is variable from 5 to 70 ft/s.

2.1 Flow Quality

Constant temperature hot-wire anemometry[5] (using Dantec model 55M01) was used to determine turbulence levels in the freestream. At all conditions the wire was operated at an overheat of 0.8. The frequency response was optimized using the standard test in which a square wave in voltage is injected at the Wheatstone bridge to simulate an impulse in velocity. The -3 dB point of the response curve was 33 kHz for chord Reynolds numbers of 100k, 200k, and 300k; and 25 kHz for a Reynolds number of 60k. As will be shown shortly, these frequencies are well above the energy-containing frequencies of the turbulence.

A common problem when measuring turbulence levels in low-speed facilities is determining the lowest frequency of interest. Usually, the anemometer signal is high-pass filtered. This procedure reduces the apparent RMS turbulence level by removing low-frequency fluctuations which may be important to boundary layer transition. In this work, however, no high-pass filter was used. Instead, the DC component (the mean) of the anemometer signal was subtracted ("bucked off") using an operational amplifier of an analog computer. The remaining signal was then amplified to fill the ± 10 volt range of the 14-bit analog-to-digital converter and sampled at frequencies from 10 Hz to 10 kHz. By sampling over a range of frequencies, high resolution of the spectra was obtained. In each case the low-pass frequency of the filter was set to somewhat less than the Nyquist sampling frequency to eliminate aliasing errors. A sampling frequency of 100 Hz resolved the high-frequency end of the spectrum and extended down to sufficiently low frequencies.

All spectra presented here were found using a sampling frequency of 100 Hz with the hot wire located 3 in below the center of the tunnel. This location was

representative of the turbulence characteristics throughout the central region of the test section. For each run, 9216 points were taken and then broken into ensembles of 1024 to calculate spectra. Spectra at several different Reynolds numbers are shown in Figs. 2.2 (*a–d*). Power spectral density multiplied by frequency is plotted against the logarithm of frequency. In this way, the area under the curve is directly proportional to $(u'_{rms})^2/V_\infty^2$—the square of the turbulence intensity. As can be clearly seen, the majority of the energy is found at frequencies below 1 Hz. If the signal were high-passed at 1 Hz, this contribution to the turbulence would be lost. Perhaps fluctuations at frequencies this low have quasi-steady effects; in any event it is currently unclear what cut-off frequency should be used so both numbers are presented. The unfiltered turbulence levels at various Reynolds numbers are given below. Note that these levels correspond to a very low cut-off frequency of 0.01 Hz due to the sampling interval. Turbulence levels are also indicated below for the case of a cut-off frequency of 1 Hz.

RMS Turbulence Intensities		
Rn	$\geq$ 0.01 Hz	$\geq$ 1 Hz
60k	0.563	0.050
100k	0.358	0.064
200k	0.188	0.017
300k	0.170	0.008

Mean-pressure surveys to determine the uniformity of the freestream were taken in the test section throughout a plane perpendicular to the flow. Less than 4% variation was found in the static pressure and there was no measurable total pressure variation. These surveys indicate a 2% variation in the velocity which was deemed sufficiently uniform.

2.2 Wind Tunnel Models

In selecting the model size to obtain the desired Reynolds number, several tradeoffs were considered. To achieve a given test Reynolds number, the measured forces increase with decreasing chord. While large forces are desirable, models with small chords are difficult to build accurately. For this work, a model shop was not used; rather, experienced model sailplane enthusiasts were solicited to build the models. Consequently, construction tolerances were on the order of that found on model sailplanes. For these reasons a 12 in chord was selected as a compromise between the two competing effects. The model span was 33 $\frac{3}{8}$ in. Construction techniques ranged from all-balsa with ribs, spars and open bays, to fiberglass-covered foam. All models were fully-sheeted except one, which had open-bay construction (see NACA 6409).

2.2.1 Digitized Profiles

As a check for model accuracy and for later airfoil performance computations, every model was profiled using a digitizing Coordinate Measuring Machine (CMM) to obtain the actual airfoil shape. A comparison was then made with the desired airfoil shape to determine the accuracy of the model. Profiling was performed at Fraser-Volpe Corporation in Warminster Pennsylvania using a Helmel Checkmaster CMM with full computer software for measurement processing. This machine and software made it possible to determine the location of a point in space within 0.0005 in absolute and 0.0003 in typical for all three axes.

A drawing of the CMM is shown in Fig. 2.3. The machine itself consists of a marble slab which is finished to a high surface flatness. On the slab is a gantry which can traverse the length of the table. Mounted on this gantry is a second gantry which in turn holds a vertical column to which the probe is attached. This arrangement allows the probe to be positioned anywhere within a large volume beginning at the surface of the slab. The probe consists of a hard plastic ball mounted to the end of a steel shaft which is screwed into a precision motion detector. The equivalent measuring diameter of a probe is found (the probe is said to be "qualified") by touching it to a sphere of precisely known diameter. The computer then calculates the measuring diameter using basic geometry. Coordinates are read from the sensors when the probe is deflected in any direction by approximately 0.0003 in from its rest position. (This deflection is automatically accounted for by the CMM software.)

Outputs from the three sensors are routed to a computer which runs commercial software allowing one to reduce the raw information from the three axes to determine diameters, lengths, angles, differential locations, rotations, many different kinds of deviations from standard shapes, and so on. It will refer all measurements either to the table itself or to an arbitrary coordinate system based on the part or its fixtures. Indeed, setting up this coordinate system, or reference frame as it is called, is a major part of any measurement.

In addition to simply making a measurement, the computer can be "taught" a program of steps which represent a specific series of measurements. The computer will then prompt the operator for what point to measure next, and "knows" what to do with the measurement once it is taken. This capability was used here, allowing the entire process of measuring a model to be completed in about 25 minutes, including fixturing and post-measurement data reduction.

The machine is routinely calibrated to standards traceable to the National Bureau of Standards.

2.2.2 Digitizing Procedure

The complete procedure from selecting the airfoil model to the end of the data reduction was standardized. The procedure was as follows: Since measurements

were generally taken at only one spanwise location, the airfoil was examined to be sure that this location was representative of the total section. If the covering had wrinkled, it was smoothed. Small, local distortions were excluded from measuring; however, larger distortions which covered most of the span, such as a flap joint or a long crack in the sheeting, were included.

The airfoil was held in two identical fixtures that supported the model in a level attitude on three points, see Fig. 2.4. These fixtures were designed so that when they were turned over the model was still supported on three points. Because of the impossibility of measuring both sides of the airfoil in a single position, machined reference blocks were permanently attached to the fixtures. These blocks could be touched by the probe with the fixture and model in either position (up or down). Consequently, when the section was turned over these blocks made it possible to maintain a single reference frame for both sides. The leading edge of the airfoil was aligned with one axis of the CMM table so the measured chord direction was perpendicular to the span, and so the same chord would be measured on both sides of the model. All the sections were of a constant chord so this point is not particularly important, but this method made it possible to check that nothing had moved during the measurements. (Because of the relatively non-rigid construction of the models compared to metal parts, the fixturing was free-standing on the machine's table. There will be more on this later.)

As mentioned above, blocks mounted to the fixtures were used to establish the reference coordinate system for the upper surface. All points on the airfoil were referred by the software to the blocks, so the actual position of the airfoil and fixtures on the machine was unimportant. The chordwise location of the trailing edge was then determined by touching it with the probe from directly behind. This point was used to determine the actual chord of the section. Between 20 and 30 points were then touched on the upper surface. The spacing of points was more or less proportional to the local curvature; near the leading and trailing edges the spacing was small, over the central parts of the airfoil it was as great as $\frac{3}{4}$ in. The final point touched in the upper surface sequence was the leading edge. This was detected by moving the probe vertically past it with the vernier lead screw at progressively closer settings until it touched.

Because of the possibility of distorting the model, the stands could not be rigidly held down to the CMM table. Consequently, any inadvertent movement during the data collection was detected by comparing the leading and trailing edge points as measured from both sides. If they were at the same points with respect to the reference frame established by the blocks on the fixtures, then no motion that could affect the measurement had occurred.

After the upper surface was done, the model and fixtures were turned over as a unit and the leading edge was once again aligned. Measuring continued at the leading edge, the first point here duplicating the last point on the upper surface,

and the final point duplicating the first point on the upper surface (the trailing edge).

Of the 67 duplicated leading edge pairs, 46 were within 0.001 in, 52 within 0.002, 59 within 0.003, 65 within 0.005 and all within 0.0057 in. Part of the difference within any pair is due to the impossibility of finding the exact point that was measured from the other orientation, because of the nature of the leading edge. However, since a chordwise error translates to a much smaller vertical error except at the leading edge, these accuracies imply a general thickness measurement error of under 0.001 in. On a 12 in chord this is trivial.

The results of the measurements were collected on a Leading Edge personal computer, which was also used to reduce the data. All the output from the CMM was saved on a disk file. Typical output of the CMM software is shown in Fig. 2.5.

The CMM data are the locations of the center of the ball at the end of the probe, not the surface itself. Consequently, a second program was used to reduce the CMM output to the actual coordinates of the airfoil, to rotate the actual chord so it was parallel to the reference axis, and to normalize the airfoil to coordinates between 0 and 1. This data was also saved as a file. A header was added to identify the airfoil and show the actual chord. A typical output file from this program is shown in Fig. 2.6.

2.2.3 Digitizer Results

(Note, "-PT" (Princeton Tests) is appended to the airfoil name to distinguish the digitized coordinates from the nominal coordinates.)

In Chapters 10 and 11, each of the actual sections is plotted against the nominal coordinates at half scale (6 vs 12 in). The legend inside the airfoils shows what is being compared; the solid line is always the first airfoil, normally the prototype, and the broken line the second, normally the test section. In a few cases different prototypes are compared. Before they are plotted, the two airfoils are fitted in a least squares sense. The fitting uses two variables—relative vertical location of the entire section and relative rotation of the entire section—to produce the lowest possible RMS difference without distorting the airfoil. This difference is shown under the trailing edge of the upper plot.

The lower plot shows the difference, or error between the two airfoils on a much expanded scale. The upper surface difference is the solid line and the lower surface the broken one. If the two sections were perfectly matched, the plot would be two straight lines lying on the horizontal axis. A displacement above or below the axis means the test section surface lies above or below the nominal, respectively. If the solid line is above (or below) the broken one, regardless of its position with respect to the axis, the section is too thick (or thin) at that point. If both lines sweep up or down together then the camber is in error. Camber error as well as thickening is frequently seen at the trailing edge.

The short, inward-facing tics show the positions of the leading and trailing edges. The most difficult point to measure is the vertical position of the leading edge. (It is quite possible for a model to have more than one leading edge.) This is because the slope becomes infinite and a very small change in the chordwise position of the probe produces inordinately large changes in the measured thickness. Consequently, the vertical locations of the exact edges, as shown by the position of the tics, have somewhat reduced accuracy. However, because many points were digitized near the leading and trailing edges and because the contribution of each point to the overall accuracy number was weighted in proportion to the distance between it and the adjacent points, the effect of the end points on the overall error is very small. In addition, the most forward and most rearward points themselves were not included in the error calculation.

As a check on the digitizing procedure, two of the models were digitized more than once: the SD7080-PT and the SD7003-PT. The SD7080 pair was done early in the profiling as a general check for repeatability, but the spanwise stations were not the same. Even so, the agreement was within 0.003 in. The SD7003-PT was digitized six times; once at the beginning of the profiling, five times at the end (a time span of about 75 days). Two profiles, the SD7003-PT and SD7003-PT (R) were taken at the same station and are a good indication of the overall repeatability of the measurement setup—about 0.0007 in, 0.006% of chord. The remaining four profiles were taken at 3 in intervals centered on the span and were intended to discover how much spanwise variation a good airfoil model might show. As can be seen in Figs. 10.46–10.49, it is very small indeed.

Several observations can be made about methods of construction based upon the models digitized in this study. Built-up, sheeted models tended to have a problem with the blend between the leading edge and the beginning of the sheeting. The trailing edge also tended to be thick. Foam core sections usually had sharper trailing edges, but any errors in contour were more prolonged; with built-up sections the errors were more local. One model had excellent contours for the separately molded upper and lower surfaces, except the joint at the leading edge was too wide. Because of the type of construction, the increased thickness at the leading edge carried back through a large part of the airfoil. This was a problem that was not present in models that used a single piece—usually wood—leading edge. The open-bay models have no single profile—over the ribs it can be accurate, but inevitably there is sag between the ribs.

Neither the cost nor the type of construction was a good indicator of the accuracy. For example, a balsa-sheeted, rib and spar section built over a weekend for under $10 had one of the most accurate profiles measured. On the other hand, the accuracy of some models costing many times this amount was only average.

Trailing edges are a problem for all types of construction. As can be seen from the plots, the most common error is a poorly contoured trailing edge; it is warped either up or down, with the preponderance being up. Since the

sensitivity of performance to trailing edge location is high, clearly there is a general problem here. One model, the S4180-PT, had a very thin trailing edge which was so warped that it was meaningless to measure it at all; there simply was no representative section. (This was the only model with such a major contour discrepancy.)

Some of the nominal airfoils differ less between themselves than the models do with the ideal coordinates. The HQ2/9, RG15, and S2048 are an example of this, and several plots compare these prototype sections. This has significance when comparing polars, because *small* differences in performance on similar sections could be a result of the inaccuracy of the model or random variations in the test results rather than an indication of the superiority of one prototype section over another. One model, the E193-PT, was actually a better fit to the E205 than to its true nominal coordinates (see Figs. 10.5 and 11.12). These airfoils are, of course, quite similar, but the point is that one must be careful in claiming performance for the prototype based on the model's performance. In cases where the model is inaccurate, the performance applies to the model airfoil and not necessarily to the nominal airfoil.

One section, a SD7032, was first tested in the tunnel with no covering over the sanded balsa sheeting (version A: SD7032A-PT), then with Monokote covering (SD7032B-PT), and finally with a flap (SD7032C-PT). Only the flapped version was digitized.

The DF102-PT and DF103-PT are compared to the DF101-PT, not to a nominal airfoil. (The DF101-PT is compared to the nominal.) Since the point of these variants was to explore the effects of changes on the forward upper surface, the relevant prototype is the DF101-PT. The plots show what and how much was added or removed in that area. The minor differences along the rest of the airfoil are due to the fact that the sample chords were not all at the same spanwise stations, and because the fitting routine tends to distribute the deliberate "error" over the entire airfoil so as to keep the RMS error down.

For a few airfoils (SPICA, WB135/35, and WB140/35/FB) the coordinates were supplied by the builders. In these cases small errors in fit are not meaningful because hand-generated coordinates are not smooth in the mathematical sense, and therefore the spline routine that compares the airfoils can have residuals of the order of the errors. This is particularly noticeable on the upper surface of the WB135/35 between 1% and 3% chord, where the model is smoother than the nominal.

2.3 Force Measurement Technique and Instrumentation

Lift was measured directly using an electro-mechanical force balance, and the drag was found indirectly using the momentum method[6]. Rather than computing the drag based on just *one* vertical survey, the wake was surveyed and the drag computed at *four* spanwise locations and then averaged.

A sketch of the apparatus used to measure lift is shown in Fig. 2.7. The airfoil model was mounted horizontally in the tunnel between two $\frac{3}{8}$ in clear plastic (Plexiglas) end plates (omitted for clarity) to isolate the model ends from the tunnel side-wall boundary layers and the support hardware. One side pivoted, and the other was free to move vertically on a precision ground shaft. Two linear ball bearings spaced 8 in apart provided essentially frictionless movement for a carriage which held the airfoil and angle of attack control hardware. Spherical bearings were used to minimize moments transmitted to each linear bearing. A force transducer coupled to the carriage through a pushrod sensed the lift (actually half the total model lift was transmitted to the transducer).

The force transducer in this study was a servo balance rather than a standard strain gauge or capacitance type transducer. As with a standard beam balance, the dead weight of the airfoil and the support structure are counterbalanced with weights. The remaining forces (the lift and residual imbalance) are balanced by the torque from a brushless DC torque motor mounted on the beam axis. Any angular displacement from a reference zero is sensed by an AC potentiometer, and the error signal is used to drive the torque motor until the error disappears. The torque required to do this is directly related to the lift. The current needed to generate the torque is a very linear analog of the torque, and therefore of the lift.

In practice several problems occur, the most difficult being to meet the requirement of low system friction. To achieve this, precision ball bearings were used throughout. The residual friction (as well as some magnetic hysteresis) was further reduced by adding a small amount of electrical dither to the torque motor. As built, the system was capable of measuring 7 lb (half of the lift) with stiction and hysteresis limited to 0.002 lb at the lowest Reynolds number. The overall system had an accuracy of $\pm 0.25\%$ of full scale or $\pm$ 0.002 lb, whichever is larger. The term full scale here refers to the maximum force experienced over a given run at constant Rn. This corresponds to ± 0.0135 of C_l at $Rn = 60$k and ± 0.0055 at 300k. Nine-point calibrations of the force balance were performed frequently to minimize the effects of drift.

The drag was measured using the momentum deficit method because the mechanical one is both difficult and expensive. In addition, drag obtained by mechanical means includes three-dimensional effects due to the side walls. These effects can be reduced by using a three-piece model with only the central panel connected to the force balance; however, the angle of attack of the two tips must be kept equal to that of the central portion and the gaps must be minimized. Althaus[7] investigated the effect of a gap on the drag at low Rn and found that with a 0.5 mm (0.3%) gap and 250 mm (156%) span, the drag was increased 12% at an angle of attack of 9°.

To compute drag using the momentum method, a pitot tube was surveyed through the wake 1.25 chord lengths downstream of the trailing edge to find

the deficit. (Using a single pitot tube and moving it through the wake provided better spatial resolution of the wake than using a rake with multiple, fixed pitot tube locations.) Based on the application of the two-dimensional momentum and continuity equations to a control volume about the airfoil[6], the drag force per unit span can be found as:

$$d = \rho \int_{-\infty}^{\infty} u(V_\infty - u)dy \tag{1}$$

where the integral is performed perpendicular to the freestream, downstream of the airfoil. The freestream velocity is V_∞, y is in the direction normal to the freestream, and u is the x-component of velocity at the downstream location.

This method of determining the drag is valid only if the wake survey is made in a region where the static pressure is equal to that in the freestream. Surveys on several airfoils indicated that static pressures in the wake were nearly equal to the freestream static pressure.

For pitot tube misalignments of less than 10°, the measured total pressure is essentially independent of flow angle. The drag calculation requires only the streamwise component of the velocity; thus, transverse velocity components at the survey location can decrease the measured drag. Drag values were found to remain constant as the survey location was moved upstream and downstream of the 1.25 chord location, indicating that it was sufficiently far from the trailing edge so that transverse velocity components were negligible.

Drag was calculated using the difference between the total pressure upstream of the airfoil and that in the wake. Equation (1) can be rewritten to give:

$$d = 2 \int_{-\infty}^{\infty} (\sqrt{P_{d\infty} - \Delta P_0})(\sqrt{P_{d\infty}} - \sqrt{P_{d\infty} - \Delta P_0})dy \tag{2}$$

where $P_{d\infty}$ is the freestream dynamic pressure measured with a pitot tube which was 15 in upstream of the airfoil and 8 in below the centerline, and ΔP_0 is the difference between the total pressure in the freestream and the total pressure in the wake. This pressure difference is small and difficult to measure, requiring a sensitive transducer. A Baratron model 220B unit made by MKS Instruments, Inc. was used for this purpose with a full-scale range of 1 mm Hg and an accuracy of 0.15% of reading. It was factory calibrated against a standard traceable to the National Bureau of Standards.

Spanwise non-uniformity in the wake is well known[7,8]. Indeed, the drag variation can be more than 50% at the lower Reynolds numbers. As mentioned previously, four spanwise stations spaced uniformly over the central 1 ft of the airfoil were used, and they were averaged to provide a better measure of the airfoil performance.

A two-axis traversing mechanism provided position control for the downstream pitot tube (see Fig. 2.8). The important features and accuracies of this positioner are:

Spanwise motion: 24 in
Vertical motion: 14 in
Resolution:
    less than 0.001 in, both directions
Readout accuracy:
    spanwise: 0.020 in
    vertical: 0.002 in
Setability:
    0.005 in, both directions

Each axis was instrumented with a precision DC potentiometer and was driven by a small, geared, DC motor. The carriage which held the pitot tube ran on precision bushings around centerless ground and polished rods, and the motors drove the carriage and potentiometers through a linkless steel and plastic chain. For stability, the entire carriage was mounted on a large aluminum "U" channel which was mounted to the bottom of the tunnel floor. The arm that carried the pitot tube projected into the tunnel through a slot cut in the floor, and both the arm and slot were sealed to prevent air leakage into the tunnel.

Each motor and potentiometer together with associated electronics formed a position servo loop. The open-loop gain was quite high; however, the accuracy of the reading was independent of the gain, since it was read directly from the feedback potentiometers. Analog inputs to the positioner were provided by a computer with two digital-to-analog converters. Because accuracy was the design goal, there was no attempt to make the positioning particularly fast. This decision to ignore speed was soon regretted when it became apparent how long each run in the tunnel required. (Changes were made later that resulted in some improvement in the speed.)

Using this two-axis positioner, the surveys were made through the wake at four spanwise locations. Each survey consisted of between 20 and 80 pressure measurements (depending on the wake thickness) with points nominally spaced 0.08 in apart. A typical survey through the wake took two minutes, which effectively yielded a time-averaged drag value for each spanwise station.

Three pressure transducers (MKS model 220B) were used in this study. A 1 mm Hg full-scale unit measured the difference in total pressure between the wake and freestream as previously mentioned. Another 1 mm Hg unit measured the difference between the test section stagnation pressure and atmospheric pressure to allow an accurate calculation of the density in the test section. The third transducer had a 10 mm Hg full scale and was used to measure the dynamic pressure at the upstream pitot tube.

Due to the tunnel blockage from the lift apparatus installed in the test section, the velocity at the airfoil was greater than that upstream where the freestream dynamic pressure was measured. Since the upstream pitot-static probe did not sense the dynamic pressure at the airfoil, a calibration was performed to correct its reading. Using the continuity equation, it can be seen that the velocity ratio between the velocity at the airfoil and the velocity upstream of the blockage is simply the ratio of effective areas. Because the effective area of the apparatus is clearly a function of Reynolds number, a velocity ratio based on the Reynolds number was determined before every run. A velocity was found with the fixed upstream pitot-static probe and with the downstream pitot-static probe placed near the tunnel centerline with the airfoil installed but generating no lift. The ratio was determined at several speeds in the neighborhood of the actual run speed. A linear interpolation based on Reynolds number was then used during the run to determine the velocity at the airfoil based on the dynamic pressure of the upstream pitot-static probe. Throughout this work, the velocity difference between the upstream location and the airfoil was less than 6%.

During a run, which usually took about 1.7 hours, the tunnel velocity drifted slightly, depending on atmospheric conditions. To ensure an accurate determination of the lift and drag coefficients, the measured lift and the ΔP_0 were normalized by the instantaneous value of the freestream dynamic pressure. Thus, slow fluctuations in tunnel speed affected only the Reynolds number and not the determination of the aerodynamic coefficients.

Wind-tunnel corrections[6] were applied to values of C_l and C_d and were approximately 4% and 2%, respectively. Error estimates indicate that the accuracy of the measured C_l is $\pm 1\%$ and that of the C_d is $\pm 4\%$. The angle of attack of the airfoil was controlled using a gear motor with a worm drive and a sector gear and was sensed using an angular transformer like that used in the force balance. The accuracy in determining α was $\pm 0.02°$.

All transducer voltages were recorded using a Scientific Solutions, Inc. 14-bit analog-to-digital converter interfaced to an IBM PC. The PC controlled the wake pitot tube position and the airfoil angle of attack. After manually setting the tunnel speed to achieve the desired Reynolds number, the data collection was completely automated and proceeded as follows: The first angle of attack was set, and the location of the wake was found. Next, the four wake surveys were performed. When they were complete, the angle of attack was increased and the process repeated. Usually, a polar at a given Reynolds number consisted of between 15 and 20 angles of attack from $-3°$ to $15°$. In all cases, this process continued into stall.

Drag was measured only for increasing angles of attack, so hysteresis was not examined. This was done for two reasons. First, the amount of run time would have doubled to 3.4 hours on average. Second, hysteresis is a sign of gross laminar separation—a high-drag condition. This investigation was directed towards

the characteristics of low-drag airfoils in application to RC sailplanes; hence, high-drag conditions were of little interest. Furthermore, if the measured drag coefficient exceeded approximately 0.050 the run was stopped, again because there was no interest in high-drag conditions and also due to time constraints.

In addition to taking lift and drag data simultaneously, which was relatively slow, in many cases a second run was made in which just lift was measured, allowing the angle of attack to be incremented relatively rapidly. In this mode of operation, the angle of attack was increased up to a pre-set value and then decreased. Hysteresis loops present in the lift behavior were then sometimes observed. Approximately 140 data points were taken, and this process usually required 5 minutes—much less than the 3.4 hours that would have been required to obtain a complete drag polar at 1° increments in α. This lift data is included along with the polar data in Chapter 12. Increasing and decreasing angles of attack are denoted by solid-circle and open-square symbols, respectively. See Fig. 12.2 for example.

2.4 Comparison with Other Facilities

Measurements in other facilities can provide a basis of comparison for the lift and drag obtained in this project. Unfortunately, it is difficult to make a broad range of systematic comparisons because relatively few of the airfoils tested in this project have been tested in other facilities at the same Reynolds numbers. Until recently the primary application for airfoils operating at Reynolds numbers considered here was for model aircraft. Consequently, little effort was directed at designing and testing airfoils in the Reynolds number range $60k \leq Rn \leq 300k$. The majority of available data with which to compare the Princeton data is from the Model Wind Tunnel at Stuttgart[7,9,10]; however, comparisons were also made to data obtained from NASA Langley[11], Delft[8,12], and Notre Dame[13,14].

Comparisons of the available drag polars are shown in Figs. 2.9 through 2.20, and comments are provided in several cases. A listing is given at the end of the discussion.

Fig. 2.10 compare drag polars obtained in the Princeton tunnel (using the E205B-PT model) with those in the Delft tunnel[8] and in the Model Wind Tunnel at Stuttgart[7] for the E205 at Reynolds numbers of 60k, 100k, and 200k. At 200k all three facilities agree to within 10% over the central region of the lift range. The agreement between Delft and Princeton data at 100k is also quite good. However, at 60k the agreement is worse.

Stuttgart tests of the S3021 in 1986 are compared to the Princeton data in Fig. 2.20 for Reynolds numbers of 100k and 200k. Overall agreement is reasonable; however, the Princeton drag values are generally lower. A comparison with Stuttgart data from 1980 on the NACA 0009 is shown in Fig. 2.18. In this case, the Stuttgart data indicates lower drag throughout much of the lift range. Results of the S2091 are compared with Stuttgart (1986) in Fig. 2.19.

At Reynolds numbers of 100k and below, the agreement is poor, with Stuttgart generally finding higher drag. By 200k, the agreement is quite good.

Comparisons were also made with data from Notre Dame as shown in Figs. 2.16 and 2.17. In the case of the FX63-137, the Notre Dame data indicates a significantly higher drag than either the Stuttgart or Princeton values.

Fig. 2.13 shows a comparison of the E387 data from the present work to that from the NASA Langley[11], Delft[12], and Stuttgart[9]. Note that the E387 model used in the Princeton test (E387A-PT) is decambered (see Fig. 10.13) which is reflected by a shift in the polar to lower lift values. The camber error is approximately 0.4%. Nevertheless, the general agreement between the data from the NASA Langley, Delft, and Princeton is good.

The discrepancies found in these comparisons are primarily due to differences in (1) flow quality, (2) accuracy of measurements, (3) methods of measurement, and (4) model accuracy. At this time it is difficult to determine how much of the disagreement is due to each of these areas, but we have documented those of the present project to allow for future comparisons.

Fig. 2.9 CLARK-Y-PT vs CLARK-Y (Althaus, 1980)[9]
Fig. 2.10 E205B-PT vs E205 comparisons [7,8]
Fig. 2.11 E214B-PT vs E214 (Althaus, 1986)[7]
Fig. 2.12 E374B-PT vs E374 (Althaus, 1985)[10]
Fig. 2.13 E387A-PT vs E387 comparisons [9,11,12]
Fig. 2.14 FX60-100-PT vs FX60-100 (Althaus, 1980)[9]
Fig. 2.15 FX63-137B-PT vs FX63-137 (Althaus, 1980)[9]
Fig. 2.16 FX63-137B-PT vs FX63-137 (Bastedo and Mueller, 1985)[14]
Fig. 2.17 M06-13-128-PT vs M06-13-128 (Pohlen and Mueller, 1983)[13]
Fig. 2.18 NACA 0009-PT vs NACA 0009 (Althaus, 1980)[9]
Fig. 2.19 S2091B-PT vs S2091 (Althaus, 1986)[7]
Fig. 2.20 S3021A-PT vs S3021 (Althaus, 1986)[7]

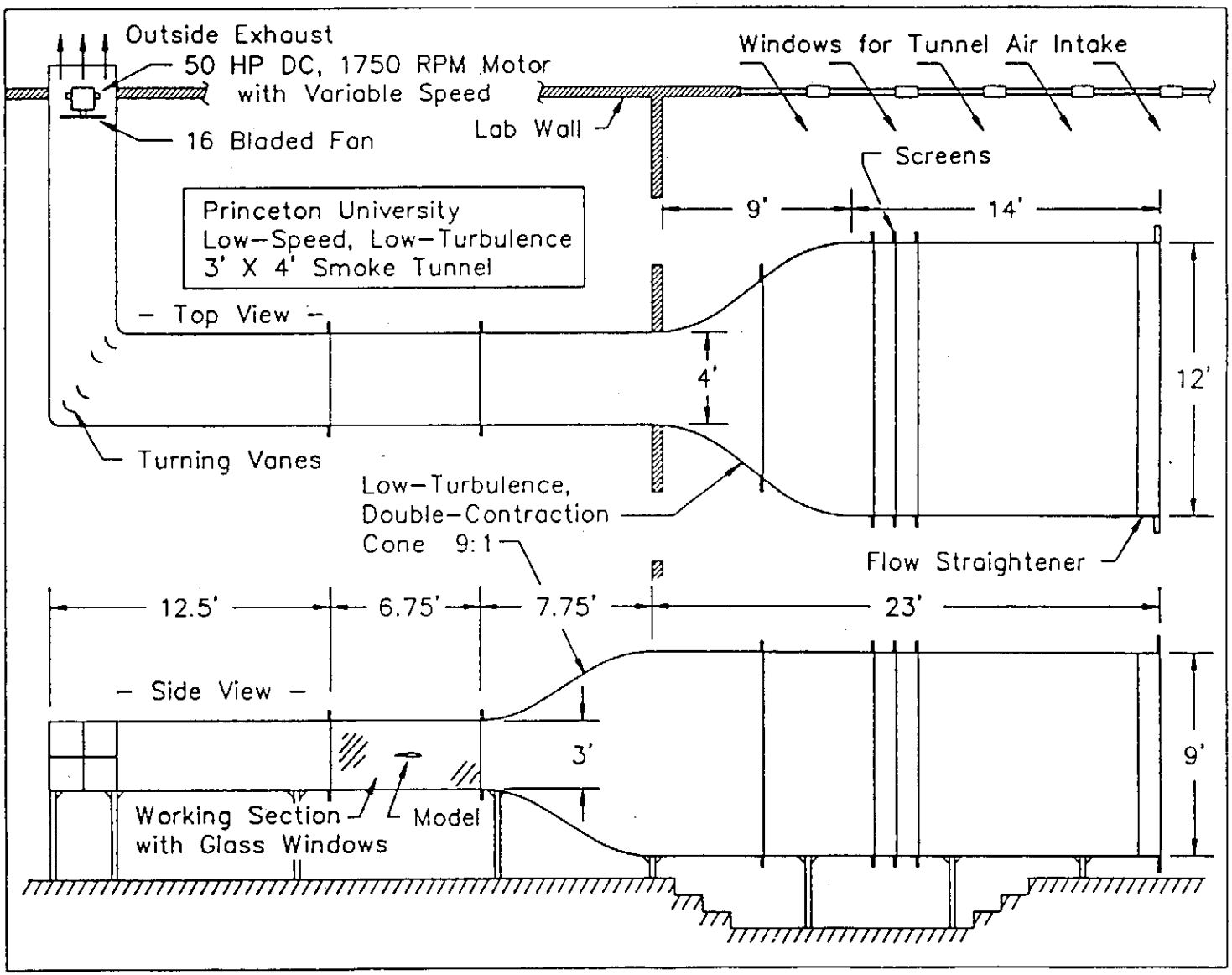

Fig. 2.1 Diagram of the Princeton University low speed wind tunnel (not to scale).

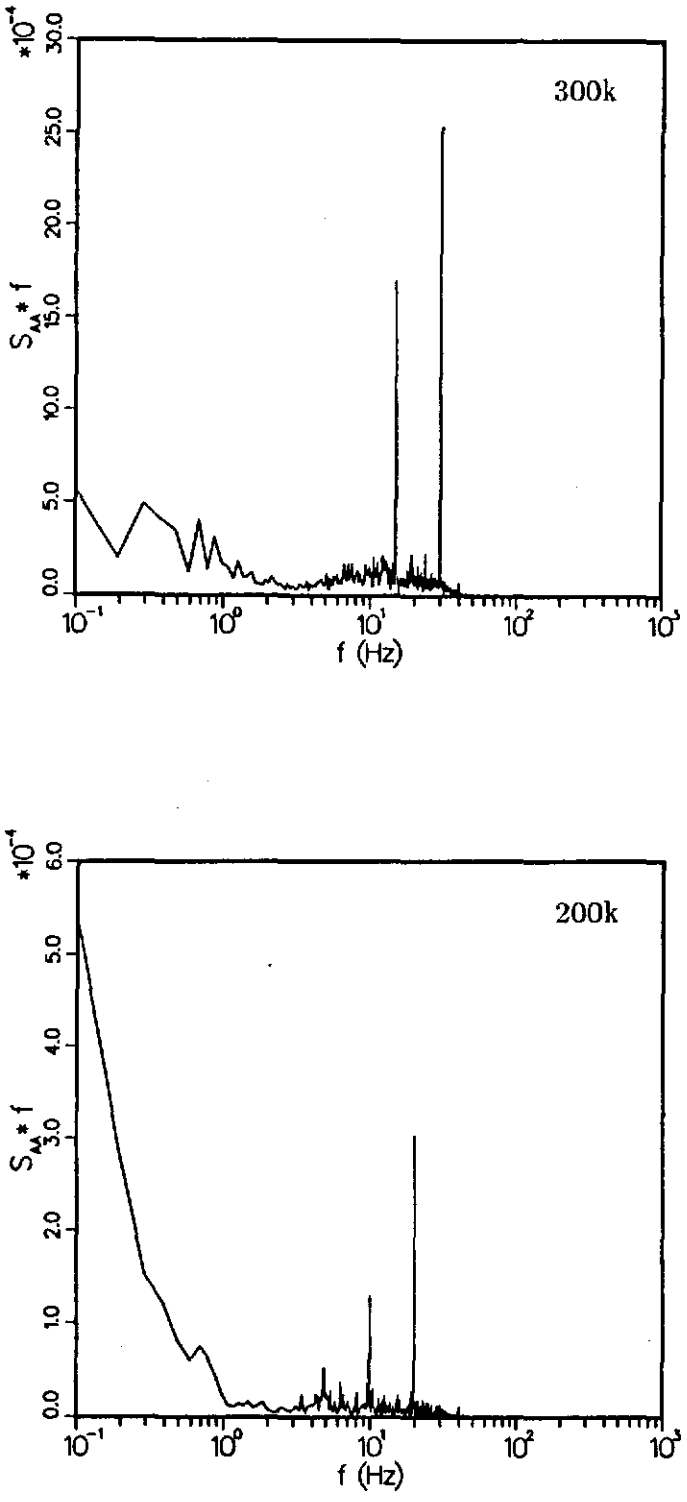

Fig. 2.2 Fluctuating velocity energy spectra in the freestream

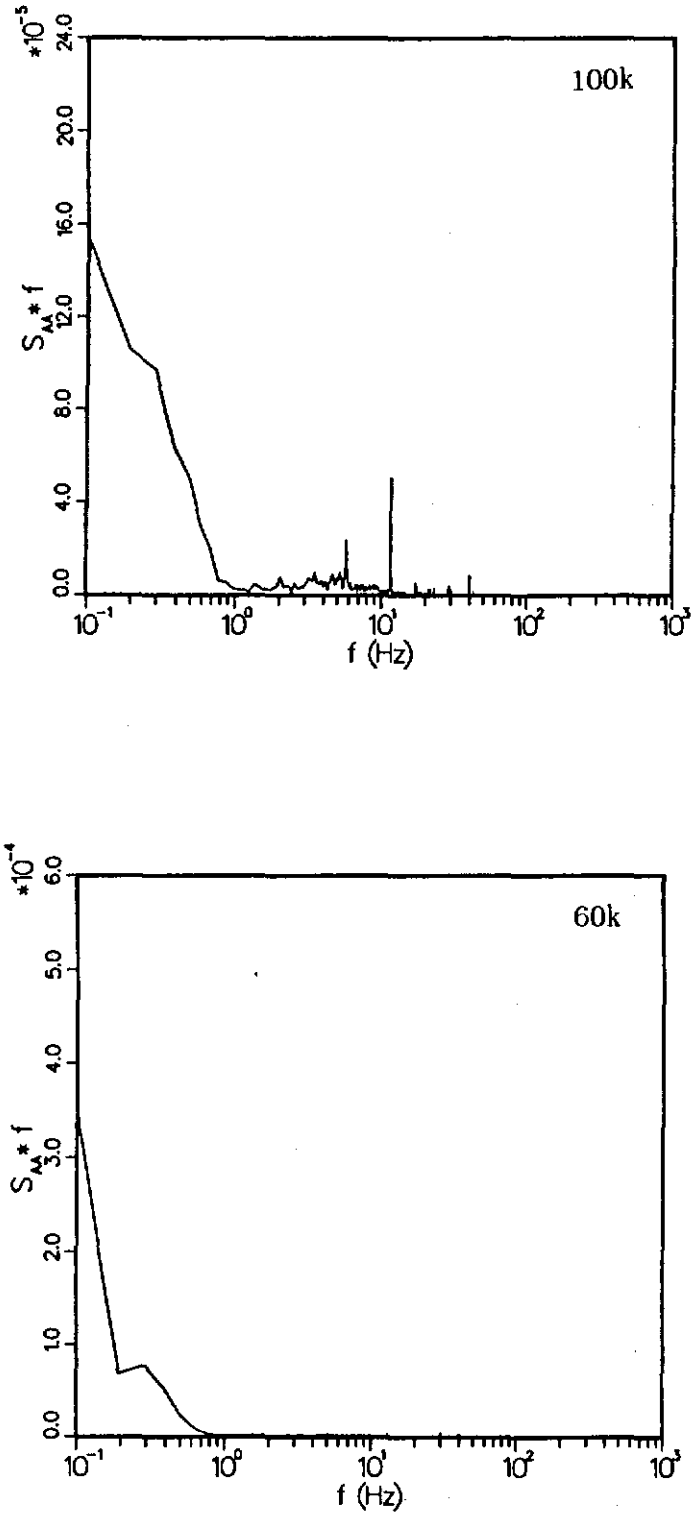

Fig. 2.2 Fluctuating velocity energy spectra (concluded).

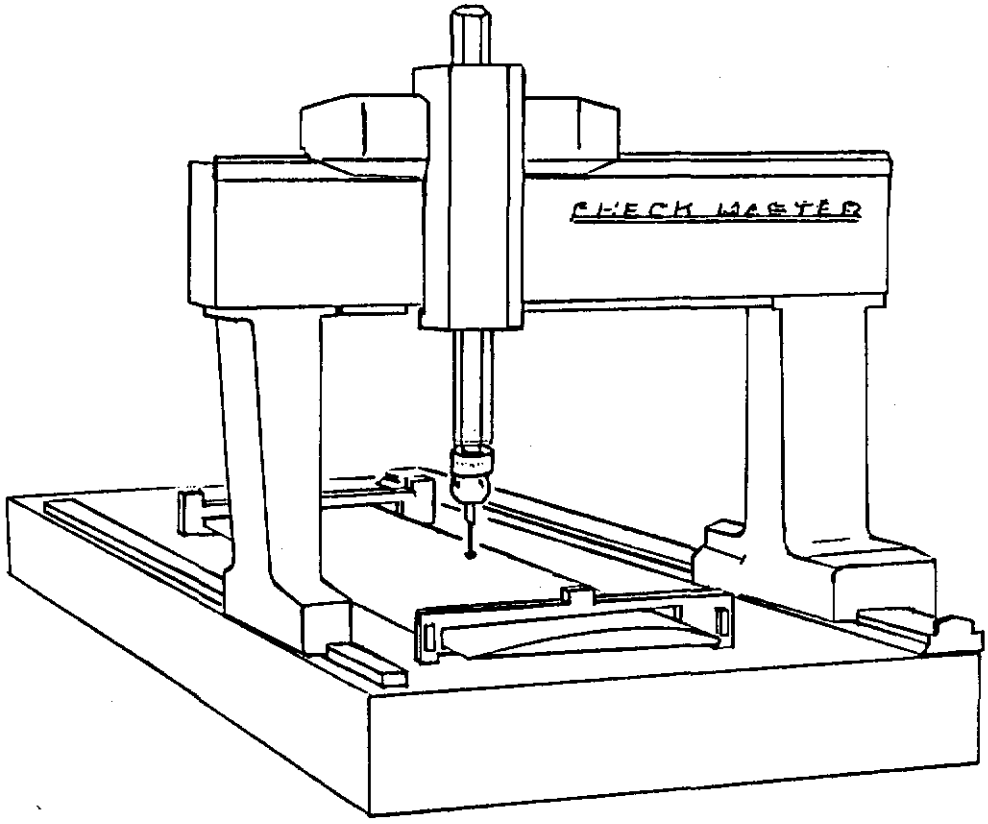

Fig. 2.3 Coordinate Measuring Machine (CMM) used for digitizing.

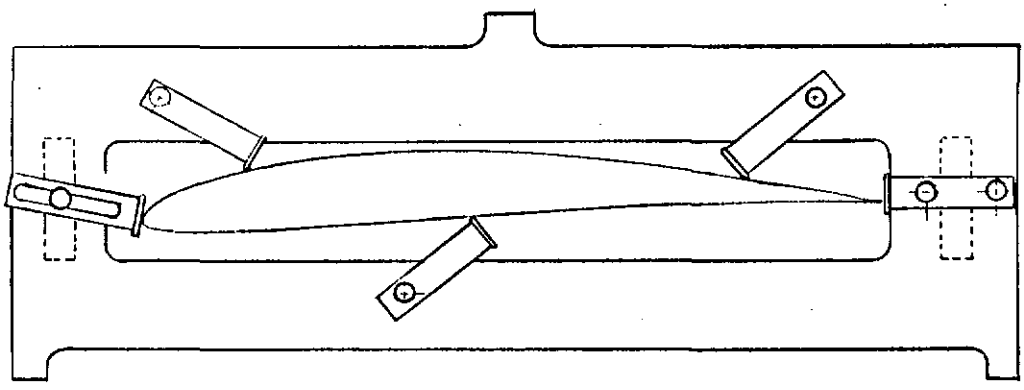

Fig. 2.4 Holding fixture for digitizing the test sections.

```
37      31/1  XZ POINT
                 X=  13.6939
                 Z=  -1.1266

38      32/1  X Z POINT        ! Upper L.E.
                 X=  13.7193
                 Z=  -1.2182
----------------------
13       7/1  XZ POINT         ! Lower L.E.
                 X=  13.7199
                 Z=  -0.7423

15       9/1  XZ POINT
                 X=  13.6941
                 Z=  -0.6770
```

Fig. 2.5 Typical CMM digitized data.

```
AQUILA profiler data.  Chord = 11.990
1.00000  0.00000                    0.00106  -.00259
0.99746  0.00123                    0.00435  -.00553
0.98829  0.00238                    0.01274  -.00714
0.97400  0.00453                    0.05262  -.00657
0.94486  0.00884                    0.13491  -.00665
0.90040  0.01570                    0.24506  -.00748
0.86567  0.02142                    0.38540  -.00767
0.83894  0.02575                    0.53849  -.00721
0.82217  0.02951                    0.70417  -.00651
0.80749  0.03199                    0.79285  -.00587
0.76590  0.03831                    0.83603  -.00546
0.69655  0.04901                    0.88509  -.00464
0.62461  0.06080                    0.94190  -.00375
0.54502  0.07190                    0.97800  -.00237
0.49234  0.07805                    0.99740  -.00083
0.39368  0.08685                    1.00000  0.00000
0.31264  0.08876
0.23528  0.08634
0.14185  0.07430
0.07922  0.05817
0.04595  0.04561
0.02491  0.03337
0.01583  0.02617
0.00659  0.01576
0.00169  0.00753
0.00000  -.00000
```

Fig. 2.6 Typical normalized coordinates from the digitized data.

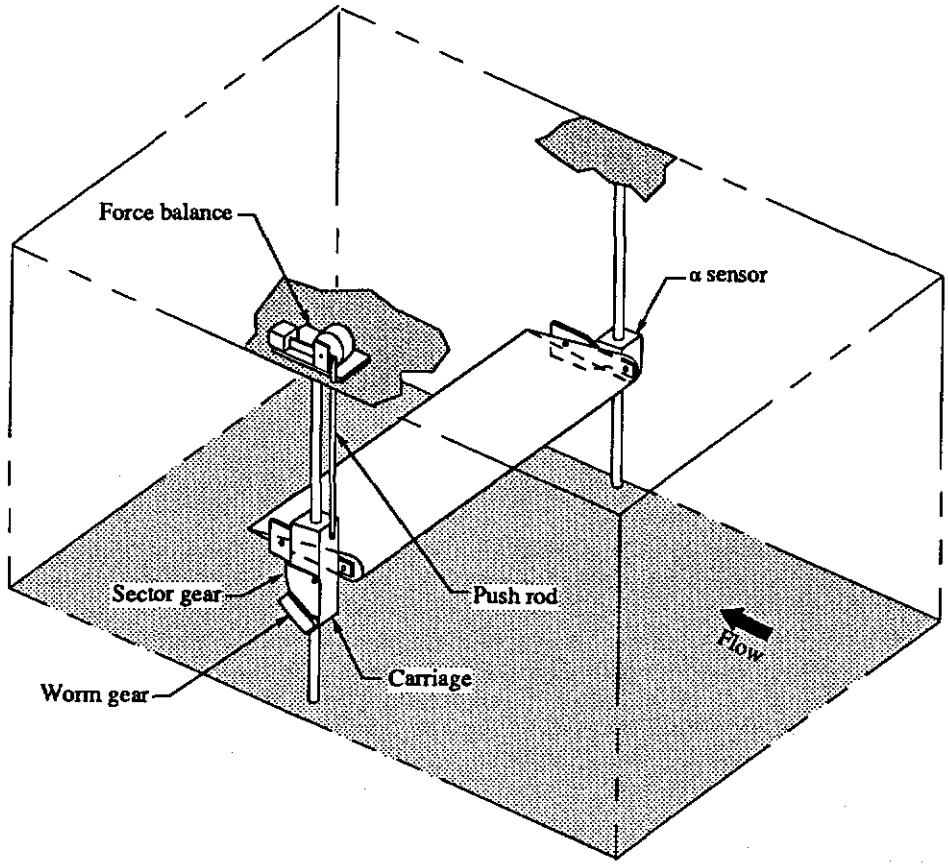

Fig. 2.7 Test rig indicating model orientation and lift measurement method. (Plexiglas end plates are not shown for clarity.)

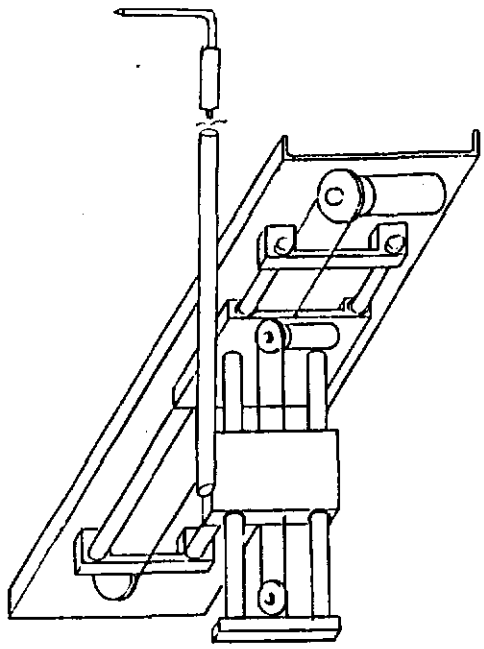

Fig. 2.8 Sketch of the X-Y traversing mechanism.

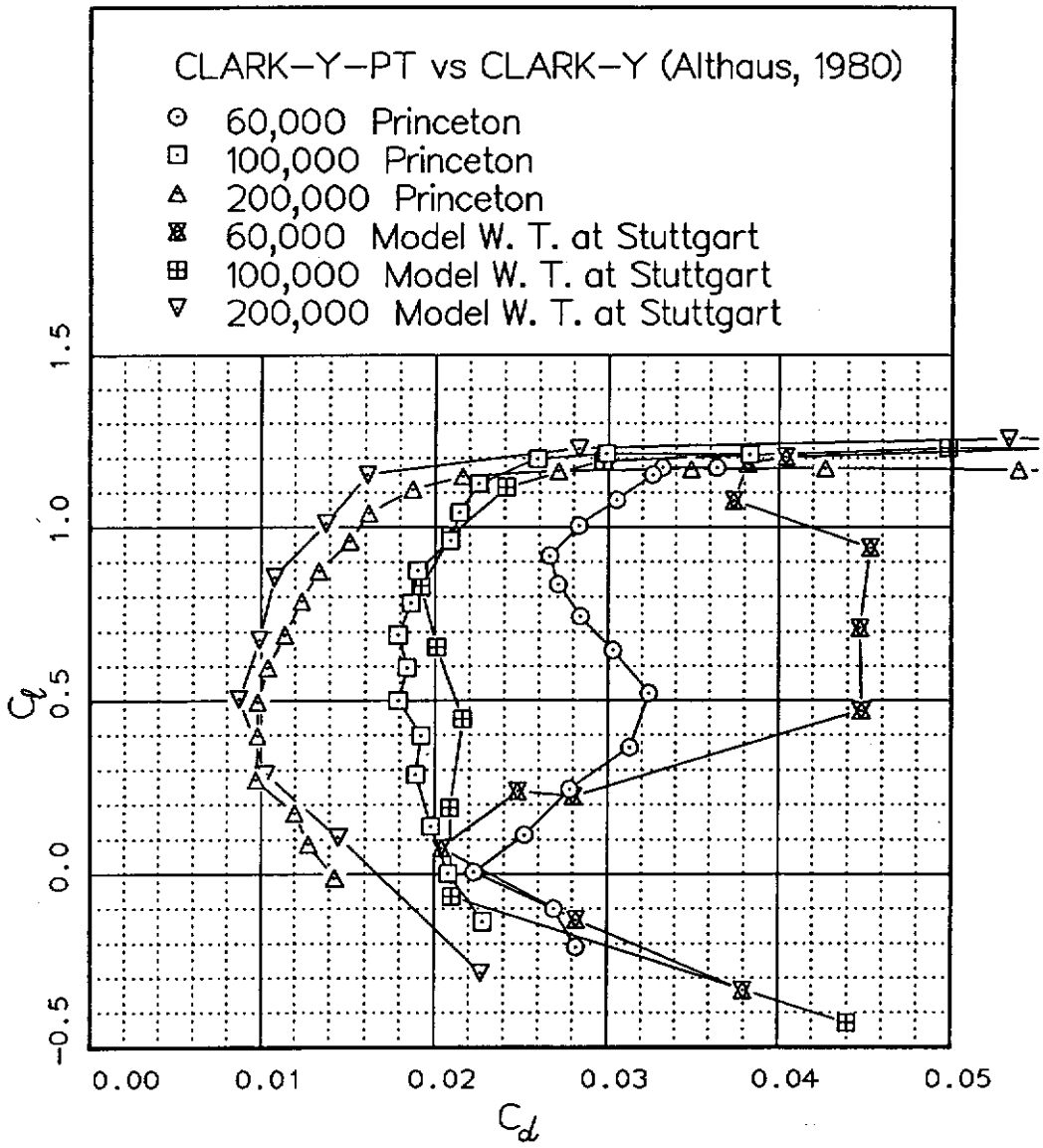

Fig. 2.9 Comparison polars: CLARK-Y-PT vs Stuttgart[9].

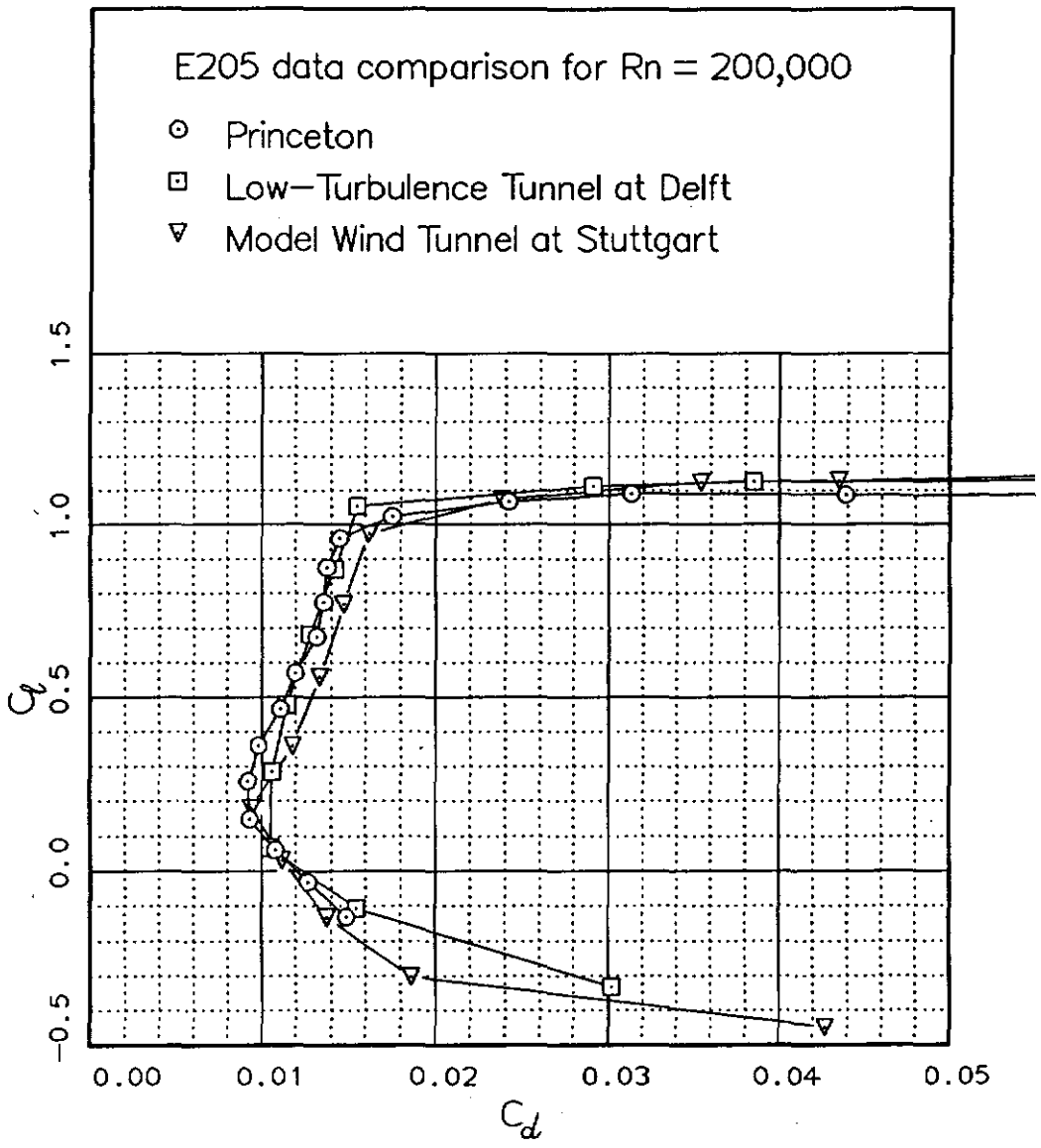

Fig. 2.10 Comparison polars: E205B-PT vs Delft[12] and Stuttgart[13]

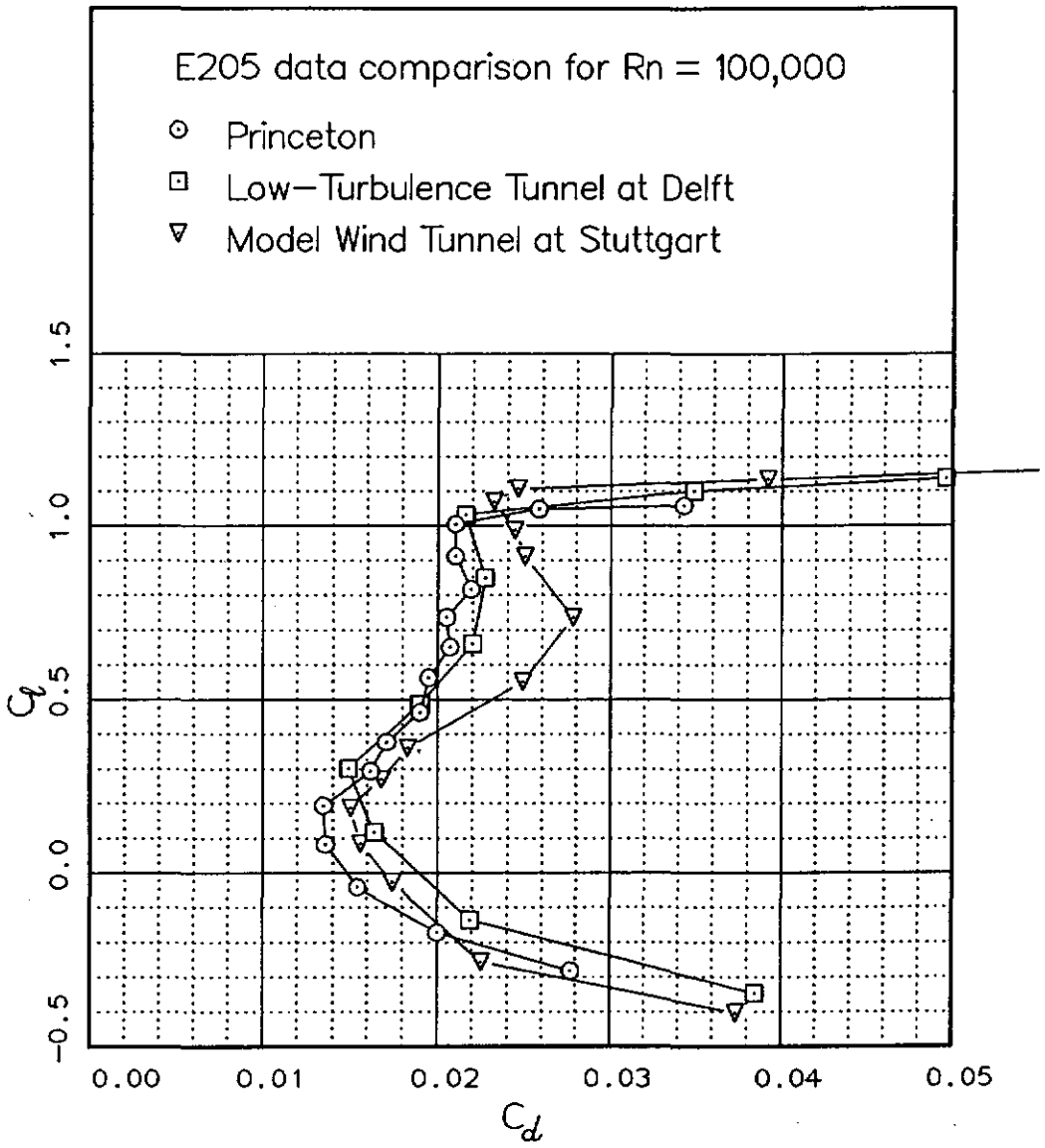

Fig. 2.10 Comparison polars (continued).

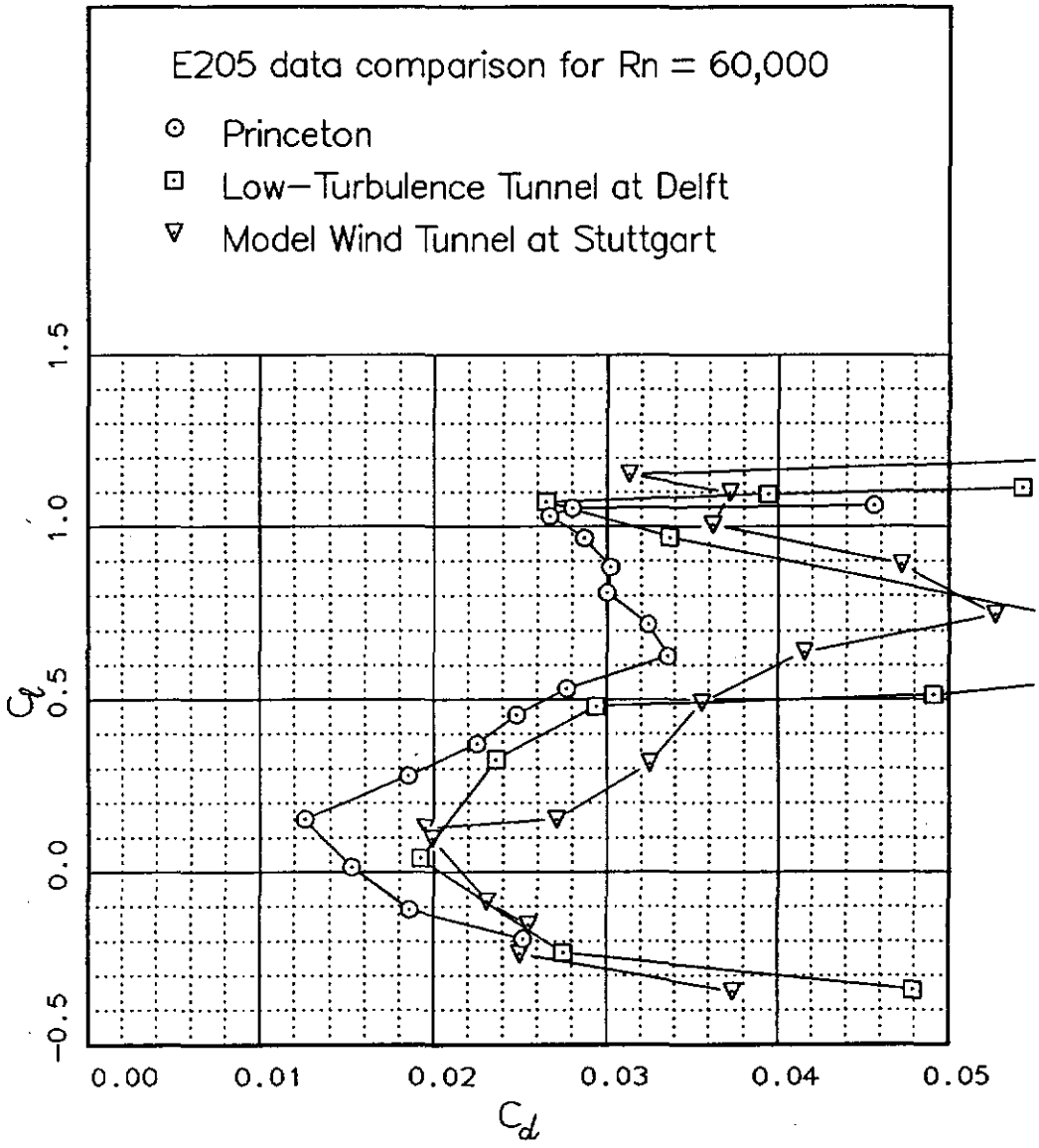

Fig. 2.10 Comparison polars (concluded).

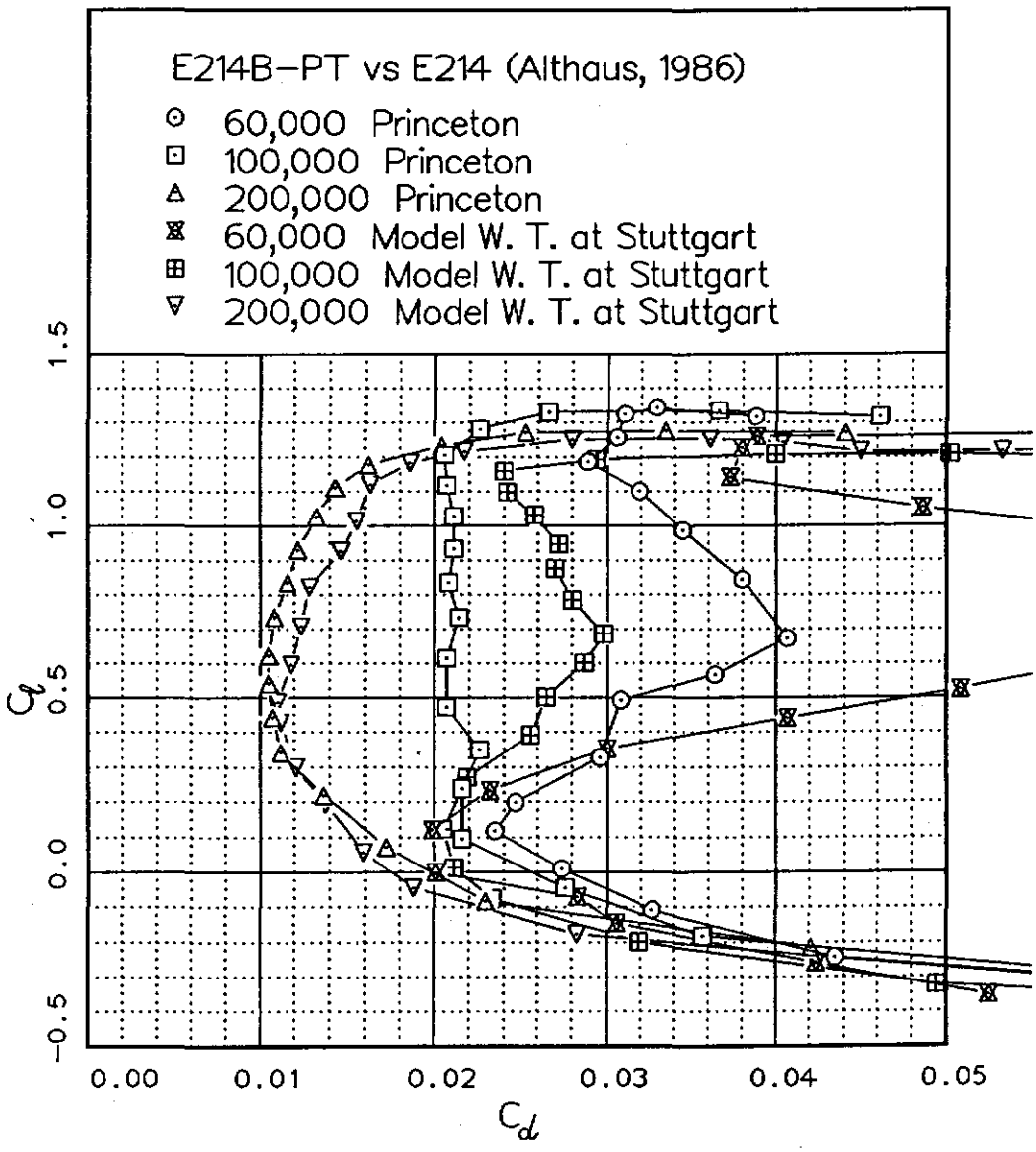

Fig. 2.11 Comparison polars: E214B-PT vs Stuttgart.

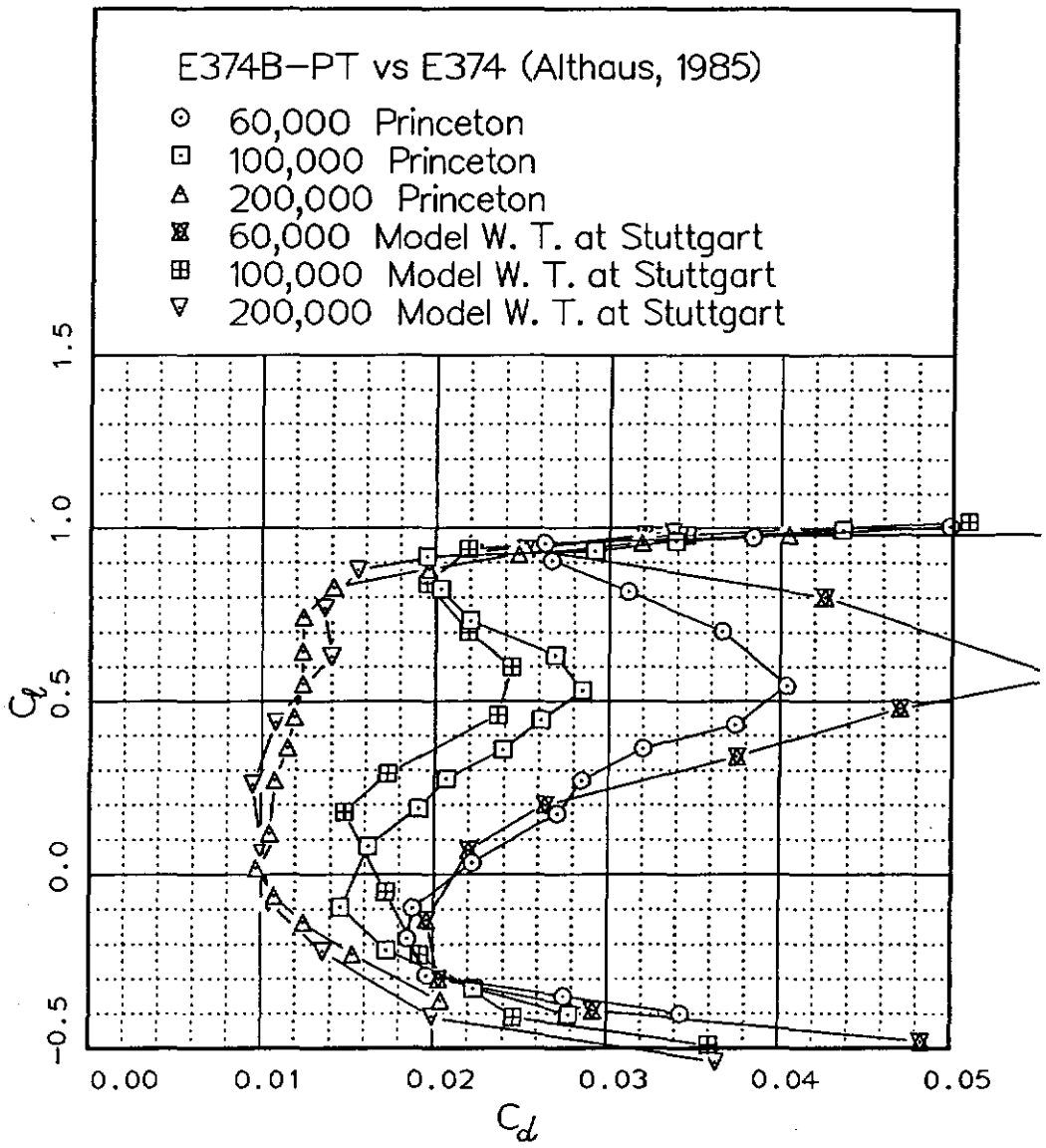

Fig. 2.12 Comparison polars: E374B-PT vs Stuttgart.

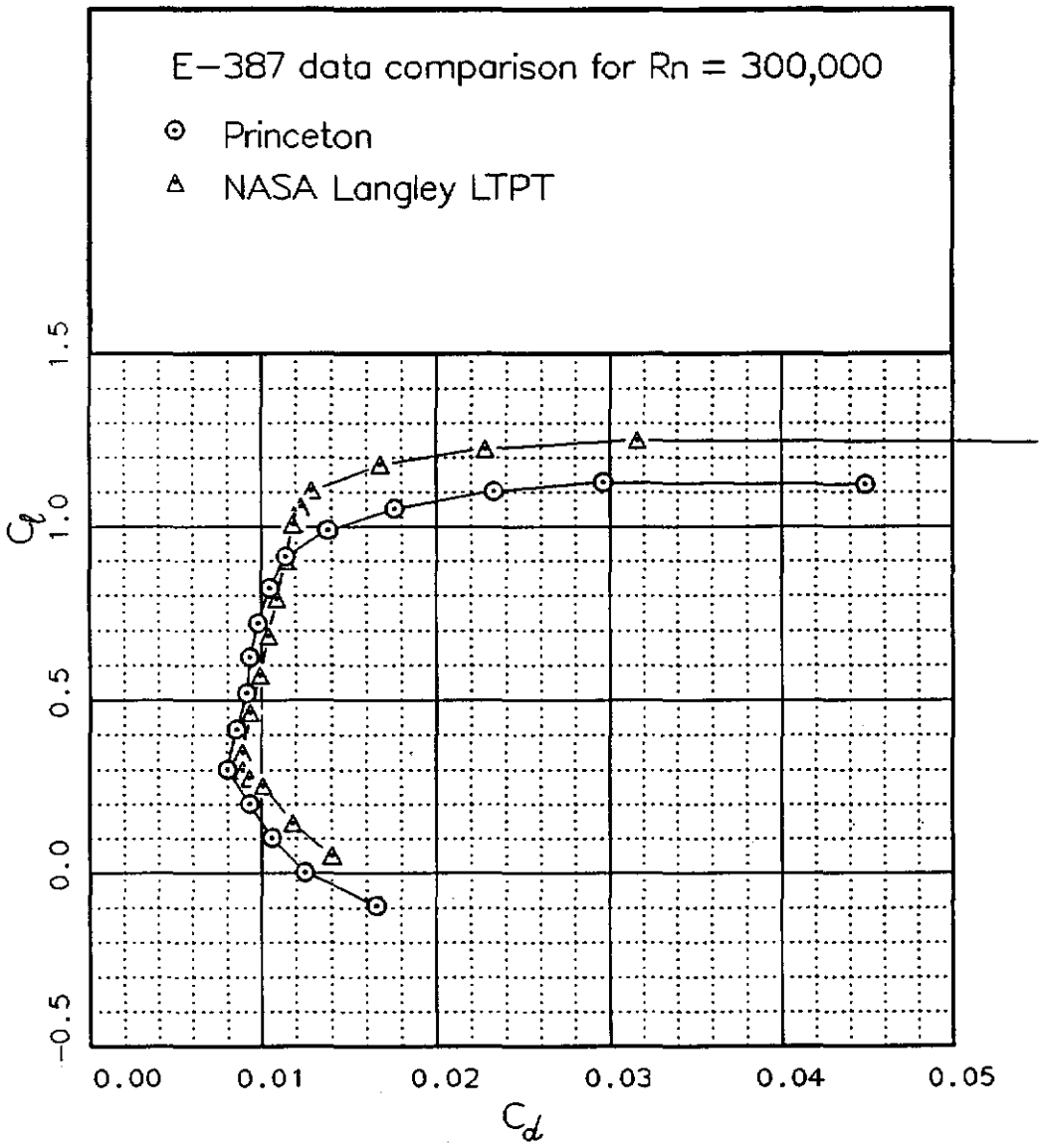

Fig. 2.13 Comparison polars: E387A-PT vs NASA LTPT, Delft University, and Stuttgart.

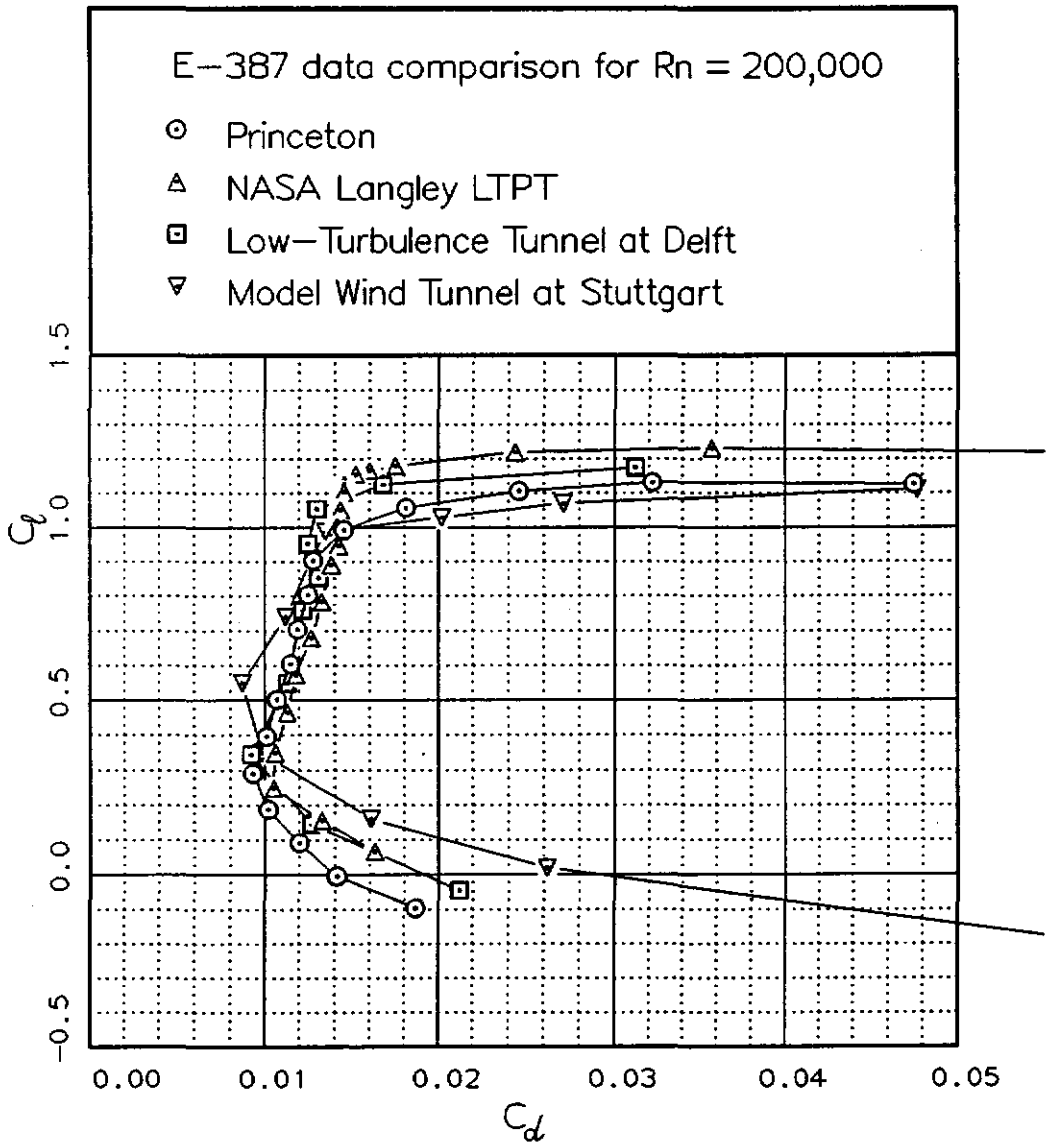

Fig. 2.13 Comparison polars: (continued).

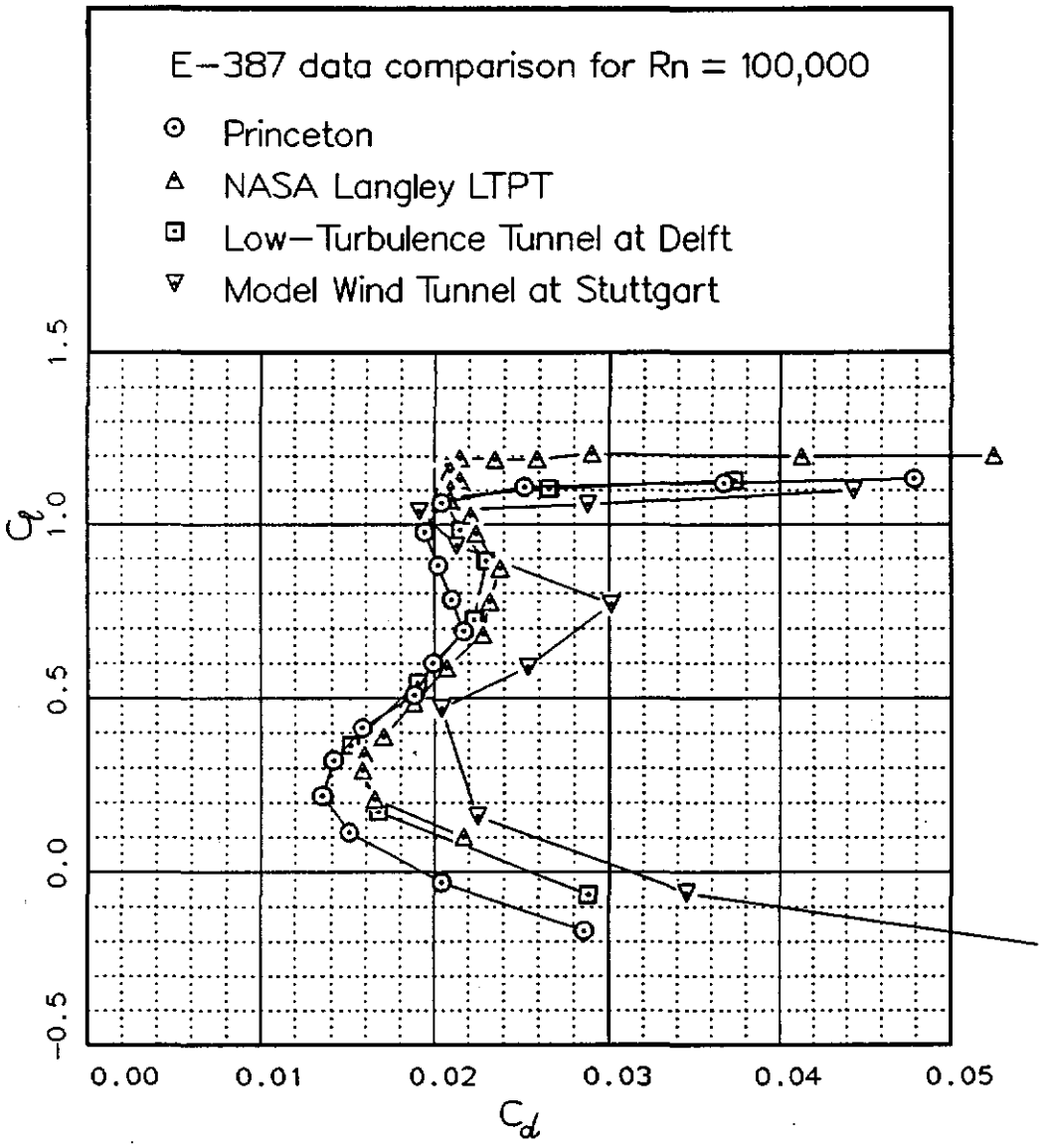

Fig. 2.13 Comparison polars: (continued).

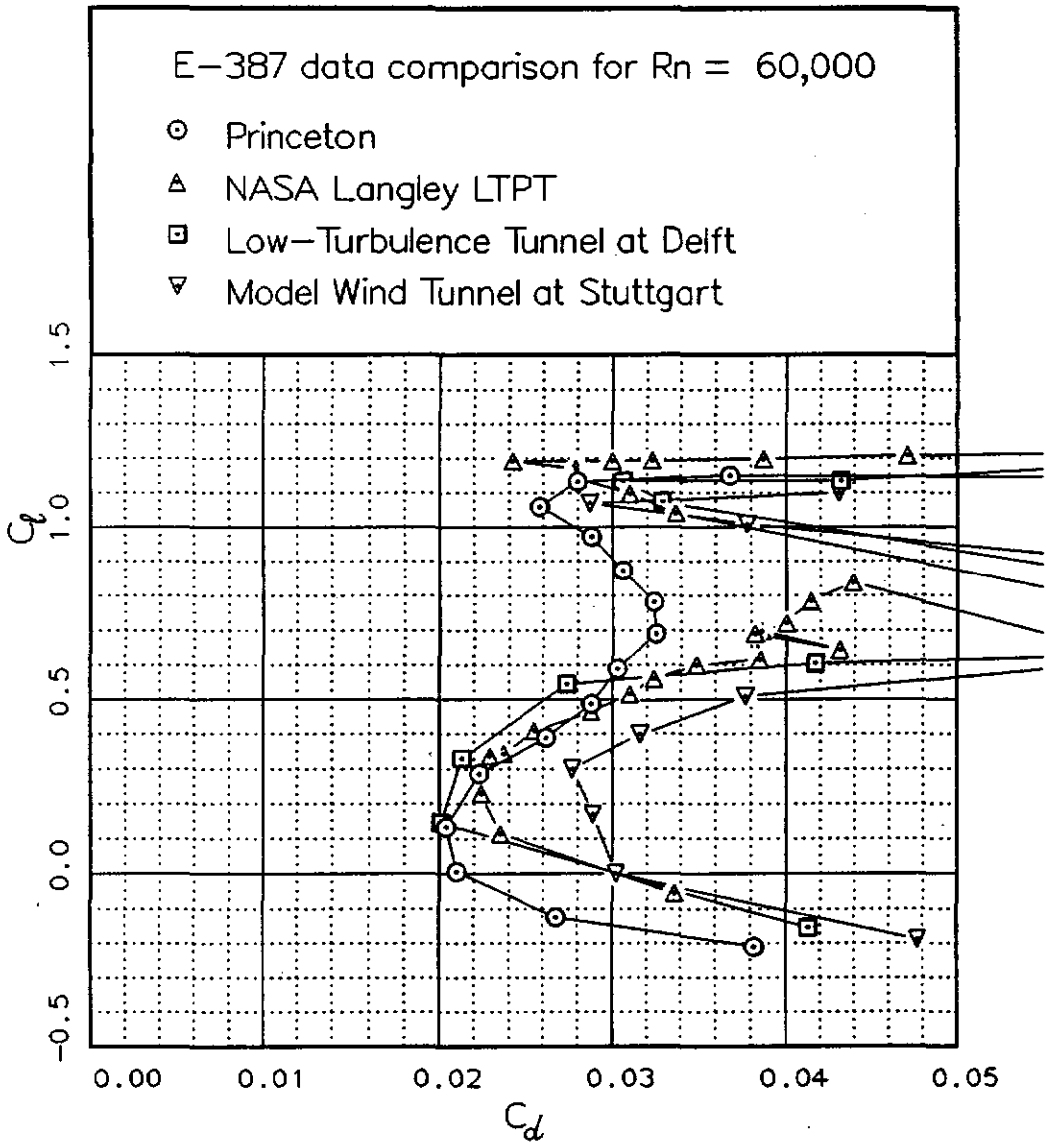

Fig. 2.13 Comparison polars: (concluded).

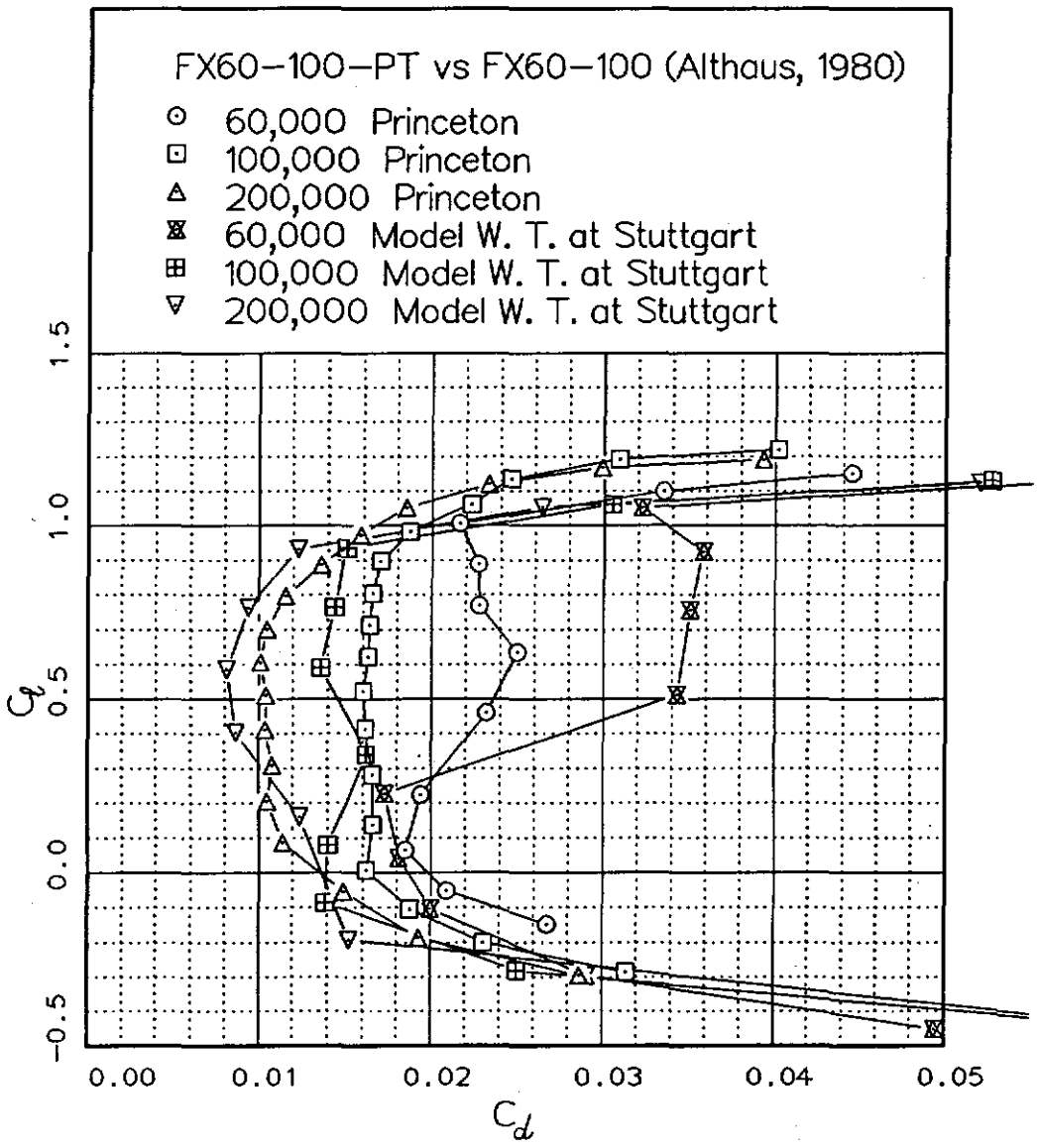

Fig. 2.14 Comparison polars: FX60-100-PT vs Stuttgart.

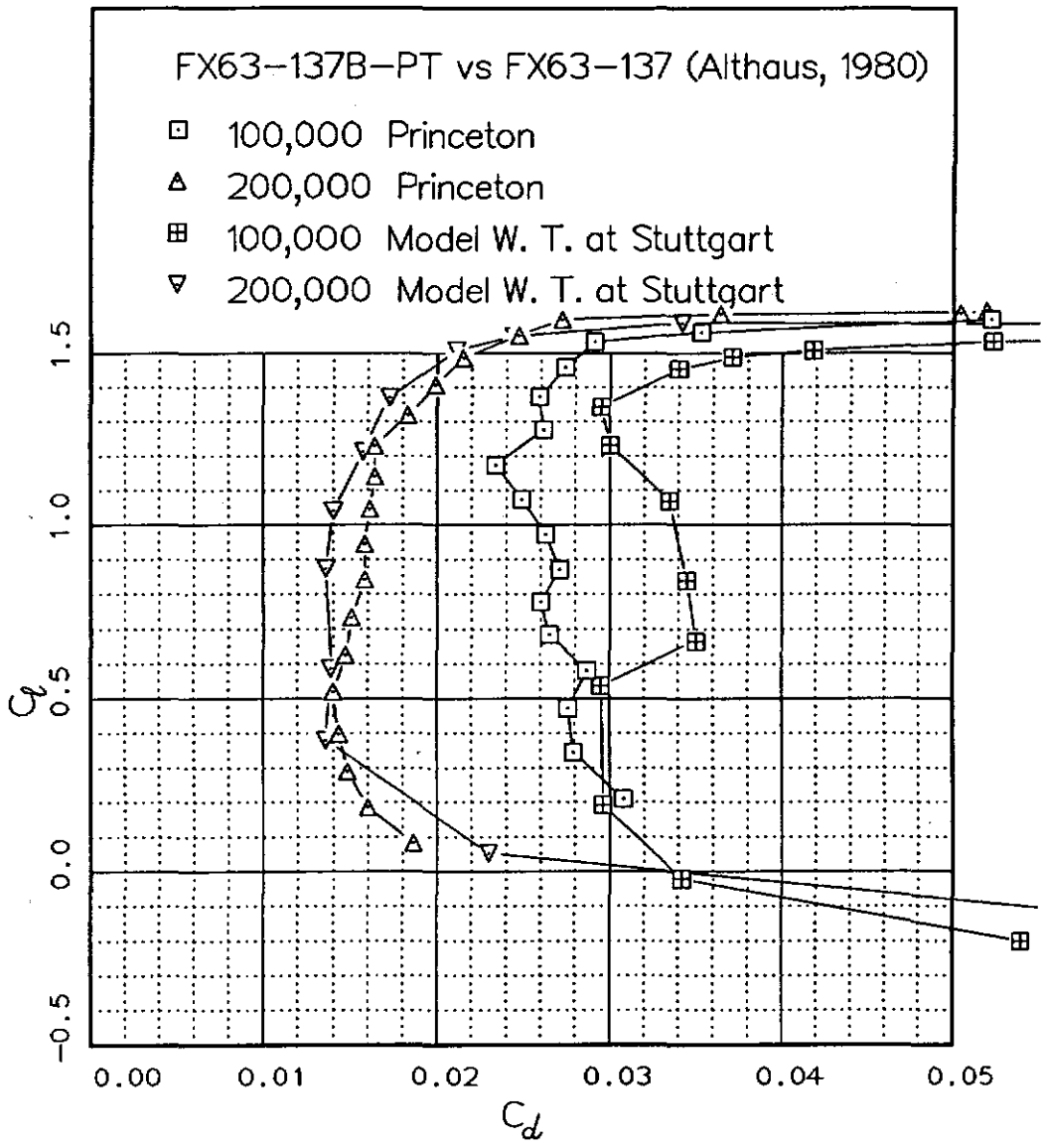

Fig. 2.15 Comparison polars: FX63-137-PT vs Stuttgart.

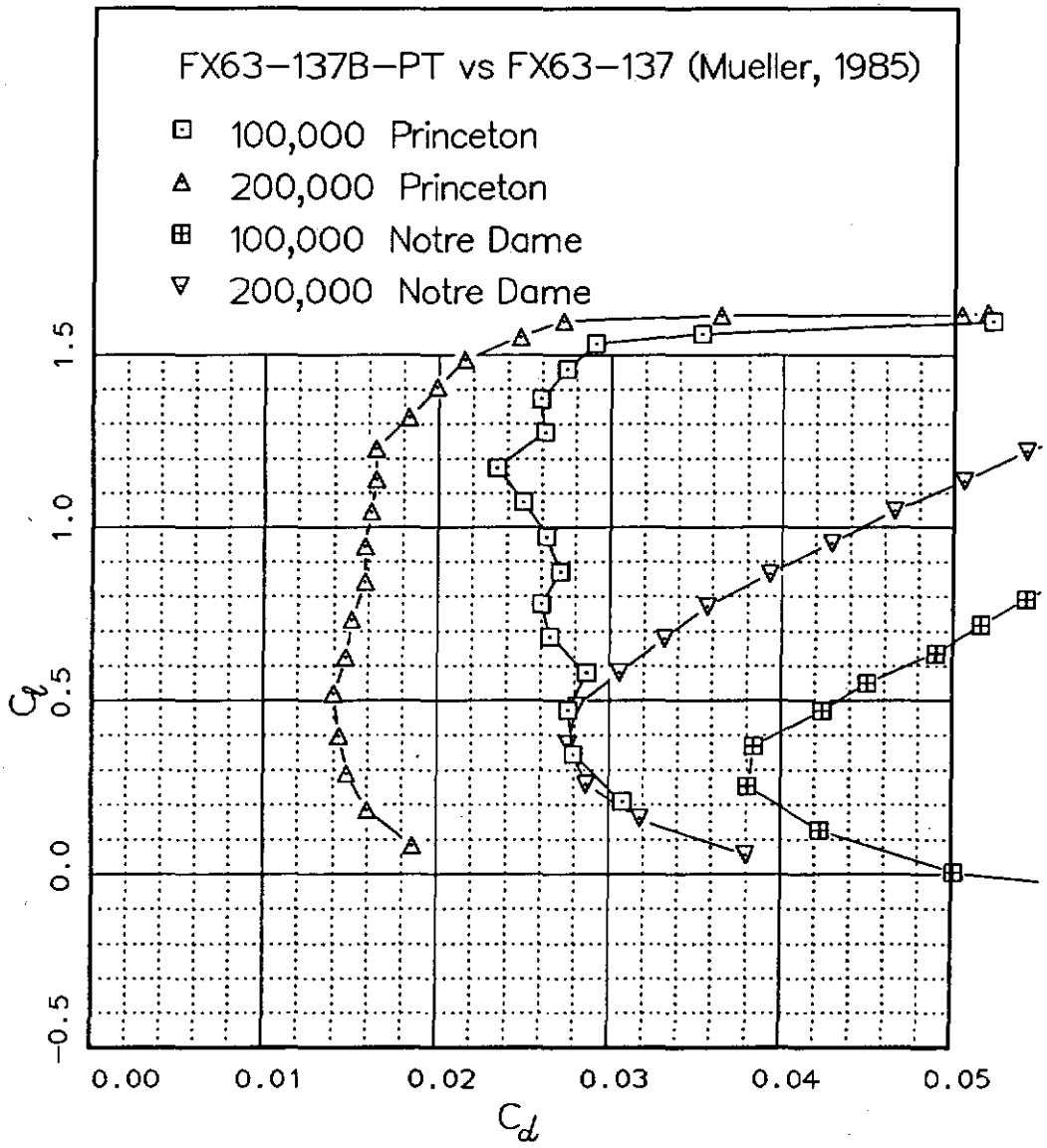

Fig. 2.16 Comparison polars: FX63-137-PT vs Notre Dame.

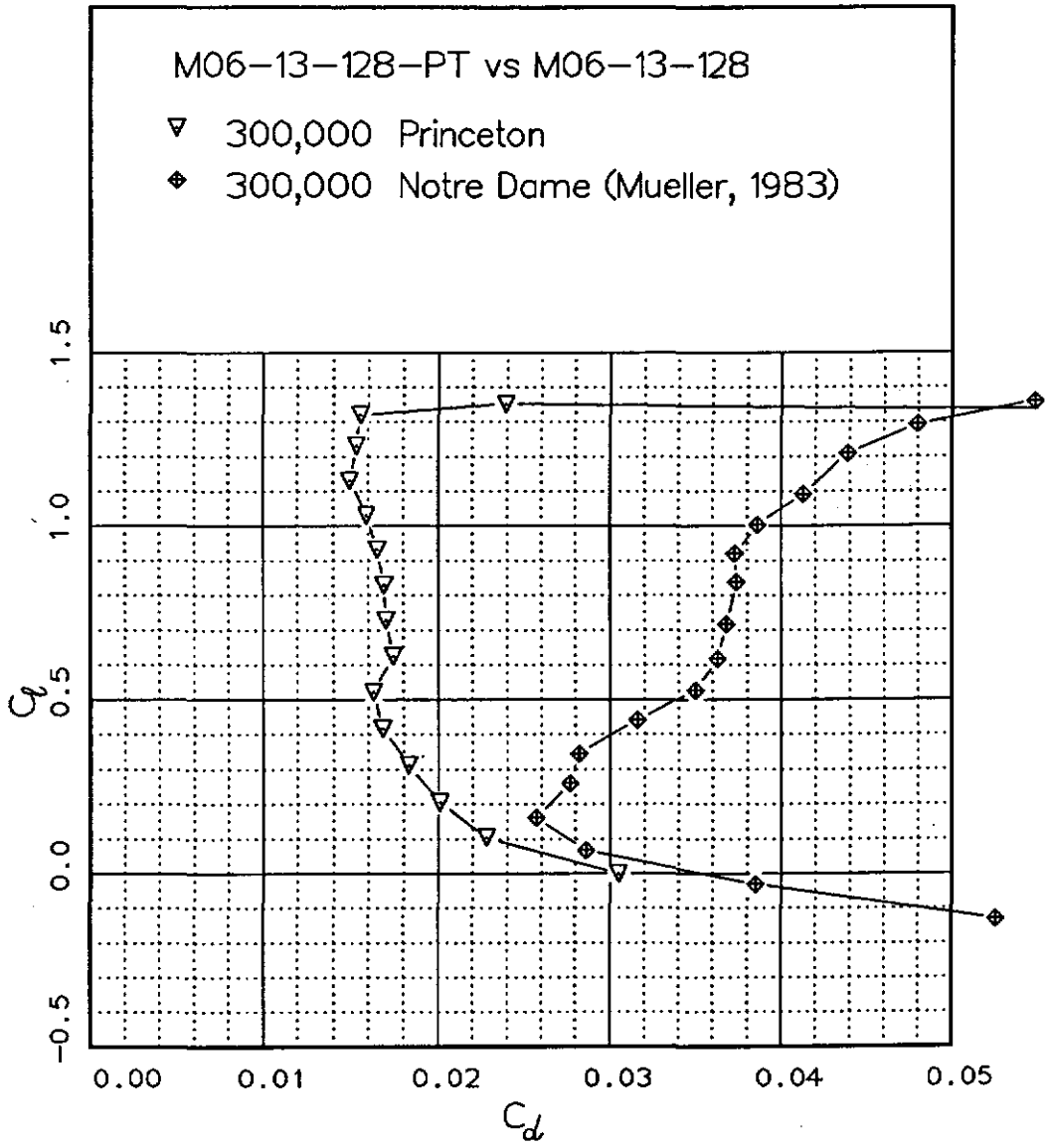

Fig. 2.17 Comparison polars: M06-13-128-PT vs Notre Dame.

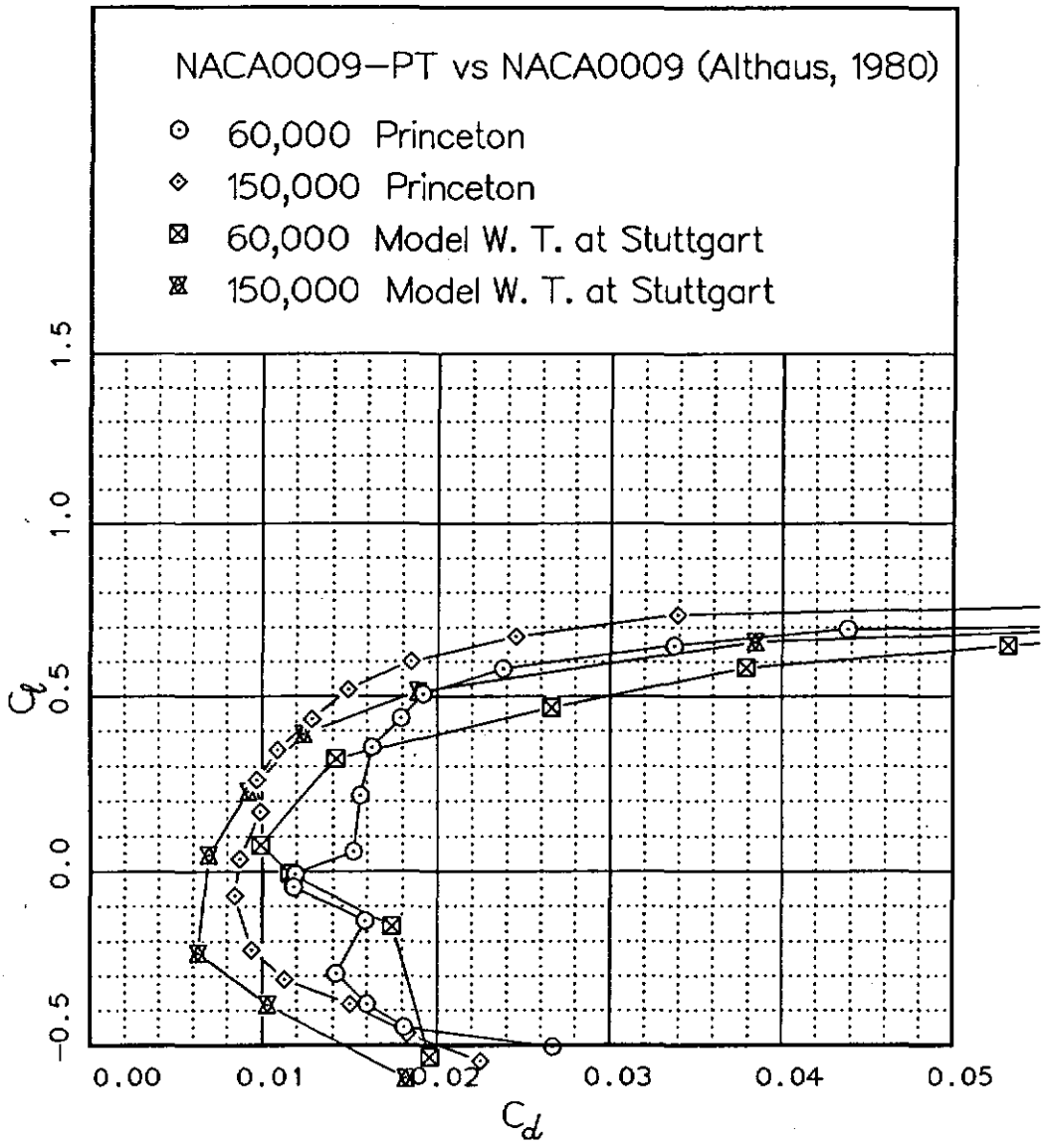

Fig. 2.18 Comparison polars: NACA 0009-PT vs Stuttgart.

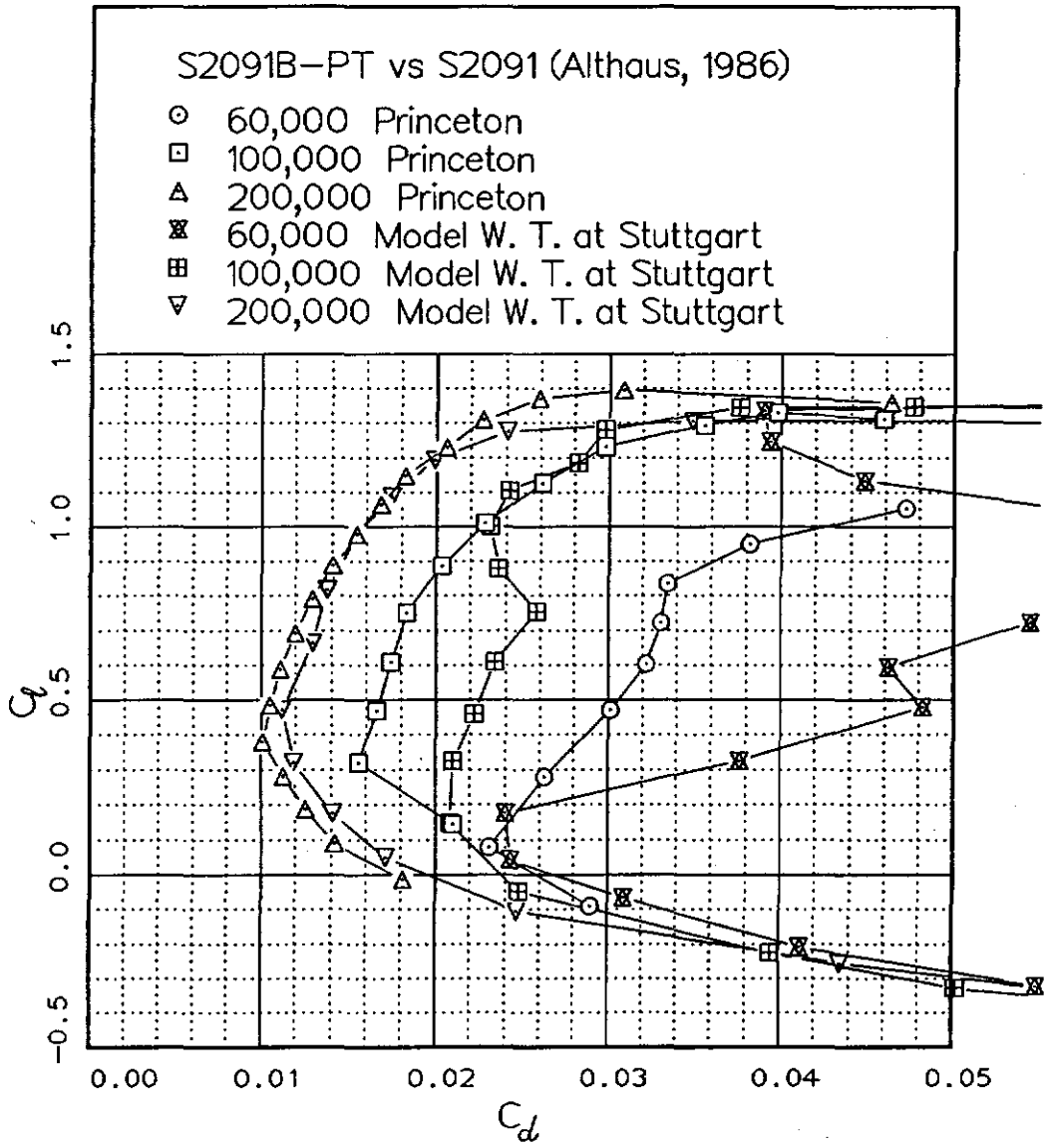

Fig. 2.19 Comparison polars: S2091B-PT vs Stuttgart.

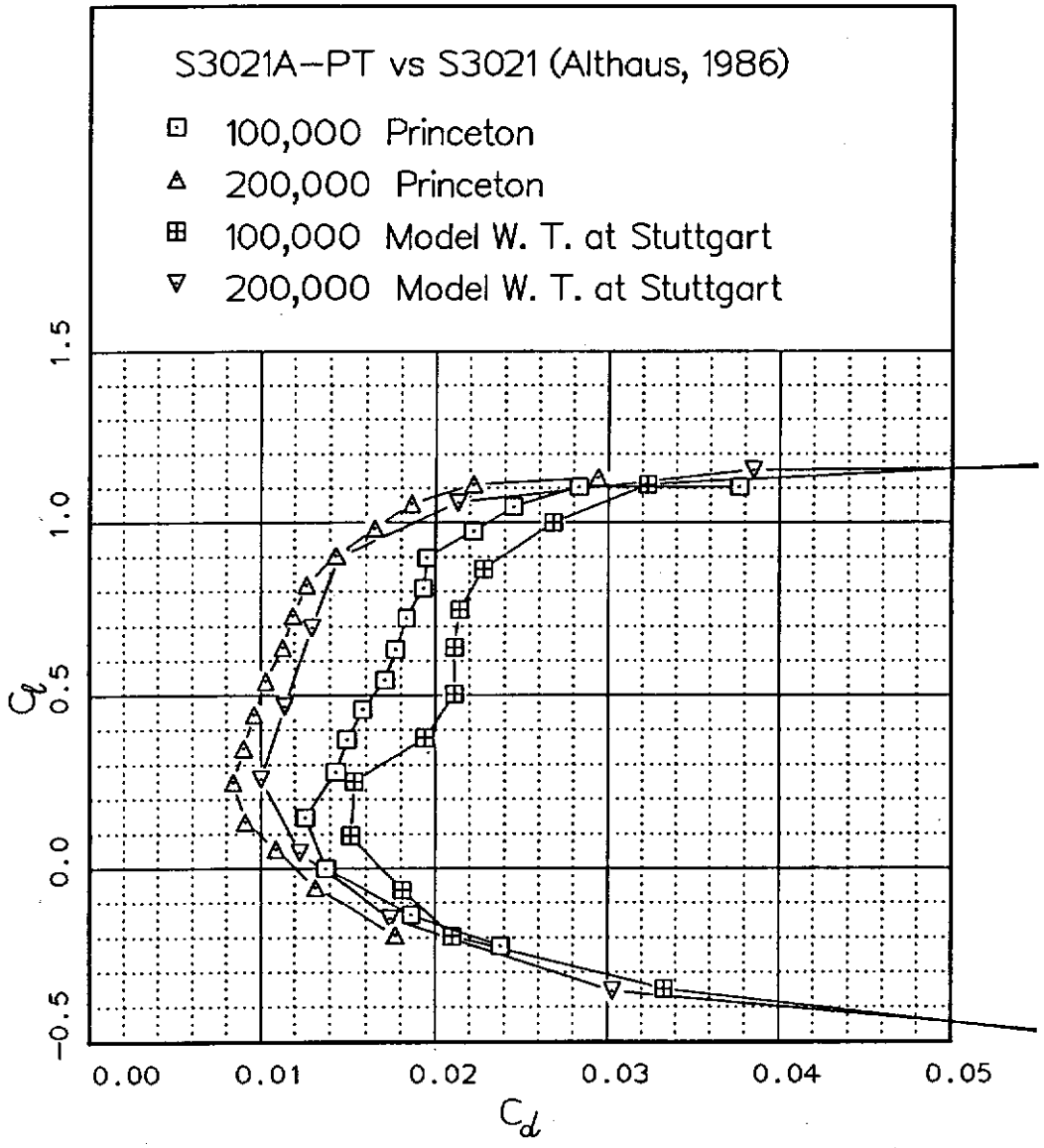

Fig. 2.20 Comparison polars: S3021A-PT vs Stuttgart.

Chapter 3

Low Reynolds Number Terminology

The concepts of modern airfoil design and the attendant jargon are familiar mostly to specialists. In addition, some of the terms commonly used even by aerodynamicists have modified or expanded meanings when applied to low Reynolds number airfoils. For example, the concept of a bubble ramp is derived from a transition ramp, but they are not synonymous. To assist the general reader and to avoid confusion we here define those terms that are specific to low Reynolds number aerodynamics in order to supplement what can be found in textbooks[15,16]. We also have gone into greater detail in the earlier airfoil discussions in Section 5.1 so that the concepts will be familiar when they are referred to more briefly in the later ones.

3.1 Laminar Separation Bubbles

As described in Chapter 1, laminar separation takes place at low Rn due to the reluctance of the boundary layer to make a natural transition from laminar to turbulent flow on the airfoil surface. This type of separation and the subsequent formation of a laminar separation bubble are the principal reasons for the degradation in airfoil performance with decreasing Rn.

At high Rn (greater than 1 million) a graph of C_l vs C_d for most airfoils shows a rounded appearance with the convex side towards the C_l axis. See References 15 and 17 for examples of polars at higher Rn's. At low Rn the situation is often markedly different. Here, separation is a major factor and can contribute a large increment of drag not normally found at higher Rn's. The effect on the shape of the polar is to produce a bulge in the mid-C_l range that is concave towards the C_l axis (see Fig. 12.13). Interestingly, with increasing C_l the drag decreases again just before stall.

Because of these effects, the shape of the polar clearly reveals the severity of the laminar separation bubble. For example, the E214 has a major problem with this at Rn's of 60k and 100k. (This will be discussed in Section 5.1.) If one compares the tripped and untripped cases (Figs. 12.19 and 12.22) the difference in shape illustrates the difference in the separation—the polar changes from concave for the untripped (separated) case, to a more favorable convex shape for the tripped case.

Separation can, however, be minimized by proper design. For such airfoils, e.g. the SD7003, the graphs, even without trips, are more typical of those for higher Rn's.

3.2 Trips and Bubble Ramps

Several means can be used to destabilize the laminar boundary layer and promote an early transition. The most direct means of doing this is through the airfoil shape. At higher Rn's than those found on model aircraft, a short, gradual pressure recovery, called a transition or instability ramp, is sometimes used before the steeper main recovery. The purpose of the ramp in this case is to ensure that the boundary layer is fully turbulent and energetic before reaching the main pressure recovery. At low Rn, the transition ramp is still useful, although it needs to be longer, and may be more appropriately called a "bubble" ramp. The gradual pressure recovery of the ramp in this case shortens the length of the bubble by shortening the distance required for reattachment. As the Rn decreases, more and more of the airfoil surface is required for the bubble ramp[18,19]. In fact, for a Rn near 60k and at moderate lift coefficients, almost the entire upper surface of the airfoil is needed to ensure transition and subsequent reattachment.

Another method of inducing transition is through the use of a turbulator or trip. Typically, these are external ridges or bumps applied to the surface of the airfoil in a direction parallel to the span. They protrude into the boundary layer in such a way as to energize it sufficiently to promote transition. Many free-flight model aircraft employ turbulators to improve performance. Several detailed experiments, as summarized by Mueller[4], have amply demonstrated that if an airfoil has high drag and hysteresis owing to a laminar separation bubble, a turbulator often alleviates these adverse effects by shortening the length of the bubble.

Currently at issue in the design of low Reynolds number airfoils are the factors governing the use of bubble ramps and turbulators. At very low Reynolds numbers, turbulators may be better than bubble ramps, but as the Rn increases, the bubble shortens naturally. Thus, the turbulator becomes unnecessary and handicaps the performance by making transition happen too early. In this case the ramp would probably be better. In the middle of the low-Rn range, the question remains unclear. Is it better to use only a bubble ramp or only a turbulator or a combination of both? Usually airfoil turbulators are simple two-dimensional strips, but some three-dimensional trips (such as zig-zag tape and bump tape) have proved highly successful in application to modern, full-size sailplane airfoils. In our research, trips and ramps were used to *begin* to explore their respective benefits and operating regimes.

3.3 Airfoil Hysteresis

The term hysteresis, as applied to airfoil aerodynamics, means the difference in C_l, C_d, or $C_{m_{c/4}}$ at a given angle of attack when this angle of attack is approached from a higher and then a lower value. This behavior may be seen

in the in the C_l vs α plot. See for example Fig. 12.2. In cases with hysteresis, as the angle of attack is increased from zero to stall, the C_l will usually reach a maximum value and then drop off at some particular α. However, when α is decreased, the C_l will not retrace its original curve; rather it will stay at the "stall" C_l until α is somewhat below the previous stall value, and then suddenly jump up to rejoin the original C_l vs α curve. Hysteresis in the aerodynamic coefficients with both Reynolds number and angle of attack is common to many of the airfoils tested.

Invariably, hysteresis is a sign of a large, laminar separation which in turn yields high bubble drag. Since this effort concentrated on those airfoils with low bubble drag, the detailed effects of hysteresis were not closely examined. In general, airfoils with hysteresis in the middle of the Rn-envelope of the aircraft should be avoided.

Chapter 4

Project Design Methods and Goals

Three main tools were used to design new airfoils: the Eppler and Somers design code[20], the ISES code written by Drela and Giles[21,22], and the wind tunnel described previously. The Eppler and Somers code formulates the design problem in a way that allows quick and easy manipulation of the airfoil shape. With a minimum number of parameters, almost any desired velocity distribution can be obtained. However, because this code does not accurately predict the performance of airfoils in the Reynolds number range considered here, it was used mainly to obtain the inviscid velocity distributions and to give an estimate of the transition point behavior.

The ISES code solves the two-dimensional Euler equations coupled with a momentum integral boundary layer formulation using a global Newton method. Over the Reynolds number range considered in this investigation, it predicts airfoil performance more accurately than the current version of the Eppler and Somers code. In particular, the agreement with the experiment at Reynolds numbers of 200k and greater is very good. However, the agreement depends on the choice of the n value used in the e^n transition criterion. While the ISES code provided a relatively good estimate of the performance, wind tunnel results were the ultimate test of an airfoil.

The design approach was to generate an airfoil with the desired inviscid velocity distribution using the Eppler and Somers code, and then predict the performance at a Reynolds number of 200k using the ISES code. If the performance was poor, the new airfoil was redesigned and the process repeated. Upon reaching a suitable design through this iteration process, a wind tunnel model was built and tested. Based upon the wind tunnel results, the new airfoils were further refined and the process repeated.

Before discussing airfoil design, it should be pointed out that for any aircraft in straight and level flight the relation between C_l and chord Reynolds number is given by:

$$Rn \propto \frac{1}{\sqrt{C_l}} .$$

This relation emphasizes the fact that the C_d should be minimized for a value of C_l and the corresponding Rn. Thus, the optimum airfoil design is clearly dependent upon the configuration and desired tasks of the aircraft for which it is designed. The designs discussed below are based upon RC sailplane

configurations; however, the general principles apply to any type of low-Reynolds number aircraft.

A popular RC soaring, cross-country airfoil is the E374. It is commonly used on aircraft intended for high speeds, with relatively little importance placed on the performance at low speeds. The experimentally determined drag polars for this airfoil are shown in Figs. 12.24–12.29. This airfoil works well at high speeds because of the small values of the drag coefficient at the higher Reynolds numbers throughout a range of low C_l values. At lower Reynolds numbers, the drag increases dramatically as C_l moves from 0.0 to 0.5, and then decreases from 0.5 to 0.8. This behavior indicates the formation of a large laminar separation bubble on the upper surface.

The inviscid velocity distribution about the E374 for a C_l of 0.55 is shown in Fig. 4.1. A "kink" in the upper-surface velocity distribution beginning at 40% separates it into two distinct regions. Over the forward 40%, the velocity changes little, and the majority of recovery takes place over the aft 50% with a relatively strong adverse pressure gradient. At low Reynolds numbers, this pressure gradient results in a large laminar separation bubble. To reduce the drag, the pressure gradient should be reduced. However, if the same pressure differential is to be recovered, then the recovery region must start farther upstream, as shown by the dashed line in Fig. 4.1. This longer region of smaller adverse pressure gradient is termed a bubble ramp. Before this point is discussed further, it is important to observe the behavior of the transition point on the upper surface with increasing C_l.

As a result of the kink in the velocity distribution at 40% chord, the transition point moves rapidly forward with C_l as shown in Fig. 4.2. (Of course, transition does not occur at a point but rather over some finite distance.) In this case the point refers to the location at which transition was predicted to occur by the Eppler and Somers code using a method based on the boundary layer shape factor for Rn of 200,000. Knowledge of the shape of the transition-point curve is helpful when designing with the Eppler and Somers code because it is similar to the distribution of design parameters which specify the airfoil (α^* with ν)[20]. In the "redesign" of the E374, the kink in the velocity distribution was removed to define a new airfoil—the SD6060. The resulting transition point behavior and velocity distribution are shown by the dashed lines in Figs. 4.1 and 4.2, respectively. Removing the kink shifted the transition point farther forward for C_l greater than 0.5. In this case, separation will occur earlier because of the steeper initial gradient, but with the transition point farther forward, the separation bubble will be shorter and the drag will be lower.

A comparison between the experimentally determined drag polars for the E374 and SD6060 is shown in Fig. 4.3. There has been a reduction in drag throughout the central portion of the polars for all Reynolds numbers because the bubble ramp has reduced the length of the separation bubble. (Some of this

reduction in drag is due to a thinning of the airfoil; the E374 is 10.9% thick and the SD6060 is 10.4% thick.) In addition to the decrease in drag in the central region, the increase in drag as C_l approaches 1.0 is more gradual in the case of the SD6060, which is consistent with the smoother forward movement of the transition point.

A further example illustrating the effectiveness of a bubble ramp in the upper-surface velocity distribution can be seen by comparing the E205 and the S3021[23]. The E205 is usually used as a "multi-task" airfoil because of its relatively good performance at both high and low lift. This airfoil has an upper-surface velocity distribution which is similar to the E374 in that it also contains a kink. The velocity distribution of the S3021 is essentially the same as that of the E205 except the kink has been replaced with a bubble ramp as in the SD6060. Figure 4.4 shows a comparison between the drag polars of the E205 and S3021 at several Reynolds numbers. The differences are similar to those noted between the E374 and SD6060, that is, at all Reynolds numbers the drag of the S3021 is lower than that of the E205 in the central region of the polars. However, at the highest Reynolds number (300k) the E205 has lower drag than the S3021 for $C_l = 0.9$. As discussed earlier, as the speed increases, the lift coefficient decreases so that for typical low Reynolds number configurations, at 300k the lift coefficient would be considerably less than 0.9. Thus, for low Reynolds number aircraft, the S3021 will perform better than the E205.

These examples illustrate that significant improvements can be made over existing designs by relatively minor changes in the velocity distributions (which, of course, directly alter the airfoil shape). Other airfoils, such as the SD7003, demonstrate that if sufficient attention is paid to the control of the bubble, it is possible to design entirely new, low Reynolds number airfoils that show little or no evidence of increased drag due to the bubble, even at 60k. What is not known at this point is how far this design philosophy can be "pushed". Even though improvements have already been demonstrated, the optimum shape and location of the ramp remain to be determined. Employing airfoils with bubble ramps on model aircraft will provide further insight into the benefits of this type of design and will help guide further study.

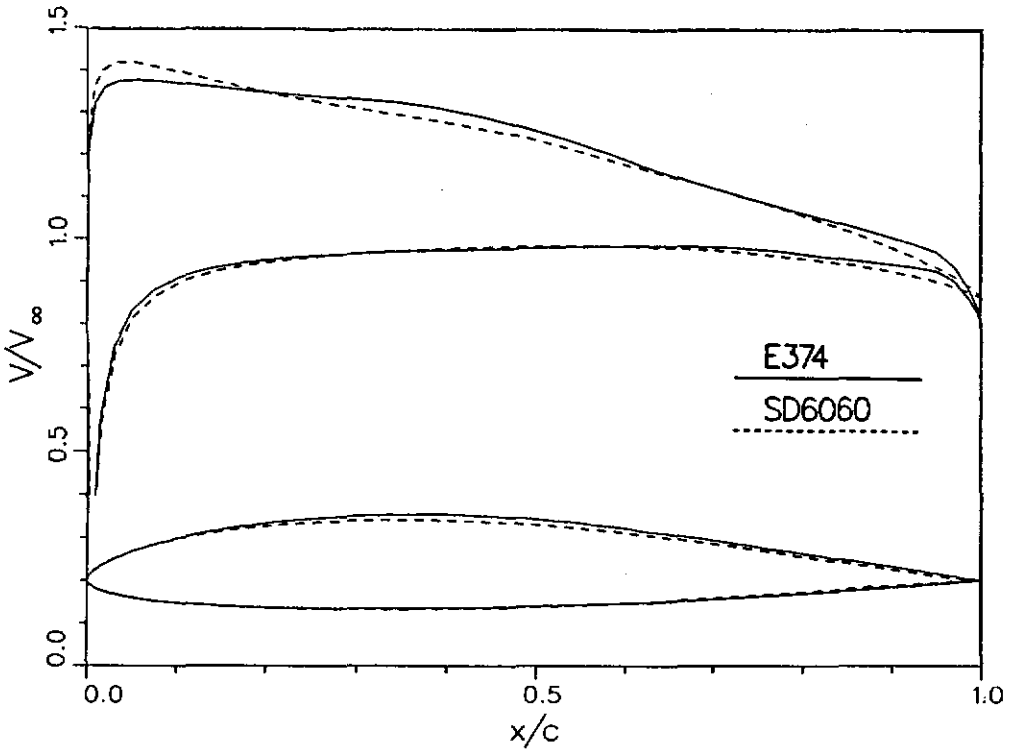

Fig. 4.1 Inviscid velocity distributions: $\alpha_{w.r.t.0L} = 5°$ $(C_l = 0.55)$.

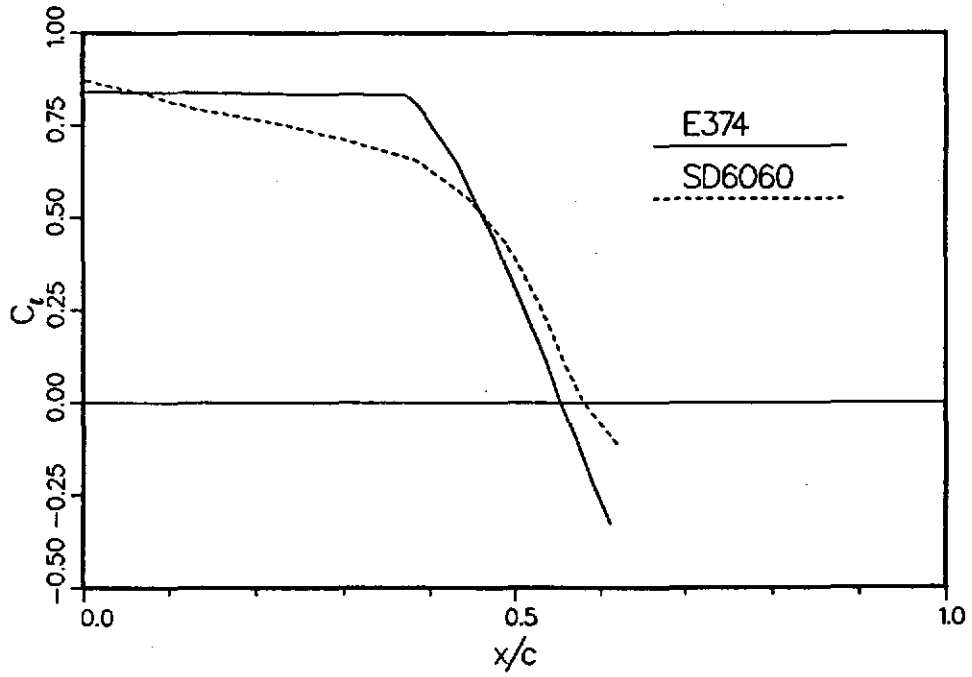

Fig. 4.2 Upper surface transition point at $Rn = 200,000$ as predicted by the Eppler code.

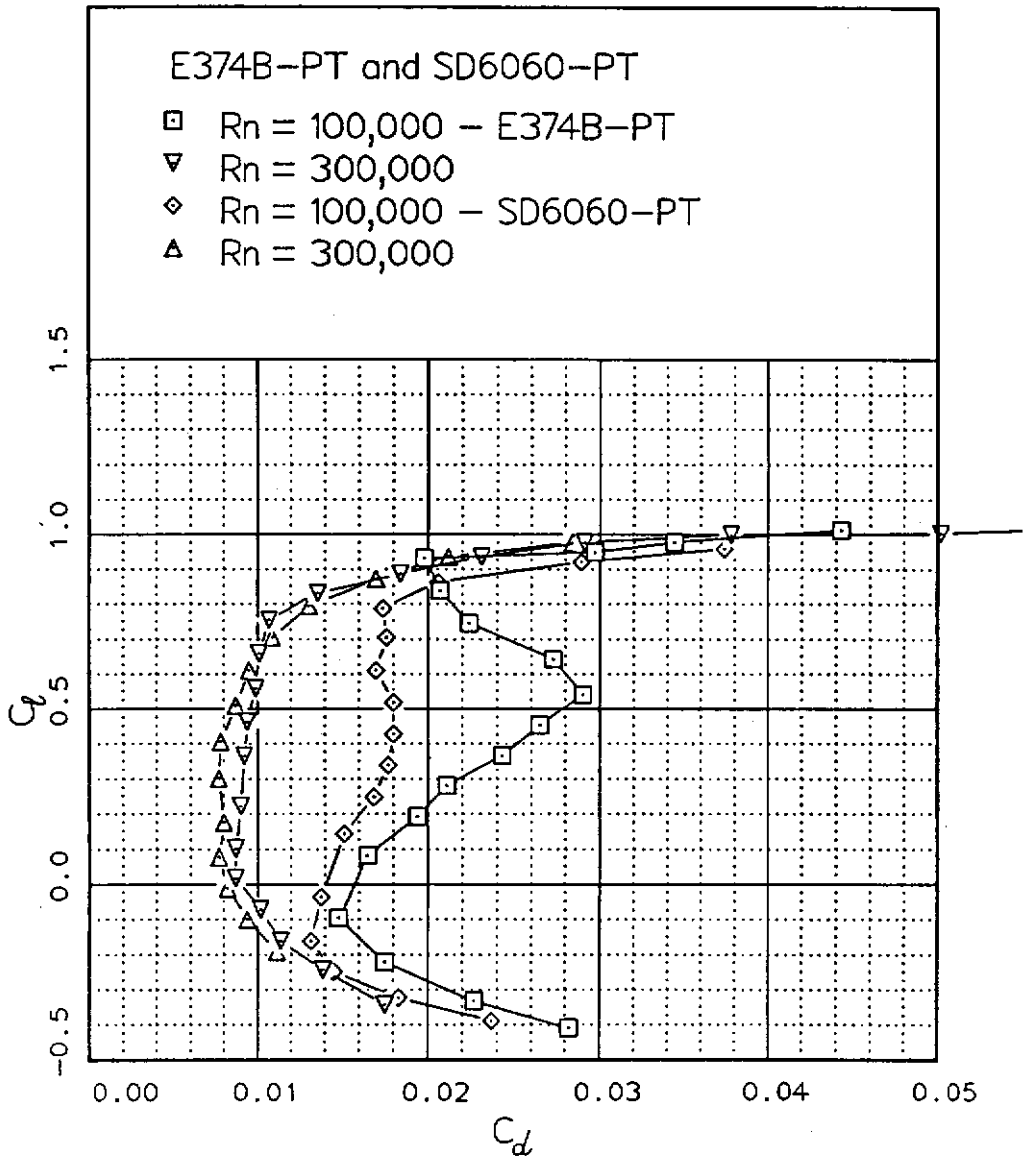

Fig. 4.3 Comparison polars: E374B-PT and SD6060-PT at two Reynolds numbers.

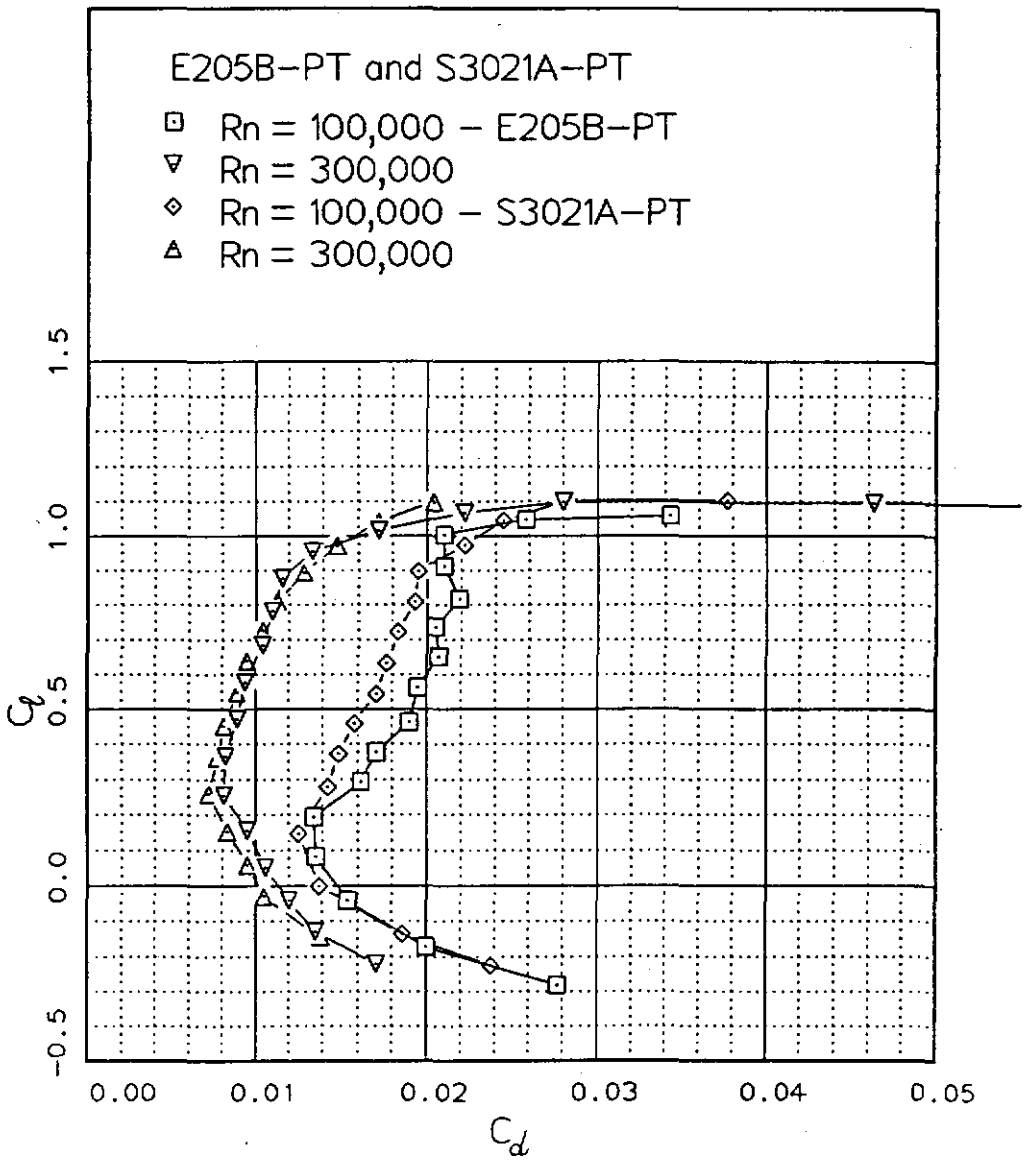

Fig. 4.4 Comparison polars: E205B-PT and S3021A-PT at two Reynolds numbers.

Chapter 5
Comments on Airfoils

In this section the performance of each airfoil is discussed in detail. Emphasis is placed on highlighting the important characteristics with respect to the other airfoils. Following these comments, smaller sections discuss:

(1) stall behavior
(2) trips and surface roughness
(3) trailing edge thickness
(4) surface waviness and contour accuracy.

In some of the airfoil discussions we give examples of sailplane performance in order to compare one airfoil with another. It should be noted in these examples that while one airfoil may be good for a particular configuration, it does not necessarily follow that it is good for all configurations. This is one of the reasons why there are so many "favorite" airfoils. In light of this, the reader is left to make the final decision as to which airfoil is best suited for a particular sailplane. To this end, a computer and an accurate performance prediction program are invaluable aids in the airfoil/aircraft integration process.

Even though most of the discussions are related to the RC sailplane, the airfoils are by no means restricted to this use. Furthermore, the aerodynamic phenomena described are common to all airfoils operating at low Reynolds numbers.

Many of the airfoils tested were not originally intended for use on RC sailplanes, but have come to be used for this application by trial and error. On the other hand, the new SD-airfoils (as well as the DF-series) were designed for the RC sailplane. Rather than tailor a design to one, particular aircraft, the SD-series airfoils were designed for different, general classes of flying; for example, thermal-duration, F3B, multi-task, etc. Additional improvements in performance can probably be made by properly integrating the initial airfoil design process into the overall aircraft design[24].

Some miscellaneous notes follow:

(1) For several of the airfoils camber-changing flaps are recommended for best performance. In these cases, "flaps" and "full-span flaps" and "camber-changing flaps" are used interchangeably.
(2) At the end of each airfoil discussion is a list of related airfoils given in order of decreasing similarity to aid the reader in the selection process.

(3) As previously mentioned in Section 2.2.3, the designation "-PT" (for Princeton Tests) is used after the names of the actual airfoils tested to distinguish them from the nominal or ideal airfoils. Depending on the accuracy of the wind tunnel model, one may chose to build using the actual coordinates (with the PT-designation) listed in Chapter 7 for this purpose. Also, the actual coordinates should be used for any theoretical computations, since in some cases the deviation from the nominal is large.

(4) The nominal Reynolds number is used in the labels of the airfoil polar plots while the actual Reynolds number is listed with the tabulated data.

(5) The airfoil maximum thickness and camber is listed at the end of each airfoil discussion for quick reference; they are also listed in tabular form in Chapter 9.

(6) If two or more models of the same airfoil were built, the designation A, B, C, etc. is used to indicate the different models. In some cases the versions may differ by the type of surface finish, the addition of a flap, or some other major modification.

(7) In addition to testing the plain airfoils, the effects of a number of different boundary layer trips were examined in a search for improved performance. Figure 13.7 shows the geometry of the plain, zig-zag, bump, and blowing trips. Note that the trip "type" designations A, B, C, etc. should not be confused with the model "version" designations A, B, C, etc.

(8) Airfoil moment data were not taken. For an estimate of the moment about the quarter-chord point, Chapter 8 lists the average moment coefficients over the range $0.2 < C_l < 0.8$ for Rn of 200k for some of the airfoils, as predicted by the Drela and Giles ISES code.

(9) Airfoil polars and lift plots are given separately in Chapter 12.

(10) An abbreviated description of the trips is found in the figure titles. These abbreviations have the following meanings:

u.s.	upper surface
u.s.t.	upper surface trip
l.s.	lower surface
l.s.t.	lower surface trip
x/c	normalized trip position measured from the model leading edge to the trip leading edge
h/c	normalized trip height
w/c	normalized trip width.

When the trip type is not explicitly stated, the trip is the simple two-dimensional trip strip. For example see Fig. 12.22.

(11) Although some of the discussions of the airfoils deal with the effects of bubble ramps, these are not important with regards to building and actually using the airfoils. Therefore, no specific details of the ramps are provided and airfoil velocity distributions are not given.

(12) There are plots comparing the nominal and actual airfoils (termed here "digitizer plots") in Chapter 10, and plots comparing different nominal and actual airfoils in Chapter 11.

(13) The data used in generating the polar plots is tabulated in Chapter 13 and is keyed according to the airfoil name and figure number. The data is ordered as it appears in the figure title.

(14) The aircraft polars in this chapter were made with SAILPLANE DESIGN, a computer program (available from Fraser) for evaluating and comparing sailplane performance. Although SAILPLANE DESIGN allows the user to vary any parameter, the polars presented here compare aircraft that are identical except for the airfoil and weight. The configuration is shown on the graph. The profile drag of the wing is taken from the tunnel data and the induced drag is calculated using lifting line theory[15] for both the wing and horizontal stabilizer. The fuselage and empennage profile drags are calculated using equation 5.18 of Reference 15. No allowances are made for parasitic drags nor is any correction applied for a non-elliptical lift distribution. (The former are impossible to accurately quantify and the latter would be very small in any case.) Neither is significant when comparing similar aircraft. The three sloping lines are lines of constant sink speed: 1.0, 1.25, and 1.5 ft/s. All units are feet, pounds, seconds.

5.1 Airfoil Discussions

AQUILA

• AQUILA-PT (Fig. 12.1)

With the level of sophistication in F3B today, it is hard to believe that in 1977 Skip Miller flew his "modified" Airtronics AQUILA sailplane to a first place finish at the first F3B RC Soaring World Championships. One can only speculate on the performance differences between Skip Miller's "modified" AQUILA and the stock version; nevertheless, the stock AQUILA was a formidable RC sailplane from the mid 70's to early 80's.

In comparison to other popular airfoils of the time, the AQUILA airfoil gave excellent thermal performance. However, the high camber was a handicap at high speed. Recognizing this deficiency, Airtronics introduced the SAGITTA with the Eppler 205 airfoil, which had the desired high-speed qualities. The popularity of the AQUILA waned, and production was finally discontinued.

Also see: S2091, SD7032, SD7037, FX60-100
Digitizer plot: Fig. 10.1
Polar plot: Fig. 12.1
Lift plot: Fig. 12.2
Thickness: 9.38% Camber: 4.05%

CLARK-Y

• CLARK-Y-PT (Fig. 12.3)

The famed CLARK-Y airfoil needs no introduction; it is perhaps the most popular airfoil ever used on both full-scale and model aircraft. As compared with the AQUILA, the high-speed, low-lift performance is superior. What is surprising is the small price for the improved performance—the maximum lift coefficient ($C_{l_{max}}$) is a mere 0.1 less than the AQUILA.

The effects of a laminar separation bubble are apparent only at a Rn of 60k through the mid-lift range, where the drag coefficient reaches a maximum of 0.032 at a C_l of 0.5. However this bubble does not necessarily detract from the performance since the drag rise occurs mostly in the mid-lift range, a range not used by the vast majority of sailplanes at 60k.

At the high-lift, low-Rn regime of the RC sailplane, the drag reduces as the bubble shortens, reaching a minimum of 0.027 at a C_l of 0.9 for 60k. No doubt the CLARK-Y will stay popular for some time to come.

Also see: DF101, S3010, S3021, SD5060
Digitizer plot: Fig. 10.2
Polar plot: Fig. 12.3
Lift plot: Fig. 12.4
Thickness: 11.72% Camber: 3.55%

DAE51

• DAE51-PT (Fig. 12.5)

The DAE51, along with several other DAE airfoils, was designed by Mark Drela using the ISES code developed by him and Giles[21,22]. As was mentioned in Chapter 1, this same code was used to analyze the new SD-series of airfoils.

The DAE51 was designed for the propeller of the DAEDALUS, human-powered aircraft[25]. Thus it was not designed for one operating point, but rather for the range of anticipated conditions. The requirements were[26]:

1. $C_{l_{max}} \geq 1.2$
2. Transition ramp optimized for Rn = 125k, $0.5 \leq C_l \leq 1.0$
3. No bubble "bursting" for Rn greater than 75k
4. Thickness less than 9%

The achievement of these design goals was demonstrated by no less than a record 74-mile flight from Crete to Santorini across the Mediterranean, a flight that duplicated in reality the mythical flight of Daedalus and his son, Icarus. Although only the third airfoil to be discussed, the variety of performances and the trade-offs made to achieve them are becoming clear. The drag of the DAE51 at Rn of 300k is considerably lower than the AQUILA and CLARK-Y, but the range of lift is significantly less. For application to RC sailplanes a broad lift range can sometimes be recovered by use of a full-span flaps, while maintaining

the low-drag characteristics of the unflapped airfoil. With a 20% flap, the low-drag range could probably be extended up to C_l of 1.1, which would make it competitive against the unflapped AQUILA and CLARK-Y.

• DAE51-PT thickened trailing edge (Fig. 12.6)

The DAE51 was tested with a substantially thickened trailing edge (see Fig. 5.1 for contour) to measure the possible loss in performance. Over most of the low-drag range, a 4–5% increase in drag was found. As further examples, the E374 and SD6080 were also tested with thickened trailing edges, and the same trends were observed. Similar results were observed by Althaus at Reynolds numbers 1–3 million[27].

Also see: S4061, SD6080, E387, E193
Digitizer plot: Fig. 10.3
Polar plot: Figs. 12.5, 12.6
Lift plot: Fig. 12.7
Thickness: 9.37% Camber: 3.98%

DAVID FRASER AIRFOILS (DF)

This series of airfoils was designed for very large sailplanes where thin airfoils are not structurally possible. The starting seed was the SD5060; however, the DF-series is thicker and has a different thickness distribution.

The design requirements were:

1. 11% thick
2. flat bottom aft of 30%
3. minimum drag at $C_l = 0.2$.

The DF101 is the initial design; the DF102 and DF103 are variations on the basic airfoil. The DF102 has an increased thickness (about $\frac{1}{16}$ in max., 0.5%) between 2% and 30% on the upper surface. The DF103 has its thickness decreased by approximately the same amount in the same place. See Figs. 11.1 and 11.2.

The purpose of the variations was to test the effects of a controlled contour change in a region previously recognized as important to performance. To make the test more precise, the same physical section was used for all three; it was modified once and became the DF102, and modified a second time to become the DF103. Besides demonstrating the effects of minor, local changes in the airfoil contour, these airfoils as a group provide a measure of the sensitivity of the airfoil performance to surface modifications, whether deliberate or inadvertent.

• DF101-PT (Fig. 12.8)

As the polars show, the initial design is the best, suggesting that deviations either way from a good nominal design are as likely to hurt performance as to help it. Compared to other airfoils, the DF101's performance is quite good; in

particular, it has a remarkable lift range for the 11% thickness. At low speed it performs better than the NACA 2.5411 and not quite as well as the CLARK-Y, something that could be expected from the CLARK-Y's much higher camber (3.55% for the CLARK-Y vs 2.30% for the DF101). At high speeds it is the equal of the NACA 2.5411 and better than the CLARK-Y.

Also see: SD5060, DF102, DF103, CLARK-Y, S3010, S3021
Digitizer plot: Fig. 10.4
Airfoil comparision plot: Figs. 11.1, 11.2
Polar plot: Fig. 12.8
Thickness: 11.00% Camber: 2.30%

- DF102-PT (Fig. 12.9)

Contrary to what might be expected, the addition of upper-surface thickness did not change the low-lift characteristics. Instead, the lift range was extended by 0.1 at the high end. But this is not the aerodynamicist's "free lunch," since overall the drag has increased for lift coefficients above 0.5. Furthermore, at *Rn's* of 60k and 100k the stall occurs earlier than at the higher *Rn's*, a condition that can cause the wing tips to stall before the inboard sections, leading to "tip stall" problems. In conclusion, the DF101 is a better airfoil.

Also see: DF101, DF103, CLARK-Y, S3010
Airfoil comparision plot: Fig. 11.1
Polar plot: Fig. 12.9
Thickness: 11.00% Camber: 2.30%

- DF103-PT (Fig. 12.10)

As compared with the DF102, removing thickness has produced the opposite effect. The maximum lift is reduced, but the stall behavior has improved over the DF101. Still, the DF101 seems to be the best choice of the three.

Also see: DF101, DF102, NACA 2.5411
Airfoil comparision plot: Fig. 11.2
Polar plot: Fig. 12.10
Thickness: 11.00% Camber: 2.30%

E193 *and* E193MOD

- E193-PT (Fig. 12.11)

The E193 has been used on a wide variety of designs from hand-launch gliders to large cross-country ships. In this sense, it may be considered as a multi-task airfoil. What makes the E193 a popular choice is not the performance in terms of drag, but rather the low-drag range from C_l of 0.1 to 1.1. With this range a sailplane will have good wind penetration and thermal performance under most

weather conditions. Of course an airfoil with the same lift range but with lower drag will always be a better choice.

In terms of the overall accuracy of the E193-PT, it should be noted that the E193-PT matches the E205 better than the intended E193 (Fig 11.12).

Also see: E205, S3021, E387, E193MOD
Digitizer plot: Fig. 10.5
Airfoil comparision plot: Fig. 11.12
Polar plot: Fig. 12.11
Thickness: 10.22% Camber: 3.57%

- E193MOD-PT (Fig. 12.12)

Dale Folkening generated the E193MOD by scaling the ordinates of the E193 by a factor of 1.19, effectively adding camber and thickness. The result increases the lift (as indicated by the change in the zero-lift angle of attack) and the width of the polar. There is an associated slight increase in drag, owing mostly to the added thickness.

Also see: E193, S4233, E205, E387
Digitizer plot: Fig. 10.6
Polar plot: Fig. 12.12
Thickness: 11.85% Camber: 4.15%

E205

- E205A-PT (Fig. 12.13)
- E205B-PT (Fig. 12.14)

The popularity of the E205 grew tremendously with the introduction of the Airtronics SAGITTA standard class sailplane. Since this time, the E205 has become one of the most favored RC soaring airfoils. The SAGITTA, which was designed to compete effectively in multi-task events as well as F3B competition, owes much of its success to the E205. As compared with the E193, the better low-lift performance of the E205 offers improved wind penetration.

Of the two models constructed, the B version was the more accurate, especially near the leading edge. Not surprisingly the drag of the B version is everywhere lower than the A.

From the polar it can be seen that the drag curves bunch at the lowest drag point near C_l of 0.25. Compare this to the AQUILA, where not only is the minimum drag at any Rn reached at a C_l of about 0.6, but it is also higher there than the E205 is at 0.25. Because the lift coefficient of a RC sailplane is about 0.2 when flying at high-speed cruise, the E205 is clearly better here than the AQUILA. This illustrates the general rule that good multi-task airfoils have the low drag region shifted to lower C_l's than thermal soaring airfoils.

Also see: S3021, RG15, E374, E193, SD5060, DF101, SD7080, SD7084
Digitizer plot: Figs. 10.7, 10.8
Airfoil comparision plot: Fig. 11.12
Polar plot: Figs. 12.13, 12.14
Lift plot: Fig. 12.15
Aircraft polar: Fig. 5.9
Thickness: 10.48% Camber: 3.01%

E214

- E214A-PT (Fig. 12.16)
- E214B-PT (Fig. 12.17)

By inspection of the E214 contour, it is clear that it not designed like the E193, E205, E374, or E387. The large amount of aft camber (sometimes called aft loading) markedly distinguishes the E214 from the others. On a more subtle level, the E214 is designed with a laminar separation bubble ramp—a mild pressure recovery on the aft upper surface.

While the bubble ramp is good for performance, the large aft camber leads to some trouble. Notice that at lift coefficients below 1.0, the lift at a given angle of attack decreases as the *Rn* is reduced. This loss in lift is due to a large, upper-surface separation over the aft end of the airfoil. (A more thorough discussion is given below in the discussion on tripping the E214.)

It should be noted that for the E214 this loss in lift at low *Rn's* does not necessarily hamper the performance of a sailplane using this airfoil. Since the operating Reynolds numbers of a RC sailplane decreases (along with the speed) as the lift coefficient increases, the mid-range lift coefficients at low *Rn* are not used. Low drag is, however, desirable at high lift and low *Rn*, and this the E214 has.

Two models of the E214 were constructed. Version A had a little less aft camber than the true E214, and version B a little more. The additional camber of version B produces a slight increase in lift, much like that produced by a small, positive (downward) flap deflection. Aside from these small differences the two models are excellent reproductions of the E214.

The E214 is used primarily for thermal-duration flying, owing to the excellent low-drag, high-lift capability. To improve the high speed characteristics full-span flaps are often employed.

- E214C-PT 3° flap (Fig. 12.18)
- E214C-PT 0° flap (Fig. 12.19)
- E214C-PT −3° flap (Fig. 12.20)
- E214C-PT −6° flap (Fig. 12.21)

A 22% flap with a lower-surface tape hinge was added to the B model (see Fig. 5.4 for flap configuration). Tests were performed for flap settings of 3°, 0°, −3° and −6°, covering a range typically used in practice. The flap setting was accurate to within $\pm\frac{1}{2}^\circ$.

It is instructive to start with the 0° case. Compared with the unflapped version, there are no detrimental effects on performance. At the location of the hinge line the upper-surface boundary layer is turbulent and therefore insensitive to the small, 0.03% (0.004 in) step of the flap seal. Although the boundary layer on the lower surface may be laminar at the location of the flap hinge at high angles of attack, a small step at this location typically has little influence on the drag. Note that the lift range is shifted downward slightly, probably because the flap was set at a small, negative angle rather than exactly zero.

For the 3° setting, the lift curve is shifted upward by about 0.2, but the increase in maximum lift is hardly noticeable. There is little change in the drag. In short, for the E214 positive flap deflections do not lead to improved thermalling performance.

On the other hand, the −3° flap deflection leads to improved high-speed performance by shifting the polar downward. In some areas the drag is reduced, while in others it is increased. Interestingly, for the −6° case nothing is gained over the −3° deflection.

• E214C-PT u.s.t. $x/c = 20\%, h/c = .17\%, w/c = 1.0\%$ (Fig. 12.22)

For *Rn's* less than 200k, a two-dimensional trip strip or turbulator placed on the upper surface at 20% chord leads to substantial improvements in the E214's performance. The advantage is seen by comparing the 100k data with Fig. 12.19. (It can be reasonably assumed that at 60k a similar performance gain takes place.) As will be discussed later (see SD7090) the height of the trip is an important parameter. The height,0.17% of chord,was found necessary in order to achieve the indicated drag reduction.

A trip or turbulator is not a panacea; its purpose is to promote transition which shortens the separation bubble. This decreases drag provided that the trip drag is smaller than the bubble drag. For some airfoils tripping the flow either had no effect at any Reynolds number or actually increased the drag. In fact, 200k is the break-even point for most of the airfoils tested; only in a few cases, such as the MILEY, did a trip reduce the drag at 300k. It appears that at 300k the longer length of turbulent flow behind the trip generates more drag than the untripped bubble. For the E214 we recommend that trips be used only for *Rn's* below 200k.

Recalling that for the untripped E214 at a given angle of attack the lift decreases with decreasing *Rn*, the tripped E214 offers insight into this phenomenon. By tripping the boundary layer, transition to turbulent flow takes place sooner than without tripping. As a result, the boundary layer approaches the trailing

edge with more energy to negotiate the sharp pressure recovery over the aft 5% or so of the airfoil. With the trip, the flow can stay attached and maintain the lift (compare Figs. 12.19 and 12.22). Only below C_l of 0.35 does the lift at 100k begin to depart from the other curves, probably because of separation on the lower surface which effectively decambers the airfoil. In summary, the trip reduces not only the size of the separation bubble but also the extent of the turbulent trailing-edge separation.

Also see: SD7032, SD7043, S2091, AQUILA
Digitizer plot: Figs. 10.9, 10.10
Polar plot: Figs. 12.16–12.22
Lift plot: Fig. 12.23
Thickness: 11.10% Camber: 4.03%

E374

- E374A-PT (Fig. 12.24)
- E374B-PT (Fig. 12.25)

The E374 is often selected because its low camber (2.2%) makes it more of a high-speed type than a floater, and because its thickness (10.9%) allows it to be used for the large spans found in cross-country sailplanes. Recently, for example, Joe Wurts flew the E374 to a new cross country distance record of 141 miles. As with the E205, E193, and E387, the E374 shows the effects of a laminar separation bubble through the mid-lift range at the lower *Rn's*.

Two models of the E374 were produced for these tests. Overall, both models were very accurate; the A version has slightly more aft camber and is slightly thinner rearward of 50% chord than the B. For reasons that cannot be satisfactorily explained, the A version is marginally the better of the two in terms of performance, even at the lower C_l's where it would be thought that the additional camber would be detrimental.

- E374B-PT u.s. bumps $x/c = 50\%$, type A (Fig. 12.26)
- E374B-PT u.s.t. $x/c = 20\%, h/c = .17\%, w/c = 1.0\%$ (Fig. 12.27)

On the more accurate E374B model, two kinds of trips were tested: upper-surface, three-dimensional bumps (type A) and the more commonly tested two-dimensional trip strip. It is a widely held view that three- dimensional boundary layer disturbances produced by bumps or zig-zag tape are more unstable than the initially two-dimensional disturbance produced by a continuous trip strip[28]. Because the trips were placed at different locations, comparisons of their relative effectiveness cannot be made. What can clearly be seen from these results is that a trip strip at 20% leads to improved performance for *Rn* less than 200k. For the bumps, the 150k case is most interesting. Below C_l of 0.5 the bubble is effectively tripped; however, above 0.5, there is no benefit. Most likely the leading edge of

the bubble is upstream of the trip, which makes it ineffective because it is in the recirculating region of the bubble.

- E374B-PT u.s. wavy clay, $x/c = 0\%$ to $15\%, h/c = .20\%$ (Fig. 12.28)

To investigate the sensitivity in performance to gross, upper-surface waviness near the leading edge, a generous amount of artist's clay was smeared over the forward 15%. The wavelength, which was random, was on the order of 7% with a maximum height of 0.2%. All edges were carefully smoothed. Although the waviness was greater than anything expected in typical construction, the results do provide clues to potential performance losses due to, say, hasty repairs near the leading edge. Interestly, as Fig. 12.28 shows, there are no large adverse effects.

- E374B-PT thickened trailing edge (Fig. 12.29)

The effect of a thickened trailing edge was also measured. The shape is given in Fig. 5.2. As with the DAE51, there is a small drag increment everywhere, indicating once again that a thin trailing edge is better.

Also see: SD6060, SD7090, E205, NACA 2.5411, CLARK-Y
Digitizer plot: Figs. 10.11, 10.12
Polar plot: Figs. 12.24–12.29
Lift plot: Fig. 12.30
Thickness: 10.91% Camber: 2.24%

E387

- E387A-PT (Fig. 12.31)
- E387A-PT repeated (Fig. 12.32)

The E387A-PT built by Bob Champine was used to compare our data with E387 data taken in other facilities. It also served as one of two calibration models used to check for measurement repeatability over the course of the six-month testing schedule.

The first data set (Fig. 12.31) was taken very early in the schedule and the second (Fig. 12.32) was taken near the end. In general the agreement is good. However, at low-lift coefficients the disagreement is larger than we found elsewhere. The discrepancy may be related to a spanwise twist in the model. For the first run, the twist was removed by applying an opposite twist over a two day period. No attempt was made to untwist the model for the repeated runs or for the tripped and high-turbulence runs.

- E387A-PT u.s.t. $x/c = 20\%, h/c = 0.17\%, w/c = 1.0\%$ (Fig. 12.33)

Figure 12.33 shows that the addition of an upper-surface trip at 20% lowers the drag over the entire range except at high lift and at 300k.

• E387A-PT high turbulence (Fig. 12.34)

To test the E387 under high turbulence conditions, a screen was placed in the test section 3 ft upstream of the model leading edge. As expected, the high turbulence leads to lower drag because the turbulence shortens the bubble in a way much like that produced by the upper-surface trip. No turbulence measurements were taken under these conditions as this was done merely to compare the data with that taken under the normal, low-turbulence test conditions.

• E387B-PT (Fig. 12.36)

The E387 version B data provides some measure of the need for accuracy. Since the camber of this model is substantially less than that of the prototype, large differences in performance can been expected and were measured. An inaccurate copy of an airfoil will probably share few traits with the parent section, as this model illustrates. While it may be possible in some cases to improve an airfoil by modifying its shape, clearly if the airfoil is a good one to begin with, any modification will usually degrade its performance.

Also see: E193, SD6080, S4061, SD7037, S2091
Digitizer plot: Figs. 10.13, 10.14
Polar plot: Figs. 12.31–12.34, 12.36
Lift plot: Fig. 12.35
Thickness: 9.06% Camber: 3.80%

Flat Plate

• Flat Plate-PT (Fig. 12.37)

This airfoil was the only one machined from solid metal. It was $\frac{1}{4}$ in thick, had a rounded leading edge, and the aft 3 in were tapered to a $\frac{1}{32}$ in trailing edge. Since this model was completely symmetrical, the data served to check several aspects of the instrumentation.

The geometry of the flat plate is typical of that used for slab, sheet-balsa stabilizers. The polar data is representative of a full-flying stabilator. In other words, there was no elevator deflection, only angle of attack changes.

As shown in the polars, the lift and drag coefficients are practically the same over the *Rn* range tested. From both theory and many previous measurements it is known that for a flat plate developing lift, the recovery pressure gradients on the suction side are both early and steep. This promotes a rapid transition to turbulent flow. The independence of drag with *Rn* and the relatively high value of the drag are commonly found when the flow is turbulent, as it is here.

Comparing the data with the symmetrical SD8020, for example, shows that the drag of the flat plate is considerably higher. Consequently we recommend a more streamlined airfoil like the SD8020 for stabilizers.

Also see: SD8020
Polar plot: Fig. 12.37
Lift plot: Fig. 12.38
Thickness: 2.08% Camber: 0.00%

FX60-100

- FX60-100-PT (Fig. 12.39)

From a quick glance the FX60-100 looks like a good airfoil; there are no signs of excessive bubble drag, and the width of the low-drag portion of the polar is similar to other 10% sections. Despite these qualities, the FX60-100 has not received wide acclaim. Possibly the unusually prolonged, thin trailing edge presents more of a construction problem than is warranted by the good performance. Or perhaps it was simply overlooked when the E214 became popular.

Also see: SD7037, SD6080, E387
Digitizer plot: Fig. 10.15
Polar plot: Fig. 12.39
Thickness: 9.97% Camber: 3.55%

FX63-137

- FX63-137A-PT (Fig. 12.40)
- FX63-137B-PT (Fig. 12.41)

The high-lift, 13.6% thick Wortmann FX63-137 is often selected in feasibility studies of high altitude, long endurance, unmanned aircraft[24]. Such aircraft are envisioned for missions where manned platforms are impractical, for example: long-duration reconnaissance, surveillance, search and rescue, meteorology and mapping, relay of radio and television, etc. Because of the strong interest in the FX63-137, it has been widely tested in other facilities. At Princeton the FX63-137 was used to make comparisons with the other tunnels (see Section 2.4).

The FX63-137 was first tested without Monokote covering (version A) and then with covering (B). As it came from the builder, the model was sheeted with heavy grain obeche which was varnished smooth; however, the grain was not completely filled by the varnish. With the Monokote covering the wood grain was effectively filled, but this had little effect on the airfoil performance. It will later be shown (see SD7032) that the differences between smooth and rough surfaces can have measurable effects on performance by influencing transition.

Also see: SD7062, S4233, MB253515, SD7043, SPICA
Digitizer plot: Fig. 10.16
Polar plot: Figs. 12.40, 12.41
Thickness: 13.59% Camber: 5.94%

HELMUT QUABECK AIRFOILS (HQ)

The HQ-series of airfoils are apparently generated in a manner similar to the NACA four- and five-digit airfoils. In this method, the thickness distribution is wrapped around a camber line. Although no details of Quabeck's method have been given, based on the lack of smoothness of the coordinates it appears that neither the thickness distribution nor the camber are analytical functions, as they are with the NACA sections.

Quabeck's design philosophy, which has been widely published in the European model press, concentrates largely on the effects of the camber distribution on the airfoil pitching moment[29]. Although it is not often mentioned, Quabeck has been guided by his prolific building and expert flying skills.

The airfoils themselves are characterized by a fair amount of aft loading. For some of them, the upper-surface velocity distribution has a gradual pressure recovery region which lowers drag. In our opinion this feature is the principal key to the success of Quabeck's more popular sections.

Finally, it should be noted that the airfoil designation "HQ" is also used by Horstmann and Quast, who collaborate in the design of airfoils for full-scale competition sailplanes (for example, the Ventus, ASW-22, and ASH-25).

HQ2/9

- HQ2/9A-PT (Fig. 12.42)
- HQ2/9A-PT u.s.t. $x/c = 20\%, h/c = .17\%, w/c = 1.0\%$ (Fig. 12.43)
- HQ2/9A-PT u.s.t. $x/c = 40\%, h/c = .17\%, w/c = 1.0\%$ (Fig. 12.44)
- HQ2/9A-PT l.s.t. $x/c = 50\%, h/c = .17\%, w/c = 1.0\%$ (Fig. 12.45)

Before discussing the lift-drag characteristics of the HQ2/9, one very important point needs to be made. The differences between the nominal HQ2/9, RG15, and S2048 are small. Moreover, these differences are of the same order as the differences between the nominal airfoils and the models of the HQ2/9, RG15, and S2048 actually tested.

To illustrate, Figs. 11.3 and 11.4 compare the nominal HQ2/9 with the nominal RG15 and S2048. As for the actual airfoils tested, Figs. 11.5, 11.6, and 11.7 compare the HQ2/9B-PT with the HQ2/9A-PT, RG15-PT, and S2048-PT. Looking at the figures, one arrives at the conclusion that the nominal airfoils were not really tested; rather a group of very similar airfoils was tested instead.

Another important point, which immediately follows, is that the performance differences between these models are probably not meaningful (at least as they apply to RC sailplane performance) despite the fact that some differences in the overall shape and appearance of the polars are apparent. When all the other components of drag are factored into the performance of the sailplane—induced drag, wing/body interference drag, fuselage drag, etc.—the subtle differences between similar polars tend to be lost. And even though the airfoils were not

tested with flaps (though flaps are usually used) it is doubtful that any one of them would have a decided advantage, even with a flap.

Two versions of the HQ2/9 were tested. The first model, version A, was found to be inaccurate and was later modified to become version B. The polar taken on the plain A model is shown in Fig. 12.42, while Figs. 12.43–12.45 show data taken with trips.

What stands out is that the drag is quite low, especially when compared with the Eppler airfoils. There are two reasons for this:

1. First, this type of airfoil, which is popular in F3B type flying, is intended for use with flaps in order to achieve a wide lift range, while the Eppler airfoils (E205, E193 type) are designed for a wide speed range without flaps. If an airfoil is intended to be used with flaps then a certain amount of lift range (at any given position of the flap) can be traded for lower drag, since the flaps will be used to recover the range. This is the approach taken by Quabeck.
2. The second reason was described in the overview of the HQ-series airfoils; that is, the upper surface pressure gradient is rather gradual, which improves the management of the laminar separation bubble.

Trips were placed on the upper surface at 20% and 40% chord. For the 20% case shown in Fig. 12.43, there is an improvement only for *Rn's* of 150k or less. For the 40% case shown in Fig. 12.44 the break-even point seems to be between 150k and 200k. For the HQ2/9, therefore, it is generally advisable to use trips on any portion of the wing that usually operates at *Rn* less than 150k–200k. With a tapered wing, the trip location near the root should be further aft (in percent of chord) than it is at the tip, since the tip operates at a lower *Rn*.

Figure 12.45 shows the effect of a trip at 50% chord on the lower surface. If anything, the drag has increased around C_l of 0.5.

- HQ2/9B-PT (Fig. 12.47)
- HQ2/9B-PT u.s.t. $x/c = 50\%, h/c = .17\%, w/c = 1.0\%$ (Fig. 12.48)

The untripped HQ2/9B-PT has performance much like the (less accurate) HQ2/9A-PT. An upper surface trip at 50% improves performance below *Rn* of 200k, and only slightly hurts the performance at 300k.

- HQ2/9B-PT u.s. blowing $x/c = 50\%$, type B (Fig. 12.49)
- HQ2/9B-PT trips, $Rn = 200{,}000$ (Fig. 12.50)

The A/B model was hollow so that tests involving boundary layer blowing through a row of spanwise holes could be conducted. The blowing configuration is shown in Fig. 5.7. As depicted in Fig. 5.8 ram air from a single "total head tube" fixed to the lower surface of the model was used for the air supply.

A complete polar for the type B blowing is shown in Fig. 12.49. Even though tripping the boundary layer with a trip strip improved the performance of the airfoil (Fig. 12.47) at low *Rn*, tripping by blowing degraded it. Perhaps the amount of blowing was too large.

Figure 12.50, which compares the blowing data with the cases with and without trips, shows that all of the trips are worse than the untripped case at 200k. Since this model arrived late in the experiments, extensive testing was not possible.

Also see: RG15, S2048, SD8000, S2030, S2055, SD2083, S3021
Digitizer plot: Figs. 10.17, 10.18
Airfoil comparision plot: Figs. 11.3–11.7
Polar plot: Figs. 12.42–12.45, 12.47–12.50
Lift plot: Figs. 12.46, 12.51
Thickness: 8.97% Camber: 1.99%

J5012

• J5012-PT (Fig. 12.52)

The J5012 is a 12% thick, symmetric section designed by Jef Raskin. The airfoil is intended for aerobatic slope soaring where inverted flying is as important as normal flight.

Beside this application, the airfoil is a candidate for use on tail surfaces. In this regard, however, the J5012, as well as some other symmetric airfoils (NACA 0009, NACA 64A010), has an undesirable characteristic if it is to be used as a full-flying surface, e.g. a stabilator. At Rn of 60k near zero angle of attack, the lift curve is nearly flat. Consequently a stabilator deflection around zero lift produces little response. This "deadband" is a common characteristic of symmetric airfoils, although it is not always present (compare the SD8020). As an aside, the aerodynamic characteristics are not quite symmetric about zero angle of attack because, as shown in Fig. 10.19, the airfoil profile itself is not symmetric.

Also see: SD8020, NACA 0009, NACA 64A010
Digitizer plot: Fig. 10.19
Polar plot: Fig. 12.52
Thickness: 12.00% Camber: 0.00%

MB253515

• MB253515-PT (Fig. 12.53)

The MB253515 (designed by Michael Bame) was one of the most intriguing of all the airfoils tested. The relatively high drag of this 15% section leaves much to be desired; nevertheless, it is favored by some.

It may be that the attraction has more to do with the lift characteristics than the drag. Under most types of flying conditions the RC sailplane spends considerable time climbing in thermals, with the wing operating very near the maximum lift coefficient. Unfortunately for most airfoils, just beyond $C_{l_{max}}$ the

airfoil stalls, posing handling problems. In a thermal the turbulence is quite high and, for a sailplane operating close to its stall angle of attack, the turbulent conditions can cause portions of the wing to stall intermittently. The problem is further aggravated by the lower tip chord *Rn's* because with most airfoils the stall angle of attack decreases with *Rn*. The net effect of the local stalling and tendency to tip stall makes efficient thermalling difficult.

Although the drag characteristics of the MB253515 are hardly dazzling, the airfoil may make up for this deficiency with good handling. (See also Section 5.2.) In Fig. 12.55, the lift characteristics of the MB253515 are shown for *Rn* from 30k to 100k. Note that the stall angle of attack is at least 18°—very far from the thermal operating point. This large angle of attack margin gives the MB253515 section a docile feel in thermals and ultimately helps the thermaling efficiency, not through low drag but through handling—by decreasing the work load of the pilot.

This characteristic of the MB253515 separates it from most low-*Rn* airfoils. Usually the lift increases smoothly with angle of attack and finally breaks away, with a stall following shortly thereafter. The highly desirable stall characteristics of the MB253515 may explain why it is favored by some flyers.

Referring to Fig. 12.55 for $Rn = 100$k, the lift increases rapidly between $-2°$ and 0°, flattens between 0° and 3°, then becomes more typical above 3°. When separation begins to take place, maximum lift ($C_{l_{max}} = 1.0$) is reached at 10°, followed by a dip and a long plateau which is maintained down to as low as 30k.

Note also that as the *Rn* is decreased the lift characteristics change markedly. Comparing the 100k, 90k and 40k cases, two important observations can be made. First, below the angle of attack at $C_{l_{max}}$ ($\alpha \approx 10°$), the lift decreases with *Rn*, which indicates the presence of a large bubble or large trailing edge separation or both. Some type of separation may also be deduced from the high drag below $C_{l_{max}}$ shown in Fig. 12.53. The second observation is the well-defined hysteresis loop in lift which is clear indication of laminar separation. Hence the relatively high drag can be attributed to a laminar separation bubble, suggesting that the airfoil could be improved with a trip.

- MB253515-PT u.s.t. $x/c = 20\%, h/c = .17\%, w/c = 1.0\%$ (Fig. 12.54)

Figure 12.54 shows that a trip at 20% chord improves the performance for *Rn* less than 200k. For airplanes using this airfoil, therefore, a trip should be used at least on the wing tips, and possibly on the entire wing, depending on the expected speed range.

Also see: S4233, SD7062, E193MOD, WB135/35, WB140/35/FB
Digitizer plot: Fig. 10.20
Airfoil comparision plot: Fig. 11.11

Polar plot: Figs. 12.53, 12.54
Lift plot: Fig. 12.55
Thickness: 14.96% Camber: 2.43%

M06-13-128 (MILEY)

In 1972, S.J. Miley[30] received his Ph.D. from Mississippi State University with a thesis titled "Analysis of the Design of Airfoil Sections for Low Reynolds Numbers." His thesis culminated with an example airfoil, the M06-13-128, designed for *Rn's* greater than 600k. As the title may suggest, there has been no consensus as to how the term low *Rn's* should be defined. A simple way would be to state a cut-off Reynolds number number below which everything is considered low *Rn's*. But low *Rn's* usually implies laminar separation and high drag. Thus another definition is *Rn's* where laminar separation is significant. However, with this definition the *Rn* would be different for each airfoil. As with any definition, there is some degree of ambiguity, and it may simply be best to state first what *Rn's* are being considered, and second, whether or not laminar separation is included in the particular problem under study. In Miley's case, laminar and turbulent separation were assumed negligible and were ignored in the anaylsis.

- M06-13-128-PT (Fig. 12.56)

As shown in Fig. 12.56, the MILEY airfoil was tested below its design *Rn* of 600k. At all *Rn's* the MILEY airfoil has a high-drag laminar separation bubble as indicated by the large bulge in the polar. In fact for a *Rn* of 200k, the drag between the stall limits was the highest of any airfoil tested. Consequently we do not recommend it for model sailplanes.

- M06-13-128-PT u.s. bumps $x/c = 31\%$, type A (Fig. 12.57)
- M06-13-128-PT u.s. trips, $x/c = 31\%, Rn = 200{,}000$ (Fig. 12.58)
  (A-trip) $h/c = .17\%, w/c = .52\%$
  (B-trip) $h/c = .08\%, w/c = .52\%$
  (C-trip) zig-zag tape, type B
  (D-trip) bumps

An upper-surface trip on the MILEY airfoil at 31% produces a dramatic drag reduction—up to 73% at $Rn = 200$k. For all the cases shown, the A-trip works the best, with the zig-zag tape (C-trip) being next. The B-trip is apparently not high enough (half that of A-trip), as the drag is slightly greater. As for the bumps (D-trip), they do not work as well as the others at high lift, although elsewhere they are as effective as the A- and B-trips. The exact mechanism of these performance differences and how it relates to the shape of the trip is still not well understood.

Also see: SD7003, FX63-137, SD7062
Digitizer plot: Fig. 10.21
Polar plot: Figs. 12.56–12.58
Lift plot: Fig. 12.59
Thickness: 12.81% Camber: 5.16%

NACA 0009

• NACA 0009-PT (Fig. 12.60)

The NACA four-digit symmetric airfoils are often used on tail surfaces, most commonly the stabilizer. As expected, the drag of the 9% thick NACA 0009 is lower than the 12% symmetric J5012. It is interesting to note, however, that the lift range of the thinner NACA 0009 is on a par with the J5012.

Again, as with the J5012, there is a deadband in lift about 0°, but as shown in Figs. 12.61 the deadband for the NACA 0009 is worse than the J5012. As mentioned before, any substantial nonlinearity in the lift-curve slope is caused by some type of laminar or turbulent separation. Also, between approximately −2° and 2°, the lift characteristics are slightly asymmetric. For the NACA 0009 at low *Rn's*, a long, thin bubble forms on both the upper and lower surfaces. Any slight asymmetries present (either in contour or surface finish) will alter the boundary layer behavior, thereby affecting the symmetry of lift. In fact, as Fig. 10.22 reveals, the NACA 0009-PT is not perfectly symmetric which leads to the asymmetric lift and drag characteristics about 0°.

Also see: SD8020, NACA 64A010, J5012
Digitizer plot: Fig. 10.22
Polar plot: Fig. 12.60
Lift plot: Fig. 12.61
Thickness: 9.00% Camber: 0.00%

NACA 2.5411

• NACA 2.5411-PT (Fig. 12.62)

The NACA 2.5411 is a four-digit NACA section with 2.5% maximum camber at 40% of chord, and 11% thickness.

The drag polar shows that the overall drag is low, and this gives a good first impression. However as shown in Fig. 12.63, the stall characteristics are undesirable. There is a smooth, continuous increase in lift up to a sharp and abrupt stall. Flight near maximum lift with this section would be exceedingly difficult because there is virtually no angle of attack margin between maximum lift and stall.

As mentioned in the discussion of the MB253515, a lift plateau with the associated high drag is desirable, as it provides warning that stall is imminent. Unless

measures such as stall strips on the leading edge are used to alleviate this problem, the NACA 2.5411 and closely related sections (NACA 2412, NACA 2415[9]) are not recommended for slow, thermal duration flying. However, its performance at high speed, such as is needed in windy conditions, is very good, and stall strips make the thermalling performance at least acceptable.

Also see: E374, CLARK-Y, DF101, SD5060
Digitizer plot: Fig. 10.23
Polar plot: Fig. 12.62
Lift plot: Fig. 12.63
Thickness: 11.00% Camber: 2.50%

NACA 64A010

• NACA 64A010-PT (Fig. 12.64)

Compared to the two symmetric airfoils discussed so far (J5012, NACA 0009), the 10% thick NACA 64A010 is the worst for low-*Rn* applications. The shape of the polar, with the large decrease in drag just before the stall, is caused by a long run of a favorable pressure gradient followed by a steep recovery region. In the design of this airfoil, the intention was to achieve long runs of laminar flow for low drag. While this design approach works for high *Rn's*, the same line of reasoning cannot be applied at low *Rn's*.

Figure 12.65 shows the lift characteristics for *Rn's* of 100k, 80k and 60k. At 60k the presence of a long bubble can be inferred from the nonlinearities around zero angle of attack. It is interesting that for *Rn's* of 100k and 80k the nonlinearities almost vanish. This does not mean that the separation has vanished; instead, the separation on the upper and lower surfaces apparently have the combined effect of cancelling each other out.

Also see: NACA 0009, SD8020, J5012
Digitizer plot: Fig. 10.24
Polar plot: Fig. 12.64
Lift plot: Fig. 12.65
Thickness: 10.00% Camber: 0.00%

NACA 6409

• NACA 6409-PT (Fig. 12.66)

The NACA 6409 is considered more of a free-flight airfoil than one for RC soaring. The actual wind tunnel section was the only model that had open bay construction from leading to trailing edge. The ribs were $\frac{1}{8}$ in (1% chord) thick and had a spacing of 3 in (25%), giving an open-bay cell aspect ratio of 1:4. The sagging of the covering was about 0.025 in (0.2%) worst case, and generally much

less—0.005 to 0.015 in. Due to the lack of torsional rigidity, data was taken only up to 200k.

As Fig. 12.66 shows, the airfoil stalls at 8° at 60k; however, in Fig. 12.67, which shows lift data only, the premature stall is not found. The lack of repeatability may have been caused by the gusty weather at the time of the lift run.

As for the performance, the NACA 6409 is an excellent low speed, floater airfoil, but, much like the AQUILA airfoil, the large camber severely limits the high speed performance.

Also see: AQUILA, S2091, SD7043
Digitizer plot: Fig. 10.25
Polar plot: Fig. 12.66
Lift plot: Fig. 12.67
Thickness: 9.00% Camber: 6.00%

RG15

- RG15-PT (Fig. 12.68)
- RG15-PT u.s.t. $x/c = 20\%, h/c = .17\%, w/c = 1.0\%$ (Fig. 12.69)
- RG15-PT u.s.t. $x/c = 40\%, h/c = .17\%, w/c = 1.0\%$ (Fig. 12.70)
- RG15-PT u.s.t. $x/c = 60\%, h/c = .17\%, w/c = 1.0\%$ (Fig. 12.71)
- RG15-PT u.s.t. $x/c = 70\%, h/c = .17\%, w/c = 1.0\%$ (Fig. 12.72)

The RG15 was tested extensively with trips because the performance of the untripped model (shown in Fig. 12.68) was relatively good. We asked ourselves: when one starts with a "good" airfoil (the RG15-PT), can trips still make modest improvements in performance? Note that the question is specific to this airfoil and cannot be generalized.

It is instructive to begin with the trip at 70% chord shown in Fig. 12.72. At this location, it has virtually no effect since it is downstream of laminar separation. In other words, it is either inside the laminar separation bubble or immersed in the turbulent boundary layer.

At 60% chord, the trip causes the 150k and 200k curves to spread apart. At 40% chord, the trip efficiently trips the boundary layer for Rn of 150k at the lower lift coefficients. As observed before, the higher-Rn polars overlap since the boundary layer is tripped too soon, producing more drag than that found for the lower Rn's (150k in this case).

At 20% chord, there is even more overlap at 300k. But the drag at 100k has decreased significantly from the untripped case as the trip moves forward. As is true with the HQ2/9, a trip should be employed for Rn less than 150k–200k. The location will depend on the average local chord Rn.

Also see: HQ2/9, S2048, SD8000, SD2030
Digitizer plot: Fig. 10.26
Airfoil comparision plot: Figs. 11.3, 11.6
Polar plot: Figs. 12.68–12.72
Lift plot: Fig. 12.73
Thickness: 8.92% Camber: 1.76%

SELIG AIRFOILS (S)

The original group of Selig airfoils[23] was designed with the aid of both the Eppler and Somers Computer Code for the Design and Analysis of Low-Speed Airfoils[20] and the experimental results of Althaus[9]. The approach taken was to compare the theoretical and experimental results of several airfoils, then to determine from these comparisons what factors (in the velocity distribution and boundary layer development) were needed to produce good, low-Rn airfoils. These factors were subsequently incorporated into the design of several new airfoils for RC sailplanes.

A common feature of most of the Selig airfoils is a long, gradual pressure recovery region on the upper surface called a bubble ramp. As a result of this ramp, the upper-surface transition point moves forward slowly and continuously with increasing angle of attack. This feature usually gives the polars an appearance more closely resembling those measured at high Rn. These are general design principles. Surprisingly, even today the details of how "gradual" and how "slowly", and how best to achieve this are topics of research.

The performance of the Selig airfoils is often markedly different from one to the next. This is because the airfoils were designed to have a variety of characteristics in the hope that trends would emerge, leading ultimately to a better understanding of low-Rn airfoils. Implicit in this approach is the recognition that low-Rn airfoil design is still in the early stages of development.

The S-designation is also used by Somers; however, Selig uses four digits in the airfoil name, while Somers uses only three.

S2048

- S2048-PT (Fig. 12.74)
- S2048-PT with trips (Fig. 12.75)
- S2048-PT misc. trips (Fig. 12.76)

The S2048 was originally presented at the 1985 MARCS Symposium held in Madison, Wisconsin and has been used on the Synergy F3B sailplanes that have represented the U.S. at the World F3B Championships held in recent years (1987 and 1989). The airfoil is a "redesigned" HQ2/9 with slightly longer bubble ramps on the upper and lower surfaces (i.e. more gradual pressure gradients). Because the performance improvement due to changing these ramps was expected to be

small in any case, more accurate models than the ones we tested would be required to detect and measure it. And even if it could be measured, actually realizing or maintaining that difference would be difficult. Nonetheless the possibility of bettering existing F3B airfoil designs may still yield to investigation at another time.

The effects of trips on the upper and lower surfaces are shown in Fig. 12.75; results of miscellaneous trip locations are shown in Fig. 12.76. Although no attempt was made to systematically study the effects of trip location on this airfoil, it does seem that a slight improvement in high-speed performance can be obtained through the use of an upper-surface trip around 60–70% chord combined with a lower-surface trip near 60%. As with the RG15 and HQ2/9, trips nearer the leading edge can be expected to produce lower drag at lower *Rn's*.

Also see: HQ2/9, RG15, S2055, SD8000, SD2030
Digitizer plot: Fig. 10.27
Airfoil comparision plot: Figs. 11.4, 11.7
Polar plot: Figs. 12.74–12.76
Lift plot: Fig. 12.77
Thickness: 8.63% Camber: 1.94%

S2055

- S2055-PT (Fig. 12.78)

The S2055 is a slightly thinned and decambered S2048. The results of this small perturbation in shape are marginally lower drag and a downward shift of the lift range. As with other F3B airfoils, flaps are necessary to fully realize the capabilities of the airfoil.

Of all the airfoils tested, the S2055-PT had the lowest drag at 300k. Although several attempts were made to reduce the drag further through the use of trips, none worked. Instead, the drag was increased except when the trip was far aft, and then it had no effect.

Although this is the lowest drag airfoil tested and should do very well on sailplanes where speed is paramount, the 8% thickness offers a significant construction challenge.

Also see: SD2030, S2048, RG15, HQ2/9, SD8000
Digitizer plot: Fig. 10.28
Polar plot: Fig. 12.78
Thickness: 7.99% Camber: 1.66%

S2091

As mentioned in the discussion of the AQUILA airfoil, its high-speed performance is severely compromised by its high-camber. The S2091 was designed

primarily to be an improvement over the AQUILA by extending the polar to lower lift, while maintaining the AQUILA's low-speed, high-lift characteristics. Details of how this was achieved through airfoil design may be found in Reference 23.

- S2091A-PT (Fig. 12.79)
- S2091B-PT (Fig. 12.80)

Data on two models are shown. The first model, version A, was found to be too thin as verified by hand-held templates. In addition, the leading edge was rough in certain areas from the fiberglass beneath the paint. Undoubtedly this influenced transition in a manner similar to that of a trip strip. The model was later re-contoured and given the B designation. Only the B version was digitized for coordinates.

The effect of the roughness of version A as compared with the smooth version B is to decrease the drag at 60k. Smaller improvements are found for 100k, while no improvement exists at 200k.

Referring to the B version data (Fig. 12.80), the goal of extending the low-lift end of the polar beyond that of the AQUILA airfoil has been achieved. Futhermore, it comes as some surprise that at *Rn's* above 60k the maximum lift coefficient is increased by 0.1 over that of the AQUILA. In summary, the S2091 is an advance in performance over the AQUILA, but this comes mostly through the relaxation of the flat-bottom requirement. Of course a flat lower surface does not necessarily mean the airfoil is deficient, as illustrated by the performance of the DF101 and the nearly flat-bottom S3021.

- S2091B-PT Gurney Flap type A (Fig. 12.81)
- S2091B-PT Gurney Flap type B (Fig. 12.82)
- S2091B-PT Gurney Flap type C (Fig. 12.83)

The S2091B-PT was tested with a so-called Gurney flap, often used on racing car wings which develop a download to increase traction. As can be seen in Fig. 5.5, a Gurney flap is a simple, thin tab on the order of 1% chord, which is perpendicular to the lower side of the airfoil at the trailing edge. For these tests the tab was 0.017% chord thick (0.002 in) brass shim stock with a length of 0.6% chord for type A, 1.2% for B, and 2.6% for C.

For the type A Gurney flap, the whole polar is shifted upwards in lift coefficient by 0.1—an impressive result for such a simple modification. Similar results are found for type B, but diminishing returns begin to appear for type C. It can be reasonably expected that the efficiency of the small 0.6% and 1.2% Gurney flaps in increasing lift is not unique to the S2091. (Note that there is a small drag penalty associated with the Gurney flap.)

Also see: AQUILA, E214, SD7037, SD7032
Digitizer plot: Fig. 10.29
Polar plot: Figs. 12.79–12.83
Lift plot: Fig. 12.84
Thickness: 10.10% Camber: 3.91%

S3010

- S3010-PT (Fig. 12.85)

The S3010 is the first example of a Selig airfoil that has a lift range much like the E193 and E205 airfoils. Other examples include the flat-bottom S3014, S3016, and S3021. All these designs took advantage of the increased understanding of the laminar separation bubble, and as a result the high-drag bulges in the middle of the low-*Rn* polars are virtually gone. Instead, the polar and its edges are more rounded, and in most places the drag of the S3010 is lower than the E205. It is interesting to note that in many respects the S3010 performance characteristics are very similar to the DF101, although as shown in Fig. 11.8, a comparison of the profiles actually tested reveals that the S3010 and DF101 shapes are very different.

Also see: S3021, CLARK-Y, DF101, S3014, S3016, E205
Digitizer plot: Fig. 10.30
Airfoil comparision plot: Fig. 11.8
Polar plot: Fig. 12.85
Lift plot: Fig. 12.86
Thickness: 10.32% Camber: 2.82%

S3014 *and* S3016

- S3014-PT (Fig. 12.87)
- S3016-PT (Fig. 12.89)

The S3010, S3014 and S3016 are quite similar aerodynamically since the latter two were derived from the first with only minor modifications. Although the S3016 has a slight edge over the S3010 and S3014 at high speed and the S3014 looks best at a *Rn* of 60k, none of the three has a decided advantage over the others.

Also see: S3021, E205, SD7080
Digitizer plot: Figs. 10.31, 10.32
Polar plot: Figs. 12.87, 12.89
Lift plot: Fig. 12.88
S3014 Thickness: 9.46% Camber: 2.57%
S3016 Thickness: 9.52% Camber: 2.09%

S3021

- S3021A-PT (Fig. 12.90)
- S3021B-PT (Fig. 12.92)

The S3021 has a bubble ramp longer than the transition ramp on the E205, and the resulting reduction in drag is dramatic. Certainly some of the reduction is because the S3021 is thinner than the E205, but, from the shape of the airplane polar shown in Fig. 5.9, it is clear that most of the drag reduction comes from better management of the laminar separation bubble.

Two models of the S3021 were built; version A is the more accurate one. Version B has a reflexed trailing edge which produces a steeper pressure recovery on the upper surface—a change which leads to a higher bubble drag.

Fig. 4.4 compares the data from the S3021A-PT and the E205B-PT (Figs. 12.90 and 12.14 respectively) and shows that the drag of the S3021A-PT is almost everywhere lower than that of the E205B-PT. The ISES code predicted a similar drag reduction when it was used to compare the nominal airfoils.

Also see: E205, S3014, S3010, SD7080, SD7084
Digitizer plots: Fig. 10.33, 10.34
Airfoil comparision plot: Fig. 11.9
Polar plot: Figs. 12.90, 12.92
Lift plot: Fig. 12.91
Aircraft polar: Fig. 5.9
Thickness: 9.47% Camber: 2.96%

S4061

Although originally intended as a cross-country airfoil, the S4061 has since demonstrated it's versatility under a variety of conditions. At a recent AMA Nationals (the NATS), Paul Carlson, founder of Off the Ground Models, flew his newly designed and kitted PRODIGY sailplane to a first place finish in the 2-Meter class, a second in Standard, and a third in Unlimited. To date over 3500 PRODIGY kits have been produced, and the popularity of the S4061 has grown proportionally.

- S4061A-PT (Fig. 12.93)
- S4061B-PT (Fig. 12.94)

The version A model of the S4061 is inaccurate. The more accurate version B shows lift and drag characteristics much different than those of the A. As was amply demonstrated in other examples, these differences in the data come as no surprise.

- S4061B-PT u.s.t. $x/c = 45\%, h/c = .17\%, w/c = 1.0\%$ (Fig. 12.95)
- S4061B-PT u.s.t. $x/c = 45\%$, Rn = 150,000 (Fig. 12.96)
- S4061B-PT u.s.t. $x/c = 45\%$, Rn = 150,000 and 300,000 (Fig. 12.97)

As shown in Fig. 12.95, a trip with height of 0.17% reduces drag for Rn less than 150k. Figures 12.96 and 12.97 show that a two-dimensional trip produces the same result as zig-zag tape (type A).

Also see: SD6080, DAE51, S4062, SD7037, E387, E193, E214
Digitizer plot: Figs. 10.35, 10.36
Polar plot: Figs. 12.93–12.97
Lift plot: Fig. 12.98
Thickness: 9.60% Camber: 3.90%

S4062

- S4062-PT (Fig. 12.99)

The S4062 was intended to be an improvement over the S4061. The major modification is a longer run of laminar flow designed into the S4062. But as the data shows, this design change has not lead to improved performance. Rather, the S4062 has higher drag owing to a larger laminar separation bubble. It is interesting to note that this problem is also predicted by the ISES code which was not available when the S4062 was designed.

Also see: S4061, SD6080, DAE51
Digitizer plot: Fig. 10.37
Polar plot: Fig. 12.99
Thickness: 9.53% Camber: 4.14%

S4180

- S4180-PT (Fig. 12.100)

The thin trailing edge of this model was wavy for the aft 25% chord along the entire span. Because of the significant three-dimensionality, nothing conclusive can be said about the two-dimensional airfoil characteristics. The model coordinates were not digitized because there is no representative section.

Also see: S4061
Polar plot: Fig. 12.100
Thickness: 9.77% Camber: 4.36%

S4233

- S4233-PT (Fig. 12.101)
- S4233-PT u.s.t. $x/c = 20\%, h/c = .17\%, w/c = 1.0\%$ (Fig. 12.102)

The S4233 was designed to be an improvement over the MB253515. To date the S4233 has probably been most used by Bob Champine, retired NACA/NASA test pilot, who recently achieved his *second* LSF level 5 flying his "stretched" GEMINI with the S4233. His enthusiasm for this airfoil is reflected in the accuracy of the wind tunnel model which he built.

Note that the 13.6% thick S4233 has a wider lift range and lower drag than the 15% thick MB253515. As with the MB253515, the S4233 shows a bulge in the drag at a *Rn* of 100k, so one would expect a trip to improve matters. Fig. 12.102 shows that the low-*Rn* drag can indeed be reduced using a trip, but the performance with the trip is slightly worse at *Rn* of 300k.

Also see: MB253515, E193MOD, WB135/35, SD7062
Digitizer plot: Fig. 10.38
Polar plot: Figs. 12.101, 12.102
Lift plot: Fig. 12.103
Thickness: 13.64% Camber: 3.26%

SELIG AND DONOVAN AIRFOILS (SD)

A discussion of the design philosophy used behind the SD designs is given in Chapter 4.

SD2030

• SD2030-PT (Fig. 12.104)

The SD2030 was designed for operation at speeds higher than those typically found on most RC sailplanes. For this reason it is suitable for high-wing-loading F3B and F3E type aircraft. Since the lift range is narrow, camber-changing flaps are recommended.

Also see: SD2083, S2055, RG15, S3021
Digitizer plot: Fig. 10.39
Polar plot: Fig. 12.104
Lift plot: Fig. 12.105
Thickness: 8.56% Camber: 2.25%

SD2083

• SD2083-PT (Fig. 12.106)

The SD2083 was an early and not very successful attempt at an F3B design. The airfoil suffers from a fairly large separation bubble, and there is too much camber (2.85%) for good, high-speed performance.

Also see: S2055, SD2030, SD8000, HQ2/9
Digitizer plot: Fig. 10.40
Polar plot: Fig. 12.106
Thickness: 8.96% Camber: 2.85%

SD5060

• SD5060-PT (Fig. 12.107)

For operation at *Rn's* from 100k down (e.g. hand-launch RC sailplanes) the SD5060 is an improvement over the S3021. The stall characteristics of the SD5060, however, are not as benign as the S3021. In fact the airfoil stalls abruptly, much like the NACA 2.5411.

Also see: S3021, DF101, CLARK-Y
Digitizer plot: Fig. 10.41
Polar plot: Fig. 12.107
Lift plot: Fig. 12.108
Thickness: 9.45% Camber: 2.30%

SD6060

• SD6060-PT (Fig. 12.109)

The SD6060 was designed to be an improvement over the E374 for cross-country flying. The E374 clearly shows large drag at low *Rn's* due to bubble losses. To alleviate these effects, the SD6060 was designed with a longer bubble ramp than the E374.

By comparing the E374 (Fig. 12.25) with the SD6060 (Fig. 12.109), one can see the advantages of the SD6060. Almost everywhere it has lower drag than the E374, especially at the high *Rn's*, which are important for cross-country flying.

• SD6060-PT u.s.t. $x/c = 20\%, h/c = .17\%, w/c = 1.0\%$ (Fig. 12.110)
• SD6060-PT u.s.t. $x/c = 40\%, h/c = .17\%, w/c = 1.0\%$ (Fig. 12.111)

A trip placed at 40% reduces the drag at 100k by shortening the bubble. Moving the trip forward to 20% further reduces the drag at 100k, although at 200k and 300k the drag is increased.

It is not surprising to find that the SD6060 and E374 are quite similar when both are tripped at 20% (compare Figs. 12.27 and 12.110). At high-Rn/low-C_l, the E374 has a slight advantage over the SD6060, although in the same regime the plain SD6060 has the lowest drag of both airfoils, tripped or untripped.

Also see: E374, E205, NACA 2.5411, SD7090
Digitizer plot: Fig. 10.42
Polar plot: Figs. 12.109–12.111
Lift plot: Fig. 12.112
Thickness: 10.37% Camber: 1.84%

SD6080

- SD6080-PT (Fig. 12.113)

The SD6080 is an improvement over the S4061. Although the high-lift characteristics of the two airfoils are much alike, the SD6080 offers improvements at the low-lift end of the flight envelope.

Figures 12.94 and 12.113 show that the lower part of the SD6080 polar is extended over that of the S4061. Besides this extension, the drag over most of the polar is lower, particularly in those areas which are used by a typical RC sailplane.

- SD6080-PT u.s.t. $x/c = 10\%, h/c = .17\%, w/c = 1.0\%$ (Fig. 12.114)
- SD6080-PT u.s.t. $x/c = 20\%, h/c = .17\%, w/c = 1.0\%$ (Fig. 12.115)
- SD6080-PT u.s.t. $x/c = 30\%, h/c = .17\%, w/c = 1.0\%$ (Fig. 12.116)

As shown in Figs. 12.114–12.116, trips were placed on the SD6080 at 10%, 20%, and 30% chord. Of the three cases, the trip at 30% is the best between *Rn's* of 100k and 300k. As expected, the trip farthest forward is best at lower *Rn's*. When the polars for the 30% trip and the untripped case are compared (Figs. 12.113 and 12.116), a 30% trip should clearly be used for *Rn* at and below 150k.

- SD6080-PT thickened trailing edge (Fig. 12.117)

As observed with the DAE51 and E374, the thickened trailing edge increases the overall drag on the order of 5%. It should be noted that the "thickened trailing edge" was slightly different for each of the three airfoils, but the effect of increased drag is common to all. The shape of the trailing edge is shown in Fig. 5.3.

Also see: S4061, E387, SD7037, SD7032
Digitizer plot: Fig. 10.43
Polar plot: Figs. 12.113–12.117
Thickness: 9.18% Camber: 3.74%

SD7003

- SD7003-PT (Fig. 12.118)
- SD7003-PT repeated (Fig. 12.119)

The SD7003 was designed to have a very long and gradual upper-surface bubble ramp. In fact, it may be considered to span the entire upper surface. The resulting effect is particularly apparent in the overall smoothness of the polar which shows no trace of high drag due to a laminar separation bubble. However this does not mean there is no bubble. Rather, the bubble losses are small. At *Rn's* of 60k and 100k, the drag is especially low when compared with all the other airfoils tested.

The polars shown in Fig. 12.119 are from a second series of runs to provide a measure of the overall repeatability. Other than a few small discrepancies, the agreement is quite good and typical of repeated runs (see the E387A-PT).

- SD7003-PT u.s.t. $x/c = 60\%, h/c = .17\%, w/c = 1.0\%$ (Fig. 12.120)
- SD7003-PT u.s.t. $x/c = 70\%, h/c = .17\%, w/c = 1.0\%$ (Fig. 12.121)
- SD7003-PT u.s. bumps $x/c = 50\%$, type A (Fig. 12.122)
- SD7003-PT u.s. bumps $x/c = 60\%$, type A (Fig. 12.123)
- SD7003-PT u.s. bumps $x/c = 70\%$, type A (Fig. 12.124)

Several attempts were made to reduce the drag through the use of trips, but they either increased the drag or had no effect. One is tempted to ask whether this means that the SD7003 is optimized for ramps such that no further improvements can be made. It seems unlikely, but it is an interesting question nonetheless. (See Section 5.3.)

Also see: SD8000, RG15, S3021, MILEY
Digitizer plot: Figs. 10.44–10.49
Polar plot: Figs. 12.118–12.124
Lift plot: Fig. 12.125
Thickness: 8.51% Camber: 1.46%

SD7032

The SD7032 is among the best of the thermal-duration type airfoils (such as the AQUILA, E214, S2091, S4061, SD6080). The design of this new airfoil incorporates what is presently known about mitigating laminar separation problems through the use of a bubble ramp.

The data show that control of the bubble has been achieved. For example, in contrast to the untripped E214, there is little evidence of separated flow even at Rn of 60k. At moderate to high Rn's, the performance is generally better than the E214. As compared to the E214 with a trip (which is another way to control separation), the untripped SD7032 is about the same at the lower Rn's, but considerably better at Rn of 300k.

It should be mentioned that the angle of attack at stall decreases with Rn, and for Rn of 60k the stall is relatively sharp, as shown in Figs. 12.133. This needs to be considered primarily for wings operating at very low Rn's, such as with hand-launch sailplanes.

- SD7032A-PT (Fig. 12.126)
- SD7032B-PT (Fig. 12.127)
- SD7032D-PT (Fig. 12.134)

There were two test sections of the SD7032 built. The first was initially covered in balsa only (version A), leaving a relatively rough aerodynamic surface. The model was then covered in Monokote (version B), and finally a 21% flap

was added (version C). The flap configuration is shown in Fig. 5.6. The nominal SD7032 coordinates for the A/B/C model were modified slightly by the addition of a linear thickness increase from the leading to the trailing edge. At the leading edge the added thickness was zero and at the trailing edge it was $\frac{1}{32}$ in, to give a finite trailing edge thickness. The second, more accurate model is version D. This model used the nominal coordinates.

Figs. 12.126 and 12.127 show that the balsa surface acts in a manner similar to that of a trip. The drag curves for the model A at Rn of 200k and 300k are nearly coincident which indicates premature transition at 300k. As shown in Fig. 12.127, adding the smooth Monokote covering reduces the drag by up to 20% at 300k.

For version B, the 300k polar exhibits about a 10% drag increase in the range $0.60 < C_l < 0.95$ when compared with the SD7032D-PT. Fig. 10.50 shows that the A/B/C model has a flat spot on the upper surface near 45% which affects the laminar separation bubble. This, in turn, leads to the differences in drag at 300k. This is still another illustration of how a relatively small surface difference can affect performance. Having said that, note that both the A and B versions out-perform the D version at low to moderate Rn (with only a small penalty at high speed). This is because of the way the wing "flies through" the polars, in this case taking advantage of the low-drag areas. See Fig. 5.10.

- SD7032C-PT 6° flap (Fig. 12.128)
- SD7032C-PT 3° flap (Fig. 12.129)
- SD7032C-PT 0° flap (Fig. 12.130)
- SD7032C-PT −3° flap (Fig. 12.131)
- SD7032C-PT −6° flap (Fig. 12.132)

Flaps on the SD7032 extend the useful high-speed range. As with the E214, the flap is intended to be used only in the reflexed position. What is also of interest is that the −6° flap deflection is too much of a good thing; −3° provides lower drag at high Rn/low C_l.

- SD7032D-PT u.s.t. $x/c = 45\%, h/c = .17\%, w/c = 1.0\%$ (Fig. 12.135)

A trip at 45% offers only marginal improvements. This is to be expected, given an airfoil that is designed with a bubble ramp. For C_l of 0.35, the drag is decreased for Rn's less than 200k. This small improvement does not warrant the use of trips for the type of flying typically encountered.

Also see: E214, S2091, AQUILA, SD7037
Digitizer plot: Figs. 10.50, 10.51
Polar plot: Figs. 12.126–12.132, 12.134, 12.135
Lift plot: Fig. 12.133
Aircraft polar: Fig. 5.10
Thickness: 9.95% Camber: 3.66%

SD7037

- SD7037-PT (Fig. 12.136)

The SD7037 is a thinner, decambered SD7032. As would be expected, the drag is lower, the polar is shifted downward in lift, and the lift range is less. To increase the lift range, flaps would be useful.

The relatively low drag at C_l near 0.3 offers good L/D performance which, together with low drag at high lift, should make the SD7037 a popular airfoil, especially for thermal-duration flying. For weak thermal conditions common to east coast soaring in the U.S., the SD7037 would make an excellent cross-country airfoil, but flaps in this case are almost essential to improve high-speed, between-thermal performance.

- SD7037-PT u.s.t. $x/c = 30\%, h/c = .17\%, w/c = 1.0\%$ (Fig. 12.137)

An upper-surface trip at 30% reduces the drag at lower *Rn's* only slightly. Although it was not measured, one would expect the drag at 300k to be increased. As with the SD7032, trips are of little benefit.

Also see: FX60-100, SD6080, SD7032, E214
Digitizer plot: Fig. 10.52
Polar plot: Figs. 12.136, 12.137
Thickness: 9.20% Camber: 3.02%

SD7043

- SD7043-PT (Fig. 12.138)
- SD7043-PT u.s.t. $x/c = 20\%, h/c = .17\%, w/c = 1.0\%$ (Fig. 12.139)

The shapes of the untripped SD7043 polars are indicative of a laminar separation bubble that would be amenable to control by a trip. This airfoil reaches a high lift coefficient which produces a low sink speed if flown just above stall speed. Due to time limitations, it was not tested with the trip at the lower *Rn's* (60k, 100k, and 150k), but it is reasonable to assume that the tripped version would maintain most of this high lift while substantially decreasing the drag. If so, the SD7043 could be a good performer on small-to-medium size airplanes, but with the caveat that the stall, which is moderately abrupt, probably needs to be controlled with leading edge stall strips. (See Section 5.2.)

Also see: SPICA, E214, SD7032
Digitizer plot: Fig. 10.53
Polar plot: Figs. 12.138, 12.139
Lift plot: Fig. 12.140
Thickness: 9.13% Camber: 3.51%

SD7062

- SD7062-PT (Fig. 12.141)
- SD7062-PT u.s.t. $x/c = 15\%, h/c = .17\%, w/c = 1.0\%$ (Fig. 12.142)
- SD7062-PT u.s.t. $x/c = 15\%, h/c = .08\%$ and $.17\%, w/c = 1.0\%$ (Fig. 12.143)

The SD7062 is a thick (14%), highly cambered (4%) airfoil. In some ways it is comparable to the S4233, but when untripped it performs considerably better than the S4233, except at high Rn. When both airfoils are tripped (see Figs. 12.102 and 12.142), the situation reverses; the S4233 has lower drag, although not much. As Fig. 12.143 shows, at 200k a trip placed at 15% increases the drag with respect to the untripped case.

Also see: FX63-137, S4233, E193MOD, MB253515
Digitizer plot: Fig. 10.54
Polar plot: Figs. 12.141–12.143
Thickness: 13.98% Camber: 3.97%

SD7080

- SD7080-PT (Fig. 12.144)

The SD7080 has a lift range much like the S3021 but with slightly lower maximum lift. At low lift coefficients and high Rn's, the drag is quite low, which will lead to excellent wind penetration. A flap, although not necessary, is recommended to improve thermalling performance.

There are some significant differences between the actual and nominal airfoils. In particular, the model was too thick (except at the leading edge) and had a turned-up trailing edge. If the usual trends apply, the model would have a little wider lift range and slightly higher drag than the nominal. This should be considered when building.

Also see: SD7084, S3021, E205, S3014, SD5060, DF101
Digitizer plot: Figs. 10.55, 10.56
Polar plot: Fig. 12.144
Lift plot: Fig. 12.145
Aircraft polar: Fig. 5.11
Thickness: 9.15% Camber: 2.48%

SD7084

- SD7084-PT (Fig. 12.146)

The SD7084 is a slightly modified SD7080. The primary differences are that the SD7084 is about 10% thicker, its lift range is greater, and the minimum drag is higher than the SD7080. The interesting result is that the two airfoils perform almost identically provided the SD7084 wing loading is about 10% greater. See Fig. 5.11.

Also see: SD7080, S3021, E205
Digitizer plot: Fig. 10.57
Polar plot: Fig. 12.146
Lift plot: Fig. 12.147
Aircraft polar: Fig. 5.11
Thickness: 9.63% Camber: 2.31%

SD7090

- SD7090-PT (Fig. 12.148)

At first glance the SD7090 appears to be a lower lift version of the S3021. A comparison plot of the profiles (see Fig. 11.9) shows that the SD7090 has less camber than the S3021, is somewhat thicker, and the thickness distribution is significantly different along the forward, upper surface. For the SD7090 this part of the airfoil plays an important role in the stall characteristics.

As Fig. 12.151 shows, the SD7090 has a fairly sharp stall, unlike the S3021. This is caused by a sudden "bursting" of the leading edge separation bubble at high angle of attack.

- SD7090-PT loose/tight covering, $Rn = 300,000$ (Fig. 12.149)

As received, the covering on the surface was typical of plastic film over balsa—somewhat wavy, with a wavelength longer than that of the raw balsa grain. After the model was tested in this condition the Monokote was shrunk tightly over the surface sheeting and made to follow the balsa grain by firmly pressing a cloth over the hot Monokote as it cooled. The resulting surface showed a marbled appearance.

As Fig. 12.149 shows for a Rn of 300k, this difference between the surface finishes did not affect the performance. (The shift in the angle of attack was caused by an inadvertent sharp jolt to the angle of attack sensor prior to the start of the run.)

- SD7090-PT trips, $Rn = 300{,}000$ (Fig. 12.150)

At 300k various size trips were tested at 30% chord. The lowest trip was 0.04% (0.005 in) and had only a small effect. But as the trip height increased so did the drag, especially at low angles of attack where the flow would otherwise have been laminar to almost 60% chord. These tests illustrate how even small roughness elements effect performance. This should mainly be considered for F3B and cross-country flying where Rn's of 300k and higher are common.

Also see: E374, SD6060, NACA 2.5411, CLARK-Y
Digitizer plot: Fig. 10.58
Airfoil comparision plot: Fig. 11.9

Polar plot: Figs. 12.148–12.150
Lift plot: Fig. 12.151
Thickness: 9.99% Camber: 1.87%

SD8000

- SD8000-PT (Fig. 12.152)
- SD8000-PT u.s.t. $x/c = 20\%, h/c = .17\%, w/c = 1.0\%$ (Fig. 12.153)
- SD8000-PT u.s.t. $x/c = 40\%, h/c = .17\%, w/c = 1.0\%$ (Fig. 12.154)
- SD8000-PT u.s.t. $x/c = 70\%, h/c = .17\%, w/c = 1.0\%$ (Fig. 12.155)

Although the shape of the SD8000 is quite different from the HQ2/9–RG15–S2048 group of airfoils (see Fig. 11.10), the performance is strikingly similar. As with the RG15 and HQ2/9, trips do not produce dramatic improvements at the higher *Rn's*. At and below 150k, there is some advantage to using a trip.

Also see: HQ2/9, RG15, S2048, S2055, SD2030
Digitizer plot: Fig. 10.59
Airfoil comparision plot: Fig. 11.10
Polar plot: Figs. 12.152–12.155
Lift plot: Fig. 12.156
Thickness: 8.86% Camber: 1.71%

SD8020

- SD8020-PT (Fig. 12.157)

The 10% thick SD8020 is a symmetric airfoil specifically designed for use on tail surfaces at low *Rn's*. As shown in Fig. 12.157, the lift and drag characteristics compare favorably with the other symmetric sections tested, i.e. the J5012, NACA 0009 and NACA 64A010. The lift range between *Rn's* of 100k and 300k is comparable to the J5012. At 60k, however, separation at the higher angles of attack limits $C_{l_{max}}$, making it more like the NACA 64A010. But it is the lift characteristics shown in Fig. 12.158 that are most interesting.

There is no significant deadband, even at a *Rn* of 40k. (The offset in lift for *Rn* of 40k was probably caused by operator error when the tare-weight entry was made.) The nearly linear C_l vs α characteristics and acceptably low drag should lead to smooth handling qualities.

Also see: J5012, NACA 0009, NACA 64A010
Digitizer plot: Fig. 10.60
Polar plot: Fig. 12.157
Lift plot: Fig. 12.158
Thickness: 10.10% Camber: 0.00%

SD8040

• SD8040-PT (Fig. 12.159)

The SD8040 was an attempt at an F3B type airfoil, but the SD8000 along with the HQ2/9, RG15, and S2048 show better performance. Unfortunately, low Reynolds number airfoil design is still far from a precise science.

Also see: HQ2/9, RG15, S2048
Digitizer plot: Fig. 10.61
Polar plot: Fig. 12.159
Thickness: 9.99% Camber: 2.65%

SPICA

• SPICA-PT (Fig. 12.160)

The SPICA airfoil was designed by Chuck Anderson in 1978 as a flat-bottom, trainer airfoil. He reports that his SPICA sailplane which uses this airfoil has consistently placed high in the standings at thermal-duration contests. This is probably a result of the high lift coefficients produced and the airfoil's gentle stall characteristics. These two qualities combine to improve the chance of successfully completing tight, low-level turns in small, turbulent thermals. As for wind-penetration, however, the SPICA airfoil has high drag at low lift coefficients, which would make cross-country flying at high speed difficult.

Also see: SD7043, E214, SD7032
Digitizer plot: Fig. 10.62
Polar plot: Fig. 12.160
Lift plot: Fig. 12.161
Thickness: 11.72% Camber: 4.74%

WB135/35 *and* WB140/35/FB

• WB135/35-PT (Fig. 12.162)
• WB140/35/FB-PT (Fig. 12.164)

These two airfoils were designed by "Woody" Blanchard Jr. The first is the original and the second is a modified, flat-bottom version with the same camber line as the original. Consequently the second has more aft thickness which leads to substantially different performance.

It is interesting to note that although the WB135/35 and MB253515 have similar upper-surface contours, the behavior of the airfoils is quite different (see Fig. 11.11). The MB253515 shows the strong effects of a laminar separation bubble at *Rn* of 100k, whereas the WB135/35 shows just the opposite trend—relatively low drag at 100k. The modified version, however, does have a drag-producing laminar separation bubble at 100k. Other than for ease of building, the flat bottom does not appear to be advantageous.

Also see: MB253515, S4233, E193MOD, SD7062, FX63-137
Digitizer plot: Figs. 10.63, 10.64
Airfoil comparision plot: Fig. 11.11
Polar plot: Figs. 12.162, 12.164
Lift plot: Fig. 12.163
WB135/35 Thickness: 13.53% Camber: 3.75%
WB140/35/FB Thickness: 13.92% Camber: 3.70%

5.2 Stall Behavior

In the quest for lower drag it is easy to forget the importance of the stall. An airfoil may have a very low drag coefficient, but if the airplane abruptly tip stalls while thermalling, far more altitude will be lost trying to recover than might have been gained by the marginally lower drag.

There are two phases to most stalls. The first occurs when the lift developed by the wing no longer increases with angle of attack—the lift curve rounds over. The second phase occurs when the lift suddenly falls back to a lower level as the angle of attack increases—the true stall.

What are the desirable stall characteristics that one should look for in the shape of the lift curve near stall? First of all, for a typical tapered wing (which closely approximates the "ideal" elliptic planform), the three-dimensional stall will be quite similar to the two-dimensional one. Thus the two-dimensional lift data shown in Chapter 12 provides a good indication of what will be experienced in flight. To illustrate both good and bad stall characteristics, the MB253515 and NACA 2.5411 respectively, serve as examples. The S2091 is an example of the intermediate case.

The stall characteristics of the MB253515 at Rn of 100k are excellent (see Fig. 12.55). "Phase 1"—the rounding of the lift curve—occurs at approximately 10°, but the actual stall which marks "phase 2" does not occur until at least 18° (the limit of the measurement). The 8° difference provides a broad, easily flown plateau with only a slight loss of lift from the maximum, even though flight in this region is inefficient because the drag is very high. For the MB253515 this angle of attack margin is quite large in comparison to most other airfoils.

On the other hand, the angle of attack margin of the NACA 2.5411 shown in Fig. 12.63 exemplifies the opposite end of the spectrum. This airfoil loses lift with no warning whatever (essentially zero angle of attack margin). Many airfoils show intermediate behavior, and some exhibit hysteresis as well at the stall. A typical example is the S2091B-PT at Rn = 100k, Fig. 12.84. While this airfoil exhibits a reasonable rounding of the lift curve, the sudden drop in C_l is over 0.3. What is more, there is hysteresis of almost 4°.

Left uncorrected, poor stall characteristics seriously compromise the controllability at low speed. Of course these problems are not unique to low-Rn airfoils; many "full-size" airfoils have similar problems. Over the years several remedies

have been developed to improve poor stall characteristics. Progressive spanwise twist, change of section (e.g. drooped leading edges) and stall strips are common, and two of these methods are often used together. For model sailplanes the most common approach is to use spanwise twist; however, it is not always effective. Flight tests on a model sailplane using a NACA 2512 (which is very similar to the NACA 2.5411) showed almost no improvement with changes in spanwise twist. Stall strips, on the other hand, were quite effective in alleviating the adverse stall characteristics.

In summary, many low-drag airfoils that might otherwise be reluctantly discarded because a deficient stall can be made usable, given the ability to improve the stall with these techniques.

5.3 Trips and Surface Roughness

As amply demonstrated in the airfoil polars, turbulators placed upstream of the laminar separation bubble may improve performance. While it is known that some airfoils benefit from trips at and above a *Rn* of 300k, for the airfoils tested in this study, trips were generally effective only below 300k. It is possible that different heights and chordwise locations might further improve the airfoils tested, but this was not systematically studied in this project.

For *Rn* below 300k performance gains were achieved, but these gains were highly dependent on the trip height and position. In addition, no "miracle" trip shape was found. Rather, it appears that if the boundary layer was sufficiently tripped, regardless of how, the performance gain was independent of the particular method. The conclusion is that elaborate turbulator devices are not warranted; the simple two-dimensional trip strip is satisfactory. We should point out that other investigators[31] have found differences in performance and recommend specific types of trips.

The MILEY airfoil and the SD7003 are two extreme examples of the effectiveness of trips. The MILEY airfoil, as may be deduced from the upper-surface shape, has a steep pressure recovery region. Consequently the laminar flow separates to form a large bubble. The polars show that trips, when placed upstream of this point, dramatically improve the performance.

The SD7003 represents the other extreme. On this airfoil the pressure recovery region is so gradual that most of the upper surface may be considered a bubble ramp. As a result, the bubble is so shallow and reattaches so quickly that the drag of a trip is about the same as the drag of the bubble it might prevent. At a *Rn* of 60k, where one would normally expect bubble drag to be high, the SD7003 had the lowest drag of any airfoil tested, and over the entire *Rn* range the presence of a bubble cannot be deduced from the polars alone (which is in sharp contrast to the MILEY airfoil).

Finally, the usefulness of a trip (on either surface) depends on the severity of the pressure recovery. Since the newer, low-drag airfoils presented here generally have a gradual recovery, one would expect trips to be of marginal value. Nonetheless trips are useful to "repair" an otherwise poor performer, typically an airfoil designed for a higher Rn. When they are properly used in this context they can produce substantial improvements. Furthermore some low-Rn airfoils are designed expressly for use with trips[31]. In these cases trips are, of course, essential.

The effects of a discrete trip can also be produced by distributed roughness. Much like single roughness elements—trips strips, bumps, blowing through holes—distributed roughness acts to promote transition. In these experiments "sheet balsa roughness" (no plastic film covering) was tested and, as expected, produced results qualitatively like that found for the trip strips. However, distributed roughness apparently does not provide any advantage over discrete roughness elements.

5.4 Trailing Edge Thickness

Test on three airfoils (DAE51, E374, and SD6080) showed that thick trailing edges produce measurable drag penalties. In order to achieve maximum performance, at least at the higher Rn's, it is necessary to have the thinnest possible trailing edges.

5.5 Surface Waviness and Contour Accuracy

So long as an airfoil surface is smooth, that is, free of sharp edges protruding into the boundary layer, surface waviness of the type produced by Monokote over balsa appears to have no measurable impact on performance. For a 12 in chord, the Monokote/balsa waviness has a peak-to-peak amplitude on the order of 0.02% chord. On the other hand, the warping of the covering in open-bay construction as it stretches over the cells alters the airfoil contour beyond what is normally considered waviness. In such cases, the airfoil really has no single shape and one can expect its performance to be significantly different from the nominal.

Based on our measurements, the best modern-day construction techniques used by modelers are capable of yielding contours accurate to ± 0.004 in. For a 12 in chord an error of ± 0.004 in is only 0.033% chord. Although at present there is no criterion on the accuracy necessary to meet the nominal performance, all indications are that errors of this order have only a small affect. On the other hand, errors two to four times this amount (which are more common) do begin to effect performance. Error in contour is undoubtedly one of the factors that explains differences in performance between two different models of the same RC sailplane.

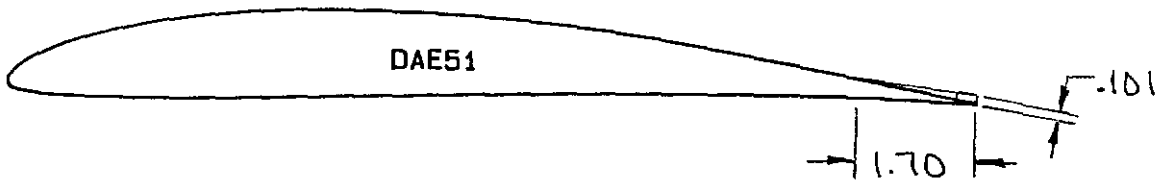

Fig. 5.1 DAE51-PT with thickened trailing edge.

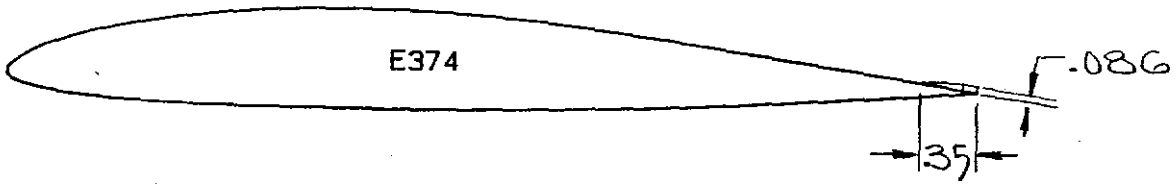

Fig. 5.2 E374B-PT with thickened trailing edge.

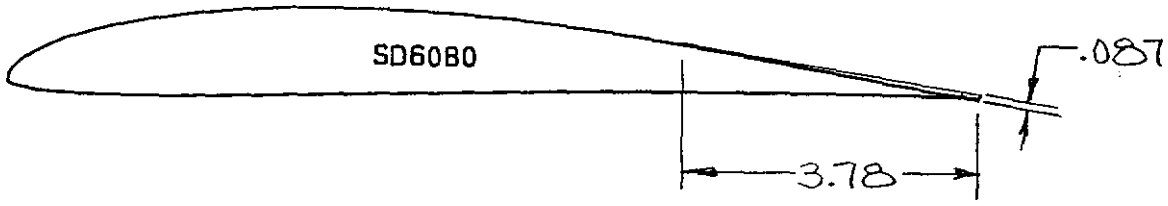

Fig. 5.3 SD6080-PT with thickened trailing edge.

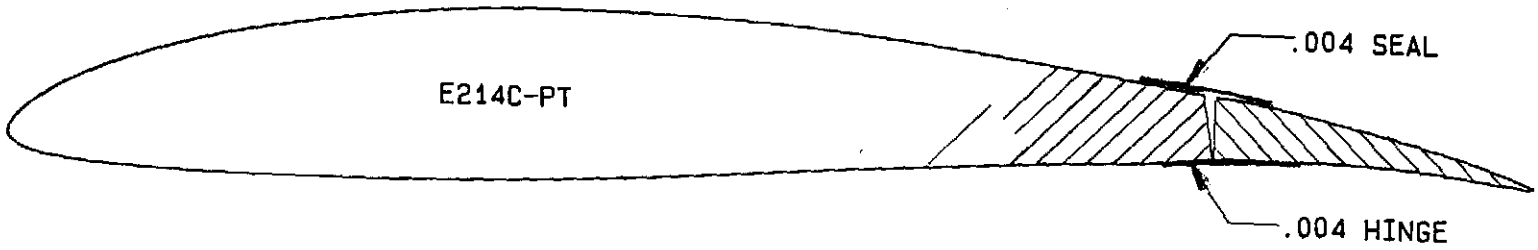

Fig. 5.4 Flap configuration: E214C-PT.

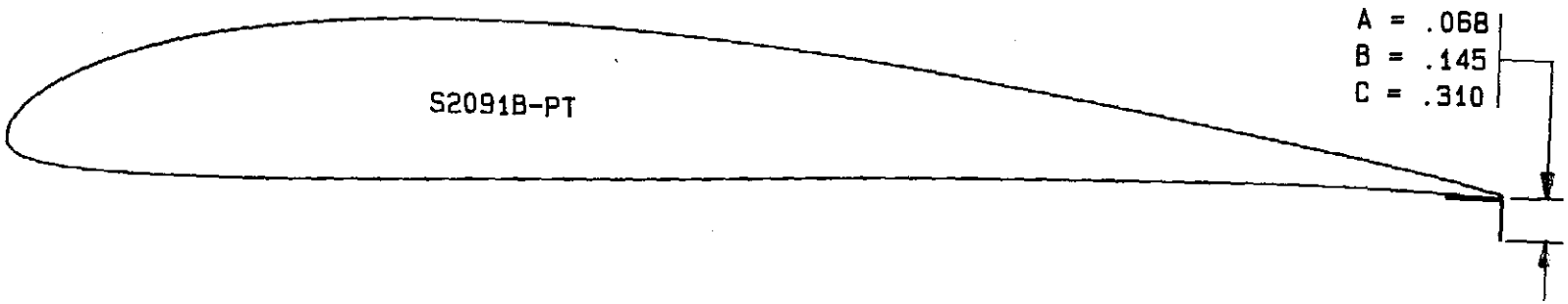

Fig. 5.5 Flap configurations: S2091B-PT.

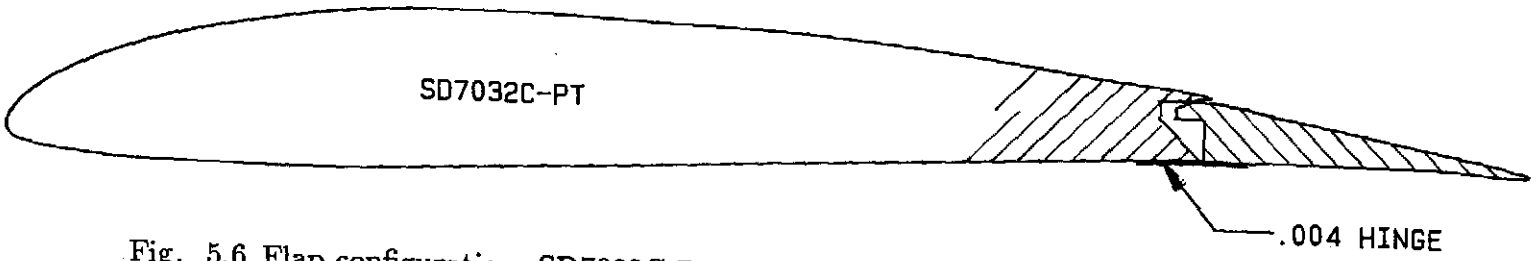

Fig. 5.6 Flap configuration: SD7032C-PT.

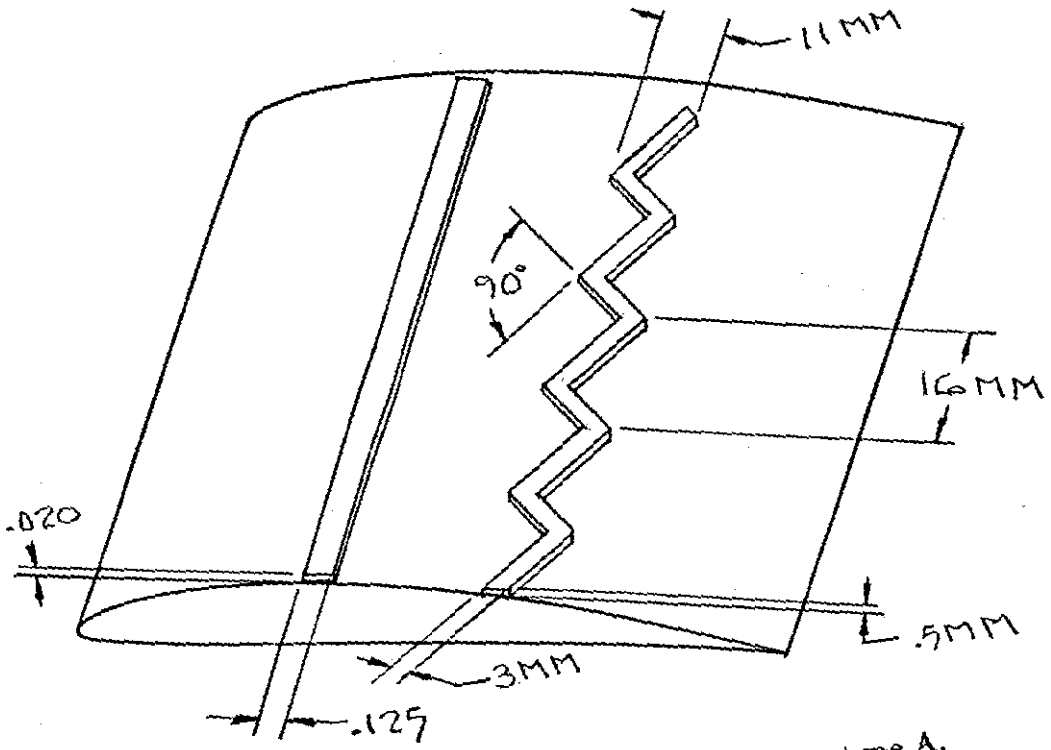

Fig. 5.7 (a) Trip configuration: Plain and zig-zag type A.

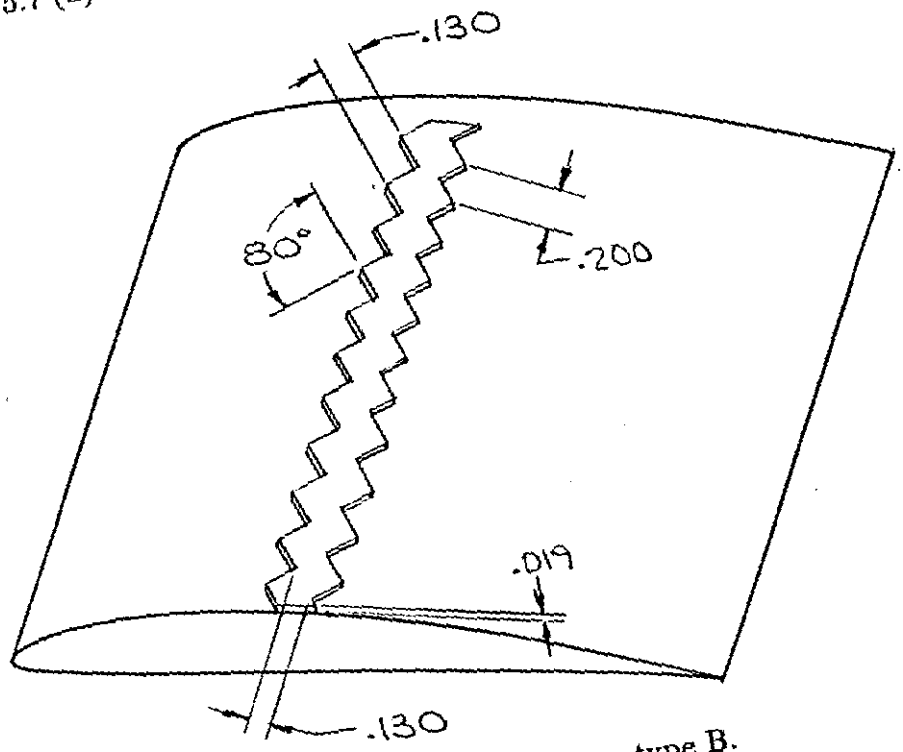

Fig. 5.7 (b) Trip configuration: zig-zag type B.

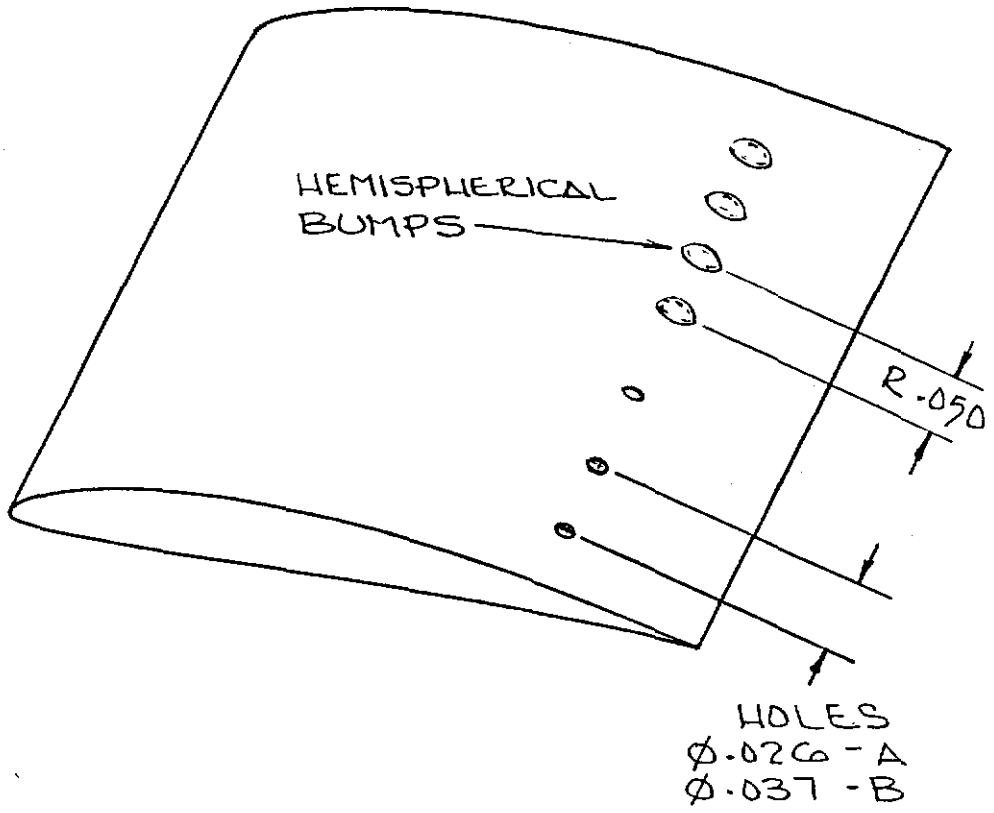

Fig. 5.7 (c) Trip configuration: Bumps and holes (blowing).

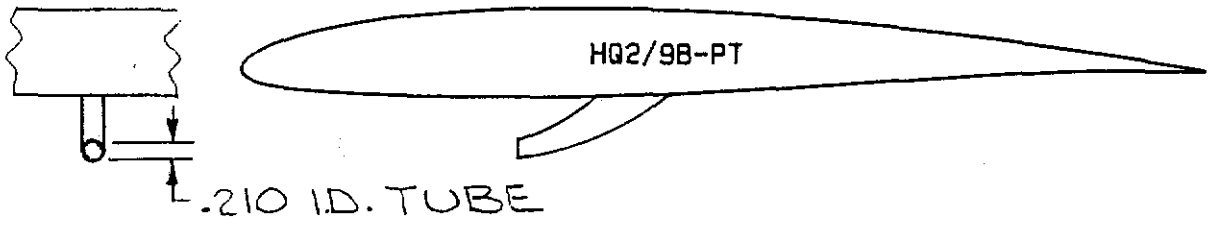

Fig. 5.8 Ram configuration.

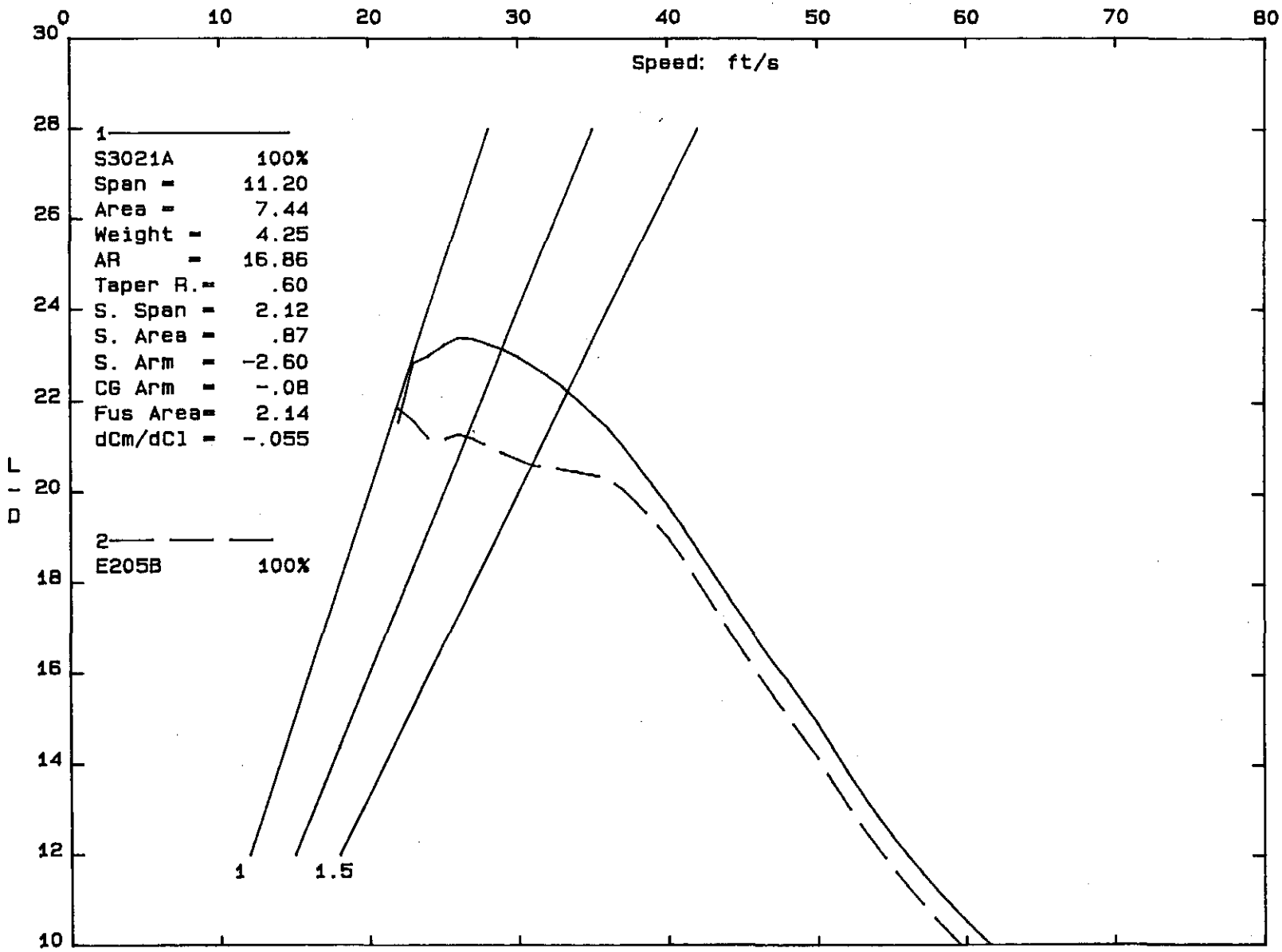

Fig. 5.9 (a) Aircraft Polar: S3021A-PT vs E205B-PT

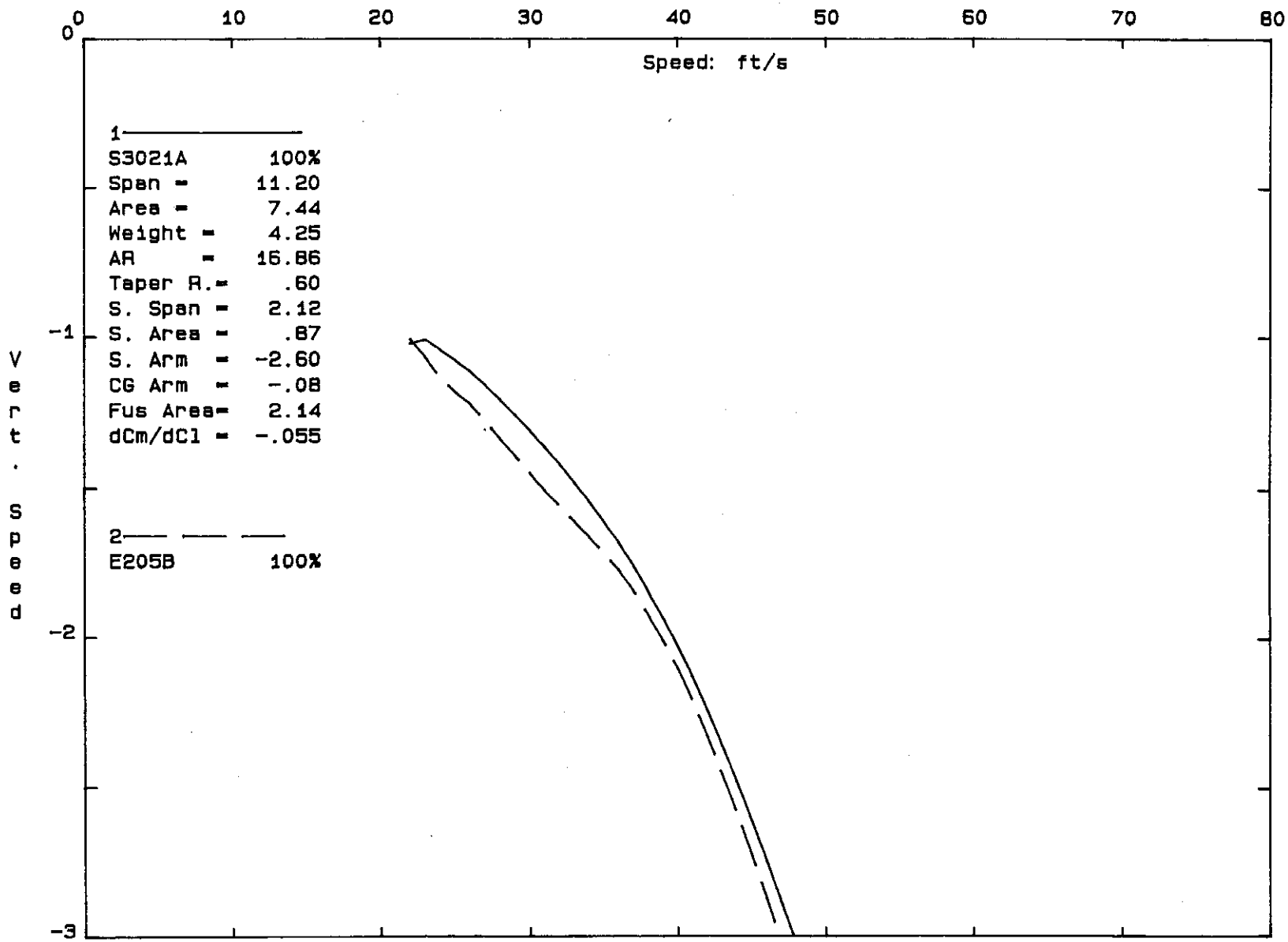

Fig. 5.9 (b) Aircraft Polar: S3021A-PT vs E205B-PT

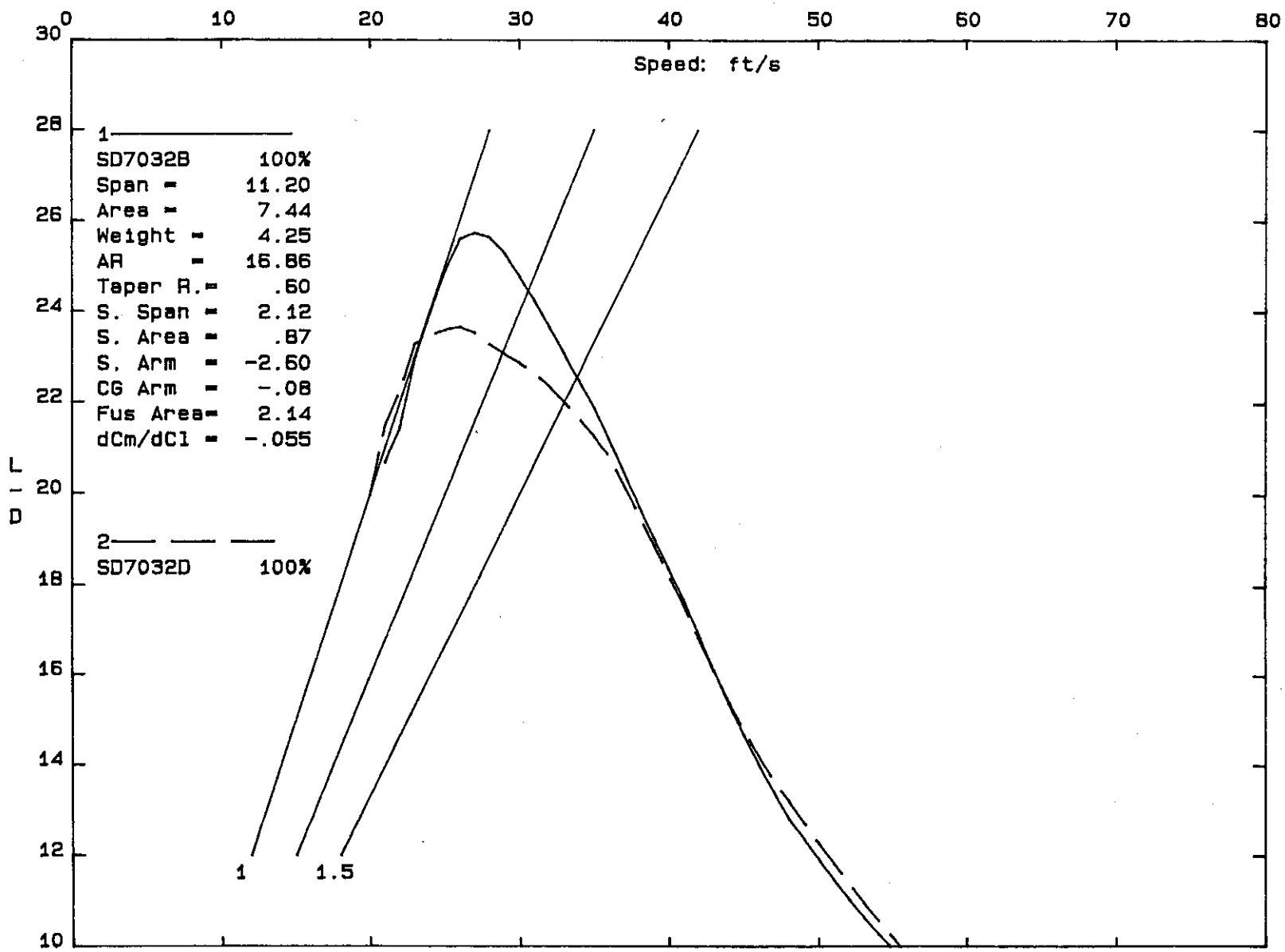

Fig. 5.10 (a) Aircraft Polar: SD7032B-PT vs SD7032D-PT

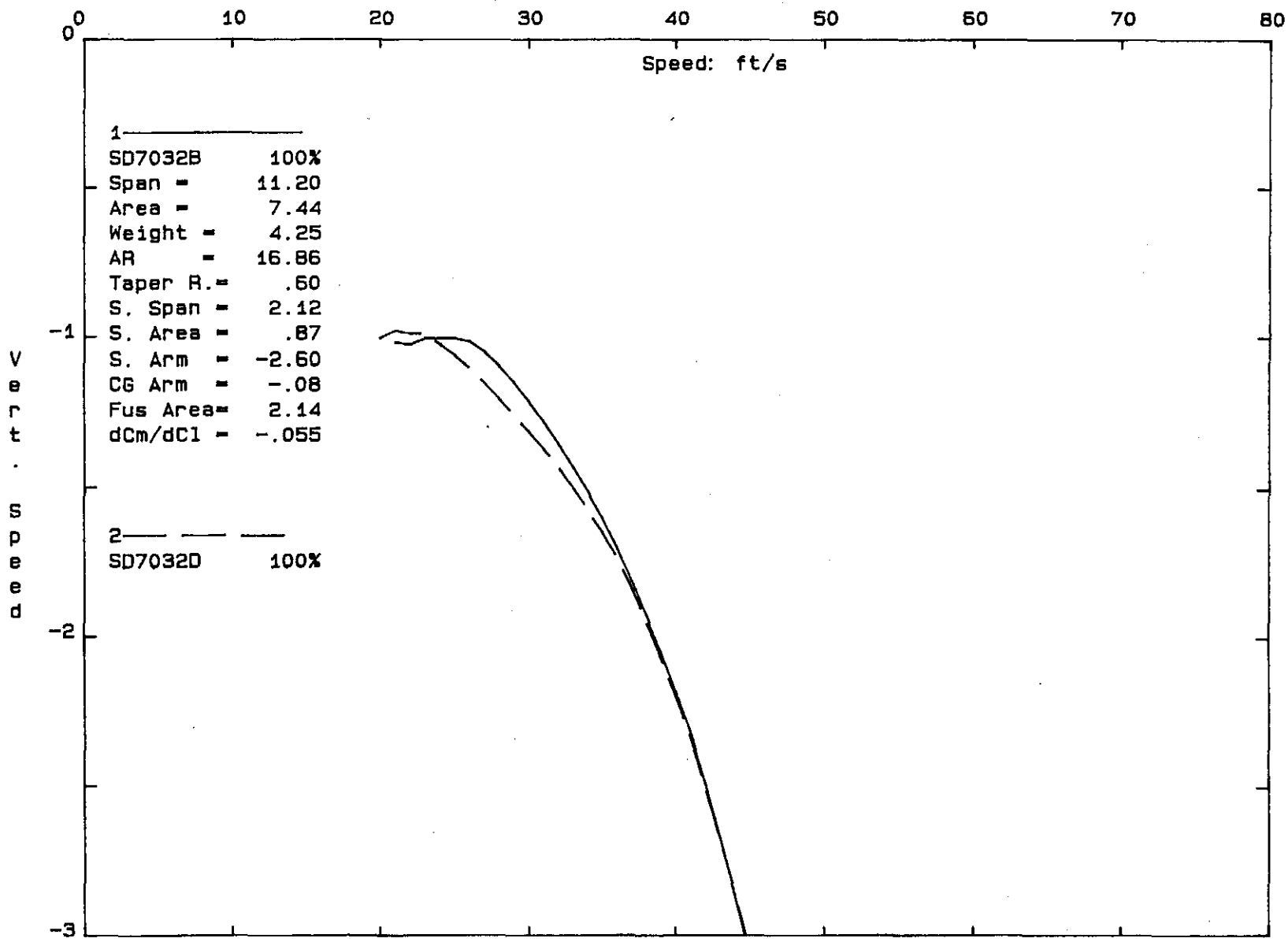

Fig. 5.10 (b) Aircraft Polar: SD7032B-PT vs SD7032D-PT

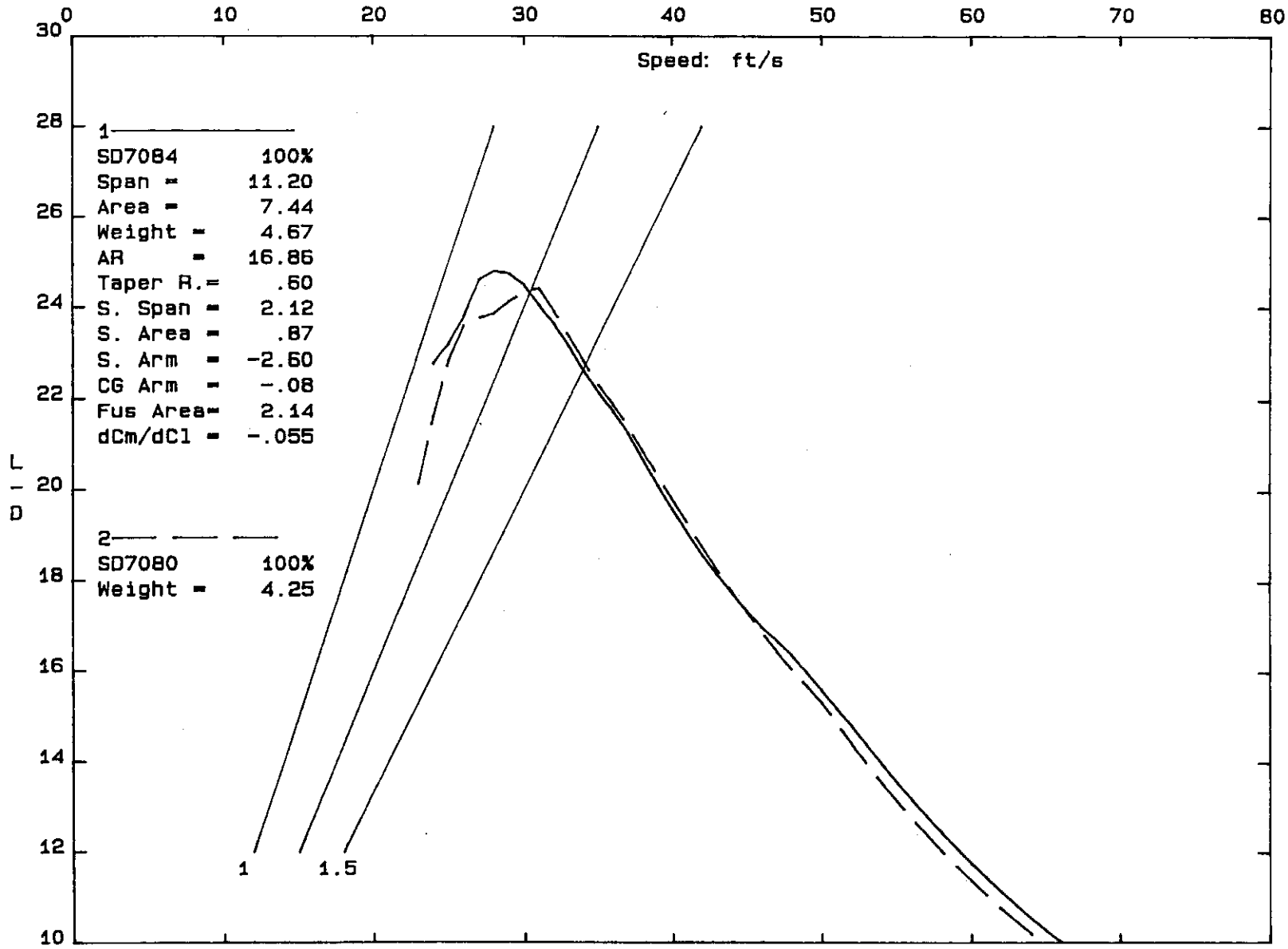

Fig. 5.11 (a) Aircraft Polar: SD7084-PT vs SD7080-PT

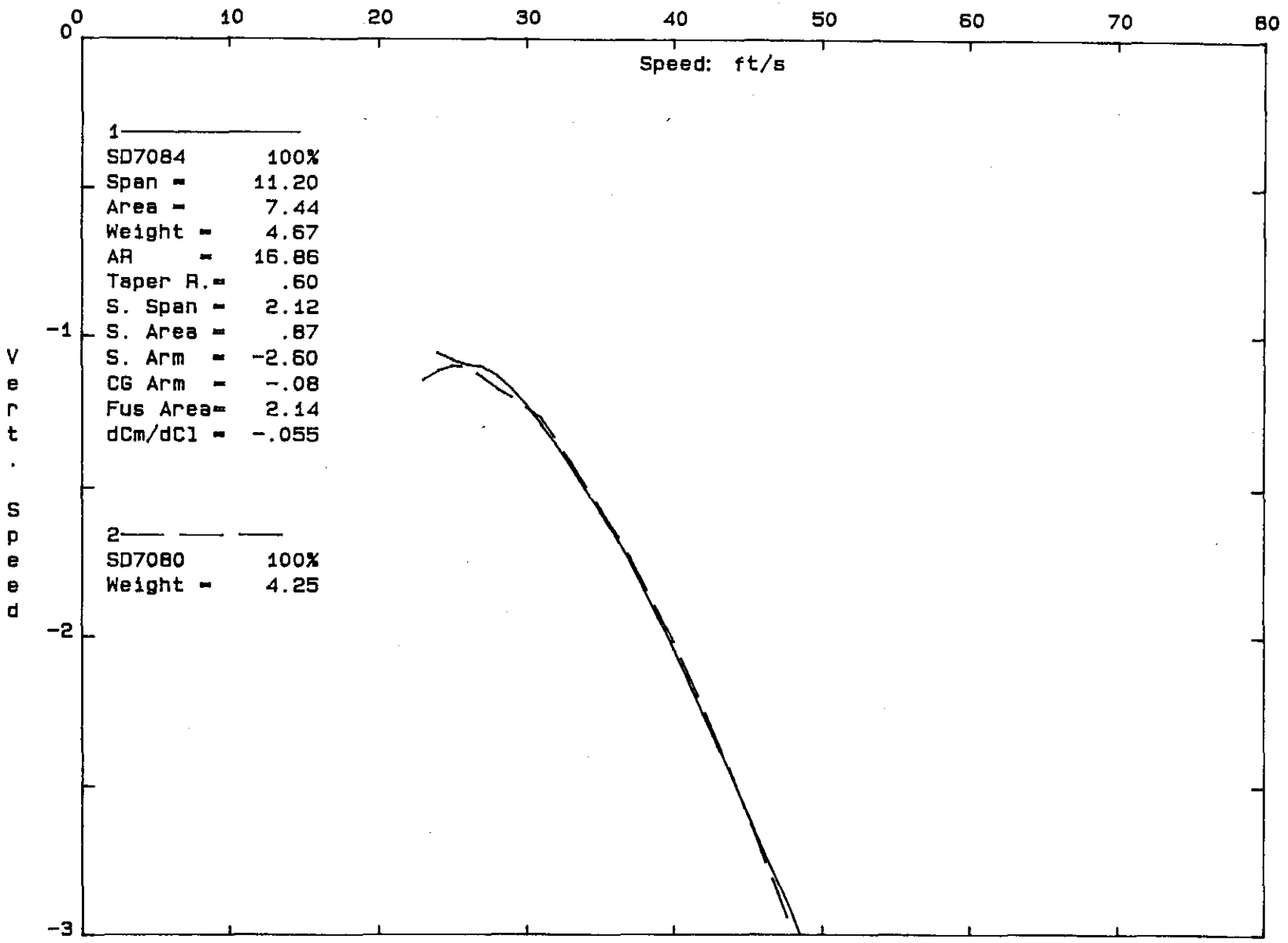

Fig. 5.11 (b) Aircraft Polar: SD7084-PT vs SD7080-PT

Chapter 6

References

[1] *Proceedings of the Conference on Low Reynolds Number Airfoil Aerodynamics*, UNDAS-CP-77B123, Notre Dame, Indiana, June 1985.

[2] *Proceedings of the Aerodynamics at Low Reynolds Numbers* $10^4 < Re < 10^6$ *International Conference*, London, October 1986.

[3] *Proceedings of the Conference on Low Reynolds Number Aerodynamics*, The University of Notre Dame, Notre Dame, Indiana, June 1989.

[4] Mueller, T.J., *Low Reynolds Number Vehicles*, AGARDograph No. 288, Feb. 1985.

[5] Perry, A. E., *Hot-Wire Anemometry*, Oxford University Press, 1982.

[6] Rae, H. and Pope, A., *Low-Speed Wind Tunnel Testing*, John Wiley & Sons, second ed., 1984.

[7] Althaus, D., "Recent Wind Tunnel Experiments at Low Reynolds Numbers," *Proceedings of the Aerodynamics at Low Reynolds Numbers* $10^4 < Re < 10^6$ *International Conference*, London, October 1986.

[8] van Ingen, J. L. and Boermans, L. M. M., "Aerodynamics at Low Reynolds Numbers: A Review of Theoretical and Experimental Research at Delft University of Technology," *Proceedings of the Aerodynamics at Low Reynolds Numbers* $10^4 < Re < 10^6$ *International Conference*, London, October 1986.

[9] Althaus, D., *Profilpolaren fur den Modellflug*, Necker-Verlag, Villingen-Schwenningen, FRG, 1980.

[10] Althaus, D., *Profilpolaren fur den Modellflug*, Vol. 2, Necker-Verlag, Villingen-Schwenningen, FRG, 1985.

[11] McGhee, R.J., Jones, G.S., and Jouty, R., "Performance Characteristics from Wind-Tunnel Tests of a Low-Reynolds-Number Airfoil," AIAA Paper 88-0607, January 1988.

[12] Volkers, D. F., "Preliminary Results of Wind Tunnel Measurements on Some Airfoil Sections at Reynolds Numbers between 0.6×10^5 and 5.0×10^5," Memo M-276, Delft University of Technology, The Netherlands, 1977.

[13] Pohlen, L.J., and Mueller, T.J., "Boundary Layer Characteristics of the Miley Airfoil at Low Reynolds Numbers," AIAA paper 83-1795.

[14] Bastedo, W.G., and Mueller, T.J., "Performance of Finite Wings at Low Reynolds Numbers," *Proceedings of the Conference on Low Reynolds Number Airfoil Aerodynamics*, UNDAS-CP-77B123, Notre Dame, Indiana, June 1985.

[15] Abbott, I.H. and von Doenhoff, A.E., *Theory of Wing Sections*, Dover Publications, Inc. New York, 1959.

[16] McCormick, B.W., *Aerodynamics, Aeronautics, and Flight Mechanics*, John Wiley & Sons, 1979.

[17] Althaus, D. and Wortmann F.X., *Stuttgarter Profilkatalog I*, Friedr. Vieweg & Sohn Verlagsgesellschaft mbH, Braunschweig, 1981.

[18] Eppler, R. and Somers, D. M., "Airfoil Design for Reynolds Numbers Between 50,000 and 500,000," *Proceedings of the Conference on Low Reynolds Number Airfoil Aerodynamics*, UNDAS-CP-77B123, Notre Dame, Indiana, June 1985.

[19] Eppler, R., "Recent Developments in Boundary Layer Computation," *Proceedings of the Aerodynamics at Low Reynolds Numbers* $10^4 < Re < 10^6$ *International Conference*, London, October 1986.

[20] Eppler, R. and Somers, D. M., "A Computer Program for the Design and Analysis of Low-Speed Airfoils, Including Transition," NASA TM 80210, August 1980.

[21] Drela, M. and Giles, M. B., "Two-Dimensional Transonic Aerodynamic Design Method," *AIAA Journal*, Vol. 25, No. 9, September 1987.

[22] Drela, M. and Giles, M. B., "ISES: A Two-Dimensional Viscous Aerodynamic Design and Analysis Code," AIAA Paper 87-0424, January 1987.

[23] Selig, M. S., "The Design of Airfoils at Low Reynolds Numbers," *Soartech 3*, published by H. A. Stokely, 1504 North Horseshoe Circle, Virginia Beach, VA 23451, U.S.A., July 1984. Also AIAA-85-0074.

[24] Maughmer, M.D. and Somers, D.M., "Figures of Merit for Airfoil/Aircraft Design Integration," AIAA paper 88-4416.

[25] Drela, M., "Low-Reynolds-Number Airfoil Design for the M.I.T. Daedalus Prototype: A Case Study," *AIAA Journal*, Vol. 25, No. 8, August 1988.

[26] Drela, M., private communications, 1989.

[27] Althaus, D., "Effects on the Polar Due To Changes or Disturbances To The Contour of the Wing Profile," *Technical Soaring*, Vol. 10, No. 1, January 1986.

[28] Hama, F. R. "An Efficient Tripping Device," *Journal of the Aeronautical Sciences (Readers' Forum)*, Vol. 24, No. 3, pp 236-237.

[29] *Modell-Technik-Berater 7: HQ Profile*, Verlag für Technik und Handwerk GmbH, 1983.

[30] Miley, S. J., "On the Design of Airfoils for Low Reynolds Numbers," AIAA Paper 74-1017, September 1974.

[31] Boermans, L.M.M., Donker Duyvis, F.J., van Ingen, J.L., and Timmer, W.A., "Experimental Aerodynamic Characteristics of the Airfoils LA 5055 and DU 86-084/18 at Low Reynolds Numbers," *Proceedings of the Conference on Low Reynolds Number Aerodynamics*, The University of Notre Dame, Notre Dame, Indiana, June 1989.

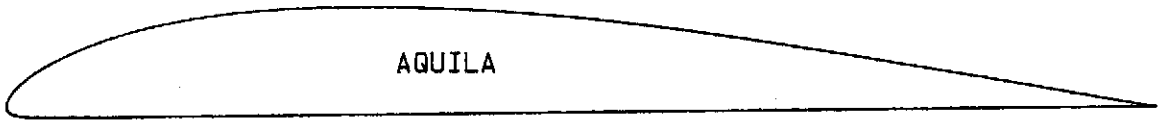

AQUILA

1	1.00000	0.00000	19	0.31333	0.08735	37	0.00667	-.00725	55	0.49333	-.00480
2	0.99667	0.00057	20	0.27333	0.08655	38	0.01000	-.00810	56	0.54667	-.00430
3	0.99333	0.00114	21	0.23333	0.08438	39	0.01333	-.00862	57	0.60000	-.00380
4	0.99000	0.00171	22	0.19333	0.08055	40	0.02000	-.00917	58	0.65333	-.00330
5	0.98667	0.00228	23	0.16000	0.07577	41	0.02667	-.00940	59	0.70667	-.00279
6	0.98000	0.00340	24	0.12667	0.06914	42	0.03333	-.00947	60	0.76000	-.00229
7	0.92667	0.01240	25	0.09333	0.06012	43	0.04667	-.00939	61	0.82000	-.00173
8	0.87333	0.02150	26	0.06000	0.04786	44	0.06000	-.00920	62	0.87333	-.00122
9	0.82000	0.03065	27	0.04667	0.04171	45	0.09333	-.00866	63	0.92667	-.00070
10	0.76000	0.04077	28	0.03333	0.03454	46	0.12667	-.00821	64	0.98000	-.00019
11	0.70667	0.04945	29	0.02667	0.03045	47	0.16000	-.00787	65	0.98667	-.00013
12	0.65333	0.05768	30	0.02000	0.02587	48	0.19333	-.00758	66	0.99000	-.00009
13	0.60000	0.06530	31	0.01333	0.02052	49	0.23333	-.00724	67	0.99333	-.00006
14	0.54667	0.07214	32	0.01000	0.01739	50	0.27333	-.00688	68	0.99667	-.00003
15	0.49333	0.07799	33	0.00667	0.01377	51	0.31333	-.00650	69	1.00000	0.00000
16	0.44000	0.08263	34	0.00333	0.00929	52	0.34667	-.00618			
17	0.39333	0.08551	35	0.00000	0.00000	53	0.39333	-.00574			
18	0.34667	0.08710	36	0.00333	-.00572	54	0.44000	-.00530			

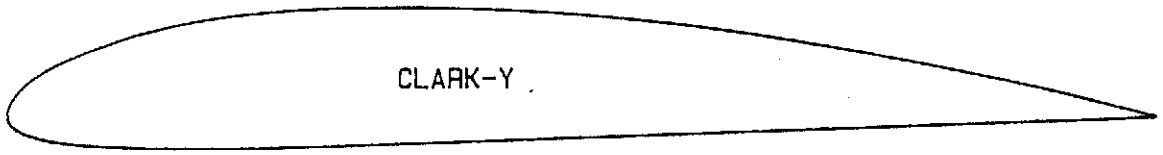

CLARK-Y

1	1.00000	0.00000	19	0.25000	0.08996	37	0.00428	-.00898	55	0.37059	-.02242
2	0.99572	0.00115	20	0.22221	0.08774	38	0.00961	-.01296	56	0.43474	-.02018
3	0.98296	0.00448	21	0.19562	0.08483	39	0.01704	-.01651	57	0.50000	-.01792
4	0.96194	0.00972	22	0.17033	0.08113	40	0.02653	-.01959	58	0.56526	-.01566
5	0.93301	0.01656	23	0.14645	0.07660	41	0.03806	-.02214	59	0.62941	-.01345
6	0.89668	0.02475	24	0.12408	0.07134	42	0.05156	-.02414	60	0.69134	-.01131
7	0.85355	0.03400	25	0.10332	0.06552	43	0.06699	-.02567	61	0.75000	-.00928
8	0.80438	0.04394	26	0.08427	0.05939	44	0.08427	-.02680	62	0.80438	-.00741
9	0.75000	0.05412	27	0.06699	0.05313	45	0.10332	-.02763	63	0.85355	-.00575
10	0.69134	0.06405	28	0.05156	0.04677	46	0.12408	-.02816	64	0.89668	-.00429
11	0.62941	0.07319	29	0.03806	0.04027	47	0.14645	-.02839	65	0.93301	-.00302
12	0.56526	0.08105	30	0.02653	0.03352	48	0.17033	-.02832	66	0.96194	-.00190
13	0.50000	0.08719	31	0.01704	0.02652	49	0.19562	-.02795	67	0.98296	-.00094
14	0.43474	0.09128	32	0.00961	0.01943	50	0.22221	-.02734	68	0.99572	-.00025
15	0.37059	0.09312	33	0.00428	0.01254	51	0.25000	-.02653	69	1.00000	0.00000
16	0.33928	0.09318	34	0.00107	0.00616	52	0.27886	-.02559			
17	0.30866	0.09266	35	0.00000	0.00047	53	0.30866	-.02458			
18	0.27886	0.09158	36	0.00107	-.00453	54	0.33928	-.02351			

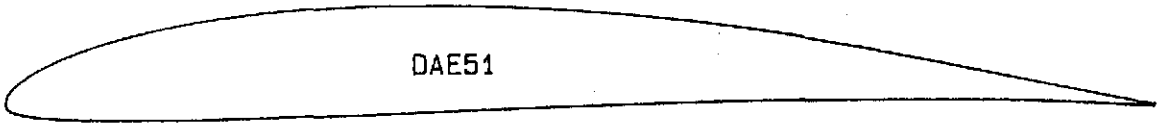

DAE51

1	1.00000	0.00000	31	0.46067	0.08312	61	0.00000	-.00009	91	0.47256	-.00300
3	0.98041	0.00369	33	0.42284	0.08460	63	0.00209	-.00569	93	0.51050	-.00155
5	0.94717	0.01002	35	0.38500	0.08527	65	0.00955	-.00991	95	0.54844	-.00021
7	0.91022	0.01729	37	0.34716	0.08505	67	0.02575	-.01314	97	0.58637	0.00102
9	0.87302	0.02477	39	0.30935	0.08389	69	0.05638	-.01544	99	0.62431	0.00210
11	0.83580	0.03224	41	0.27159	0.08172	71	0.09341	-.01617	101	0.66225	0.00300
13	0.79857	0.03957	43	0.23394	0.07845	73	0.13122	-.01593	103	0.70019	0.00369
15	0.76130	0.04663	45	0.19643	0.07396	75	0.16912	-.01514	105	0.73812	0.00414
17	0.72399	0.05331	47	0.15916	0.06807	77	0.20704	-.01400	107	0.77606	0.00431
19	0.68660	0.05948	49	0.12227	0.06051	79	0.24496	-.01261	109	0.81399	0.00418
21	0.64912	0.06508	51	0.08605	0.05086	81	0.28289	-.01107	111	0.85191	0.00372
23	0.61158	0.07004	53	0.05141	0.03860	83	0.32082	-.00943	113	0.88981	0.00286
25	0.57394	0.07431	55	0.02301	0.02458	85	0.35876	-.00777	115	0.92759	0.00155
27	0.53623	0.07793	57	0.00795	0.01353	87	0.39670	-.00613	117	0.96431	-.00012
29	0.49848	0.08088	59	0.00172	0.00596	89	0.43463	-.00453	119	0.99200	-.00158
30	0.47958	0.08209	60	0.00040	0.00281	90	0.45360	-.00376	120	1.00000	-.00200

Note: Several of the original 120 coordinates were removed due to space limitations.

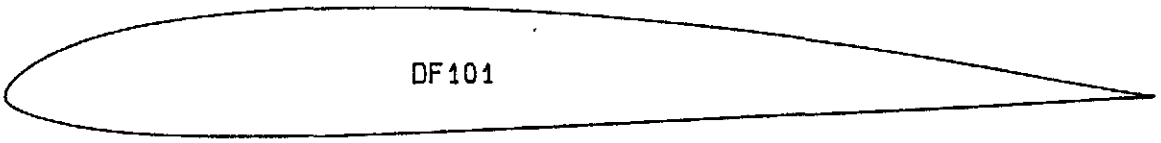

DF101

1	1.00000	0.00000	17	0.43513	0.07436	33	0.00478	-.00767	49	0.61295	-.01953
2	0.99680	0.00043	18	0.38578	0.07605	34	0.01512	-.01350	50	0.66543	-.01689
3	0.98727	0.00187	19	0.33765	0.07652	35	0.02987	-.01893	51	0.71618	-.01444
4	0.97163	0.00435	20	0.29125	0.07580	36	0.04877	-.02398	52	0.76453	-.01218
5	0.95030	0.00793	21	0.24708	0.07397	37	0.07192	-.02849	53	0.80990	-.01004
6	0.92375	0.01258	22	0.20557	0.07109	38	0.09940	-.03216	54	0.85165	-.00793
7	0.89245	0.01818	23	0.16715	0.06717	39	0.13128	-.03475	55	0.88918	-.00585
8	0.85697	0.02450	24	0.13208	0.06211	40	0.16755	-.03611	56	0.92195	-.00391
9	0.81783	0.03123	25	0.10063	0.05581	41	0.20782	-.03629	57	0.94943	-.00229
10	0.77558	0.03809	26	0.07308	0.04827	42	0.25158	-.03547	58	0.97128	-.00114
11	0.73072	0.04484	27	0.04975	0.03970	43	0.29833	-.03397	59	0.98715	-.00046
12	0.68375	0.05129	28	0.03082	0.03046	44	0.34758	-.03205	60	0.99677	-.00015
13	0.63525	0.05731	29	0.01637	0.02109	45	0.39883	-.02988	61	1.00002	-.00007
14	0.58567	0.06279	30	0.00647	0.01226	46	0.45162	-.02751			
15	0.53552	0.06757	31	0.00107	0.00454	47	0.50533	-.02496			
16	0.48520	0.07149	32	-.00010	-.00089	48	0.55933	-.02226			

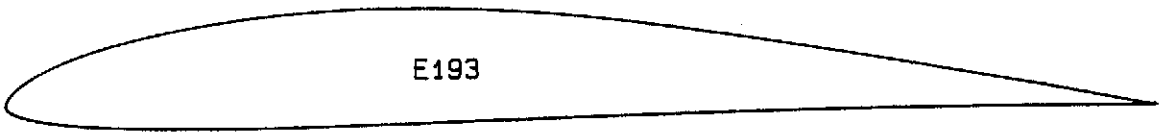

E193

1	1.00000	0.00000	17	0.44673	0.08332	33	0.00000	0.00000	49	0.55630	-.00824
2	0.99661	0.00051	18	0.39979	0.08551	34	0.00129	-.00375	50	0.61059	-.00645
3	0.98674	0.00220	19	0.35402	0.08603	35	0.00819	-.00838	51	0.66364	-.00486
4	0.97108	0.00522	20	0.30967	0.08487	36	0.02044	-.01252	52	0.71479	-.00350
5	0.95023	0.00932	21	0.26696	0.08213	37	0.03791	-.01588	53	0.76339	-.00239
6	0.92452	0.01415	22	0.22620	0.07805	38	0.06049	-.01841	54	0.80882	-.00153
7	0.89414	0.01957	23	0.18780	0.07284	39	0.08801	-.02010	55	0.85050	-.00091
8	0.85945	0.02558	24	0.15218	0.06663	40	0.12026	-.02098	56	0.88788	-.00048
9	0.82096	0.03214	25	0.11967	0.05957	41	0.15697	-.02112	57	0.92048	-.00018
10	0.77923	0.03914	26	0.09061	0.05181	42	0.19778	-.02061	58	0.94794	0.00010
11	0.73484	0.04642	27	0.06525	0.04352	43	0.24227	-.01955	59	0.97003	0.00032
12	0.68859	0.05381	28	0.04383	0.03487	44	0.28998	-.01807	60	0.98640	0.00034
13	0.64052	0.06112	29	0.02652	0.02608	45	0.34035	-.01628	61	0.99655	0.00014
14	0.59186	0.06808	30	0.01344	0.01740	46	0.39280	-.01430	62	1.00000	0.00000
15	0.54306	0.07436	31	0.00465	0.00915	47	0.44672	-.01224			
16	0.49458	0.07954	32	0.00026	0.00190	48	0.50145	-.01019			

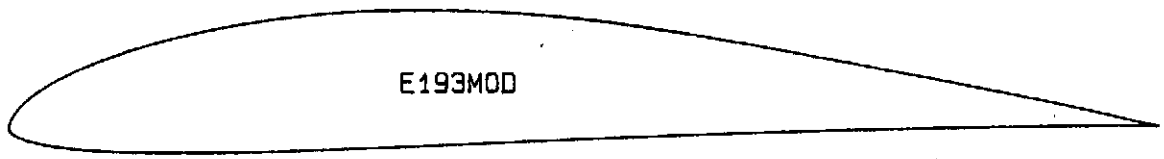

E193MOD

1	1.00000	0.00000	17	0.44673	0.09665	33	0.00000	0.00000	49	0.55630	-.00956
2	0.99661	0.00059	18	0.39979	0.09919	34	0.00129	-.00435	50	0.61059	-.00748
3	0.98674	0.00255	19	0.35402	0.09979	35	0.00819	-.00972	51	0.66364	-.00564
4	0.97108	0.00606	20	0.30967	0.09845	36	0.02044	-.01452	52	0.71479	-.00406
5	0.95023	0.01081	21	0.26696	0.09527	37	0.03791	-.01842	53	0.76339	-.00277
6	0.92452	0.01641	22	0.22620	0.09054	38	0.06049	-.02136	54	0.80882	-.00177
7	0.89414	0.02270	23	0.18780	0.08449	39	0.08801	-.02332	55	0.85050	-.00106
8	0.85945	0.02967	24	0.15218	0.07729	40	0.12026	-.02434	56	0.88788	-.00056
9	0.82096	0.03728	25	0.11967	0.06910	41	0.15697	-.02450	57	0.92048	-.00021
10	0.77923	0.04540	26	0.09061	0.06010	42	0.19778	-.02391	58	0.94794	0.00012
11	0.73484	0.05385	27	0.06525	0.05048	43	0.24227	-.02268	59	0.97003	0.00037
12	0.68859	0.06242	28	0.04383	0.04045	44	0.28998	-.02096	60	0.98640	0.00039
13	0.64052	0.07090	29	0.02652	0.03025	45	0.34035	-.01888	61	0.99655	0.00016
14	0.59186	0.07897	30	0.01344	0.02018	46	0.39280	-.01659	62	1.00000	0.00000
15	0.54306	0.08626	31	0.00465	0.01061	47	0.44672	-.01420			
16	0.49458	0.09227	32	0.00026	0.00220	48	0.50145	-.01182			

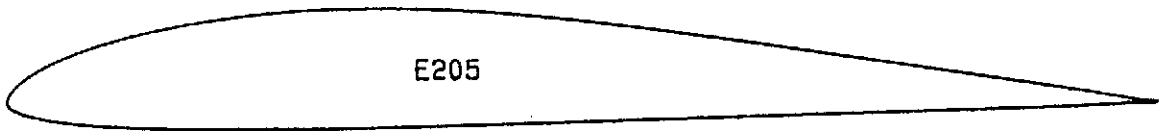

E205

1	1.00000	0.00000	17	0.43410	0.07785	33	0.00000	0.00000	49	0.56591	-.01516
2	0.99655	0.00039	18	0.38680	0.08081	34	0.00233	-.00506	50	0.61938	-.01345
3	0.98649	0.00174	19	0.34101	0.08214	35	0.01065	-.00988	51	0.67149	-.01180
4	0.97049	0.00427	20	0.29699	0.08177	36	0.02419	-.01420	52	0.72160	-.01023
5	0.94916	0.00778	21	0.25496	0.07970	37	0.04291	-.01776	53	0.76911	-.00876
6	0.92285	0.01196	22	0.21508	0.07606	38	0.06669	-.02053	54	0.81343	-.00740
7	0.89175	0.01668	23	0.17764	0.07111	39	0.09534	-.02252	55	0.85400	-.00614
8	0.85624	0.02199	24	0.14302	0.06507	40	0.12864	-.02378	56	0.89034	-.00497
9	0.81684	0.02786	25	0.11157	0.05811	41	0.16627	-.02436	57	0.92195	-.00380
10	0.77412	0.03419	26	0.08360	0.05040	42	0.20783	-.02435	58	0.94860	-.00252
11	0.72866	0.04088	27	0.05937	0.04211	43	0.25290	-.02384	59	0.97017	-.00125
12	0.68108	0.04777	28	0.03909	0.03344	44	0.30097	-.02292	60	0.98635	-.00036
13	0.63204	0.05470	29	0.02292	0.02461	45	0.35149	-.02168	61	0.99651	-.00003
14	0.58218	0.06147	30	0.01097	0.01589	46	0.40388	-.02021	62	1.00000	0.00000
15	0.53217	0.06782	31	0.00331	0.00766	47	0.45751	-.01859			
16	0.48265	0.07342	32	0.00002	0.00055	48	0.51174	-.01689			

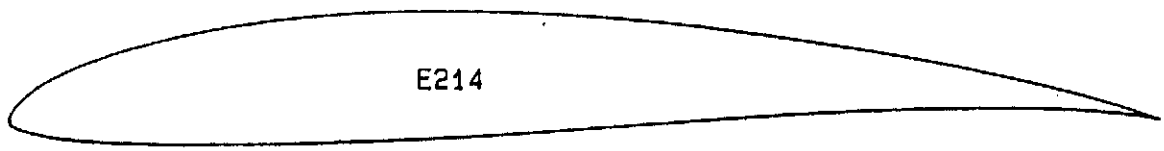

E214

1	1.00000	0.00000	17	0.47142	0.09093	33	0.00000	0.00000	49	0.52450	-.00678
2	0.99669	0.00104	18	0.42346	0.09281	34	0.00005	-.00086	50	0.57932	-.00245
3	0.98737	0.00422	19	0.37645	0.09332	35	0.00360	-.00632	51	0.63400	0.00155
4	0.97312	0.00916	20	0.33076	0.09241	36	0.01326	-.01087	52	0.68770	0.00495
5	0.95431	0.01501	21	0.28674	0.09008	37	0.02830	-.01475	53	0.73959	0.00756
6	0.93081	0.02139	22	0.24474	0.08639	38	0.04858	-.01784	54	0.78883	0.00923
7	0.90279	0.02833	23	0.20510	0.08142	39	0.07390	-.02011	55	0.83461	0.00994
8	0.87072	0.03576	24	0.16816	0.07532	40	0.10406	-.02161	56	0.87612	0.00970
9	0.83508	0.04344	25	0.13424	0.06822	41	0.13874	-.02236	57	0.91265	0.00862
10	0.79626	0.05102	26	0.10365	0.06028	42	0.17759	-.02245	58	0.94352	0.00684
11	0.75457	0.05841	27	0.07665	0.05168	43	0.22017	-.02193	59	0.96809	0.00461
12	0.71040	0.06544	28	0.05349	0.04258	44	0.26599	-.02086	60	0.98582	0.00235
13	0.66430	0.07207	29	0.03434	0.03321	45	0.31449	-.01928	61	0.99646	0.00065
14	0.61682	0.07813	30	0.01934	0.02379	46	0.36508	-.01721	62	1.00000	0.00000
15	0.56852	0.08344	31	0.00856	0.01465	47	0.41714	-.01453			
16	0.51991	0.08776	32	0.00210	0.00619	48	0.47030	-.01100			

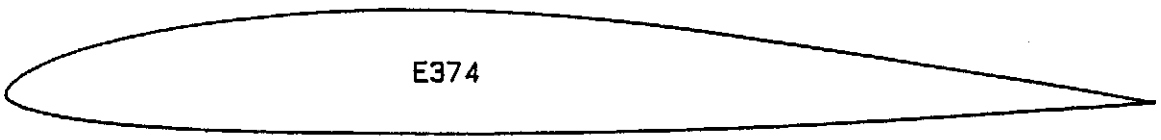

E374

1	1.00000	0.00000	17	0.43681	0.07543	33	0.00437	-.00624	49	0.62336	-.02570
2	0.99640	0.00045	18	0.38939	0.07684	34	0.01427	-.01133	50	0.67382	-.02334
3	0.98610	0.00204	19	0.34312	0.07669	35	0.02935	-.01602	51	0.72243	-.02060
4	0.97000	0.00485	20	0.29824	0.07506	36	0.04949	-.02017	52	0.76874	-.01760
5	0.94864	0.00846	21	0.25510	0.07215	37	0.07454	-.02371	53	0.81228	-.01451
6	0.92214	0.01264	22	0.21415	0.06815	38	0.10428	-.02662	54	0.85254	-.01153
7	0.89077	0.01747	23	0.17583	0.06317	39	0.13845	-.02892	55	0.88892	-.00882
8	0.85508	0.02297	24	0.14053	0.05732	40	0.17669	-.03062	56	0.92085	-.00643
9	0.81560	0.02905	25	0.10860	0.05071	41	0.21861	-.03177	57	0.94783	-.00432
10	0.77292	0.03559	26	0.08035	0.04349	42	0.26374	-.03240	58	0.96958	-.00241
11	0.72769	0.04245	27	0.05605	0.03578	43	0.31158	-.03256	59	0.98594	-.00091
12	0.68053	0.04943	28	0.03589	0.02778	44	0.36159	-.03230	60	0.99637	-.00016
13	0.63210	0.05628	29	0.02003	0.01970	45	0.41320	-.03165	61	1.00000	0.00000
14	0.58308	0.06268	30	0.00862	0.01183	46	0.46580	-.03065			
15	0.53397	0.06820	31	0.00178	0.00457	47	0.51877	-.02932			
16	0.48511	0.07251	32	0.00014	-.00124	48	0.57150	-.02768			

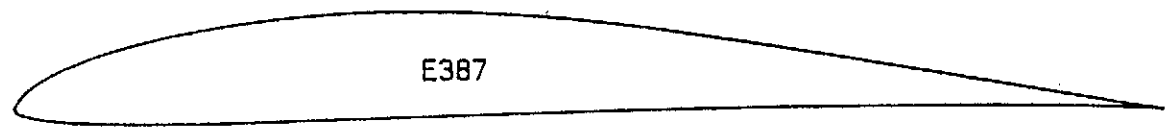

E387

1	1.00000	0.00000	17	0.44767	0.07936	33	0.00000	0.00000	49	0.50182	-.00228
2	0.99677	0.00043	18	0.40077	0.08173	34	0.00000	0.00000	50	0.55694	-.00065
3	0.98729	0.00180	19	0.35505	0.08247	35	0.00091	-.00286	51	0.61147	0.00074
4	0.97198	0.00423	20	0.31078	0.08156	36	0.00717	-.00682	52	0.66472	0.00186
5	0.95128	0.00763	21	0.26813	0.07908	37	0.01890	-.01017	53	0.71602	0.00268
6	0.92554	0.01184	22	0.22742	0.07529	38	0.03596	-.01265	54	0.76475	0.00320
7	0.89510	0.01679	23	0.18906	0.07037	39	0.05827	-.01425	55	0.81027	0.00342
8	0.86035	0.02242	24	0.15345	0.06448	40	0.08569	-.01500	56	0.85202	0.00337
9	0.82183	0.02866	25	0.12094	0.05775	41	0.11800	-.01502	57	0.88944	0.00307
10	0.78007	0.03540	26	0.09185	0.05033	42	0.15490	-.01441	58	0.92205	0.00258
11	0.73567	0.04249	27	0.06643	0.04238	43	0.19599	-.01329	59	0.94942	0.00196
12	0.68922	0.04975	28	0.04493	0.03408	44	0.24083	-.01177	60	0.97118	0.00132
13	0.64136	0.05696	29	0.02748	0.02562	45	0.28892	-.00998	61	0.98705	0.00071
14	0.59272	0.06390	30	0.01423	0.01726	46	0.33968	-.00804	62	0.99674	0.00021
15	0.54394	0.07020	31	0.00700	0.01100	47	0.39252	-.00605	63	1.00000	0.00000
16	0.49549	0.07546	32	0.00090	0.00245	48	0.44679	-.00410			

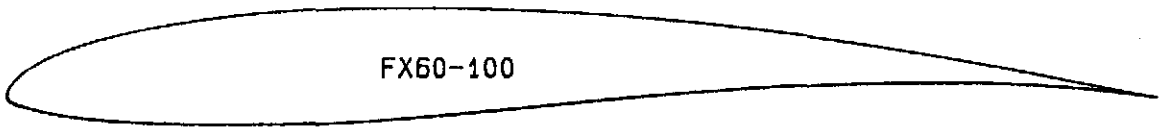

FX60-100

1	1.00000	0.00000	19	0.25000	0.07543	37	0.00428	-.00503	55	0.37059	-.01617
2	0.99572	0.00087	20	0.22221	0.07326	38	0.00961	-.00751	56	0.43474	-.01029
3	0.98296	0.00344	21	0.19562	0.07059	39	0.01704	-.00991	57	0.50000	-.00404
4	0.96194	0.00765	22	0.17033	0.06743	40	0.02653	-.01235	58	0.56526	0.00192
5	0.93301	0.01342	23	0.14645	0.06383	41	0.03806	-.01482	59	0.62941	0.00702
6	0.89668	0.02056	24	0.12408	0.05982	42	0.05156	-.01719	60	0.69134	0.01081
7	0.85355	0.02875	25	0.10332	0.05545	43	0.06699	-.01933	61	0.75000	0.01305
8	0.80438	0.03754	26	0.08427	0.05078	44	0.08427	-.02115	62	0.80438	0.01367
9	0.75000	0.04643	27	0.06699	0.04584	45	0.10332	-.02265	63	0.85355	0.01281
10	0.69134	0.05491	28	0.05156	0.04064	46	0.12408	-.02381	64	0.89668	0.01080
11	0.62941	0.06255	29	0.03806	0.03517	47	0.14645	-.02464	65	0.93301	0.00808
12	0.56526	0.06902	30	0.02653	0.02937	48	0.17033	-.02510	66	0.96194	0.00514
13	0.50000	0.07402	31	0.01704	0.02331	49	0.19562	-.02518	67	0.98296	0.00250
14	0.43474	0.07735	32	0.00961	0.01715	50	0.22221	-.02483	68	0.99572	0.00066
15	0.37059	0.07880	33	0.00428	0.01123	51	0.25000	-.02402	69	1.00000	0.00000
16	0.33928	0.07876	34	0.00107	0.00589	52	0.27886	-.02273			
17	0.30866	0.07819	35	0.00000	0.00142	53	0.30866	-.02096			
18	0.27886	0.07708	36	0.00107	-.00216	54	0.33928	-.01874			

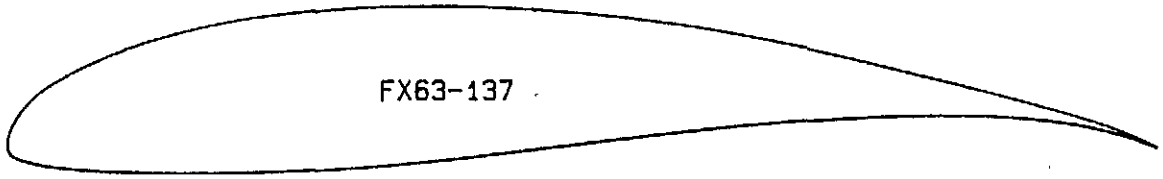

FX63-137

1	1.00000	0.00000	19	0.25000	0.11492	37	0.00428	-.00702	55	0.37059	-.01118
2	0.99572	0.00226	20	0.22221	0.11122	38	0.00961	-.01016	56	0.43474	-.00421
3	0.98296	0.00822	21	0.19562	0.10680	39	0.01704	-.01275	57	0.50000	0.00341
4	0.96194	0.01642	22	0.17033	0.10169	40	0.02653	-.01503	58	0.56526	0.01092
5	0.93301	0.02581	23	0.14645	0.09591	41	0.03806	-.01706	59	0.62941	0.01760
6	0.89668	0.03615	24	0.12408	0.08955	42	0.05156	-.01879	60	0.69134	0.02287
7	0.85355	0.04757	25	0.10332	0.08270	43	0.06699	-.02018	61	0.75000	0.02629
8	0.80438	0.06001	26	0.08427	0.07552	44	0.08427	-.02123	62	0.80438	0.02758
9	0.75000	0.07305	27	0.06699	0.06812	45	0.10332	-.02199	63	0.85355	0.02661
10	0.69134	0.08596	28	0.05156	0.06052	46	0.12408	-.02248	64	0.89668	0.02343
11	0.62941	0.09788	29	0.03806	0.05264	47	0.14645	-.02272	65	0.93301	0.01841
12	0.56526	0.10799	30	0.02653	0.04430	48	0.17033	-.02267	66	0.96194	0.01229
13	0.50000	0.11562	31	0.01704	0.03548	49	0.19562	-.02230	67	0.98296	0.00623
14	0.43474	0.12031	32	0.00961	0.02636	50	0.22221	-.02157	68	0.99572	0.00170
15	0.37059	0.12180	33	0.00428	0.01742	51	0.25000	-.02043	69	1.00000	0.00000
16	0.33928	0.12130	34	0.00107	0.00927	52	0.27886	-.01884			
17	0.30866	0.11998	35	0.00000	0.00241	53	0.30866	-.01675			
18	0.27886	0.11785	36	0.00107	-.00296	54	0.33928	-.01418			

HQ2/9

1	1.00000	0.00000	11	0.30000	0.06300	21	0.00500	-.00510	31	0.40000	-.02480
2	0.95000	0.00710	12	0.25000	0.06090	22	0.01250	-.00870	32	0.50000	-.02080
3	0.90000	0.01490	13	0.20000	0.05760	23	0.02500	-.01220	33	0.60000	-.01490
4	0.85000	0.02230	14	0.15000	0.05240	24	0.05000	-.01630	34	0.70000	-.00760
5	0.80000	0.02950	15	0.10000	0.04450	25	0.10000	-.02070	35	0.80000	-.00170
6	0.70000	0.04280	16	0.05000	0.03190	26	0.15000	-.02320	36	0.85000	0.00010
7	0.60000	0.05360	17	0.02500	0.02240	27	0.20000	-.02480	37	0.90000	0.00110
8	0.50000	0.06060	18	0.01250	0.01560	28	0.25000	-.02570	38	0.95000	0.00110
9	0.40000	0.06370	19	0.00500	0.00950	29	0.30000	-.02610	39	1.00000	0.00000
10	0.35000	0.06390	20	0.00000	0.00000	30	0.35000	-.02580			

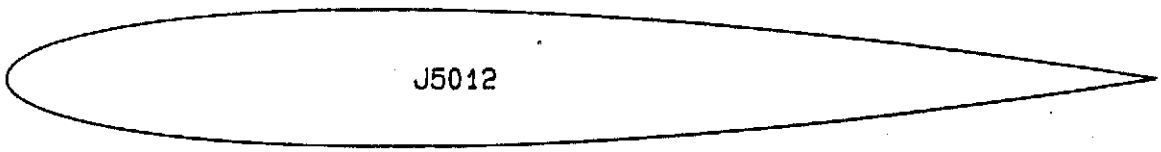

J5012

1	1.00000	0.00000	17	0.44774	0.05763	33	0.01093	-.01612	49	0.65451	-.04359
2	0.99726	0.00043	18	0.39604	0.05928	34	0.02447	-.02380	50	0.70337	-.03880
3	0.98907	0.00169	19	0.34549	0.06000	35	0.04323	-.03102	51	0.75000	-.03377
4	0.97553	0.00377	20	0.29663	0.05975	36	0.06699	-.03766	52	0.79389	-.02864
5	0.95677	0.00659	21	0.25000	0.05849	37	0.09549	-.04359	53	0.83456	-.02357
6	0.93301	0.01009	22	0.20611	0.05621	38	0.12843	-.04871	54	0.87157	-.01870
7	0.90451	0.01416	23	0.16544	0.05294	39	0.16543	-.05294	55	0.90451	-.01416
8	0.87157	0.01870	24	0.12843	0.04871	40	0.20611	-.05621	56	0.93301	-.01009
9	0.83457	0.02357	25	0.09549	0.04359	41	0.25000	-.05849	57	0.95677	-.00659
10	0.79389	0.02864	26	0.06699	0.03766	42	0.29663	-.05975	58	0.97553	-.00377
11	0.75000	0.03377	27	0.04323	0.03102	43	0.34549	-.06000	59	0.98907	-.00169
12	0.70337	0.03880	28	0.02447	0.02380	44	0.39604	-.05928	60	0.99726	-.00043
13	0.65451	0.04359	29	0.01093	0.01612	45	0.44774	-.05763	61	1.00000	0.00000
14	0.60396	0.04800	30	0.00274	0.00814	46	0.50000	-.05514			
15	0.55226	0.05189	31	0.00000	0.00000	47	0.55226	-.05189			
16	0.50000	0.05514	32	0.00274	-.00814	48	0.60396	-.04800			

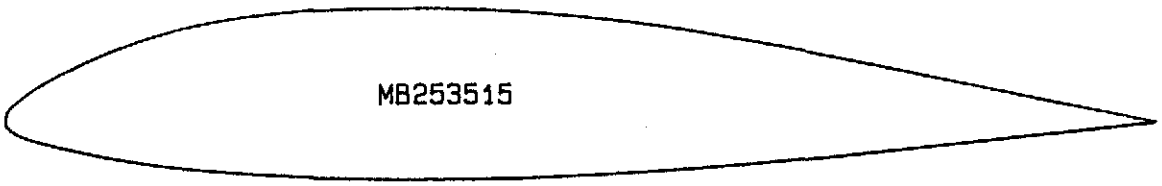

MB253515

1	1.00000	0.00000	18	0.30000	0.09788	35	0.01000	-.01223	52	0.35000	-.05054
2	0.95000	0.01032	19	0.27500	0.09660	36	0.02500	-.01809	53	0.37500	-.05035
3	0.90000	0.02033	20	0.25000	0.09473	37	0.03750	-.02159	54	0.40000	-.04997
4	0.85000	0.03052	21	0.22500	0.09211	38	0.05000	-.02461	55	0.42500	-.04941
5	0.80000	0.04079	22	0.20000	0.08861	39	0.06250	-.02739	56	0.45000	-.04866
6	0.75000	0.05095	23	0.17500	0.08410	40	0.07500	-.03001	57	0.50000	-.04660
7	0.70000	0.06078	24	0.15000	0.07844	41	0.08750	-.03246	58	0.55000	-.04383
8	0.65000	0.07005	25	0.12500	0.07146	42	0.10000	-.03472	59	0.60000	-.04036
9	0.60000	0.07849	26	0.10000	0.06296	43	0.12500	-.03861	60	0.65000	-.03628
10	0.55000	0.08582	27	0.08750	0.05807	44	0.15000	-.04175	61	0.70000	-.03169
11	0.50000	0.09174	28	0.07500	0.05274	45	0.17500	-.04425	62	0.75000	-.02669
12	0.45000	0.09602	29	0.06250	0.04696	46	0.20000	-.04622	63	0.80000	-.02144
13	0.42500	0.09748	30	0.05000	0.04072	47	0.22500	-.04776	64	0.85000	-.01606
14	0.40000	0.09847	31	0.03750	0.03393	48	0.25000	-.04892	65	0.90000	-.01070
15	0.37500	0.09898	32	0.02500	0.02636	49	0.27500	-.04974	66	0.95000	-.00544
16	0.35000	0.09904	33	0.01000	0.01521	50	0.30000	-.05026	67	1.00000	0.00000
17	0.32500	0.09868	34	0.00000	-.00041	51	0.32500	-.05052			

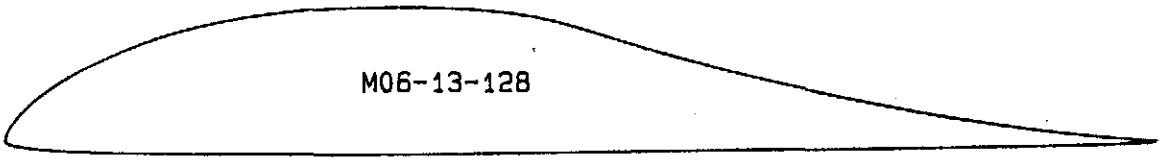

M06-13-128

1	1.00000	0.00000	17	0.43510	0.11094	33	0.00098	0.00452	49	0.49338	-.01053
2	0.99896	0.00015	18	0.39263	0.11489	34	0.00005	0.00087	50	0.54820	-.00972
3	0.99152	0.00088	19	0.35032	0.11617	35	0.00030	-.00183	51	0.60242	-.00890
4	0.97756	0.00198	20	0.30873	0.11531	36	0.00233	-.00372	52	0.65541	-.00809
5	0.95718	0.00370	21	0.26838	0.11256	37	0.01203	-.00669	53	0.70652	-.00729
6	0.93068	0.00631	22	0.22975	0.10814	38	0.02803	-.00901	54	0.75516	-.00652
7	0.89849	0.01002	23	0.19328	0.10220	39	0.04987	-.01077	55	0.80073	-.00577
8	0.86112	0.01499	24	0.15942	0.09487	40	0.07718	-.01203	56	0.84269	-.00506
9	0.81923	0.02139	25	0.12857	0.08605	41	0.10959	-.01287	57	0.88053	-.00437
10	0.77354	0.02930	26	0.10057	0.07583	42	0.14667	-.01333	58	0.91379	-.00370
11	0.72493	0.03878	27	0.07558	0.06460	43	0.18796	-.01349	59	0.94205	-.00302
12	0.67434	0.04980	28	0.05382	0.05305	44	0.23296	-.01339	60	0.96496	-.00228
13	0.62288	0.06225	29	0.03551	0.04122	45	0.28111	-.01308	61	0.98232	-.00147
14	0.57180	0.07584	30	0.02083	0.02960	46	0.33185	-.01260	62	0.99393	-.00073
15	0.52265	0.09002	31	0.00994	0.01862	47	0.38456	-.01200	63	0.99942	-.00014
16	0.47756	0.10309	32	0.00296	0.00878	48	0.43862	-.01129	64	1.00000	0.00000

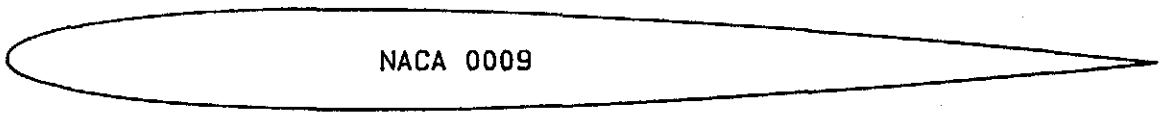

NACA 0009

1	1.00000	0.00000	19	0.25000	0.04466	37	0.00428	-.00767	55	0.37059	-.04431
2	0.99572	0.00057	20	0.22221	0.04397	38	0.00961	-.01214	56	0.43474	-.04248
3	0.98296	0.00218	21	0.19562	0.04295	39	0.01704	-.01646	57	0.50000	-.03978
4	0.96194	0.00463	22	0.17033	0.04161	40	0.02653	-.02039	58	0.56526	-.03638
5	0.93301	0.00770	23	0.14645	0.03994	41	0.03806	-.02395	59	0.62941	-.03247
6	0.89668	0.01127	24	0.12408	0.03795	42	0.05156	-.02720	60	0.69134	-.02823
7	0.85355	0.01522	25	0.10332	0.03564	43	0.06699	-.03023	61	0.75000	-.02384
8	0.80438	0.01945	26	0.08427	0.03305	44	0.08427	-.03305	62	0.80438	-.01945
9	0.75000	0.02384	27	0.06699	0.03023	45	0.10332	-.03564	63	0.85355	-.01522
10	0.69134	0.02823	28	0.05156	0.02720	46	0.12408	-.03795	64	0.89668	-.01127
11	0.62941	0.03247	29	0.03806	0.02395	47	0.14645	-.03994	65	0.93301	-.00770
12	0.56526	0.03638	30	0.02653	0.02039	48	0.17033	-.04161	66	0.96194	-.00463
13	0.50000	0.03978	31	0.01704	0.01646	49	0.19562	-.04295	67	0.98296	-.00218
14	0.43474	0.04248	32	0.00961	0.01214	50	0.22221	-.04397	68	0.99572	-.00057
15	0.37059	0.04431	33	0.00428	0.00767	51	0.25000	-.04466	69	1.00000	0.00000
16	0.33928	0.04484	34	0.00107	0.00349	52	0.27886	-.04504			
17	0.30866	0.04509	35	0.00000	0.00000	53	0.30866	-.04509			
18	0.27886	0.04504	36	0.00107	-.00349	54	0.33928	-.04484			

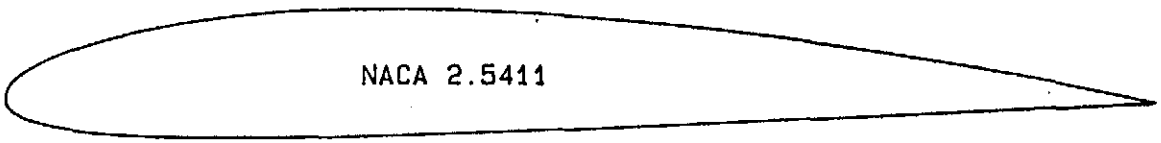

NACA 2.5411

1	1.00000	0.00000	17	0.44807	0.07606	33	0.01290	-.01483	49	0.65320	-.01677
2	0.99730	0.00059	18	0.39597	0.07830	34	0.02723	-.02061	50	0.70198	-.01436
3	0.98918	0.00235	19	0.34455	0.07912	35	0.04662	-.02531	51	0.74862	-.01208
4	0.97578	0.00520	20	0.29485	0.07831	36	0.07080	-.02893	52	0.79257	-.00994
5	0.95720	0.00906	21	0.24745	0.07588	37	0.09948	-.03151	53	0.83337	-.00798
6	0.93365	0.01380	22	0.20292	0.07193	38	0.13238	-.03310	54	0.87053	-.00621
7	0.90535	0.01927	23	0.16175	0.06659	39	0.16912	-.03379	55	0.90368	-.00463
8	0.87260	0.02532	24	0.12448	0.06006	40	0.20932	-.03368	56	0.93238	-.00326
9	0.83577	0.03175	25	0.09148	0.05253	41	0.25255	-.03291	57	0.95633	-.00211
10	0.79520	0.03839	26	0.06317	0.04427	42	0.29842	-.03165	58	0.97528	-.00120
11	0.75138	0.04506	27	0.03985	0.03553	43	0.34642	-.03005	59	0.98895	-.00054
12	0.70475	0.05158	28	0.02170	0.02654	44	0.39612	-.02830	60	0.99723	-.00013
13	0.65583	0.05777	29	0.00897	0.01752	45	0.44740	-.02637	61	1.00000	0.00000
14	0.60513	0.06347	30	0.00172	0.00862	46	0.49933	-.02415			
15	0.55322	0.06852	31	0.00000	0.00000	47	0.55132	-.02174			
16	0.50067	0.07276	32	0.00375	-.00794	48	0.60280	-.01925			

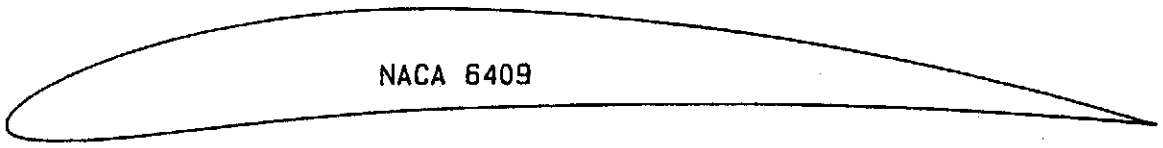

NACA 6409

1	1.00000	0.00000	17	0.44840	0.10152	33	0.01467	-.00956	49	0.65193	0.01880
2	0.99732	0.00084	18	0.39590	0.10360	34	0.02973	-.01157	50	0.70065	0.01780
3	0.98930	0.00333	19	0.34367	0.10352	35	0.04970	-.01192	51	0.74728	0.01634
4	0.97603	0.00737	20	0.29315	0.10086	36	0.07428	-.01080	52	0.79130	0.01451
5	0.95760	0.01284	21	0.24502	0.09584	37	0.10317	-.00844	53	0.83223	0.01241
6	0.93423	0.01954	22	0.19988	0.08874	38	0.13607	-.00513	54	0.86957	0.01017
7	0.90615	0.02724	23	0.15830	0.07992	39	0.17257	-.00119	55	0.90288	0.00791
8	0.87357	0.03571	24	0.12080	0.06982	40	0.21235	0.00307	56	0.93180	0.00576
9	0.83690	0.04464	25	0.08780	0.05889	41	0.25498	0.00729	57	0.95593	0.00383
10	0.79647	0.05378	26	0.05968	0.04762	42	0.30012	0.01112	58	0.97503	0.00221
11	0.75272	0.06283	27	0.03677	0.03646	43	0.34730	0.01425	59	0.98883	0.00101
12	0.70608	0.07153	28	0.01920	0.02581	44	0.39618	0.01639	60	0.99722	0.00025
13	0.65710	0.07961	29	0.00720	0.01603	45	0.44707	0.01772	61	1.00000	0.00000
14	0.60627	0.08684	30	0.00080	0.00737	46	0.49868	0.01871			
15	0.55413	0.09302	31	0.00000	0.00000	47	0.55040	0.01925			
16	0.50132	0.09796	32	0.00467	-.00573	48	0.60167	0.01929			

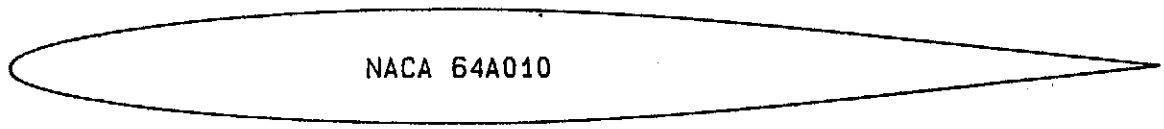

NACA 64A010

1	1.00000	0.00000	29	0.03000	0.01842	57	0.00025	-.00189	85	0.05000	-.02331
3	0.90000	0.01063	31	0.01000	0.01117	59	0.00075	-.00327	87	0.07000	-.02720
5	0.80000	0.02102	33	0.00900	0.01065	61	0.00125	-.00421	89	0.09000	-.03052
7	0.70000	0.03124	35	0.00800	0.01010	63	0.00175	-.00495	91	0.12000	-.03471
9	0.60000	0.04021	37	0.00700	0.00950	65	0.00225	-.00559	93	0.16000	-.03918
11	0.50000	0.04683	39	0.00600	0.00886	67	0.00300	-.00642	95	0.20000	-.04274
13	0.40000	0.04995	41	0.00500	0.00815	69	0.00400	-.00735	97	0.30000	-.04837
15	0.30000	0.04837	43	0.00400	0.00735	71	0.00500	-.00815	99	0.40000	-.04995
17	0.20000	0.04274	45	0.00300	0.00642	73	0.00600	-.00886	101	0.50000	-.04683
19	0.16000	0.03918	47	0.00225	0.00559	75	0.00700	-.00950	103	0.60000	-.04021
21	0.12000	0.03471	49	0.00175	0.00495	77	0.00800	-.01010	105	0.70000	-.03124
23	0.09000	0.03052	51	0.00125	0.00421	79	0.00900	-.01065	107	0.80000	-.02102
25	0.07000	0.02720	53	0.00075	0.00327	81	0.01000	-.01117	109	0.90000	-.01063
27	0.05000	0.02331	55	0.00025	0.00189	83	0.03000	-.01842	111	1.00000	0.00000
28	0.04000	0.02103	56	0.00000	0.00000	84	0.04000	-.02103			

Note: Several of the original 120 coordinates were removed due to space limitations.

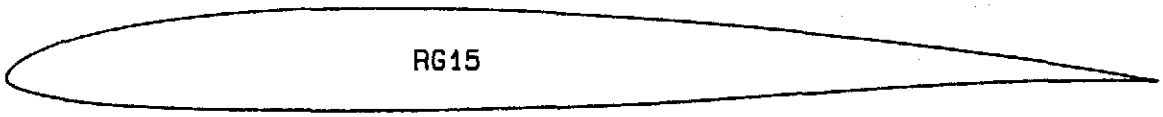

RG15

1	1.00000	0.00000	17	0.44676	0.05966	33	0.00002	-.00048	49	0.55944	-.02025
2	0.99671	0.00054	18	0.39727	0.06123	34	0.00336	-.00534	50	0.61128	-.01717
3	0.98726	0.00229	19	0.34902	0.06190	35	0.01247	-.01006	51	0.66244	-.01366
4	0.97237	0.00514	20	0.30248	0.06162	36	0.02670	-.01436	52	0.71237	-.01015
5	0.95248	0.00865	21	0.25809	0.06036	37	0.04596	-.01811	53	0.76037	-.00691
6	0.92764	0.01254	22	0.21624	0.05810	38	0.07010	-.02123	54	0.80575	-.00413
7	0.89810	0.01685	23	0.17730	0.05486	39	0.09896	-.02372	55	0.84779	-.00192
8	0.86427	0.02152	24	0.14161	0.05068	40	0.13224	-.02559	56	0.88583	-.00034
9	0.82660	0.02644	25	0.10945	0.04564	41	0.16963	-.02688	57	0.91925	0.00062
10	0.78557	0.03149	26	0.08108	0.03985	42	0.21073	-.02762	58	0.94748	0.00101
11	0.74165	0.03654	27	0.05673	0.03343	43	0.25509	-.02785	59	0.97003	0.00097
12	0.69537	0.04146	28	0.03658	0.02654	44	0.30221	-.02762	60	0.98652	0.00064
13	0.64723	0.04612	29	0.02076	0.01935	45	0.35156	-.02696	61	0.99660	0.00021
14	0.59778	0.05039	30	0.00932	0.01214	46	0.40257	-.02590	62	1.00000	0.00000
15	0.54753	0.05414	31	0.00235	0.00526	47	0.45463	-.02446			
16	0.49702	0.05727	32	0.00000	0.00000	48	0.50713	-.02262			

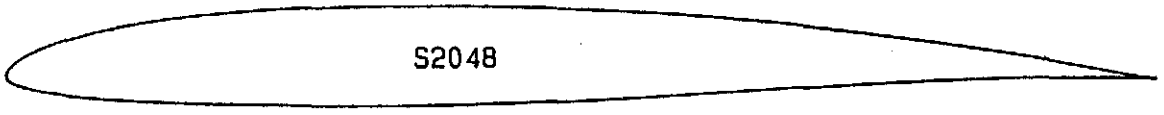

S2048

1	1.00000	0.00000	17	0.45172	0.06025	33	0.00307	-.00506	49	0.61084	-.01395
2	0.99671	0.00045	18	0.40212	0.06093	34	0.01200	-.00943	50	0.66260	-.01049
3	0.98710	0.00196	19	0.35350	0.06086	35	0.02603	-.01339	51	0.71302	-.00724
4	0.97174	0.00470	20	0.30640	0.06004	36	0.04518	-.01667	52	0.76139	-.00439
5	0.95126	0.00855	21	0.26132	0.05849	37	0.06942	-.01934	53	0.80700	-.00208
6	0.92617	0.01320	22	0.21878	0.05621	38	0.09852	-.02152	54	0.84914	-.00040
7	0.89683	0.01825	23	0.17925	0.05318	39	0.13210	-.02327	55	0.88712	0.00067
8	0.86343	0.02345	24	0.14319	0.04935	40	0.16972	-.02461	56	0.92036	0.00120
9	0.82623	0.02877	25	0.11087	0.04457	41	0.21096	-.02553	57	0.94833	0.00127
10	0.78572	0.03418	26	0.08232	0.03887	42	0.25531	-.02600	58	0.97059	0.00102
11	0.74243	0.03954	27	0.05765	0.03256	43	0.30225	-.02600	59	0.98681	0.00060
12	0.69691	0.04467	28	0.03715	0.02590	44	0.35127	-.02546	60	0.99669	0.00018
13	0.64968	0.04934	29	0.02106	0.01905	45	0.40189	-.02432	61	1.00001	0.00000
14	0.60115	0.05332	30	0.00950	0.01218	46	0.45363	-.02260			
15	0.55171	0.05649	31	0.00249	0.00552	47	0.50596	-.02030			
16	0.50176	0.05879	32	0.00001	-.00028	48	0.55846	-.01736			

S2055

1	1.00000	0.00000	17	0.44602	0.05552	33	0.00403	-.00537	49	0.62337	-.01794
2	0.99670	0.00037	18	0.39625	0.05623	34	0.01374	-.00952	50	0.67376	-.01604
3	0.98702	0.00164	19	0.34755	0.05624	35	0.02855	-.01321	51	0.72225	-.01380
4	0.97150	0.00400	20	0.30044	0.05557	36	0.04846	-.01620	52	0.76843	-.01130
5	0.95075	0.00738	21	0.25546	0.05420	37	0.07349	-.01855	53	0.81187	-.00870
6	0.92529	0.01151	22	0.21310	0.05215	38	0.10338	-.02043	54	0.85210	-.00617
7	0.89548	0.01607	23	0.17385	0.04939	39	0.13776	-.02187	55	0.88861	-.00389
8	0.86156	0.02081	24	0.13818	0.04585	40	0.17622	-.02292	56	0.92087	-.00205
9	0.82383	0.02571	25	0.10633	0.04135	41	0.21835	-.02358	57	0.94834	-.00075
10	0.78279	0.03074	26	0.07830	0.03594	42	0.26365	-.02390	58	0.97046	-.00003
11	0.73898	0.03577	27	0.05421	0.02992	43	0.31161	-.02387	59	0.98671	0.00019
12	0.69297	0.04061	28	0.03433	0.02356	44	0.36169	-.02354	60	0.99666	0.00009
13	0.64527	0.04504	29	0.01890	0.01704	45	0.41332	-.02293	61	1.00001	0.00000
14	0.59634	0.04884	30	0.00803	0.01051	46	0.46591	-.02205			
15	0.54654	0.05187	31	0.00174	0.00423	47	0.51885	-.02092			
16	0.49629	0.05408	32	0.00012	-.00101	48	0.57154	-.01955			

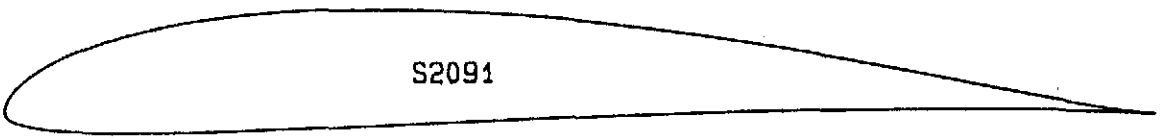

S2091

1	1.00000	0.00000	17	0.44220	0.08415	33	0.00058	-.00312	49	0.60607	0.00025
2	0.99674	0.00035	18	0.39450	0.08676	34	0.00575	-.00864	50	0.66007	0.00182
3	0.98707	0.00150	19	0.34805	0.08804	35	0.01662	-.01315	51	0.71218	0.00296
4	0.97126	0.00367	20	0.30323	0.08793	36	0.03263	-.01645	52	0.76169	0.00367
5	0.94970	0.00699	21	0.26043	0.08643	37	0.05397	-.01844	53	0.80796	0.00397
6	0.92292	0.01150	22	0.22002	0.08355	38	0.08063	-.01935	54	0.85037	0.00391
7	0.89147	0.01713	23	0.18232	0.07933	39	0.11237	-.01939	55	0.88835	0.00354
8	0.85595	0.02373	24	0.14765	0.07381	40	0.14884	-.01872	56	0.92142	0.00295
9	0.81694	0.03107	25	0.11622	0.06708	41	0.18960	-.01750	57	0.94912	0.00222
10	0.77501	0.03888	26	0.08823	0.05927	42	0.23417	-.01580	58	0.97110	0.00144
11	0.73071	0.04688	27	0.06384	0.05059	43	0.28206	-.01373	59	0.98706	0.00073
12	0.68455	0.05478	28	0.04320	0.04130	44	0.33272	-.01141	60	0.99675	0.00020
13	0.63701	0.06231	29	0.02645	0.03168	45	0.38556	-.00894	61	1.00001	0.00000
14	0.58856	0.06920	30	0.01374	0.02204	46	0.43996	-.00642			
15	0.53966	0.07525	31	0.00517	0.01269	47	0.49529	-.00397			
16	0.49073	0.08028	32	0.00076	0.00401	48	0.55090	-.00170			

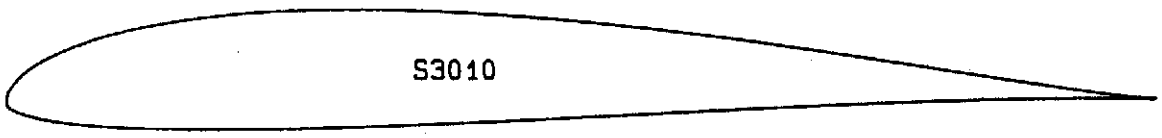

S3010

1	1.00000	0.00000	17	0.43275	0.07422	33	0.00181	-.00543	49	0.61127	-.00994
2	0.99674	0.00027	18	0.38438	0.07706	34	0.00932	-.01048	50	0.66399	-.00749
3	0.98706	0.00118	19	0.33750	0.07870	35	0.02239	-.01506	51	0.71495	-.00526
4	0.97122	0.00293	20	0.29250	0.07902	36	0.04061	-.01894	52	0.76350	-.00332
5	0.94959	0.00564	21	0.24970	0.07796	37	0.06381	-.02203	53	0.80901	-.00172
6	0.92264	0.00936	22	0.20944	0.07556	38	0.09180	-.02427	54	0.85087	-.00051
7	0.89090	0.01405	23	0.17206	0.07184	39	0.12435	-.02567	55	0.88851	0.00031
8	0.85493	0.01960	24	0.13785	0.06689	40	0.16119	-.02625	56	0.92140	0.00075
9	0.81531	0.02585	25	0.10706	0.06076	41	0.20200	-.02610	57	0.94905	0.00086
10	0.77261	0.03259	26	0.07990	0.05360	42	0.24635	-.02531	58	0.97104	0.00072
11	0.72739	0.03958	27	0.05655	0.04556	43	0.29376	-.02399	59	0.98703	0.00042
12	0.68021	0.04658	28	0.03713	0.03683	44	0.34371	-.02221	60	0.99674	0.00013
13	0.63158	0.05337	29	0.02173	0.02766	45	0.39565	-.02009	61	1.00000	0.00000
14	0.58203	0.05971	30	0.01042	0.01835	46	0.44899	-.01769			
15	0.53204	0.06541	31	0.00319	0.00927	47	0.50312	-.01514			
16	0.48213	0.07029	32	0.00005	0.00100	48	0.55743	-.01252			

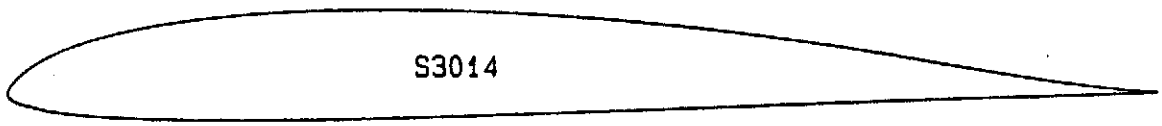

S3014

1	1.00000	0.00000	17	0.43477	0.06988	33	0.00284	-.00526	49	0.62242	-.01246
2	0.99663	0.00021	18	0.38629	0.07166	34	0.01183	-.00972	50	0.67431	-.01064
3	0.98667	0.00099	19	0.33908	0.07235	35	0.02610	-.01383	51	0.72423	-.00893
4	0.97044	0.00264	20	0.29354	0.07192	36	0.04545	-.01731	52	0.77158	-.00736
5	0.94840	0.00532	21	0.25011	0.07043	37	0.06973	-.02006	53	0.81577	-.00595
6	0.92108	0.00911	22	0.20924	0.06790	38	0.09879	-.02204	54	0.85625	-.00472
7	0.88906	0.01394	23	0.17136	0.06434	39	0.13239	-.02329	55	0.89250	-.00367
8	0.85297	0.01970	24	0.13682	0.05971	40	0.17024	-.02386	56	0.92405	-.00277
9	0.81342	0.02617	25	0.10585	0.05403	41	0.21197	-.02385	57	0.95049	-.00199
10	0.77104	0.03310	26	0.07864	0.04741	42	0.25713	-.02335	58	0.97151	-.00124
11	0.72642	0.04012	27	0.05535	0.03997	43	0.30520	-.02244	59	0.98699	-.00052
12	0.68001	0.04685	28	0.03607	0.03190	44	0.35564	-.02120	60	0.99668	-.00010
13	0.63214	0.05301	29	0.02088	0.02344	45	0.40787	-.01970	61	1.00001	0.00000
14	0.58321	0.05850	30	0.00978	0.01492	46	0.46129	-.01801			
15	0.53368	0.06322	31	0.00278	0.00682	47	0.51527	-.01620			
16	0.48405	0.06704	32	0.00000	-.00003	48	0.56920	-.01433			

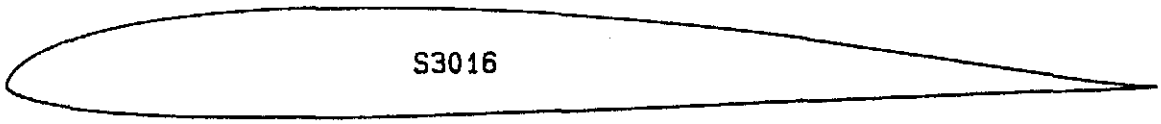

S3016

1	1.00000	0.00000	17	0.43144	0.06528	33	0.00391	-.00606	49	0.62352	-.01588
2	0.99664	0.00017	18	0.38265	0.06707	34	0.01386	-.01088	50	0.67514	-.01363
3	0.98669	0.00085	19	0.33517	0.06783	35	0.02891	-.01543	51	0.72484	-.01147
4	0.97048	0.00233	20	0.28946	0.06755	36	0.04888	-.01941	52	0.77202	-.00946
5	0.94843	0.00476	21	0.24593	0.06624	37	0.07362	-.02271	53	0.81607	-.00763
6	0.92107	0.00821	22	0.20504	0.06396	38	0.10296	-.02526	54	0.85645	-.00602
7	0.88898	0.01266	23	0.16726	0.06066	39	0.13666	-.02705	55	0.89264	-.00462
8	0.85274	0.01798	24	0.13288	0.05631	40	0.17444	-.02807	56	0.92414	-.00344
9	0.81299	0.02400	25	0.10216	0.05092	41	0.21598	-.02839	57	0.95055	-.00242
10	0.77035	0.03047	26	0.07529	0.04459	42	0.26085	-.02810	58	0.97154	-.00148
11	0.72541	0.03706	27	0.05240	0.03743	43	0.30857	-.02729	59	0.98700	-.00063
12	0.67865	0.04337	28	0.03358	0.02964	44	0.35862	-.02604	60	0.99668	-.00012
13	0.63040	0.04917	29	0.01892	0.02146	45	0.41044	-.02442	61	1.00000	0.00000
14	0.58106	0.05437	30	0.00839	0.01321	46	0.46345	-.02251			
15	0.53112	0.05885	31	0.00203	0.00544	47	0.51705	-.02040			
16	0.48109	0.06252	32	0.00007	-.00095	48	0.57061	-.01816			

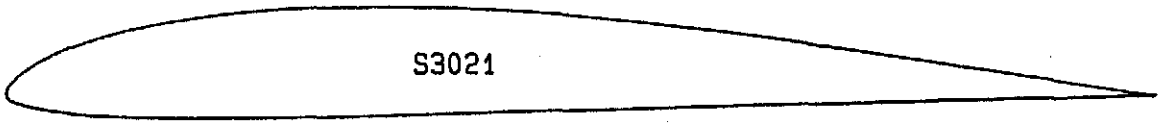

S3021

1	1.00000	0.00000	17	0.43996	0.07312	33	0.00191	-.00427	49	0.61834	-.00963
2	0.99663	0.00039	18	0.39190	0.07536	34	0.00984	-.00852	50	0.67056	-.00821
3	0.98679	0.00172	19	0.34513	0.07632	35	0.02320	-.01232	51	0.72079	-.00690
4	0.97104	0.00419	20	0.29999	0.07596	36	0.04178	-.01547	52	0.76840	-.00570
5	0.94996	0.00769	21	0.25685	0.07433	37	0.06542	-.01789	53	0.81283	-.00462
6	0.92398	0.01193	22	0.21611	0.07151	38	0.09395	-.01957	54	0.85355	-.00365
7	0.89336	0.01670	23	0.17816	0.06753	39	0.12712	-.02053	55	0.89005	-.00278
8	0.85840	0.02198	24	0.14331	0.06243	40	0.16464	-.02085	56	0.92187	-.00193
9	0.81959	0.02776	25	0.11182	0.05631	41	0.20614	-.02059	57	0.94876	-.00107
10	0.77748	0.03393	26	0.08392	0.04930	42	0.25118	-.01986	58	0.97048	-.00035
11	0.73266	0.04038	27	0.05983	0.04156	43	0.29928	-.01876	59	0.98660	0.00003
12	0.68572	0.04694	28	0.03968	0.03329	44	0.34988	-.01742	60	0.99661	0.00006
13	0.63730	0.05341	29	0.02358	0.02472	45	0.40237	-.01592	61	1.00001	0.00000
14	0.58801	0.05954	30	0.01160	0.01615	46	0.45612	-.01433			
15	0.53839	0.06504	31	0.00374	0.00799	47	0.51047	-.01273			
16	0.48891	0.06964	32	0.00008	0.00099	48	0.56476	-.01115			

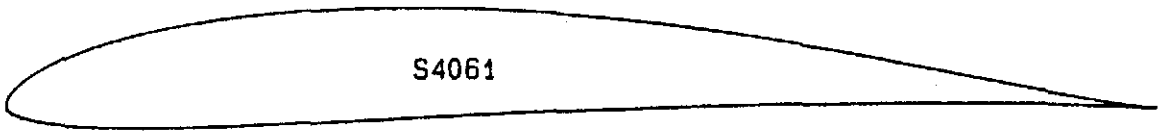

S4061

1	1.00000	0.00000	17	0.44716	0.08301	33	0.00079	-.00320	49	0.60777	0.00107
2	0.99675	0.00034	18	0.39979	0.08491	34	0.00681	-.00787	50	0.66164	0.00245
3	0.98709	0.00147	19	0.35348	0.08542	35	0.01835	-.01209	51	0.71357	0.00342
4	0.97129	0.00363	20	0.30862	0.08453	36	0.03499	-.01545	52	0.76289	0.00400
5	0.94977	0.00698	21	0.26554	0.08227	37	0.05666	-.01780	53	0.80895	0.00419
6	0.92304	0.01156	22	0.22460	0.07876	38	0.08329	-.01907	54	0.85115	0.00405
7	0.89171	0.01729	23	0.18619	0.07414	39	0.11475	-.01932	55	0.88894	0.00363
8	0.85637	0.02403	24	0.15074	0.06848	40	0.15086	-.01864	56	0.92184	0.00301
9	0.81765	0.03151	25	0.11855	0.06186	41	0.19130	-.01724	57	0.94940	0.00225
10	0.77610	0.03945	26	0.08988	0.05437	42	0.23566	-.01527	58	0.97127	0.00146
11	0.73227	0.04752	27	0.06493	0.04616	43	0.28346	-.01291	59	0.98714	0.00074
12	0.68665	0.05541	28	0.04385	0.03741	44	0.33414	-.01034	60	0.99678	0.00020
13	0.63971	0.06283	29	0.02676	0.02838	45	0.38708	-.00771	61	1.00001	0.00000
14	0.59189	0.06949	30	0.01380	0.01937	46	0.44161	-.00516			
15	0.54359	0.07519	31	0.00502	0.01069	47	0.49704	-.00279			
16	0.49522	0.07974	32	0.00046	0.00283	48	0.55267	-.00069			

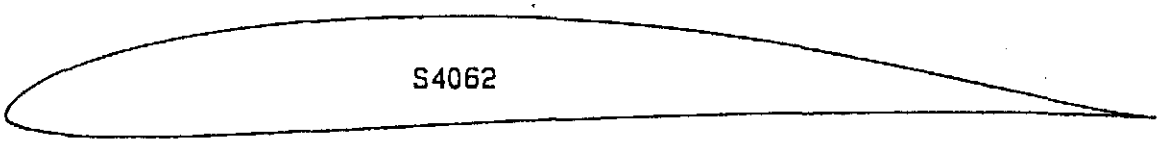

S4062

1	1.00000	0.00000	17	0.45626	0.08630	33	0.00061	-.00262	49	0.60436	0.00196
2	0.99671	0.00041	18	0.40887	0.08717	34	0.00608	-.00725	50	0.65845	0.00337
3	0.98696	0.00178	19	0.36217	0.08673	35	0.01719	-.01145	51	0.71066	0.00437
4	0.97107	0.00438	20	0.31661	0.08510	36	0.03342	-.01482	52	0.76031	0.00495
5	0.94954	0.00836	21	0.27271	0.08239	37	0.05470	-.01716	53	0.80673	0.00511
6	0.92297	0.01374	22	0.23092	0.07864	38	0.08097	-.01844	54	0.84932	0.00491
7	0.89200	0.02036	23	0.19171	0.07393	39	0.11211	-.01868	55	0.88751	0.00439
8	0.85727	0.02799	24	0.15550	0.06828	40	0.14793	-.01800	56	0.92078	0.00364
9	0.81936	0.03628	25	0.12259	0.06173	41	0.18813	-.01659	57	0.94869	0.00273
10	0.77881	0.04487	26	0.09326	0.05435	42	0.23229	-.01462	58	0.97086	0.00178
11	0.73609	0.05339	27	0.06769	0.04627	43	0.27993	-.01224	59	0.98695	0.00090
12	0.69165	0.06147	28	0.04604	0.03765	44	0.33049	-.00965	60	0.99673	0.00025
13	0.64586	0.06881	29	0.02843	0.02876	45	0.38336	-.00700	61	1.00000	0.00000
14	0.59909	0.07513	30	0.01499	0.01986	46	0.43788	-.00441			
15	0.55168	0.08024	31	0.00578	0.01124	47	0.49336	-.00199			
16	0.50397	0.08399	32	0.00081	0.00339	48	0.54909	0.00015			

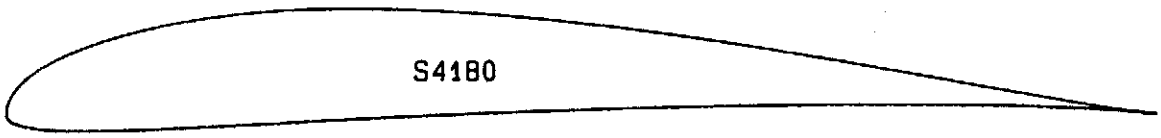

S4180

1	1.00000	0.00000	17	0.44203	0.08471	33	0.00016	-.00200	49	0.60221	0.00602
2	0.99684	0.00036	18	0.39426	0.08828	34	0.00377	-.00814	50	0.65661	0.00709
3	0.98746	0.00156	19	0.34797	0.09049	35	0.01306	-.01234	51	0.70909	0.00775
4	0.97208	0.00376	20	0.30354	0.09117	36	0.02779	-.01523	52	0.75899	0.00801
5	0.95106	0.00702	21	0.26125	0.09017	37	0.04791	-.01669	53	0.80565	0.00787
6	0.92482	0.01132	22	0.22126	0.08751	38	0.07351	-.01680	54	0.84849	0.00736
7	0.89384	0.01661	23	0.18382	0.08329	39	0.10453	-.01584	55	0.88694	0.00652
8	0.85861	0.02279	24	0.14915	0.07770	40	0.14066	-.01416	56	0.92048	0.00541
9	0.81970	0.02971	25	0.11756	0.07095	41	0.18140	-.01201	57	0.94864	0.00407
10	0.77768	0.03718	26	0.08934	0.06322	42	0.22624	-.00956	58	0.97094	0.00263
11	0.73313	0.04497	27	0.06475	0.05468	43	0.27460	-.00696	59	0.98704	0.00131
12	0.68660	0.05280	28	0.04398	0.04553	44	0.32586	-.00432	60	0.99676	0.00035
13	0.63859	0.06041	29	0.02725	0.03596	45	0.37937	-.00177	61	1.00001	0.00000
14	0.58961	0.06761	30	0.01466	0.02605	46	0.43446	0.00061			
15	0.54018	0.07420	31	0.00607	0.01606	47	0.49043	0.00274			
16	0.49082	0.07996	32	0.00129	0.00643	48	0.54659	0.00456			

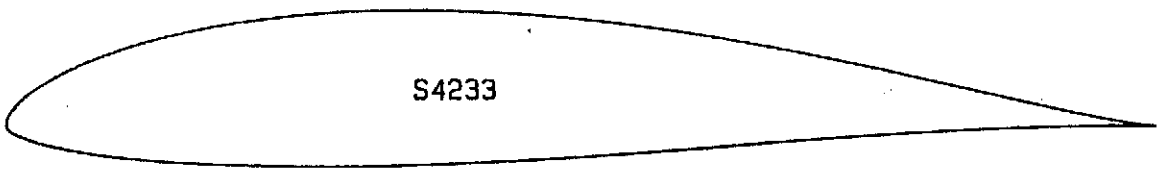

S4233

1	1.00000	0.00000	17	0.44078	0.09770	33	0.00156	-.00488	49	0.59939	-.02139
2	0.99650	0.00042	18	0.39411	0.09969	34	0.00916	-.01058	50	0.65200	-.01703
3	0.98618	0.00186	19	0.34856	0.10001	35	0.02237	-.01621	51	0.70342	-.01286
4	0.96949	0.00461	20	0.30450	0.09867	36	0.04069	-.02144	52	0.75290	-.00910
5	0.94698	0.00881	21	0.26227	0.09570	37	0.06388	-.02609	53	0.79967	-.00592
6	0.91927	0.01444	22	0.22218	0.09118	38	0.09171	-.03003	54	0.84300	-.00337
7	0.88703	0.02138	23	0.18457	0.08523	39	0.12392	-.03321	55	0.88220	-.00149
8	0.85089	0.02939	24	0.14971	0.07798	40	0.16018	-.03559	56	0.91665	-.00026
9	0.81146	0.03817	25	0.11788	0.06963	41	0.20013	-.03714	57	0.94576	0.00040
10	0.76933	0.04740	26	0.08934	0.06040	42	0.24338	-.03782	58	0.96905	0.00058
11	0.72503	0.05674	27	0.06437	0.05055	43	0.28950	-.03768	59	0.98608	0.00043
12	0.67908	0.06585	28	0.04319	0.04033	44	0.33802	-.03672	60	0.99650	0.00014
13	0.63196	0.07443	29	0.02602	0.02999	45	0.38846	-.03497	61	1.00001	0.00000
14	0.58414	0.08218	30	0.01300	0.01986	46	0.44032	-.03249			
15	0.53609	0.08881	31	0.00433	0.01032	47	0.49308	-.02934			
16	0.48820	0.09405	32	0.00017	0.00183	48	0.54626	-.02558			

SD2030

1	1.00000	0.00000	17	0.45282	0.06415	33	0.00249	-.00501	49	0.61621	-.01471
2	0.99665	0.00049	18	0.40336	0.06478	34	0.01071	-.00935	50	0.66738	-.01286
3	0.98686	0.00212	19	0.35488	0.06460	35	0.02419	-.01306	51	0.71670	-.01076
4	0.97128	0.00510	20	0.30788	0.06360	36	0.04296	-.01601	52	0.76373	-.00848
5	0.95059	0.00930	21	0.26288	0.06179	37	0.06693	-.01829	53	0.80802	-.00616
6	0.92535	0.01438	22	0.22034	0.05917	38	0.09584	-.01997	54	0.84906	-.00398
7	0.89593	0.01992	23	0.18069	0.05576	39	0.12941	-.02113	55	0.88632	-.00210
8	0.86252	0.02564	24	0.14432	0.05157	40	0.16727	-.02183	56	0.91925	-.00066
9	0.82542	0.03150	25	0.11158	0.04664	41	0.20896	-.02213	57	0.94728	0.00024
10	0.78512	0.03742	26	0.08273	0.04100	42	0.25401	-.02207	58	0.96985	0.00059
11	0.74219	0.04320	27	0.05798	0.03475	43	0.30191	-.02170	59	0.98643	0.00049
12	0.69709	0.04856	28	0.03752	0.02803	44	0.35208	-.02106	60	0.99659	0.00017
13	0.65019	0.05328	29	0.02150	0.02096	45	0.40396	-.02018	61	1.00001	0.00000
14	0.60189	0.05724	30	0.00995	0.01371	46	0.45693	-.01908			
15	0.55259	0.06038	31	0.00281	0.00657	47	0.51038	-.01780			
16	0.50273	0.06268	32	0.00000	0.00017	48	0.56368	-.01634			

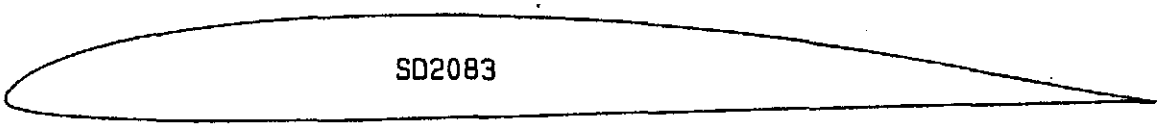

SD2083

1	1.00000	0.00000	17	0.44755	0.07162	33	0.00220	-.00437	49	0.61905	-.00939
2	0.99669	0.00035	18	0.39913	0.07251	34	0.01032	-.00853	50	0.67117	-.00782
3	0.98686	0.00152	19	0.35168	0.07236	35	0.02369	-.01213	51	0.72136	-.00637
4	0.97089	0.00374	20	0.30568	0.07121	36	0.04234	-.01491	52	0.76901	-.00509
5	0.94929	0.00716	21	0.26160	0.06908	37	0.06624	-.01696	53	0.81350	-.00397
6	0.92265	0.01176	22	0.21990	0.06601	38	0.09515	-.01844	54	0.85428	-.00304
7	0.89158	0.01741	23	0.18101	0.06203	39	0.12868	-.01937	55	0.89084	-.00226
8	0.85666	0.02384	24	0.14532	0.05718	40	0.16649	-.01977	56	0.92270	-.00157
9	0.81846	0.03078	25	0.11313	0.05143	41	0.20818	-.01970	57	0.94955	-.00094
10	0.77745	0.03791	26	0.08464	0.04489	42	0.25331	-.01921	58	0.97108	-.00044
11	0.73412	0.04489	27	0.06004	0.03772	43	0.30137	-.01837	59	0.98693	-.00015
12	0.68886	0.05146	28	0.03952	0.03010	44	0.35182	-.01725	60	0.99670	-.00004
13	0.64208	0.05737	29	0.02319	0.02224	45	0.40406	-.01592	61	1.00001	0.00000
14	0.59415	0.06243	30	0.01113	0.01440	46	0.45750	-.01439			
15	0.54546	0.06655	31	0.00338	0.00698	47	0.51157	-.01274			
16	0.49645	0.06964	32	0.00003	0.00060	48	0.56563	-.01105			

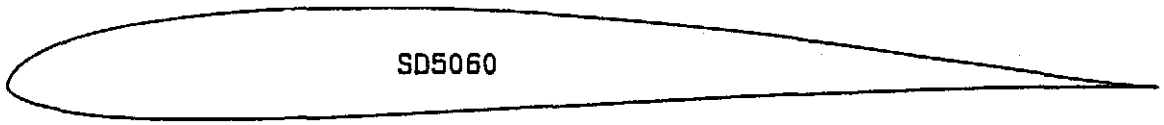

SD5060

1	1.00000	0.00000	17	0.43508	0.06536	33	0.00334	-.00656	49	0.61416	-.01020
2	0.99678	0.00023	18	0.38632	0.06730	34	0.01244	-.01208	50	0.66680	-.00772
3	0.98720	0.00102	19	0.33882	0.06816	35	0.02641	-.01729	51	0.71760	-.00551
4	0.97149	0.00256	20	0.29301	0.06793	36	0.04507	-.02178	52	0.76592	-.00361
5	0.95002	0.00500	21	0.24931	0.06664	37	0.06835	-.02538	53	0.81113	-.00206
6	0.92326	0.00838	22	0.20814	0.06433	38	0.09613	-.02795	54	0.85265	-.00089
7	0.89173	0.01268	23	0.16992	0.06105	39	0.12829	-.02938	55	0.88992	-.00008
8	0.85600	0.01778	24	0.13504	0.05683	40	0.16475	-.02973	56	0.92244	0.00039
9	0.81664	0.02351	25	0.10383	0.05168	41	0.20524	-.02920	57	0.94974	0.00057
10	0.77422	0.02967	26	0.07656	0.04565	42	0.24935	-.02795	58	0.97144	0.00051
11	0.72929	0.03600	27	0.05343	0.03875	43	0.29661	-.02611	59	0.98721	0.00032
12	0.68236	0.04227	28	0.03444	0.03104	44	0.34651	-.02384	60	0.99679	0.00010
13	0.63396	0.04824	29	0.01954	0.02280	45	0.39845	-.02126	61	1.00001	0.00000
14	0.58457	0.05370	30	0.00878	0.01443	46	0.45183	-.01851			
15	0.53465	0.05847	31	0.00223	0.00637	47	0.50602	-.01568			
16	0.48468	0.06239	32	0.00003	-.00066	48	0.56034	-.01288			

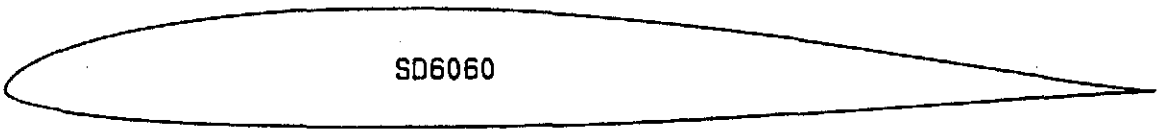

SD6060

1	1.00000	0.00000	17	0.43386	0.06866	33	0.00495	-.00647	49	0.62223	-.02527
2	0.99661	0.00023	18	0.38566	0.07003	34	0.01525	-.01148	50	0.67254	-.02231
3	0.98660	0.00108	19	0.33862	0.07020	35	0.03068	-.01612	51	0.72116	-.01906
4	0.97033	0.00283	20	0.29316	0.06922	36	0.05114	-.02025	52	0.76761	-.01568
5	0.94829	0.00559	21	0.24976	0.06715	37	0.07648	-.02381	53	0.81133	-.01236
6	0.92100	0.00941	22	0.20883	0.06402	38	0.10645	-.02678	54	0.85176	-.00922
7	0.88905	0.01419	23	0.17076	0.05988	39	0.14078	-.02919	55	0.88838	-.00638
8	0.85301	0.01977	24	0.13589	0.05480	40	0.17909	-.03105	56	0.92070	-.00399
9	0.81346	0.02595	25	0.10456	0.04887	41	0.22096	-.03238	57	0.94818	-.00214
10	0.77096	0.03248	26	0.07700	0.04218	42	0.26592	-.03321	58	0.97032	-.00090
11	0.72602	0.03912	27	0.05344	0.03486	43	0.31347	-.03354	59	0.98661	-.00024
12	0.67917	0.04563	28	0.03399	0.02710	44	0.36306	-.03338	60	0.99662	-.00002
13	0.63091	0.05177	29	0.01879	0.01913	45	0.41413	-.03273	61	1.00001	0.00000
14	0.58174	0.05738	30	0.00790	0.01132	46	0.46614	-.03159			
15	0.53222	0.06225	31	0.00148	0.00411	47	0.51852	-.02995			
16	0.48283	0.06606	32	0.00025	-.00159	48	0.57073	-.02784			

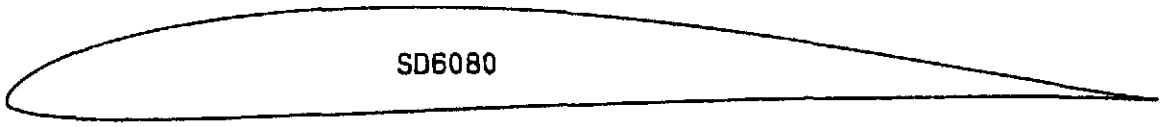

SD6080

1	1.00000	0.00000	17	0.44730	0.07980	33	0.00082	-.00296	49	0.61136	-.00020
2	0.99676	0.00037	18	0.39986	0.08176	34	0.00692	-.00710	50	0.66463	0.00099
3	0.98716	0.00159	19	0.35351	0.08234	35	0.01860	-.01060	51	0.71596	0.00189
4	0.97155	0.00383	20	0.30859	0.08154	36	0.03565	-.01322	52	0.76470	0.00250
5	0.95032	0.00717	21	0.26547	0.07941	37	0.05796	-.01494	53	0.81024	0.00282
6	0.92396	0.01160	22	0.22453	0.07607	38	0.08539	-.01581	54	0.85200	0.00287
7	0.89301	0.01704	23	0.18616	0.07160	39	0.11771	-.01592	55	0.88944	0.00267
8	0.85799	0.02332	24	0.15071	0.06609	40	0.15462	-.01539	56	0.92207	0.00228
9	0.81945	0.03025	25	0.11851	0.05965	41	0.19573	-.01433	57	0.94944	0.00175
10	0.77793	0.03758	26	0.08984	0.05238	42	0.24059	-.01285	58	0.97121	0.00118
11	0.73396	0.04508	27	0.06490	0.04442	43	0.28870	-.01109	59	0.98707	0.00063
12	0.68807	0.05250	28	0.04387	0.03595	44	0.33948	-.00916	60	0.99675	0.00018
13	0.64077	0.05960	29	0.02684	0.02720	45	0.39233	-.00717	61	1.00001	0.00000
14	0.59257	0.06613	30	0.01391	0.01844	46	0.44662	-.00519			
15	0.54399	0.07185	31	0.00509	0.01004	47	0.50168	-.00334			
16	0.49546	0.07646	32	0.00045	0.00260	48	0.55682	-.00166			

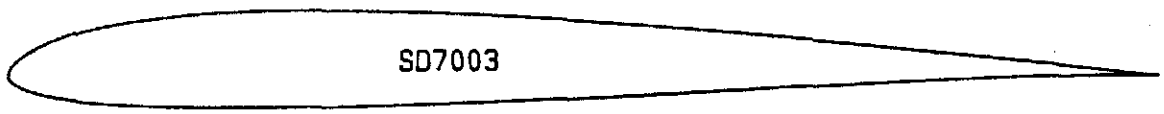

SD7003

1	1.00000	0.00000	17	0.43249	0.05171	33	0.00457	-.00741	49	0.61748	-.01450
2	0.99681	0.00031	18	0.38250	0.05415	34	0.01408	-.01285	50	0.66898	-.01167
3	0.98745	0.00132	19	0.33405	0.05581	35	0.02839	-.01759	51	0.71883	-.00887
4	0.97235	0.00310	20	0.28760	0.05658	36	0.04763	-.02141	52	0.76644	-.00628
5	0.95193	0.00547	21	0.24358	0.05639	37	0.07182	-.02438	53	0.81118	-.00403
6	0.92639	0.00824	22	0.20240	0.05518	38	0.10073	-.02660	54	0.85241	-.00220
7	0.89600	0.01139	23	0.16442	0.05292	39	0.13407	-.02809	55	0.88957	-.00082
8	0.86112	0.01494	24	0.12993	0.04961	40	0.17150	-.02888	56	0.92210	0.00008
9	0.82224	0.01884	25	0.09921	0.04526	41	0.21268	-.02900	57	0.94952	0.00052
10	0.77985	0.02304	26	0.07244	0.03993	42	0.25719	-.02852	58	0.97134	0.00057
11	0.73449	0.02744	27	0.04978	0.03372	43	0.30456	-.02752	59	0.98718	0.00037
12	0.68673	0.03197	28	0.03130	0.02677	44	0.35426	-.02608	60	0.99679	0.00011
13	0.63717	0.03649	29	0.01702	0.01932	45	0.40572	-.02428	61	1.00001	0.00000
14	0.58641	0.04086	30	0.00697	0.01172	46	0.45837	-.02217			
15	0.53499	0.04494	31	0.00127	0.00438	47	0.51161	-.01980			
16	0.48350	0.04859	32	0.00025	-.00186	48	0.56484	-.01723			

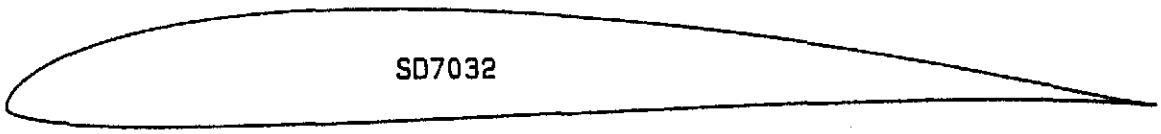

SD7032

1	1.00000	0.00000	17	0.45058	0.08154	33	0.00038	-.00223	49	0.60112	-.00190
2	0.99674	0.00048	18	0.40222	0.08385	34	0.00532	-.00701	50	0.65469	0.00030
3	0.98712	0.00204	19	0.35506	0.08500	35	0.01649	-.01088	51	0.70664	0.00224
4	0.97155	0.00485	20	0.30953	0.08493	36	0.03308	-.01403	52	0.75634	0.00379
5	0.95054	0.00894	21	0.26604	0.08359	37	0.05491	-.01635	53	0.80313	0.00485
6	0.92464	0.01420	22	0.22499	0.08096	38	0.08180	-.01787	54	0.84635	0.00535
7	0.89436	0.02041	23	0.18671	0.07703	39	0.11351	-.01862	55	0.88534	0.00526
8	0.86021	0.02731	24	0.15146	0.07182	40	0.14974	-.01867	56	0.91942	0.00458
9	0.82264	0.03460	25	0.11948	0.06548	41	0.19010	-.01810	57	0.94797	0.00350
10	0.78208	0.04199	26	0.09105	0.05809	42	0.23420	-.01699	58	0.97054	0.00226
11	0.73892	0.04925	27	0.06627	0.04976	43	0.28153	-.01547	59	0.98684	0.00113
12	0.69356	0.05620	28	0.04524	0.04078	44	0.33154	-.01363	60	0.99670	0.00030
13	0.64646	0.06270	29	0.02812	0.03145	45	0.38364	-.01152	61	1.00001	0.00000
14	0.59812	0.06861	30	0.01502	0.02206	46	0.43724	-.00922			
15	0.54902	0.07381	31	0.00606	0.01293	47	0.49176	-.00678			
16	0.49967	0.07816	32	0.00115	0.00448	48	0.54659	-.00430			

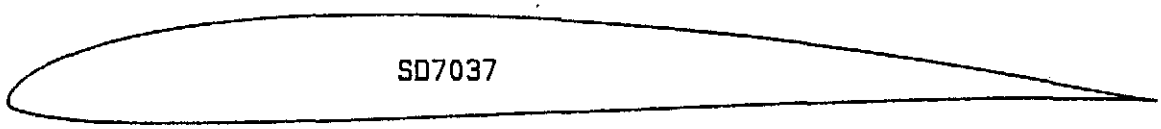

SD7037

1	1.00000	0.00000	17	0.44745	0.07211	33	0.00127	-.00393	49	0.60914	-.00549
2	0.99672	0.00042	18	0.39862	0.07410	34	0.00806	-.00839	50	0.66197	-.00349
3	0.98707	0.00180	19	0.35101	0.07504	35	0.02038	-.01227	51	0.71305	-.00168
4	0.97146	0.00436	20	0.30508	0.07488	36	0.03800	-.01541	52	0.76178	-.00014
5	0.95041	0.00811	21	0.26125	0.07358	37	0.06074	-.01777	53	0.80752	0.00104
6	0.92450	0.01295	22	0.21989	0.07113	38	0.08844	-.01934	54	0.84964	0.00182
7	0.89425	0.01865	23	0.18137	0.06754	39	0.12084	-.02017	55	0.88756	0.00220
8	0.86015	0.02490	24	0.14601	0.06286	40	0.15765	-.02032	56	0.92071	0.00218
9	0.82261	0.03141	25	0.11410	0.05715	41	0.19850	-.01987	57	0.94859	0.00185
10	0.78201	0.03788	26	0.08586	0.05049	42	0.24296	-.01891	58	0.97077	0.00132
11	0.73865	0.04413	27	0.06146	0.04300	43	0.29055	-.01754	59	0.98690	0.00071
12	0.69294	0.05011	28	0.04102	0.03486	44	0.34071	-.01586	60	0.99671	0.00021
13	0.64539	0.05572	29	0.02462	0.02632	45	0.39288	-.01396	61	1.00001	0.00000
14	0.59655	0.06085	30	0.01232	0.01770	46	0.44643	-.01190			
15	0.54693	0.06538	31	0.00418	0.00936	47	0.50074	-.00976			
16	0.49706	0.06917	32	0.00021	0.00185	48	0.55519	-.00760			

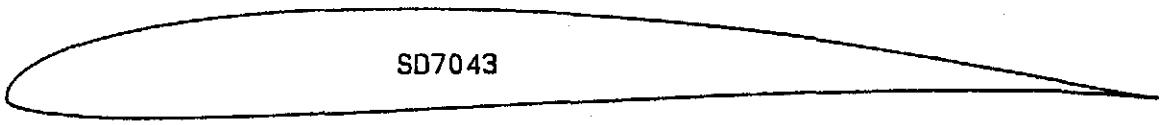

SD7043

1	1.00000	0.00000	17	0.45282	0.07620	33	0.00052	-.00278	49	0.60146	0.00096
2	0.99681	0.00046	18	0.40422	0.07789	34	0.00555	-.00770	50	0.65530	0.00311
3	0.98736	0.00191	19	0.35665	0.07850	35	0.01669	-.01150	51	0.70751	0.00487
4	0.97202	0.00451	20	0.31056	0.07802	36	0.03324	-.01452	52	0.75740	0.00615
5	0.95121	0.00828	21	0.26639	0.07645	37	0.05501	-.01669	53	0.80430	0.00688
6	0.92544	0.01315	22	0.22457	0.07382	38	0.08183	-.01802	54	0.84755	0.00703
7	0.89522	0.01897	23	0.18549	0.07015	39	0.11345	-.01856	55	0.88650	0.00654
8	0.86108	0.02553	24	0.14954	0.06549	40	0.14956	-.01839	56	0.92047	0.00546
9	0.82351	0.03256	25	0.11702	0.05989	41	0.18979	-.01756	57	0.94881	0.00400
10	0.78301	0.03979	26	0.08821	0.05340	42	0.23374	-.01617	58	0.97110	0.00248
11	0.74004	0.04690	27	0.06331	0.04612	43	0.28094	-.01429	59	0.98713	0.00119
12	0.69500	0.05362	28	0.04249	0.03818	44	0.33088	-.01204	60	0.99678	0.00031
13	0.64825	0.05974	29	0.02581	0.02975	45	0.38302	-.00951	61	1.00001	0.00000
14	0.60019	0.06515	30	0.01334	0.02106	46	0.43678	-.00683			
15	0.55127	0.06975	31	0.00509	0.01236	47	0.49153	-.00412			
16	0.50199	0.07347	32	0.00083	0.00404	48	0.54665	-.00148			

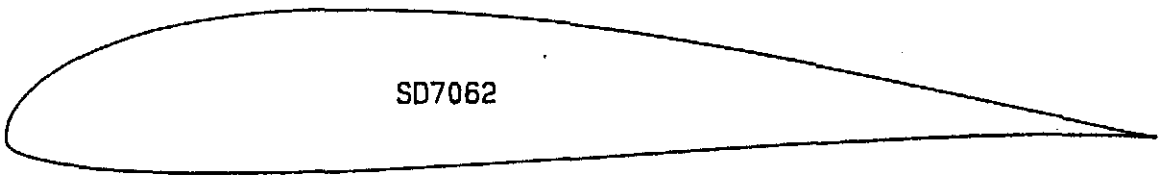

SD7062

1	1.00000	0.00000	17	0.43540	0.10229	33	0.00027	-.00327	49	0.58975	-.01295
2	0.99652	0.00057	18	0.38779	0.10592	34	0.00425	-.01115	50	0.64403	-.00927
3	0.98634	0.00242	19	0.34159	0.10801	35	0.01414	-.01701	51	0.69692	-.00593
4	0.97004	0.00571	20	0.29720	0.10846	36	0.02991	-.02205	52	0.74768	-.00307
5	0.94818	0.01036	21	0.25496	0.10722	37	0.05099	-.02623	53	0.79557	-.00079
6	0.92127	0.01615	22	0.21521	0.10428	38	0.07710	-.02948	54	0.83990	0.00087
7	0.88967	0.02289	23	0.17825	0.09965	39	0.10798	-.03179	55	0.87998	0.00189
8	0.85381	0.03049	24	0.14432	0.09340	40	0.14328	-.03319	56	0.91518	0.00230
9	0.81427	0.03885	25	0.11363	0.08562	41	0.18265	-.03367	57	0.94491	0.00216
10	0.77166	0.04778	26	0.08637	0.07647	42	0.22570	-.03327	58	0.96864	0.00163
11	0.72662	0.05702	27	0.06269	0.06616	43	0.27199	-.03206	59	0.98593	0.00092
12	0.67973	0.06626	28	0.04272	0.05491	44	0.32105	-.03010	60	0.99646	0.00027
13	0.63154	0.07517	29	0.02650	0.04300	45	0.37238	-.02747	61	1.00001	0.00000
14	0.58254	0.08347	30	0.01410	0.03081	46	0.42547	-.02426			
15	0.53322	0.09089	31	0.00562	0.01871	47	0.47979	-.02064			
16	0.48402	0.09723	32	0.00103	0.00711	48	0.53477	-.01680			

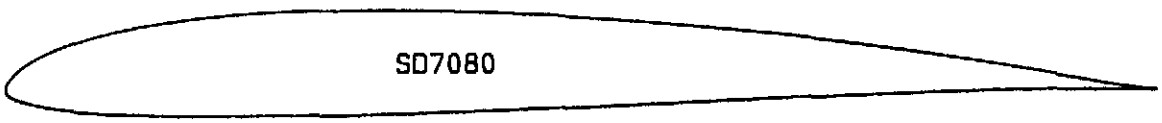

SD7080

1	1.00000	0.00000	17	0.44370	0.06680	33	0.00216	-.00492	49	0.61281	-.01015
2	0.99671	0.00037	18	0.39448	0.06871	34	0.01016	-.00948	50	0.66505	-.00783
3	0.98701	0.00162	19	0.34656	0.06969	35	0.02347	-.01354	51	0.71557	-.00564
4	0.97133	0.00395	20	0.30040	0.06966	36	0.04198	-.01694	52	0.76376	-.00366
5	0.95018	0.00743	21	0.25644	0.06858	37	0.06549	-.01962	53	0.80900	-.00201
6	0.92413	0.01195	22	0.21509	0.06641	38	0.09383	-.02156	54	0.85068	-.00072
7	0.89372	0.01728	23	0.17670	0.06312	39	0.12676	-.02279	55	0.88820	0.00017
8	0.85943	0.02313	24	0.14157	0.05875	40	0.16397	-.02337	56	0.92104	0.00069
9	0.82169	0.02919	25	0.10996	0.05334	41	0.20508	-.02338	57	0.94871	0.00087
10	0.78084	0.03519	26	0.08210	0.04699	42	0.24962	-.02289	58	0.97079	0.00076
11	0.73720	0.04097	27	0.05814	0.03983	43	0.29710	-.02194	59	0.98689	0.00047
12	0.69117	0.04647	28	0.03821	0.03203	44	0.34700	-.02059	60	0.99671	0.00015
13	0.64326	0.05163	29	0.02237	0.02383	45	0.39877	-.01891	61	1.00001	0.00000
14	0.59402	0.05635	30	0.01068	0.01558	46	0.45183	-.01696			
15	0.54399	0.06052	31	0.00322	0.00763	47	0.50559	-.01480			
16	0.49371	0.06404	32	0.00003	0.00061	48	0.55945	-.01250			

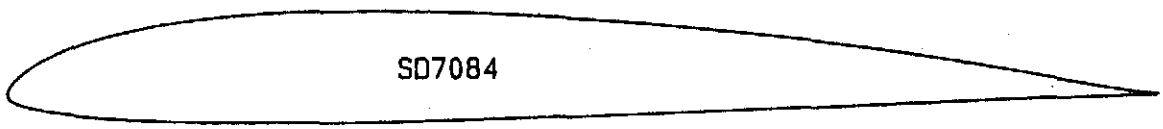

SD7084

1	1.00000	0.00000	17	0.43785	0.06786	33	0.00294	-.00551	49	0.61943	-.01520
2	0.99658	0.00030	18	0.38874	0.06978	34	0.01167	-.01031	50	0.67116	-.01298
3	0.98650	0.00139	19	0.34098	0.07074	35	0.02575	-.01440	51	0.72105	-.01079
4	0.97026	0.00361	20	0.29505	0.07068	36	0.04512	-.01786	52	0.76852	-.00873
5	0.94845	0.00706	21	0.25139	0.06955	37	0.06955	-.02071	53	0.81296	-.00685
6	0.92172	0.01163	22	0.21042	0.06734	38	0.09876	-.02295	54	0.85379	-.00522
7	0.89064	0.01708	23	0.17254	0.06399	39	0.13245	-.02458	55	0.89047	-.00384
8	0.85575	0.02311	24	0.13804	0.05945	40	0.17030	-.02560	56	0.92250	-.00272
9	0.81748	0.02938	25	0.10710	0.05374	41	0.21190	-.02607	57	0.94942	-.00182
10	0.77619	0.03557	26	0.07986	0.04698	42	0.25680	-.02601	58	0.97088	-.00105
11	0.73218	0.04152	27	0.05642	0.03934	43	0.30452	-.02547	59	0.98671	-.00039
12	0.68584	0.04716	28	0.03687	0.03109	44	0.35455	-.02448	60	0.99661	-.00006
13	0.63770	0.05245	29	0.02132	0.02256	45	0.40633	-.02312	61	1.00001	0.00000
14	0.58829	0.05727	30	0.00985	0.01413	46	0.45931	-.02143			
15	0.53815	0.06151	31	0.00263	0.00631	47	0.51289	-.01951			
16	0.48783	0.06508	32	0.00000	-.00016	48	0.56647	-.01741			

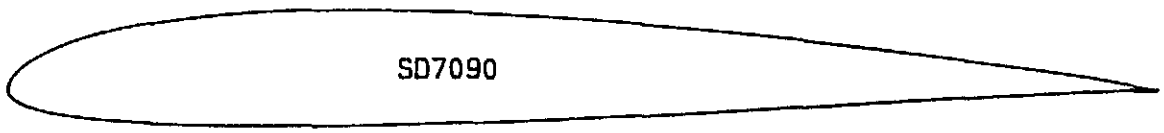

SD7090

1	1.00000	0.00000	17	0.43649	0.06457	33	0.00345	-.00734	49	0.61442	-.01948
2	0.99655	0.00050	18	0.38699	0.06674	34	0.01238	-.01318	50	0.66605	-.01658
3	0.98664	0.00219	19	0.33890	0.06795	35	0.02624	-.01834	51	0.71605	-.01363
4	0.97113	0.00512	20	0.29269	0.06814	36	0.04514	-.02262	52	0.76381	-.01083
5	0.95062	0.00882	21	0.24878	0.06724	37	0.06903	-.02605	53	0.80869	-.00829
6	0.92522	0.01284	22	0.20759	0.06522	38	0.09771	-.02873	54	0.85007	-.00609
7	0.89500	0.01718	23	0.16945	0.06206	39	0.13087	-.03067	55	0.88735	-.00426
8	0.86036	0.02188	24	0.13467	0.05780	40	0.16817	-.03188	56	0.92001	-.00279
9	0.82176	0.02691	25	0.10352	0.05249	41	0.20926	-.03240	57	0.94757	-.00160
10	0.77972	0.03218	26	0.07624	0.04621	42	0.25371	-.03229	58	0.96974	-.00066
11	0.73479	0.03760	27	0.05297	0.03907	43	0.30106	-.03161	59	0.98622	-.00009
12	0.68754	0.04304	28	0.03384	0.03125	44	0.35077	-.03046	60	0.99650	0.00004
13	0.63860	0.04834	29	0.01891	0.02298	45	0.40227	-.02889	61	1.00001	0.00000
14	0.58850	0.05329	30	0.00827	0.01458	46	0.45499	-.02696			
15	0.53777	0.05773	31	0.00196	0.00637	47	0.50832	-.02472			
16	0.48692	0.06153	32	0.00005	-.00097	48	0.56166	-.02221			

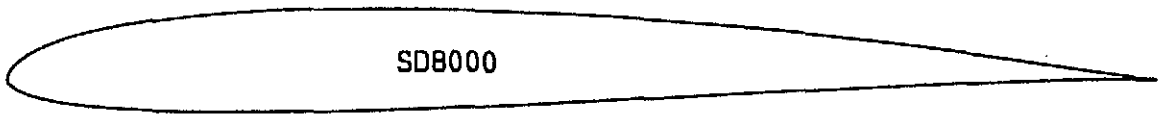

SD8000

1	1.00000	0.00000	17	0.43875	0.05780	33	0.00440	-.00749	49	0.61566	-.01459
2	0.99674	0.00030	18	0.38905	0.05929	34	0.01370	-.01315	50	0.66757	-.01179
3	0.98711	0.00130	19	0.34062	0.05996	35	0.02780	-.01814	51	0.71773	-.00910
4	0.97148	0.00321	20	0.29395	0.05978	36	0.04677	-.02225	52	0.76556	-.00662
5	0.95032	0.00607	21	0.24951	0.05872	37	0.07058	-.02544	53	0.81047	-.00445
6	0.92413	0.00984	22	0.20775	0.05675	38	0.09914	-.02776	54	0.85185	-.00268
7	0.89343	0.01434	23	0.16906	0.05389	39	0.13219	-.02929	55	0.88910	-.00132
8	0.85871	0.01936	24	0.13380	0.05012	40	0.16941	-.03008	56	0.92170	-.00040
9	0.82042	0.02466	25	0.10229	0.04548	41	0.21041	-.03020	57	0.94916	0.00013
10	0.77899	0.03000	26	0.07476	0.04000	42	0.25477	-.02969	58	0.97105	0.00032
11	0.73481	0.03521	27	0.05142	0.03377	43	0.30202	-.02864	59	0.98700	0.00026
12	0.68831	0.04017	28	0.03238	0.02686	44	0.35163	-.02710	60	0.99673	0.00009
13	0.63998	0.04478	29	0.01766	0.01948	45	0.40307	-.02514	61	1.00001	0.00000
14	0.59034	0.04894	30	0.00729	0.01194	46	0.45576	-.02284			
15	0.53991	0.05256	31	0.00136	0.00460	47	0.50913	-.02024			
16	0.48921	0.05553	32	0.00022	-.00175	48	0.56263	-.01744			

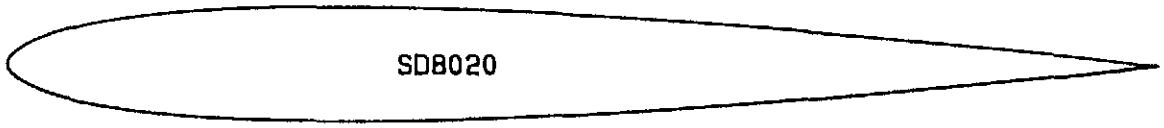

SD8020

1	1.00000	0.00000	17	0.42116	0.04770	33	0.01066	-.01345	49	0.62778	-.03534
2	0.99646	0.00027	18	0.37077	0.04938	34	0.02319	-.02041	50	0.67790	-.03135
3	0.98625	0.00131	19	0.32196	0.05034	35	0.04024	-.02697	51	0.72629	-.02722
4	0.97017	0.00330	20	0.27523	0.05051	36	0.06180	-.03287	52	0.77238	-.02308
5	0.94885	0.00591	21	0.23106	0.04982	37	0.08774	-.03802	53	0.81561	-.01907
6	0.92247	0.00876	22	0.18987	0.04824	38	0.11790	-.04233	54	0.85539	-.01532
7	0.89118	0.01188	23	0.15203	0.04574	39	0.15204	-.04574	55	0.89119	-.01188
8	0.85538	0.01532	24	0.11789	0.04233	40	0.18987	-.04824	56	0.92248	-.00876
9	0.81560	0.01908	25	0.08774	0.03802	41	0.23107	-.04982	57	0.94886	-.00591
10	0.77237	0.02308	26	0.06179	0.03287	42	0.27524	-.05051	58	0.97018	-.00330
11	0.72627	0.02722	27	0.04024	0.02697	43	0.32197	-.05034	59	0.98626	-.00131
12	0.67789	0.03135	28	0.02318	0.02041	44	0.37077	-.04938	60	0.99647	-.00027
13	0.62777	0.03535	29	0.01065	0.01345	45	0.42117	-.04769	61	1.00001	0.00000
14	0.57647	0.03909	30	0.00276	0.00645	46	0.47262	-.04536			
15	0.52456	0.04246	31	0.00000	0.00000	47	0.52457	-.04246			
16	0.47261	0.04536	32	0.00276	-.00645	48	0.57648	-.03908			

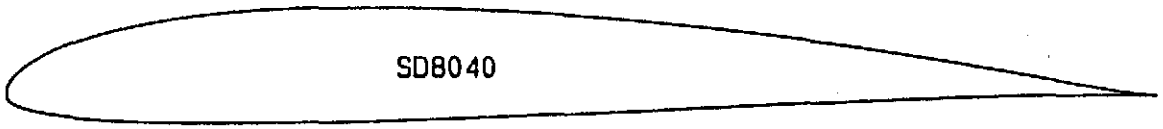

SD8040

1	1.00000	0.00000	17	0.43970	0.07233	33	0.00157	-.00582	49	0.60999	-.01193
2	0.99667	0.00037	18	0.39070	0.07444	34	0.00845	-.01097	50	0.66249	-.00943
3	0.98684	0.00162	19	0.34300	0.07552	35	0.02120	-.01542	51	0.71327	-.00704
4	0.97093	0.00397	20	0.29706	0.07550	36	0.03925	-.01911	52	0.76174	-.00487
5	0.94946	0.00748	21	0.25332	0.07434	37	0.06241	-.02202	53	0.80726	-.00301
6	0.92299	0.01208	22	0.21218	0.07201	38	0.09046	-.02413	54	0.84921	-.00153
7	0.89205	0.01757	23	0.17398	0.06850	39	0.12317	-.02546	55	0.88700	-.00044
8	0.85717	0.02369	24	0.13903	0.06386	40	0.16023	-.02609	56	0.92010	0.00026
9	0.81881	0.03018	25	0.10761	0.05814	41	0.20125	-.02610	57	0.94803	0.00062
10	0.77739	0.03675	26	0.07994	0.05144	42	0.24576	-.02558	58	0.97036	0.00064
11	0.73331	0.04321	27	0.05620	0.04389	43	0.29326	-.02456	59	0.98668	0.00044
12	0.68699	0.04942	28	0.03653	0.03565	44	0.34324	-.02311	60	0.99665	0.00014
13	0.63893	0.05527	29	0.02099	0.02694	45	0.39513	-.02130	61	1.00000	0.00000
14	0.58966	0.06060	30	0.00967	0.01809	46	0.44836	-.01921			
15	0.53969	0.06530	31	0.00271	0.00938	47	0.50232	-.01690			
16	0.48953	0.06925	32	0.00004	0.00101	48	0.55640	-.01445			

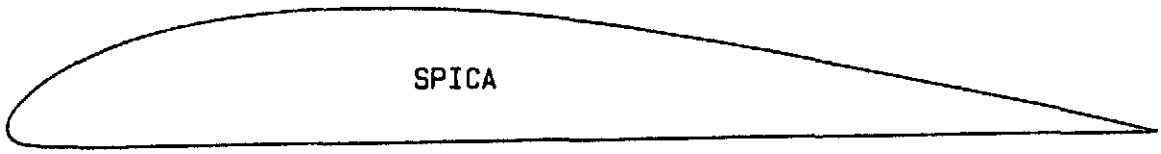

SPICA

1	1.00000	0.00000	14	0.35000	0.10583	27	0.02000	-.01510	40	0.55000	-.00765
2	0.95000	0.01195	15	0.30000	0.10530	28	0.04000	-.01632	41	0.60000	-.00680
3	0.90000	0.02270	16	0.25000	0.10242	29	0.06000	-.01590	42	0.65000	-.00595
4	0.85000	0.03275	17	0.20000	0.09690	30	0.08000	-.01564	43	0.70000	-.00510
5	0.80000	0.04260	18	0.15000	0.08805	31	0.10000	-.01530	44	0.75000	-.00425
6	0.75000	0.05238	19	0.10000	0.07400	32	0.15000	-.01445	45	0.80000	-.00340
7	0.70000	0.06190	20	0.08000	0.06634	33	0.20000	-.01360	46	0.85000	-.00255
8	0.65000	0.07107	21	0.06000	0.05704	34	0.25000	-.01275	47	0.90000	-.00170
9	0.60000	0.07970	22	0.04000	0.04560	35	0.30000	-.01190	48	0.95000	-.00085
10	0.55000	0.08773	23	0.02000	0.03042	36	0.35000	-.01105	49	1.00000	0.00000
11	0.50000	0.09490	24	0.01000	0.02053	37	0.40000	-.01020			
12	0.45000	0.10053	25	0.00000	0.00000	38	0.45000	-.00935			
13	0.40000	0.10415	26	0.01000	-.01280	39	0.50000	-.00850			

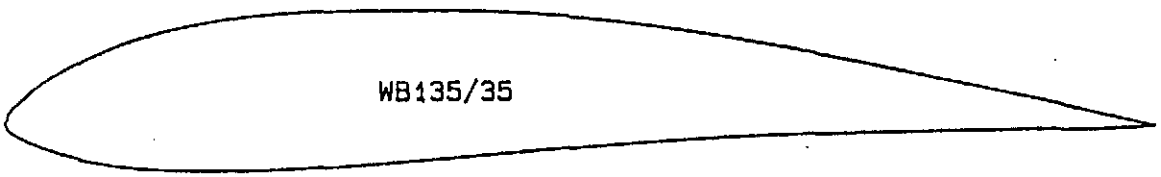

WB135/35

1	1.00000	0.00000	15	0.30000	0.09900	29	0.01250	-.01200	43	0.40000	-.02775
2	0.95000	0.01200	16	0.27500	0.09800	30	0.02500	-.01800	44	0.45000	-.02350
3	0.90000	0.02310	17	0.25000	0.09660	31	0.05000	-.02670	45	0.50000	-.01925
4	0.85000	0.03425	18	0.22500	0.09470	32	0.07500	-.03275	46	0.55000	-.01532
5	0.80000	0.04500	19	0.20000	0.09200	33	0.10000	-.03685	47	0.60000	-.01200
6	0.75000	0.05510	20	0.17500	0.08825	34	0.12500	-.03930	48	0.65000	-.00940
7	0.70000	0.06465	21	0.15000	0.08325	35	0.15000	-.04050	49	0.70000	-.00750
8	0.65000	0.07360	22	0.12500	0.07700	36	0.17500	-.04085	50	0.75000	-.00600
9	0.60000	0.08175	23	0.10000	0.06915	37	0.20000	-.04060	51	0.80000	-.00500
10	0.55000	0.08875	24	0.07500	0.05900	38	0.22500	-.03995	52	0.85000	-.00400
11	0.50000	0.09425	25	0.05000	0.04650	39	0.25000	-.03890	53	0.90000	-.00325
12	0.45000	0.09790	26	0.02500	0.03000	40	0.27500	-.03750	54	0.95000	-.00250
13	0.40000	0.09975	27	0.01250	0.01875	41	0.30000	-.03575	55	1.00000	0.00000
14	0.35000	0.10000	28	0.00000	0.00000	42	0.35000	-.03185			

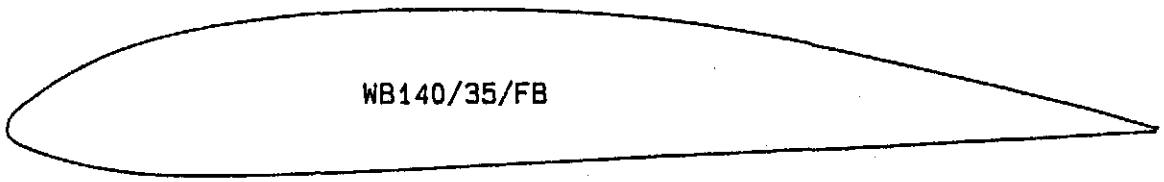

WB140/35/FB

1	1.00000	0.00250	15	0.30000	0.10225	29	0.01250	-.01350	43	0.40000	-.03225
2	0.95000	0.01475	16	0.27500	0.10050	30	0.02500	-.01800	44	0.45000	-.02975
3	0.90000	0.02775	17	0.25000	0.09775	31	0.05000	-.02650	45	0.50000	-.02750
4	0.85000	0.04000	18	0.22500	0.09550	32	0.07500	-.03275	46	0.55000	-.02475
5	0.80000	0.05150	19	0.20000	0.09225	33	0.10000	-.03675	47	0.60000	-.02275
6	0.75000	0.06275	20	0.17500	0.08830	34	0.12500	-.03950	48	0.65000	-.02050
7	0.70000	0.07100	21	0.15000	0.08325	35	0.15000	-.04050	49	0.70000	-.01800
8	0.65000	0.08300	22	0.12500	0.07700	36	0.17500	-.04075	50	0.75000	-.01575
9	0.60000	0.09100	23	0.10000	0.06950	37	0.17500	-.04050	51	0.80000	-.01300
10	0.55000	0.09725	24	0.07500	0.05900	38	0.22500	-.04025	52	0.85000	-.01025
11	0.50000	0.10125	25	0.05000	0.04630	39	0.25000	-.03950	53	0.90000	-.00800
12	0.45000	0.10365	26	0.02500	0.03000	40	0.27500	-.03800	54	0.95000	-.00500
13	0.40000	0.10450	27	0.01250	0.01875	41	0.30000	-.03700	55	1.00000	-.00250
14	0.35000	0.10450	28	0.00000	0.00000	42	0.35000	-.03475			

AQUILA-PT

1	1.00000	0.00000	12	0.69655	0.04901	23	0.01583	0.02617	34	0.53849	-.00721
2	0.99746	0.00123	13	0.62461	0.06080	24	0.00659	0.01576	35	0.70417	-.00651
3	0.98829	0.00238	14	0.54502	0.07190	25	0.00169	0.00753	36	0.79285	-.00587
4	0.97400	0.00453	15	0.49234	0.07805	26	0.00000	0.00000	37	0.83603	-.00546
5	0.94486	0.00884	16	0.39368	0.08685	27	0.00106	-.00259	38	0.88509	-.00464
6	0.90040	0.01570	17	0.31264	0.08876	28	0.00435	-.00553	39	0.94190	-.00375
7	0.86567	0.02142	18	0.23528	0.08634	29	0.01274	-.00714	40	0.97800	-.00237
8	0.83894	0.02575	19	0.14185	0.07430	30	0.05262	-.00657	41	0.99740	-.00083
9	0.82217	0.02951	20	0.07922	0.05817	31	0.13491	-.00665	42	1.00000	0.00000
10	0.80749	0.03199	21	0.04595	0.04561	32	0.24506	-.00748			
11	0.76590	0.03831	22	0.02491	0.03337	33	0.38540	-.00767			

CLARK-Y-PT

1	1.00000	0.00000	12	0.40164	0.09016	23	0.00000	0.00000	34	0.45718	-.02187
2	0.99331	0.00318	13	0.31229	0.09013	24	0.00066	-.00621	35	0.54165	-.01896
3	0.98501	0.00568	14	0.23278	0.08569	25	0.00347	-.01067	36	0.62167	-.01618
4	0.96357	0.01071	15	0.16999	0.07741	26	0.00625	-.01289	37	0.70704	-.01307
5	0.93418	0.01676	16	0.11136	0.06409	27	0.01978	-.01848	38	0.78060	-.01024
6	0.88972	0.02590	17	0.06646	0.04852	28	0.04312	-.02394	39	0.84337	-.00792
7	0.82686	0.03854	18	0.03795	0.03506	29	0.08548	-.02908	40	0.90607	-.00552
8	0.74751	0.05340	19	0.02528	0.02806	30	0.14826	-.03144	41	0.94727	-.00385
9	0.65555	0.06802	20	0.01684	0.02286	31	0.24816	-.02951	42	0.96663	-.00314
10	0.59641	0.07581	21	0.00670	0.01362	32	0.31864	-.02690	43	0.98544	-.00229
11	0.49368	0.08578	22	0.00382	0.00999	33	0.37724	-.02485	44	1.00000	0.00000

DAE51-PT

1	1.00000	0.00000	14	0.52542	0.08215	27	0.00000	0.00000	40	0.55527	-.00064
2	0.99975	0.00067	15	0.45825	0.08683	28	0.00130	-.00460	41	0.61490	0.00117
3	0.99430	0.00208	16	0.38900	0.08866	29	0.00375	-.00769	42	0.66395	0.00211
4	0.98966	0.00322	17	0.32284	0.08807	30	0.01053	-.01070	43	0.72358	0.00288
5	0.97928	0.00553	18	0.25556	0.08444	31	0.02248	-.01238	44	0.78351	0.00383
6	0.95178	0.01143	19	0.19912	0.07759	32	0.06617	-.01510	45	0.84305	0.00396
7	0.92545	0.01685	20	0.14456	0.06774	33	0.12056	-.01619	46	0.89405	0.00375
8	0.89329	0.02329	21	0.09622	0.05531	34	0.17815	-.01470	47	0.93910	0.00247
9	0.84249	0.03356	22	0.05931	0.04165	35	0.24055	-.01200	48	0.97895	0.00027
10	0.79090	0.04364	23	0.03216	0.02863	36	0.29820	-.00968	49	0.99236	-.00056
11	0.73471	0.05409	24	0.01887	0.02138	37	0.36264	-.00700	50	0.99603	-.00073
12	0.66160	0.06607	25	0.00891	0.01506	38	0.43373	-.00442	51	0.99935	-.00034
13	0.59105	0.07520	26	0.00167	0.00694	39	0.49162	-.00250	52	1.00000	0.00000

DF101-PT

1	1.00000	0.00000	14	0.32064	0.07634	27	0.00000	0.00000	40	0.53354	-.02684
2	0.99390	0.00111	15	0.25879	0.07510	28	0.00235	-.00593	41	0.60846	-.02337
3	0.97698	0.00417	16	0.17826	0.07096	29	0.00764	-.00991	42	0.67731	-.02003
4	0.95507	0.00770	17	0.13250	0.06429	30	0.02123	-.01570	43	0.75184	-.01683
5	0.92393	0.01245	18	0.10424	0.05844	31	0.03554	-.02007	44	0.81039	-.01366
6	0.88698	0.01848	19	0.08069	0.05238	32	0.06937	-.02811	45	0.85031	-.01199
7	0.83138	0.02780	20	0.05829	0.04483	33	0.11253	-.03378	46	0.89796	-.00994
8	0.77287	0.03677	21	0.03522	0.03436	34	0.16135	-.03677	47	0.92453	-.00885
9	0.71380	0.04498	22	0.02415	0.02767	35	0.22347	-.03800	48	0.94743	-.00665
10	0.64510	0.05379	23	0.01375	0.02014	36	0.29035	-.03647	49	0.97110	-.00402
11	0.58169	0.06157	24	0.00652	0.01346	37	0.36835	-.03394	50	0.98967	-.00229
12	0.49163	0.06980	25	0.00326	0.00920	38	0.42578	-.03165	51	0.99933	-.00083
13	0.40111	0.07482	26	0.00062	0.00373	39	0.48012	-.02940	52	1.00000	0.00000

DF102-PT

1	1.00000	0.00000	14	0.38465	0.07591	27	0.00067	-.00184	40	0.69649	-.01907
2	0.99758	0.00023	15	0.30177	0.07723	28	0.00507	-.00659	41	0.78261	-.01512
3	0.98684	0.00242	16	0.23713	0.07552	29	0.01516	-.01135	42	0.85031	-.01190
4	0.95862	0.00673	17	0.18776	0.07312	30	0.02851	-.01607	43	0.88932	-.01043
5	0.92933	0.01107	18	0.13114	0.06848	31	0.04978	-.02193	44	0.91774	-.00921
6	0.92050	0.01242	19	0.08774	0.06029	32	0.09129	-.02959	45	0.93667	-.00739
7	0.90822	0.01428	20	0.04747	0.04620	33	0.15210	-.03461	46	0.95726	-.00519
8	0.84695	0.02491	21	0.02653	0.03504	34	0.21567	-.03645	47	0.97224	-.00346
9	0.77960	0.03587	22	0.01628	0.02758	35	0.29604	-.03502	48	0.98520	-.00227
10	0.71918	0.04438	23	0.00930	0.02087	36	0.37094	-.03256	49	0.99197	-.00153
11	0.64174	0.05446	24	0.00374	0.01266	37	0.47468	-.02853	50	0.99915	-.00015
12	0.55087	0.06519	25	0.00122	0.00638	38	0.56072	-.02472	51	1.00000	0.00000
13	0.46035	0.07269	26	0.00000	0.00000	39	0.62900	-.02171			

DF103-PT

1	1.00000	0.00000	14	0.52020	0.06842	27	0.00531	-.00817	40	0.63510	-.02182
2	0.99839	0.00062	15	0.44983	0.07362	28	0.01343	-.01256	41	0.71830	-.01817
3	0.99344	0.00171	16	0.38151	0.07602	29	0.02464	-.01705	42	0.78521	-.01512
4	0.98725	0.00280	17	0.32115	0.07665	30	0.04527	-.02263	43	0.85325	-.01255
5	0.96137	0.00654	18	0.24545	0.07458	31	0.07923	-.02935	44	0.91451	-.01044
6	0.93023	0.01087	19	0.18323	0.06800	32	0.13321	-.03500	45	0.95585	-.00628
7	0.90275	0.01514	20	0.12250	0.05787	33	0.17245	-.03677	46	0.97433	-.00387
8	0.85245	0.02447	21	0.07474	0.04478	34	0.22188	-.03747	47	0.98913	-.00221
9	0.80273	0.03286	22	0.03718	0.02933	35	0.28975	-.03580	48	0.99488	-.00152
10	0.76033	0.03902	23	0.01256	0.01611	36	0.35733	-.03383	49	1.00000	0.00000
11	0.70203	0.04757	24	0.00321	0.00764	37	0.41728	-.03145			
12	0.64366	0.05501	25	0.00000	0.00000	38	0.48896	-.02828			
13	0.57978	0.06266	26	0.00156	-.00456	39	0.55877	-.02525			

E193-PT

1	1.00000	0.00000	13	0.27865	0.08034	25	0.00456	-.01003	37	0.65450	-.01572
2	0.99023	0.00405	14	0.20590	0.07308	26	0.00985	-.01329	38	0.71890	-.01389
3	0.97498	0.00611	15	0.14176	0.06289	27	0.02631	-.01865	39	0.78023	-.01202
4	0.93975	0.01077	16	0.09505	0.05207	28	0.04653	-.02292	40	0.83702	-.01017
5	0.89354	0.01779	17	0.06074	0.04109	29	0.07208	-.02609	41	0.89421	-.00805
6	0.83149	0.02758	18	0.03087	0.02759	30	0.11861	-.02836	42	0.94810	-.00549
7	0.76683	0.03764	19	0.01476	0.01771	31	0.17130	-.02823	43	0.97647	-.00358
8	0.69587	0.04856	20	0.00706	0.01178	32	0.24998	-.02677	44	0.98762	-.00276
9	0.62046	0.05987	21	0.00393	0.00830	33	0.33658	-.02493	45	1.00000	0.00000
10	0.53249	0.07139	22	0.00000	0.00000	34	0.41345	-.02258			
11	0.45255	0.07866	23	0.00019	-.00180	35	0.49857	-.01992			
12	0.35820	0.08223	24	0.00203	-.00710	36	0.57412	-.01772			

E193MOD-PT

1	1.00000	0.00000	13	0.45924	0.09504	25	0.00000	0.00000	37	0.63667	-.00873
2	0.99907	0.00064	14	0.36710	0.09833	26	0.00084	-.00407	38	0.70790	-.00605
3	0.98843	0.00324	15	0.29461	0.09617	27	0.00439	-.00889	39	0.77809	-.00424
4	0.97482	0.00632	16	0.22483	0.08943	28	0.01121	-.01345	40	0.84996	-.00253
5	0.94788	0.01228	17	0.16040	0.07729	29	0.02597	-.01863	41	0.89347	-.00139
6	0.90833	0.02074	18	0.11756	0.06602	30	0.06100	-.02433	42	0.94238	-.00081
7	0.86791	0.02918	19	0.07718	0.05206	31	0.11235	-.02792	43	0.97287	-.00049
8	0.80730	0.04178	20	0.04951	0.04070	32	0.19187	-.02840	44	0.99393	-.00065
9	0.74614	0.05414	21	0.02619	0.02915	33	0.27519	-.02613	45	0.99859	-.00069
10	0.68386	0.06618	22	0.01556	0.02133	34	0.36103	-.02234	46	1.00000	0.00000
11	0.61843	0.07721	23	0.00687	0.01291	35	0.45198	-.01730			
12	0.53910	0.08802	24	0.00149	0.00573	36	0.54395	-.01267			

E205A-PT

1	1.00000	0.00000	14	0.46089	0.07496	27	0.00070	-.00391	40	0.64824	-.01480
2	0.99926	0.00143	15	0.40011	0.08003	28	0.00230	-.00675	41	0.71250	-.01289
3	0.99537	0.00217	16	0.33678	0.08233	29	0.00852	-.01119	42	0.77621	-.01119
4	0.99118	0.00289	17	0.26549	0.08061	30	0.01952	-.01539	43	0.85231	-.00929
5	0.98606	0.00419	18	0.20528	0.07572	31	0.04302	-.02077	44	0.92416	-.00680
6	0.96215	0.00749	19	0.15044	0.06819	32	0.08976	-.02546	45	0.97037	-.00430
7	0.90880	0.01469	20	0.10372	0.05801	33	0.13152	-.02659	46	0.98277	-.00303
8	0.86509	0.02076	21	0.06079	0.04462	34	0.19372	-.02653	47	0.98881	-.00223
9	0.78619	0.03254	22	0.03498	0.03315	35	0.26049	-.02537	48	0.99352	-.00150
10	0.71377	0.04265	23	0.01856	0.02293	36	0.32690	-.02360	49	0.99758	-.00083
11	0.64768	0.05142	24	0.00813	0.01411	37	0.40729	-.02150	50	1.00000	0.00000
12	0.59147	0.05923	25	0.00234	0.00719	38	0.49880	-.01879			
13	0.52519	0.06792	26	0.00000	0.00000	39	0.57345	-.01676			

E205B-PT

1	1.00000	0.00000	15	0.53232	0.06738	29	0.00000	0.00000	43	0.63816	-.01012
2	0.99974	0.00085	16	0.48264	0.07291	30	0.00089	-.00334	44	0.69937	-.00831
3	0.99392	0.00159	17	0.44197	0.07676	31	0.00310	-.00596	45	0.75692	-.00681
4	0.98578	0.00307	18	0.38814	0.08039	32	0.00816	-.00968	46	0.82133	-.00505
5	0.97290	0.00499	19	0.32774	0.08186	33	0.01807	-.01343	47	0.87969	-.00361
6	0.94617	0.00876	20	0.26612	0.08023	34	0.03718	-.01680	48	0.92076	-.00233
7	0.91866	0.01274	21	0.21066	0.07548	35	0.07273	-.02114	49	0.96116	-.00099
8	0.88020	0.01864	22	0.14521	0.06478	36	0.13766	-.02413	50	0.98546	-.00048
9	0.83393	0.02611	23	0.09684	0.05300	37	0.20297	-.02449	51	0.98991	-.00068
10	0.79263	0.03228	24	0.06230	0.04164	38	0.26877	-.02305	52	0.99485	-.00044
11	0.73829	0.04008	25	0.04043	0.03241	39	0.34581	-.02057	53	0.99873	-.00063
12	0.68535	0.04742	26	0.02021	0.02210	40	0.42989	-.01762	54	1.00000	0.00000
13	0.63333	0.05440	27	0.01003	0.01499	41	0.49449	-.01526			
14	0.58021	0.06127	28	0.00152	0.00614	42	0.56883	-.01258			

E214A-PT

1	1.00000	0.00000	13	0.44143	0.08968	25	0.00000	0.00000	37	0.47023	-.01310
2	0.98921	0.00291	14	0.38189	0.09096	26	0.00033	-.00410	38	0.54246	-.00767
3	0.97156	0.00721	15	0.30797	0.08894	27	0.00063	-.00507	39	0.60567	-.00311
4	0.94593	0.01344	16	0.24597	0.08367	28	0.00418	-.00905	40	0.65865	0.00037
5	0.91110	0.02168	17	0.19136	0.07663	29	0.01395	-.01253	41	0.71106	0.00250
6	0.86106	0.03257	18	0.13199	0.06536	30	0.03006	-.01639	42	0.78073	0.00530
7	0.80668	0.04368	19	0.08756	0.05249	31	0.06052	-.02078	43	0.85444	0.00629
8	0.75150	0.05474	20	0.05881	0.04195	32	0.09479	-.02275	44	0.91581	0.00511
9	0.68560	0.06613	21	0.03272	0.02927	33	0.15454	-.02370	45	0.95562	0.00337
10	0.61533	0.07584	22	0.01429	0.01748	34	0.22884	-.02353	46	0.97958	0.00146
11	0.53834	0.08344	23	0.00723	0.01156	35	0.31157	-.02165	47	0.99116	-.00013
12	0.49264	0.08723	24	0.00246	0.00572	36	0.38703	-.01842	48	1.00000	0.00000

E214C-PT

1	1.00000	0.00000	14	0.74722	0.05912	27	0.00197	0.00620	40	0.69869	0.00535
2	0.99655	0.00141	15	0.74147	0.05939	28	0.00000	0.00000	41	0.76251	0.00846
3	0.99284	0.00303	16	0.73699	0.06017	29	0.00048	-.00258	42	0.77662	0.01014
4	0.98588	0.00572	17	0.70930	0.06458	30	0.00407	-.00709	43	0.79801	0.01166
5	0.95318	0.01654	18	0.59339	0.07982	31	0.01143	-.01086	44	0.81510	0.01110
6	0.90743	0.02863	19	0.49886	0.08847	32	0.02611	-.01491	45	0.84045	0.01110
7	0.85807	0.04006	20	0.37788	0.09241	33	0.07150	-.01977	46	0.87890	0.01069
8	0.82377	0.04717	21	0.28427	0.08863	34	0.13117	-.02223	47	0.92625	0.00763
9	0.81466	0.04885	22	0.21392	0.08093	35	0.20579	-.02260	48	0.96317	0.00317
10	0.80921	0.04985	23	0.14102	0.06849	36	0.32076	-.02002	49	0.98393	0.00053
11	0.80160	0.05061	24	0.06897	0.04741	37	0.44292	-.01278	50	0.99173	-.00042
12	0.76784	0.05523	25	0.02548	0.02647	38	0.55176	-.00430	51	0.99848	-.00106
13	0.75295	0.05802	26	0.00783	0.01291	39	0.64112	0.00192	52	1.00000	0.00000

E374A-PT

1	1.00000	0.00000	13	0.43932	0.07641	25	0.00305	-.00617	37	0.77048	-.01312
2	0.99956	0.00082	14	0.36181	0.07807	26	0.01036	-.01040	38	0.86019	-.00700
3	0.99459	0.00150	15	0.26789	0.07440	27	0.02689	-.01573	39	0.89877	-.00448
4	0.98587	0.00275	16	0.19237	0.06652	28	0.05618	-.02161	40	0.95261	-.00171
5	0.97104	0.00474	17	0.12583	0.05501	29	0.10183	-.02669	41	0.98133	-.00108
6	0.93069	0.01135	18	0.07677	0.04263	30	0.15093	-.02928	42	0.99182	-.00106
7	0.87735	0.02077	19	0.04590	0.03197	31	0.23526	-.03114	43	0.99570	-.00097
8	0.82139	0.02989	20	0.02563	0.02254	32	0.33725	-.03114	44	0.99768	-.00086
9	0.74877	0.04103	21	0.01233	0.01442	33	0.41827	-.03024	45	1.00000	0.00000
10	0.67132	0.05230	22	0.00357	0.00694	34	0.50423	-.02782			
11	0.59367	0.06283	23	0.00000	0.00000	35	0.59964	-.02386			
12	0.51772	0.07109	24	0.00058	-.00284	36	0.67810	-.01950			

E374B-PT

1	1.00000	0.00000	13	0.41722	0.07679	25	0.00454	-.00782	37	0.61172	-.02648
2	0.99993	0.00129	14	0.32904	0.07653	26	0.00927	-.01061	38	0.69039	-.02253
3	0.99430	0.00219	15	0.25364	0.07226	27	0.02052	-.01485	39	0.74960	-.01882
4	0.98514	0.00343	16	0.19283	0.06574	28	0.04315	-.02037	40	0.81443	-.01408
5	0.95128	0.00869	17	0.14024	0.05709	29	0.08539	-.02657	41	0.87169	-.00935
6	0.89135	0.01837	18	0.09328	0.04642	30	0.13467	-.03042	42	0.92030	-.00541
7	0.83110	0.02791	19	0.05724	0.03532	31	0.19350	-.03260	43	0.96395	-.00203
8	0.76815	0.03752	20	0.02726	0.02246	32	0.25247	-.03349	44	0.98292	-.00105
9	0.70590	0.04674	21	0.00983	0.01222	33	0.30895	-.03356	45	0.99096	-.00098
10	0.63671	0.05655	22	0.00219	0.00528	34	0.37453	-.03294	46	0.99772	-.00096
11	0.56544	0.06553	23	0.00000	0.00000	35	0.45910	-.03128	47	1.00000	0.00000
12	0.49001	0.07283	24	0.00090	-.00379	36	0.53883	-.02915			

E387A-PT

1	1.00000	0.00000	14	0.51616	0.06899	27	0.00000	0.00000	40	0.55808	-.00313
2	0.99924	0.00006	15	0.42894	0.07624	28	0.00013	-.00191	41	0.66477	-.00022
3	0.99533	0.00083	16	0.35996	0.07840	29	0.00069	-.00344	42	0.71808	0.00098
4	0.99099	0.00146	17	0.28899	0.07685	30	0.00192	-.00504	43	0.80195	0.00237
5	0.98425	0.00252	18	0.22957	0.07237	31	0.00540	-.00717	44	0.86350	0.00256
6	0.95748	0.00650	19	0.17031	0.06483	32	0.01115	-.00909	45	0.92373	0.00200
7	0.91799	0.01244	20	0.11571	0.05454	33	0.01982	-.01116	46	0.95595	0.00125
8	0.86352	0.02039	21	0.07836	0.04485	34	0.03719	-.01407	47	0.97517	0.00074
9	0.81249	0.02810	22	0.05443	0.03663	35	0.08786	-.01734	48	0.98369	0.00050
10	0.76066	0.03570	23	0.03539	0.02851	36	0.14326	-.01736	49	0.99004	0.00034
11	0.70352	0.04423	24	0.01771	0.01825	37	0.24611	-.01467	50	0.99546	0.00023
12	0.65172	0.05179	25	0.00888	0.01173	38	0.32673	-.01180	51	0.99789	0.00017
13	0.58767	0.06062	26	0.00339	0.00657	39	0.45261	-.00680	52	1.00000	0.00000

E387B-PT

1	1.00000	0.00000	13	0.47124	0.06943	25	0.00380	-.00669	37	0.63885	-.00583
2	0.99939	0.00097	14	0.37851	0.07326	26	0.00999	-.01023	38	0.71691	-.00548
3	0.99336	0.00137	15	0.29601	0.07379	27	0.02603	-.01471	39	0.75201	-.00489
4	0.98178	0.00244	16	0.21432	0.06883	28	0.05012	-.01874	40	0.80627	-.00381
5	0.95621	0.00540	17	0.14550	0.05900	29	0.09227	-.02218	41	0.85747	-.00376
6	0.91962	0.00938	18	0.08724	0.04501	30	0.15840	-.02327	42	0.90475	-.00380
7	0.87744	0.01463	19	0.05087	0.03312	31	0.22554	-.02082	43	0.94168	-.00295
8	0.82622	0.02133	20	0.02446	0.02177	32	0.29099	-.01859	44	0.97236	-.00170
9	0.75981	0.03170	21	0.01131	0.01339	33	0.37263	-.01471	45	0.98821	-.00091
10	0.70153	0.04153	22	0.00234	0.00503	34	0.42928	-.01243	46	0.99700	-.00066
11	0.64244	0.04991	23	0.00000	0.00000	35	0.50854	-.00893	47	1.00000	0.00000
12	0.56611	0.06005	24	0.00033	-.00174	36	0.56905	-.00730			

FX60-100-PT

1	1.00000	0.00000	13	0.34272	0.07591	25	0.01074	-.00661	37	0.74044	0.00933
2	0.99688	0.00165	14	0.25878	0.07372	26	0.02520	-.01134	38	0.80264	0.01050
3	0.98950	0.00376	15	0.19079	0.06850	27	0.04846	-.01755	39	0.85934	0.00954
4	0.97472	0.00688	16	0.11598	0.05724	28	0.07737	-.02247	40	0.92032	0.00634
5	0.93436	0.01377	17	0.06298	0.04375	29	0.12022	-.02616	41	0.95073	0.00320
6	0.87379	0.02331	18	0.04045	0.03461	30	0.17811	-.02773	42	0.97458	0.00085
7	0.82271	0.03192	19	0.02559	0.02633	31	0.24832	-.02641	43	0.98818	-.00027
8	0.74795	0.04377	20	0.01154	0.01627	32	0.35046	-.02044	44	0.99654	-.00092
9	0.67207	0.05472	21	0.00387	0.00900	33	0.42369	-.01382	45	1.00000	0.00000
10	0.57258	0.06558	22	0.00000	0.00000	34	0.50757	-.00549			
11	0.49431	0.07207	23	0.00047	-.00153	35	0.57619	0.00036			
12	0.42133	0.07508	24	0.00454	-.00463	36	0.65564	0.00596			

FX63-137B-PT (local slight bulge on lower surface near endplate)

1	1.00000	0.00000	14	0.37524	0.12111	27	0.00675	-.01148	40	0.70945	0.01889
2	0.99813	0.00273	15	0.28888	0.11925	28	0.01140	-.01432	41	0.79234	0.02205
3	0.99524	0.00403	16	0.21585	0.11169	29	0.01857	-.01727	42	0.86207	0.02006
4	0.99004	0.00599	17	0.14628	0.09767	30	0.03606	-.02178	43	0.91819	0.01416
5	0.97848	0.00989	18	0.10000	0.08367	31	0.06990	-.02781	44	0.95596	0.00762
6	0.94758	0.01889	19	0.06262	0.06835	32	0.11115	-.03047	45	0.97732	0.00321
7	0.90432	0.03103	20	0.03783	0.05437	33	0.15725	-.02833	46	0.99003	0.00034
8	0.83405	0.05027	21	0.01623	0.03577	34	0.20042	-.02754	47	0.99535	-.00083
9	0.76242	0.06743	22	0.00468	0.01975	35	0.28516	-.02414	48	0.99817	-.00141
10	0.68583	0.08408	23	0.00118	0.01032	36	0.36884	-.01684	49	1.00000	0.00000
11	0.60394	0.09972	24	0.00000	0.00000	37	0.45637	-.00716			
12	0.53476	0.10971	25	0.00160	-.00614	38	0.53717	0.00236			
13	0.45272	0.11760	26	0.00333	-.00861	39	0.63054	0.01208			

FX63-137B-PT (these coordinates used in plots given in Chapters 10 and 11)

1	1.00000	0.00000	14	0.49999	0.11363	27	0.00438	-.01147	40	0.59311	0.00682
2	0.99840	0.00244	15	0.43566	0.11855	28	0.01227	-.01669	41	0.65128	0.01304
3	0.99093	0.00525	16	0.36648	0.12072	29	0.02323	-.02029	42	0.69668	0.01722
4	0.97998	0.00914	17	0.29955	0.11902	30	0.04263	-.02406	43	0.74790	0.02021
5	0.96160	0.01489	18	0.23771	0.11343	31	0.07505	-.02797	44	0.78942	0.02129
6	0.92836	0.02478	19	0.17228	0.10221	32	0.12658	-.02927	45	0.82510	0.02089
7	0.88226	0.03794	20	0.12362	0.08959	33	0.18910	-.02901	46	0.86695	0.01920
8	0.83638	0.05017	21	0.08139	0.07484	34	0.25427	-.02696	47	0.90673	0.01549
9	0.79653	0.06001	22	0.04291	0.05552	35	0.31387	-.02330	48	0.95148	0.00796
10	0.74843	0.07127	23	0.01780	0.03516	36	0.37828	-.01728	49	0.97197	0.00378
11	0.70056	0.08163	24	0.00364	0.01477	37	0.42888	-.01159	50	0.98807	0.00018
12	0.63881	0.09386	25	0.00000	0.00000	38	0.48085	-.00562	51	0.99601	-.00142
13	0.56897	0.10530	26	0.00106	-.00654	39	0.53463	-.00015	52	1.00000	0.00000

HQ2/9A-PT

1	1.00000	0.00000	16	0.34245	0.06269	31	0.00000	0.00000	46	0.46945	-.02512
2	0.99158	0.00215	17	0.28758	0.06153	32	0.00044	-.00295	47	0.53267	-.02127
3	0.98204	0.00376	18	0.23277	0.05880	33	0.00233	-.00624	48	0.59521	-.01704
4	0.96502	0.00638	19	0.17088	0.05353	34	0.00723	-.01110	49	0.64950	-.01323
5	0.92908	0.01202	20	0.12035	0.04675	35	0.01070	-.01357	50	0.70060	-.00953
6	0.88623	0.01833	21	0.09294	0.04171	36	0.01479	-.01578	51	0.74808	-.00638
7	0.84235	0.02457	22	0.07273	0.03726	37	0.02728	-.01990	52	0.79130	-.00336
8	0.77859	0.03310	23	0.04864	0.03059	38	0.04396	-.02258	53	0.84243	-.00082
9	0.74410	0.03727	24	0.03793	0.02692	39	0.07704	-.02577	54	0.88326	0.00080
10	0.69008	0.04352	25	0.02898	0.02335	40	0.11918	-.02841	55	0.91782	0.00095
11	0.65019	0.04776	26	0.02140	0.01977	41	0.17539	-.03054	56	0.94303	0.00044
12	0.60357	0.05209	27	0.01261	0.01459	42	0.23448	-.03127	57	0.96638	0.00021
13	0.53121	0.05743	28	0.00679	0.00997	43	0.28428	-.03103	58	0.97660	0.00013
14	0.46829	0.06063	29	0.00124	0.00369	44	0.34963	-.02992	59	0.99028	-.00017
15	0.40805	0.06243	30	0.00031	0.00171	45	0.40448	-.02811	60	1.00000	0.00000

HQ2/9B-PT

1	1.00000	0.00000	13	0.52797	0.05897	25	0.00415	-.00779	37	0.57808	-.01613
2	0.99873	0.00098	14	0.45504	0.06271	26	0.01004	-.01185	38	0.67584	-.00976
3	0.99320	0.00190	15	0.36556	0.06416	27	0.01770	-.01519	39	0.76389	-.00426
4	0.98771	0.00286	16	0.29318	0.06305	28	0.03004	-.01822	40	0.84803	0.00018
5	0.97217	0.00549	17	0.19551	0.05717	29	0.05650	-.02158	41	0.90593	0.00103
6	0.93095	0.01197	18	0.12338	0.04821	30	0.09563	-.02464	42	0.95164	0.00006
7	0.87289	0.02068	19	0.07332	0.03797	31	0.14394	-.02729	43	0.97221	-.00018
8	0.81780	0.02849	20	0.03082	0.02427	32	0.20474	-.02874	44	0.98737	-.00035
9	0.76178	0.03590	21	0.01061	0.01340	33	0.26557	-.02877	45	0.99542	-.00072
10	0.70325	0.04303	22	0.00286	0.00665	34	0.32895	-.02788	46	1.00000	0.00000
11	0.65407	0.04844	23	0.00000	0.00000	35	0.40631	-.02552			
12	0.58573	0.05474	24	0.00068	-.00387	36	0.49340	-.02140			

J5012-PT

1	1.00000	0.00000	12	0.50773	0.05482	23	0.00229	-.00837	34	0.64288	-.04321
2	0.99839	0.00255	13	0.41197	0.05797	24	0.00952	-.01533	35	0.71886	-.03546
3	0.99141	0.00405	14	0.32424	0.05887	25	0.03772	-.02874	36	0.79724	-.02655
4	0.97999	0.00577	15	0.23778	0.05673	26	0.08438	-.03944	37	0.86129	-.01815
5	0.95851	0.00843	16	0.13255	0.04791	27	0.12578	-.04588	38	0.92077	-.01093
6	0.91330	0.01337	17	0.05972	0.03376	28	0.19537	-.05295	39	0.95825	-.00747
7	0.85319	0.02234	18	0.03509	0.02643	29	0.26780	-.05766	40	0.98225	-.00531
8	0.78393	0.03074	19	0.01716	0.01910	30	0.34668	-.05852	41	0.99224	-.00375
9	0.71117	0.03835	20	0.00787	0.01354	31	0.41617	-.05729	42	0.99856	-.00236
10	0.64248	0.04476	21	0.00209	0.00698	32	0.49443	-.05444	43	1.00000	0.00000
11	0.57332	0.04992	22	0.00000	0.00000	33	0.56234	-.04989			

MB253515-PT

1	1.00000	0.00000	12	0.37864	0.09873	23	0.00137	-.00627	34	0.67530	-.03477
2	0.99710	0.00083	13	0.31208	0.09826	24	0.00473	-.01046	35	0.77219	-.02482
3	0.99302	0.00166	14	0.24036	0.09369	25	0.01929	-.01795	36	0.84769	-.01665
4	0.98163	0.00402	15	0.18302	0.08585	26	0.05222	-.02720	37	0.90082	-.01083
5	0.95193	0.01000	16	0.12940	0.07307	27	0.10483	-.03726	38	0.94663	-.00586
6	0.88089	0.02430	17	0.08764	0.05829	28	0.16957	-.04517	39	0.97990	-.00226
7	0.79569	0.04146	18	0.05744	0.04435	29	0.23425	-.04944	40	0.99127	-.00103
8	0.70484	0.05945	19	0.03642	0.03266	30	0.32312	-.05123	41	0.99800	-.00026
9	0.62803	0.07353	20	0.01695	0.01982	31	0.41644	-.05061	42	1.00000	0.00000
10	0.54312	0.08641	21	0.00565	0.01039	32	0.50314	-.04751			
11	0.46570	0.09456	22	0.00000	0.00000	33	0.59102	-.04204			

M06-13-128-PT

1	1.00000	0.00000	13	0.53817	0.08761	25	0.01325	0.02401	37	0.43053	-.01263
2	0.99875	0.00110	14	0.49316	0.10041	26	0.00342	0.01037	38	0.53876	-.01121
3	0.99113	0.00249	15	0.47429	0.10527	27	0.00000	0.00000	39	0.63080	-.00961
4	0.98068	0.00416	16	0.45124	0.10986	28	0.00078	-.00284	40	0.71853	-.00741
5	0.95248	0.00743	17	0.40392	0.11643	29	0.00722	-.00669	41	0.79608	-.00539
6	0.91306	0.01267	18	0.34297	0.11964	30	0.01678	-.00880	42	0.84383	-.00380
7	0.86592	0.01884	19	0.28317	0.11754	31	0.03290	-.01102	43	0.89026	-.00218
8	0.81308	0.02712	20	0.22462	0.11054	32	0.06064	-.01306	44	0.93888	-.00112
9	0.74939	0.03782	21	0.16643	0.09933	33	0.11702	-.01410	45	0.97090	-.00067
10	0.69189	0.04962	22	0.11150	0.08380	34	0.18367	-.01460	46	0.98601	-.00046
11	0.64657	0.05965	23	0.06272	0.06139	35	0.25128	-.01439	47	0.99294	-.00009
12	0.59104	0.07291	24	0.03292	0.04183	36	0.33028	-.01360	48	1.00000	0.00000

NACA 0009-PT

1	1.00000	0.00000	14	0.43278	0.04380	27	0.01283	-.01362	40	0.65205	-.02796
2	0.99283	0.00039	15	0.35732	0.04624	28	0.02821	-.01822	41	0.70766	-.02446
3	0.98609	0.00092	16	0.29023	0.04694	29	0.04999	-.02301	42	0.77221	-.02037
4	0.96059	0.00291	17	0.23516	0.04622	30	0.07483	-.02790	43	0.82859	-.01621
5	0.92431	0.00640	18	0.16732	0.04324	31	0.10934	-.03344	44	0.87338	-.01252
6	0.87143	0.01241	19	0.10575	0.03826	32	0.14977	-.03767	45	0.91345	-.00896
7	0.81876	0.01786	20	0.05991	0.03049	33	0.19806	-.04057	46	0.94522	-.00649
8	0.75627	0.02377	21	0.02791	0.02112	34	0.24150	-.04230	47	0.96977	-.00429
9	0.69948	0.02841	22	0.01445	0.01572	35	0.30241	-.04303	48	0.98336	-.00276
10	0.63384	0.03274	23	0.00504	0.00989	36	0.36697	-.04212	49	0.99146	-.00166
11	0.58017	0.03631	24	0.00000	0.00000	37	0.44282	-.03948	50	0.99831	-.00023
12	0.52537	0.03956	25	0.00132	-.00515	38	0.51078	-.03621	51	1.00000	0.00000
13	0.47998	0.04165	26	0.00405	-.00856	39	0.58407	-.03209			

NACA 2.5411-PT

1	1.00000	0.00000	14	0.56708	0.06439	27	0.00000	0.00000	40	0.50834	-.02570
2	0.99780	0.00256	15	0.50514	0.06980	28	0.00046	-.00206	41	0.55444	-.02382
3	0.98445	0.00417	16	0.42977	0.07462	29	0.00240	-.00626	42	0.62454	-.02058
4	0.96760	0.00668	17	0.33796	0.07599	30	0.00674	-.01152	43	0.69843	-.01716
5	0.94313	0.01013	18	0.26124	0.07446	31	0.01900	-.01953	44	0.75752	-.01442
6	0.92315	0.01291	19	0.16841	0.06535	32	0.03591	-.02543	45	0.83045	-.01095
7	0.91076	0.01539	20	0.09001	0.04979	33	0.06146	-.02986	46	0.89440	-.00808
8	0.89857	0.01767	21	0.05152	0.03759	34	0.09647	-.03378	47	0.93291	-.00617
9	0.85609	0.02545	22	0.03428	0.03162	35	0.13947	-.03595	48	0.96624	-.00407
10	0.80729	0.03379	23	0.01718	0.02406	36	0.20396	-.03646	49	0.98582	-.00266
11	0.75693	0.04130	24	0.00660	0.01565	37	0.28404	-.03487	50	0.99642	-.00187
12	0.69964	0.04910	25	0.00344	0.01107	38	0.36124	-.03195	51	1.00000	0.00000
13	0.64221	0.05612	26	0.00069	0.00362	39	0.43485	-.02881			

NACA 64A010-PT

1	1.00000	0.00000	16	0.27863	0.04705	31	0.01704	-.01413	46	0.64994	-.03598
2	0.99938	0.00041	17	0.21109	0.04339	32	0.03061	-.01904	47	0.68222	-.03297
3	0.99423	0.00104	18	0.15254	0.03848	33	0.04837	-.02366	48	0.72400	-.02889
4	0.98815	0.00168	19	0.09698	0.03214	34	0.07230	-.02859	49	0.78813	-.02243
5	0.96673	0.00344	20	0.05746	0.02569	35	0.10833	-.03427	50	0.84438	-.01658
6	0.93471	0.00729	21	0.03479	0.01965	36	0.14298	-.03848	51	0.89289	-.01148
7	0.88984	0.01209	22	0.02328	0.01597	37	0.20830	-.04444	52	0.93628	-.00693
8	0.82035	0.01920	23	0.01348	0.01206	38	0.26119	-.04770	53	0.96862	-.00347
9	0.75015	0.02567	24	0.00702	0.00876	39	0.30559	-.04955	54	0.98664	-.00164
10	0.68796	0.03102	25	0.00253	0.00500	40	0.34325	-.05059	55	0.99437	-.00090
11	0.62998	0.03601	26	0.00000	0.00000	41	0.39887	-.05078	56	0.99921	-.00030
12	0.55005	0.04222	27	0.00050	-.00195	42	0.44771	-.04961	57	1.00000	0.00000
13	0.47705	0.04647	28	0.00257	-.00545	43	0.50911	-.04652			
14	0.41203	0.04818	29	0.00474	-.00733	44	0.55650	-.04345			
15	0.34783	0.04859	30	0.01005	-.01068	45	0.59897	-.04043			

NACA 6409-PT

1	1.00000	0.00000	15	0.49536	0.09820	29	0.00066	-.00353	43	0.64151	0.01793
2	0.99869	0.00088	16	0.43439	0.10309	30	0.00393	-.00760	44	0.71030	0.01617
3	0.99259	0.00301	17	0.38363	0.10438	31	0.01217	-.01115	45	0.77575	0.01371
4	0.98608	0.00531	18	0.33207	0.10346	32	0.02151	-.01308	46	0.84401	0.00993
5	0.96609	0.01146	19	0.27114	0.09920	33	0.03912	-.01485	47	0.89326	0.00723
6	0.94340	0.01768	20	0.21151	0.09209	34	0.05735	-.01490	48	0.93168	0.00442
7	0.91779	0.02418	21	0.16223	0.08208	35	0.10165	-.01161	49	0.96632	0.00192
8	0.88166	0.03290	22	0.12154	0.07046	36	0.14954	-.00674	50	0.98617	0.00039
9	0.83969	0.04276	23	0.08205	0.05676	37	0.19854	-.00039	51	0.99502	-.00020
10	0.79396	0.05290	24	0.05983	0.04756	38	0.26759	0.00752	52	0.99816	-.00077
11	0.74082	0.06381	25	0.03560	0.03414	39	0.35105	0.01340	53	1.00000	0.00000
12	0.68758	0.07337	26	0.01524	0.02074	40	0.43511	0.01665			
13	0.62605	0.08344	27	0.00588	0.01177	41	0.51627	0.01785			
14	0.54319	0.09371	28	0.00000	0.00000	42	0.57869	0.01832			

RG15-PT

1	1.00000	0.00000	17	0.26141	0.06379	33	0.00075	0.00448	49	0.33755	-.02429
2	0.97685	0.00453	18	0.22751	0.06223	34	0.00059	0.00393	50	0.41569	-.02237
3	0.94725	0.00900	19	0.19485	0.06009	35	0.00000	0.00000	51	0.48721	-.01990
4	0.91431	0.01433	20	0.16417	0.05730	36	0.00088	-.00251	52	0.56191	-.01664
5	0.87100	0.02090	21	0.12536	0.05257	37	0.00167	-.00352	53	0.61788	-.01375
6	0.83233	0.02627	22	0.09250	0.04692	38	0.00349	-.00524	54	0.67232	-.01060
7	0.79485	0.03115	23	0.06872	0.04120	39	0.00823	-.00837	55	0.72297	-.00743
8	0.74835	0.03667	24	0.05621	0.03733	40	0.01372	-.01059	56	0.78968	-.00358
9	0.70274	0.04177	25	0.04380	0.03287	41	0.02652	-.01420	57	0.86269	-.00050
10	0.64464	0.04784	26	0.03255	0.02817	42	0.04323	-.01743	58	0.92258	0.00086
11	0.58955	0.05267	27	0.02124	0.02266	43	0.06172	-.01981	59	0.95161	0.00081
12	0.52527	0.05749	28	0.01348	0.01814	44	0.08964	-.02216	60	0.96703	0.00046
13	0.45545	0.06150	29	0.00822	0.01423	45	0.12580	-.02415	61	0.97897	-.00006
14	0.39801	0.06374	30	0.00382	0.00991	46	0.16261	-.02533	62	0.98873	-.00059
15	0.34875	0.06473	31	0.00227	0.00777	47	0.22083	-.02584	63	0.99514	-.00098
16	0.29884	0.06469	32	0.00126	0.00584	48	0.27587	-.02516	64	1.00000	0.00000

S2048-PT

1	1.00000	0.00000	13	0.33249	0.06211	25	0.00579	-.00762	37	0.63109	-.01588
2	0.99877	0.00164	14	0.23428	0.05880	26	0.01268	-.01127	38	0.69126	-.01190
3	0.99320	0.00324	15	0.14340	0.05075	27	0.02975	-.01501	39	0.75073	-.00822
4	0.98831	0.00435	16	0.07235	0.03721	28	0.05444	-.01819	40	0.81098	-.00492
5	0.97708	0.00692	17	0.04544	0.02842	29	0.08654	-.02175	41	0.88816	-.00164
6	0.93558	0.01450	18	0.02968	0.02214	30	0.13059	-.02477	42	0.95036	-.00042
7	0.88316	0.02301	19	0.01619	0.01591	31	0.19111	-.02697	43	0.97854	-.00073
8	0.81545	0.03282	20	0.00593	0.00904	32	0.25652	-.02814	44	0.98990	-.00114
9	0.74217	0.04215	21	0.00125	0.00316	33	0.35344	-.02813	45	0.99425	-.00136
10	0.65783	0.05023	22	0.00000	0.00000	34	0.43114	-.02621	46	0.99770	-.00149
11	0.55386	0.05774	23	0.00067	-.00269	35	0.50087	-.02359	47	1.00000	0.00000
12	0.45158	0.06134	24	0.00233	-.00486	36	0.56192	-.02034			

S2055-PT

1	1.00000	0.00000	13	0.35868	0.05903	25	0.00364	-.00635	37	0.59785	-.01914
2	0.99877	0.00140	14	0.27485	0.05758	26	0.01121	-.01010	38	0.65640	-.01708
3	0.98528	0.00366	15	0.21531	0.05494	27	0.02071	-.01262	39	0.71940	-.01426
4	0.95559	0.00804	16	0.15430	0.04986	28	0.03715	-.01558	40	0.80215	-.00990
5	0.91492	0.01500	17	0.11011	0.04371	29	0.05514	-.01806	41	0.87321	-.00509
6	0.86076	0.02348	18	0.07451	0.03624	30	0.08242	-.02058	42	0.91194	-.00287
7	0.80484	0.03151	19	0.04421	0.02697	31	0.12571	-.02320	43	0.94297	-.00195
8	0.73201	0.04009	20	0.01919	0.01641	32	0.18074	-.02486	44	0.96810	-.00158
9	0.65915	0.04777	21	0.00906	0.01095	33	0.25713	-.02566	45	0.98432	-.00131
10	0.57721	0.05518	22	0.00328	0.00614	34	0.33256	-.02503	46	0.99176	-.00118
11	0.51605	0.05837	23	0.00000	0.00000	35	0.41100	-.02369	47	0.99792	-.00101
12	0.43705	0.05893	24	0.00044	-.00228	36	0.50148	-.02169	48	1.00000	0.00000

S2091B-PT

1	1.00000	0.00000	13	0.45554	0.08429	25	0.00140	-.00539	37	0.53852	-.00610
2	0.99863	0.00124	14	0.37549	0.08858	26	0.00498	-.00965	38	0.61380	-.00283
3	0.99247	0.00293	15	0.29967	0.08903	27	0.01294	-.01371	39	0.69005	-.00050
4	0.98180	0.00537	16	0.22796	0.08570	28	0.02635	-.01700	40	0.75738	0.00102
5	0.94359	0.01389	17	0.17229	0.07979	29	0.05539	-.02022	41	0.83165	0.00238
6	0.89665	0.02293	18	0.11658	0.06940	30	0.10538	-.02174	42	0.88976	0.00254
7	0.83696	0.03315	19	0.07098	0.05562	31	0.13942	-.02143	43	0.93487	0.00137
8	0.77627	0.04334	20	0.03719	0.03984	32	0.19379	-.02019	44	0.97173	-.00032
9	0.72031	0.05243	21	0.01763	0.02674	33	0.25957	-.01794	45	0.98802	-.00094
10	0.66347	0.06102	22	0.00547	0.01461	34	0.32532	-.01533	46	0.99373	-.00104
11	0.60612	0.06898	23	0.00163	0.00812	35	0.39702	-.01251	47	0.99953	-.00084
12	0.52556	0.07819	24	0.00000	0.00000	36	0.46777	-.00949	48	1.00000	0.00000

S3010-PT

1	1.00000	0.00000	13	0.55534	0.06086	25	0.00941	0.01692	37	0.44681	-.02288
2	0.99477	0.00032	14	0.49711	0.06652	26	0.00210	0.00804	38	0.52195	-.01813
3	0.98769	0.00130	15	0.44786	0.07044	27	0.00000	0.00000	39	0.61100	-.01316
4	0.96742	0.00384	16	0.39650	0.07352	28	0.00169	-.00721	40	0.70581	-.00793
5	0.93685	0.00770	17	0.34462	0.07523	29	0.00511	-.01193	41	0.79231	-.00390
6	0.89027	0.01405	18	0.27941	0.07562	30	0.01144	-.01640	42	0.86608	-.00126
7	0.83870	0.02140	19	0.22025	0.07333	31	0.03114	-.02300	43	0.92894	0.00010
8	0.79404	0.02812	20	0.16599	0.06825	32	0.07160	-.02901	44	0.96663	0.00030
9	0.74718	0.03532	21	0.12042	0.06093	33	0.11988	-.03185	45	0.98245	0.00016
10	0.70875	0.04113	22	0.08047	0.05141	34	0.18994	-.03216	46	0.98906	0.00011
11	0.67078	0.04647	23	0.05463	0.04271	35	0.25622	-.03103	47	0.99536	0.00011
12	0.61495	0.05398	24	0.02904	0.03041	36	0.34875	-.02806	48	1.00000	0.00000

S3014-PT

1	1.00000	0.00000	13	0.52768	0.06486	25	0.00578	0.01103	37	0.50427	-.01646
2	0.99999	0.00107	14	0.46432	0.06960	26	0.00221	0.00626	38	0.63099	-.01228
3	0.99596	0.00168	15	0.39335	0.07303	27	0.00000	0.00000	39	0.73135	-.00905
4	0.99116	0.00222	16	0.33569	0.07412	28	0.00162	-.00438	40	0.80302	-.00682
5	0.97895	0.00327	17	0.26875	0.07293	29	0.00443	-.00734	41	0.87708	-.00457
6	0.94090	0.00756	18	0.21013	0.06939	30	0.01048	-.01058	42	0.92559	-.00317
7	0.89641	0.01382	19	0.16832	0.06514	31	0.03315	-.01715	43	0.95847	-.00208
8	0.83558	0.02310	20	0.11618	0.05713	32	0.07651	-.02236	44	0.97874	-.00148
9	0.75977	0.03483	21	0.07292	0.04669	33	0.15793	-.02481	45	0.98711	-.00121
10	0.69802	0.04406	22	0.04791	0.03779	34	0.22343	-.02458	46	0.99325	-.00099
11	0.63927	0.05229	23	0.03029	0.02929	35	0.30182	-.02286	47	0.99892	-.00072
12	0.58346	0.05920	24	0.01316	0.01794	36	0.41006	-.01965	48	1.00000	0.00000

S3016-PT

1	1.00000	0.00000	15	0.44543	0.06403	29	0.00225	-.00561	43	0.56216	-.02055
2	0.99903	0.00119	16	0.38021	0.06680	30	0.00662	-.00948	44	0.63320	-.01788
3	0.99441	0.00160	17	0.32602	0.06745	31	0.01331	-.01285	45	0.71127	-.01496
4	0.98887	0.00213	18	0.25687	0.06653	32	0.02580	-.01675	46	0.77792	-.01237
5	0.98369	0.00247	19	0.18845	0.06273	33	0.04778	-.02112	47	0.84744	-.00937
6	0.96478	0.00369	20	0.12729	0.05599	34	0.07285	-.02443	48	0.90233	-.00660
7	0.91855	0.00790	21	0.07971	0.04688	35	0.10882	-.02736	49	0.94896	-.00410
8	0.87084	0.01401	22	0.04798	0.03781	36	0.14789	-.02913	50	0.97506	-.00252
9	0.82121	0.02159	23	0.02431	0.02771	37	0.18098	-.02981	51	0.98331	-.00199
10	0.75744	0.03128	24	0.01323	0.02038	38	0.23833	-.03003	52	0.98881	-.00165
11	0.70315	0.03914	25	0.00571	0.01285	39	0.31258	-.02864	53	0.99426	-.00133
12	0.63635	0.04779	26	0.00194	0.00703	40	0.37836	-.02675	54	0.99811	-.00104
13	0.57910	0.05385	27	0.00000	0.00000	41	0.43886	-.02482	55	1.00000	0.00000
14	0.52089	0.05904	28	0.00065	-.00275	42	0.50034	-.02272			

S3021A-PT

1	1.00000	0.00000	12	0.33088	0.07528	23	0.00218	-.00481	34	0.77037	-.00339
2	0.99269	0.00137	13	0.23332	0.07202	24	0.00605	-.00755	35	0.85719	-.00087
3	0.98303	0.00312	14	0.16278	0.06493	25	0.01300	-.01057	36	0.90241	0.00030
4	0.97106	0.00520	15	0.10700	0.05507	26	0.02415	-.01358	37	0.94457	0.00018
5	0.93853	0.01089	16	0.06277	0.04245	27	0.05651	-.01806	38	0.97902	0.00010
6	0.87927	0.02031	17	0.03606	0.03115	28	0.12338	-.02176	39	0.98958	0.00009
7	0.78031	0.03475	18	0.01931	0.02151	29	0.19693	-.02178	40	0.99544	0.00004
8	0.70835	0.04454	19	0.01125	0.01529	30	0.28664	-.01974	41	1.00000	0.00000
9	0.61823	0.05602	20	0.00302	0.00666	31	0.39682	-.01608			
10	0.53048	0.06542	21	0.00000	0.00000	32	0.51668	-.01198			
11	0.43335	0.07270	22	0.00069	-.00264	33	0.65450	-.00720			

S3021B-PT

1	1.00000	0.00000	14	0.39023	0.07174	27	0.00687	-.00981	40	0.59892	-.01543
2	0.99058	0.00072	15	0.33135	0.07264	28	0.02481	-.01637	41	0.67229	-.01328
3	0.96084	0.00367	16	0.28464	0.07177	29	0.05033	-.02088	42	0.75272	-.01154
4	0.91517	0.01029	17	0.21676	0.06792	30	0.07537	-.02332	43	0.82462	-.00968
5	0.86938	0.01692	18	0.16125	0.06219	31	0.10516	-.02436	44	0.88415	-.00803
6	0.82314	0.02362	19	0.10703	0.05253	32	0.14365	-.02429	45	0.91632	-.00674
7	0.77702	0.02983	20	0.07085	0.04284	33	0.18487	-.02416	46	0.95206	-.00489
8	0.72171	0.03776	21	0.03675	0.02962	34	0.23153	-.02382	47	0.97430	-.00330
9	0.68029	0.04320	22	0.01908	0.01943	35	0.25974	-.02372	48	0.98894	-.00161
10	0.62893	0.05033	23	0.00667	0.00951	36	0.30117	-.02247	49	1.00000	0.00000
11	0.58511	0.05608	24	0.00227	0.00422	37	0.37652	-.02097			
12	0.50942	0.06475	25	0.00000	0.00000	38	0.45339	-.01917			
13	0.45925	0.06833	26	0.00094	-.00398	39	0.52707	-.01735			

S4061A-PT

1	1.00000	0.00000	12	0.38353	0.07975	23	0.00105	-.00377	34	0.54661	-.00422
2	0.99673	0.00230	13	0.31736	0.08113	24	0.00471	-.00827	35	0.62422	0.00022
3	0.98570	0.00361	14	0.24629	0.07721	25	0.01160	-.01257	36	0.68944	0.00062
4	0.96705	0.00508	15	0.16873	0.06793	26	0.02467	-.01704	37	0.76627	0.00025
5	0.92527	0.00967	16	0.11572	0.05767	27	0.05029	-.02120	38	0.83860	-.00041
6	0.86284	0.01804	17	0.07883	0.04614	28	0.08856	-.02407	39	0.90270	-.00114
7	0.79417	0.02926	18	0.04869	0.03373	29	0.14436	-.02479	40	0.95973	-.00263
8	0.70452	0.04618	19	0.02569	0.02300	30	0.20789	-.02344	41	0.98139	-.00239
9	0.64995	0.05453	20	0.01128	0.01471	31	0.29093	-.01881	42	0.99103	-.00197
10	0.54327	0.06846	21	0.00276	0.00708	32	0.36256	-.01528	43	0.99778	-.00188
11	0.45623	0.07634	22	0.00000	0.00000	33	0.45217	-.00992	44	1.00000	0.00000

S4061B-PT

1	1.00000	0.00000	14	0.50745	0.08189	27	0.00247	0.00720	40	0.49771	-.00212
2	0.99856	0.00053	15	0.45525	0.08508	28	0.00000	0.00000	41	0.56052	0.00122
3	0.99229	0.00150	16	0.41078	0.08666	29	0.00182	-.00595	42	0.63379	0.00430
4	0.98413	0.00273	17	0.35388	0.08705	30	0.00549	-.00974	43	0.70802	0.00625
5	0.95858	0.00709	18	0.29739	0.08558	31	0.01174	-.01288	44	0.78775	0.00670
6	0.92449	0.01327	19	0.25310	0.08266	32	0.02599	-.01614	45	0.85749	0.00587
7	0.88177	0.02170	20	0.19704	0.07675	33	0.05660	-.01929	46	0.91202	0.00429
8	0.83273	0.03228	21	0.14752	0.06864	34	0.11239	-.02112	47	0.95693	0.00144
9	0.78644	0.04212	22	0.10590	0.05888	35	0.16687	-.01950	48	0.98563	-.00029
10	0.73718	0.05132	23	0.07171	0.04844	36	0.22327	-.01672	49	0.99253	-.00046
11	0.68253	0.06072	24	0.04062	0.03538	37	0.27919	-.01368	50	1.00000	0.00000
12	0.62974	0.06848	25	0.01859	0.02286	38	0.34892	-.00996			
13	0.56110	0.07689	26	0.00568	0.01170	39	0.41346	-.00648			

S4062-PT

1	1.00000	0.00000	14	0.49689	0.08110	27	0.00122	-.00454	40	0.57139	0.00024
2	0.99924	0.00080	15	0.41448	0.08467	28	0.00376	-.00791	41	0.63760	0.00211
3	0.99612	0.00134	16	0.33532	0.08430	29	0.01095	-.01156	42	0.69795	0.00350
4	0.99135	0.00213	17	0.25715	0.08012	30	0.01836	-.01332	43	0.76774	0.00421
5	0.98577	0.00275	18	0.19327	0.07339	31	0.04564	-.01618	44	0.83762	0.00406
6	0.95901	0.00621	19	0.13335	0.06281	32	0.07108	-.01764	45	0.88264	0.00354
7	0.91891	0.01305	20	0.08300	0.04931	33	0.11581	-.01836	46	0.92784	0.00249
8	0.87252	0.02149	21	0.04562	0.03531	34	0.18077	-.01699	47	0.96114	0.00113
9	0.81385	0.03362	22	0.02696	0.02690	35	0.24062	-.01464	48	0.97354	0.00040
10	0.76002	0.04476	23	0.01299	0.01823	36	0.30099	-.01160	49	0.98652	-.00021
11	0.69586	0.05676	24	0.00570	0.01171	37	0.36347	-.00841	50	0.99415	-.00058
12	0.63933	0.06580	25	0.00263	0.00776	38	0.42626	-.00536	51	0.99958	-.00046
13	0.56493	0.07513	26	0.00000	0.00000	39	0.50577	-.00189	52	1.00000	0.00000

S4233-PT

1	1.00000	0.00000	15	0.41487	0.09805	29	0.00423	-.00733	43	0.56063	-.02533
2	0.99965	0.00135	16	0.33847	0.09914	30	0.00787	-.01015	44	0.63022	-.02006
3	0.99675	0.00185	17	0.28714	0.09689	31	0.01462	-.01331	45	0.70793	-.01368
4	0.99208	0.00244	18	0.23126	0.09139	32	0.02719	-.01811	46	0.78274	-.00784
5	0.98292	0.00348	19	0.16785	0.08089	33	0.04099	-.02240	47	0.85409	-.00356
6	0.95407	0.00819	20	0.12159	0.06957	34	0.06320	-.02717	48	0.90758	-.00175
7	0.90598	0.01758	21	0.08679	0.05843	35	0.09827	-.03223	49	0.96048	-.00114
8	0.85668	0.02697	22	0.05274	0.04400	36	0.14049	-.03573	50	0.98223	-.00112
9	0.80341	0.03831	23	0.02774	0.02955	37	0.18760	-.03794	51	0.99184	-.00127
10	0.74226	0.05125	24	0.01569	0.02080	38	0.22910	-.03884	52	0.99655	-.00132
11	0.69122	0.06183	25	0.00690	0.01258	39	0.28748	-.03888	53	0.99937	-.00110
12	0.62493	0.07396	26	0.00258	0.00667	40	0.34399	-.03787	54	1.00000	0.00000
13	0.55767	0.08440	27	0.00000	0.00000	41	0.40654	-.03530			
14	0.48838	0.09281	28	0.00111	-.00344	42	0.46493	-.03195			

SD2030-PT

1	1.00000	0.00000	13	0.49512	0.06299	25	0.00000	0.00000	37	0.50216	-.01840
2	0.99594	0.00274	14	0.42477	0.06460	26	0.00105	-.00452	38	0.58733	-.01579
3	0.98879	0.00430	15	0.36002	0.06448	27	0.00400	-.00754	39	0.66517	-.01286
4	0.97366	0.00743	16	0.29870	0.06302	28	0.01075	-.01080	40	0.74397	-.00927
5	0.94936	0.01239	17	0.23863	0.06010	29	0.02425	-.01468	41	0.81666	-.00571
6	0.90526	0.02054	18	0.17709	0.05484	30	0.04663	-.01851	42	0.88423	-.00279
7	0.85117	0.02918	19	0.12427	0.04765	31	0.09223	-.02201	43	0.93306	-.00082
8	0.80405	0.03583	20	0.07855	0.03861	32	0.14375	-.02344	44	0.96157	-.00087
9	0.74591	0.04331	21	0.04526	0.02929	33	0.19208	-.02369	45	0.98044	-.00072
10	0.68902	0.04996	22	0.01948	0.01772	34	0.25685	-.02319	46	0.99140	-.00095
11	0.63091	0.05582	23	0.00848	0.01064	35	0.33714	-.02207	47	1.00000	0.00000
12	0.55826	0.06059	24	0.00157	0.00519	36	0.41589	-.02049			

SD2083-PT

1	1.00000	0.00000	15	0.38078	0.07015	29	0.00801	-.01151	43	0.71114	-.00949
2	0.99879	0.00061	16	0.30214	0.06862	30	0.01486	-.01407	44	0.77953	-.00781
3	0.99529	0.00103	17	0.23457	0.06485	31	0.03055	-.01738	45	0.84138	-.00654
4	0.99026	0.00171	18	0.16431	0.05695	32	0.06495	-.01998	46	0.89008	-.00617
5	0.98274	0.00265	19	0.10215	0.04537	33	0.08912	-.02138	47	0.92852	-.00528
6	0.95421	0.00665	20	0.06168	0.03381	34	0.13961	-.02268	48	0.96633	-.00309
7	0.90309	0.01436	21	0.03498	0.02403	35	0.19371	-.02278	49	0.97901	-.00225
8	0.85175	0.02310	22	0.01768	0.01655	36	0.26237	-.02177	50	0.98663	-.00151
9	0.79675	0.03244	23	0.00755	0.01073	37	0.33724	-.01967	51	0.99147	-.00111
10	0.73356	0.04255	24	0.00220	0.00564	38	0.39894	-.01832	52	0.99772	-.00034
11	0.66435	0.05292	25	0.00000	0.00000	39	0.46205	-.01617	53	1.00000	0.00000
12	0.59630	0.06096	26	0.00068	-.00376	40	0.53047	-.01435			
13	0.52505	0.06637	27	0.00183	-.00649	41	0.58338	-.01286			
14	0.45243	0.06899	28	0.00373	-.00869	42	0.65583	-.01087			

SD5060-PT

1	1.00000	0.00000	13	0.43410	0.06515	25	0.00405	-.00794	37	0.81957	-.00335
2	0.99965	0.00030	14	0.36463	0.06735	26	0.01042	-.01225	38	0.87370	-.00263
3	0.99670	0.00027	15	0.27437	0.06730	27	0.02708	-.01964	39	0.92155	-.00197
4	0.98943	0.00164	16	0.20304	0.06348	28	0.05681	-.02635	40	0.95825	-.00082
5	0.97661	0.00291	17	0.14689	0.05788	29	0.10279	-.03031	41	0.98124	-.00080
6	0.94328	0.00705	18	0.09709	0.04961	30	0.19875	-.03053	42	0.99136	-.00054
7	0.89226	0.01408	19	0.04985	0.03647	31	0.31977	-.02586	43	0.99484	-.00058
8	0.82463	0.02381	20	0.02170	0.02416	32	0.44792	-.01995	44	0.99836	-.00023
9	0.75963	0.03299	21	0.00944	0.01560	33	0.54575	-.01505	45	1.00000	0.00000
10	0.67850	0.04386	22	0.00349	0.00945	34	0.63304	-.01055			
11	0.58574	0.05443	23	0.00000	0.00000	35	0.70321	-.00780			
12	0.52135	0.05993	24	0.00062	-.00366	36	0.76889	-.00534			

SD6060-PT

1	1.00000	0.00000	14	0.54167	0.05970	27	0.00000	0.00000	40	0.46848	-.03156
2	0.99861	0.00074	15	0.46829	0.06533	28	0.00099	-.00229	41	0.54565	-.02921
3	0.99563	0.00112	16	0.39060	0.06849	29	0.00397	-.00502	42	0.62118	-.02566
4	0.99071	0.00128	17	0.31688	0.06850	30	0.00894	-.00836	43	0.69134	-.02058
5	0.98023	0.00214	18	0.24528	0.06569	31	0.01681	-.01177	44	0.75386	-.01605
6	0.96319	0.00369	19	0.17139	0.05936	32	0.03416	-.01685	45	0.81523	-.01177
7	0.92005	0.00860	20	0.12326	0.05187	33	0.07070	-.02325	46	0.88784	-.00608
8	0.88111	0.01401	21	0.09126	0.04492	34	0.11221	-.02758	47	0.93895	-.00240
9	0.82496	0.02226	22	0.06175	0.03681	35	0.16377	-.03027	48	0.97956	-.00100
10	0.76495	0.03132	23	0.03378	0.02649	36	0.21314	-.03165	49	0.98981	-.00096
11	0.71077	0.03920	24	0.01620	0.01690	37	0.26926	-.03269	50	0.99494	-.00103
12	0.65836	0.04650	25	0.00782	0.01049	38	0.33337	-.03325	51	0.99843	-.00091
13	0.60244	0.05335	26	0.00320	0.00578	39	0.40505	-.03265	52	1.00000	0.00000

SD6080-PT

1	1.00000	0.00000	15	0.40646	0.08254	29	0.01178	-.00811	43	0.69393	0.00274
2	1.00059	-.00006	16	0.34441	0.08341	30	0.02664	-.01127	44	0.75307	0.00346
3	0.99686	0.00008	17	0.27971	0.08137	31	0.05239	-.01420	45	0.81591	0.00346
4	0.98941	0.00145	18	0.21524	0.07606	32	0.08323	-.01503	46	0.87412	0.00335
5	0.97733	0.00321	19	0.15269	0.06740	33	0.12224	-.01446	47	0.91340	0.00282
6	0.94524	0.00913	20	0.09914	0.05605	34	0.17602	-.01292	48	0.95190	0.00200
7	0.90699	0.01498	21	0.05667	0.04250	35	0.23877	-.01088	49	0.97337	0.00160
8	0.85870	0.02346	22	0.03775	0.03369	36	0.30489	-.00850	50	0.98784	0.00093
9	0.80014	0.03438	23	0.01727	0.02082	37	0.36166	-.00632	51	0.99352	0.00046
10	0.74439	0.04409	24	0.01018	0.01521	38	0.41383	-.00434	52	0.99878	0.00028
11	0.69444	0.05214	25	0.00318	0.00787	39	0.47523	-.00223	53	1.00000	0.00000
12	0.65704	0.05792	26	0.00000	0.00000	40	0.53027	-.00082			
13	0.58070	0.06833	27	0.00062	-.00184	41	0.58943	0.00063			
14	0.49908	0.07682	28	0.00538	-.00581	42	0.63386	0.00166			

SD6080-PT with thickened trailing edge

1	1.00000	0.00000	15	0.48053	0.07665	29	0.00155	-.00392	43	0.63891	0.00024
2	0.99980	0.00273	16	0.42930	0.07984	30	0.00517	-.00639	44	0.67737	0.00079
3	0.99682	0.00400	17	0.34746	0.08189	31	0.01381	-.00931	45	0.71977	0.00144
4	0.99328	0.00438	18	0.29043	0.08045	32	0.02692	-.01202	46	0.76263	0.00174
5	0.98356	0.00545	19	0.23356	0.07663	33	0.04465	-.01429	47	0.81964	0.00169
6	0.96550	0.00756	20	0.18604	0.07121	34	0.08699	-.01582	48	0.86566	0.00159
7	0.92852	0.01323	21	0.14632	0.06500	35	0.13981	-.01483	49	0.91167	0.00102
8	0.87960	0.02092	22	0.10445	0.05615	36	0.19891	-.01316	50	0.95181	0.00014
9	0.83534	0.02738	23	0.06446	0.04437	37	0.26720	-.01093	51	0.97953	-.00047
10	0.77190	0.03767	24	0.03342	0.03023	38	0.32396	-.00890	52	0.99066	-.00116
11	0.72015	0.04614	25	0.01231	0.01594	39	0.39456	-.00622	53	0.99485	-.00150
12	0.66197	0.05548	26	0.00629	0.01039	40	0.46417	-.00389	54	0.99844	-.00180
13	0.59815	0.06425	27	0.00163	0.00464	41	0.52933	-.00221	55	1.00000	0.00000
14	0.54297	0.07083	28	0.00000	0.00000	42	0.59273	-.00077			

SD7003-PT

1	1.00000	0.00000	12	0.45370	0.05089	23	0.00104	-.00270	34	0.67179	-.01172
2	0.99835	0.00167	13	0.36452	0.05525	24	0.00341	-.00565	35	0.75444	-.00721
3	0.99144	0.00244	14	0.27994	0.05708	25	0.00981	-.00990	36	0.82285	-.00364
4	0.98072	0.00355	15	0.20186	0.05552	26	0.03079	-.01716	37	0.89391	-.00058
5	0.95984	0.00564	16	0.12918	0.04949	27	0.05997	-.02324	38	0.93863	0.00031
6	0.91623	0.00988	17	0.07702	0.04066	28	0.10826	-.02753	39	0.96772	-.00029
7	0.86546	0.01496	18	0.03821	0.02923	29	0.17601	-.02940	40	0.98613	-.00124
8	0.78327	0.02298	19	0.02050	0.02146	30	0.25357	-.02873	41	0.99338	-.00161
9	0.70362	0.03055	20	0.00968	0.01465	31	0.35759	-.02599	42	0.99790	-.00170
10	0.62282	0.03807	21	0.00363	0.00854	32	0.46650	-.02199	43	1.00000	0.00000
11	0.53137	0.04562	22	0.00000	0.00000	33	0.56973	-.01721			

SD7003-PT (R – repeated)

1	1.00000	0.00000	14	0.48816	0.04814	27	0.00913	-.01046	40	0.65013	-.01329
2	0.99850	0.00190	15	0.41985	0.05212	28	0.01966	-.01476	41	0.71029	-.00986
3	0.99320	0.00249	16	0.37050	0.05433	29	0.03993	-.02037	42	0.75779	-.00716
4	0.98686	0.00315	17	0.29520	0.05619	30	0.06766	-.02522	43	0.81776	-.00404
5	0.97330	0.00445	18	0.22473	0.05559	31	0.11056	-.02857	44	0.86491	-.00168
6	0.95149	0.00660	19	0.15572	0.05153	32	0.14828	-.02989	45	0.91000	0.00000
7	0.90760	0.01086	20	0.09394	0.04324	33	0.20352	-.03029	46	0.94514	0.00035
8	0.85674	0.01578	21	0.05855	0.03514	34	0.25853	-.02942	47	0.97461	-.00052
9	0.79920	0.02129	22	0.03160	0.02569	35	0.31553	-.02797	48	0.98155	-.00085
10	0.74005	0.02692	23	0.01254	0.01591	36	0.37324	-.02619	49	0.99094	-.00135
11	0.68241	0.03228	24	0.00254	0.00610	37	0.44810	-.02332	50	0.99714	-.00162
12	0.62939	0.03701	25	0.00000	0.00000	38	0.51957	-.02014	51	1.00000	0.00000
13	0.56269	0.04264	26	0.00192	-.00477	39	0.58682	-.01674			

SD7003-PT (A – 4.5 in off model centerline)

1	1.00000	0.00000	15	0.41796	0.05237	29	0.00532	-.00780	43	0.67726	-.01214
2	0.99661	0.00200	16	0.36098	0.05490	30	0.01260	-.01175	44	0.74815	-.00822
3	0.99067	0.00256	17	0.30461	0.05629	31	0.02639	-.01659	45	0.79496	-.00577
4	0.97723	0.00397	18	0.25412	0.05653	32	0.04847	-.02196	46	0.84047	-.00347
5	0.95540	0.00607	19	0.20027	0.05504	33	0.08076	-.02641	47	0.88421	-.00153
6	0.91003	0.01049	20	0.15765	0.05214	34	0.11940	-.02893	48	0.93450	-.00020
7	0.86108	0.01517	21	0.11276	0.04687	35	0.16902	-.03021	49	0.97019	-.00079
8	0.81578	0.01954	22	0.06985	0.03862	36	0.22369	-.03013	50	0.98418	-.00125
9	0.76441	0.02444	23	0.04022	0.02971	37	0.28571	-.02882	51	0.99156	-.00141
10	0.71354	0.02924	24	0.02247	0.02222	38	0.34937	-.02704	52	0.99691	-.00143
11	0.66555	0.03367	25	0.01044	0.01504	39	0.41625	-.02477	53	1.00000	0.00000
12	0.60731	0.03882	26	0.00327	0.00805	40	0.47847	-.02220			
13	0.55247	0.04341	27	0.00000	0.00000	41	0.54404	-.01916			
14	0.48492	0.04844	28	0.00091	-.00306	42	0.60577	-.01595			

SD7003-PT (B – 1.5 in off model centerline)

1	1.00000	0.00000	14	0.54410	0.04424	27	0.00588	0.01082	40	0.48216	-.02188
2	0.99706	0.00194	15	0.50917	0.04689	28	0.00000	0.00000	41	0.54957	-.01871
3	0.99177	0.00256	16	0.45985	0.05009	29	0.00115	-.00342	42	0.62788	-.01460
4	0.98594	0.00305	17	0.40213	0.05318	30	0.00463	-.00736	43	0.70836	-.01006
5	0.97274	0.00437	18	0.35423	0.05509	31	0.01251	-.01183	44	0.78332	-.00597
6	0.94989	0.00649	19	0.29665	0.05636	32	0.03496	-.01884	45	0.85627	-.00235
7	0.90395	0.01110	20	0.24408	0.05639	33	0.07172	-.02546	46	0.90913	-.00024
8	0.85172	0.01618	21	0.19715	0.05479	34	0.10740	-.02818	47	0.95169	0.00001
9	0.80116	0.02108	22	0.13869	0.05008	35	0.15204	-.02979	48	0.97479	-.00073
10	0.74091	0.02683	23	0.09631	0.04407	36	0.21359	-.03009	49	0.98972	-.00146
11	0.69316	0.03137	24	0.05435	0.03434	37	0.27920	-.02884	50	0.99628	-.00170
12	0.63904	0.03628	25	0.02838	0.02483	38	0.35010	-.02687	51	0.99810	-.00167
13	0.59240	0.04036	26	0.01480	0.01788	39	0.41691	-.02458	52	1.00000	0.00000

SD7003-PT (C – −1.5 in off model centerline)

1	1.00000	0.00000	14	0.47549	0.04979	27	0.00125	-.00358	40	0.55647	-.01802
2	0.99845	0.00201	15	0.40331	0.05380	28	0.00474	-.00728	41	0.62442	-.01438
3	0.99228	0.00280	16	0.32999	0.05645	29	0.01062	-.01092	42	0.68151	-.01119
4	0.98521	0.00358	17	0.27384	0.05722	30	0.02150	-.01520	43	0.74212	-.00781
5	0.96228	0.00590	18	0.21714	0.05631	31	0.03580	-.01929	44	0.81045	-.00423
6	0.91842	0.01039	19	0.16565	0.05338	32	0.06677	-.02489	45	0.87511	-.00112
7	0.88320	0.01377	20	0.12282	0.04885	33	0.10516	-.02798	46	0.92515	0.00044
8	0.83383	0.01858	21	0.08120	0.04177	34	0.14505	-.02946	47	0.96051	0.00002
9	0.78119	0.02367	22	0.04037	0.03021	35	0.20728	-.02988	48	0.98089	-.00092
10	0.73689	0.02792	23	0.02078	0.02178	36	0.26818	-.02895	49	0.99029	-.00148
11	0.68466	0.03279	24	0.01067	0.01557	37	0.34123	-.02692	50	0.99777	-.00172
12	0.62705	0.03803	25	0.00275	0.00752	38	0.40624	-.02465	51	1.00000	0.00000
13	0.55800	0.04386	26	0.00000	0.00000	39	0.47990	-.02164			

SD7003-PT (D – –4.5 in off model centerline)

1	1.00000	0.00000	14	0.52036	0.04599	27	0.00052	-.00209	40	0.70106	-.00963
2	0.99855	0.00149	15	0.47487	0.04907	28	0.00430	-.00684	41	0.76829	-.00594
3	0.99212	0.00234	16	0.42236	0.05208	29	0.01044	-.01078	42	0.83486	-.00251
4	0.98248	0.00344	17	0.35584	0.05490	30	0.02080	-.01484	43	0.90325	0.00029
5	0.95698	0.00593	18	0.29160	0.05629	31	0.04074	-.02025	44	0.94657	0.00075
6	0.92233	0.00942	19	0.23081	0.05585	32	0.07285	-.02533	45	0.97785	-.00039
7	0.88800	0.01279	20	0.17208	0.05294	33	0.12085	-.02853	46	0.98676	-.00087
8	0.83807	0.01758	21	0.12205	0.04779	34	0.16788	-.02964	47	0.99274	-.00120
9	0.78212	0.02294	22	0.06905	0.03790	35	0.24117	-.02918	48	0.99877	-.00125
10	0.73439	0.02746	23	0.02604	0.02320	36	0.32112	-.02725	49	1.00000	0.00000
11	0.68369	0.03221	24	0.00830	0.01252	37	0.40618	-.02430			
12	0.62807	0.03720	25	0.00135	0.00392	38	0.51949	-.01946			
13	0.57299	0.04193	26	0.00000	0.00000	39	0.62499	-.01394			

SD7032C-PT

1	1.00000	0.00000	17	0.61360	0.06784	33	0.00281	-.00770	49	0.78215	0.00364
2	0.99788	0.00150	18	0.56683	0.07258	34	0.00443	-.00918	50	0.78908	0.00300
3	0.99251	0.00285	19	0.50700	0.07732	35	0.00616	-.01015	51	0.79593	0.00234
4	0.98586	0.00478	20	0.43508	0.07985	36	0.01329	-.01253	52	0.80111	0.00223
5	0.97531	0.00727	21	0.34570	0.08308	37	0.02482	-.01518	53	0.80814	0.00207
6	0.94450	0.01314	22	0.27218	0.08262	38	0.03686	-.01677	54	0.81691	0.00278
7	0.90739	0.01983	23	0.20312	0.07780	39	0.07162	-.02038	55	0.85246	0.00324
8	0.85655	0.02948	24	0.13483	0.06655	40	0.11631	-.02138	56	0.90897	0.00279
9	0.81714	0.03716	25	0.08988	0.05568	41	0.18733	-.02248	57	0.94911	0.00209
10	0.80383	0.04006	26	0.05735	0.04380	42	0.28260	-.01935	58	0.97687	-.00031
11	0.79457	0.04116	27	0.03212	0.03167	43	0.38225	-.01518	59	0.98850	-.00097
12	0.78859	0.04499	28	0.01410	0.01936	44	0.48002	-.00990	60	0.99597	-.00111
13	0.78486	0.04581	29	0.00568	0.01110	45	0.56021	-.00575	61	0.99922	-.00107
14	0.77441	0.04768	30	0.00208	0.00602	46	0.66816	-.00074	62	1.00000	0.00000
15	0.73922	0.05186	31	0.00000	0.00000	47	0.72514	0.00185			
16	0.67833	0.05977	32	0.00094	-.00484	48	0.76998	0.00356			

SD7032D-PT

1	1.00000	0.00000	14	0.47315	0.07913	27	0.00273	0.00908	40	0.45692	-.00951
2	0.99137	0.00286	15	0.42374	0.08227	28	0.00000	0.00000	41	0.52521	-.00611
3	0.98247	0.00444	16	0.36989	0.08379	29	0.00113	-.00405	42	0.60399	-.00217
4	0.96493	0.00751	17	0.31682	0.08400	30	0.00438	-.00727	43	0.70058	0.00192
5	0.92939	0.01376	18	0.26289	0.08238	31	0.01078	-.01087	44	0.77805	0.00431
6	0.89510	0.01948	19	0.21266	0.07915	32	0.03100	-.01502	45	0.84831	0.00576
7	0.84249	0.02917	20	0.16234	0.07298	33	0.06577	-.01834	46	0.89925	0.00548
8	0.78647	0.03883	21	0.12348	0.06568	34	0.11048	-.02010	47	0.94144	0.00330
9	0.75229	0.04509	22	0.08306	0.05435	35	0.15228	-.02071	48	0.97357	0.00150
10	0.69177	0.05506	23	0.06190	0.04707	36	0.20211	-.01972	49	0.98819	0.00040
11	0.64102	0.06240	24	0.03961	0.03728	37	0.24471	-.01830	50	0.99580	0.00029
12	0.58683	0.06890	25	0.02096	0.02672	38	0.31076	-.01601	51	1.00000	0.00000
13	0.52799	0.07486	26	0.00920	0.01726	39	0.37360	-.01372			

SD7037-PT

1	1.00000	0.00000	14	0.38172	0.07208	27	0.00100	-.00303	40	0.66498	-.00611
2	0.99929	0.00005	15	0.32809	0.07272	28	0.00317	-.00580	41	0.73236	-.00418
3	0.99331	0.00138	16	0.26972	0.07146	29	0.00628	-.00805	42	0.79819	-.00285
4	0.98886	0.00195	17	0.21907	0.06820	30	0.01237	-.01065	43	0.85561	-.00190
5	0.97369	0.00400	18	0.17163	0.06320	31	0.02077	-.01283	44	0.90268	-.00145
6	0.93649	0.01081	19	0.12344	0.05527	32	0.04601	-.01597	45	0.95100	-.00090
7	0.87592	0.02111	20	0.08236	0.04579	33	0.09997	-.01955	46	0.98064	-.00040
8	0.80782	0.03232	21	0.04524	0.03382	34	0.17663	-.02114	47	0.98922	-.00028
9	0.73151	0.04406	22	0.02528	0.02568	35	0.24444	-.01983	48	0.99502	-.00040
10	0.64776	0.05466	23	0.01451	0.01930	36	0.32451	-.01786	49	0.99919	-.00001
11	0.58572	0.06081	24	0.00635	0.01251	37	0.40798	-.01490	50	1.00000	0.00000
12	0.51706	0.06670	25	0.00131	0.00565	38	0.48859	-.01220			
13	0.44411	0.07028	26	0.00000	0.00000	39	0.56361	-.00939			

SD7043-PT

1	1.00000	0.00000	13	0.35134	0.08283	25	0.00210	-.00401	37	0.75556	0.01157
2	0.99874	0.00120	14	0.27330	0.08101	26	0.00653	-.00649	38	0.82892	0.01267
3	0.99193	0.00290	15	0.19497	0.07518	27	0.01381	-.00935	39	0.89294	0.01167
4	0.98462	0.00453	16	0.12296	0.06475	28	0.02710	-.01270	40	0.93019	0.00930
5	0.96737	0.00845	17	0.06910	0.05120	29	0.05550	-.01564	41	0.96463	0.00442
6	0.92851	0.01715	18	0.04318	0.04122	30	0.11109	-.01723	42	0.97740	0.00240
7	0.88433	0.02616	19	0.02601	0.03208	31	0.19526	-.01555	43	0.98975	0.00039
8	0.81359	0.03946	20	0.01634	0.02526	32	0.27461	-.01191	44	0.99654	-.00072
9	0.73237	0.05332	21	0.00717	0.01651	33	0.37827	-.00634	45	1.00000	0.00000
10	0.64469	0.06550	22	0.00299	0.01089	34	0.46235	-.00181			
11	0.55543	0.07458	23	0.00000	0.00000	35	0.56668	0.00391			
12	0.45008	0.08110	24	0.00076	-.00234	36	0.66589	0.00861			

SD7062-PT

1	1.00000	0.00000	14	0.41947	0.10497	27	0.00464	-.01019	40	0.68761	-.00633
2	0.99858	0.00128	15	0.35724	0.10829	28	0.01147	-.01475	41	0.75148	-.00241
3	0.99093	0.00291	16	0.28393	0.10941	29	0.02707	-.02076	42	0.81902	0.00042
4	0.98251	0.00456	17	0.21095	0.10473	30	0.05446	-.02622	43	0.87480	0.00261
5	0.95556	0.01028	18	0.14450	0.09412	31	0.08914	-.02971	44	0.92416	0.00285
6	0.90289	0.02164	19	0.09052	0.07916	32	0.13205	-.03178	45	0.96263	0.00165
7	0.83860	0.03550	20	0.05381	0.06297	33	0.18926	-.03306	46	0.98036	0.00021
8	0.77121	0.04995	21	0.03165	0.04835	34	0.26367	-.03252	47	0.99012	-.00056
9	0.71025	0.06236	22	0.01436	0.03170	35	0.33088	-.03018	48	0.99375	-.00072
10	0.66158	0.07149	23	0.00394	0.01602	36	0.39758	-.02680	49	0.99747	-.00070
11	0.60375	0.08161	24	0.00068	0.00610	37	0.46365	-.02278	50	1.00000	0.00000
12	0.54144	0.09144	25	0.00000	0.00000	38	0.53611	-.01725			
13	0.47657	0.09977	26	0.00110	-.00509	39	0.60846	-.01185			

SD7080-PT

1	1.00000	0.00000	17	0.60750	0.05468	33	0.00438	0.01055	49	0.53834	-.01760
2	0.99183	0.00117	18	0.56410	0.05836	34	0.00116	0.00634	50	0.58628	-.01561
3	0.98352	0.00174	19	0.49176	0.06332	35	0.00000	0.00000	51	0.62824	-.01397
4	0.96858	0.00350	20	0.43149	0.06648	36	0.00254	-.00454	52	0.68145	-.01175
5	0.95485	0.00542	21	0.37481	0.06858	37	0.01040	-.00900	53	0.72884	-.01001
6	0.93589	0.00832	22	0.32848	0.06924	38	0.02575	-.01287	54	0.77743	-.00840
7	0.91890	0.01088	23	0.27587	0.06886	39	0.04165	-.01529	55	0.82590	-.00658
8	0.88226	0.01684	24	0.23356	0.06782	40	0.07011	-.01892	56	0.86881	-.00526
9	0.82797	0.02559	25	0.19377	0.06581	41	0.11868	-.02311	57	0.91610	-.00378
10	0.77224	0.03414	26	0.15401	0.06139	42	0.16464	-.02511	58	0.94941	-.00283
11	0.73311	0.03955	27	0.11281	0.05456	43	0.19765	-.02600	59	0.97309	-.00181
12	0.71136	0.04265	28	0.07803	0.04624	44	0.23366	-.02637	60	0.98891	-.00080
13	0.69676	0.04483	29	0.05006	0.03645	45	0.29930	-.02566	61	1.00000	0.00000
14	0.67807	0.04689	30	0.03430	0.02945	46	0.34847	-.02428			
15	0.65950	0.04850	31	0.01974	0.02177	47	0.41309	-.02221			
16	0.63631	0.05108	32	0.01025	0.01553	48	0.47835	-.01998			

SD7080-PT (R – repeated)

1	1.00000	0.00000	14	0.57352	0.05644	27	0.00098	0.00290	40	0.37210	-.02582
2	0.99990	0.00014	15	0.49992	0.06140	28	0.00000	0.00000	41	0.45218	-.02299
3	0.99376	0.00096	16	0.43739	0.06475	29	0.00159	-.00655	42	0.53688	-.01943
4	0.98594	0.00196	17	0.35012	0.06707	30	0.00555	-.01003	43	0.63455	-.01503
5	0.96163	0.00487	18	0.26596	0.06657	31	0.01333	-.01318	44	0.72084	-.01131
6	0.91714	0.01123	19	0.20697	0.06435	32	0.02421	-.01578	45	0.81907	-.00754
7	0.84994	0.02182	20	0.15342	0.05878	33	0.03589	-.01767	46	0.89835	-.00433
8	0.77406	0.03330	21	0.11012	0.05138	34	0.05181	-.01982	47	0.95343	-.00250
9	0.72826	0.03962	22	0.07047	0.04117	35	0.07084	-.02211	48	0.98508	-.00082
10	0.68963	0.04505	23	0.04668	0.03217	36	0.10893	-.02546	49	0.99711	0.00009
11	0.65702	0.04793	24	0.03308	0.02595	37	0.15520	-.02762	50	1.00000	0.00000
12	0.63630	0.05018	25	0.01511	0.01594	38	0.20519	-.02892			
13	0.61179	0.05314	26	0.00562	0.00872	39	0.28829	-.02833			

SD7084-PT

1	1.00000	0.00000	14	0.38273	0.07052	27	0.00255	-.00568	40	0.64219	-.01549
2	1.00054	0.00065	15	0.32521	0.07125	28	0.00736	-.00873	41	0.70619	-.01276
3	0.99653	0.00137	16	0.25319	0.07007	29	0.01606	-.01190	42	0.75542	-.01058
4	0.99114	0.00222	17	0.19244	0.06629	30	0.02985	-.01528	43	0.80901	-.00830
5	0.97294	0.00504	18	0.13759	0.05965	31	0.06279	-.02023	44	0.86804	-.00576
6	0.93611	0.01066	19	0.07344	0.04503	32	0.10990	-.02400	45	0.88704	-.00497
7	0.88482	0.01893	20	0.05096	0.03696	33	0.15766	-.02593	46	0.91556	-.00379
8	0.82063	0.02921	21	0.03199	0.02852	34	0.23338	-.02676	47	0.94846	-.00243
9	0.74736	0.04035	22	0.01874	0.02121	35	0.29873	-.02622	48	0.97209	-.00159
10	0.68131	0.04887	23	0.00632	0.01161	36	0.37682	-.02466	49	0.98882	-.00096
11	0.62448	0.05519	24	0.00182	0.00612	37	0.44099	-.02295	50	0.99462	-.00073
12	0.53534	0.06299	25	0.00000	0.00000	38	0.52013	-.02032	51	0.99950	-.00050
13	0.45167	0.06811	26	0.00072	-.00308	39	0.58645	-.01780	52	1.00000	0.00000

SD7090-PT

1	1.00000	0.00000	14	0.40677	0.06377	27	0.00275	-.00807	40	0.59401	-.02121
2	0.99809	0.00048	15	0.33532	0.06612	28	0.00793	-.01270	41	0.66395	-.01716
3	0.99216	0.00130	16	0.27801	0.06638	29	0.01900	-.01823	42	0.73667	-.01307
4	0.98366	0.00248	17	0.23836	0.06555	30	0.03878	-.02247	43	0.79664	-.00974
5	0.96484	0.00485	18	0.18226	0.06181	31	0.07305	-.02736	44	0.86846	-.00573
6	0.93672	0.00889	19	0.12139	0.05399	32	0.12168	-.03140	45	0.90654	-.00410
7	0.89561	0.01491	20	0.07629	0.04409	33	0.17594	-.03319	46	0.95168	-.00275
8	0.82595	0.02453	21	0.04068	0.03230	34	0.22966	-.03335	47	0.97538	-.00194
9	0.74885	0.03382	22	0.02135	0.02383	35	0.29527	-.03243	48	0.99014	-.00101
10	0.68385	0.04153	23	0.00753	0.01387	36	0.35147	-.03124	49	0.99401	-.00083
11	0.62373	0.04777	24	0.00226	0.00647	37	0.39780	-.03007	50	0.99882	-.00013
12	0.53659	0.05518	25	0.00000	0.00000	38	0.46494	-.02773	51	1.00000	0.00000
13	0.47817	0.05930	26	0.00026	-.00311	39	0.52937	-.02480			

SD8000-PT

1	1.00000	0.00000	13	0.48977	0.05786	25	0.00102	-.00319	37	0.43854	-.02091
2	1.00046	0.00111	14	0.40596	0.06130	26	0.00371	-.00622	38	0.53740	-.01575
3	0.99665	0.00195	15	0.32881	0.06252	27	0.00922	-.00961	39	0.62509	-.01101
4	0.98897	0.00307	16	0.25288	0.06117	28	0.01796	-.01358	40	0.70568	-.00666
5	0.96936	0.00554	17	0.17660	0.05690	29	0.02842	-.01697	41	0.78624	-.00248
6	0.93466	0.01027	18	0.11169	0.04938	30	0.04584	-.02041	42	0.87495	0.00048
7	0.89450	0.01624	19	0.05866	0.03824	31	0.07055	-.02359	43	0.93423	0.00087
8	0.82036	0.02689	20	0.03413	0.02978	32	0.11413	-.02689	44	0.97424	-.00016
9	0.75841	0.03476	21	0.01668	0.02080	33	0.16687	-.02834	45	0.99198	-.00099
10	0.70380	0.04128	22	0.00800	0.01455	34	0.22209	-.02834	46	0.99724	-.00115
11	0.64809	0.04662	23	0.00318	0.00899	35	0.29657	-.02675	47	0.99949	-.00113
12	0.57198	0.05264	24	0.00000	0.00000	36	0.36217	-.02436	48	1.00000	0.00000

SD8020-PT

1	1.00000	0.00000	12	0.43092	0.04660	23	0.00147	-.00625	34	0.49319	-.04514
2	0.99396	0.00191	13	0.33493	0.04972	24	0.00412	-.00985	35	0.57180	-.04045
3	0.98570	0.00275	14	0.26455	0.05010	25	0.00968	-.01413	36	0.66694	-.03329
4	0.96612	0.00430	15	0.18958	0.04800	26	0.02060	-.02008	37	0.75090	-.02598
5	0.92732	0.00795	16	0.13368	0.04383	27	0.04464	-.02910	38	0.82765	-.01870
6	0.86826	0.01364	17	0.08309	0.03709	28	0.07929	-.03733	39	0.90390	-.01106
7	0.80447	0.01961	18	0.03760	0.02616	29	0.13372	-.04507	40	0.95497	-.00571
8	0.73551	0.02585	19	0.01708	0.01766	30	0.19340	-.04970	41	0.98171	-.00275
9	0.67337	0.03114	20	0.00634	0.01068	31	0.25884	-.05173	42	0.99027	-.00195
10	0.59887	0.03672	21	0.00201	0.00586	32	0.33492	-.05100	43	0.99794	-.00110
11	0.51865	0.04194	22	0.00000	0.00000	33	0.40845	-.04886	44	1.00000	0.00000

SD8040-PT

1	1.00000	0.00000	17	0.50241	0.06120	33	0.00137	-.00569	49	0.61451	-.01724
2	0.99965	0.00040	18	0.46196	0.06398	34	0.00413	-.01087	50	0.70186	-.01217
3	0.99521	0.00063	19	0.42357	0.06621	35	0.00780	-.01426	51	0.77828	-.00785
4	0.98927	0.00169	20	0.38505	0.06785	36	0.01781	-.01932	52	0.84101	-.00515
5	0.98316	0.00231	21	0.34640	0.06855	37	0.02962	-.02226	53	0.88632	-.00448
6	0.95575	0.00536	22	0.30158	0.06867	38	0.07618	-.02874	54	0.93238	-.00406
7	0.91961	0.00936	23	0.25831	0.06831	39	0.07876	-.02907	55	0.96097	-.00276
8	0.87616	0.01531	24	0.22090	0.06686	40	0.12049	-.03167	56	0.98033	-.00192
9	0.83607	0.02078	25	0.16299	0.06167	41	0.16063	-.03279	57	0.98804	-.00097
10	0.79536	0.02660	26	0.10802	0.05288	42	0.20477	-.03241	58	0.99040	-.00123
11	0.75229	0.03293	27	0.07243	0.04403	43	0.24661	-.03109	59	0.99542	-.00056
12	0.71153	0.03874	28	0.04372	0.03340	44	0.28913	-.02979	60	0.99835	-.00037
13	0.66984	0.04431	29	0.02237	0.02376	45	0.33180	-.02825	61	1.00000	0.00000
14	0.62781	0.04995	30	0.01244	0.01812	46	0.37070	-.02704			
15	0.58684	0.05425	31	0.00365	0.01007	47	0.43114	-.02456			
16	0.54497	0.05818	32	0.00000	0.00000	48	0.51941	-.02103			

SPICA-PT

1	1.00000	0.00000	12	0.33472	0.10149	23	0.00210	-.00766	34	0.73344	-.01016
2	0.99747	0.00218	13	0.24624	0.09962	24	0.00603	-.01151	35	0.81667	-.00892
3	0.98865	0.00375	14	0.17395	0.09128	25	0.01313	-.01472	36	0.89714	-.00671
4	0.97029	0.00686	15	0.10819	0.07550	26	0.02579	-.01662	37	0.94426	-.00477
5	0.92254	0.01496	16	0.06122	0.05629	27	0.05337	-.01706	38	0.98203	-.00305
6	0.85855	0.02619	17	0.02790	0.03758	28	0.13855	-.01653	39	0.98989	-.00259
7	0.77971	0.04050	18	0.01155	0.02351	29	0.27127	-.01512	40	0.99763	-.00191
8	0.68977	0.05706	19	0.00566	0.01562	30	0.37689	-.01423	41	1.00000	0.00000
9	0.59982	0.07254	20	0.00224	0.00889	31	0.47150	-.01310			
10	0.50396	0.08771	21	0.00000	0.00000	32	0.55852	-.01217			
11	0.42396	0.09740	22	0.00060	-.00440	33	0.63629	-.01128			

WB135/35-PT

1	1.00000	0.00000	15	0.37012	0.09633	29	0.00972	-.01375	43	0.62232	-.01219
2	0.99821	0.00274	16	0.30793	0.09621	30	0.01297	-.01638	44	0.67693	-.00950
3	0.99188	0.00445	17	0.25066	0.09418	31	0.01887	-.01908	45	0.73298	-.00793
4	0.98481	0.00608	18	0.19031	0.08820	32	0.02815	-.02308	46	0.78998	-.00708
5	0.96319	0.01048	19	0.14094	0.07863	33	0.04827	-.02948	47	0.85532	-.00630
6	0.92894	0.01721	20	0.09773	0.06491	34	0.08172	-.03637	48	0.90696	-.00578
7	0.87438	0.02743	21	0.06119	0.04891	35	0.12166	-.04183	49	0.95165	-.00520
8	0.81262	0.03955	22	0.03477	0.03555	36	0.16424	-.04421	50	0.97784	-.00383
9	0.75053	0.05152	23	0.01358	0.02146	37	0.21630	-.04300	51	0.98772	-.00308
10	0.70000	0.06086	24	0.00457	0.01238	38	0.27413	-.03907	52	0.99297	-.00293
11	0.62886	0.07332	25	0.00158	0.00717	39	0.33433	-.03411	53	0.99738	-.00254
12	0.56368	0.08158	26	0.00000	0.00000	40	0.41105	-.02751	54	1.00000	0.00000
13	0.50644	0.08754	27	0.00046	-.00433	41	0.48508	-.02135			
14	0.43789	0.09367	28	0.00207	-.00719	42	0.55472	-.01631			

WB140/35/FB-PT

1	1.00000	0.00000	13	0.59546	0.09232	25	0.00000	0.00000	37	0.60202	-.02154
2	0.99723	0.00331	14	0.53052	0.09962	26	0.00139	-.00545	38	0.69153	-.01732
3	0.99072	0.00555	15	0.44053	0.10466	27	0.00482	-.00920	39	0.76755	-.01374
4	0.98199	0.00864	16	0.36440	0.10427	28	0.01433	-.01452	40	0.83783	-.01025
5	0.95585	0.01663	17	0.30002	0.10112	29	0.03152	-.02117	41	0.89180	-.00751
6	0.93184	0.02317	18	0.23707	0.09598	30	0.05959	-.02869	42	0.93869	-.00480
7	0.89998	0.03098	19	0.17643	0.08673	31	0.11668	-.03807	43	0.97036	-.00336
8	0.86854	0.03837	20	0.11345	0.06943	32	0.17375	-.04098	44	0.98701	-.00265
9	0.82209	0.04901	21	0.06669	0.05044	33	0.25293	-.03858	45	0.99303	-.00287
10	0.76684	0.06102	22	0.03588	0.03498	34	0.32927	-.03509	46	0.99700	-.00276
11	0.70863	0.07278	23	0.01392	0.02054	35	0.41526	-.03066	47	1.00000	0.00000
12	0.64966	0.08378	24	0.00542	0.01259	36	0.51953	-.02546			

Sorted by Name	
Airfoil	$C_{mc/4}$
CLARK-Y	−0.0873
DAE51	−0.1081
DF101	−0.0582
DF102	−0.0521
E205	−0.0543
E214	−0.1382
E374	−0.0556
E387	−0.0817
FX60-100	−0.1201
HQ2/9	−0.0821
MB253515	−0.0495
RG15	−0.0578
S2048	−0.0676
S2055	−0.0483
S2083	−0.0722
S2091	−0.0817
S3014	−0.0508
S3016	−0.0390
S3021	−0.0597
S4061	−0.0915
S4233	−0.0758
S8040	−0.0630
SD5060	−0.0529
SD6060	−0.0386
SD6080	−0.0822
SD7003	−0.0347
SD7032	−0.0989
SD7043	−0.1001
SD7062	−0.0831
SD7080	−0.0667
SD7090	−0.0484
SD8000	−0.0493
SPICA	−0.1024

Note: Average moment coefficient as predicted by the ISES code for $Rn = 200,000$.

Sorted by Name		
Airfoil	% Thickness	% Camber
AQUILA	9.38	4.05
CLARK-Y	11.72	3.55
DAE51	9.37	3.98
DF101	11.00	2.30
DF102	11.00	2.30
DF103	11.00	2.30
E193	10.22	3.57
E193MOD	11.85	4.15
E205	10.48	3.01
E214	11.10	4.03
E374	10.91	2.24
E387	9.06	3.80
FX60-100	9.97	3.55
FX63-137	13.59	5.94
HQ2/9	8.97	1.99
J5012	12.00	0.00
MB253515	14.96	2.43
MILEY	12.81	5.16
NACA 0009	9.00	0.00
NACA 2.5411	11.00	2.50
NACA 64A010	10.00	0.00
NACA 6409	9.00	6.00
RG15	8.92	1.76
S2048	8.63	1.94
S2055	7.99	1.66
S2091	10.10	3.91
S3010	10.32	2.82
S3014	9.46	2.57
S3016	9.52	2.09
S3021	9.47	2.96
S4061	9.60	3.90
S4062	9.53	4.14
S4180	9.77	4.36
S4233	13.64	3.26
SD2030	8.56	2.25
SD2083	8.96	2.85
SD5060	9.45	2.30
SD6060	10.37	1.84
SD6080	9.18	3.74
SD7003	8.51	1.46
SD7032	9.95	3.66
SD7037	9.20	3.02
SD7043	9.13	3.51
SD7062	13.98	3.97
SD7080	9.15	2.48
SD7084	9.63	2.31
SD7090	9.99	1.87
SD8000	8.86	1.71
SD8020	10.10	0.00
SD8040	9.99	2.65
SPICA	11.72	4.74
WB135/35	13.53	3.75
WB140/35/FB	13.92	3.70

Sorted by Thickness		
Airfoil	% Thickness	% Camber
S2055	7.99	1.66
SD7003	8.51	1.46
SD2030	8.56	2.25
S2048	8.63	1.94
SD8000	8.86	1.71
RG15	8.92	1.76
SD2083	8.96	2.85
HQ2/9	8.97	1.99
NACA 0009	9.00	0.00
NACA 6409	9.00	6.00
E387	9.06	3.80
SD7043	9.13	3.51
SD7080	9.15	2.48
SD6080	9.18	3.74
SD7037	9.20	3.02
DAE51	9.37	3.98
AQUILA	9.38	4.05
SD5060	9.45	2.30
S3014	9.46	2.57
S3021	9.47	2.96
S3016	9.52	2.09
S4062	9.53	4.14
S4061	9.60	3.90
SD7084	9.63	2.31
S4180	9.77	4.36
SD7032	9.95	3.66
FX60-100	9.97	3.55
SD7090	9.99	1.87
SD8040	9.99	2.65
NACA 64A010	10.00	0.00
SD8020	10.10	0.00
S2091	10.10	3.91
E193	10.22	3.57
S3010	10.32	2.82
SD6060	10.37	1.84
E205	10.48	3.01
E374	10.91	2.24
DF103	11.00	2.30
DF102	11.00	2.30
DF101	11.00	2.30
NACA 2.5411	11.00	2.50
E214	11.10	4.03
CLARK-Y	11.72	3.55
SPICA	11.72	4.74
E193MOD	11.85	4.15
J5012	12.00	0.00
MILEY	12.81	5.16
WB135/35	13.53	3.75
FX63-137	13.59	5.94
S4233	13.64	3.26
WB140/35/FB	13.92	3.70
SD7062	13.98	3.97
MB253515	14.96	2.43

Sorted by Camber		
Airfoil	% Thickness	% Camber
NACA 0009	9.00	0.00
NACA 64A010	10.00	0.00
SD8020	10.10	0.00
J5012	12.00	0.00
SD7003	8.51	1.46
S2055	7.99	1.66
SD8000	8.86	1.71
RG15	8.92	1.76
SD6060	10.37	1.84
SD7090	9.99	1.87
S2048	8.63	1.94
HQ2/9	8.97	1.99
S3016	9.52	2.09
E374	10.91	2.24
SD2030	8.56	2.25
SD5060	9.45	2.30
DF101	11.00	2.30
DF102	11.00	2.30
DF103	11.00	2.30
SD7084	9.63	2.31
MB253515	14.96	2.43
SD7080	9.15	2.48
NACA 2.5411	11.00	2.50
S3014	9.46	2.57
SD8040	9.99	2.65
S3010	10.32	2.82
SD2083	8.96	2.85
S3021	9.47	2.96
E205	10.48	3.01
SD7037	9.20	3.02
S4233	13.64	3.26
SD7043	9.13	3.51
FX60-100	9.97	3.55
CLARK-Y	11.72	3.55
E193	10.22	3.57
SD7032	9.95	3.66
WB140/35/FB	13.92	3.70
SD6080	9.18	3.74
WB135/35	13.53	3.75
E387	9.06	3.80
S4061	9.60	3.90
S2091	10.10	3.91
SD7062	13.98	3.97
DAE51	9.37	3.98
E214	11.10	4.03
AQUILA	9.38	4.05
S4062	9.53	4.14
E193MOD	11.85	4.15
S4180	9.77	4.36
SPICA	11.72	4.74
MILEY	12.81	5.16
FX63-137	13.59	5.94
NACA 6409	9.00	6.00

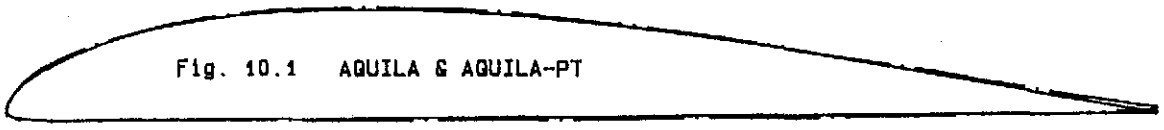

Fig. 10.1 AQUILA & AQUILA-PT

Avg. diff. = 0.0158 in.

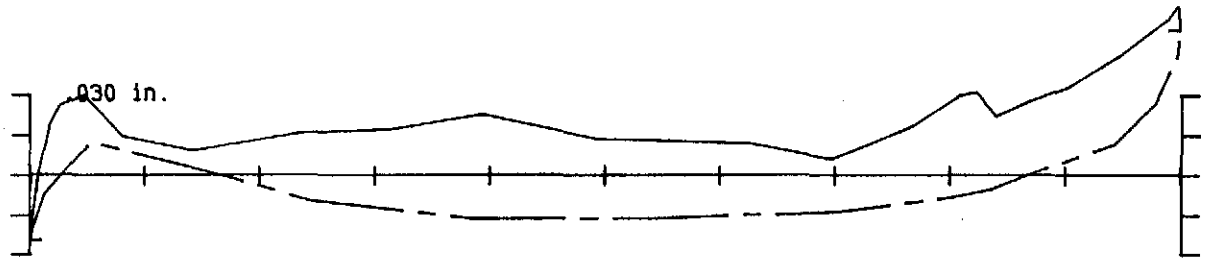

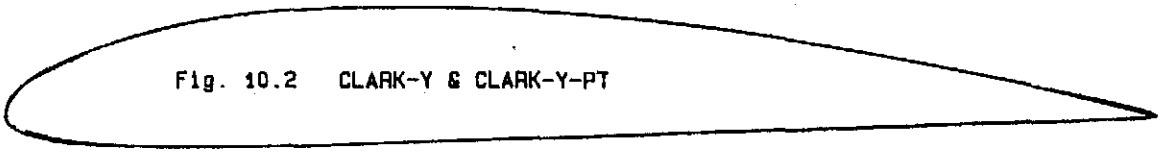

Fig. 10.2 CLARK-Y & CLARK-Y-PT

Avg. diff. = 0.0062 in.

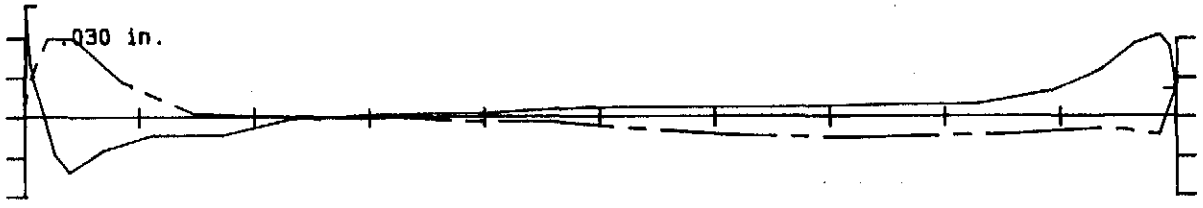

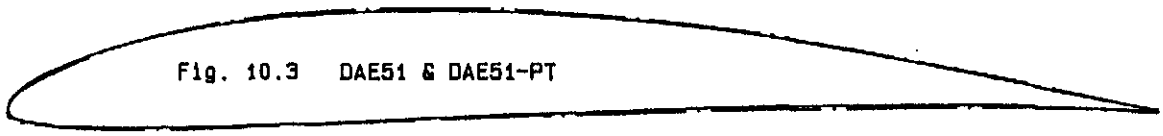

Fig. 10.3 DAE51 & DAE51-PT

Avg. diff. = 0.0172 in.

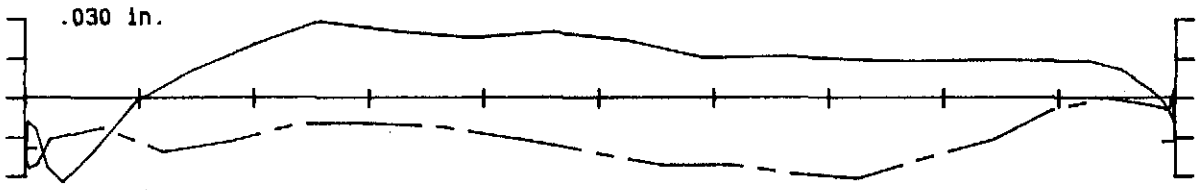

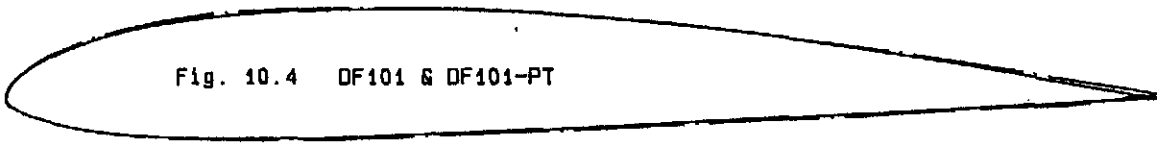

Fig. 10.4 DF101 & DF101-PT

Avg. diff. = 0.0150 in.

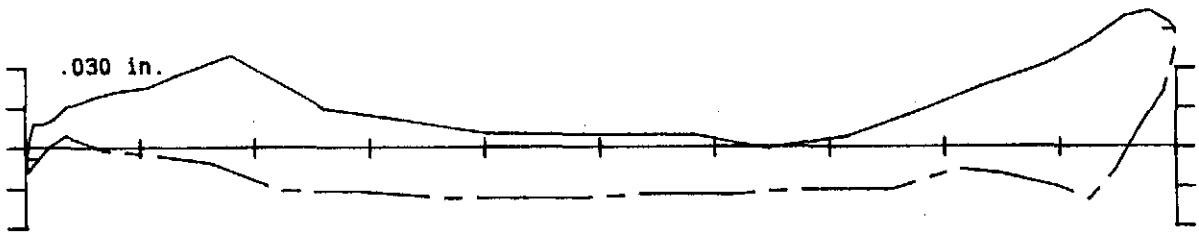

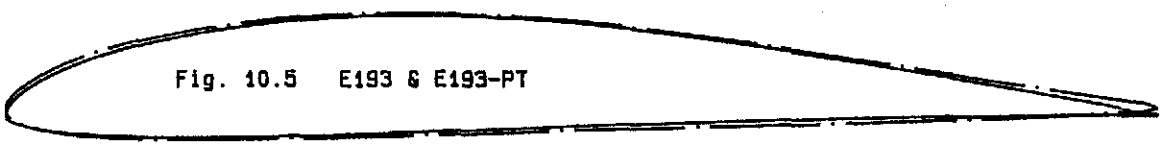

Fig. 10.5 E193 & E193-PT

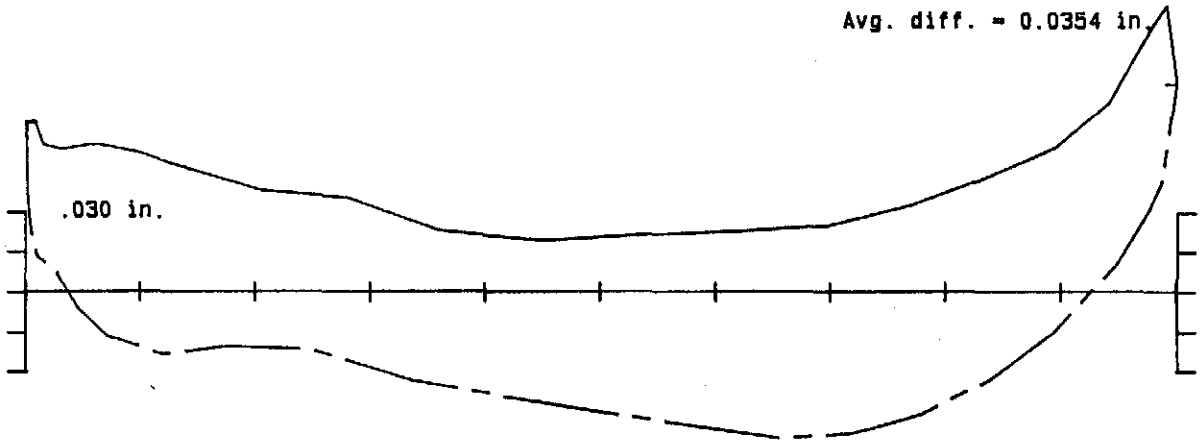

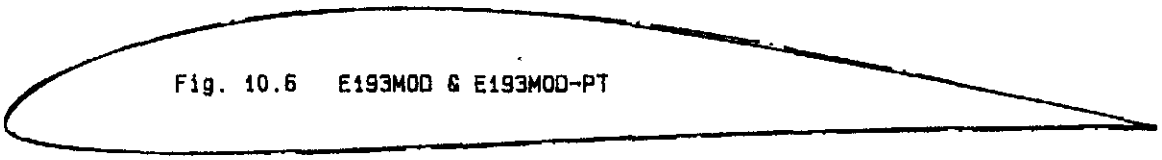

Fig. 10.6 E193MOD & E193MOD-PT

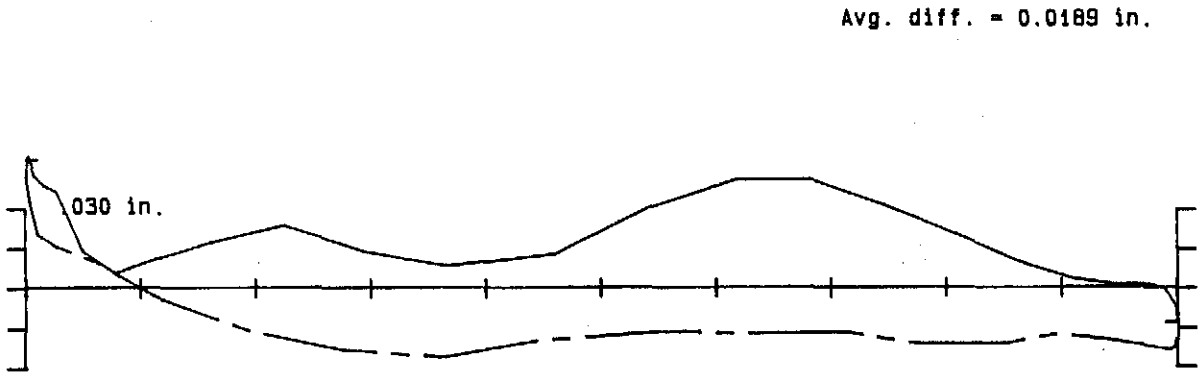

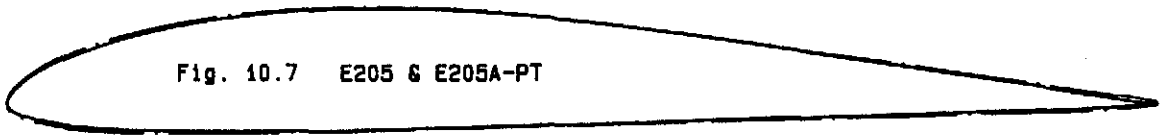

Fig. 10.7 E205 & E205A-PT

Avg. diff. = 0.0151 in.

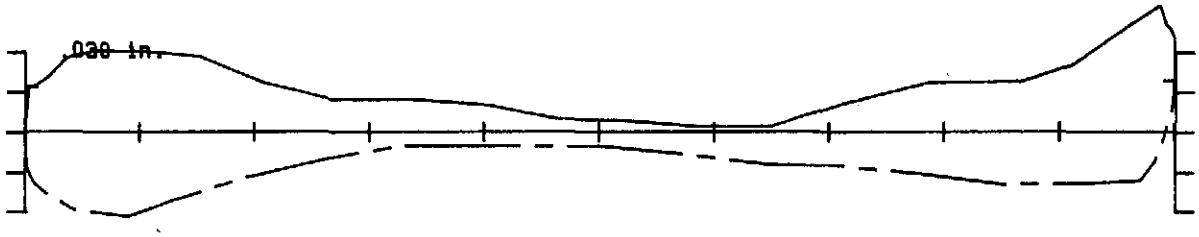

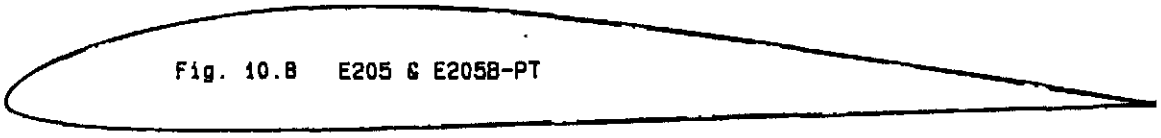

Fig. 10.8 E205 & E205B-PT

Avg. diff. = 0.0106 in.

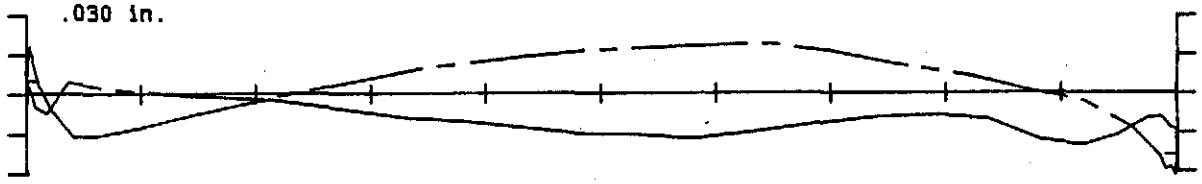

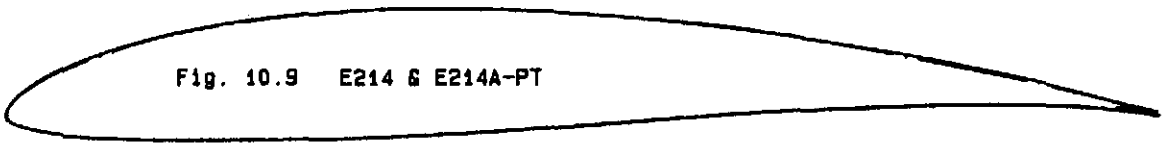

Fig. 10.9 E214 & E214A-PT

Avg. diff. = 0.0066 in.

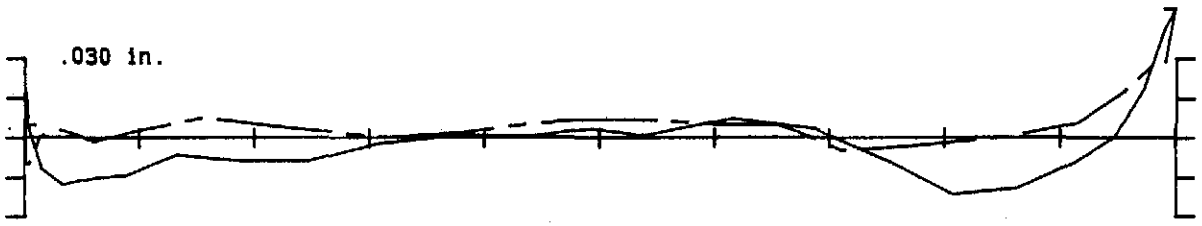

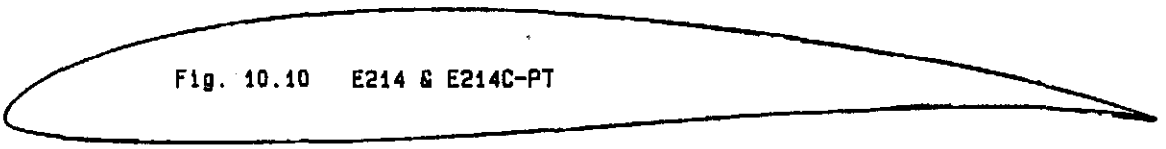

Fig. 10.10 E214 & E214C-PT

Avg. diff. = 0.0081 in.

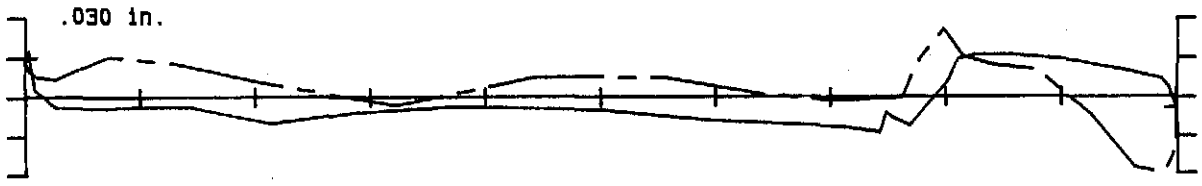

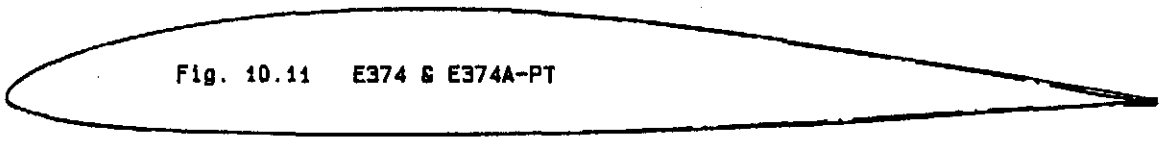

Fig. 10.11 E374 & E374A-PT

Avg. diff. = 0.0089 in.

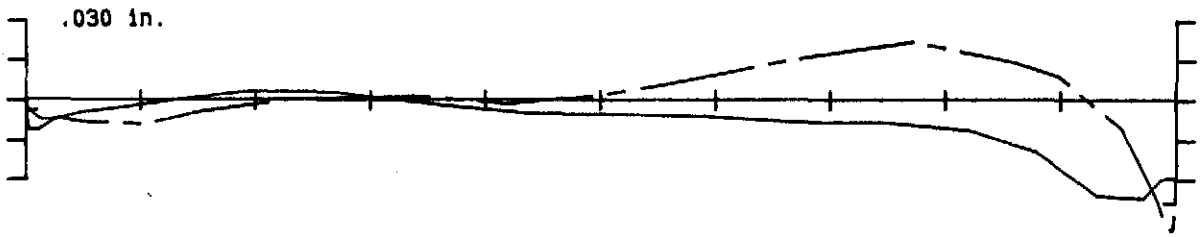

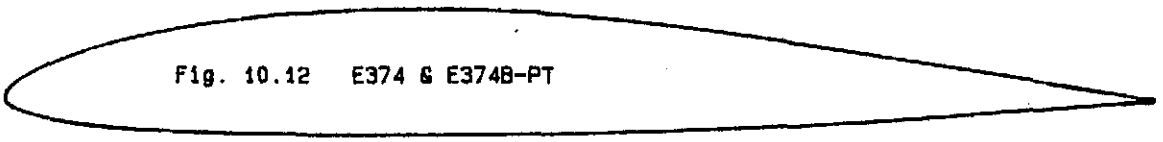

Fig. 10.12 E374 & E374B-PT

Avg. diff. = 0.0063 in.

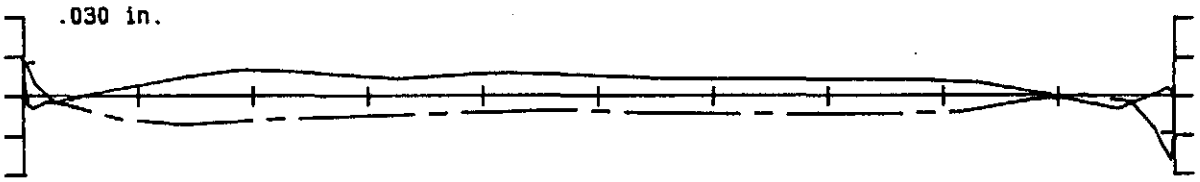

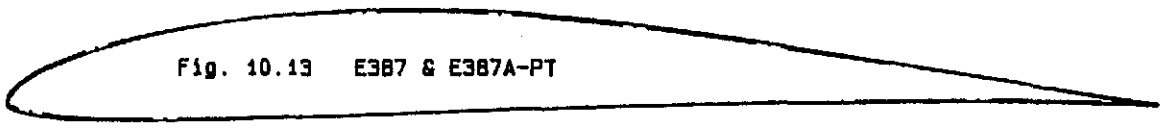

Fig. 10.13 E387 & E387A-PT

Avg. diff. = 0.0109 in.

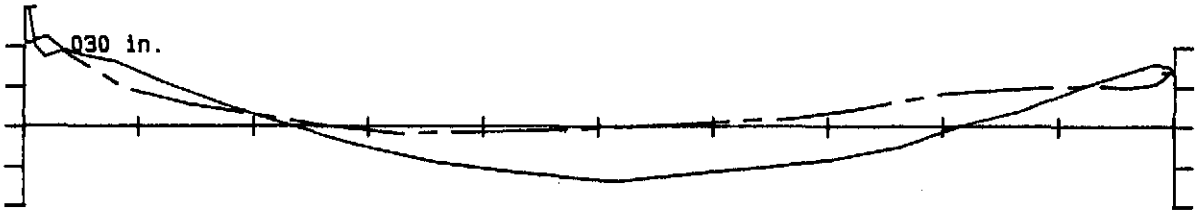

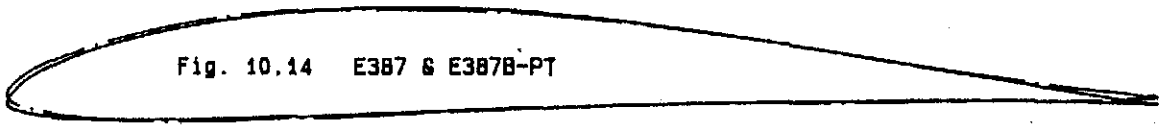

Fig. 10.14 E387 & E387B-PT

Avg. diff. = 0.0174 in.

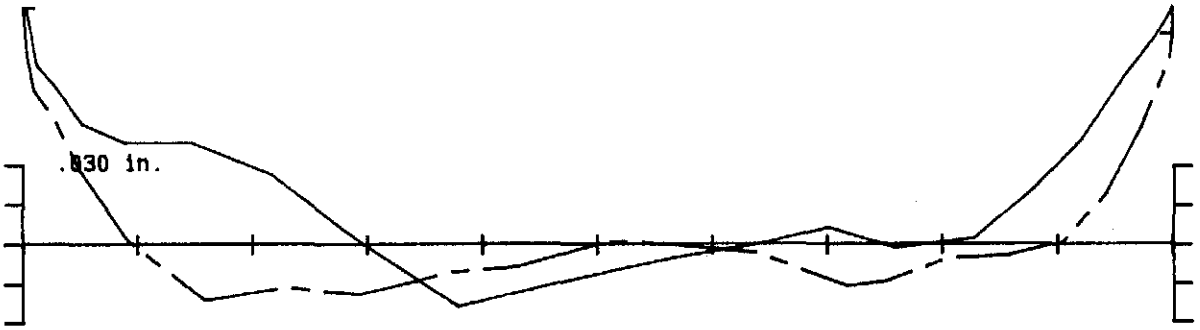

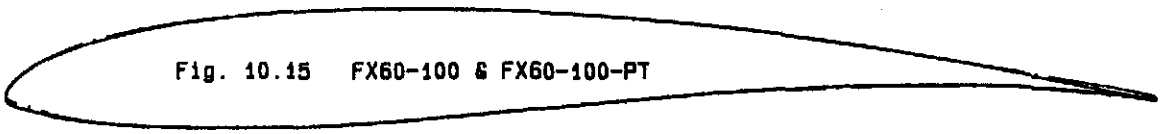

Fig. 10.15 FX60-100 & FX60-100-PT

Avg. diff. = 0.0074 in.

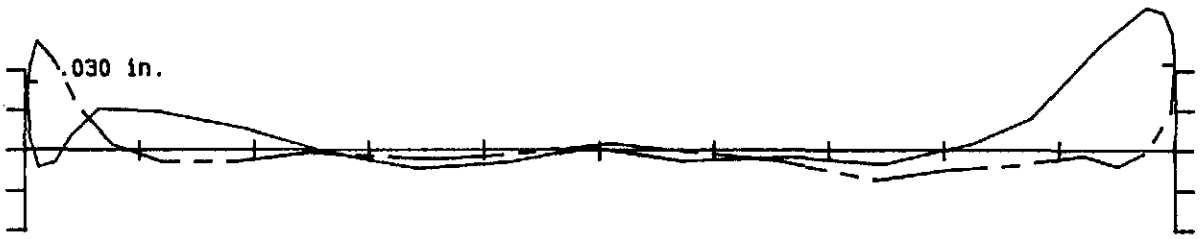

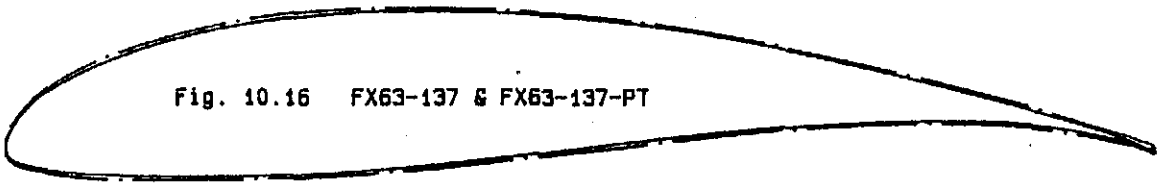

Fig. 10.16 FX63-137 & FX63-137-PT

Avg. diff. = 0.0322 in.

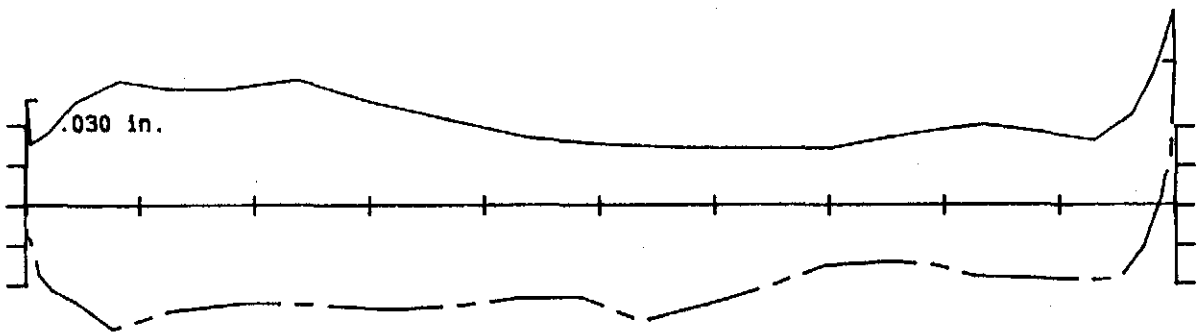

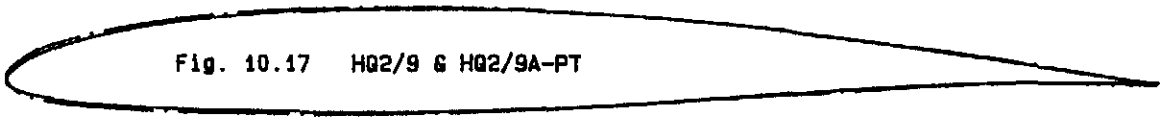

Fig. 10.17 HQ2/9 & HQ2/9A-PT

Avg. diff. = 0.0164 in.

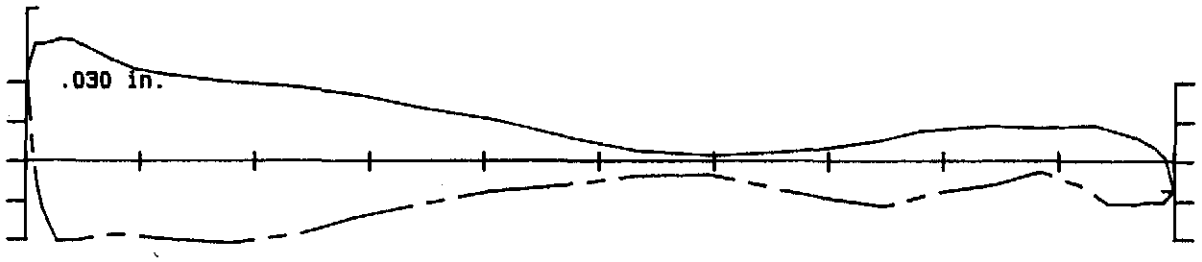

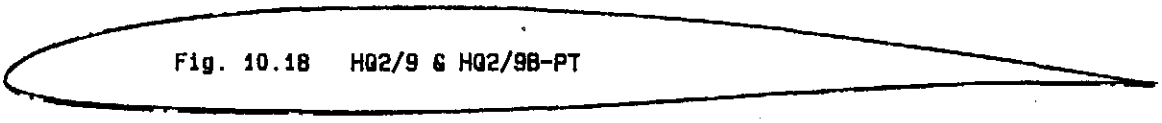

Fig. 10.18 HQ2/9 & HQ2/9B-PT

Avg. diff. = 0.0124 in.

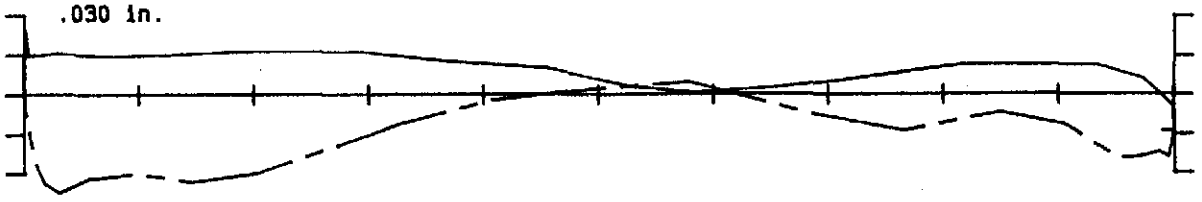

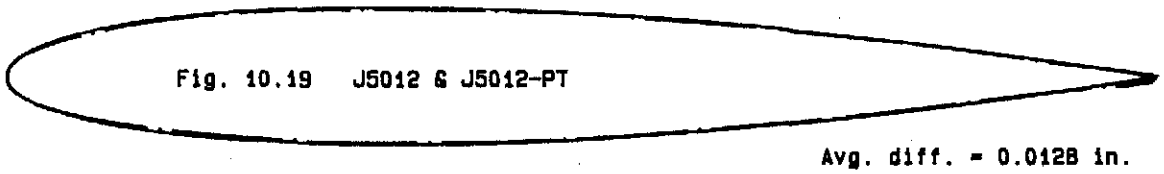

Fig. 10.19 J5012 & J5012-PT

Avg. diff. = 0.0128 in.

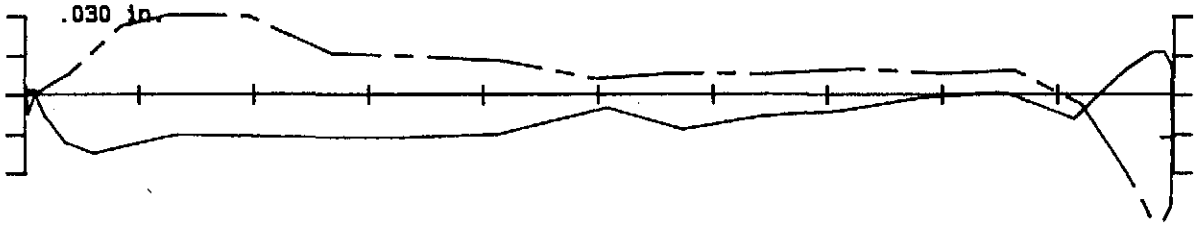

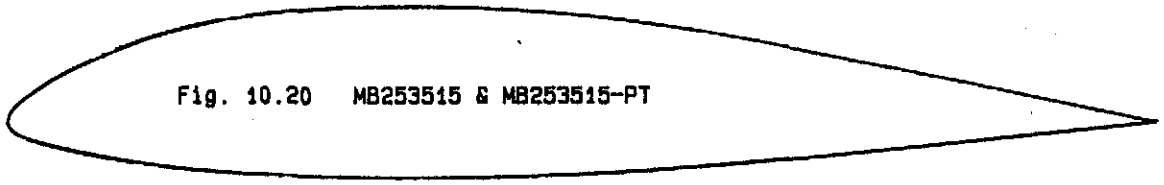

Fig. 10.20 MB253515 & MB253515-PT

Avg. diff. = 0.0047 in.

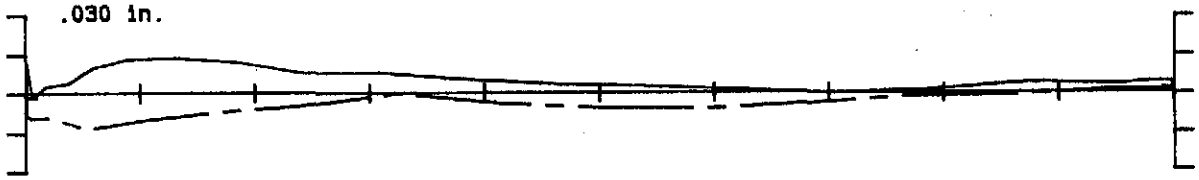

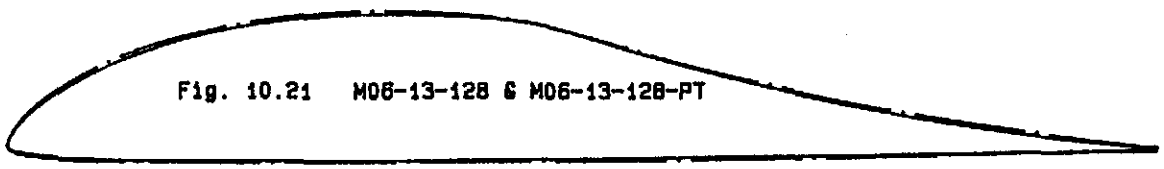

Fig. 10.21 M06-13-128 & M06-13-128-PT

Avg. diff. = 0.0221 in.

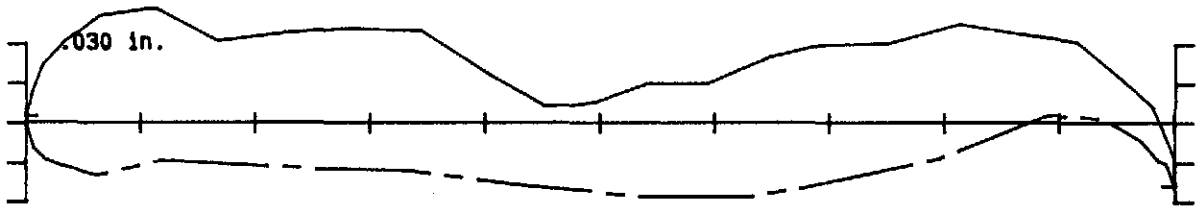

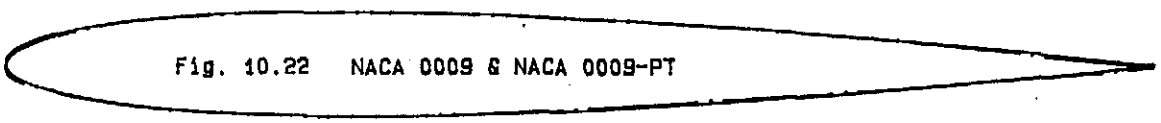

Fig. 10.22 NACA 0009 & NACA 0009-PT

Avg. diff. = 0.0080 in.

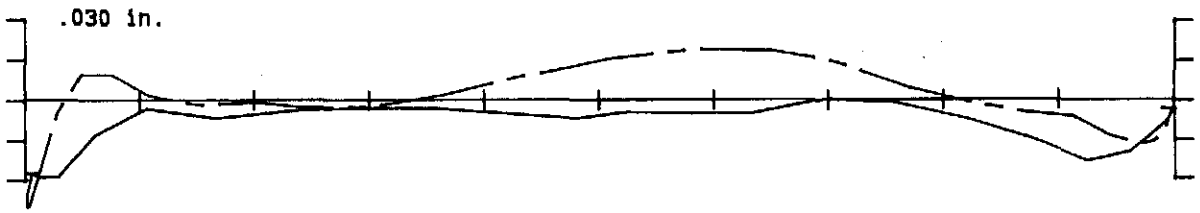

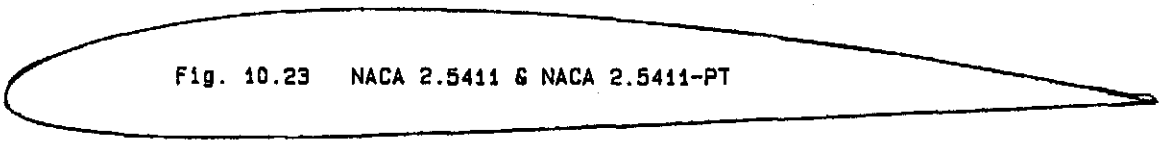

Fig. 10.23 NACA 2.5411 & NACA 2.5411-PT

Avg. diff. = 0.0046 in.

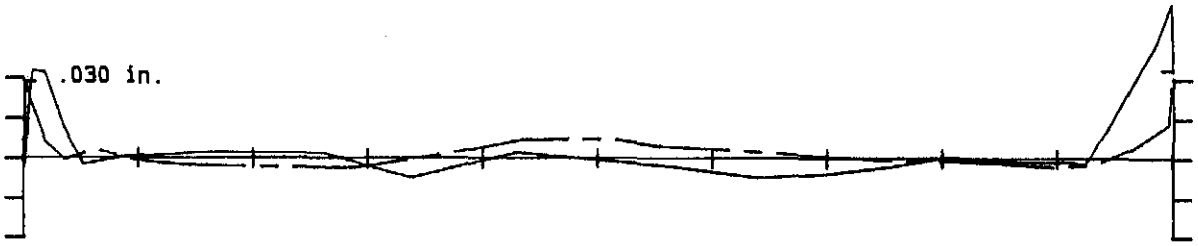

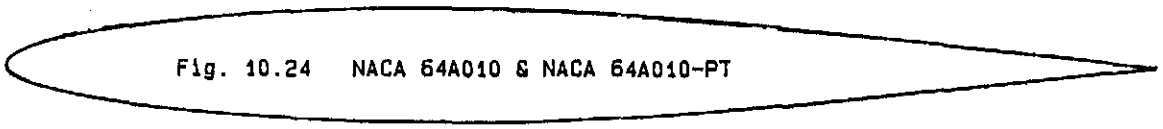

Fig. 10.24 NACA 64A010 & NACA 64A010-PT

Avg. diff. = 0.0065 in.

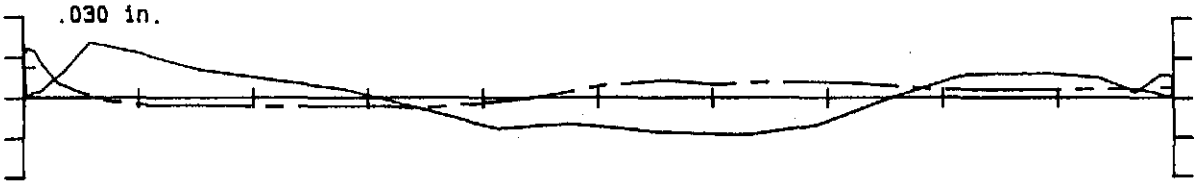

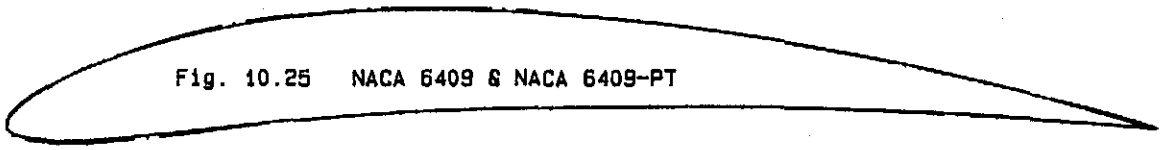

Fig. 10.25 NACA 6409 & NACA 6409-PT

Avg. diff. = 0.0097 in.

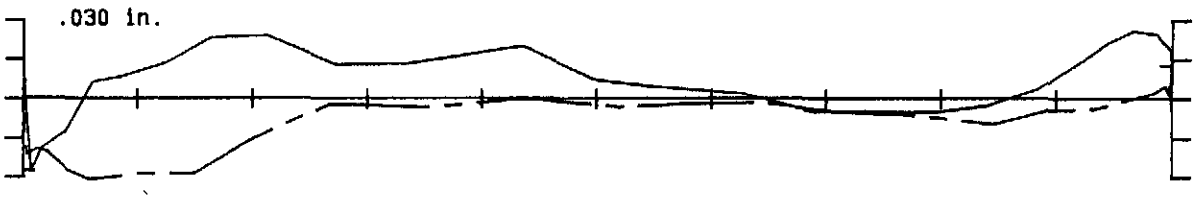

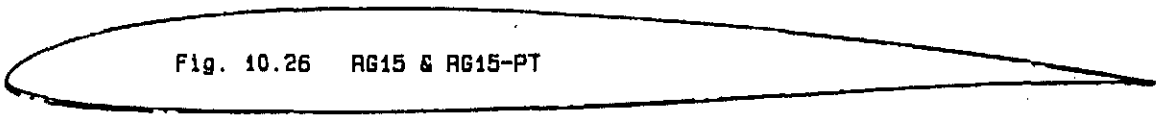

Fig. 10.26 RG15 & RG15-PT

Avg. diff. = 0.0098 in.

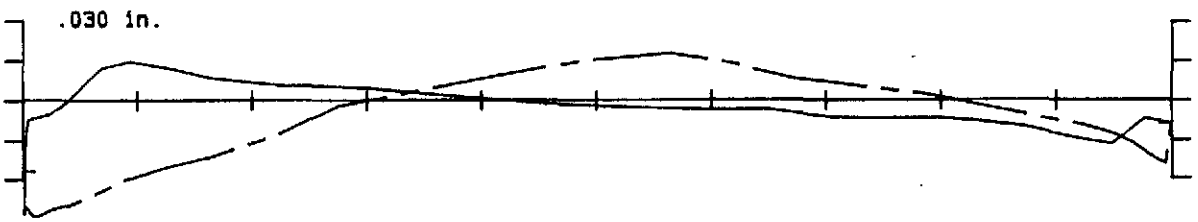

Fig. 10.27 S2048 & S2048-PT

Avg. diff. = 0.0246 in.

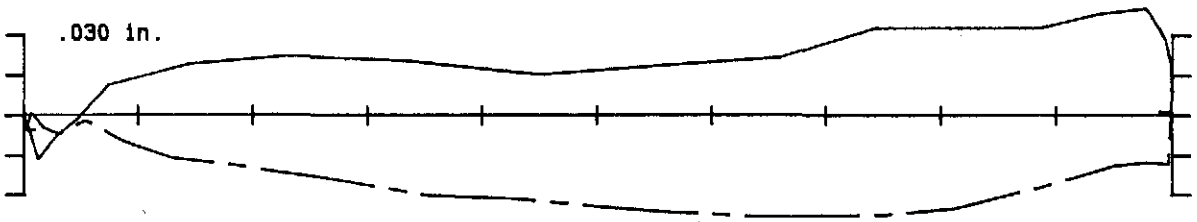

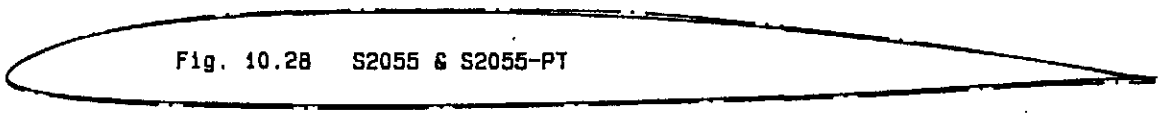

Fig. 10.28 S2055 & S2055-PT

Avg. diff. = 0.0233 in.

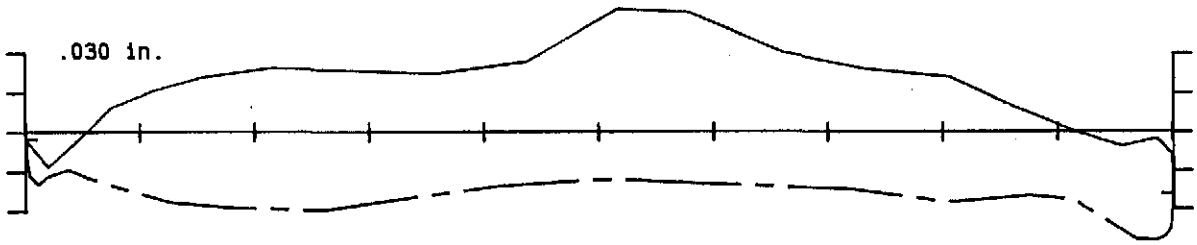

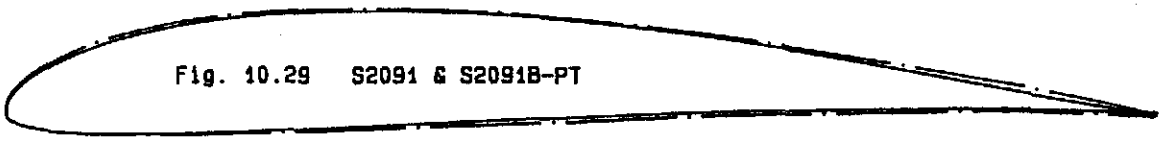

Fig. 10.29 S2091 & S2091B-PT

Avg. diff. = 0.0329 in.

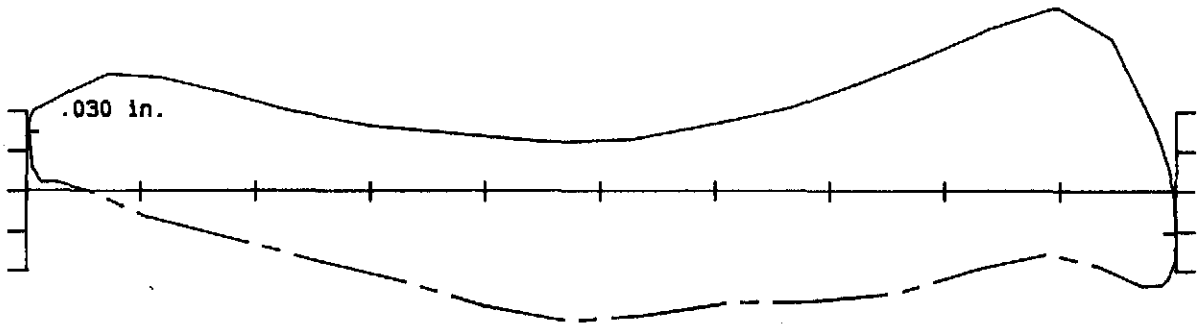

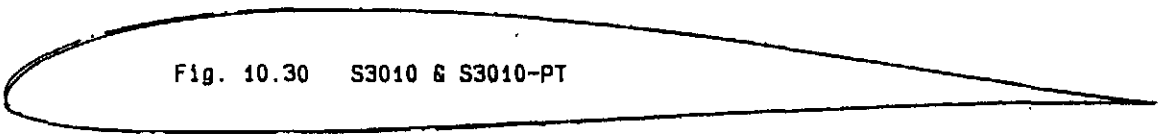

Fig. 10.30 S3010 & S3010-PT

Avg. diff. = 0.0128 in.

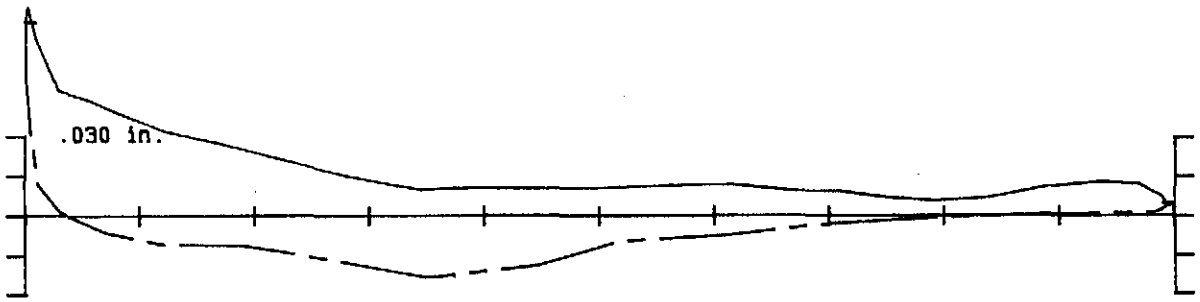

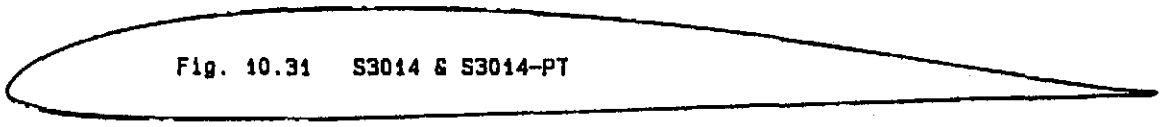

Fig. 10.31 S3014 & S3014-PT

Avg. diff. = 0.0092 in.

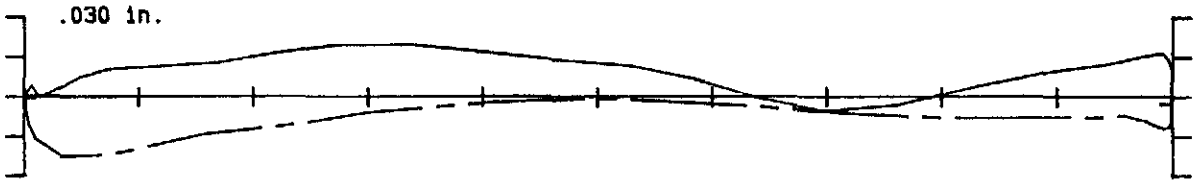

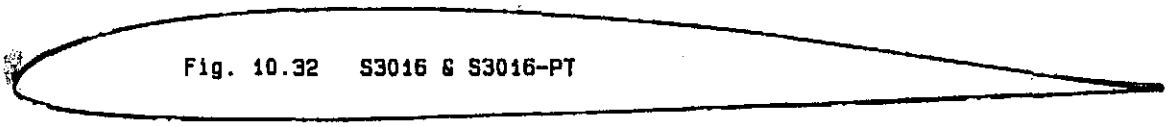

Fig. 10.32 S3016 & S3016-PT

Avg. diff. = 0.0114 in.

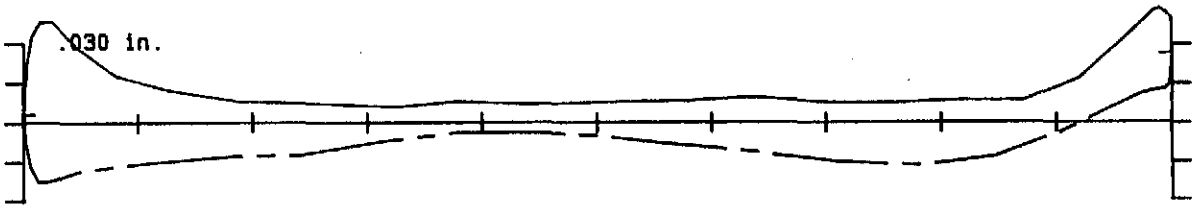

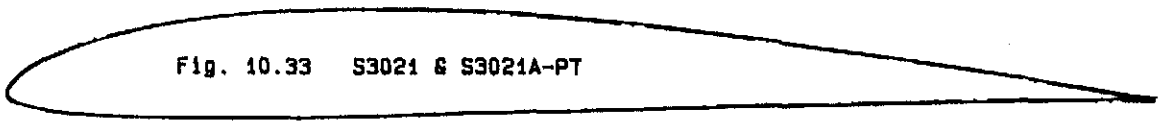

Fig. 10.33 S3021 & S3021A-PT

Avg. diff. = 0.0067 in.

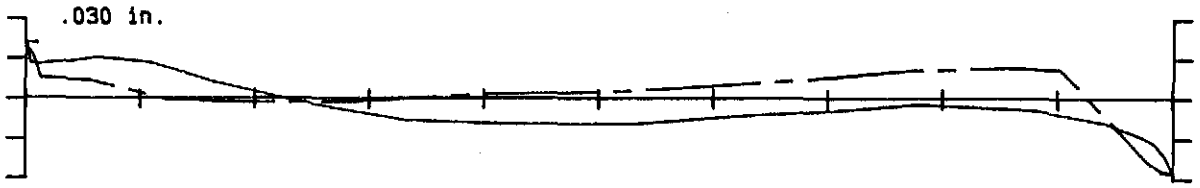

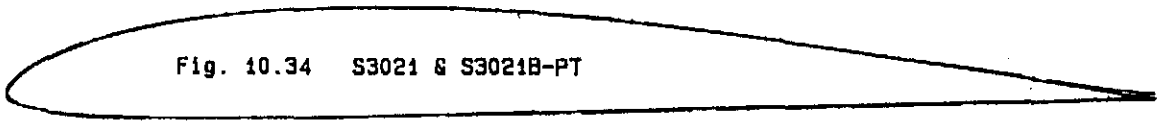

Fig. 10.34 S3021 & S3021B-PT

Avg. diff. = 0.0084 in.

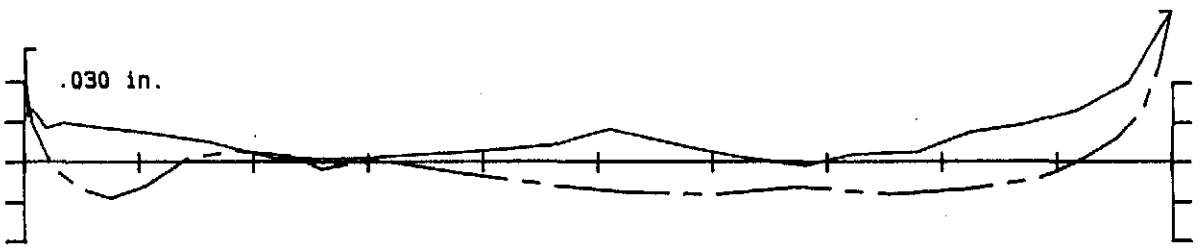

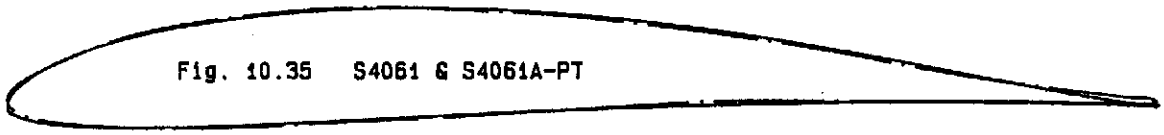

Fig. 10.35 S4061 & S4061A-PT

Avg. diff. = 0.0176 in.

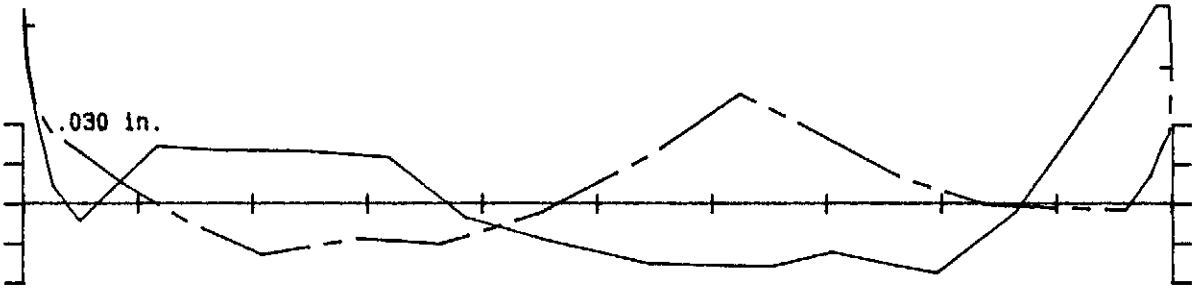

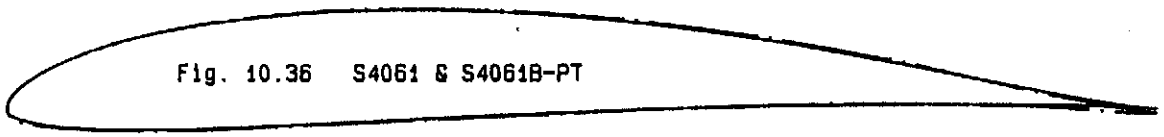

Fig. 10.36 S4061 & S4061B-PT

Avg. diff. = 0.0148 in.

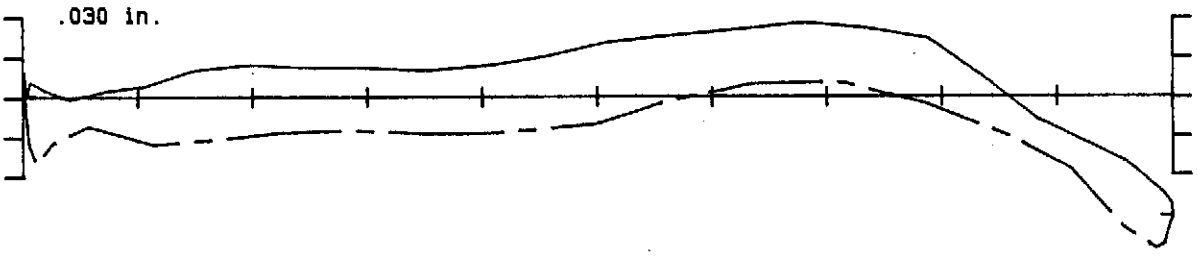

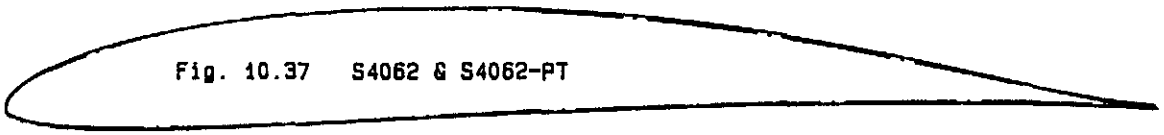

Fig. 10.37 S4062 & S4062-PT

Avg. diff. = 0.0141 in.

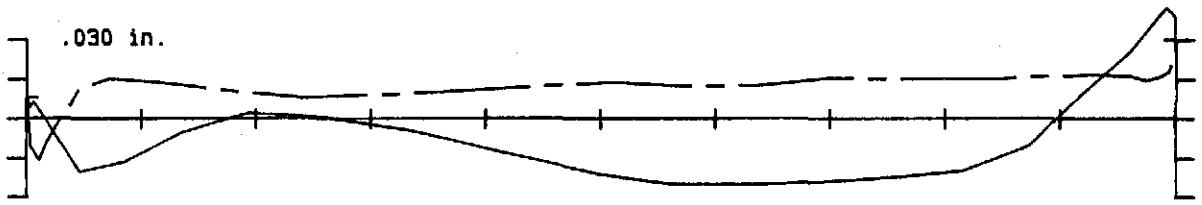

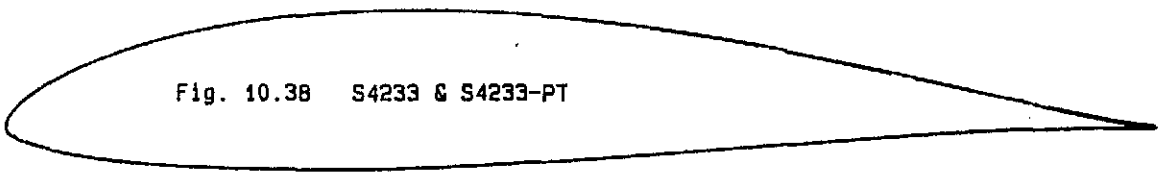

Fig. 10.38 S4233 & S4233-PT

Avg. diff. = 0.0043 in.

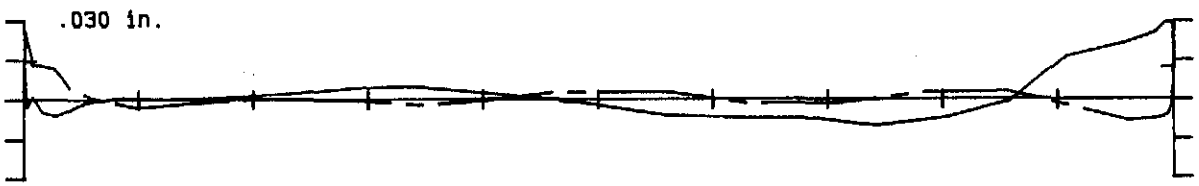

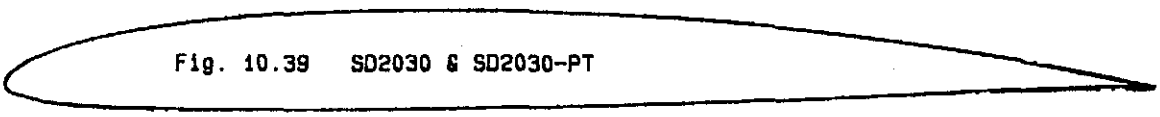

Fig. 10.39 SD2030 & SD2030-PT

Avg. diff. = 0.0067 in.

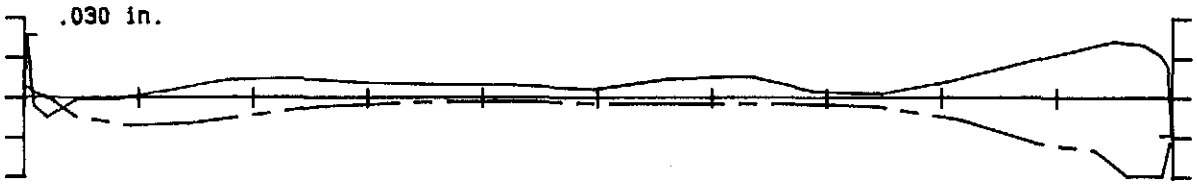

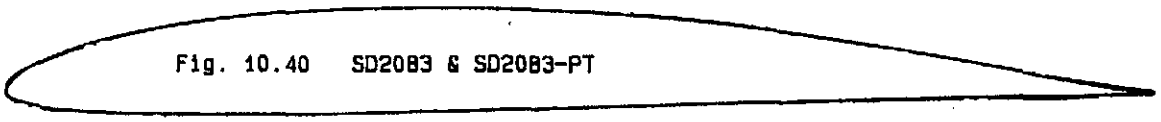

Fig. 10.40 SD2083 & SD2083-PT

Avg. diff. = 0.0072 in.

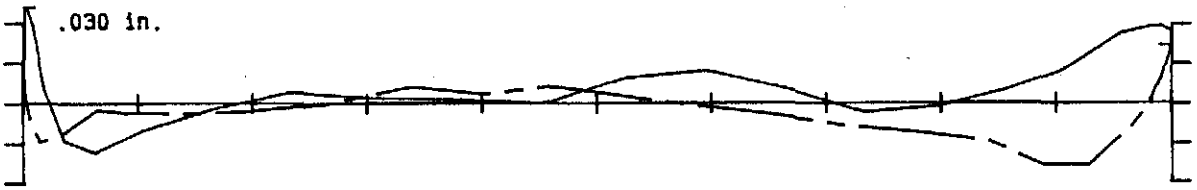

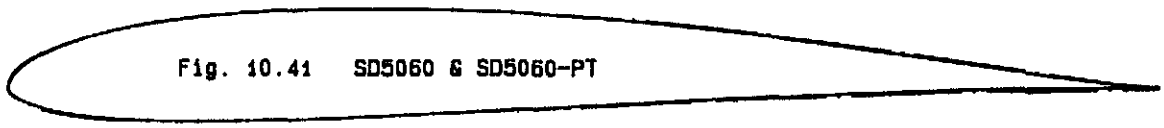

Fig. 10.41 SD5060 & SD5060-PT

Avg. diff. = 0.0110 in.

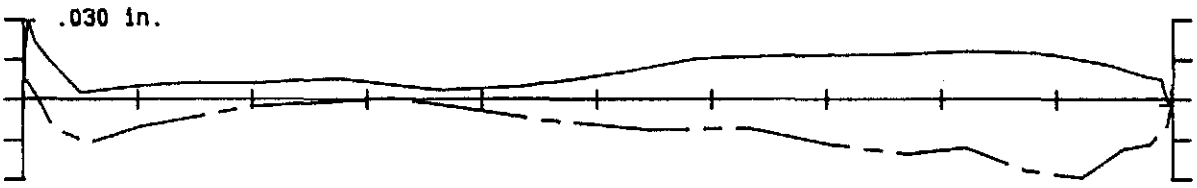

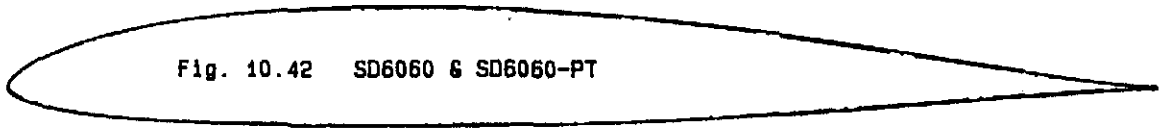

Fig. 10.42 SD6060 & SD6060-PT

Avg. diff. = 0.0095 in.

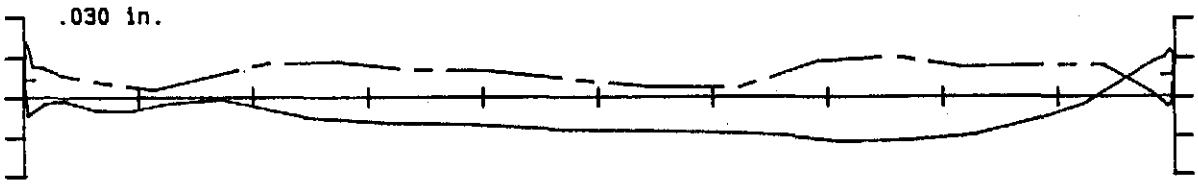

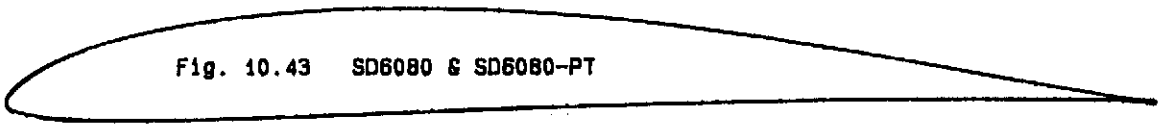

Fig. 10.43 SD6080 & SD6080-PT

Avg. diff. = 0.0052 in.

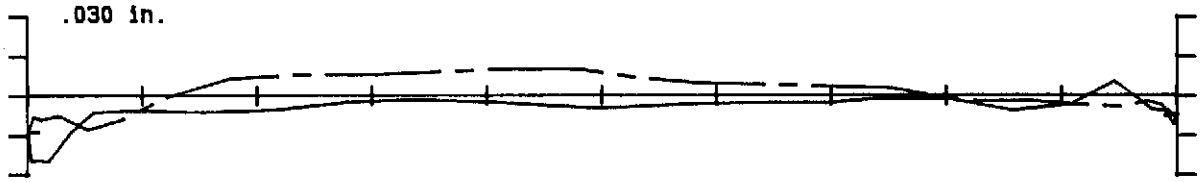

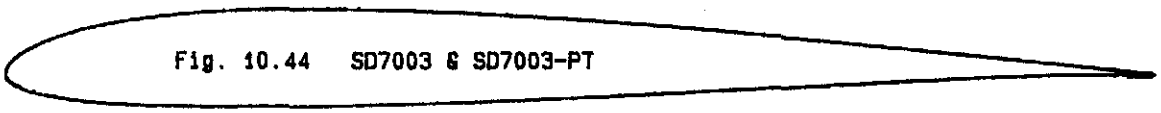

Fig. 10.44 SD7003 & SD7003-PT

Avg. diff. = 0.0041 in.

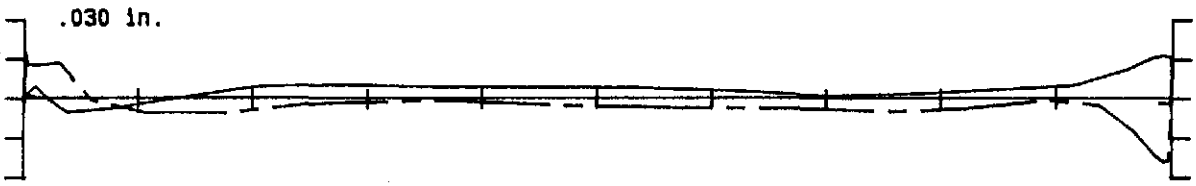

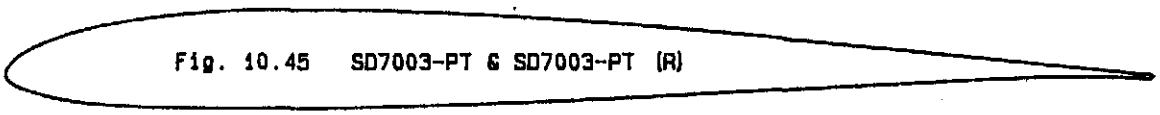

Fig. 10.45 SD7003-PT & SD7003-PT (R)

Avg. diff. = 0.0007 in.

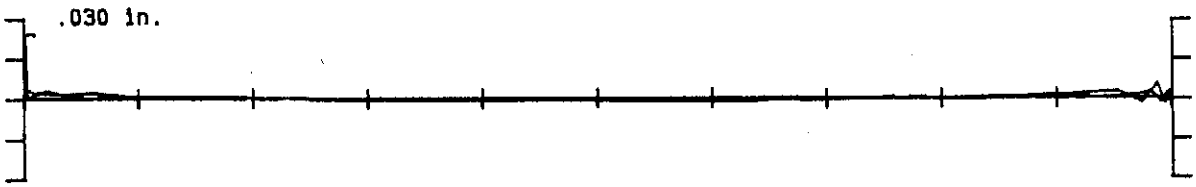

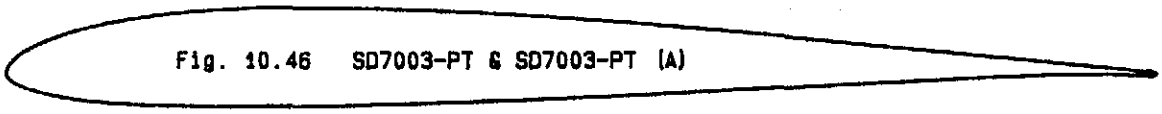

Fig. 10.46 SD7003-PT & SD7003-PT (A)

Avg. diff. = 0.0022 in.

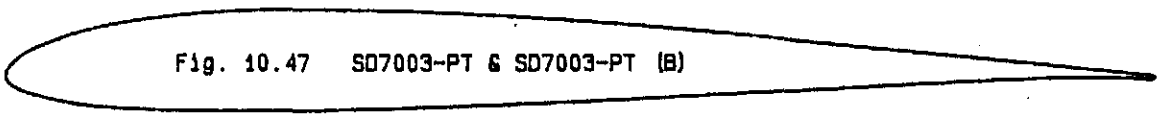

Fig. 10.47 SD7003-PT & SD7003-PT (B)

Avg. diff. = 0.0012 in.

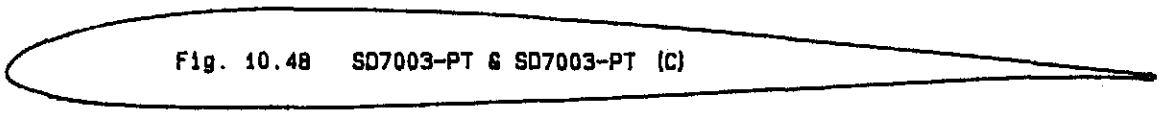

Fig. 10.48 SD7003-PT & SD7003-PT (C)

Avg. diff. = 0.0033 in.

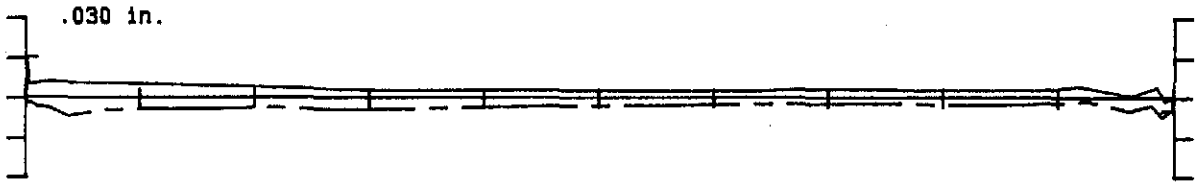

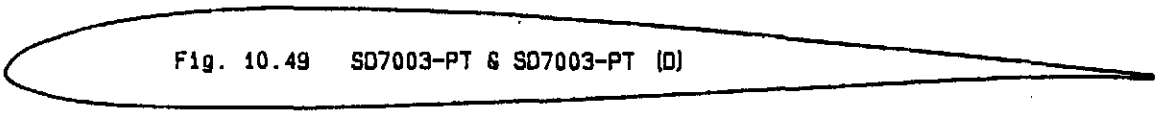

Fig. 10.49 SD7003-PT & SD7003-PT (D)

Avg. diff. = 0.0034 in.

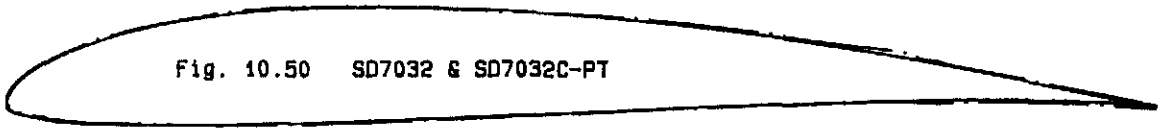

Fig. 10.50 SD7032 & SD7032C-PT

Avg. diff. = 0.0175 in.

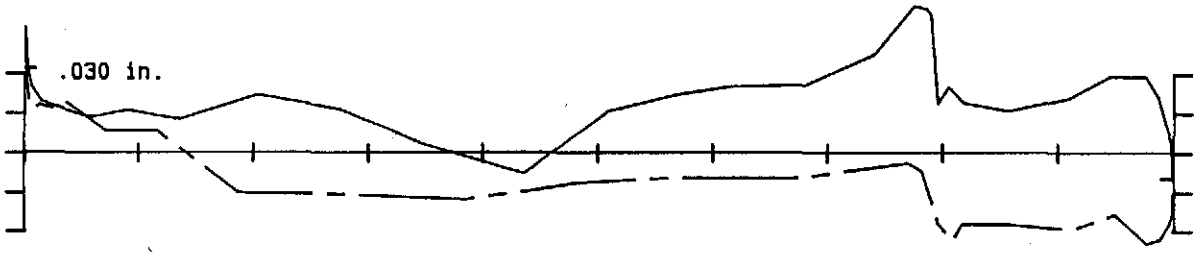

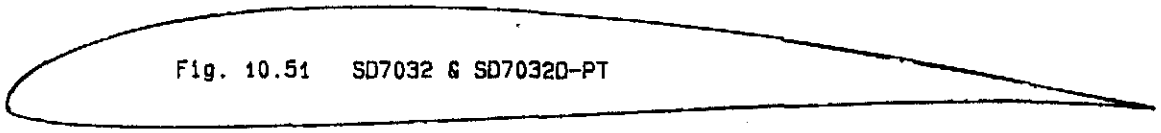

Fig. 10.51 SD7032 & SD7032D-PT

Avg. diff. = 0.0062 in.

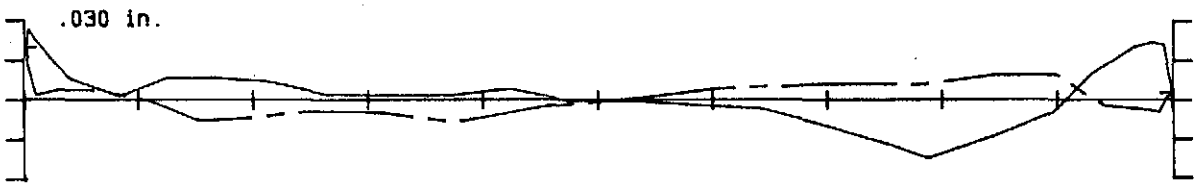

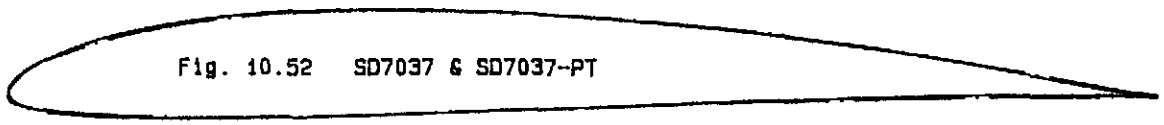

Fig. 10.52 SD7037 & SD7037-PT

Avg. diff. = 0.0120 in.

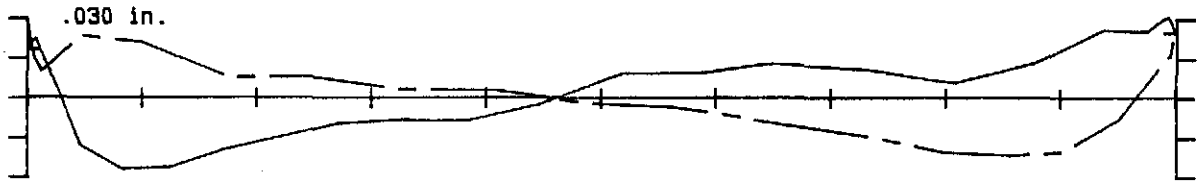

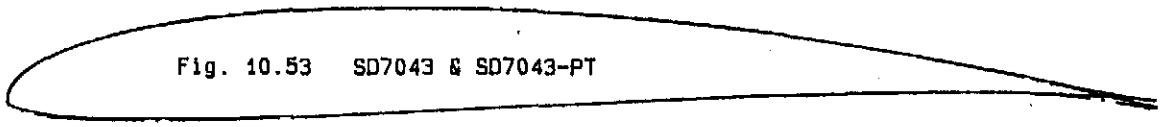

Fig. 10.53 SD7043 & SD7043-PT

Avg. diff. = 0.0099 in.

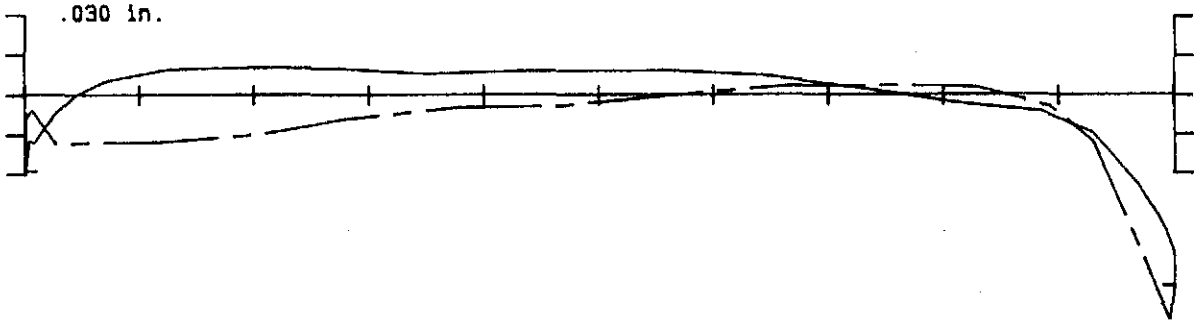

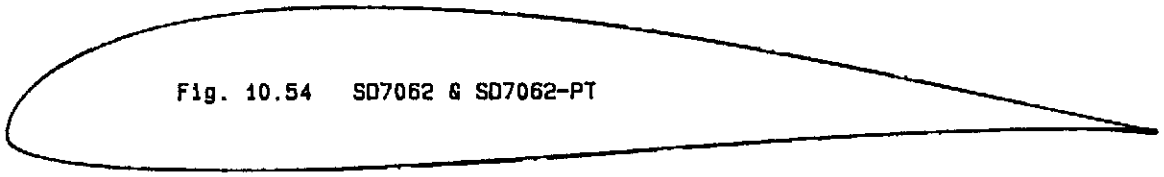

Fig. 10.54 SD7062 & SD7062-PT

Avg. diff. = 0.0093 in.

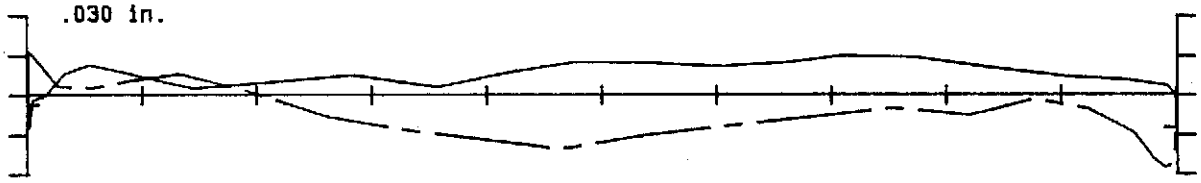

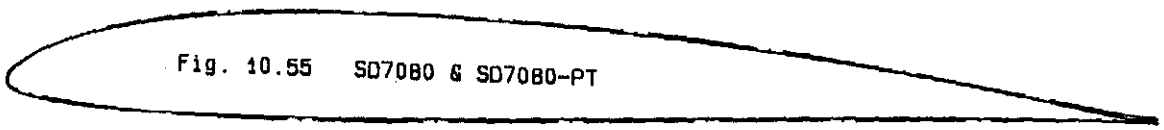

Fig. 10.55 SD7080 & SD7080-PT

Avg. diff. = 0.0185 in.

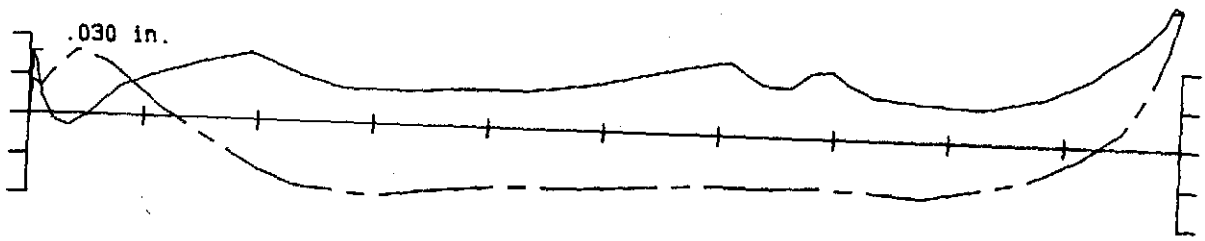

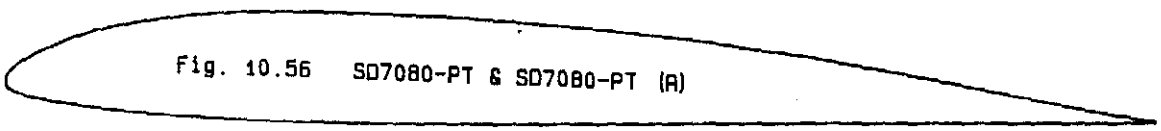

Fig. 10.56 SD7080-PT & SD7080-PT (A)

Avg. diff. = 0.0025 in.

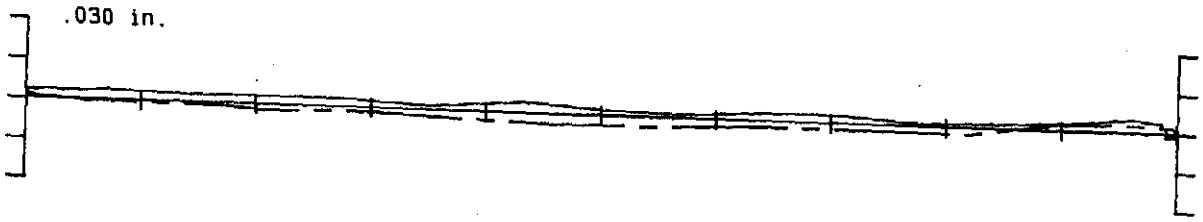

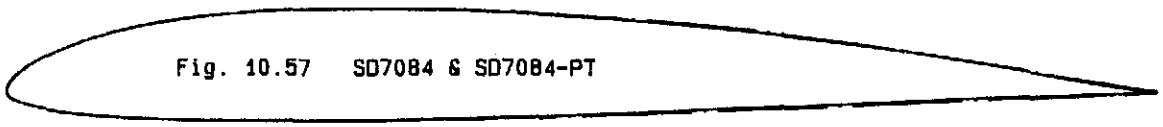

Fig. 10.57 SD7084 & SD7084-PT

Avg. diff. = 0.0097 in.

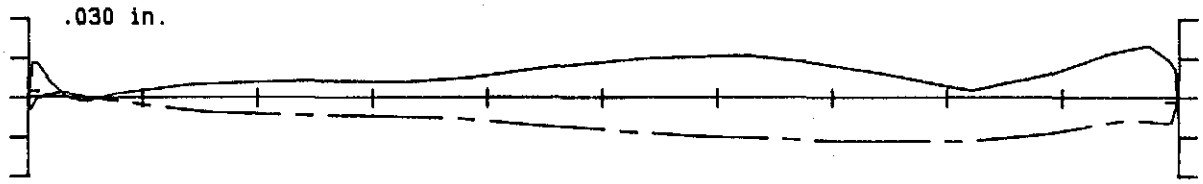

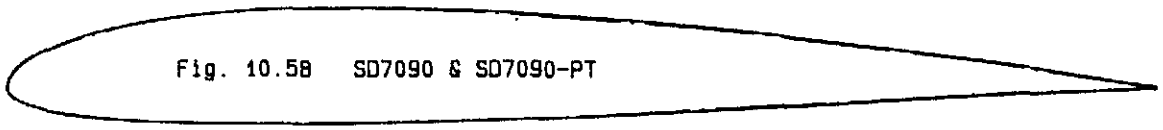

Fig. 10.58 SD7090 & SD7090-PT

Avg. diff. = 0.0071 in.

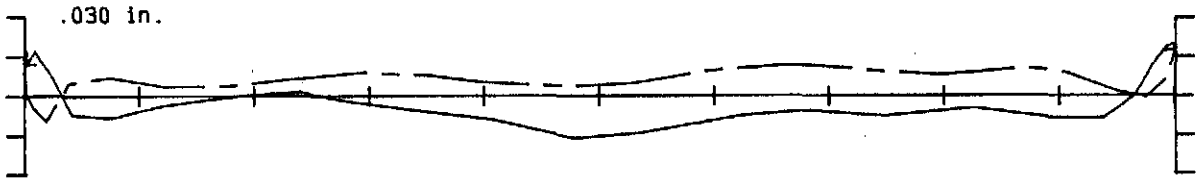

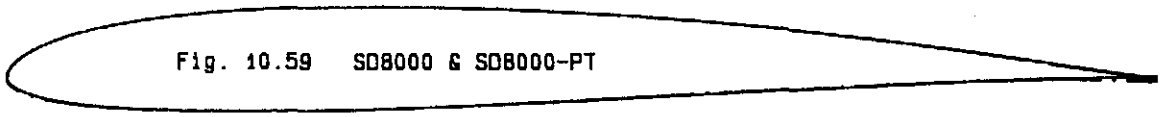

Fig. 10.59 SD8000 & SD8000-PT

Avg. diff. = 0.0050 in.

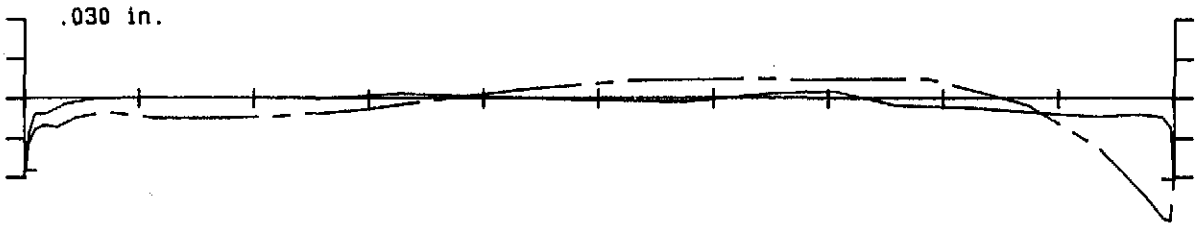

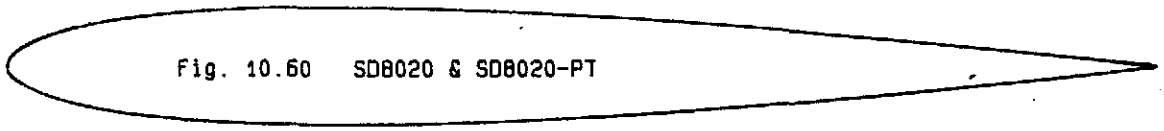

Fig. 10.60 SD8020 & SD8020-PT

Avg. diff. = 0.0037 in.

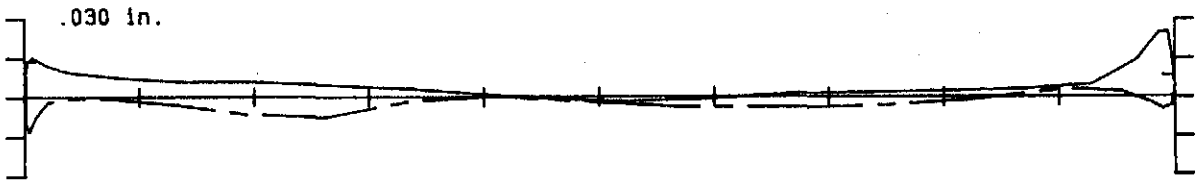

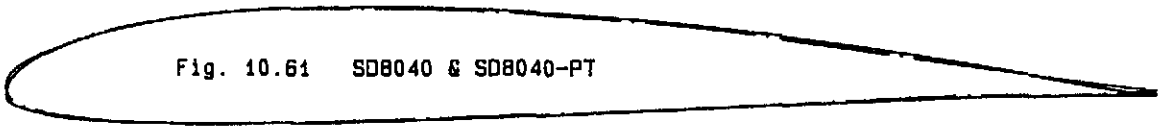

Fig. 10.61 SD8040 & SD8040-PT

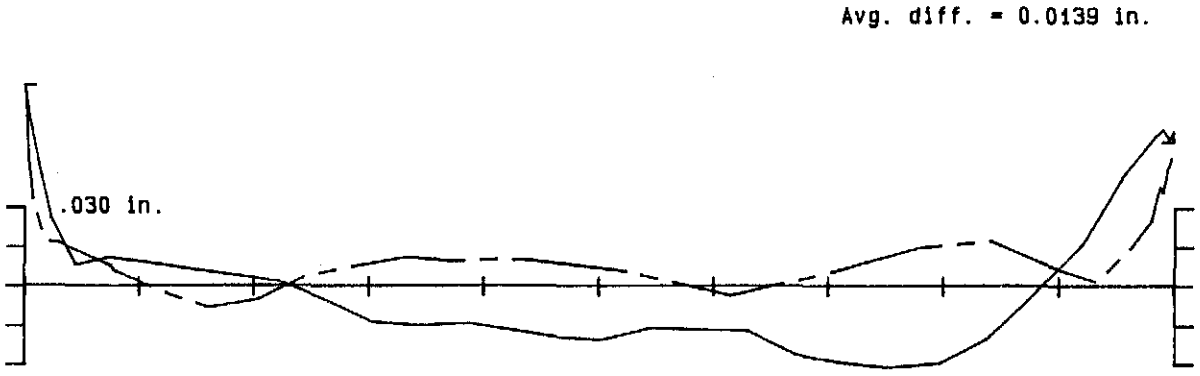

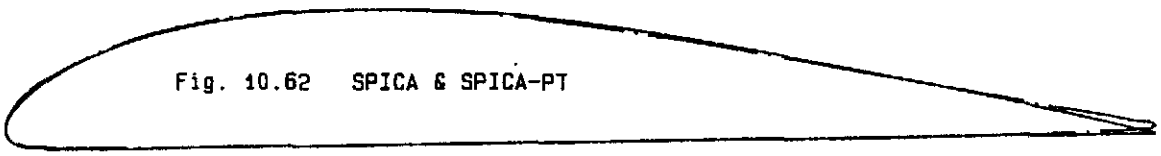

Fig. 10.62 SPICA & SPICA-PT

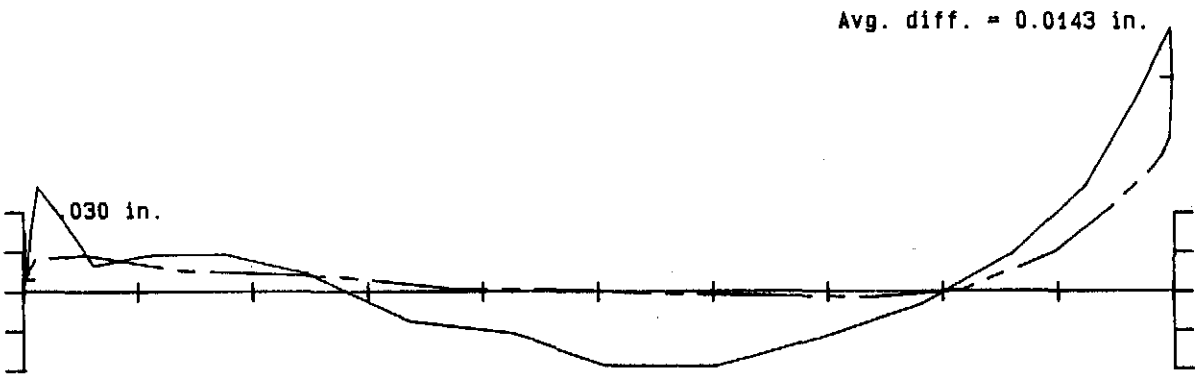

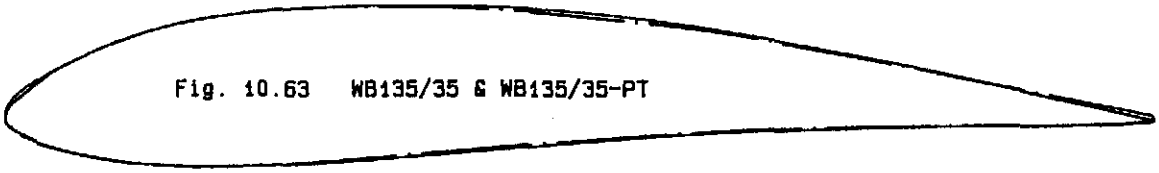

Fig. 10.63 WB135/35 & WB135/35-PT

Avg. diff. = 0.0144 in.

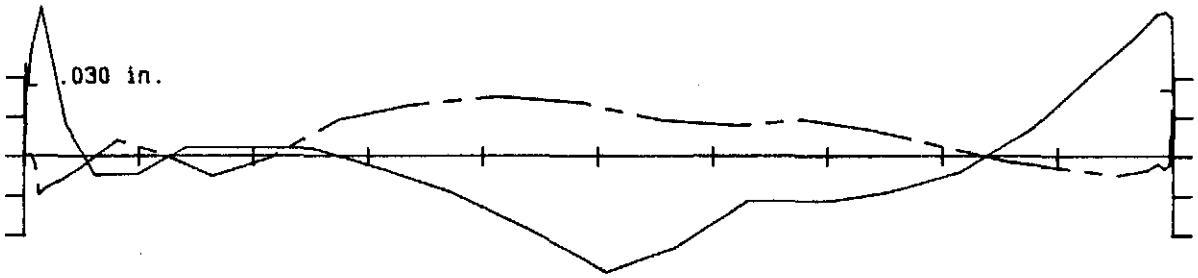

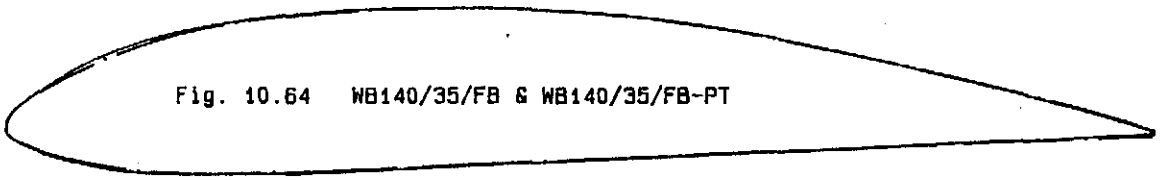

Fig. 10.64 WB140/35/FB & WB140/35/FB-PT

Avg. diff. = 0.0097 in.

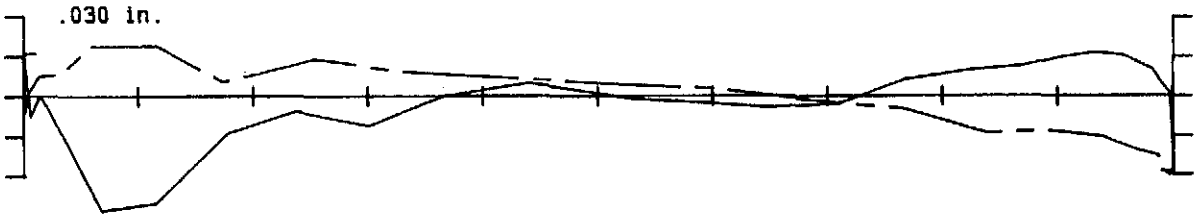

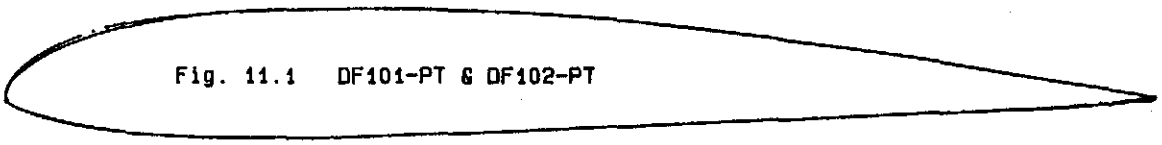

Fig. 11.1 DF101-PT & DF102-PT

Avg. diff. = 0.0065 in.

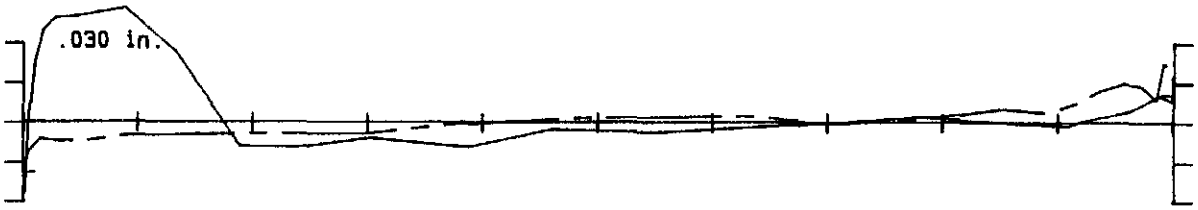

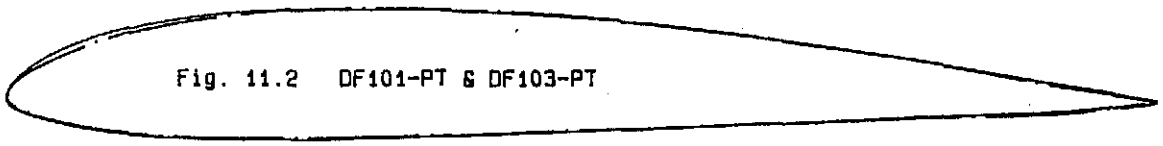

Fig. 11.2 DF101-PT & DF103-PT

Avg. diff. = 0.0131 in.

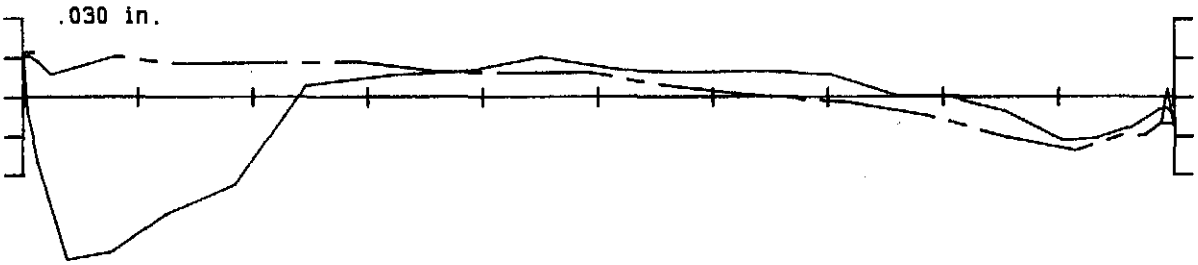

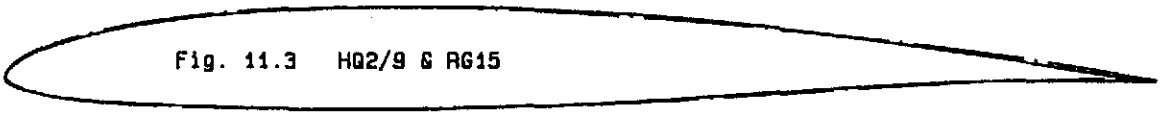

Fig. 11.3 HQ2/9 & RG15

Avg. diff. = 0.0139 in.

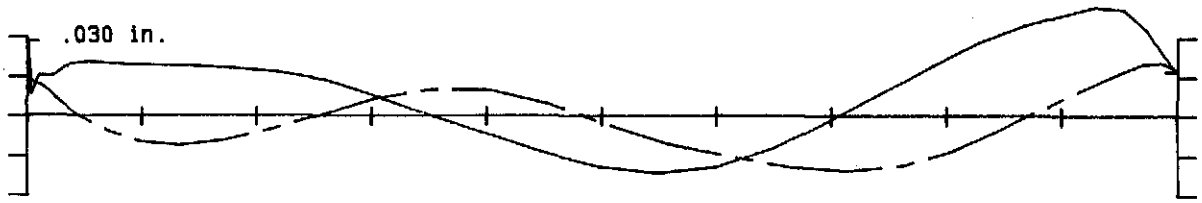

Fig. 11.4 HQ2/9 & S2048

Avg. diff. = 0.0134 in.

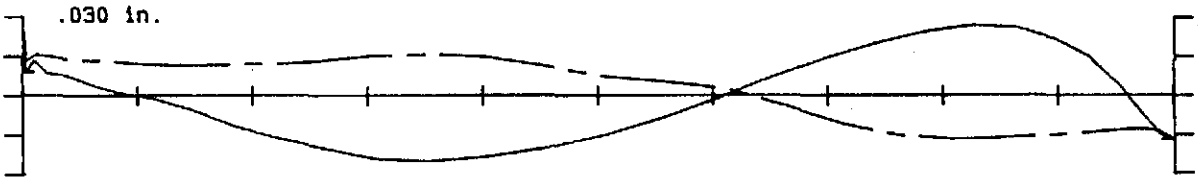

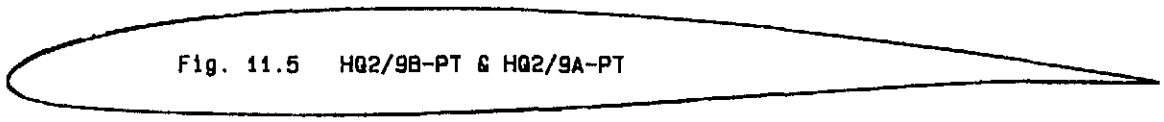

Avg. diff. = 0.0063 in.

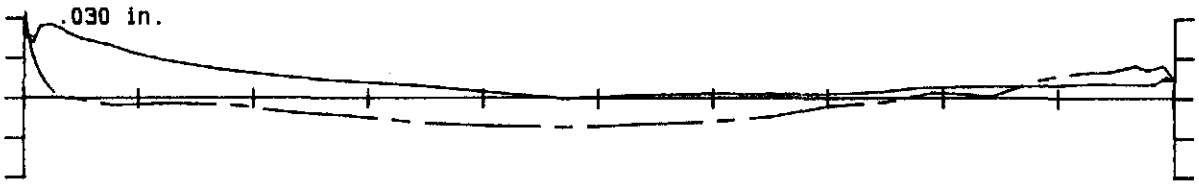

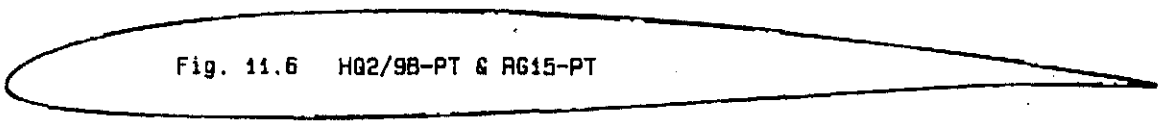

Avg. diff. = 0.0118 in.

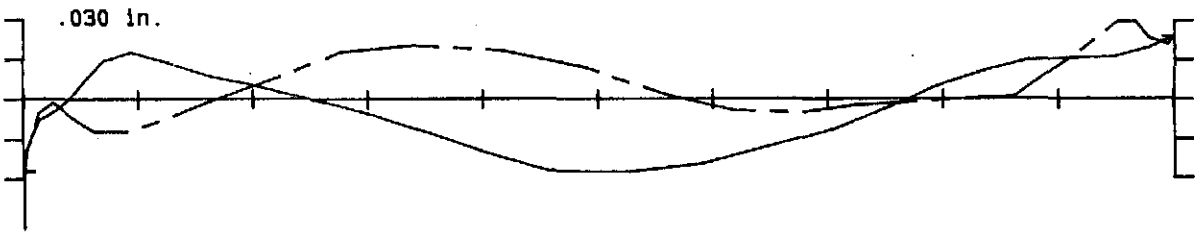

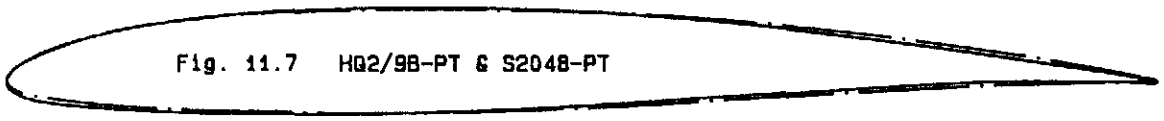

Fig. 11.7 HQ2/9B-PT & S2048-PT

Avg. diff. = 0.0240 in.

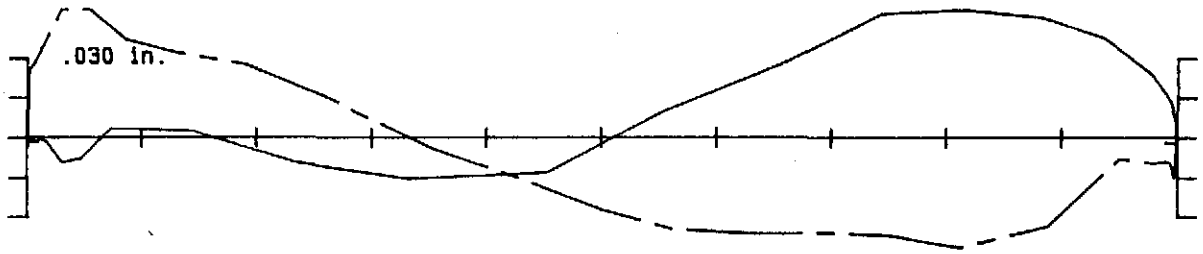

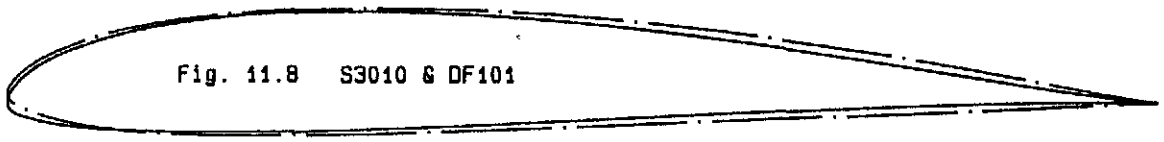

Fig. 11.8 S3010 & DF101

Avg. diff. = 0.0589 in.

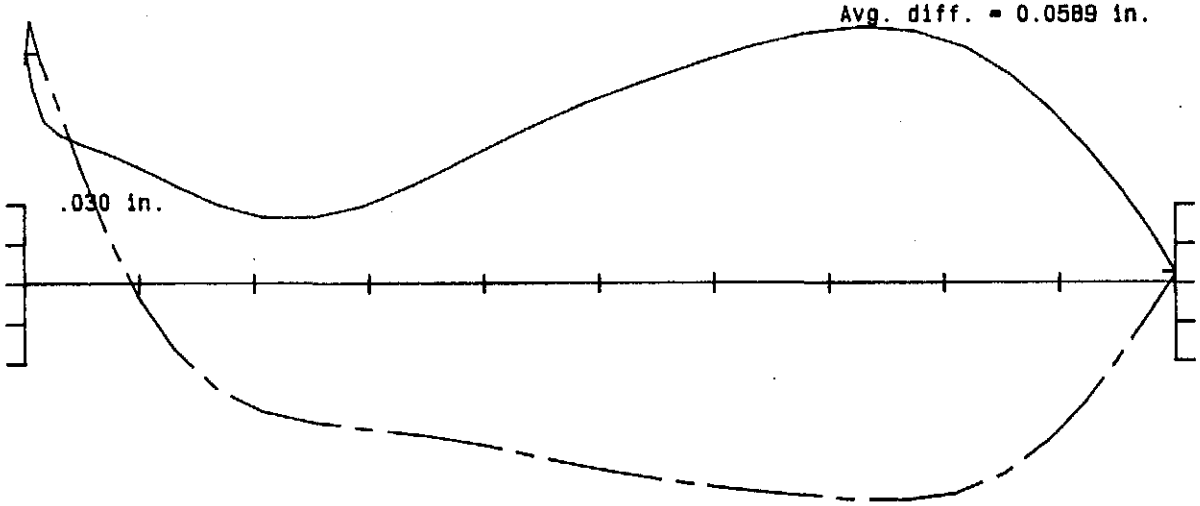

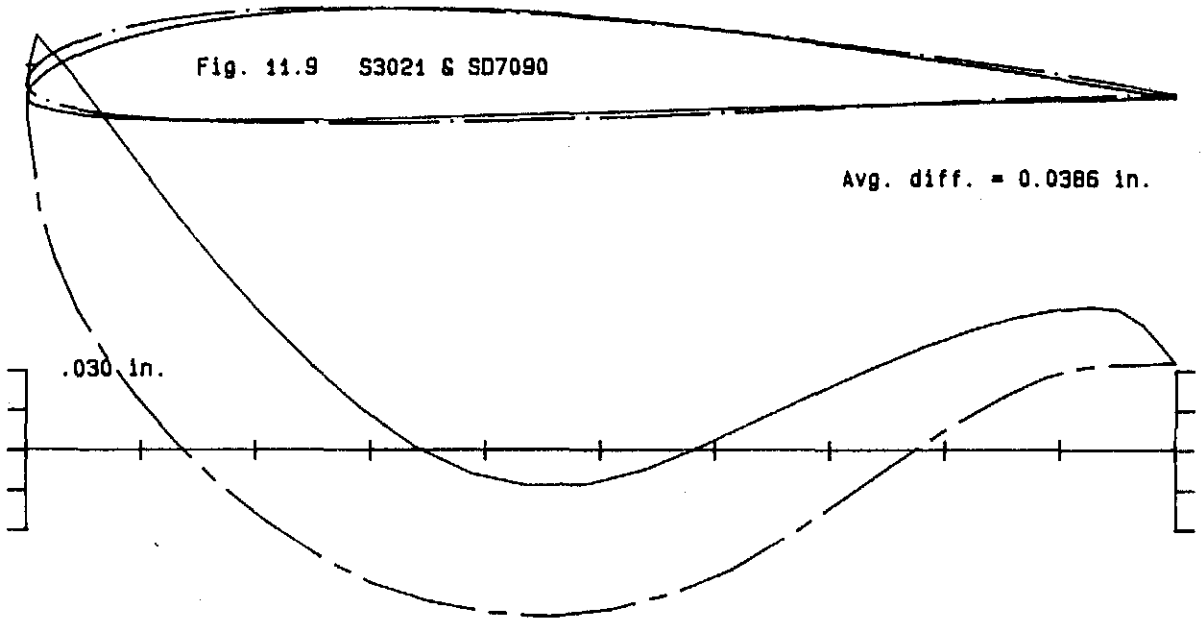
Fig. 11.9 S3021 & SD7090
Avg. diff. = 0.0386 in.
.030 in.

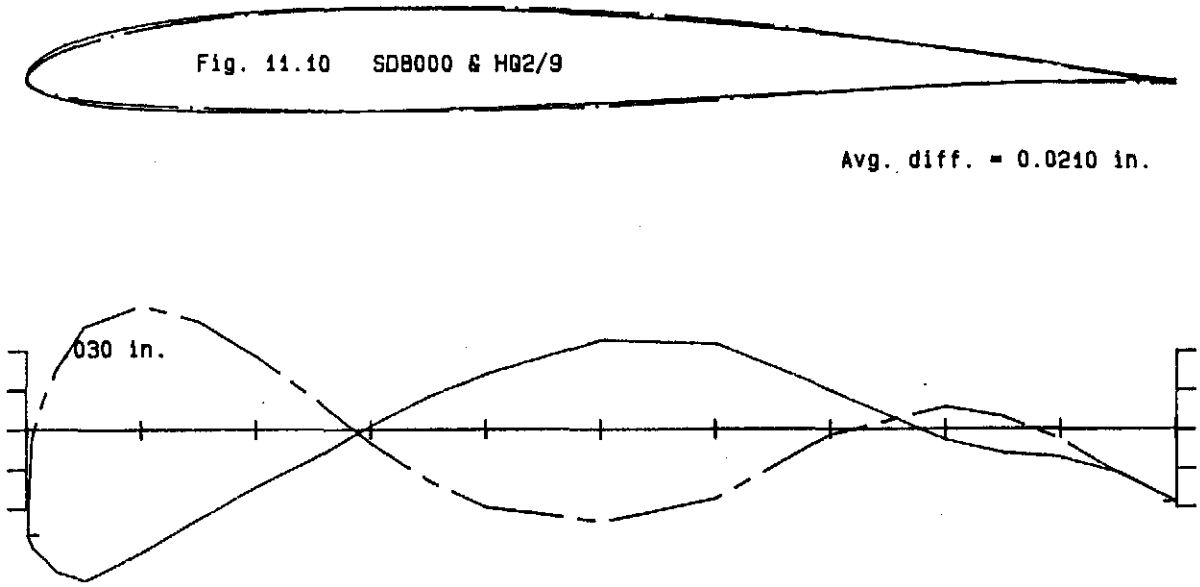
Fig. 11.10 SD8000 & HQ2/9
Avg. diff. = 0.0210 in.
.030 in.

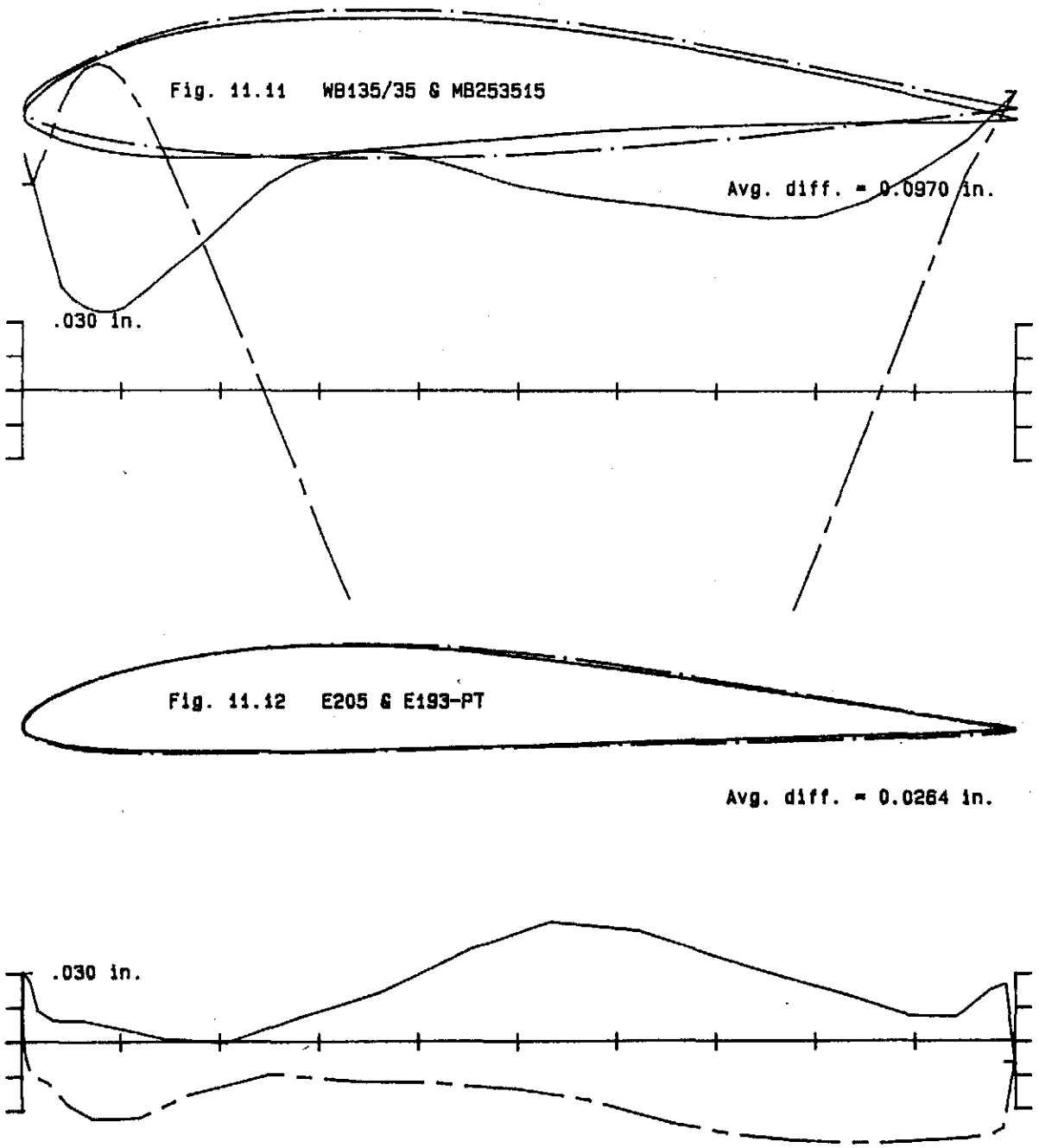
Fig. 11.11 WB135/35 & MB253515
Avg. diff. = 0.0970 in.
.030 in.
Fig. 11.12 E205 & E193-PT
Avg. diff. = 0.0264 in.
.030 in.

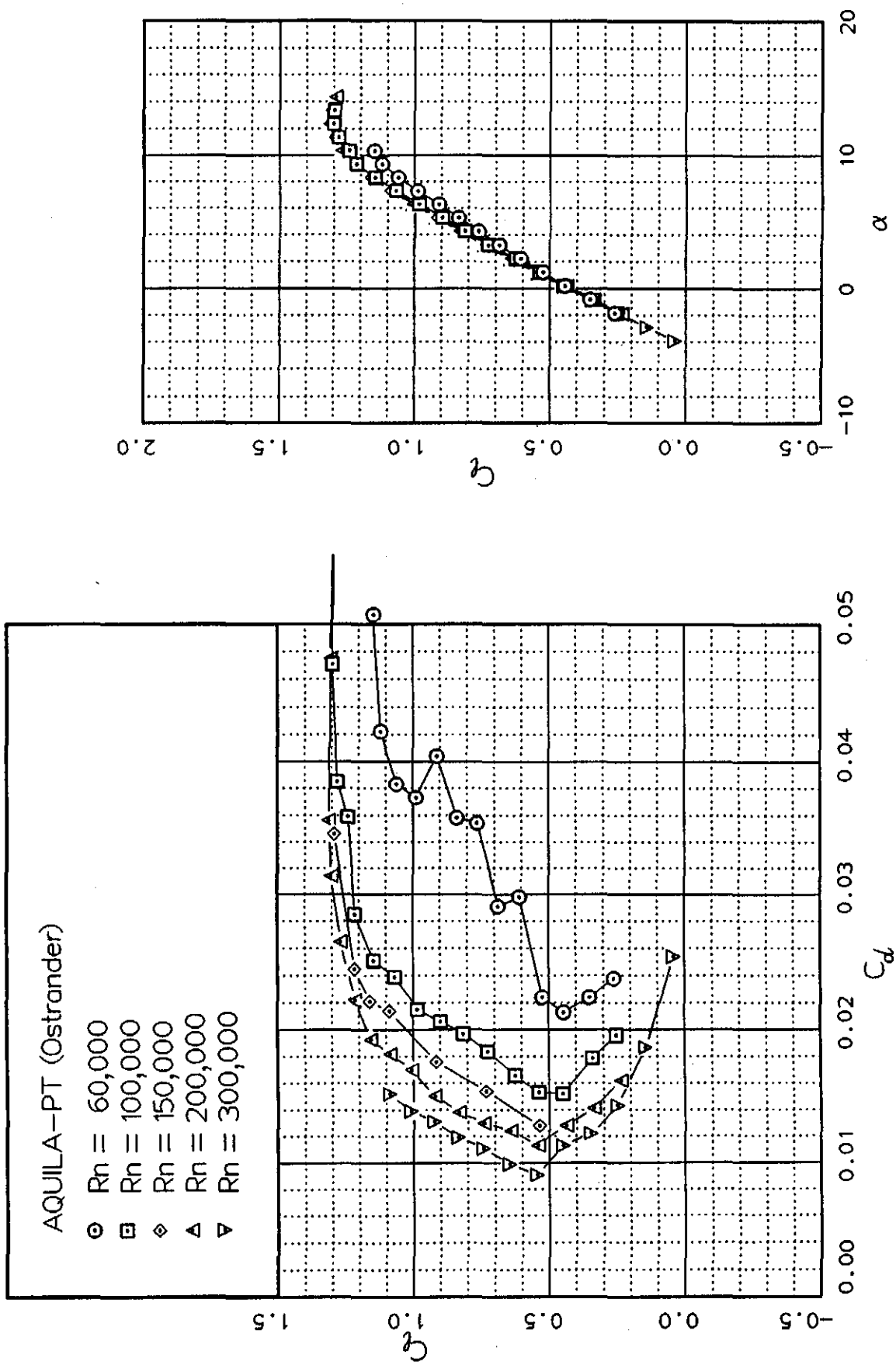
AQUILA–PT (Ostrander)
Rn = 60,000
Rn = 100,000
Rn = 150,000
Rn = 200,000
Rn = 300,000
0.00
0.01
0.02
0.03
0.04
0.05
C_d
−0.5
0.0
0.5
1.0
1.5
C_l
20
10
0
−10
α
−0.5
0.0
0.5
1.0
1.5
2.0
C_l

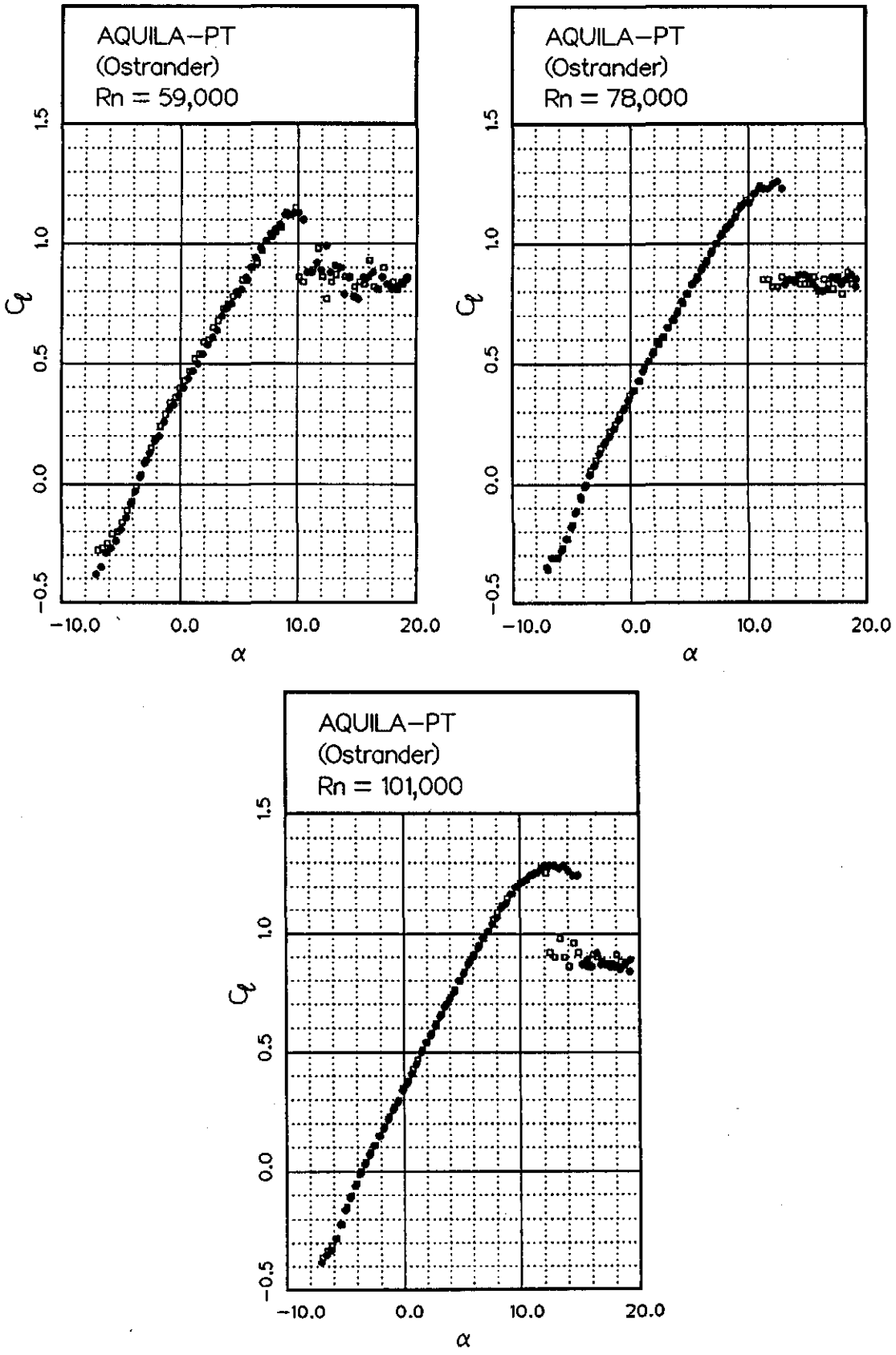
AQUILA–PT
(Ostrander)
Rn = 59,000
AQUILA–PT
(Ostrander)
Rn = 78,000
AQUILA–PT
(Ostrander)
Rn = 101,000
C_ℓ
α
1.5
1.0
0.5
0.0
−0.5
−10.0
0.0
10.0
20.0

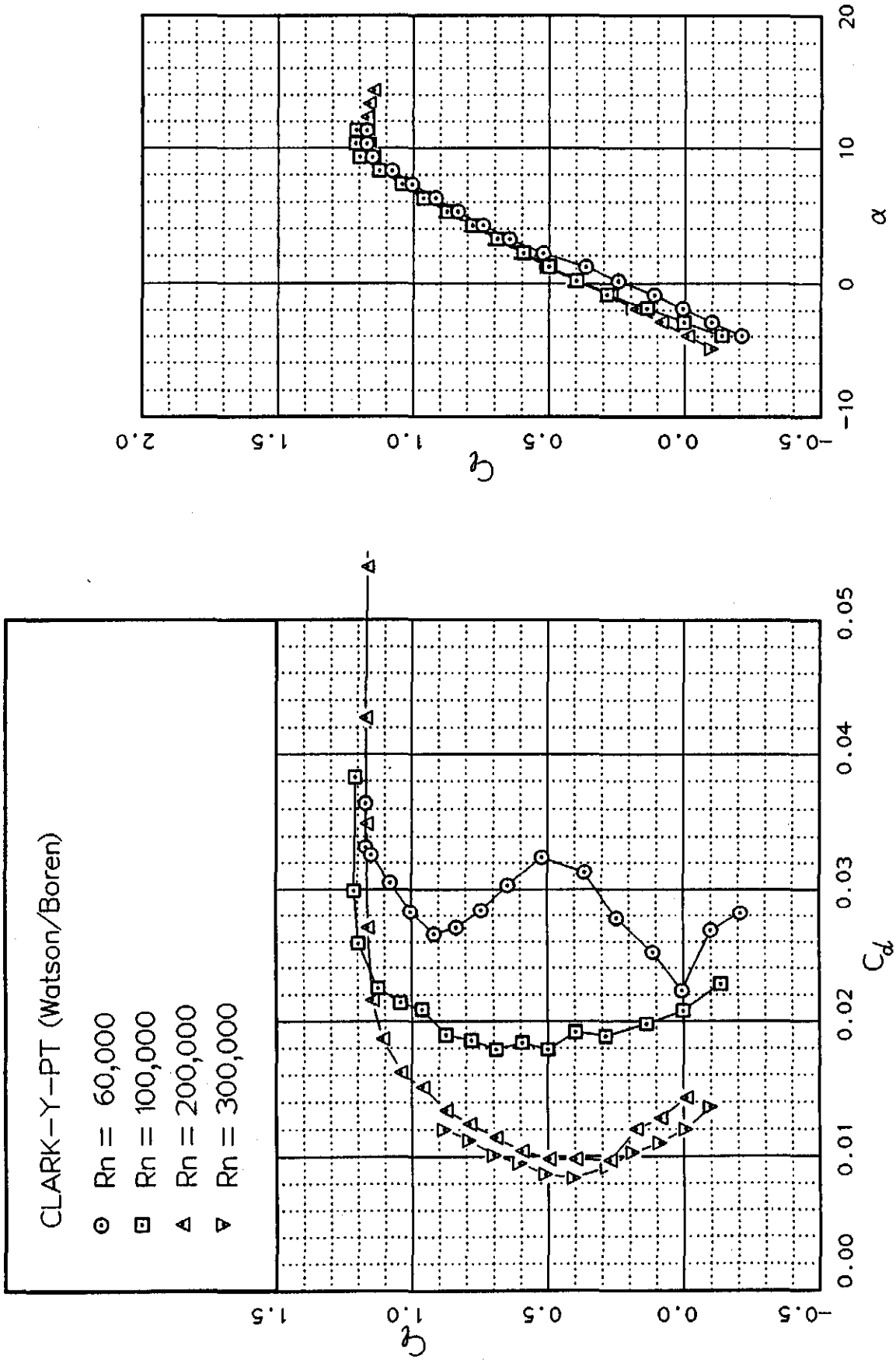
CLARK-Y-PT (Watson/Boren)
Rn = 60,000
Rn = 100,000
Rn = 200,000
Rn = 300,000
C_l
C_d
α

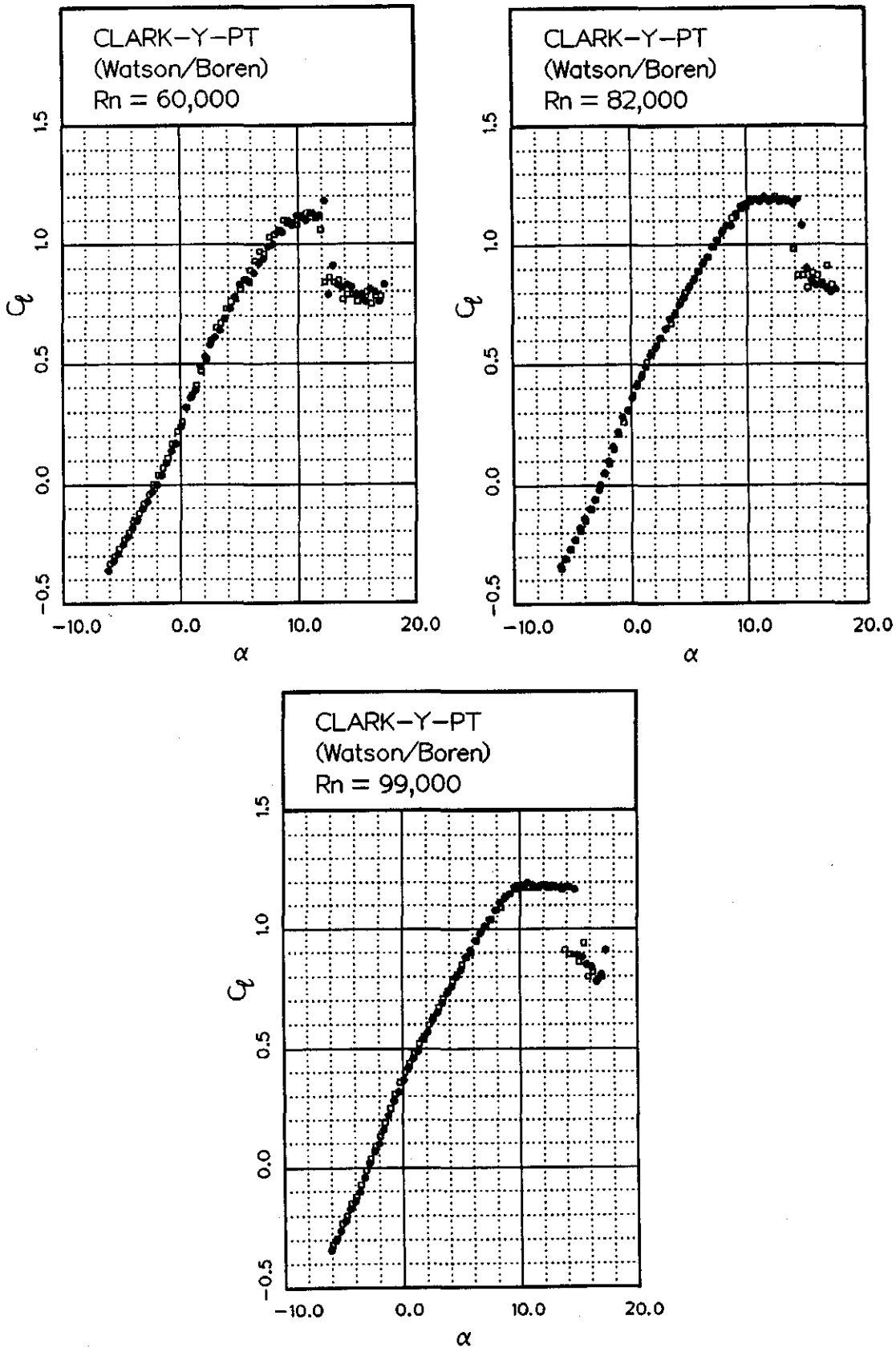
CLARK–Y–PT
(Watson/Boren)
Rn = 60,000
CLARK–Y–PT
(Watson/Boren)
Rn = 82,000
CLARK–Y–PT
(Watson/Boren)
Rn = 99,000
C_ℓ
α
1.5
1.0
0.5
0.0
−0.5
−10.0
0.0
10.0
20.0

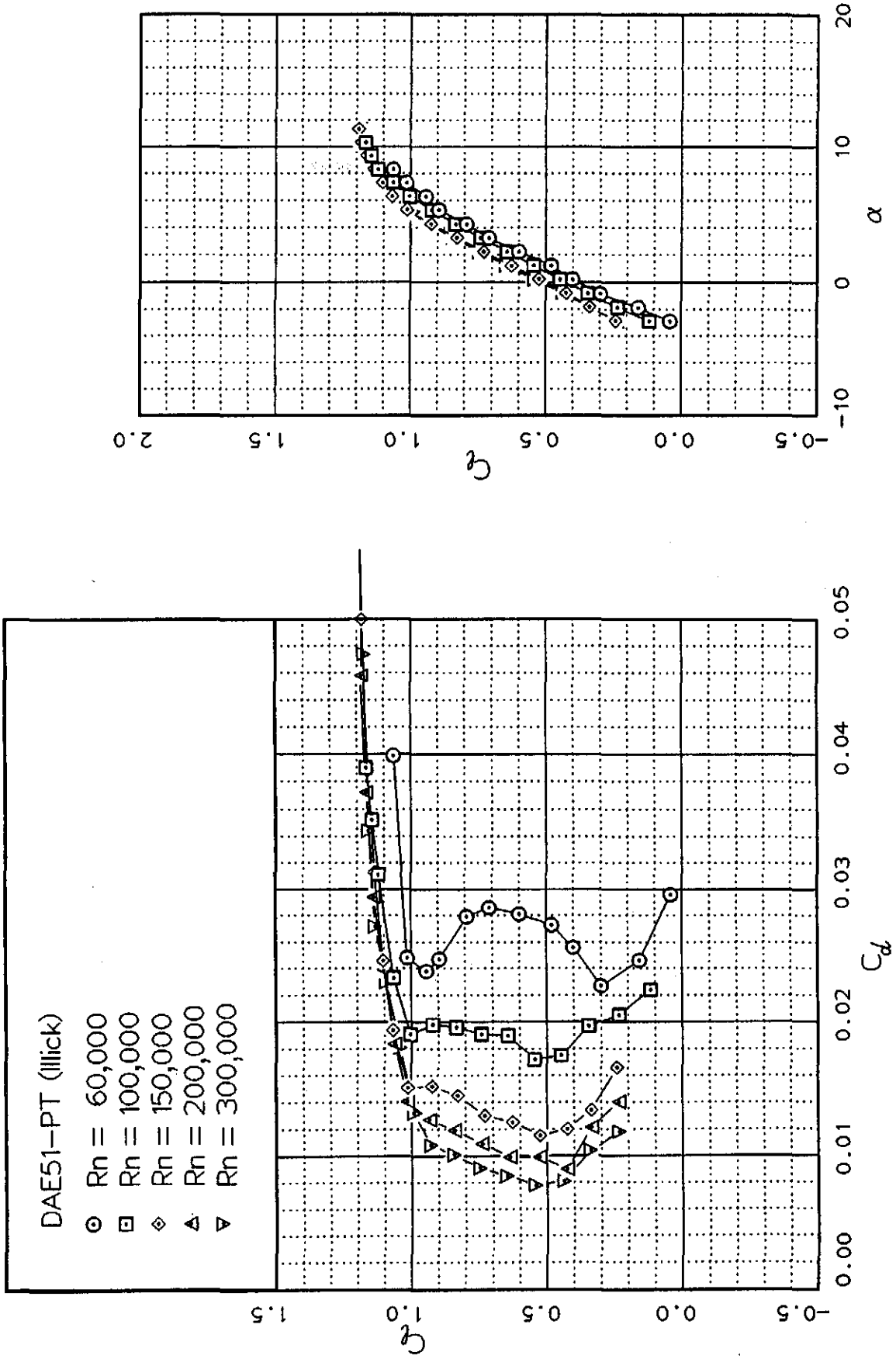
α
20
10
0
−10
−0.5
0.0
0.5
1.0
1.5
2.0
cl
DAE51−PT (Ilick)
Rn = 60,000
Rn = 100,000
Rn = 150,000
Rn = 200,000
Rn = 300,000
0.05
0.04
0.03
0.02
0.01
0.00
cd

Fig. 12.6

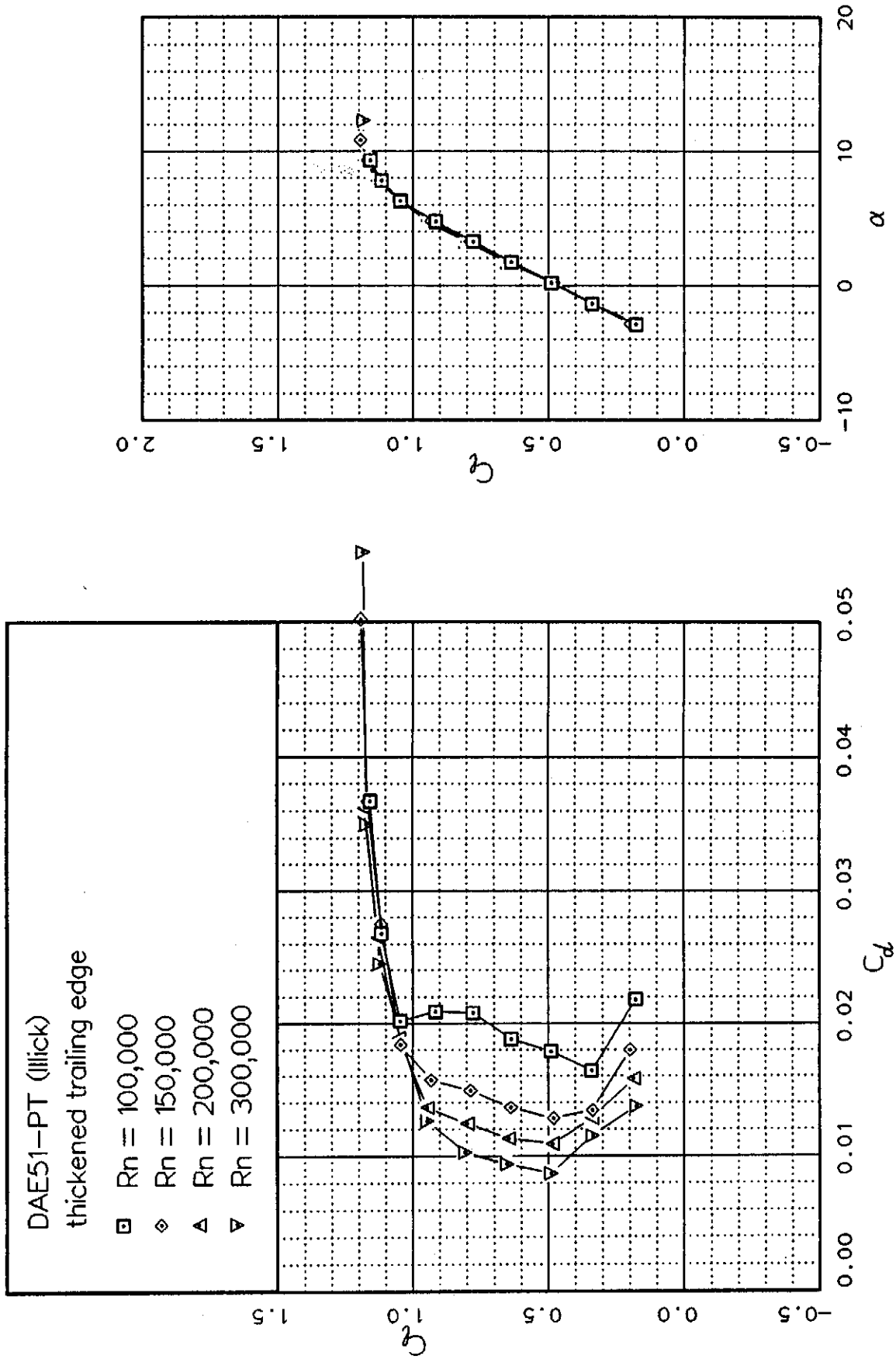
DAE51–PT (Ilick)
thickened trailing edge
Rn = 100,000
Rn = 150,000
Rn = 200,000
Rn = 300,000
C_l
C_d
α

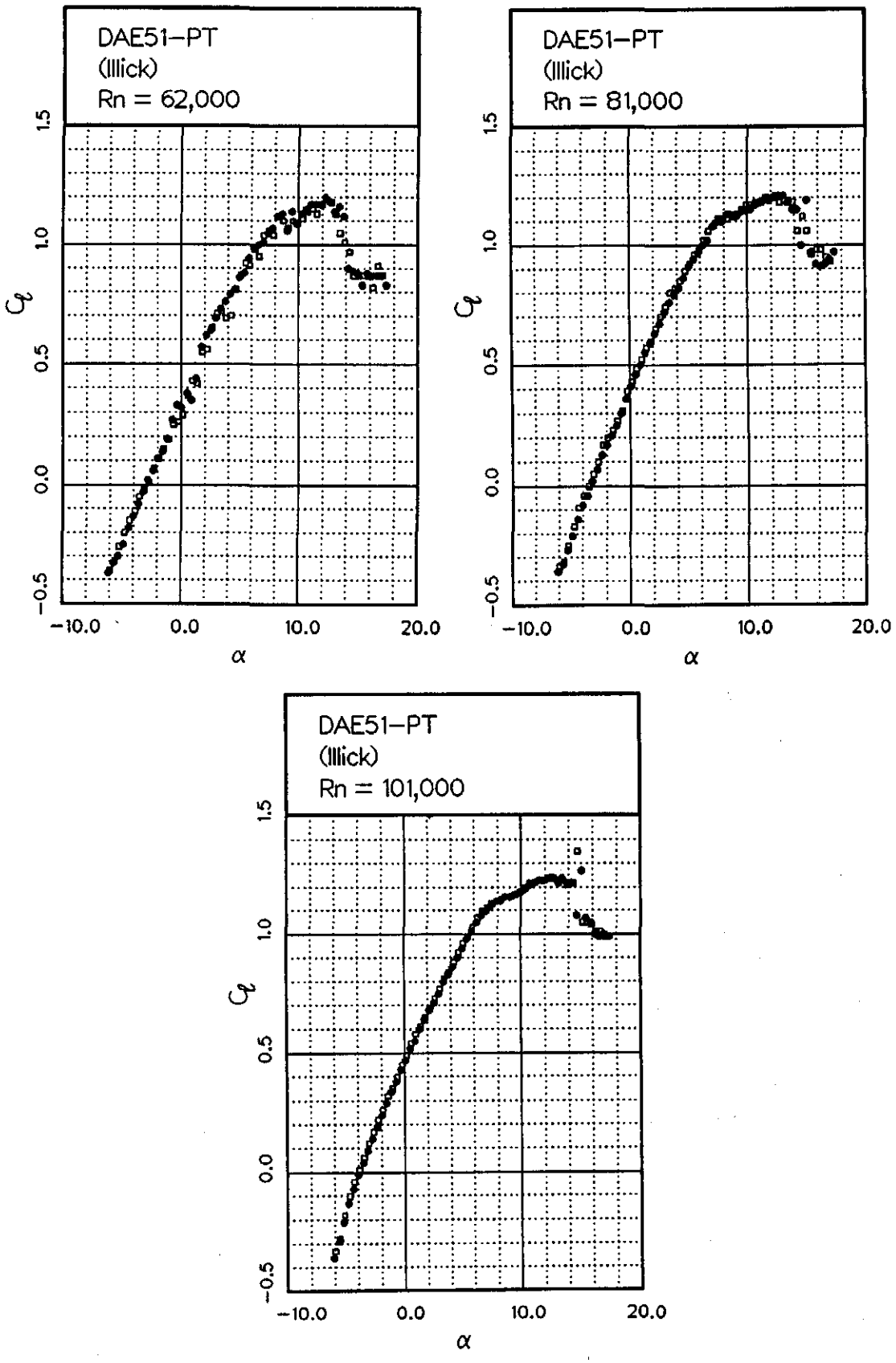
DAE51–PT
(Illick)
Rn = 62,000
DAE51–PT
(Illick)
Rn = 81,000
DAE51–PT
(Illick)
Rn = 101,000
C_l
α
1.5
1.0
0.5
0.0
−0.5
−10.0
0.0
10.0
20.0

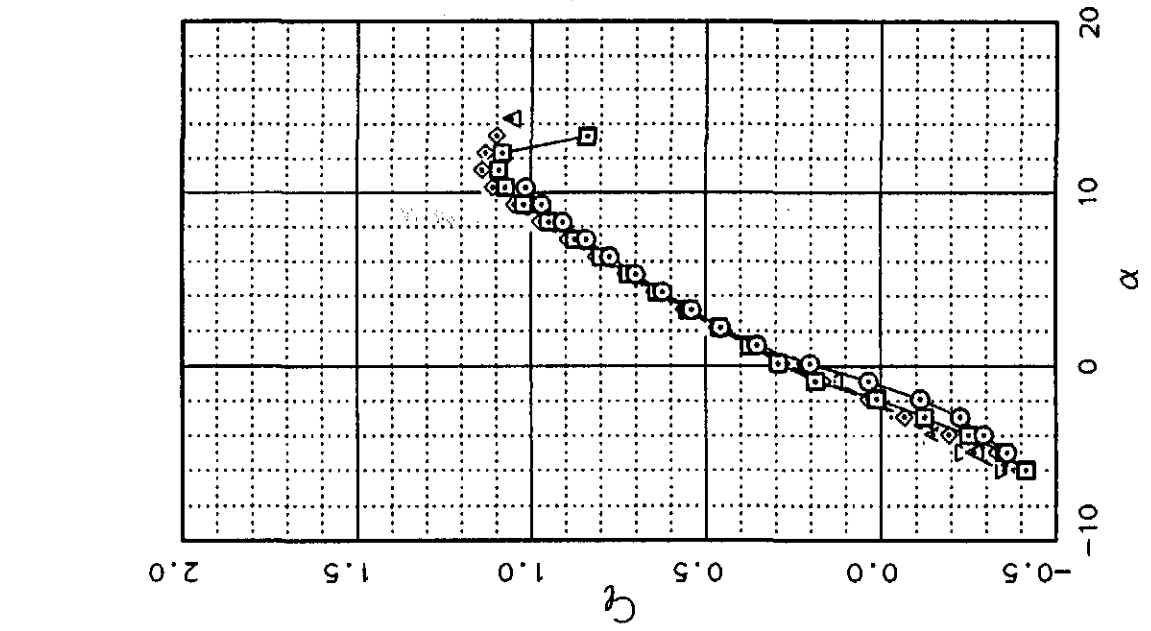
20
10
0
−10
α
−0.5
0.0
0.5
1.0
1.5
2.0
c_l

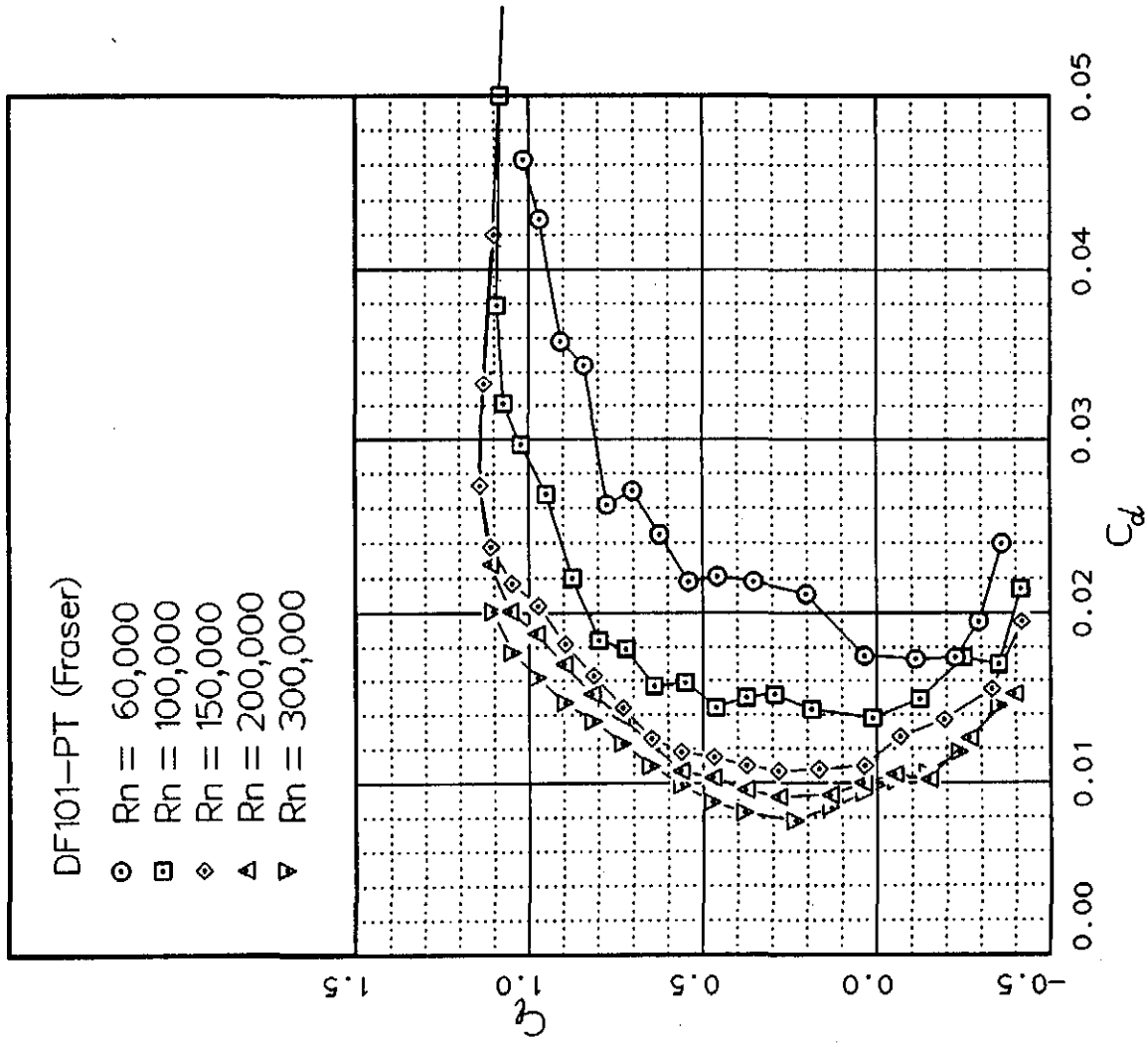
DF101–PT (Fraser)
Rn = 60,000
Rn = 100,000
Rn = 150,000
Rn = 200,000
Rn = 300,000
0.05
0.04
0.03
0.02
0.01
0.00
c_d
−0.5
0.0
0.5
1.0
1.5
c_l

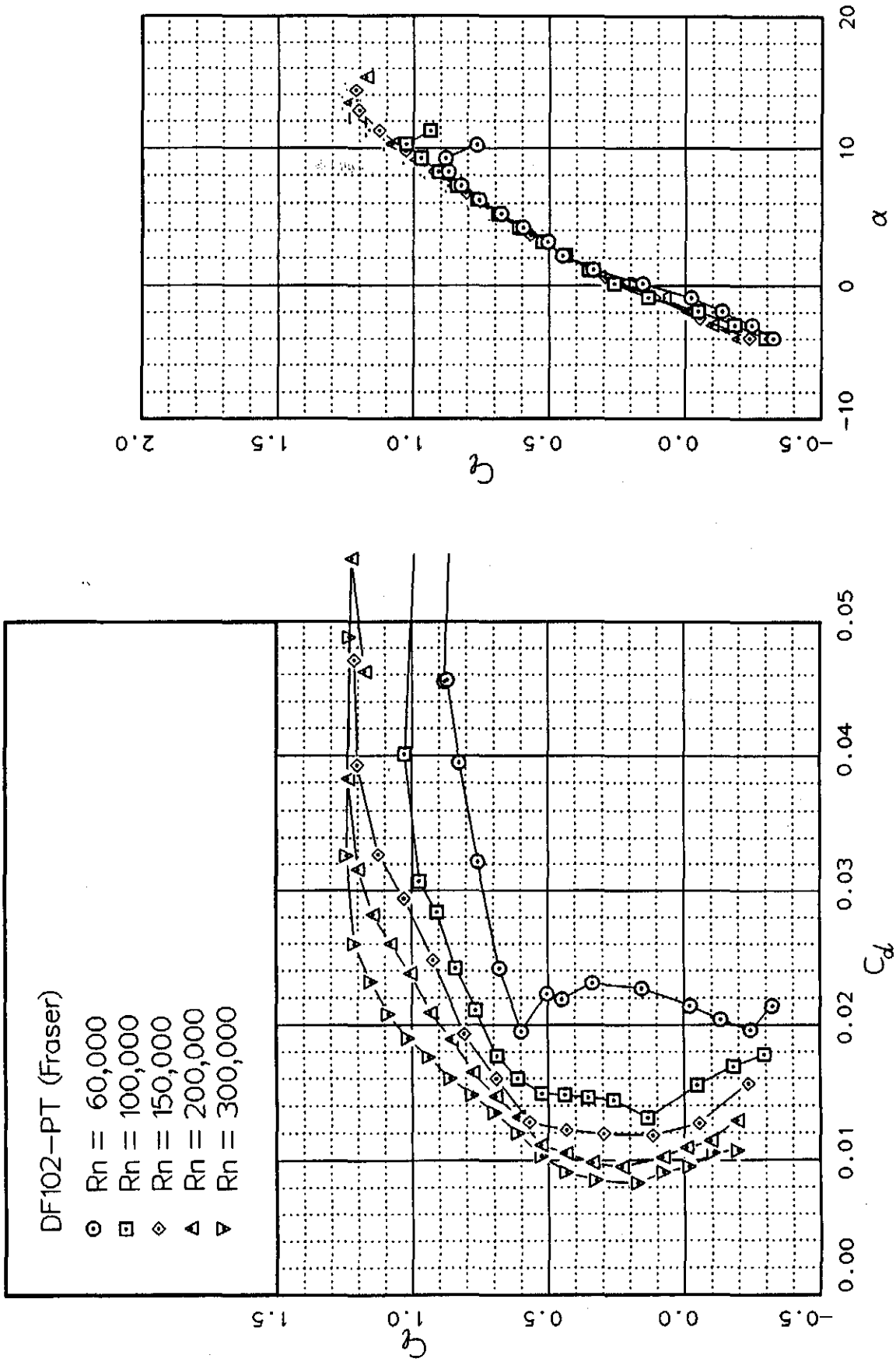
α
20
10
0
−10
−0.5
0.0
0.5
1.0
1.5
2.0
cl
DF102−PT (Fraser)
Rn = 60,000
Rn = 100,000
Rn = 150,000
Rn = 200,000
Rn = 300,000
cd
0.00
0.01
0.02
0.03
0.04
0.05

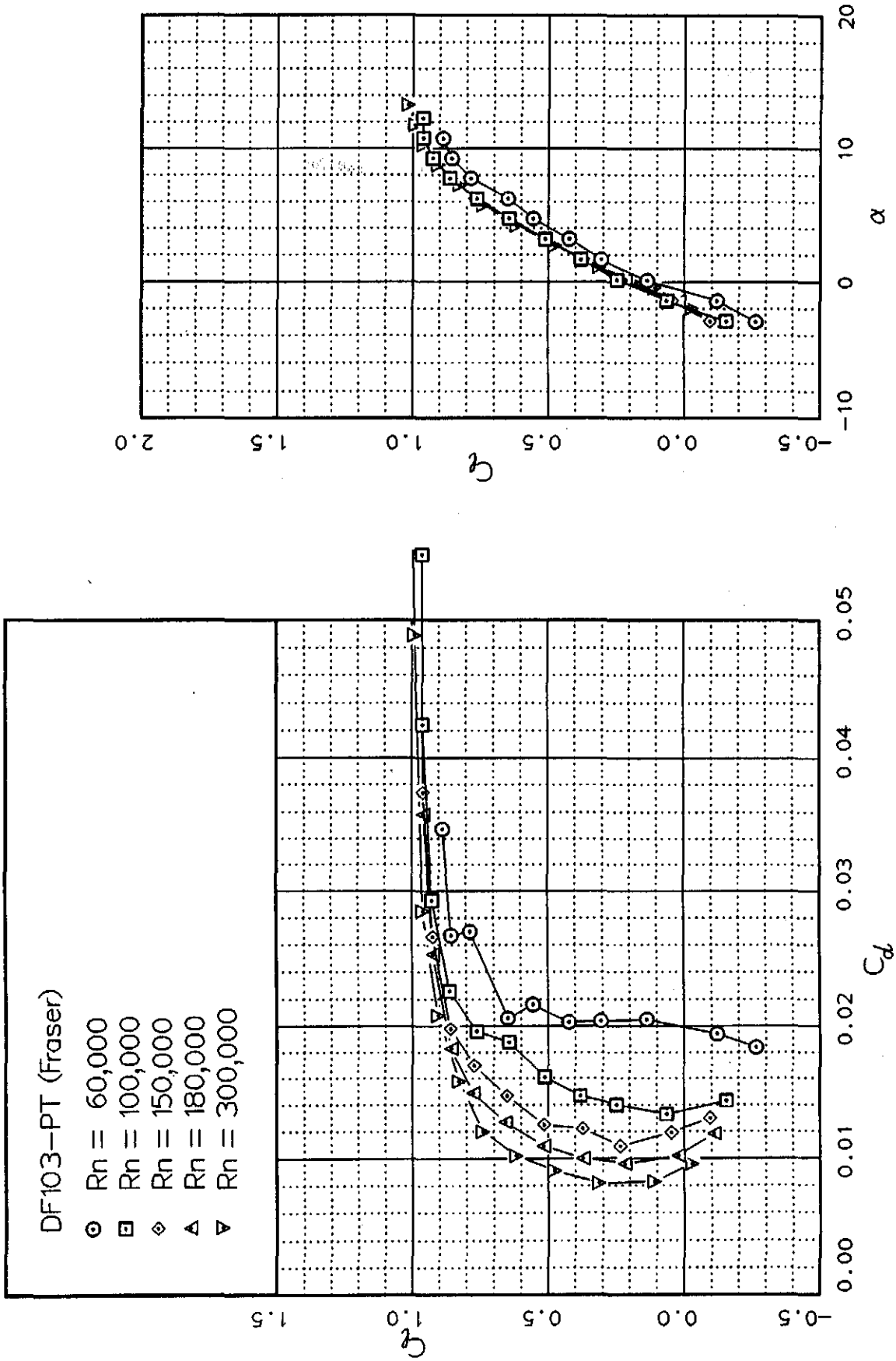
DF103-PT (Fraser)
Rn = 60,000
Rn = 100,000
Rn = 150,000
Rn = 180,000
Rn = 300,000
C_l
C_d
α

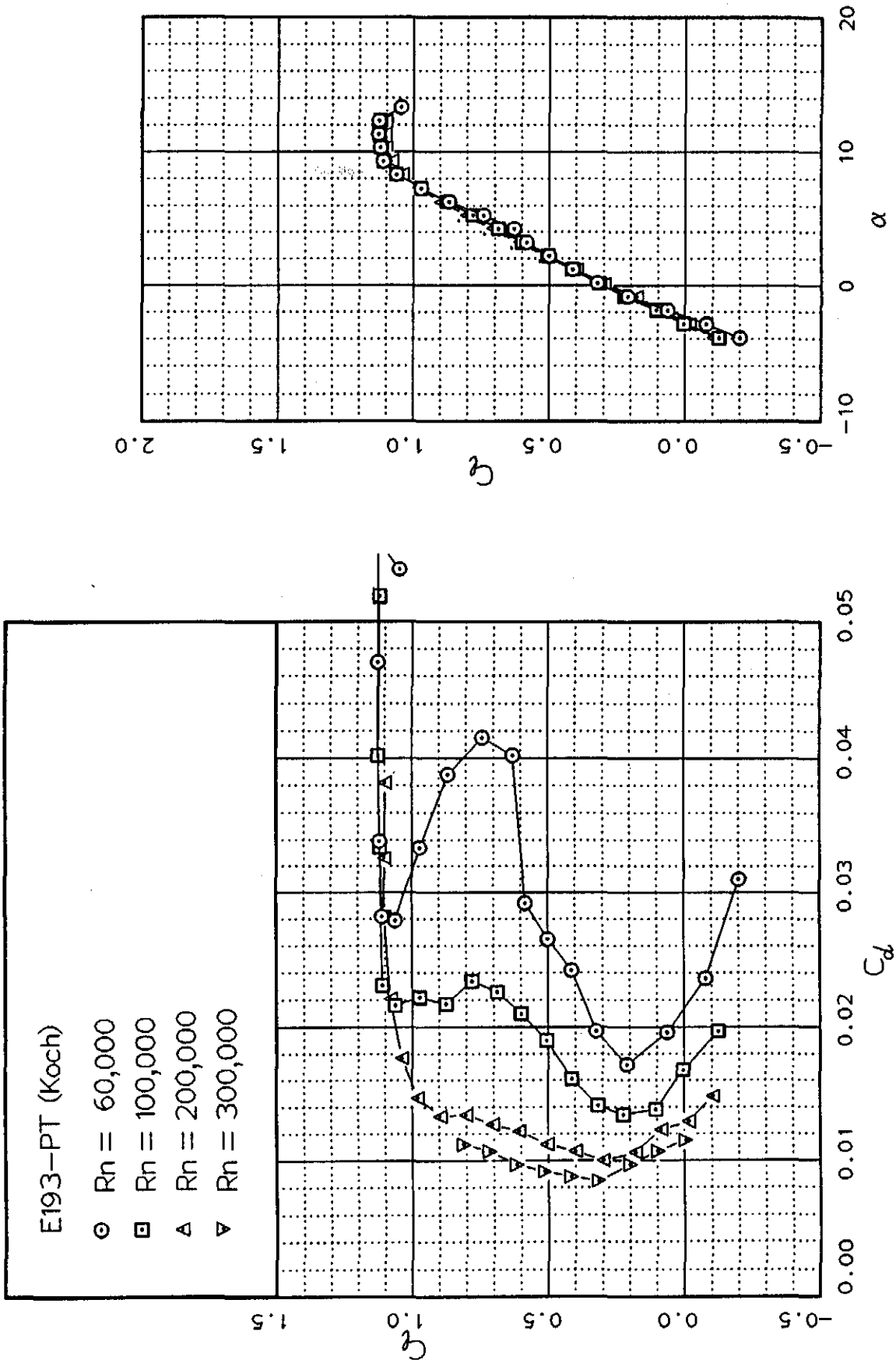
E193–PT (Koch)
Rn = 60,000
Rn = 100,000
Rn = 200,000
Rn = 300,000
α
C_l
C_d
−0.5
0.0
0.5
1.0
1.5
2.0
−10
0
10
20
0.00
0.01
0.02
0.03
0.04
0.05

Fig. 12.12

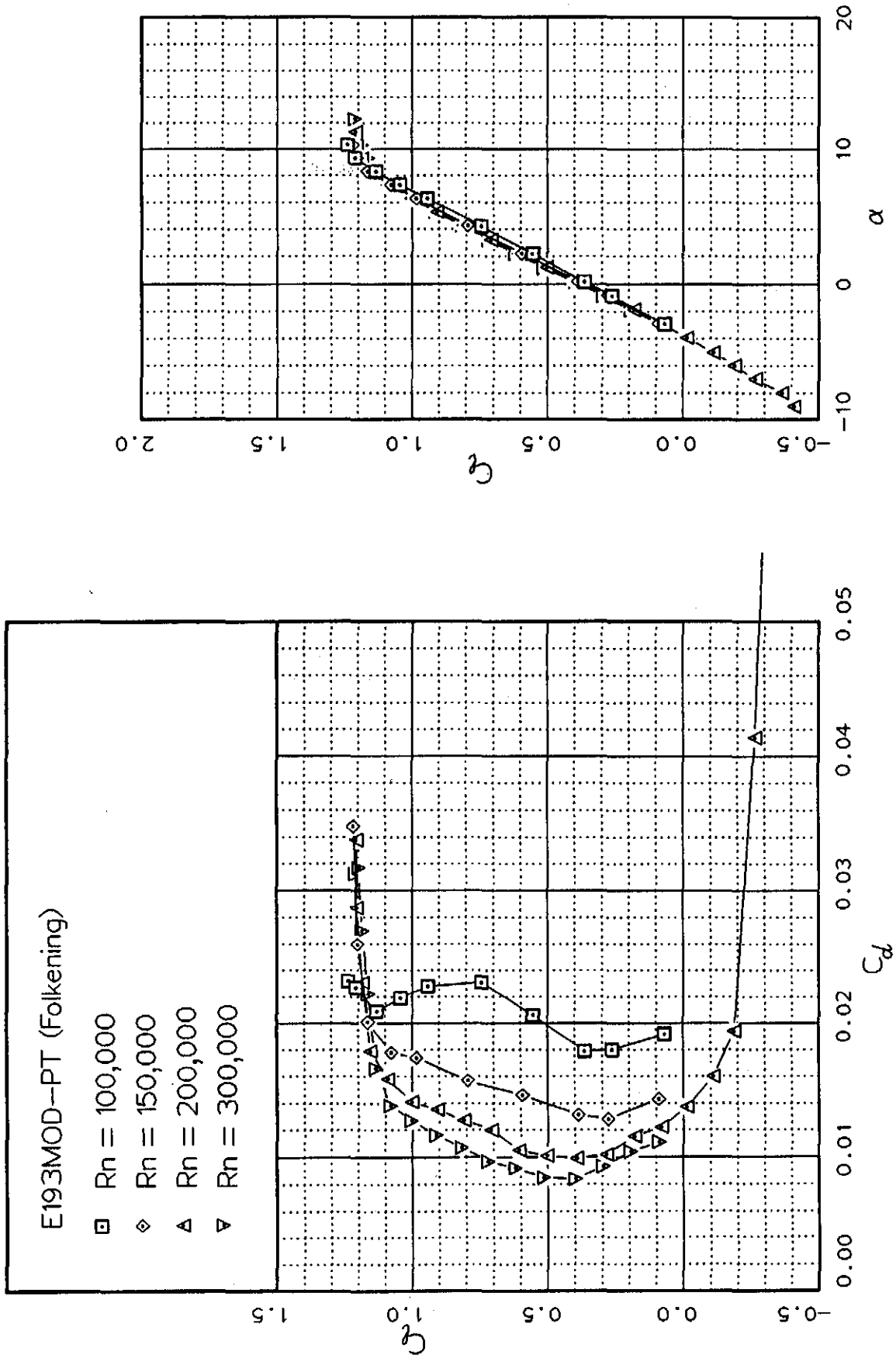
E193MOD–PT (Folkening)
Rn = 100,000
Rn = 150,000
Rn = 200,000
Rn = 300,000
−0.5
0.0
0.5
1.0
1.5
2.0
c_l
−10
0
10
20
α
0.00
0.01
0.02
0.03
0.04
0.05
c_d

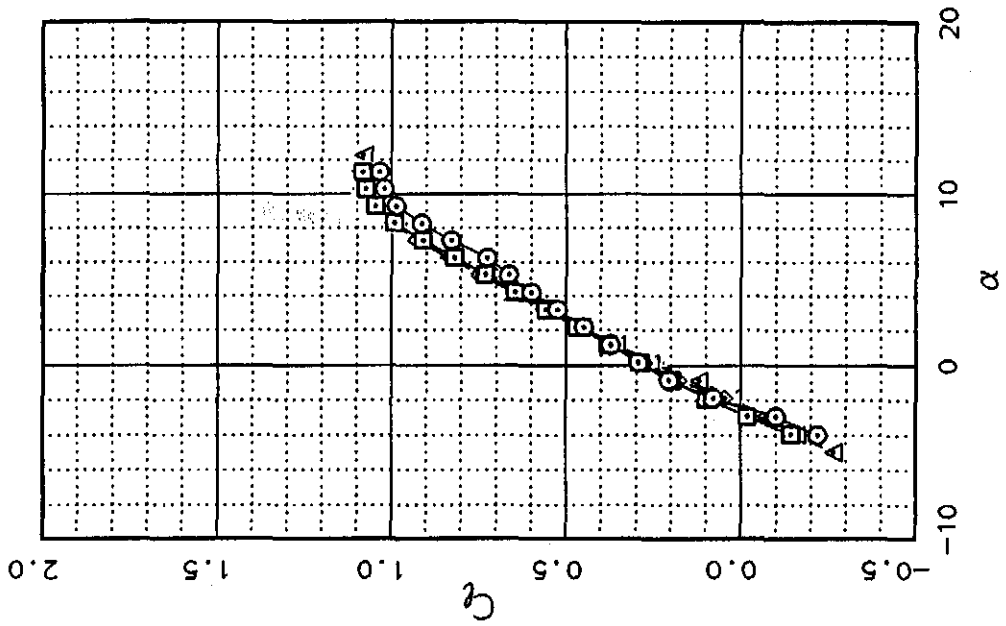
20
10
0
−10
α
−0.5
0.0
0.5
1.0
1.5
2.0
Cl

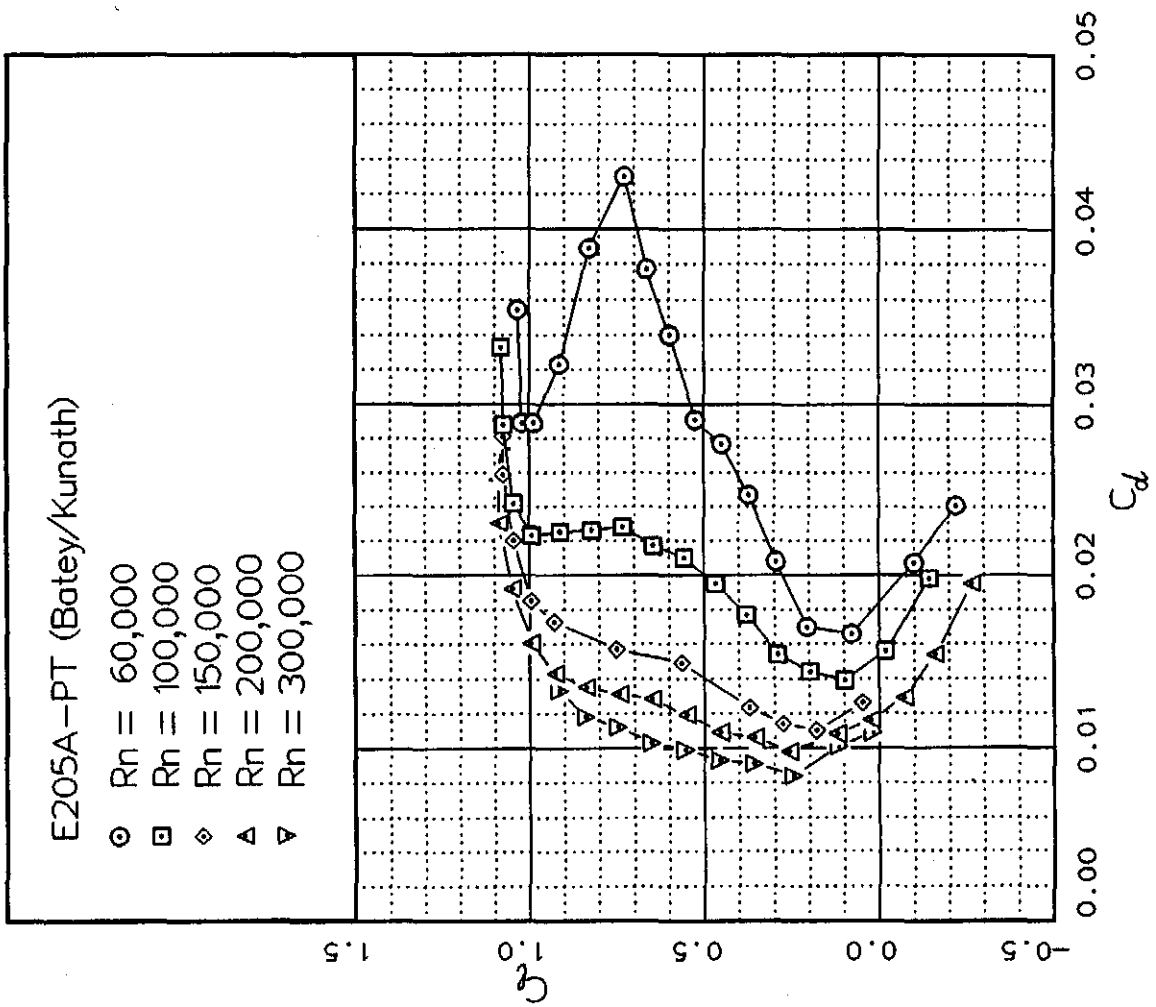
E205A−PT (Batey/Kunath)
Rn = 60,000
Rn = 100,000
Rn = 150,000
Rn = 200,000
Rn = 300,000
0.05
0.04
0.03
0.02
0.01
0.00
Cd
−0.5
0.0
0.5
1.0
1.5
Cl

Fig. 12.14

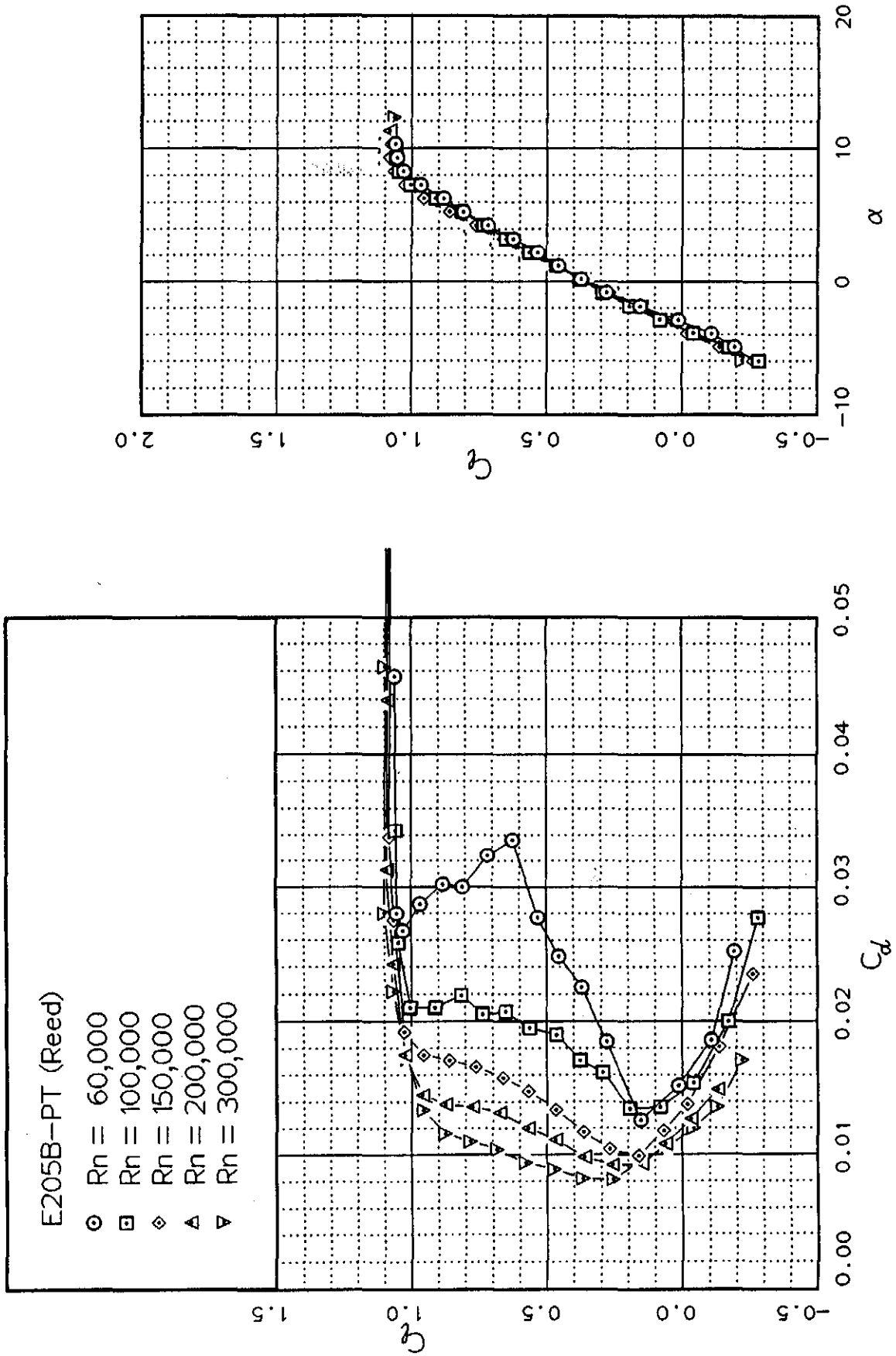
E205B–PT (Reed)
Rn = 60,000
Rn = 100,000
Rn = 150,000
Rn = 200,000
Rn = 300,000
0.00
0.01
0.02
0.03
0.04
0.05
C_d
−0.5
0.0
0.5
1.0
1.5
C_l
20
10
0
−10
α
−0.5
0.0
0.5
1.0
1.5
2.0
C_l

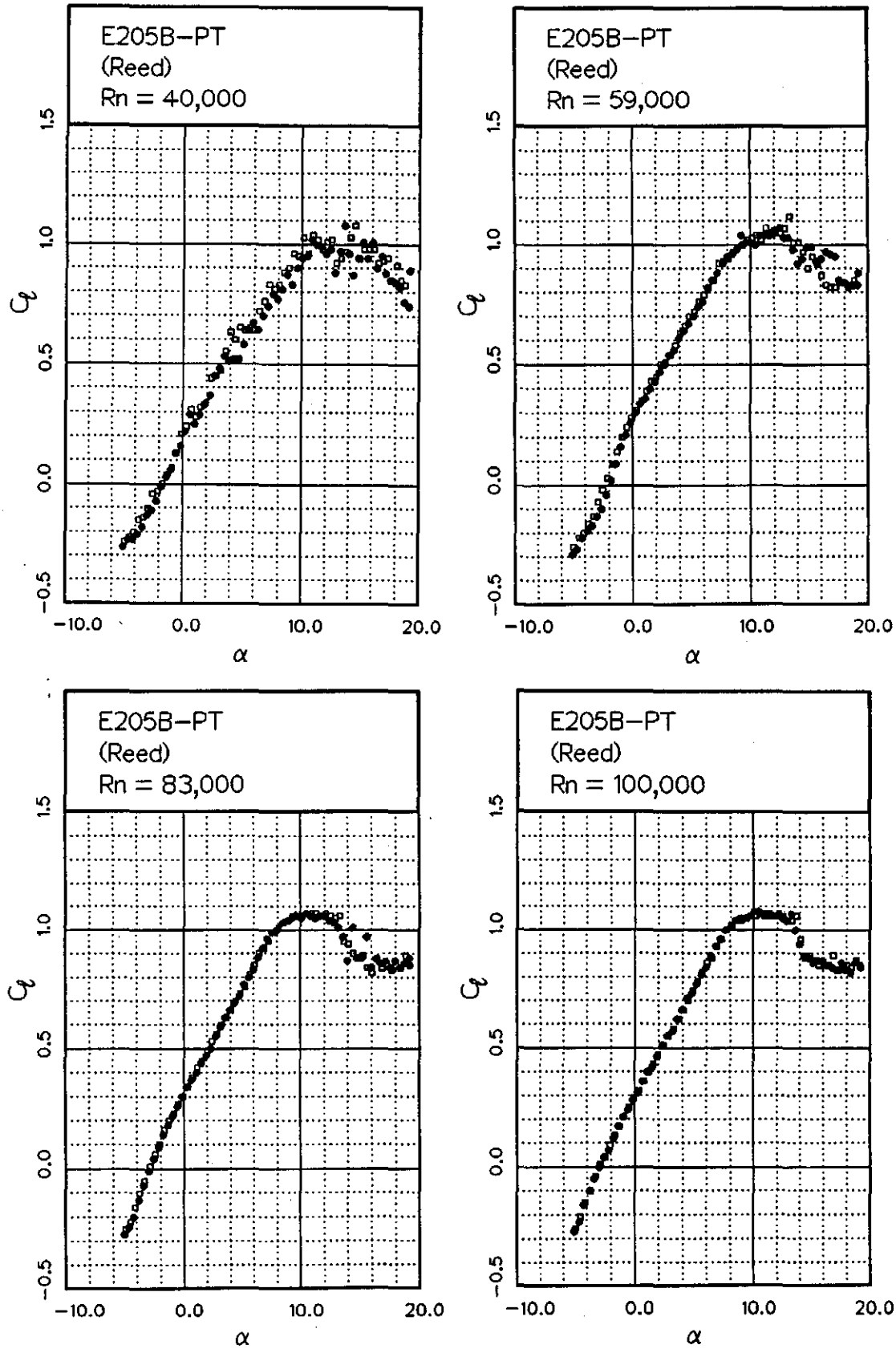
E205B–PT
(Reed)
Rn = 40,000
E205B–PT
(Reed)
Rn = 59,000
E205B–PT
(Reed)
Rn = 83,000
E205B–PT
(Reed)
Rn = 100,000
C_l
α
1.5
1.0
0.5
0.0
−0.5
−10.0
0.0
10.0
20.0

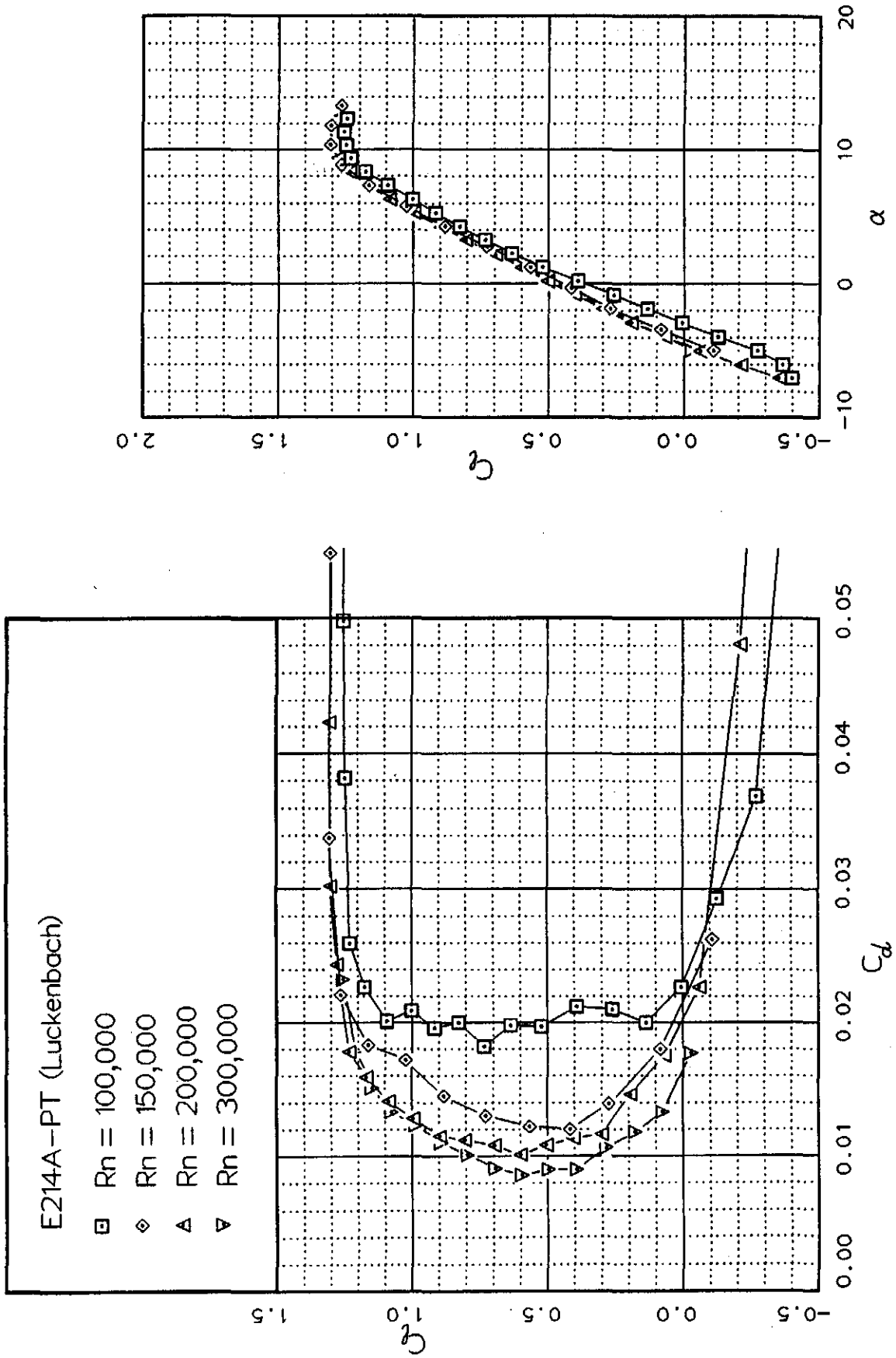
E214A-PT (Luckenbach)
Rn = 100,000
Rn = 150,000
Rn = 200,000
Rn = 300,000
C_l
C_d
α

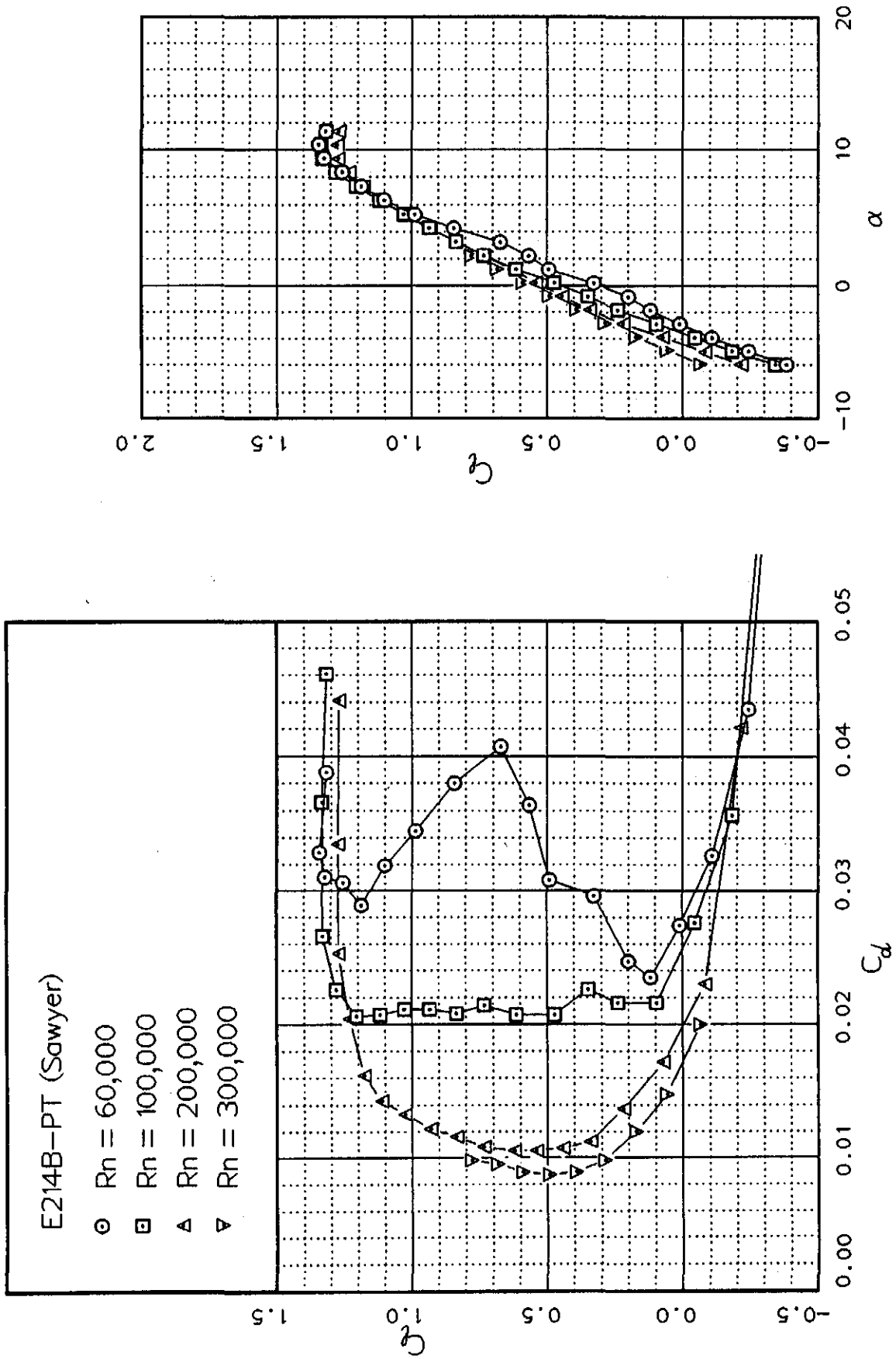
E214B–PT (Sawyer)
Rn = 60,000
Rn = 100,000
Rn = 200,000
Rn = 300,000
C_l
C_d
α
−0.5
0.0
0.5
1.0
1.5
2.0
−10
0
10
20
0.00
0.01
0.02
0.03
0.04
0.05

Fig. 12.18

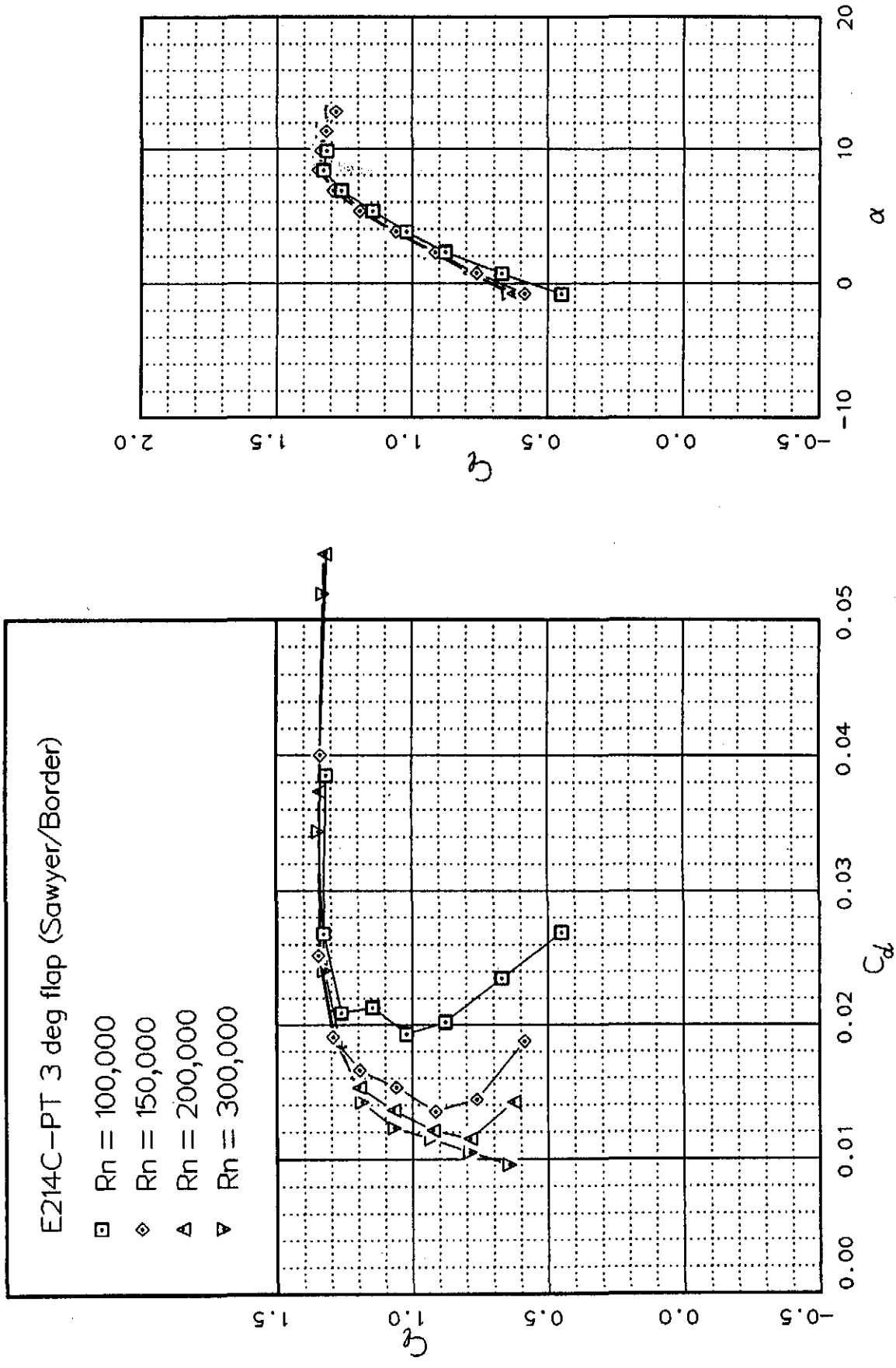
E214C–PT 3 deg flap (Sawyer/Border)
Rn = 100,000
Rn = 150,000
Rn = 200,000
Rn = 300,000
−0.5
0.0
0.5
1.0
1.5
2.0
c_l
−10
0
10
20
α
0.00
0.01
0.02
0.03
0.04
0.05
c_d

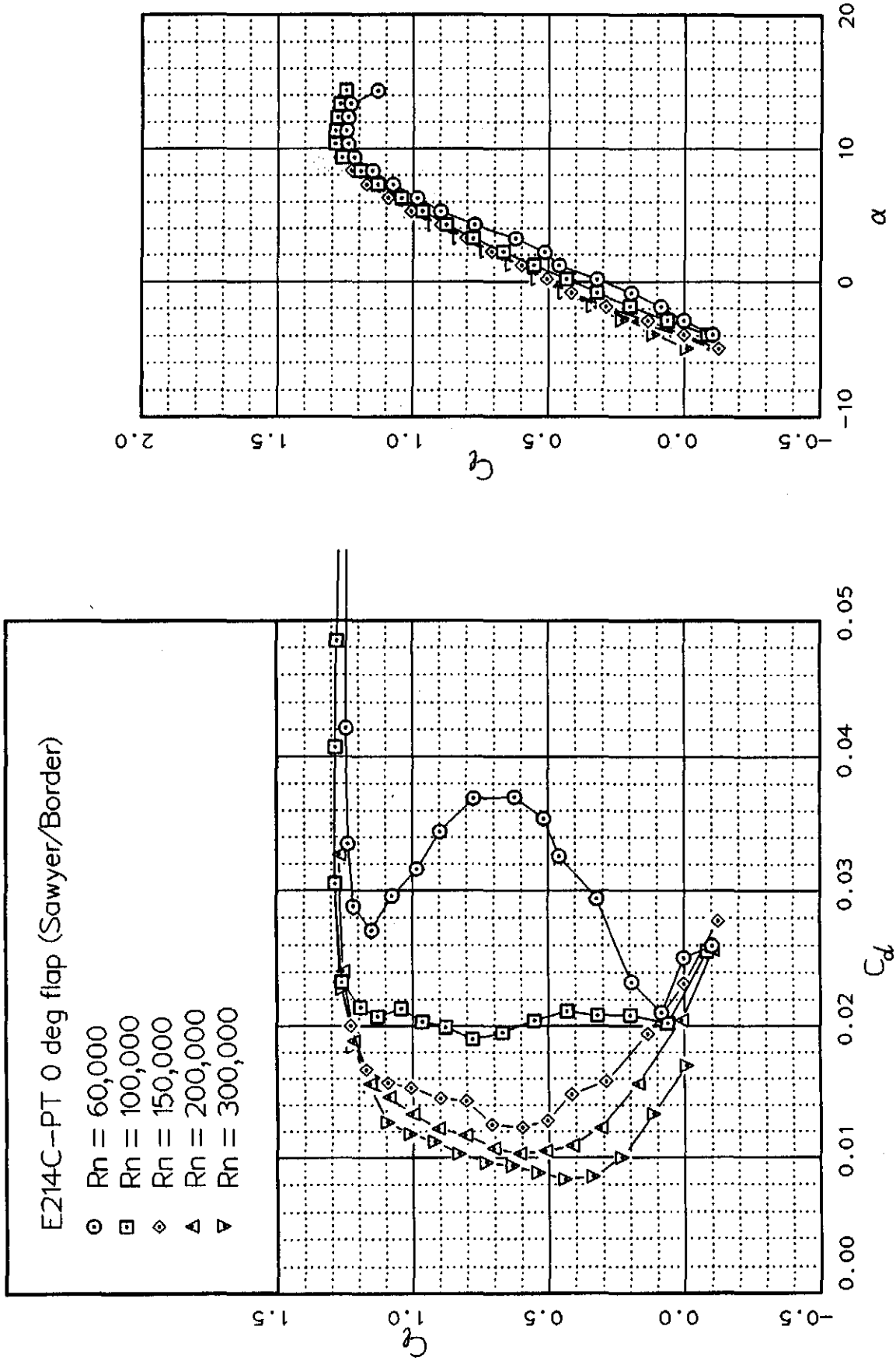
E214C-PT 0 deg flap (Sawyer/Border)
Rn = 60,000
Rn = 100,000
Rn = 150,000
Rn = 200,000
Rn = 300,000
0.05
0.04
0.03
0.02
0.01
0.00
C_d
1.5
1.0
0.5
0.0
−0.5
C_l
20
10
0
−10
α
2.0
1.5
1.0
0.5
0.0
−0.5
C_l

Fig. 12.20

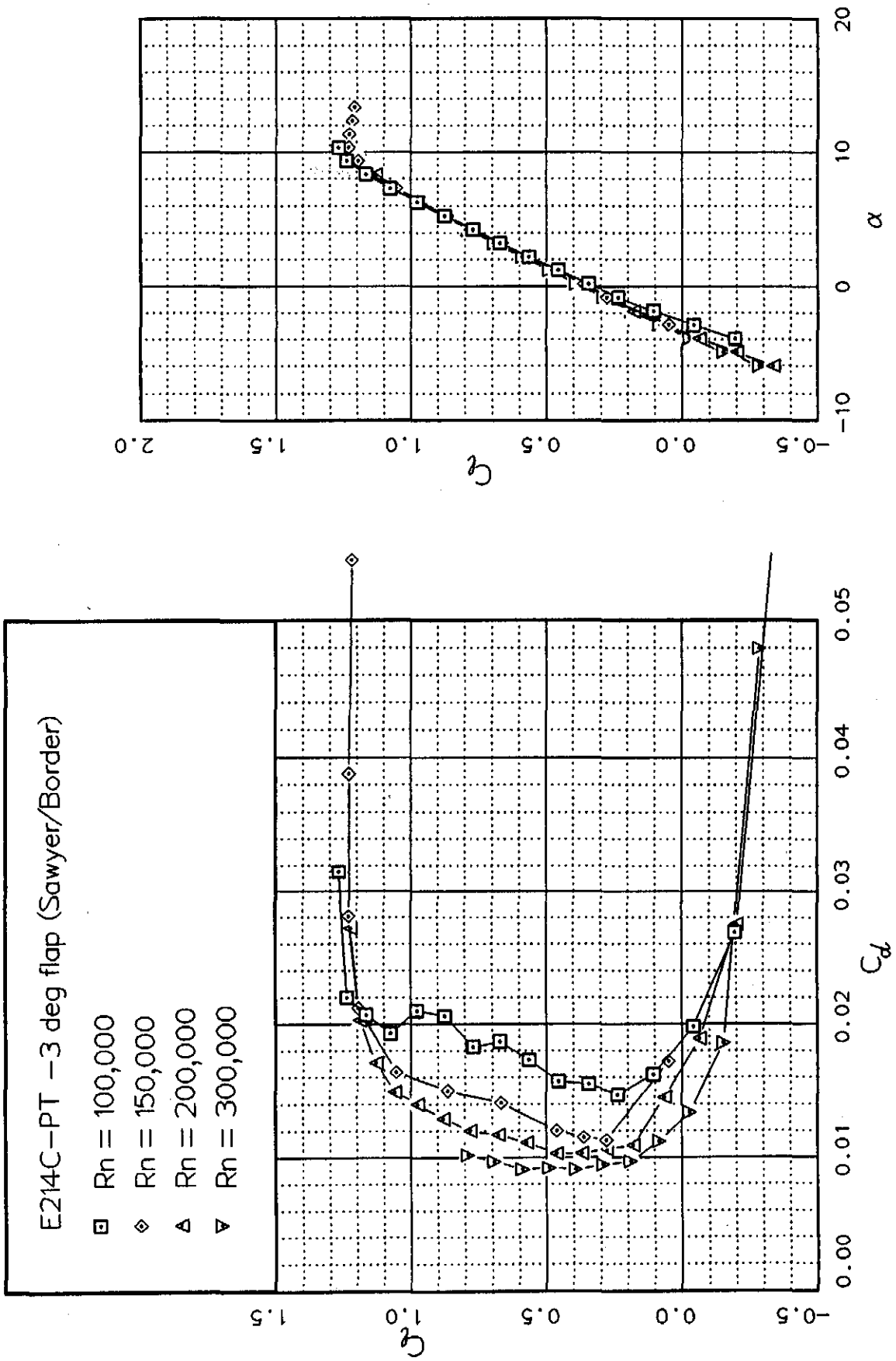
E214C-PT −3 deg flap (Sawyer/Border)
Rn = 100,000
Rn = 150,000
Rn = 200,000
Rn = 300,000
−0.5
0.0
0.5
1.0
1.5
2.0
c_l
20
10
0
−10
α
0.00
0.01
0.02
0.03
0.04
0.05
c_d

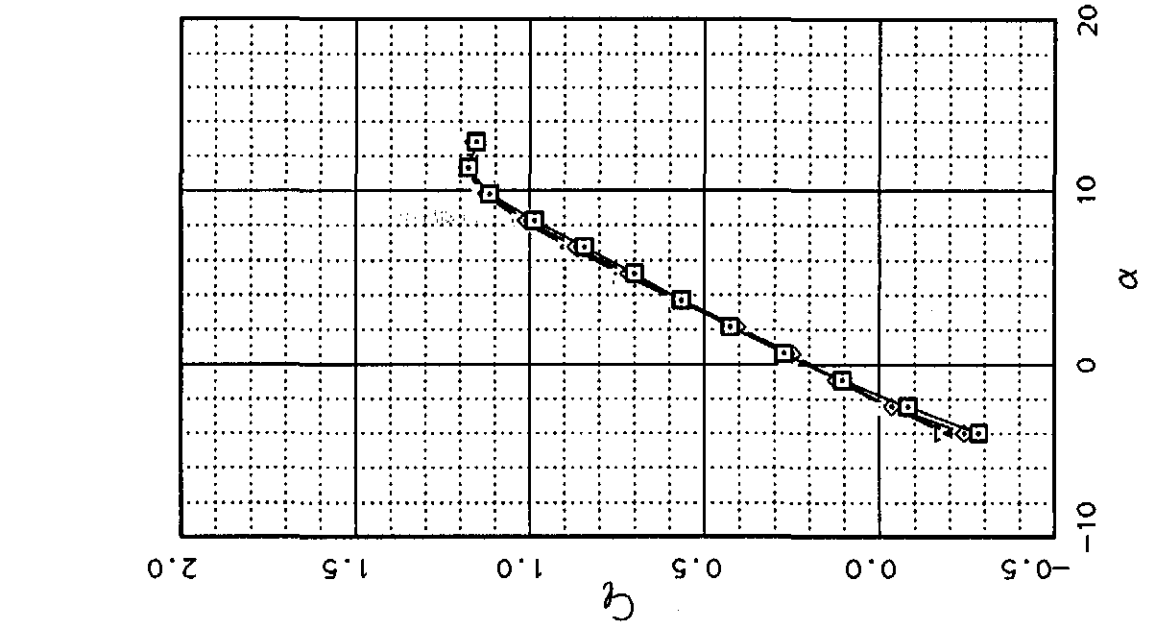
20
10
0
−10
α
−0.5
0.0
0.5
1.0
1.5
2.0
cl

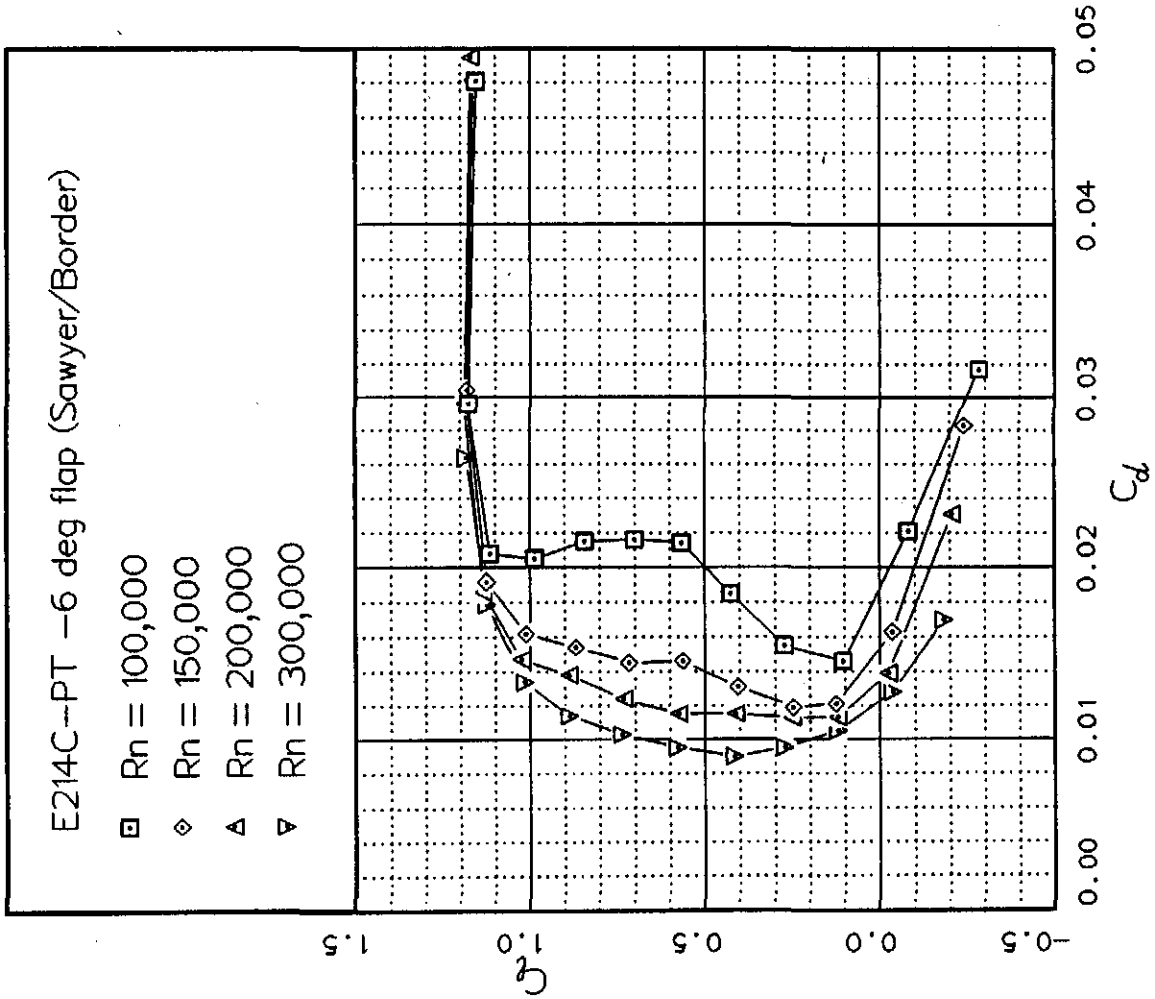
E214C-PT −6 deg flap (Sawyer/Border)
Rn = 100,000
Rn = 150,000
Rn = 200,000
Rn = 300,000
0.05
0.04
0.03
0.02
0.01
0.00
Cd
−0.5
0.0
0.5
1.0
1.5
cl

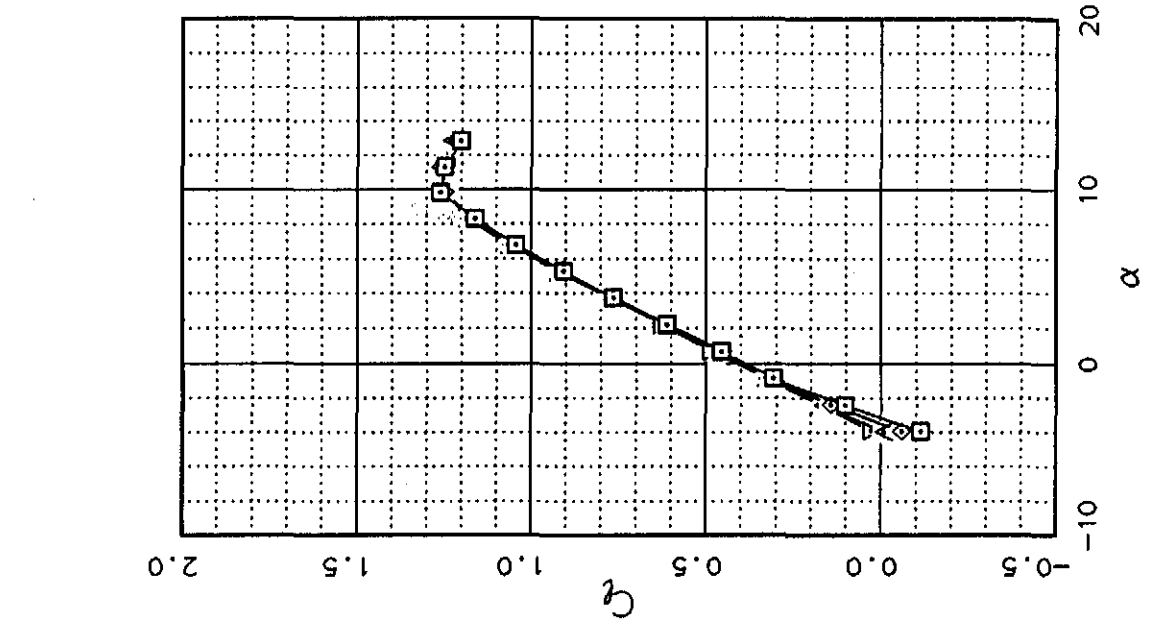
20
10
0
−10
α
−0.5
0.0
0.5
1.0
1.5
2.0
c_l

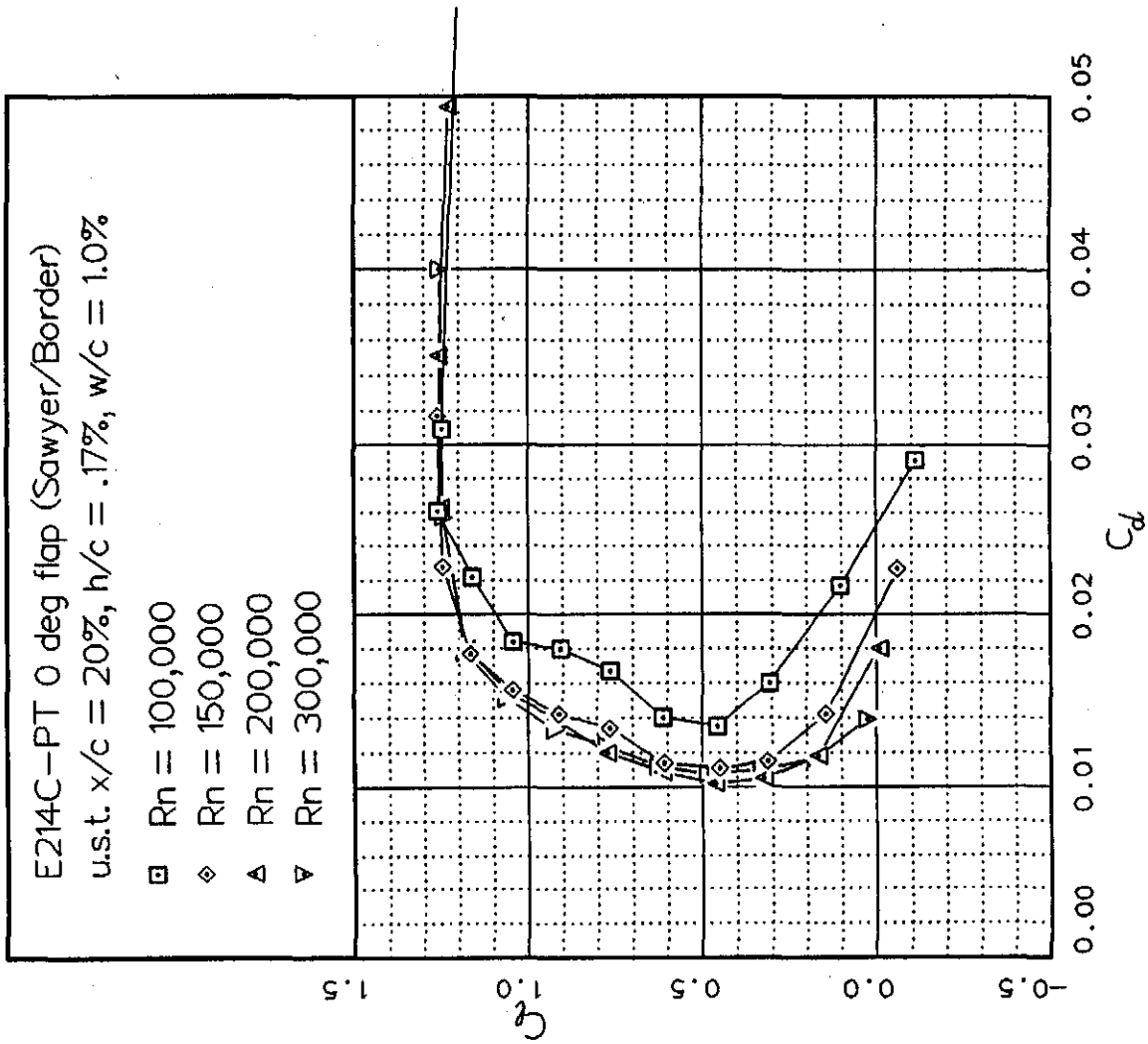
E214C–PT 0 deg flap (Sawyer/Border)
u.s.t. x/c = 20%, h/c = .17%, w/c = 1.0%
Rn = 100,000
Rn = 150,000
Rn = 200,000
Rn = 300,000
0.05
0.04
0.03
0.02
0.01
0.00
C_d
−0.5
0.0
0.5
1.0
1.5
c_l

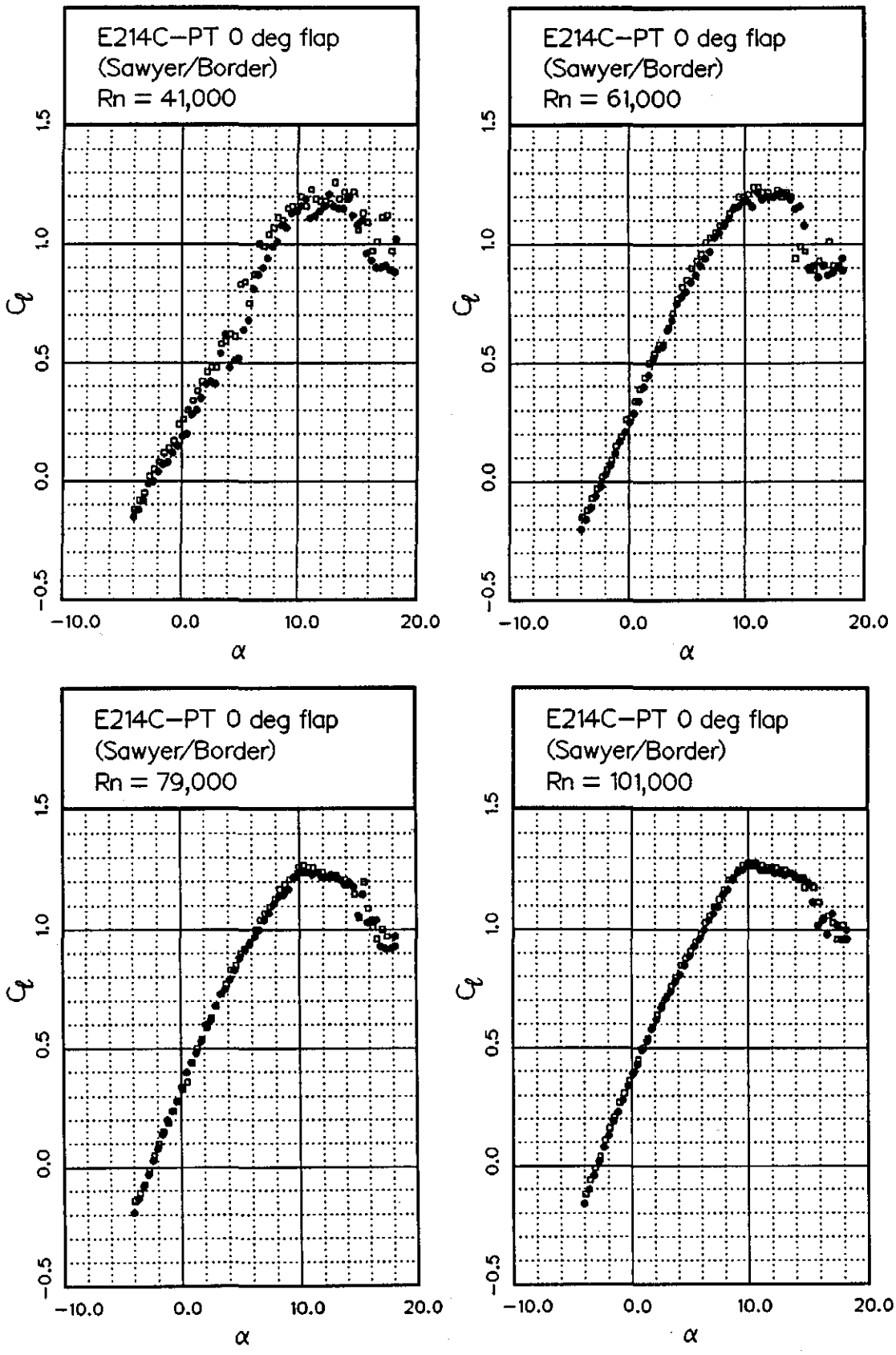
E214C–PT 0 deg flap
(Sawyer/Border)
Rn = 41,000
E214C–PT 0 deg flap
(Sawyer/Border)
Rn = 61,000
E214C–PT 0 deg flap
(Sawyer/Border)
Rn = 79,000
E214C–PT 0 deg flap
(Sawyer/Border)
Rn = 101,000
C_ℓ
α
1.5
1.0
0.5
0.0
−0.5
−10.0
0.0
10.0
20.0

Fig. 12.24

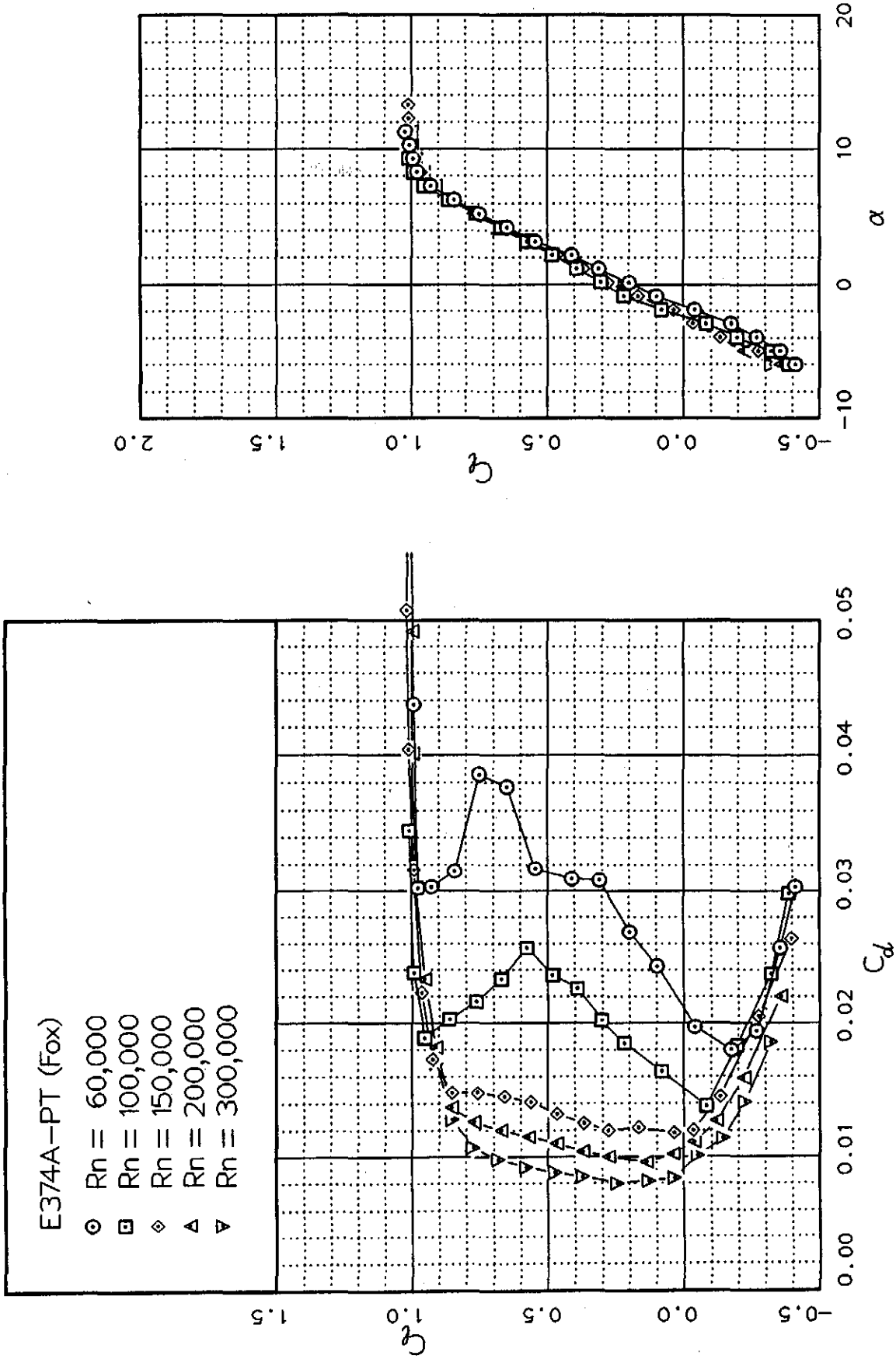
E374A–PT (Fox)
Rn = 60,000
Rn = 100,000
Rn = 150,000
Rn = 200,000
Rn = 300,000
C_l
C_d
α

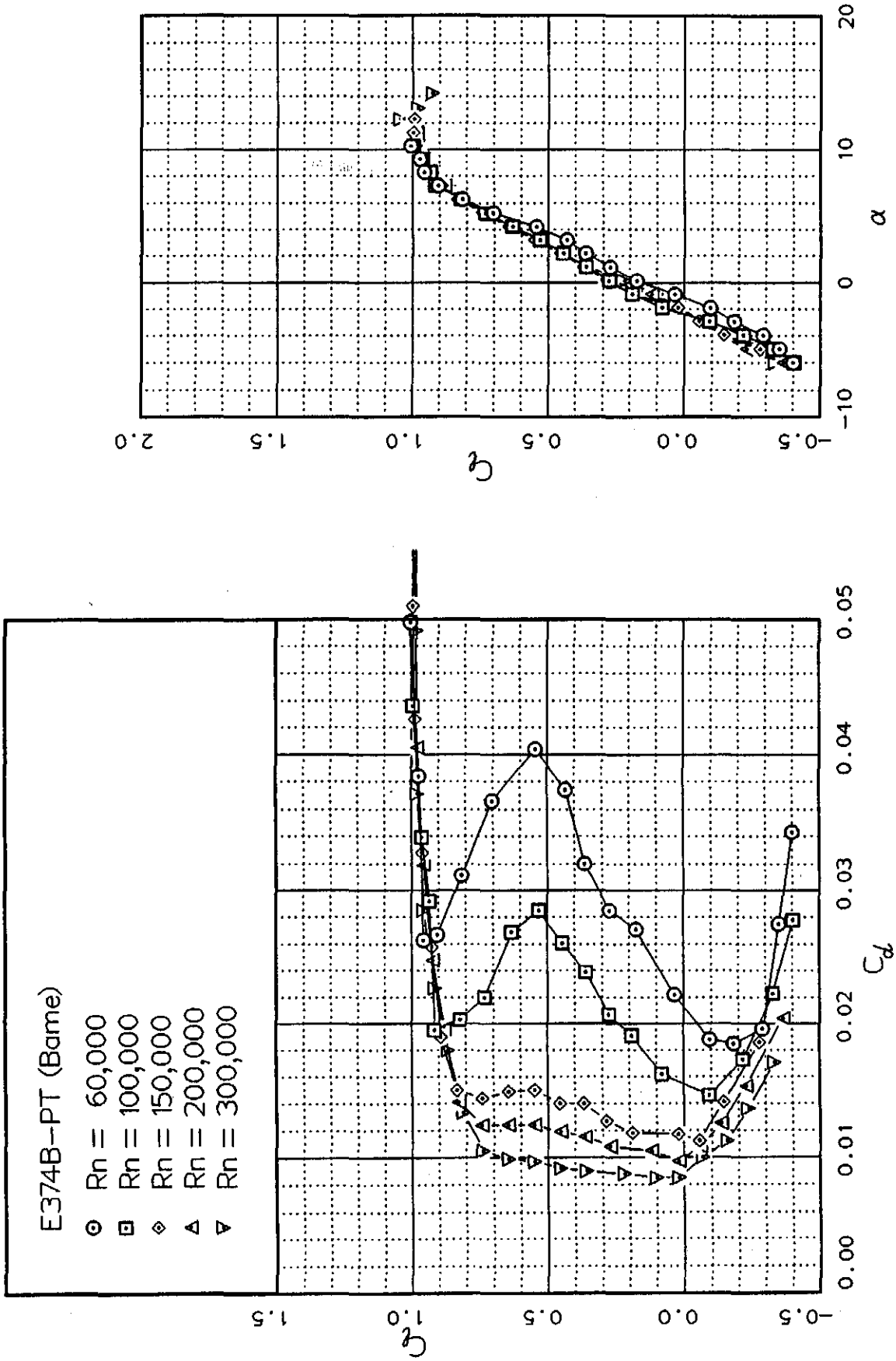
E374B-PT (Bare)
Rn = 60,000
Rn = 100,000
Rn = 150,000
Rn = 200,000
Rn = 300,000
α
C_l
C_d
20
10
0
−10
0.05
0.04
0.03
0.02
0.01
0.00
−0.5
0.0
0.5
1.0
1.5
2.0

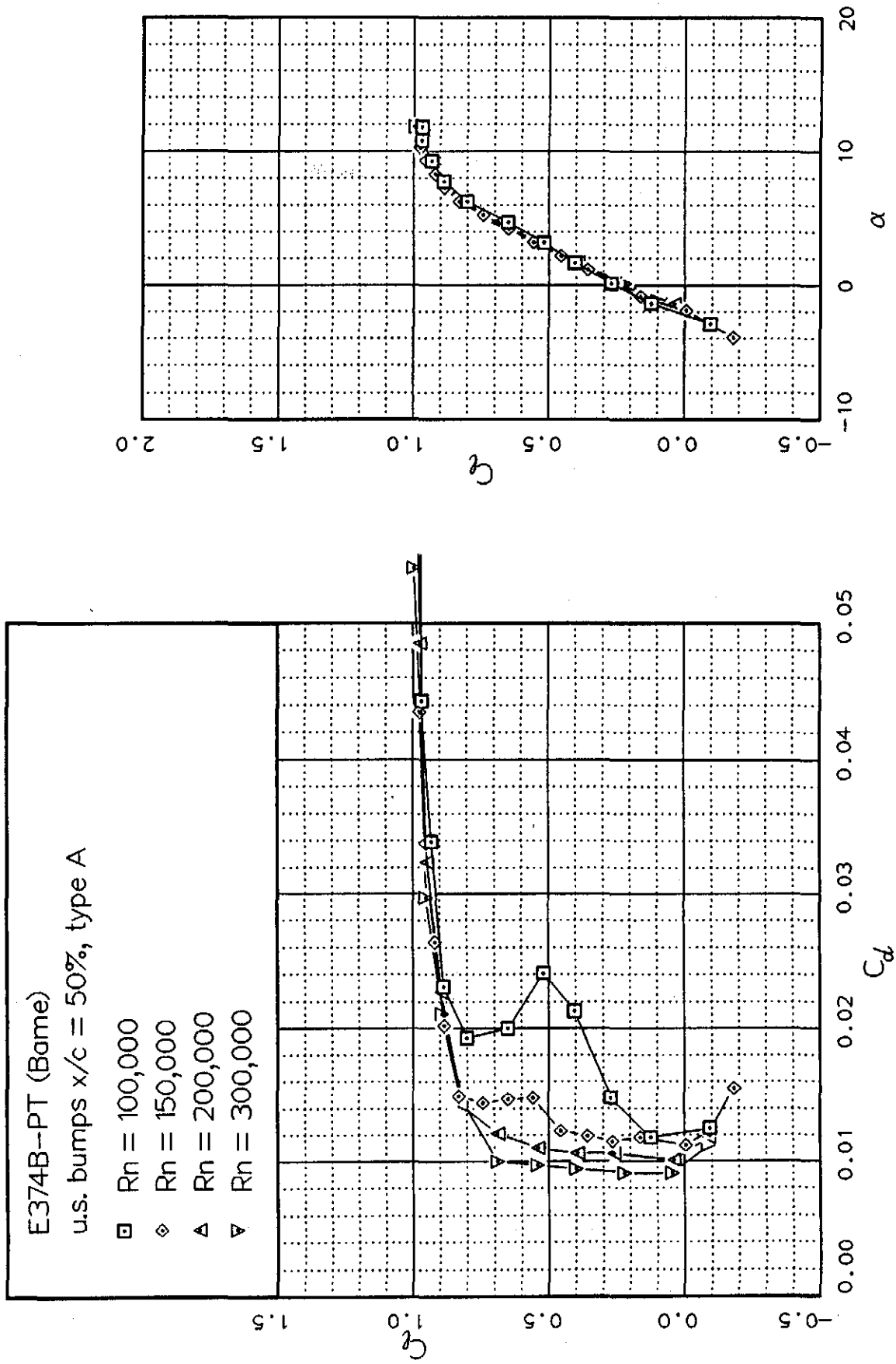
E374B-PT (Bame)
u.s. bumps x/c = 50%, type A
Rn = 100,000
Rn = 150,000
Rn = 200,000
Rn = 300,000
α
C_d
C_l
20
10
0
−10
0.05
0.04
0.03
0.02
0.01
0.00
−0.5
0.0
0.5
1.0
1.5
2.0

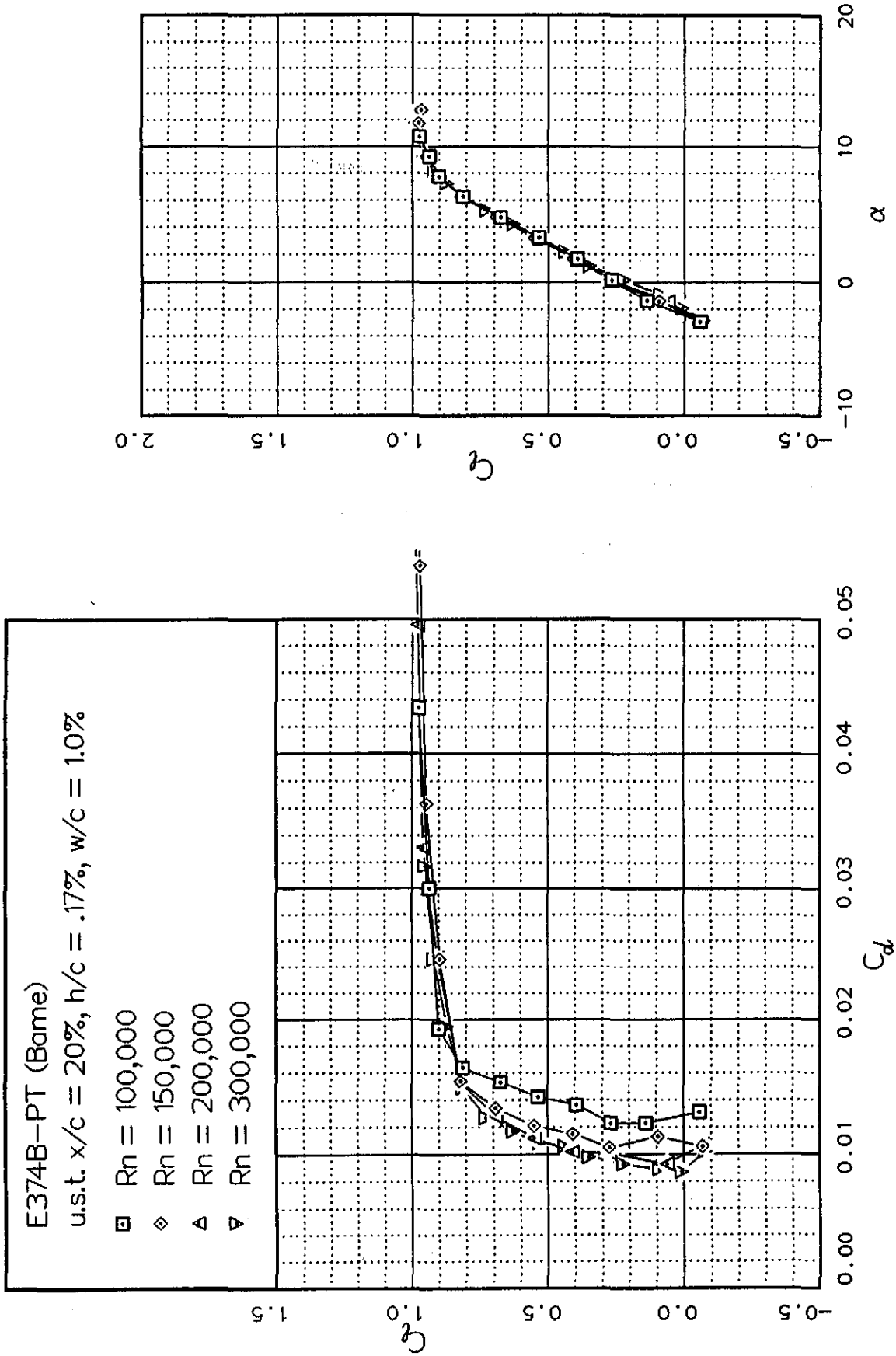
E374B–PT (Bame)
u.s.t. x/c = 20%, h/c = .17%, w/c = 1.0%
Rn = 100,000
Rn = 150,000
Rn = 200,000
Rn = 300,000
C_l
C_d
α
−0.5
0.0
0.5
1.0
1.5
2.0
−10
0
10
20
0.00
0.01
0.02
0.03
0.04
0.05

Fig. 12.28

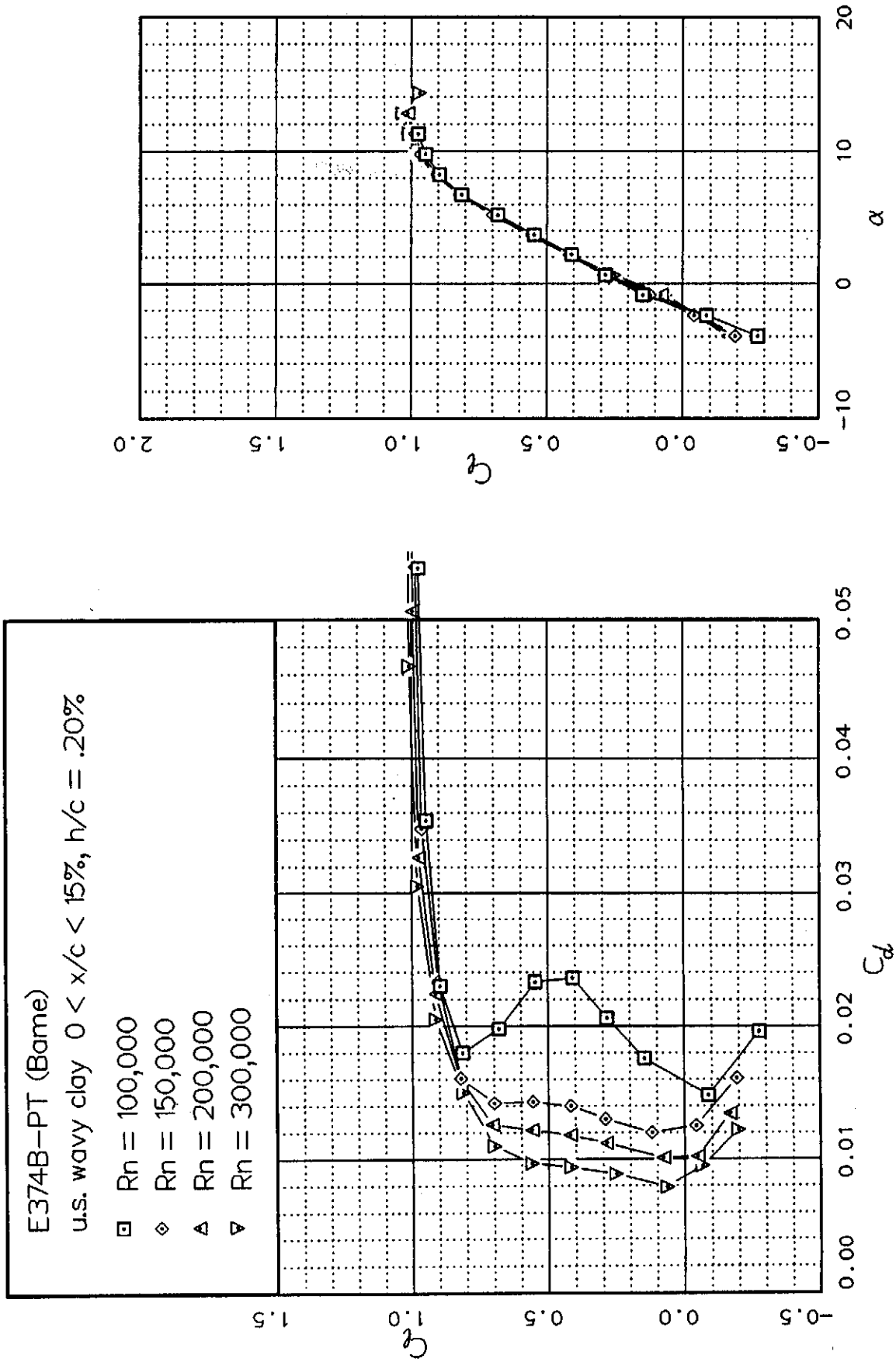
E374B–PT (Bame)
u.s. wavy clay 0 < x/c < 15%, h/c = .20%
Rn = 100,000
Rn = 150,000
Rn = 200,000
Rn = 300,000
α
C_l
C_d
20
10
0
−10
2.0
1.5
1.0
0.5
0.0
−0.5
0.05
0.04
0.03
0.02
0.01
0.00

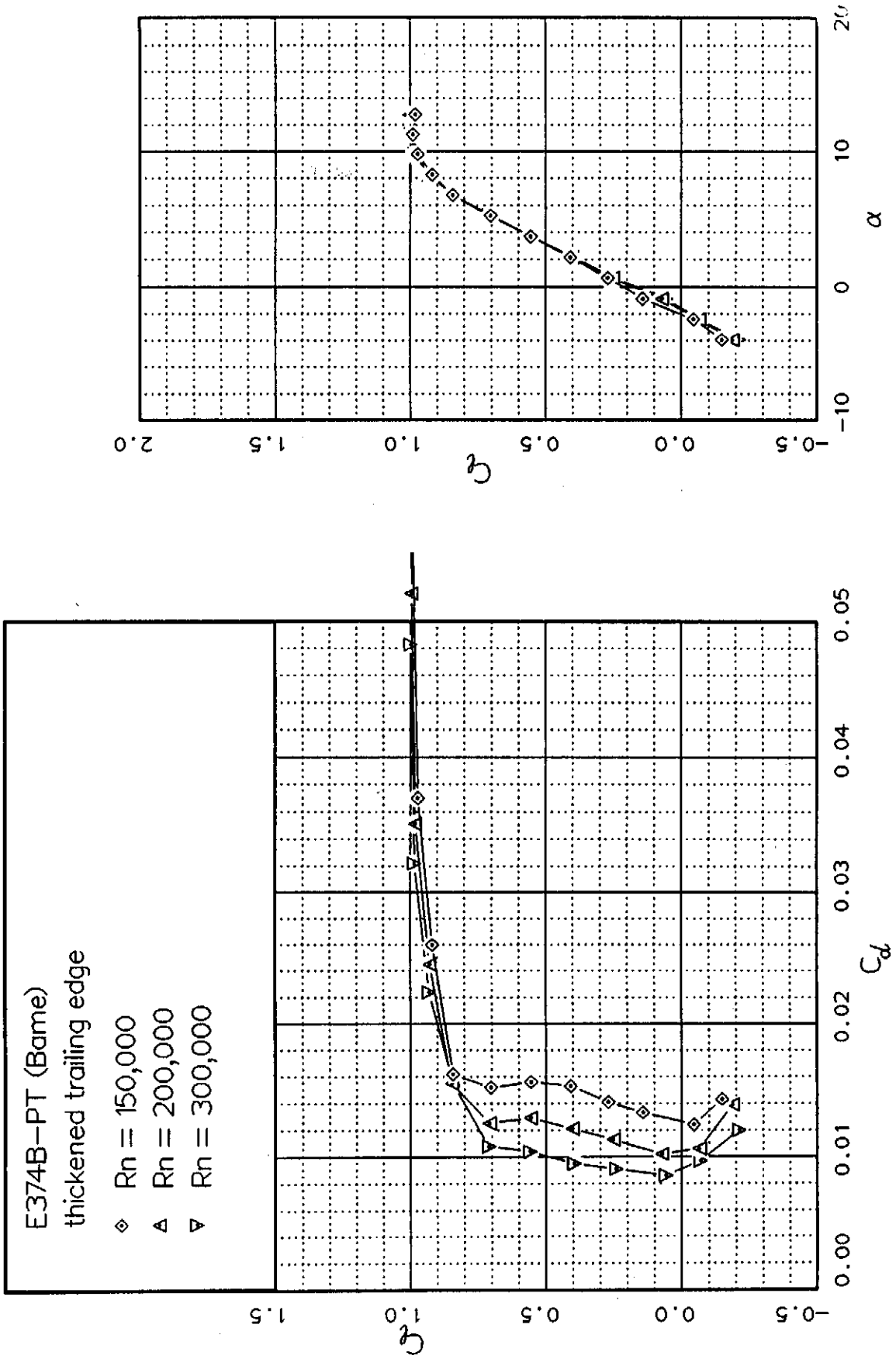
E374B–PT (Bame)
thickened trailing edge
◇ Rn = 150,000
△ Rn = 200,000
▽ Rn = 300,000
−0.5
0.0
0.5
1.0
1.5
2.0
Cl
0.00
0.01
0.02
0.03
0.04
0.05
Cd
−10
0
10
α

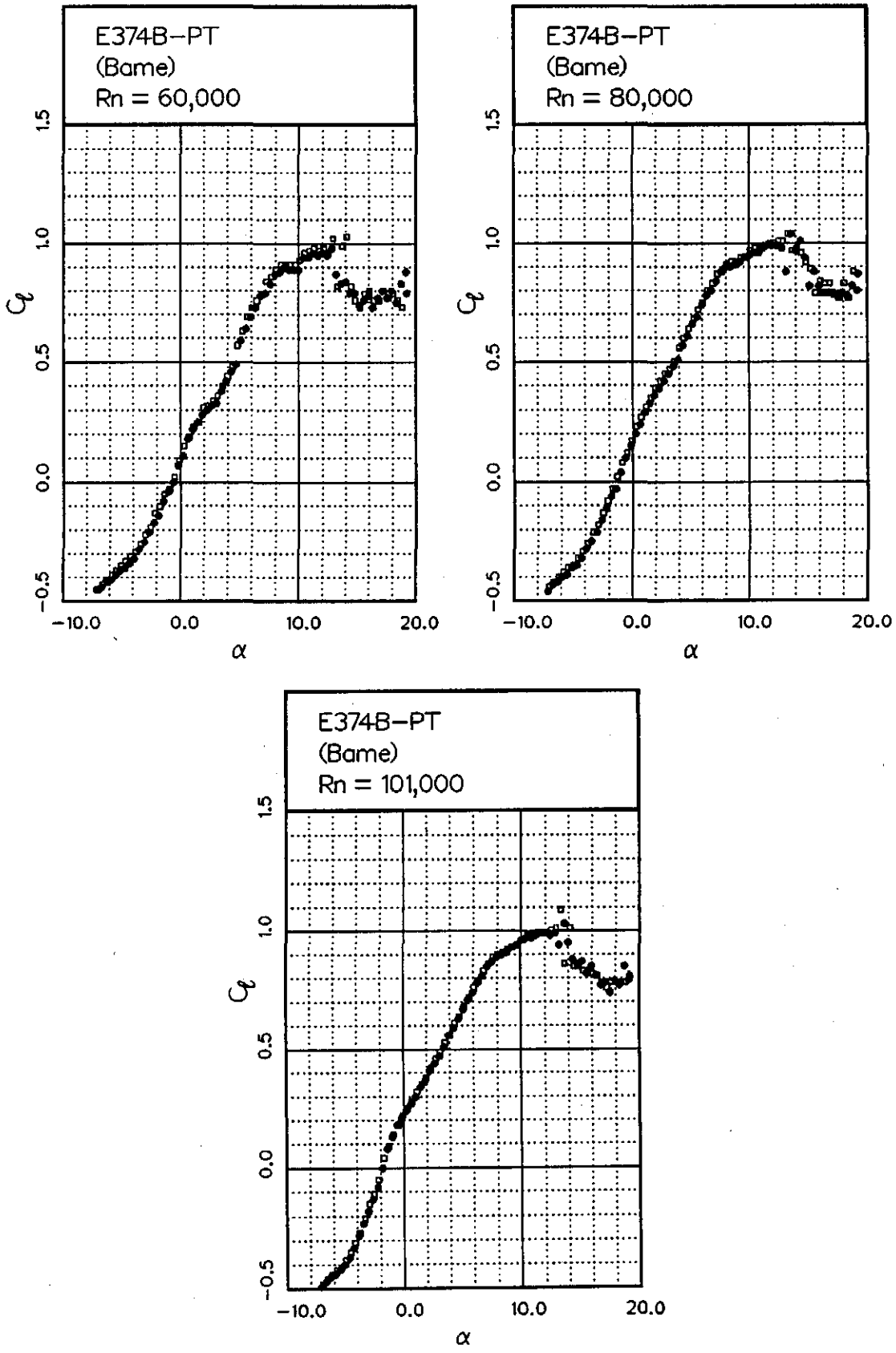
E374B–PT
(Bame)
Rn = 60,000
E374B–PT
(Bame)
Rn = 80,000
E374B–PT
(Bame)
Rn = 101,000
C_ℓ
α
1.5
1.0
0.5
0.0
−0.5
−10.0
0.0
10.0
20.0

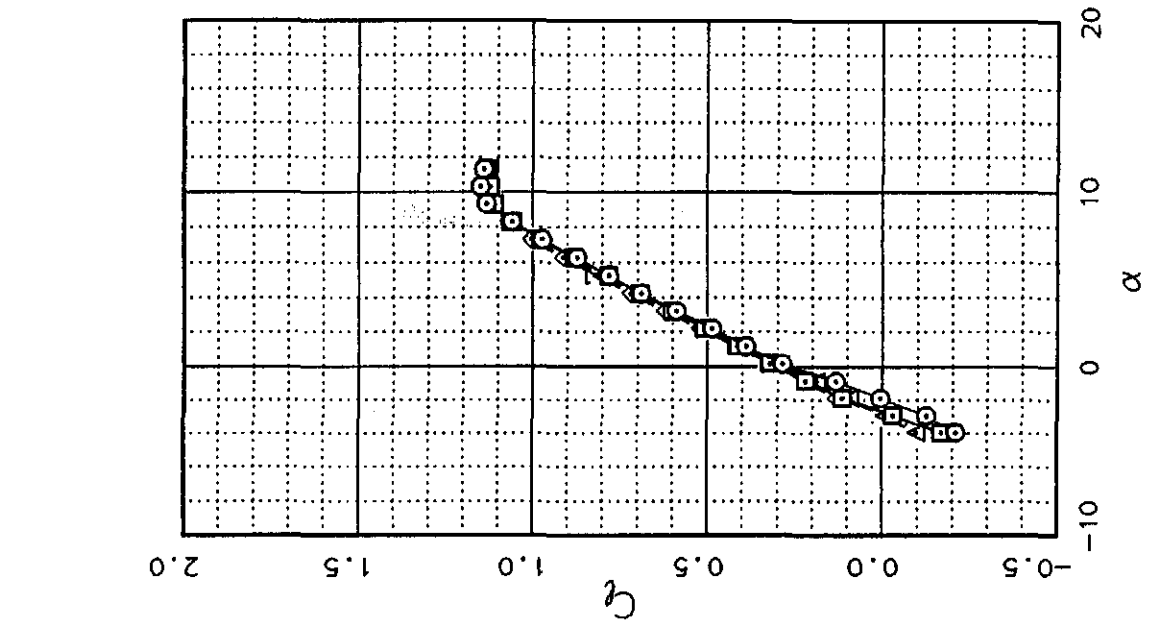
20
10
0
−10
α
−0.5
0.0
0.5
1.0
1.5
2.0
C_l

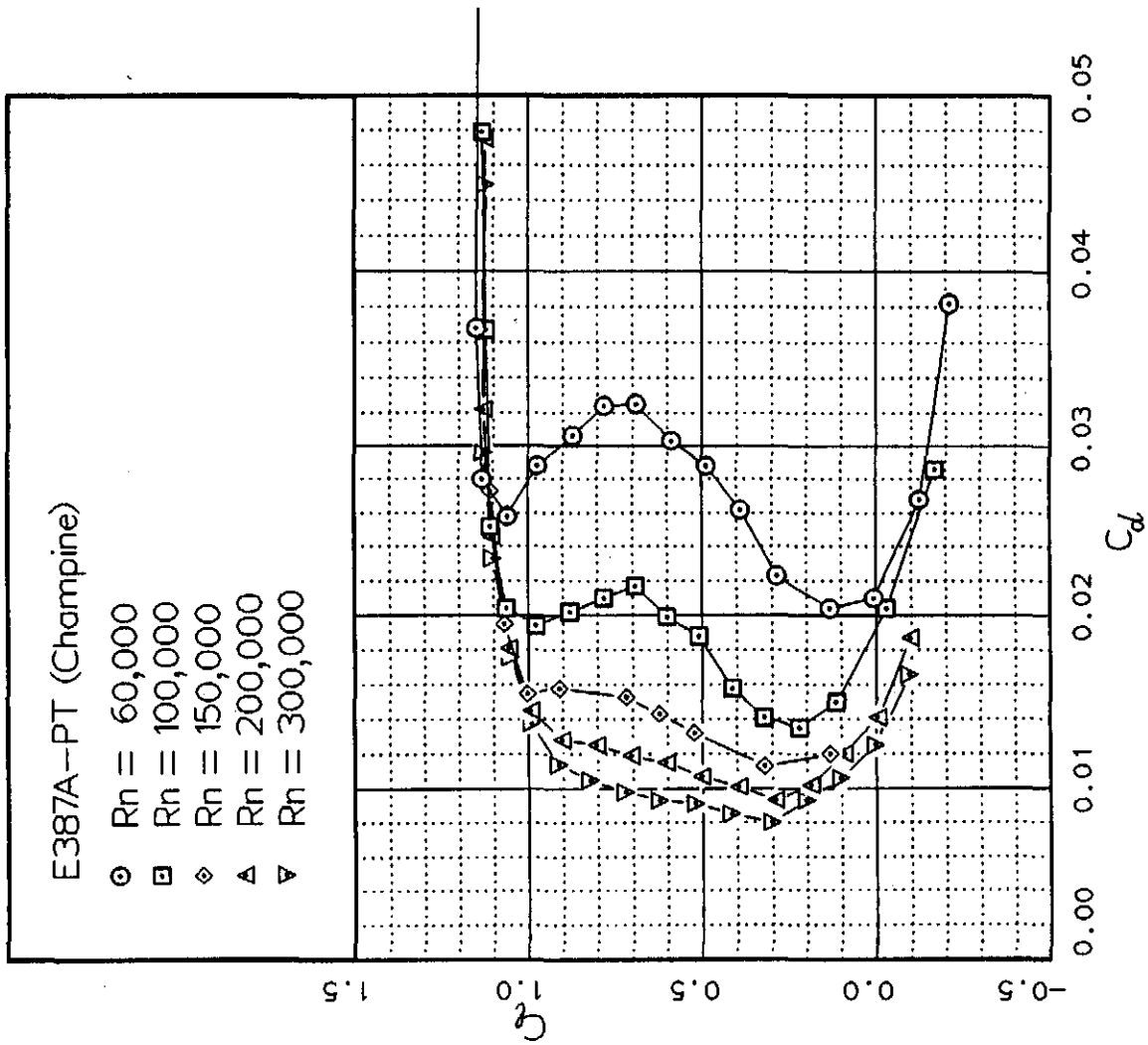
E387A–PT (Champine)
Rn = 60,000
Rn = 100,000
Rn = 150,000
Rn = 200,000
Rn = 300,000
0.05
0.04
0.03
0.02
0.01
0.00
C_d
−0.5
0.0
0.5
1.0
1.5
C_l

Fig. 12.32

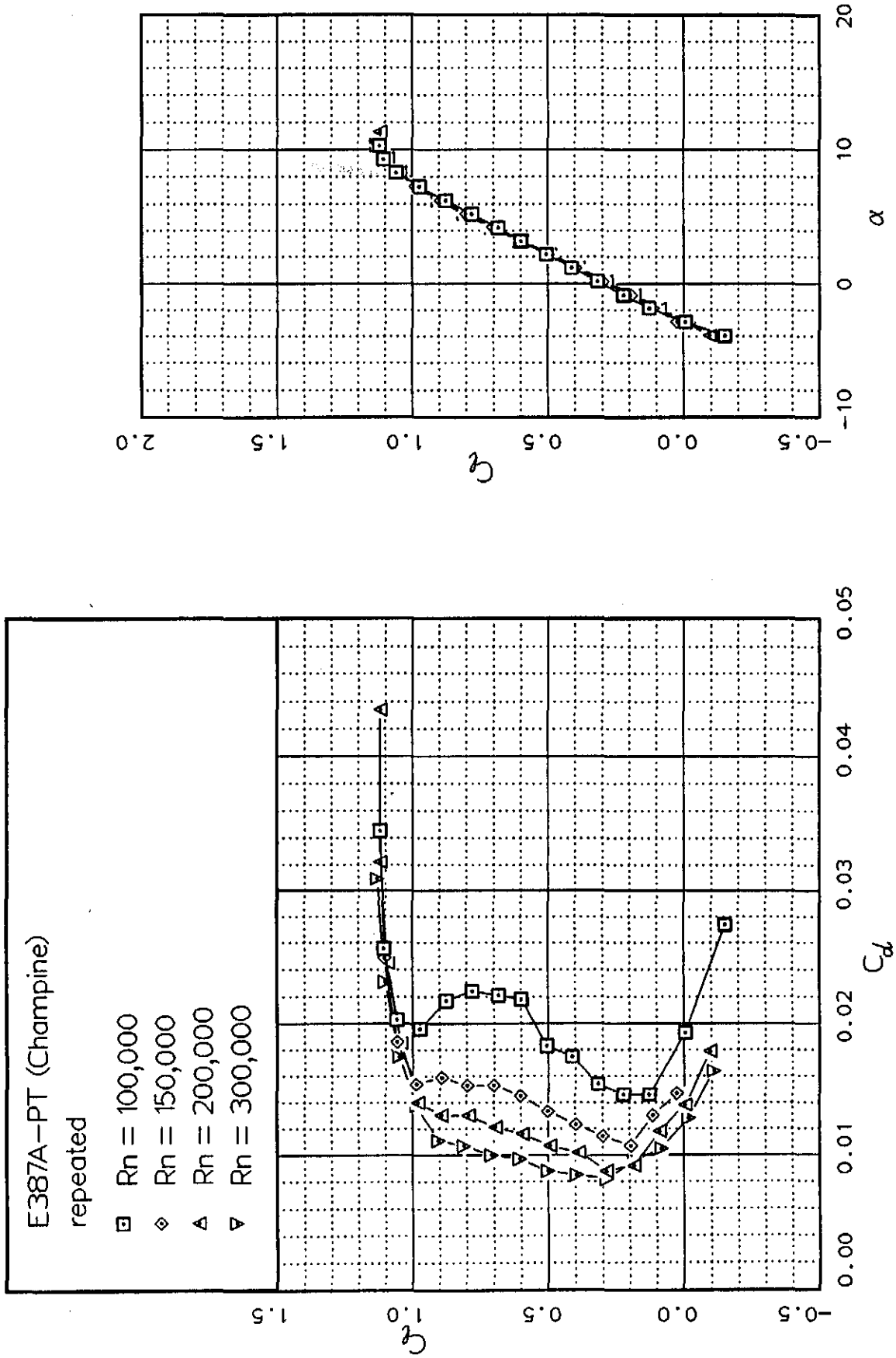
E387A–PT (Champine)
repeated
Rn = 100,000
Rn = 150,000
Rn = 200,000
Rn = 300,000
C_l
C_d
α
−0.5
0.0
0.5
1.0
1.5
2.0
0.00
0.01
0.02
0.03
0.04
0.05
−10
0
10
20

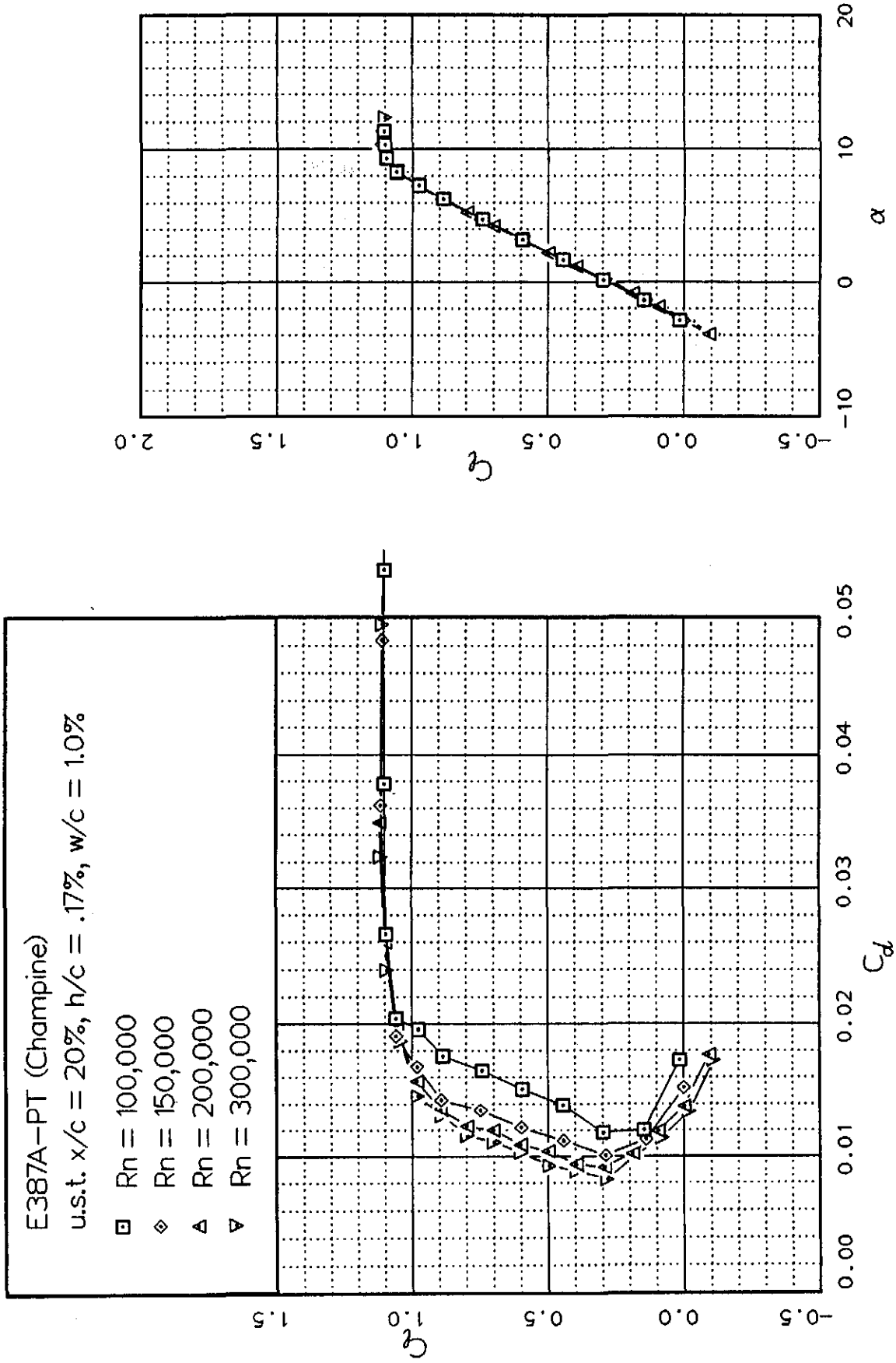
E387A–PT (Champine)
u.s.t. x/c = 20%, h/c = .17%, w/c = 1.0%
Rn = 100,000
Rn = 150,000
Rn = 200,000
Rn = 300,000
−0.5
0.0
0.5
1.0
1.5
2.0
cl
−10
0
10
20
α
0.00
0.01
0.02
0.03
0.04
0.05
cd

Fig. 12.34

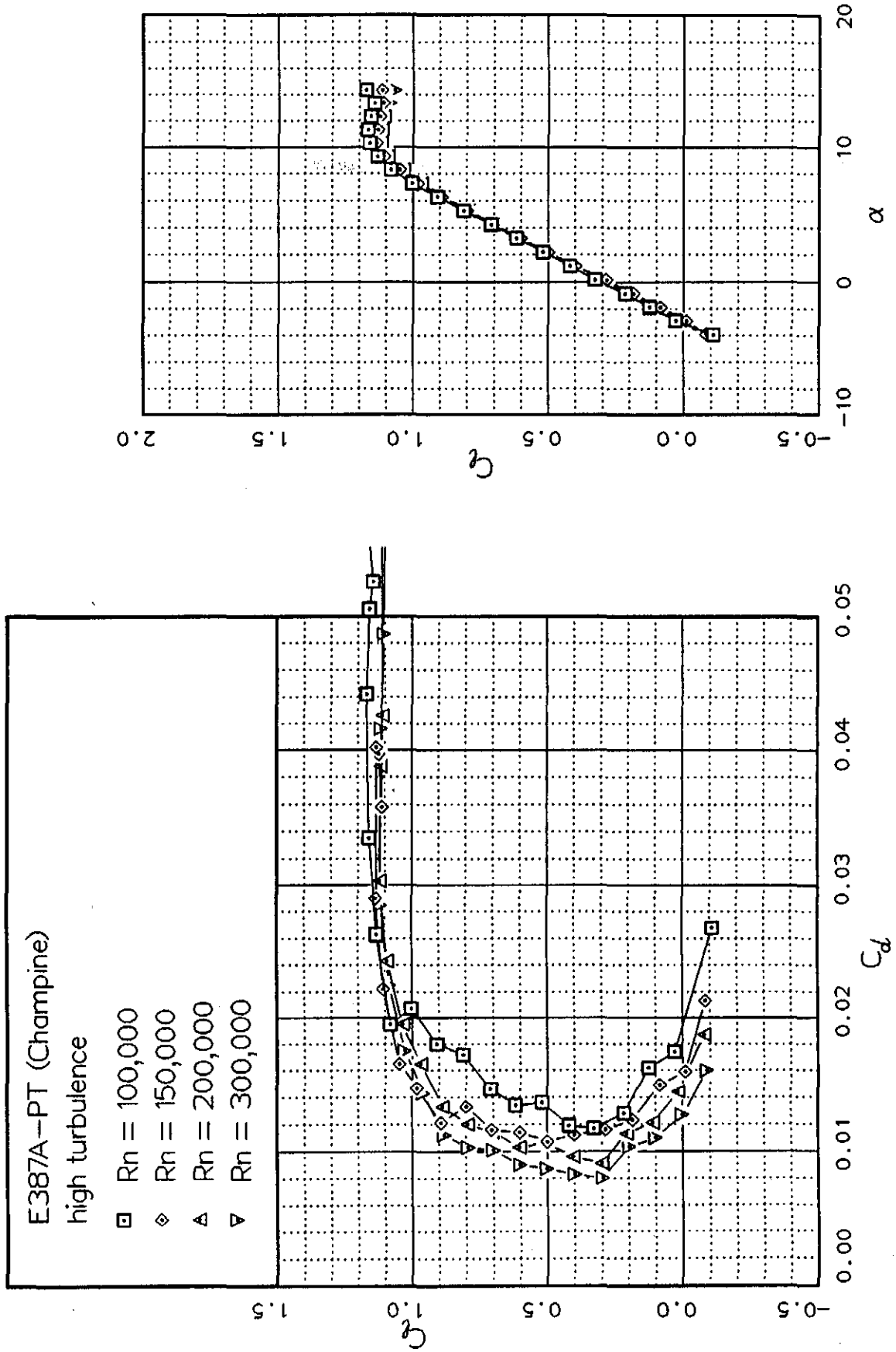
E387A–PT (Champine)
high turbulence
Rn = 100,000
Rn = 150,000
Rn = 200,000
Rn = 300,000
C_l
C_d
α

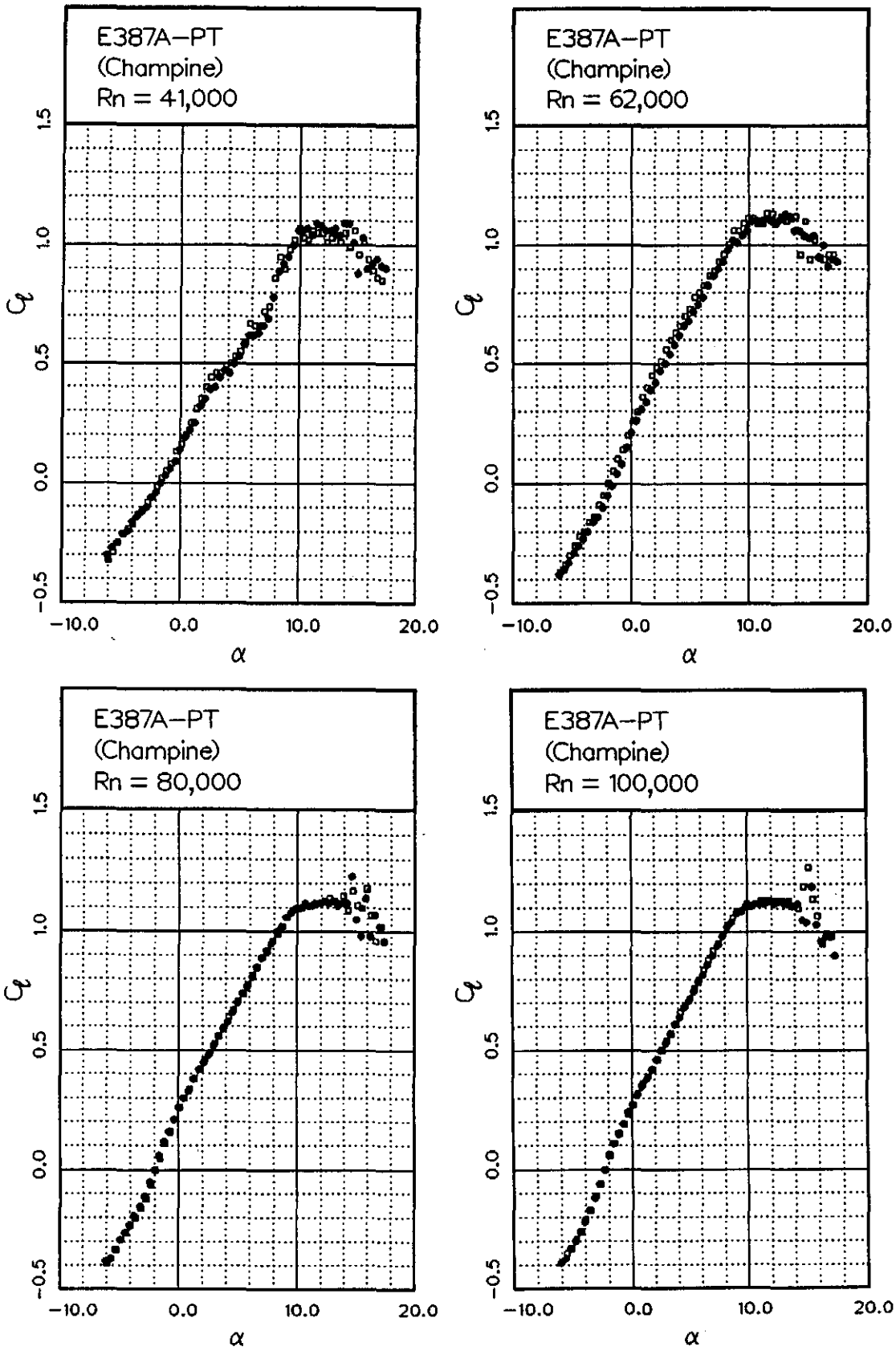
E387A–PT
(Champine)
Rn = 41,000
E387A–PT
(Champine)
Rn = 62,000
E387A–PT
(Champine)
Rn = 80,000
E387A–PT
(Champine)
Rn = 100,000
C_ℓ
α
1.5
1.0
0.5
0.0
−0.5
−10.0
0.0
10.0
20.0

Fig. 12.36

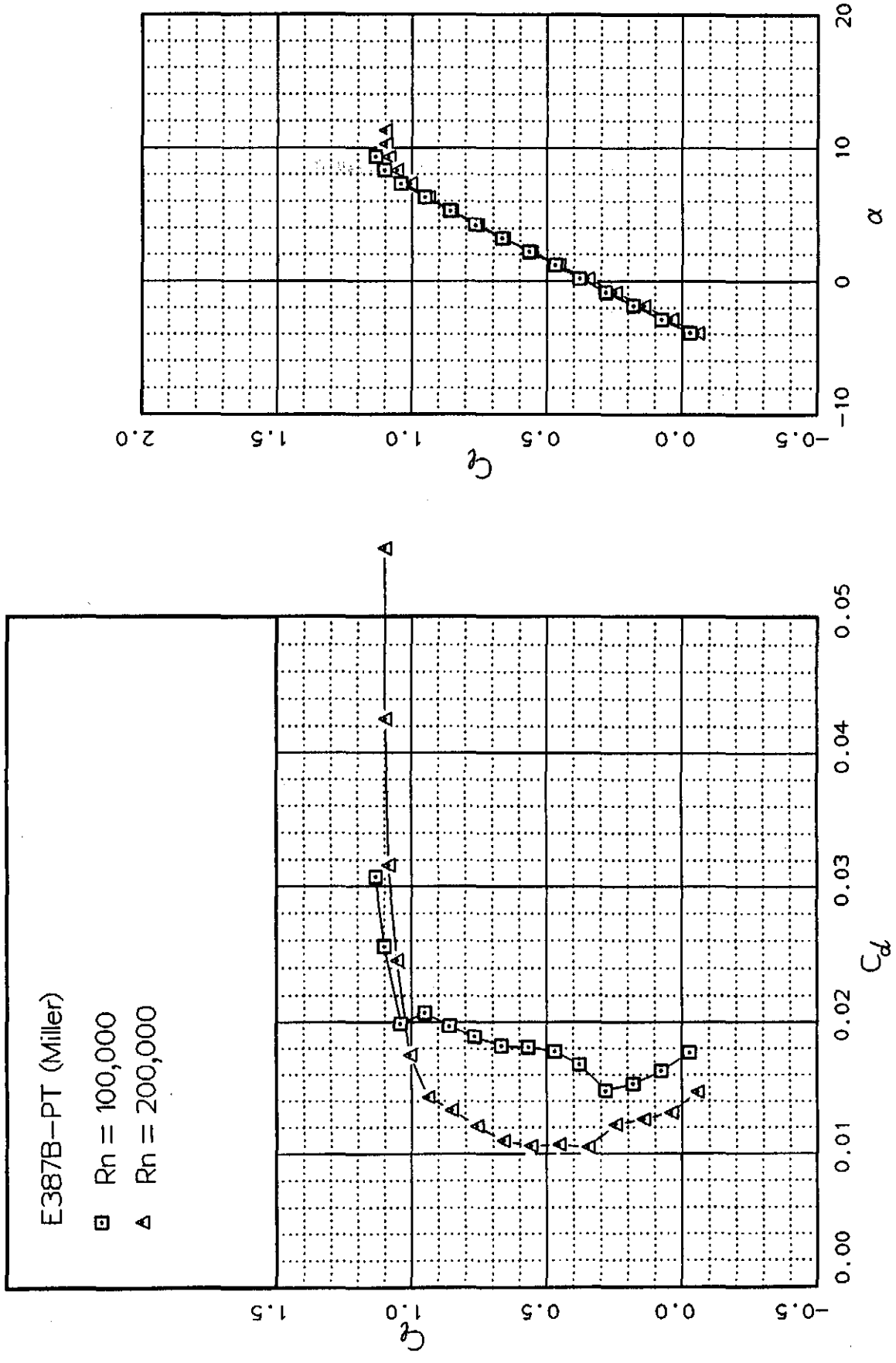
E387B-PT (Miller)
Rn = 100,000
Rn = 200,000
C_l
C_d
α
−0.5
0.0
0.5
1.0
1.5
2.0
−10
0
10
20
0.00
0.01
0.02
0.03
0.04
0.05

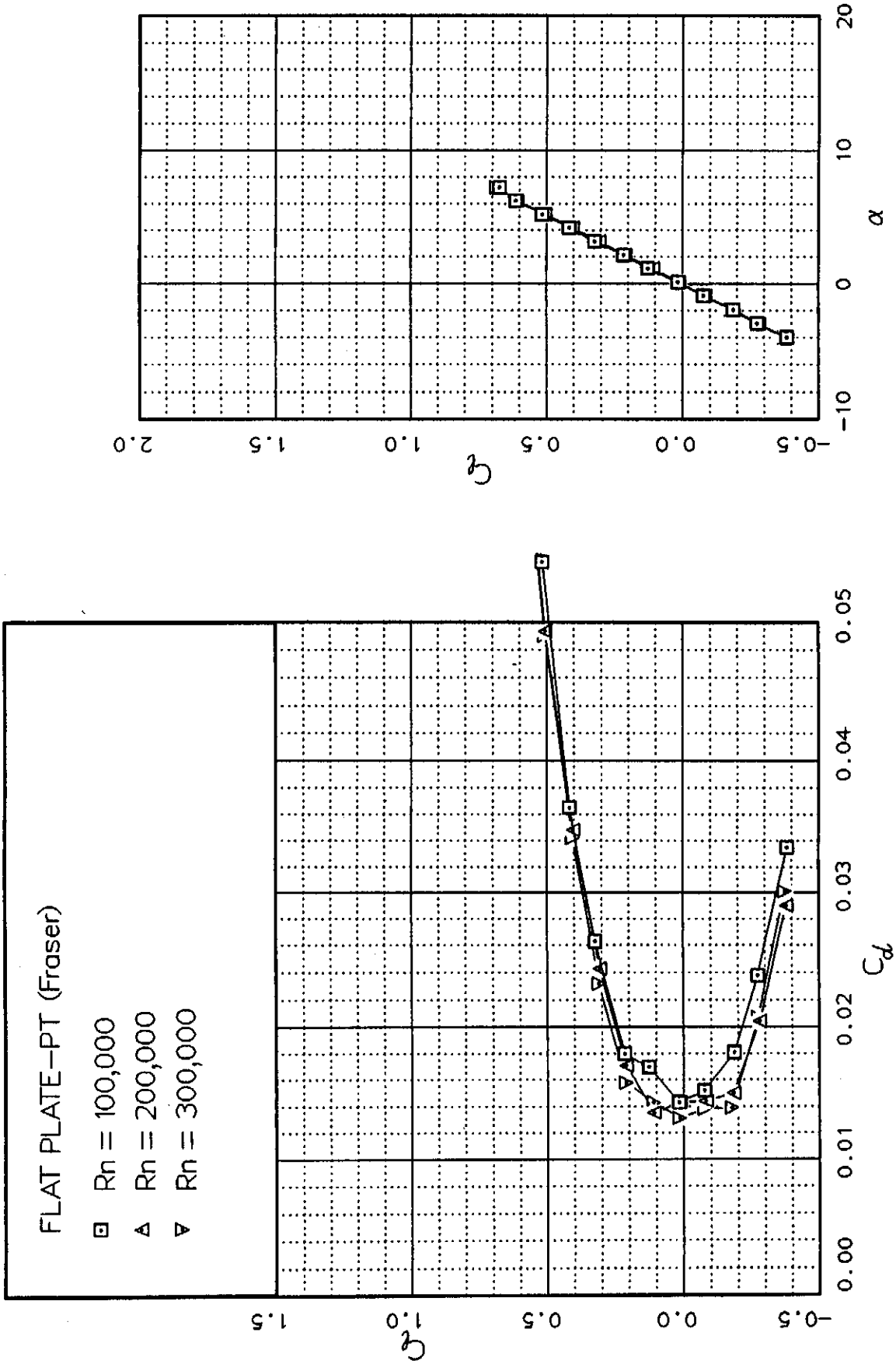
FLAT PLATE–PT (Fraser)
Rn = 100,000
Rn = 200,000
Rn = 300,000
C_l
C_d
α

Fig. 12.38

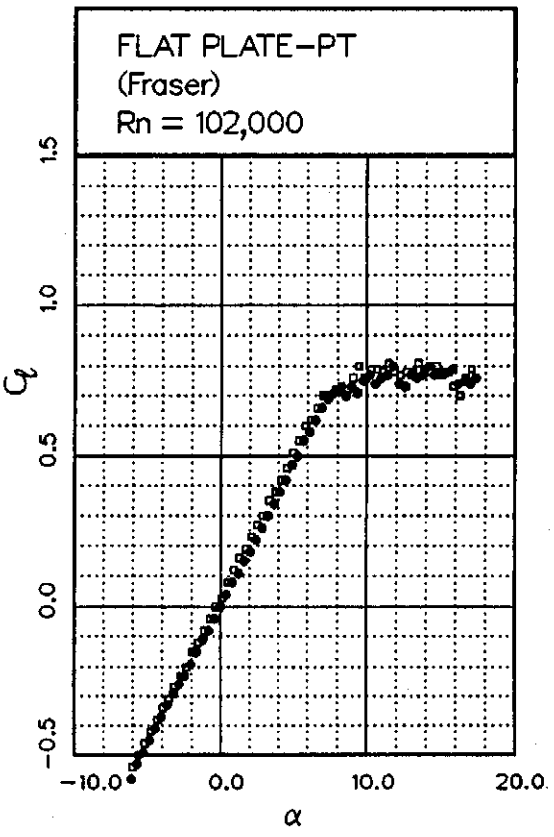

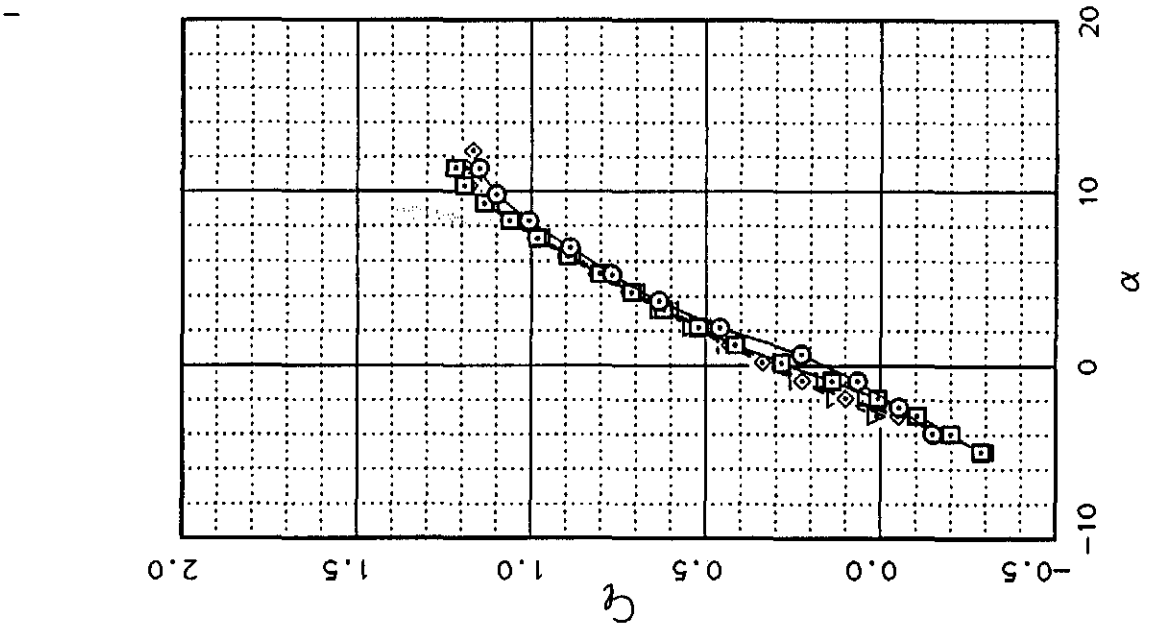
20
10
0
−10
α
−0.5
0.0
0.5
1.0
1.5
2.0
C_l

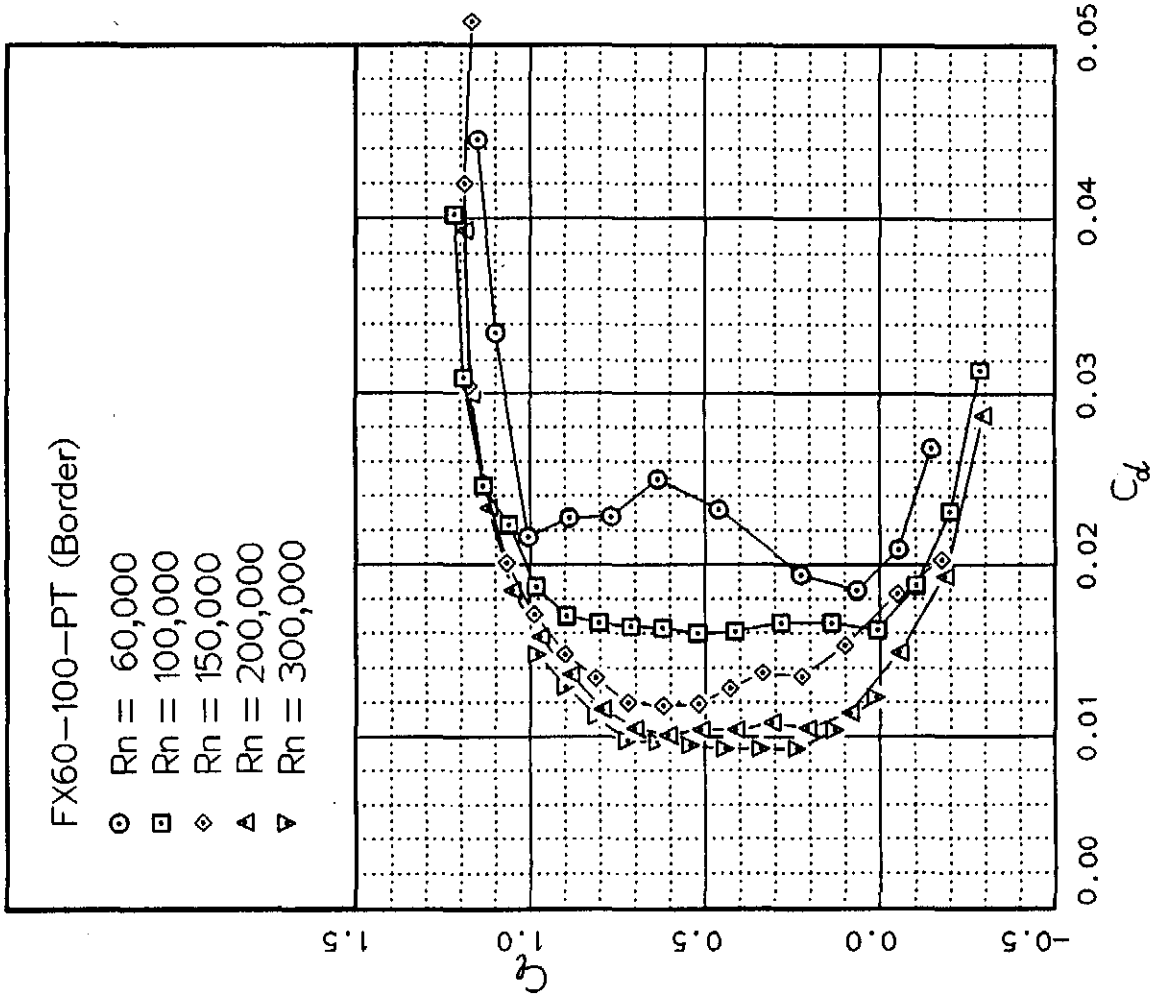
FX60−100−PT (Border)
Rn = 60,000
Rn = 100,000
Rn = 150,000
Rn = 200,000
Rn = 300,000
0.05
0.04
0.03
0.02
0.01
0.00
C_d
−0.5
0.0
0.5
1.0
1.5
C_l

Fig. 12.40

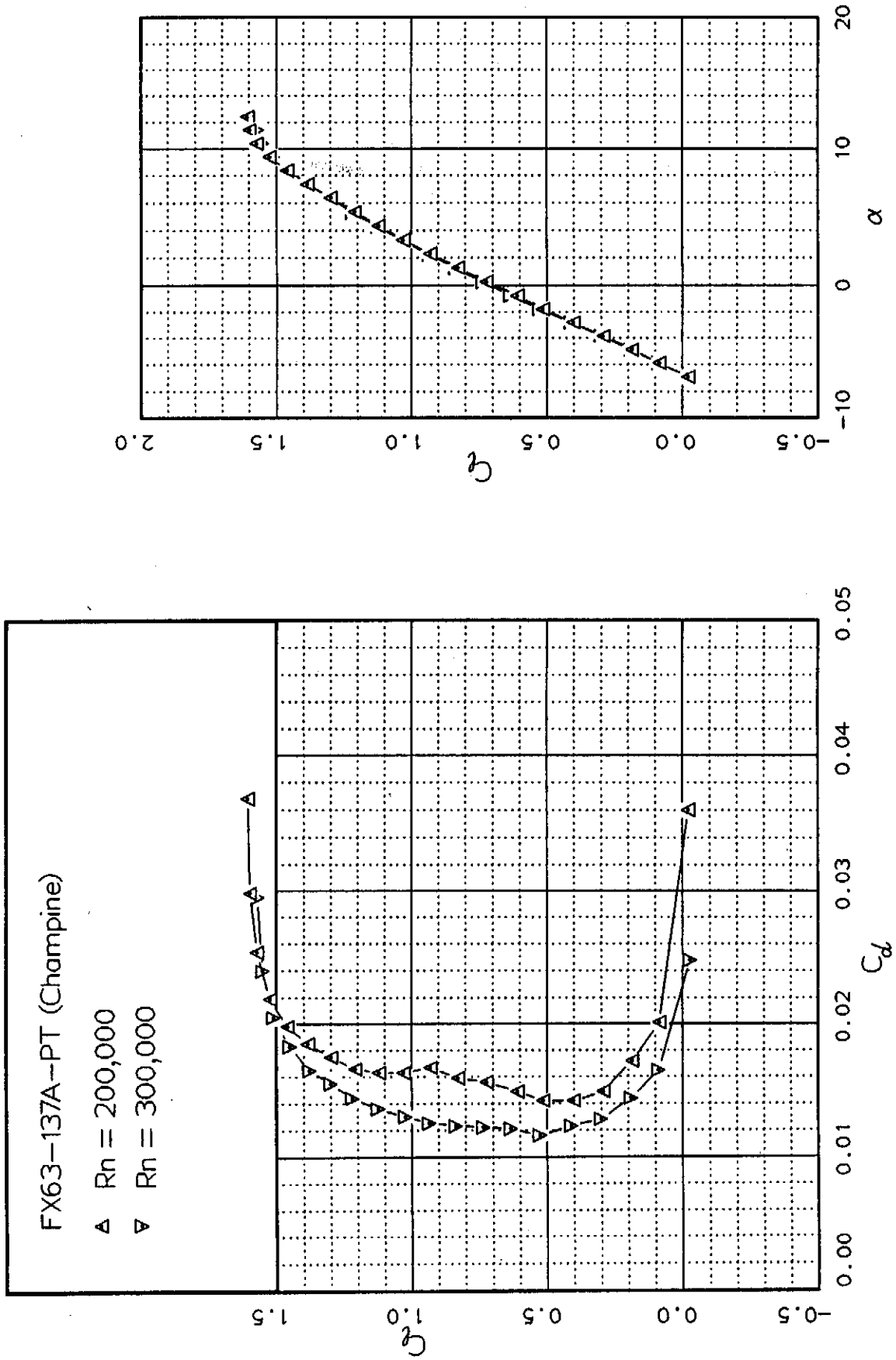
FX63–137A–PT (Champine)
Rn = 200,000
Rn = 300,000
−0.5
0.0
0.5
1.0
1.5
2.0
c_l
−10
0
10
20
α
0.00
0.01
0.02
0.03
0.04
0.05
c_d

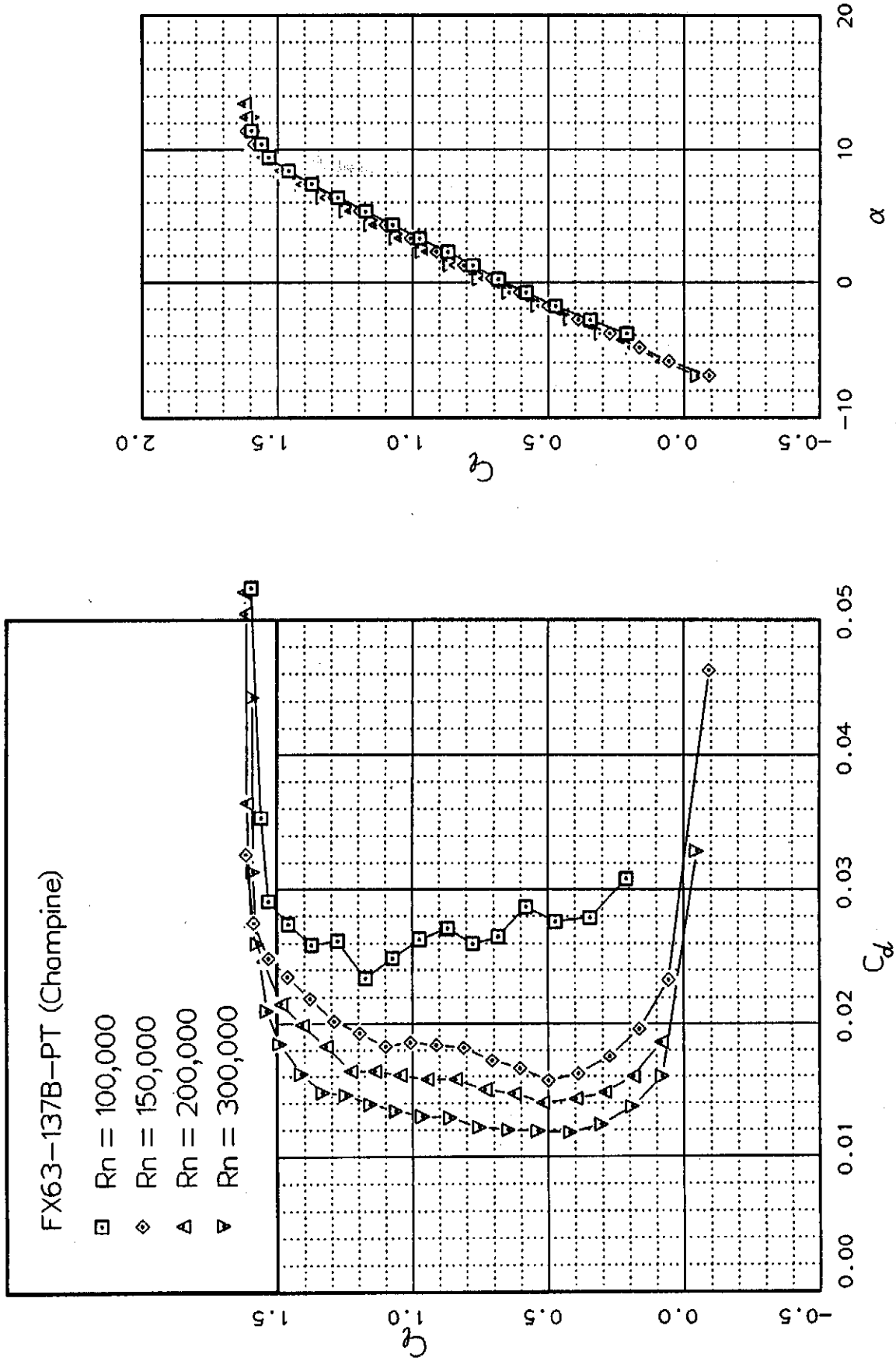
FX63-137B-PT (Champine)
Rn = 100,000
Rn = 150,000
Rn = 200,000
Rn = 300,000
α
C_d
C_l
20
10
0
−10
0.05
0.04
0.03
0.02
0.01
0.00
−0.5
0.0
0.5
1.0
1.5
2.0

Fig. 12.42

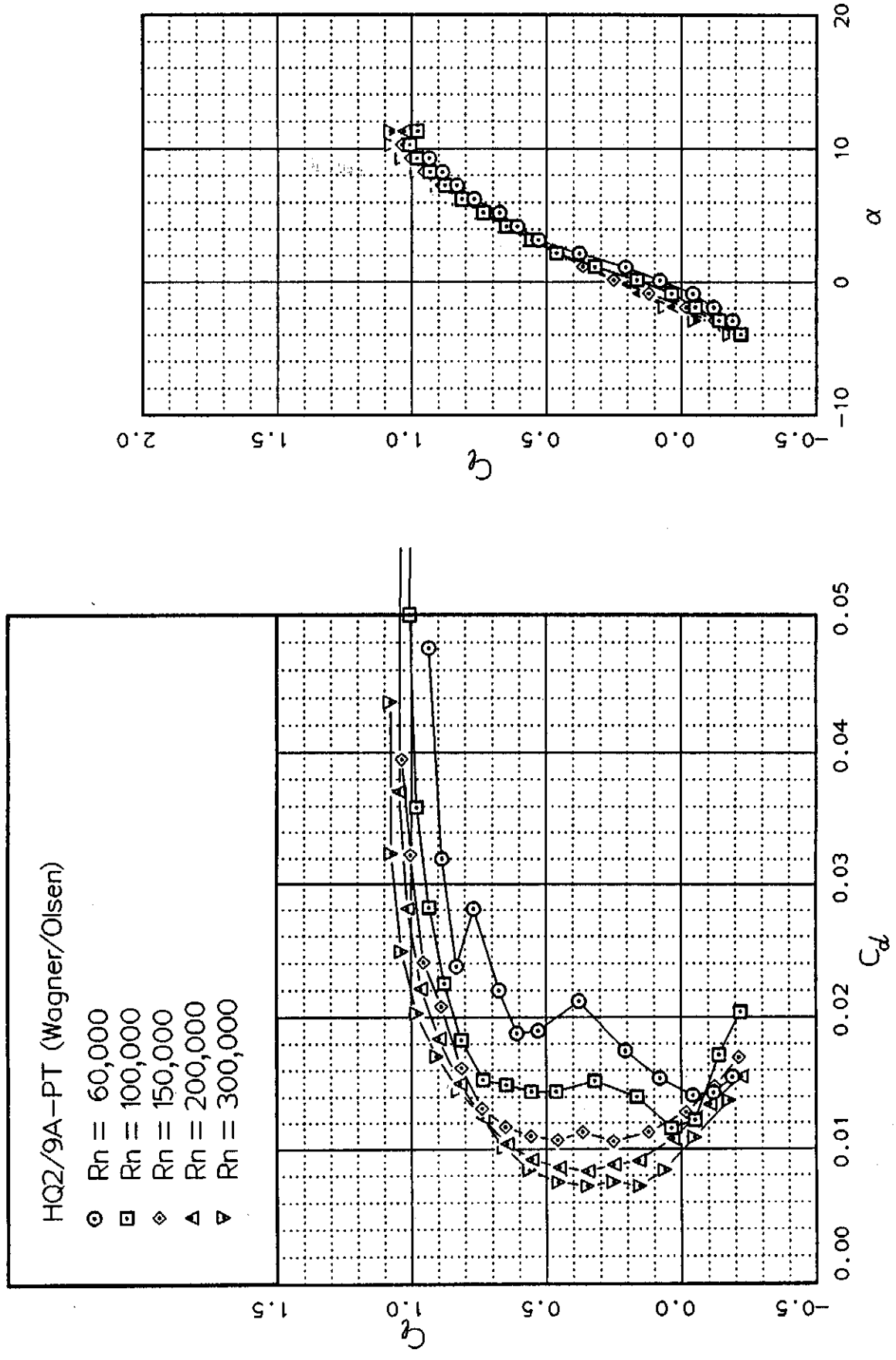
HQ2/9A–PT (Wagner/Olsen)
Rn = 60,000
Rn = 100,000
Rn = 150,000
Rn = 200,000
Rn = 300,000
c_l
α
c_d

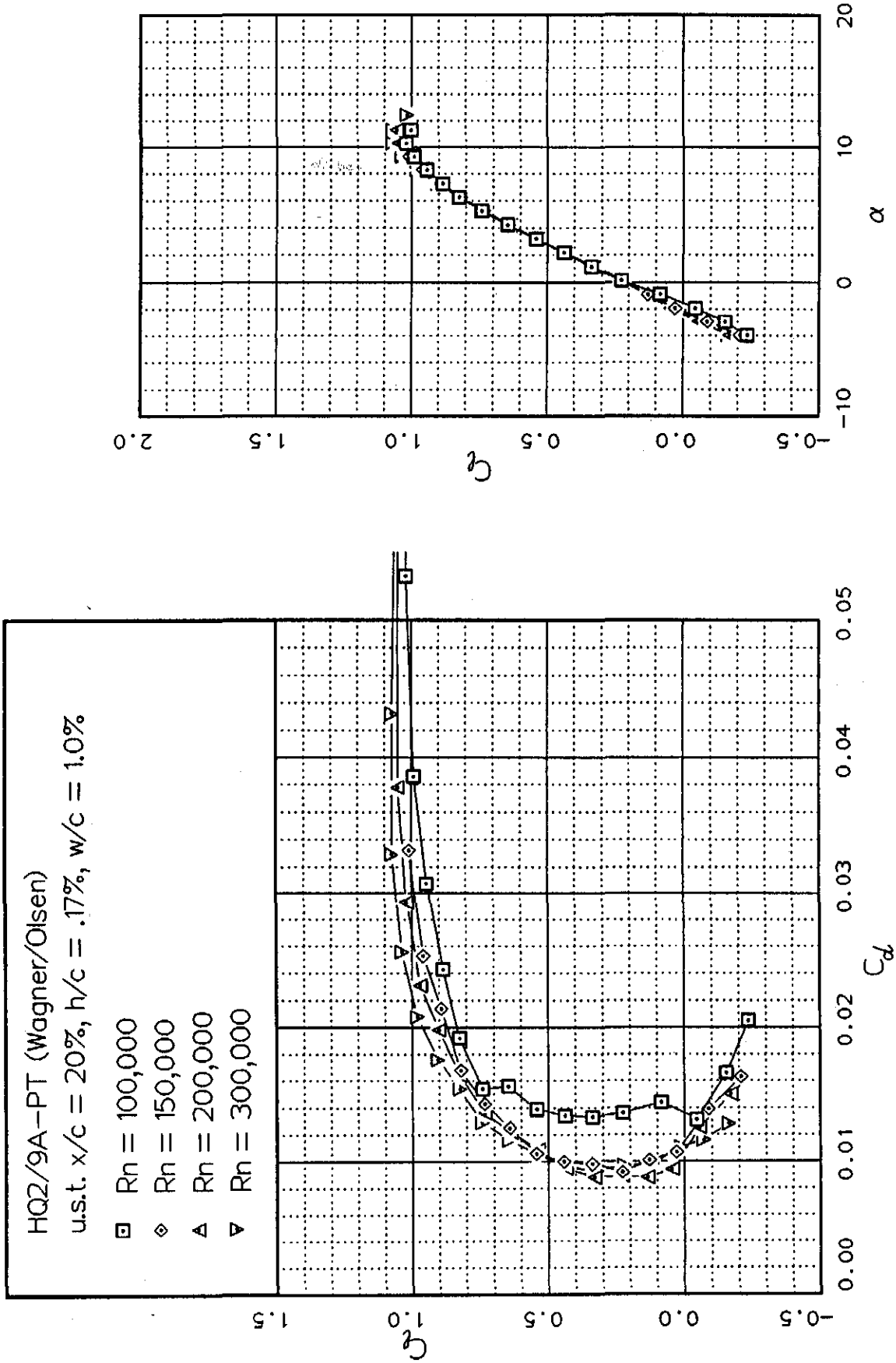
HQ2/9A–PT (Wagner/Olsen)
u.s.t. x/c = 20%, h/c = .17%, w/c = 1.0%
Rn = 100,000
Rn = 150,000
Rn = 200,000
Rn = 300,000
−0.5
0.0
0.5
1.0
1.5
2.0
c_l
−10
0
10
20
α
0.00
0.01
0.02
0.03
0.04
0.05
c_d

Fig. 12.44

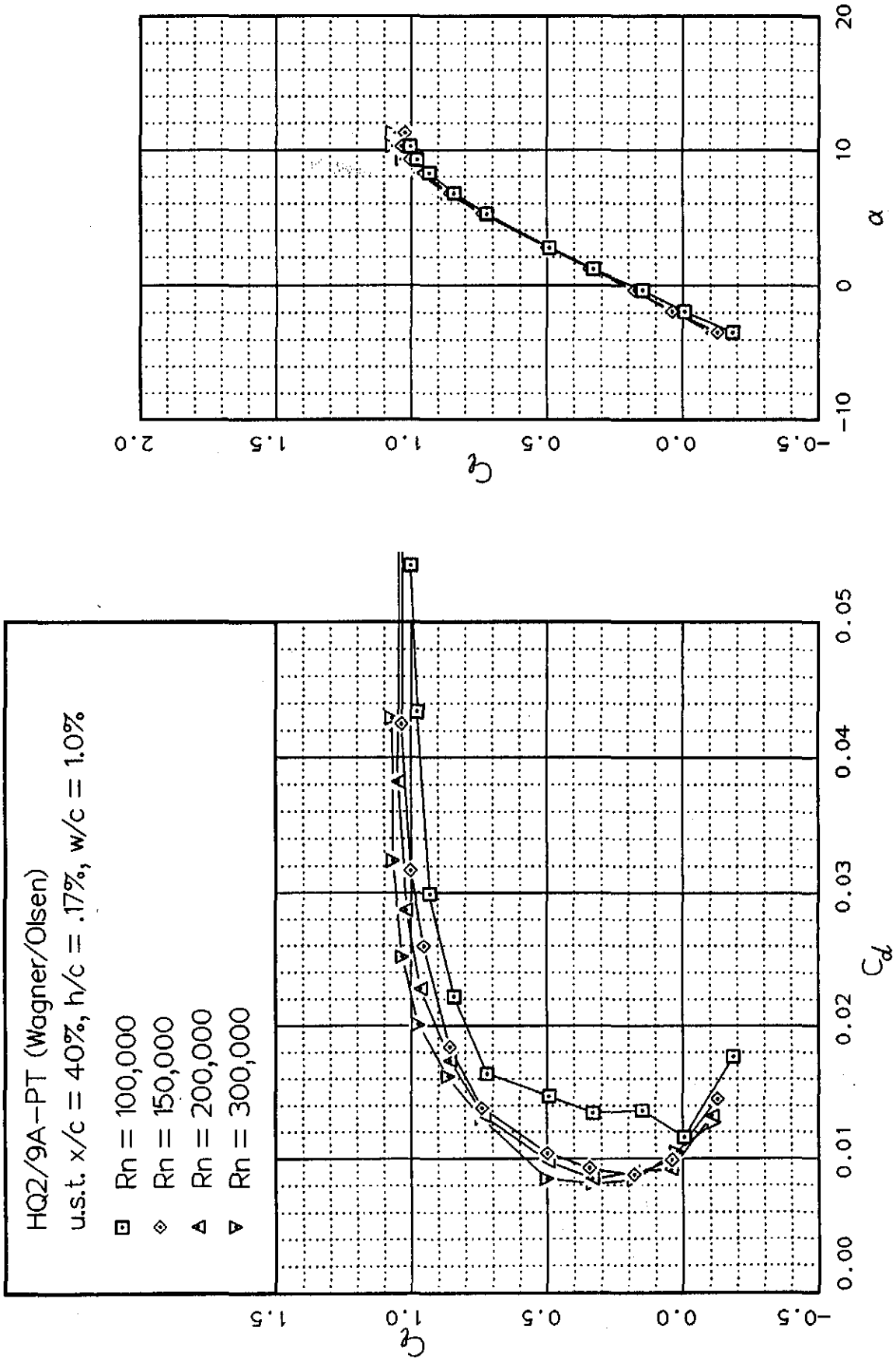
HQ2/9A-PT (Wagner/Olsen)
u.s.t. x/c = 40%, h/c = .17%, w/c = 1.0%
Rn = 100,000
Rn = 150,000
Rn = 200,000
Rn = 300,000
-0.5
0.0
0.5
1.0
1.5
2.0
c_l
20
10
0
-10
α
0.00
0.01
0.02
0.03
0.04
0.05
c_d

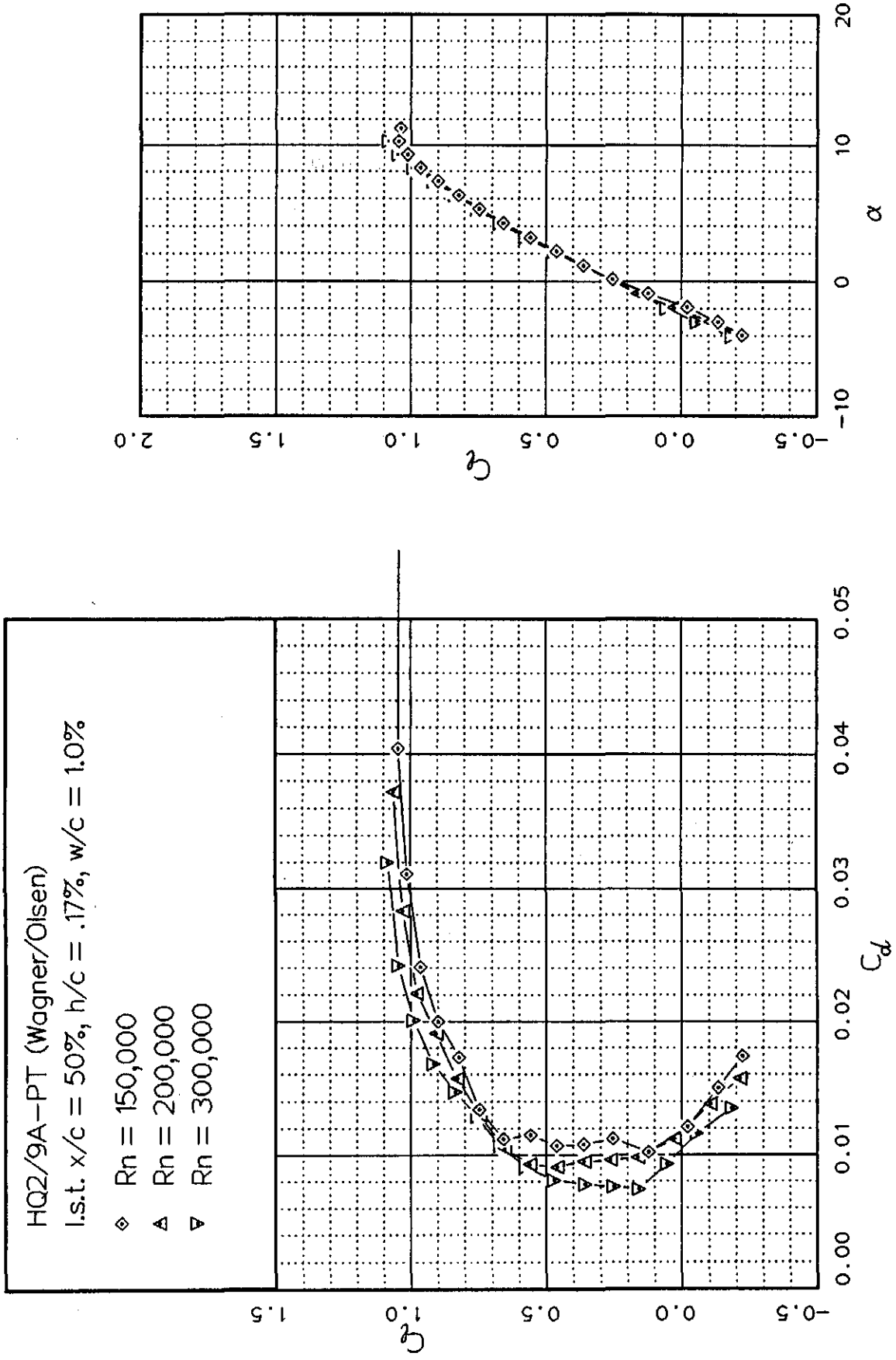
HQ2/9A–PT (Wagner/Olsen)
l.s.t. x/c = 50%, h/c = .17%, w/c = 1.0%
◇ Rn = 150,000
△ Rn = 200,000
▷ Rn = 300,000
−0.5
0.0
0.5
1.0
1.5
2.0
cl
−10
0
10
20
α
0.00
0.01
0.02
0.03
0.04
0.05
cd

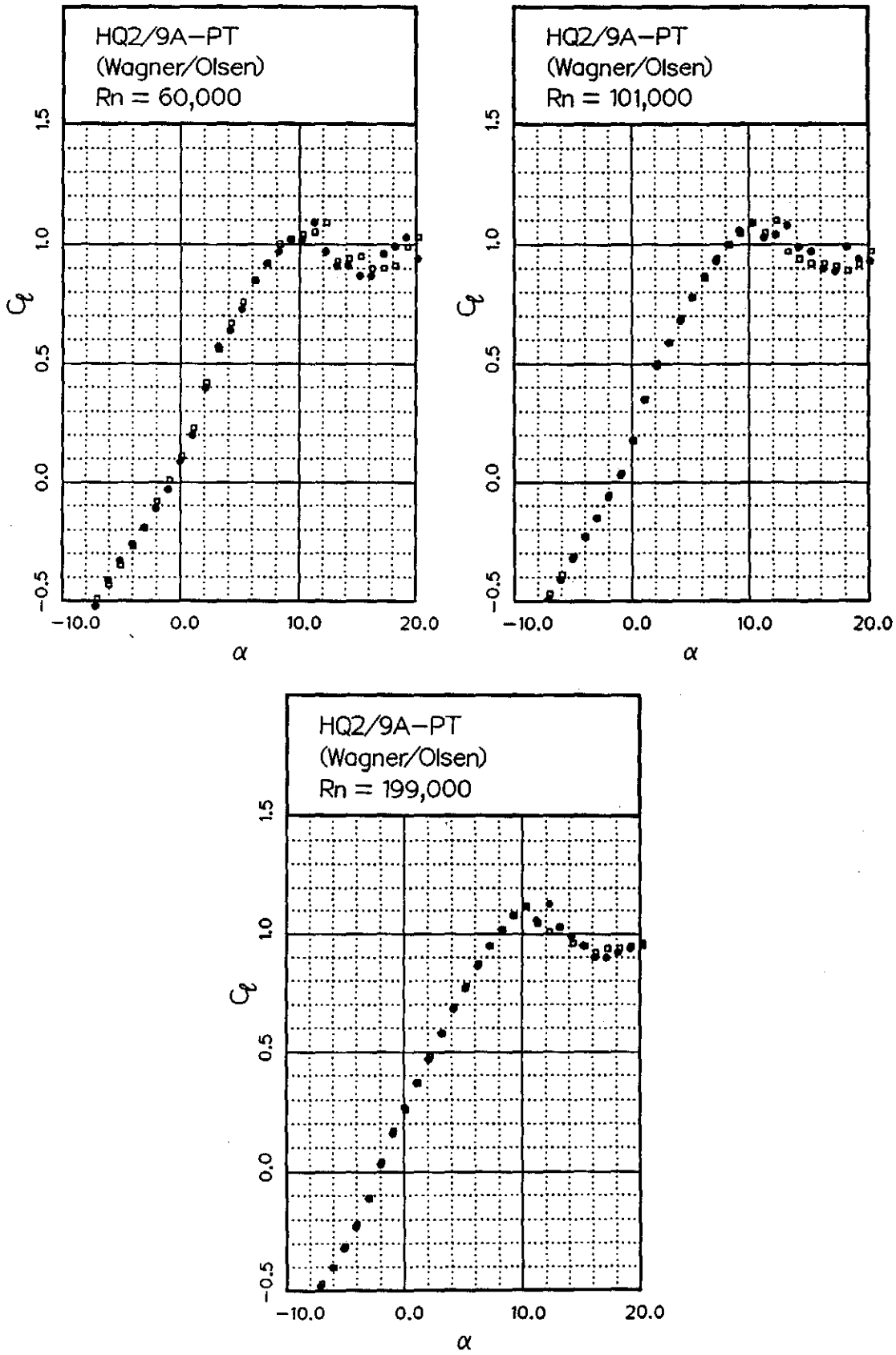
HQ2/9A–PT
(Wagner/Olsen)
Rn = 60,000
HQ2/9A–PT
(Wagner/Olsen)
Rn = 101,000
HQ2/9A–PT
(Wagner/Olsen)
Rn = 199,000
C_ℓ
α
1.5
1.0
0.5
0.0
−0.5
−10.0
0.0
10.0
20.0

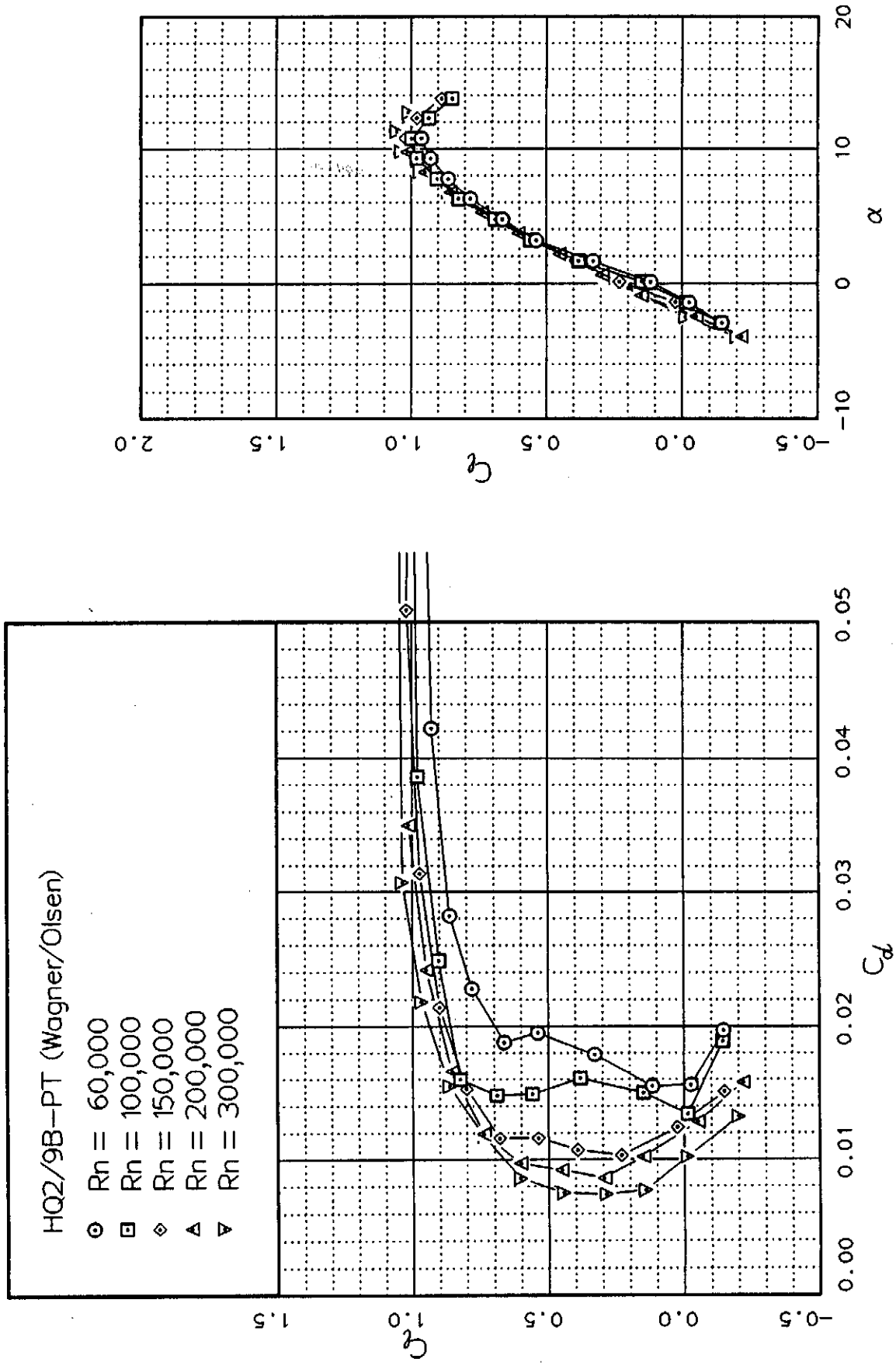
HQ2/9B–PT (Wagner/Olsen)
Rn = 60,000
Rn = 100,000
Rn = 150,000
Rn = 200,000
Rn = 300,000
−0.5
0.0
0.5
1.0
1.5
2.0
Cl
−10
0
10
20
α
0.00
0.01
0.02
0.03
0.04
0.05
Cd

Fig. 12.48

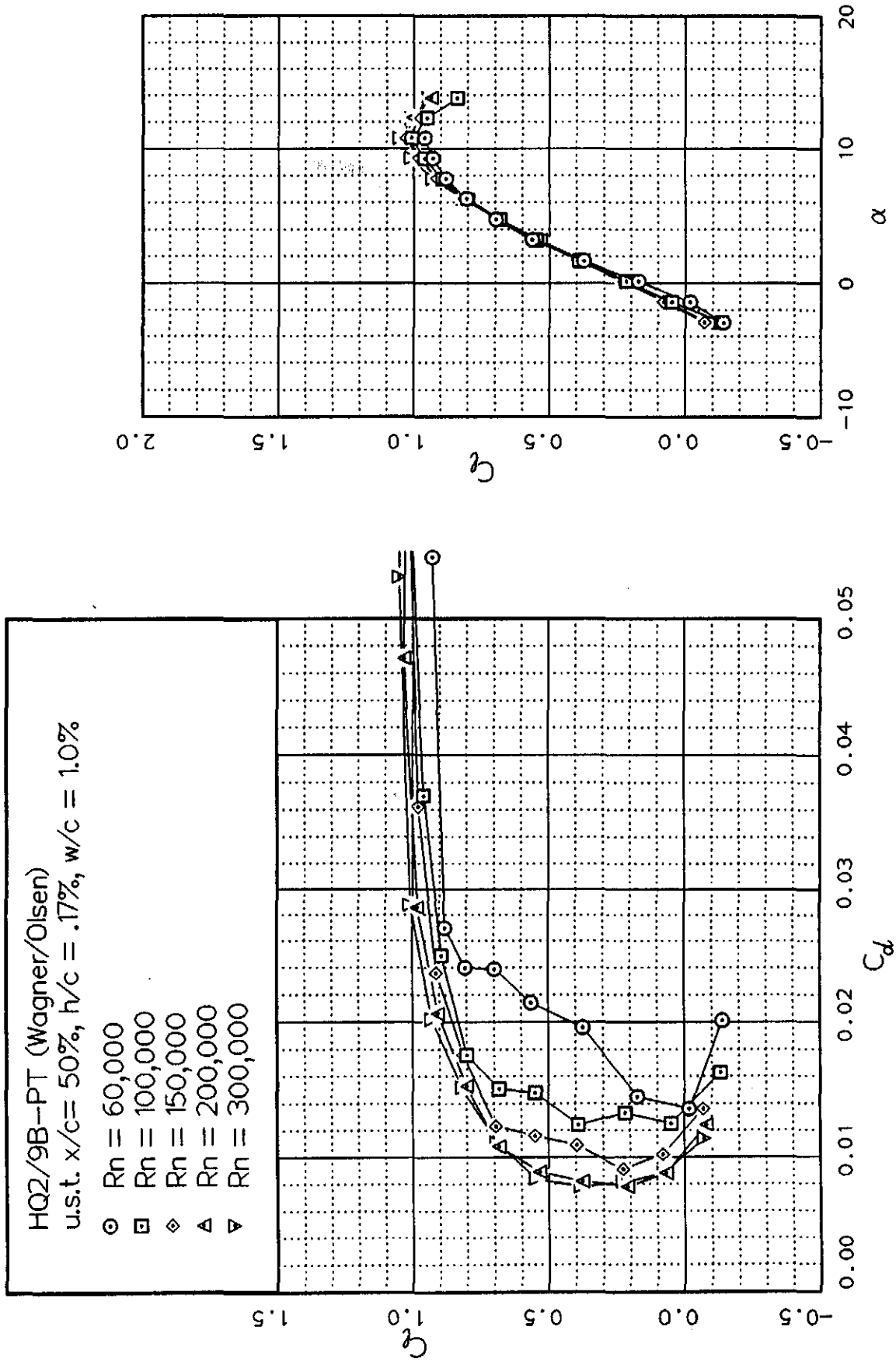
HQ2/9B–PT (Wagner/Olsen)
u.s.t. x/c= 50%, h/c = .17%, w/c = 1.0%
Rn = 60,000
Rn = 100,000
Rn = 150,000
Rn = 200,000
Rn = 300,000
−0.5
0.0
0.5
1.0
1.5
2.0
c_l
−10
0
10
20
α
0.00
0.01
0.02
0.03
0.04
0.05
c_d

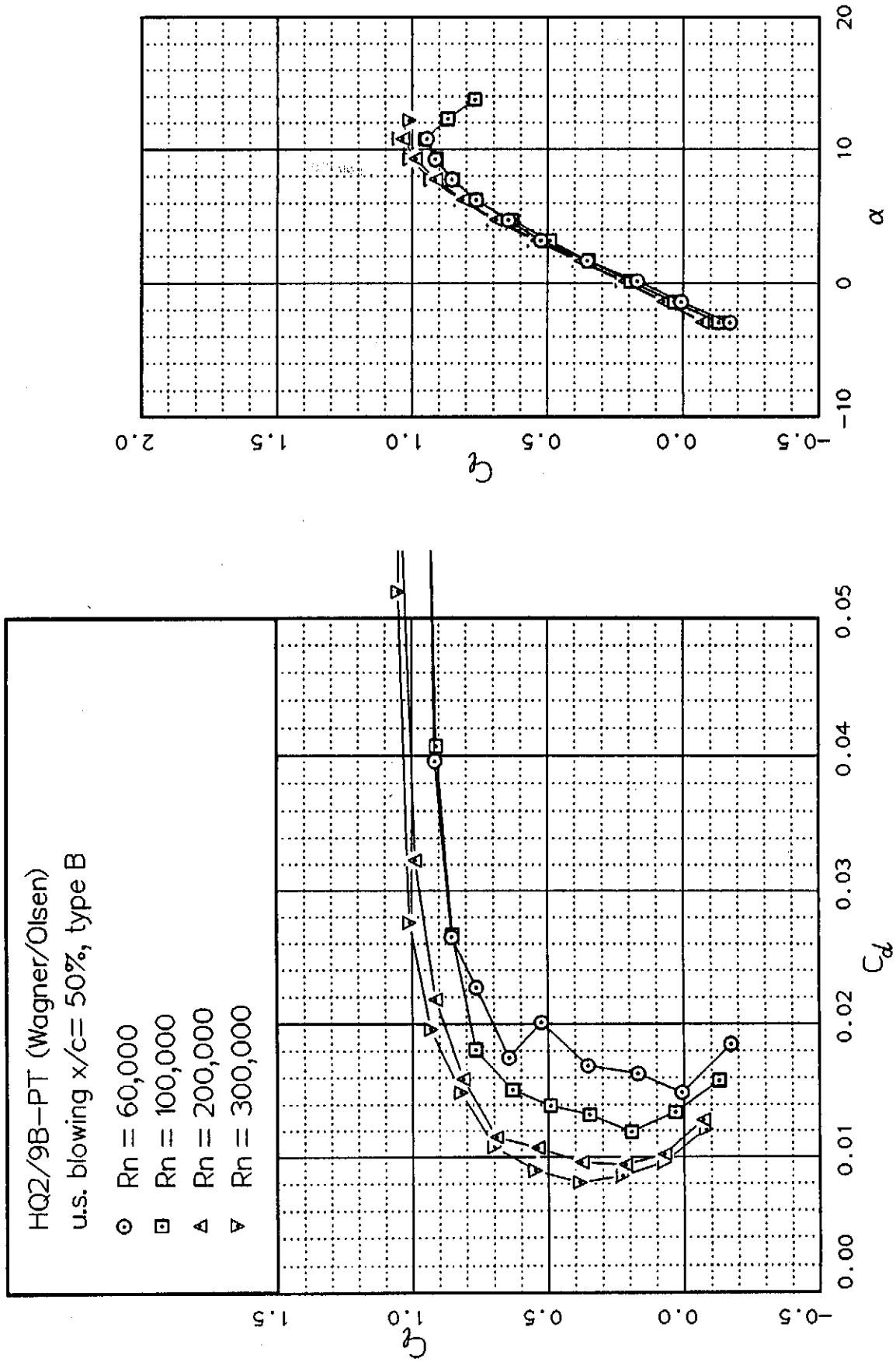
HQ2/9B–PT (Wagner/Olsen)
u.s. blowing x/c= 50%, type B
Rn = 60,000
Rn = 100,000
Rn = 200,000
Rn = 300,000
C_l
C_d
α

Fig. 12.50

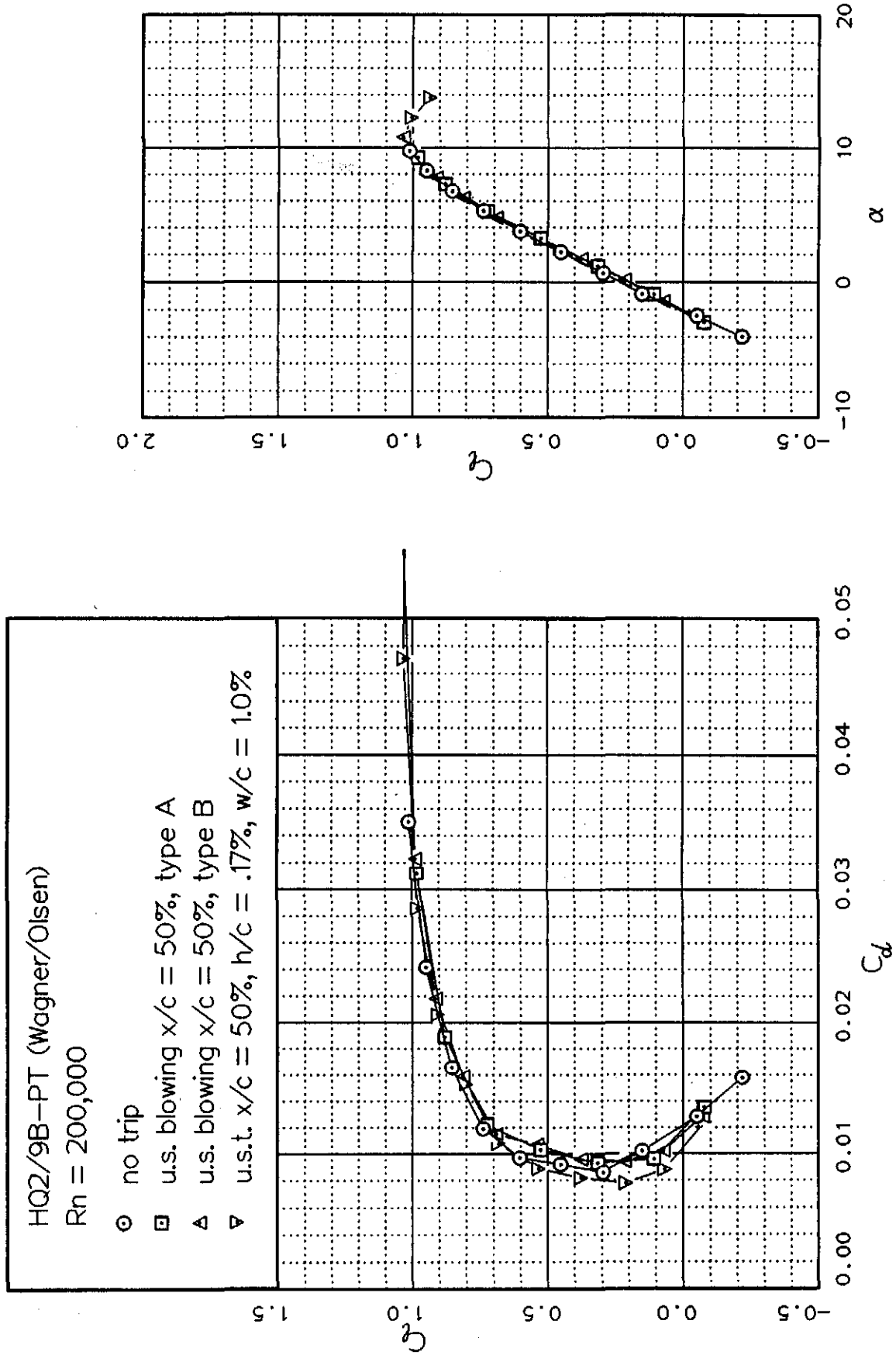
HQ2/9B–PT (Wagner/Olsen)
Rn = 200,000
no trip
u.s. blowing x/c = 50%, type A
u.s. blowing x/c = 50%, type B
u.s.t. x/c = 50%, h/c = .17%, w/c = 1.0%
c_l
c_d
α

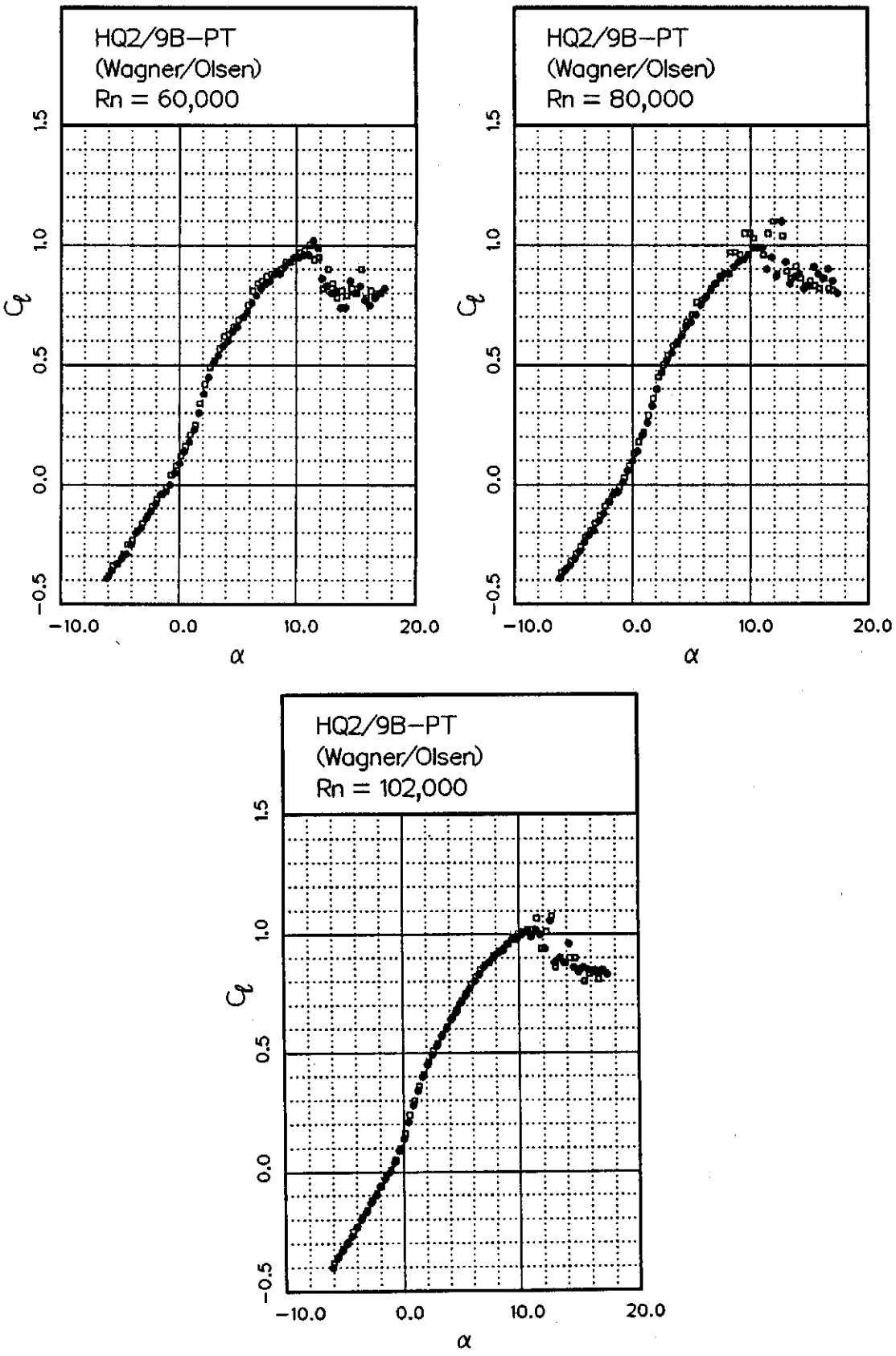
HQ2/9B–PT
(Wagner/Olsen)
Rn = 60,000
HQ2/9B–PT
(Wagner/Olsen)
Rn = 80,000
HQ2/9B–PT
(Wagner/Olsen)
Rn = 102,000
C_ℓ
α
1.5
1.0
0.5
0.0
−0.5
−10.0
0.0
10.0
20.0

Fig. 12.52

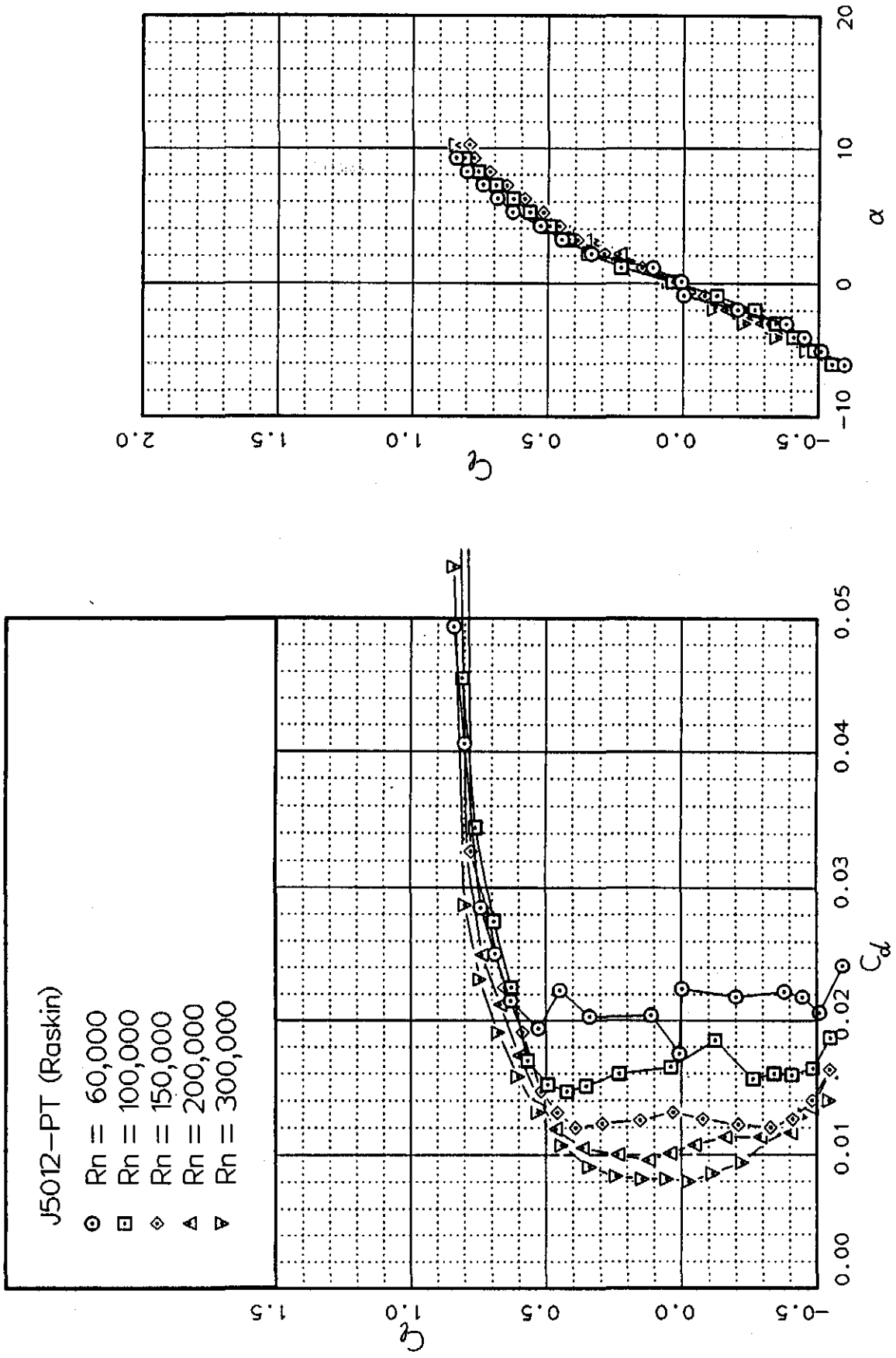
20
10
0
−10
α
−0.5
0.0
0.5
1.0
1.5
2.0
cl
0.05
0.04
0.03
0.02
0.01
0.00
cd
J5012−PT (Raskin)
Rn = 60,000
Rn = 100,000
Rn = 150,000
Rn = 200,000
Rn = 300,000

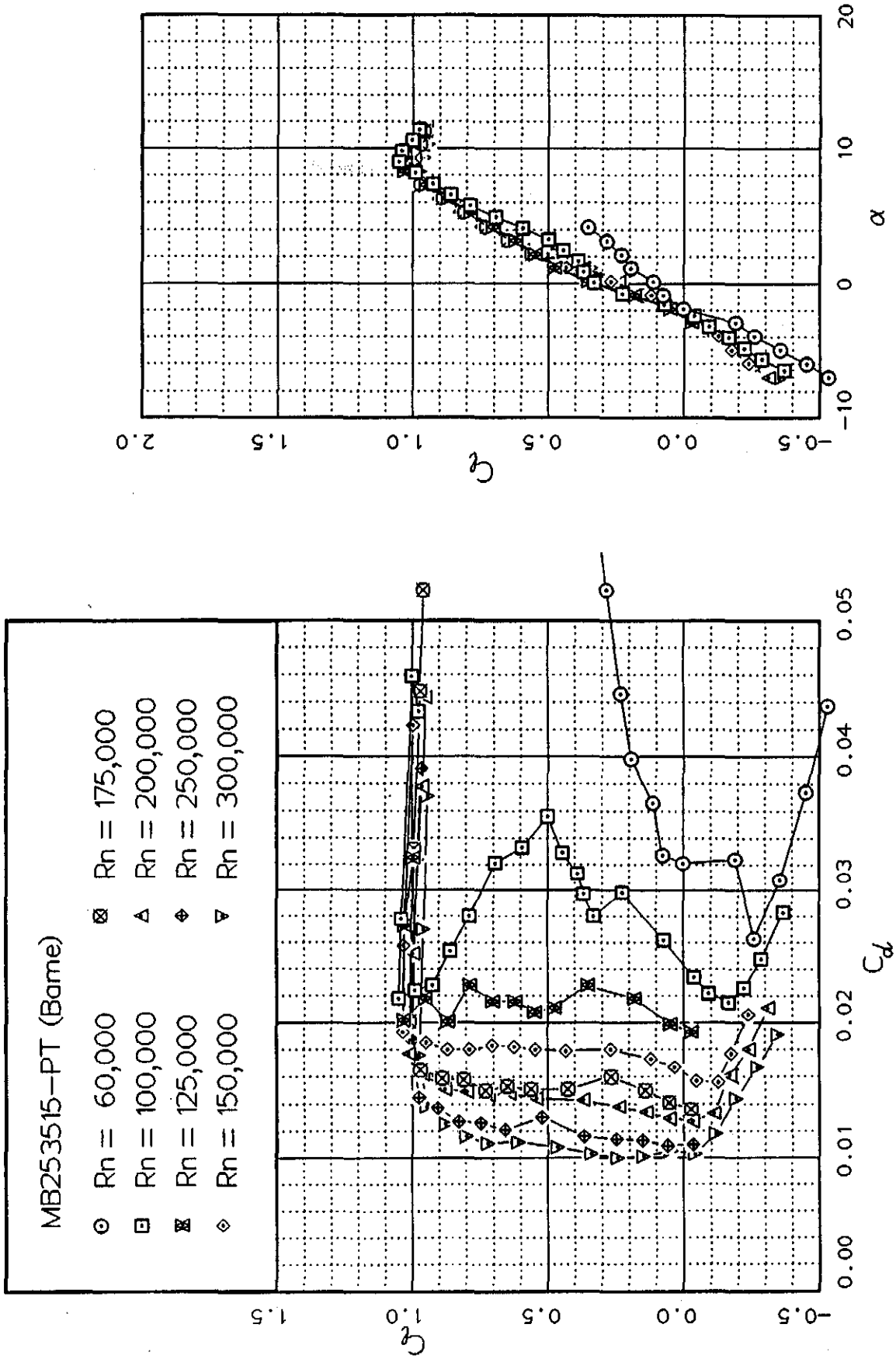
MB25 3515–PT (Bare)
Rn = 60,000
Rn = 100,000
Rn = 125,000
Rn = 150,000
Rn = 175,000
Rn = 200,000
Rn = 250,000
Rn = 300,000
C_l
α

Fig. 12.54

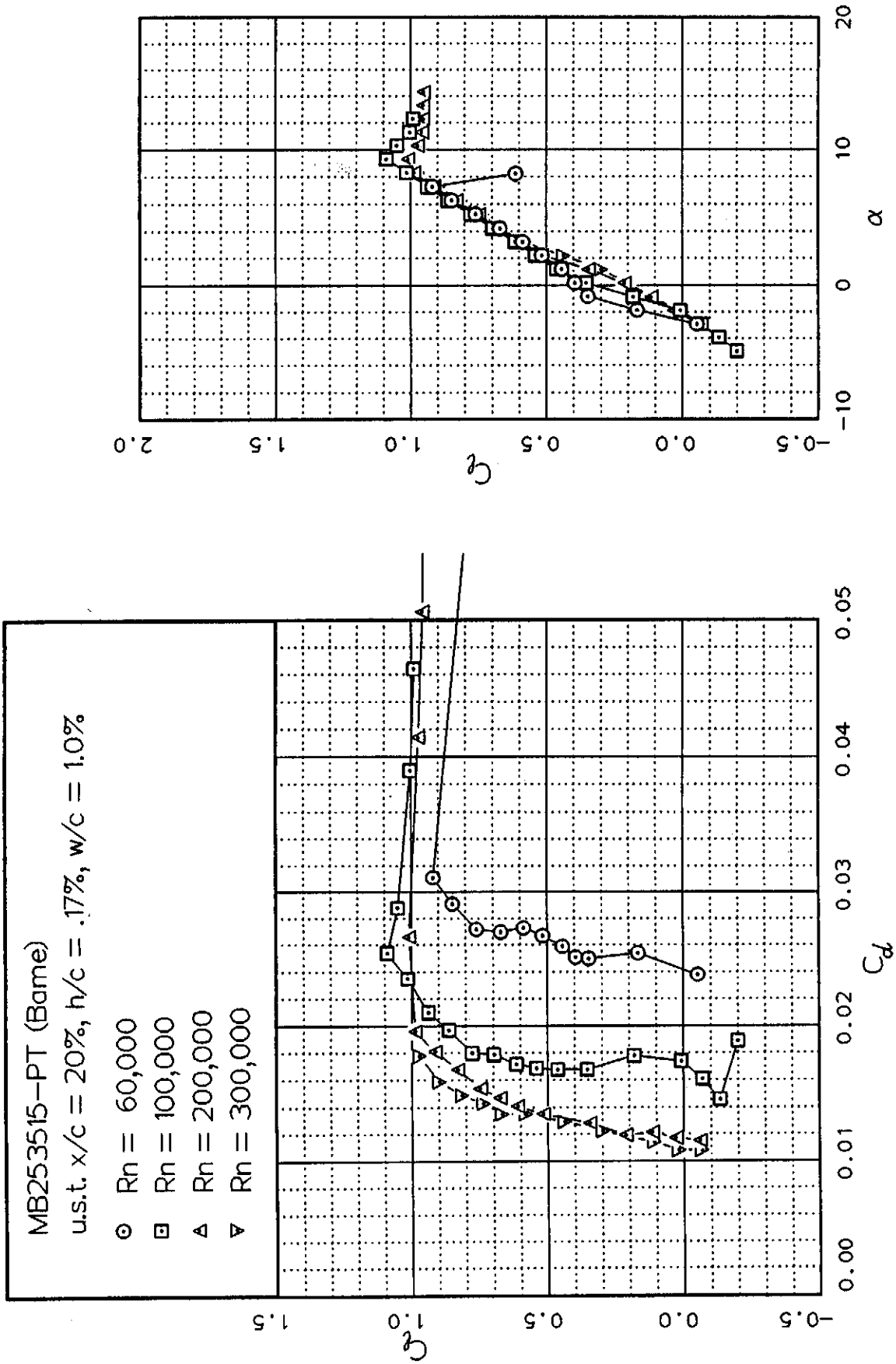
MB253515-PT (Bame)
u.s.t. x/c = 20%, h/c = .17%, w/c = 1.0%
Rn = 60,000
Rn = 100,000
Rn = 200,000
Rn = 300,000
α
C_l
C_d

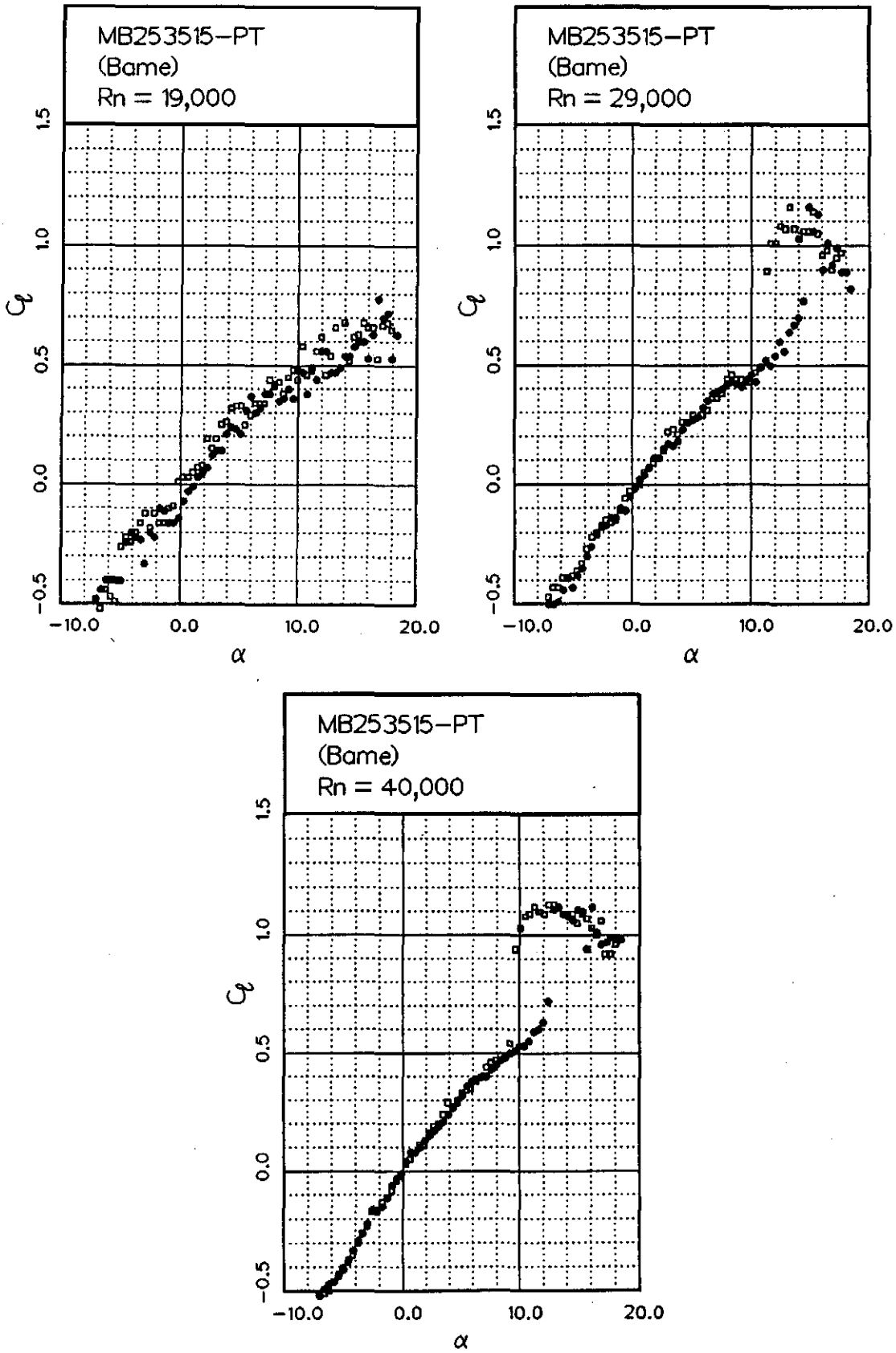
MB253515–PT
(Bame)
Rn = 19,000
MB253515–PT
(Bame)
Rn = 29,000
MB253515–PT
(Bame)
Rn = 40,000
C_ℓ
α
1.5
1.0
0.5
0.0
−0.5
−10.0
0.0
10.0
20.0

Fig. 12.55 continued

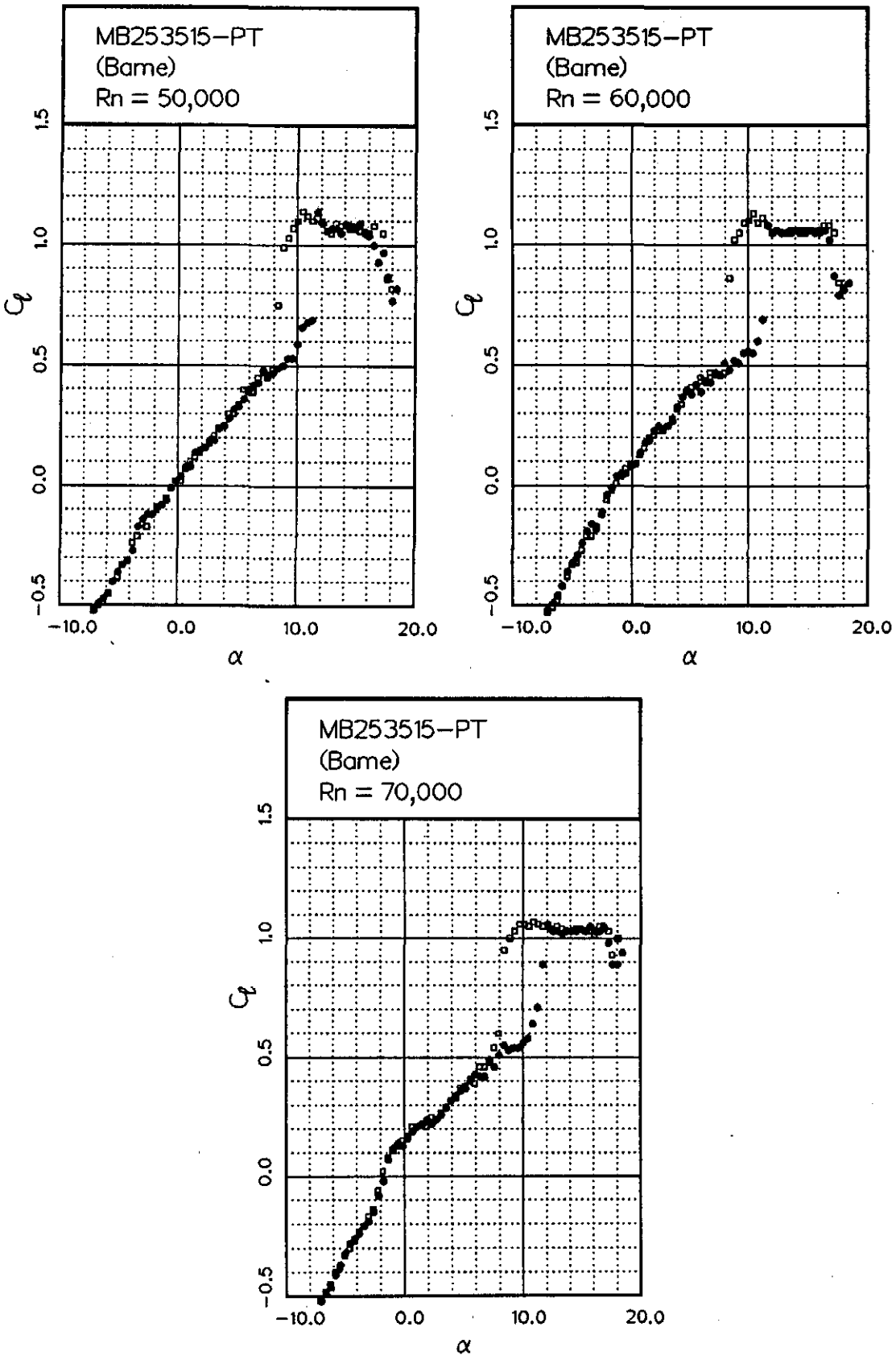

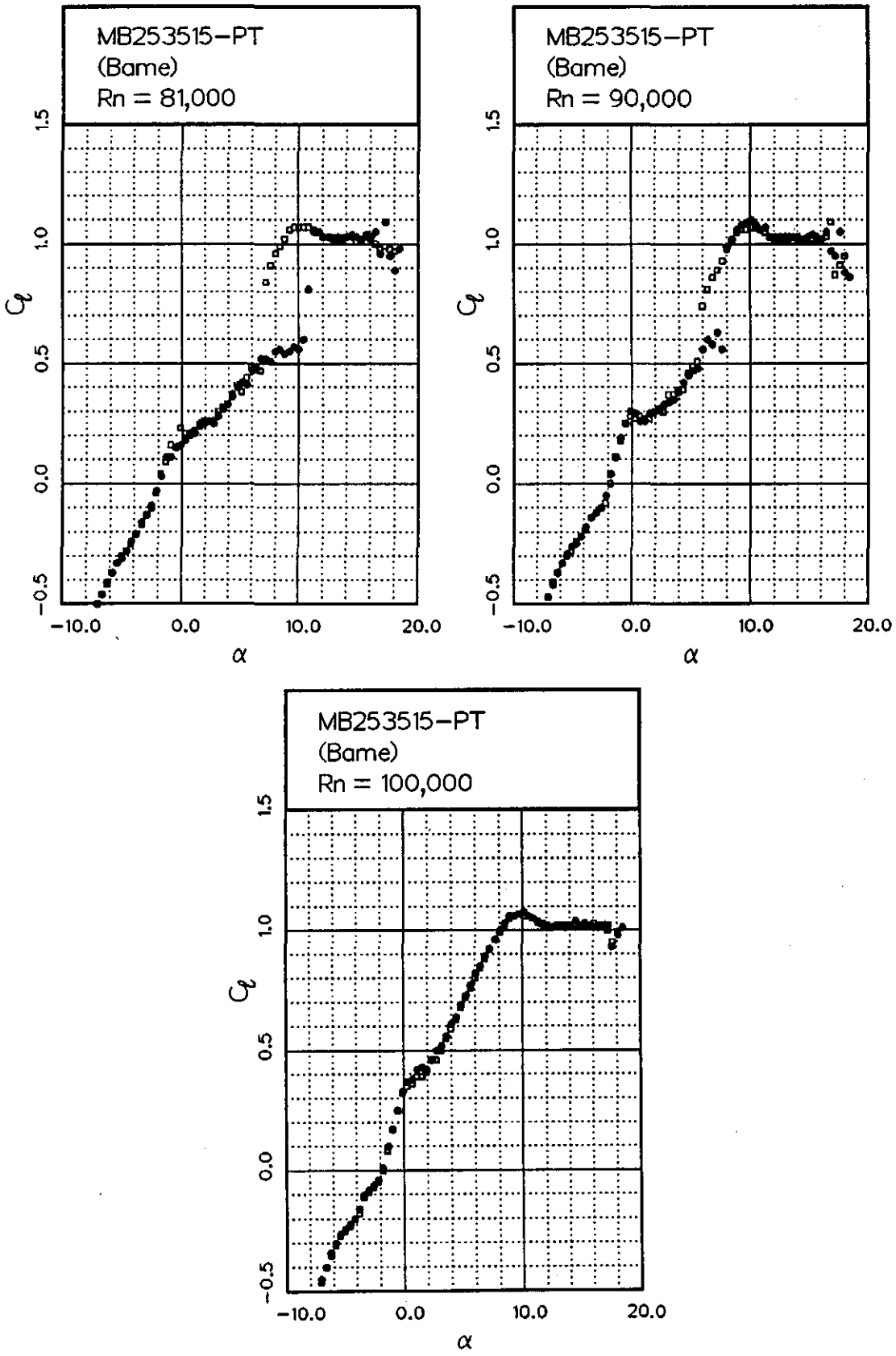
MB253515-PT
(Bame)
Rn = 81,000
MB253515-PT
(Bame)
Rn = 90,000
MB253515-PT
(Bame)
Rn = 100,000
C_ℓ
α
1.5
1.0
0.5
0.0
-0.5
-10.0
0.0
10.0
20.0

Fig. 12.56

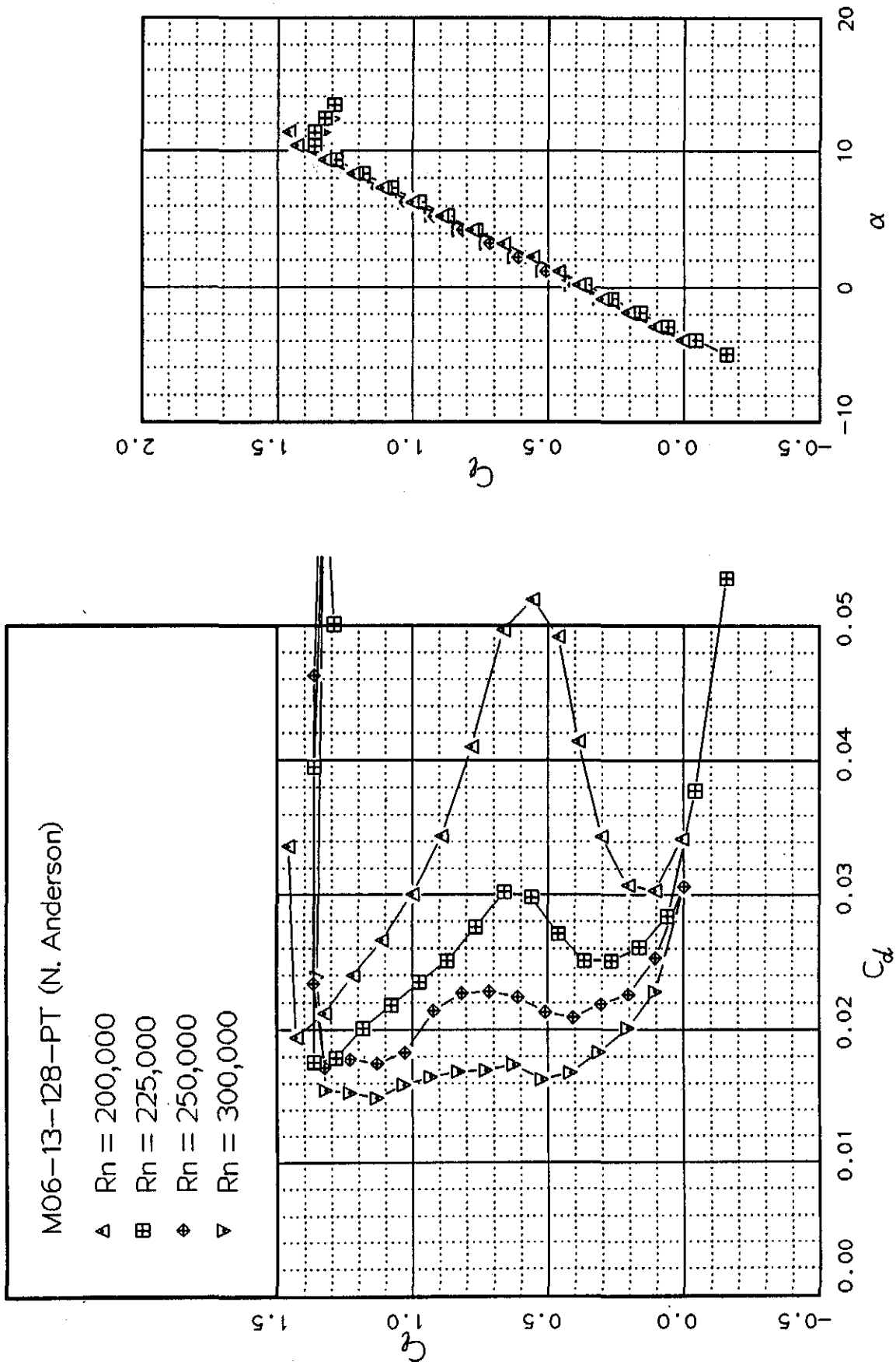
M06-13-128-PT (N. Anderson)
Rn = 200,000
Rn = 225,000
Rn = 250,000
Rn = 300,000
−0.5
0.0
0.5
1.0
1.5
2.0
cl
−10
0
10
20
α
0.00
0.01
0.02
0.03
0.04
0.05
cd

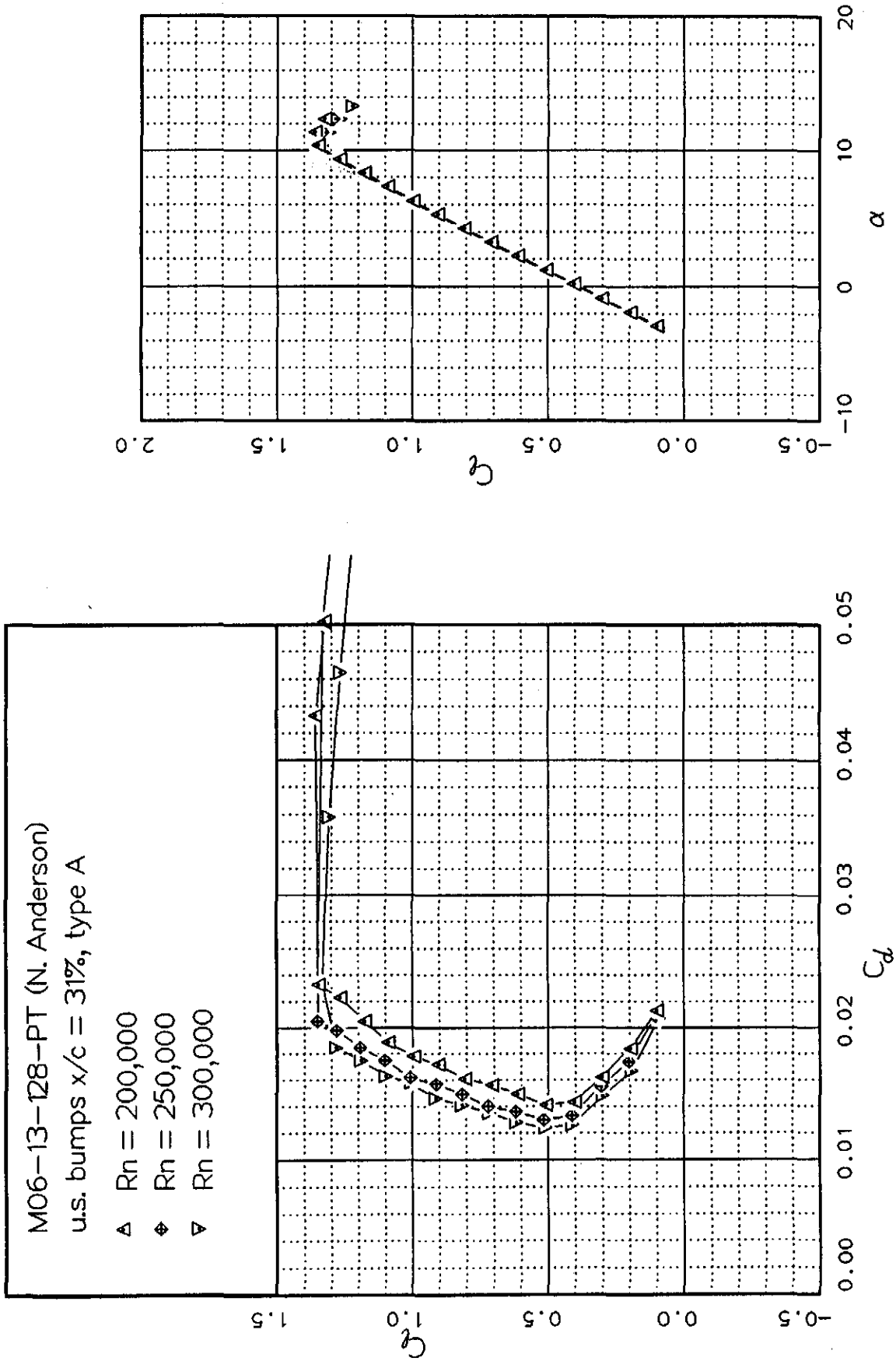
M06-13-128-PT (N. Anderson)
u.s. bumps x/c = 31%, type A
Rn = 200,000
Rn = 250,000
Rn = 300,000
C_l
C_d
α

Fig. 12.58

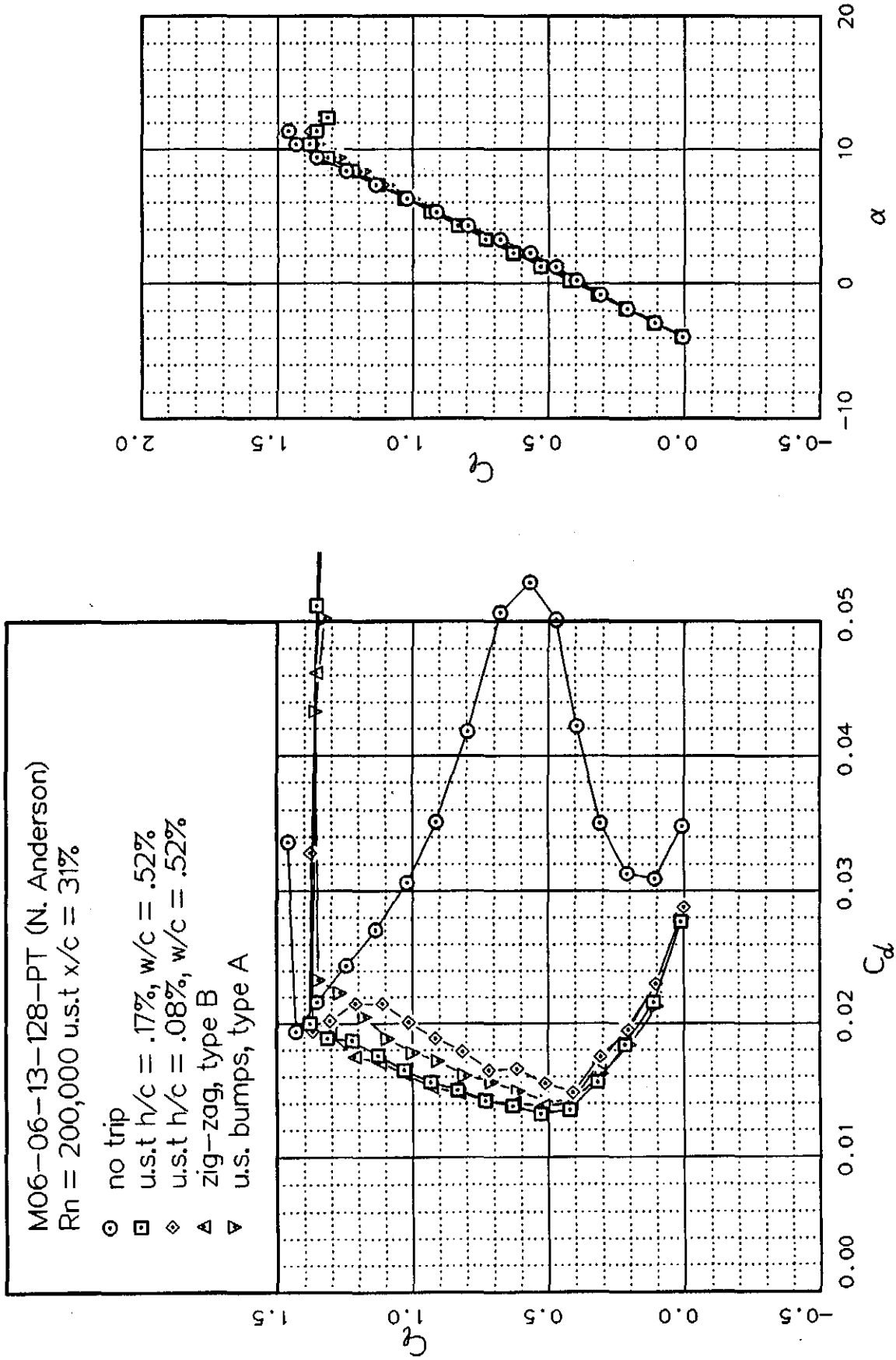
M06-06-13-128-PT (N. Anderson)
Rn = 200,000 u.s.t x/c = 31%
no trip
u.s.t h/c = .17%, w/c = .52%
u.s.t h/c = .08%, w/c = .52%
zig-zag, type B
u.s. bumps, type A
α
20
10
0
−10
−0.5
0.0
0.5
1.0
1.5
2.0
C_l
C_d
0.00
0.01
0.02
0.03
0.04
0.05

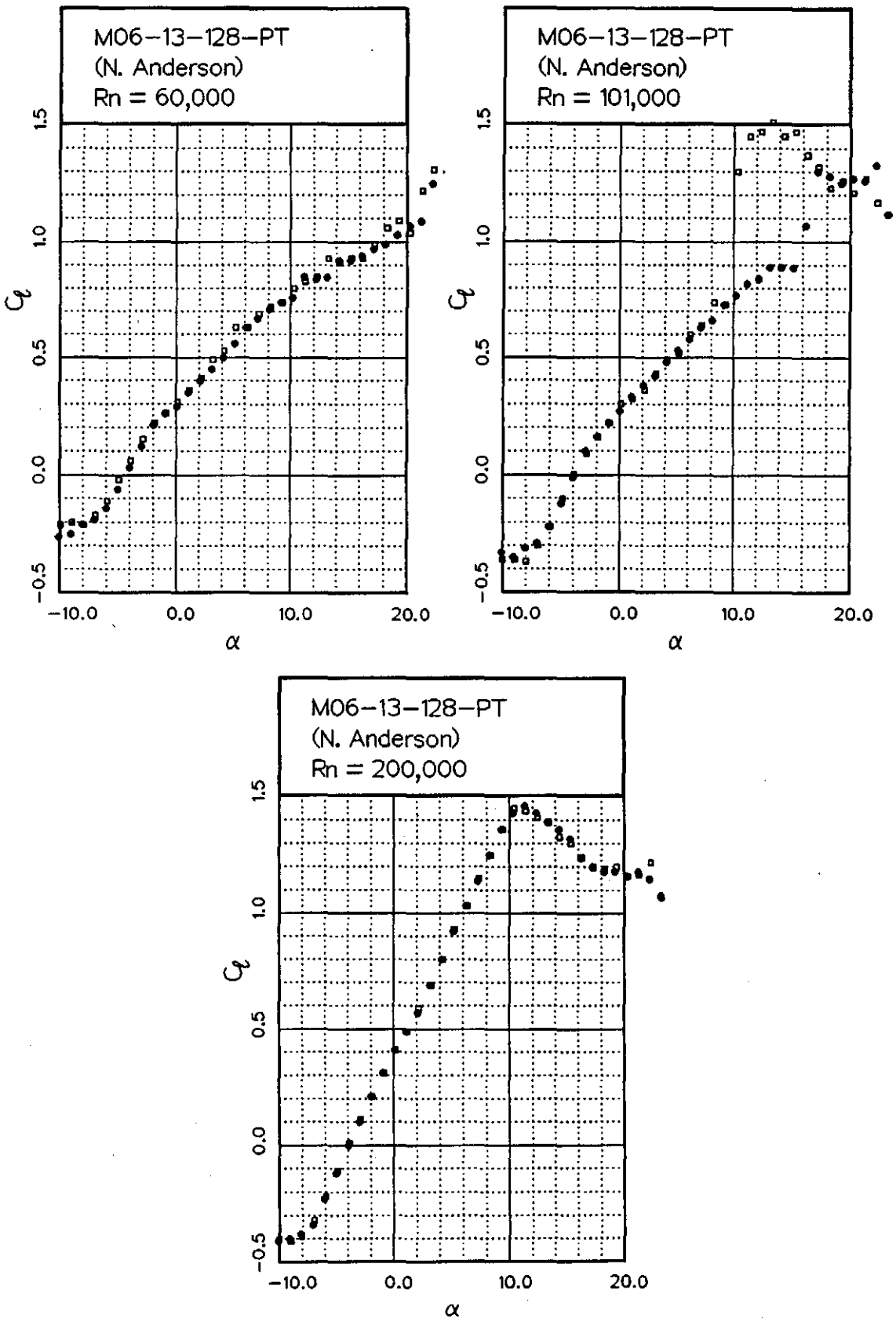
M06-13-128-PT
(N. Anderson)
Rn = 60,000
M06-13-128-PT
(N. Anderson)
Rn = 101,000
M06-13-128-PT
(N. Anderson)
Rn = 200,000
C_ℓ
α
1.5
1.0
0.5
0.0
-0.5
-10.0
0.0
10.0
20.0

Fig. 12.60

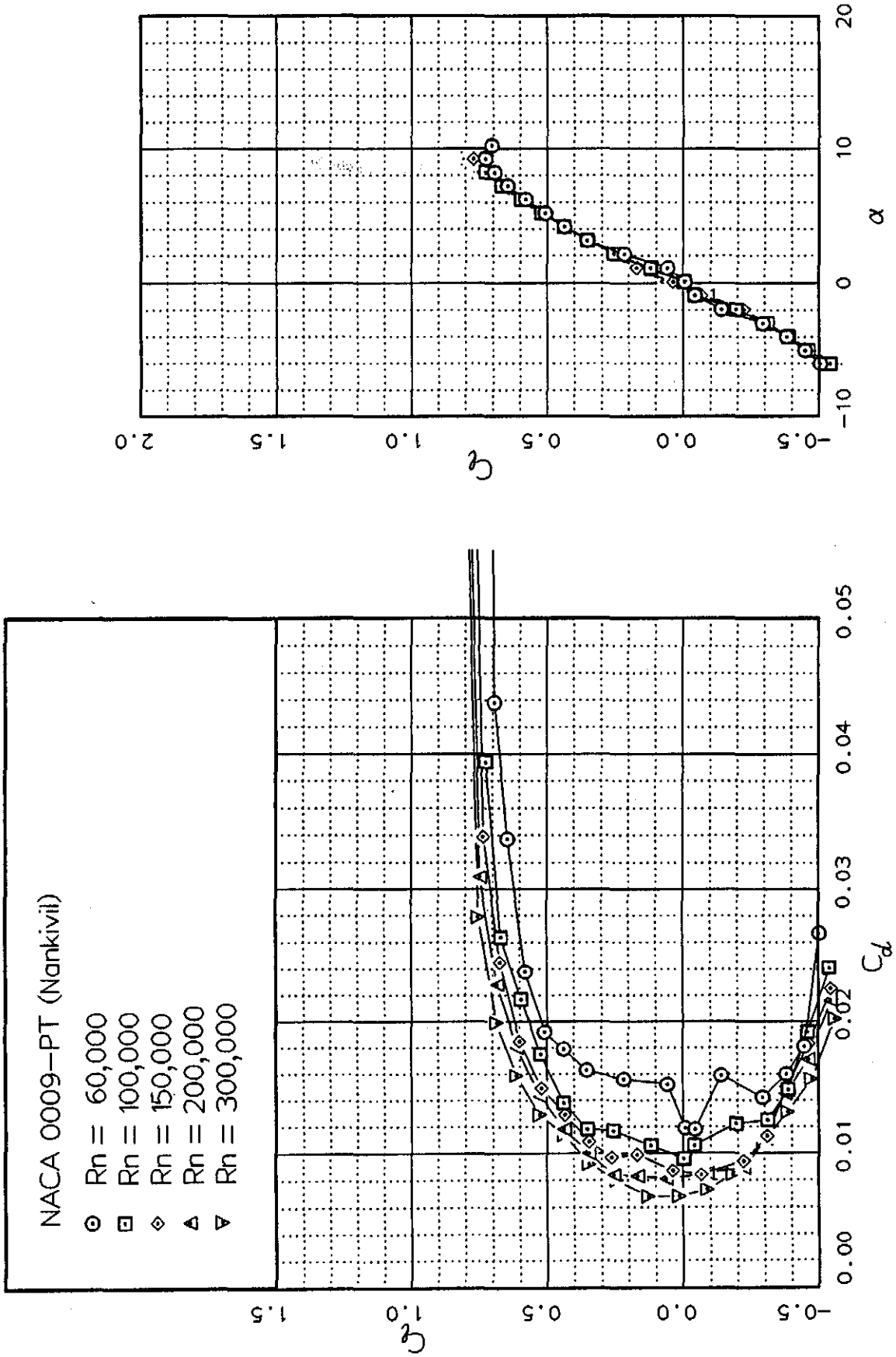
NACA 0009–PT (Nankivil)
Rn = 60,000
Rn = 100,000
Rn = 150,000
Rn = 200,000
Rn = 300,000
C_l
C_d
α

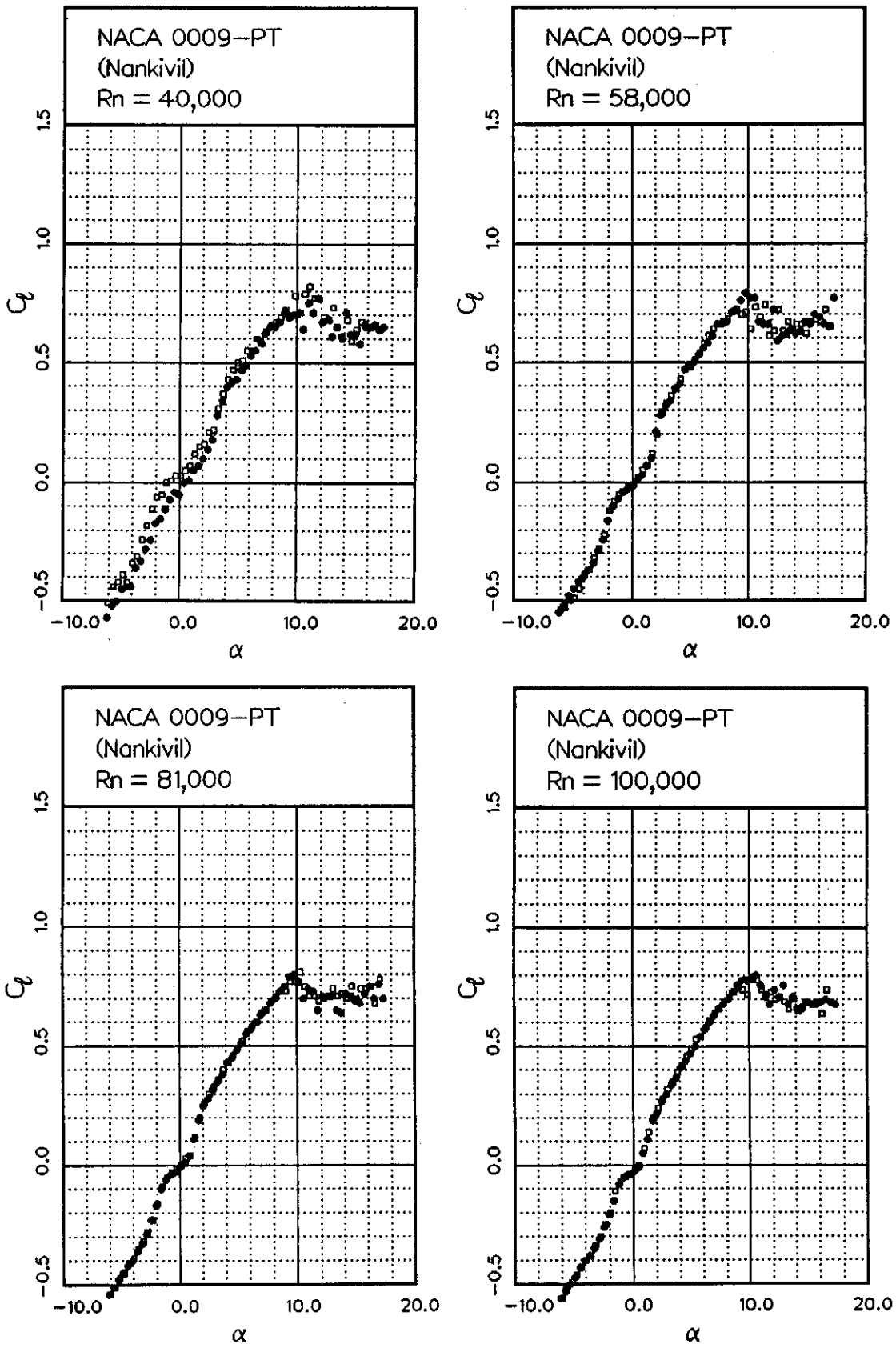
NACA 0009–PT
(Nankivil)
Rn = 40,000
NACA 0009–PT
(Nankivil)
Rn = 58,000
NACA 0009–PT
(Nankivil)
Rn = 81,000
NACA 0009–PT
(Nankivil)
Rn = 100,000
C_ℓ
α
1.5
1.0
0.5
0.0
−0.5
−10.0
0.0
10.0
20.0

Fig. 12.62

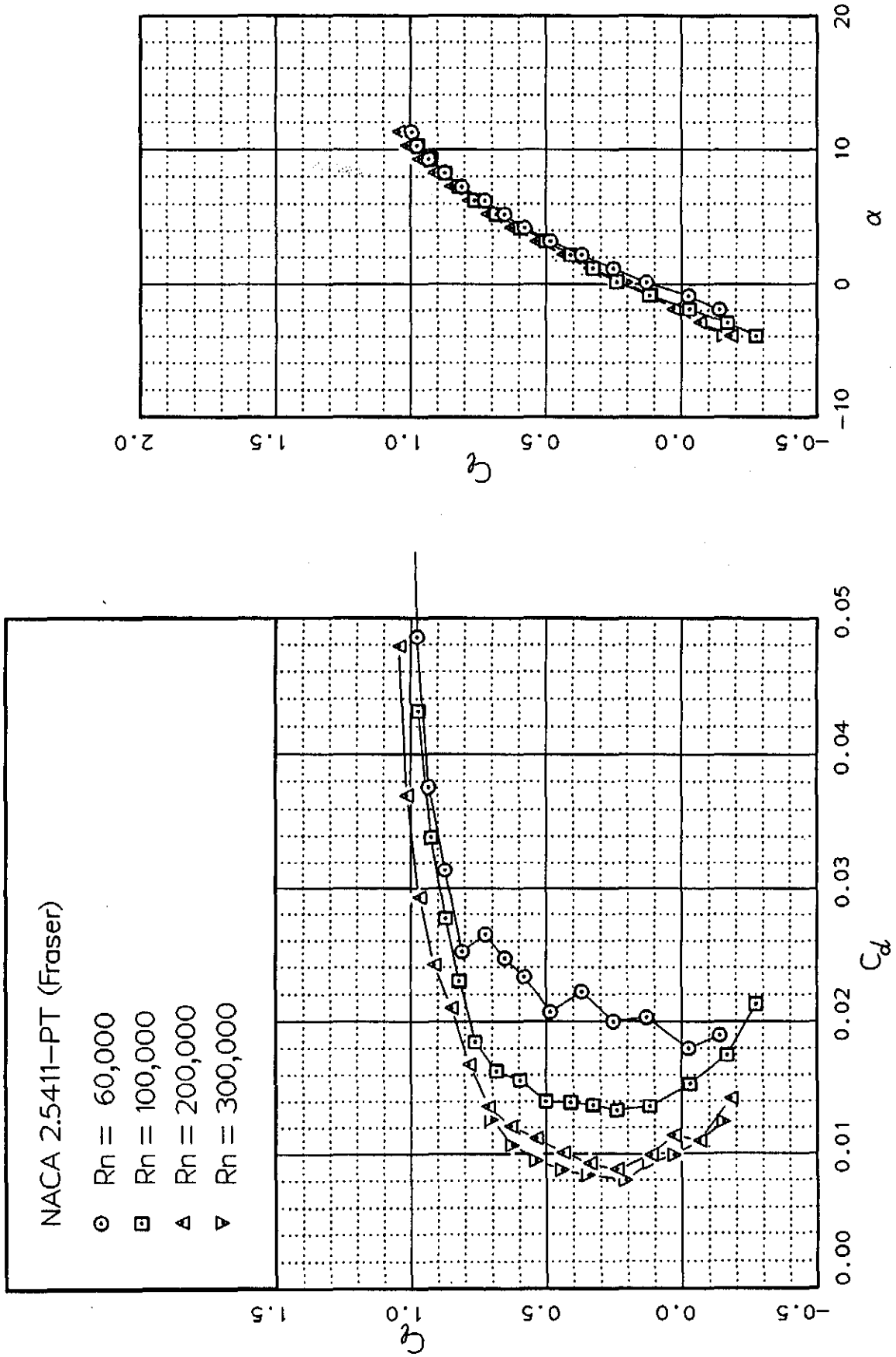
NACA 2.5411–PT (Fraser)
Rn = 60,000
Rn = 100,000
Rn = 200,000
Rn = 300,000
C_l
C_d
α
−0.5
0.0
0.5
1.0
1.5
2.0
−10
0
10
20
0.00
0.01
0.02
0.03
0.04
0.05

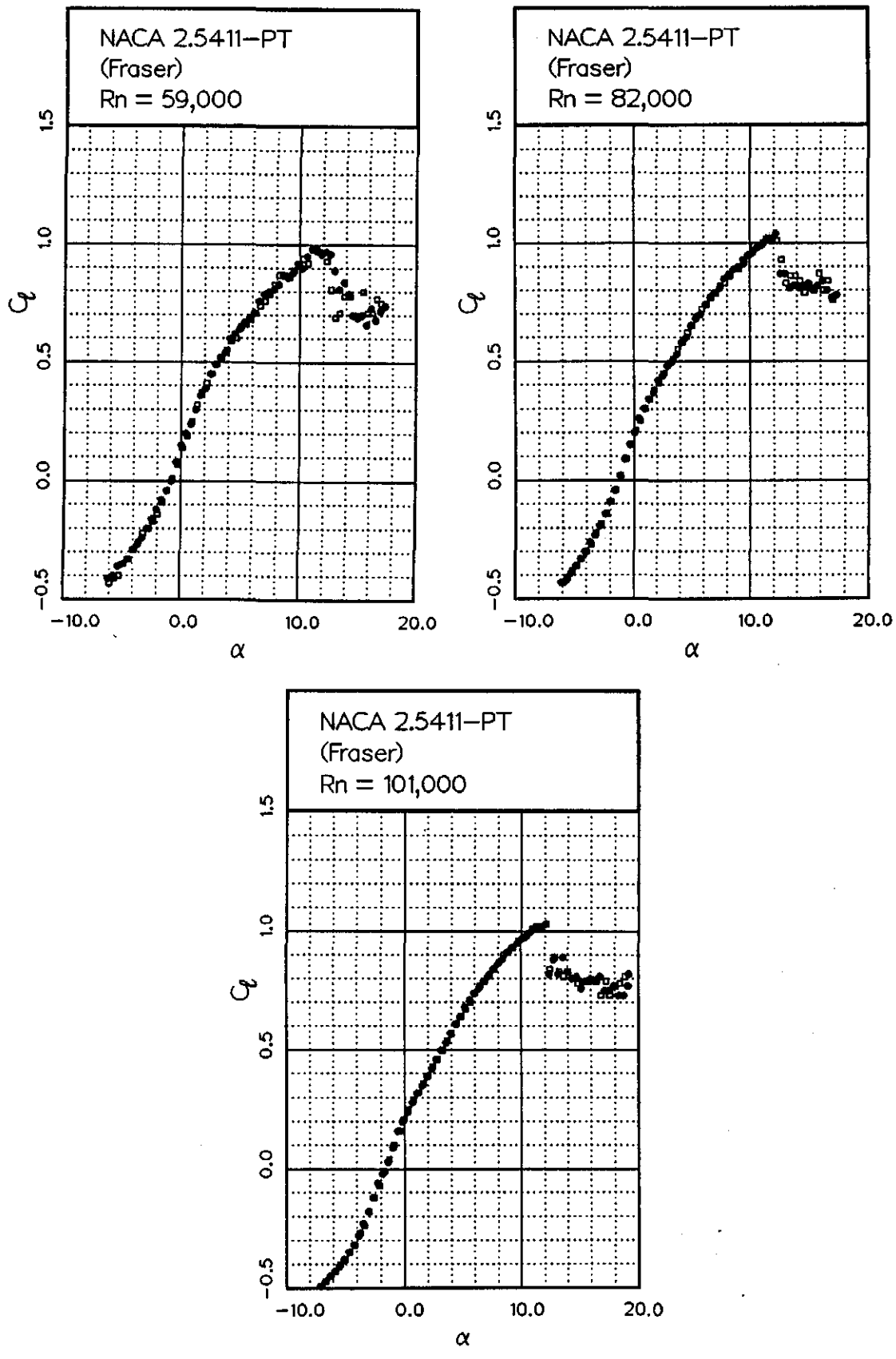
NACA 2.5411–PT
(Fraser)
Rn = 59,000
NACA 2.5411–PT
(Fraser)
Rn = 82,000
NACA 2.5411–PT
(Fraser)
Rn = 101,000
C_l
α
1.5
1.0
0.5
0.0
−0.5
−10.0
0.0
10.0
20.0

Fig. 12.64

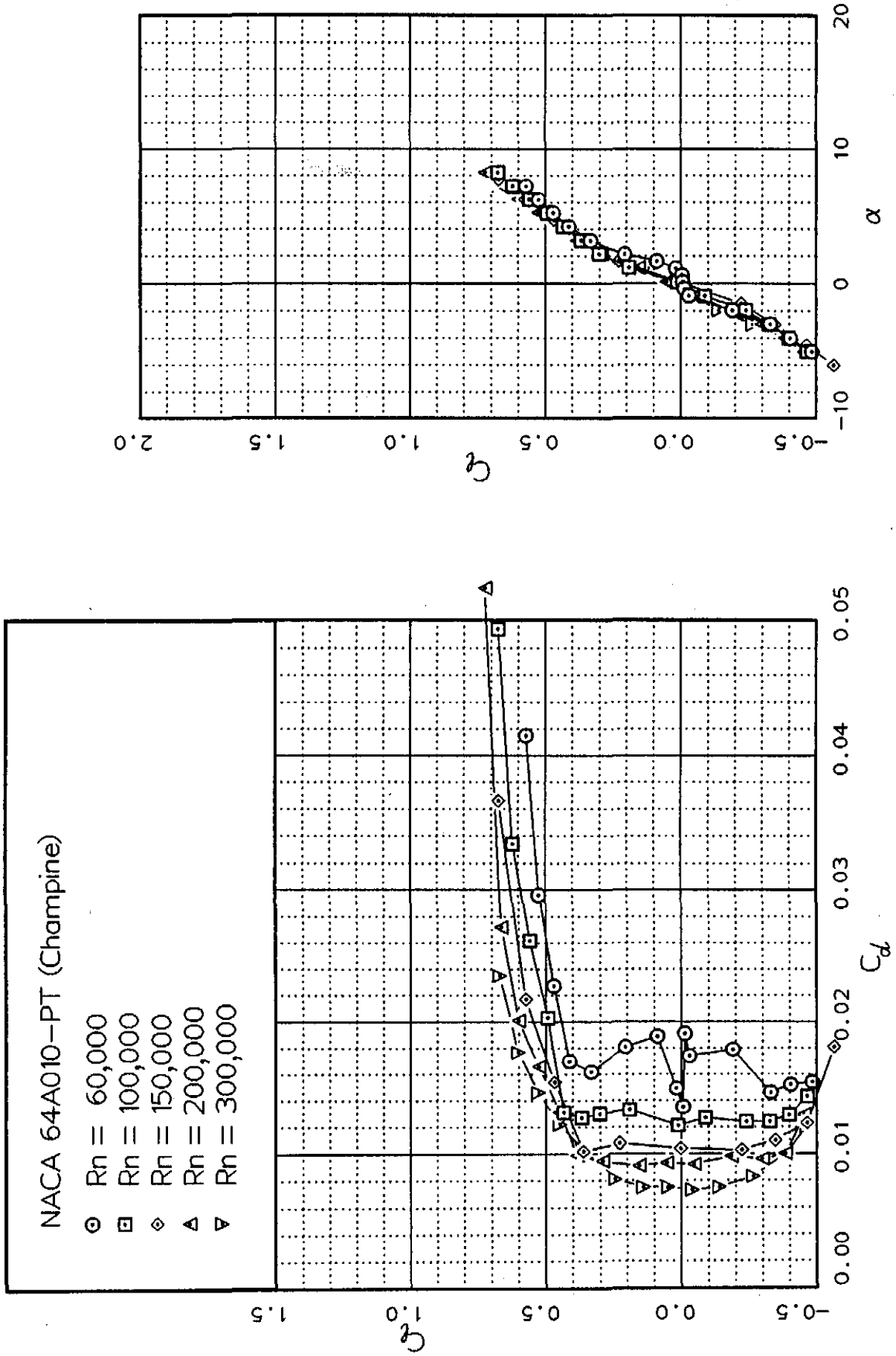
NACA 64A010–PT (Champine)
Rn = 60,000
Rn = 100,000
Rn = 150,000
Rn = 200,000
Rn = 300,000
C_l
C_d
α

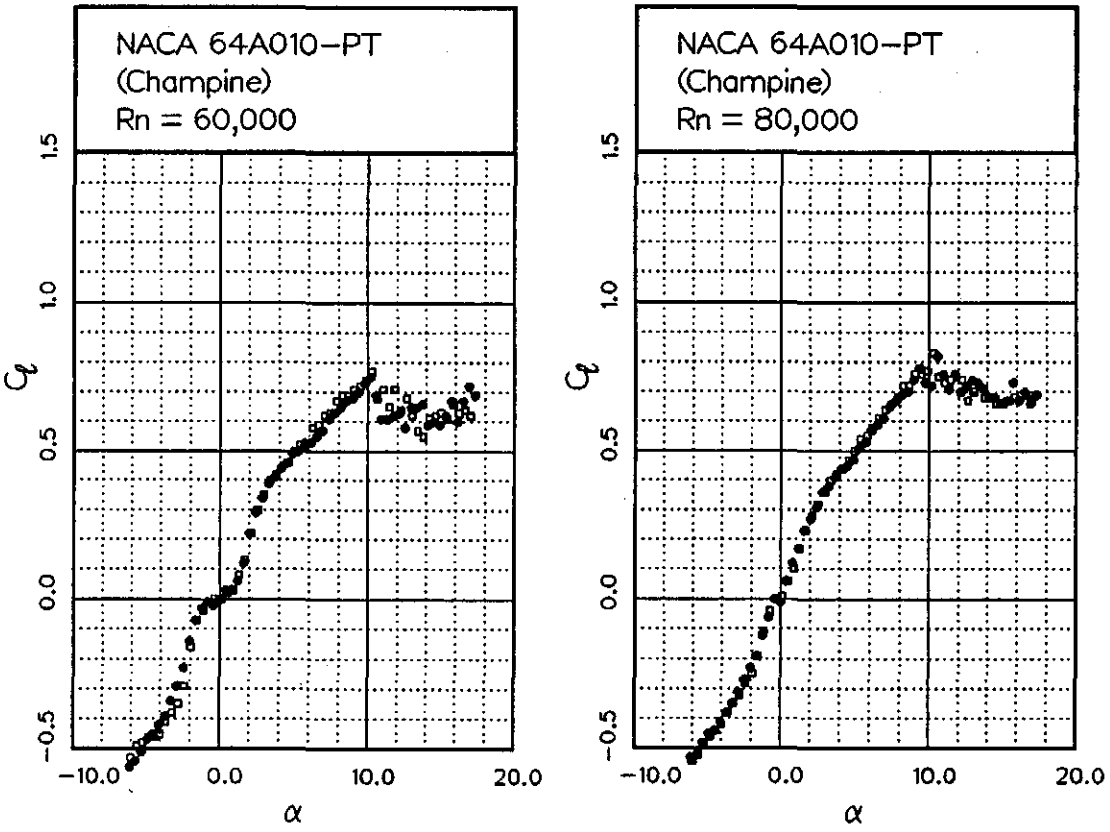
NACA 64A010–PT
(Champine)
Rn = 60,000
NACA 64A010–PT
(Champine)
Rn = 80,000
C_l
α
1.5
1.0
0.5
0.0
−0.5
−10.0
0.0
10.0
20.0

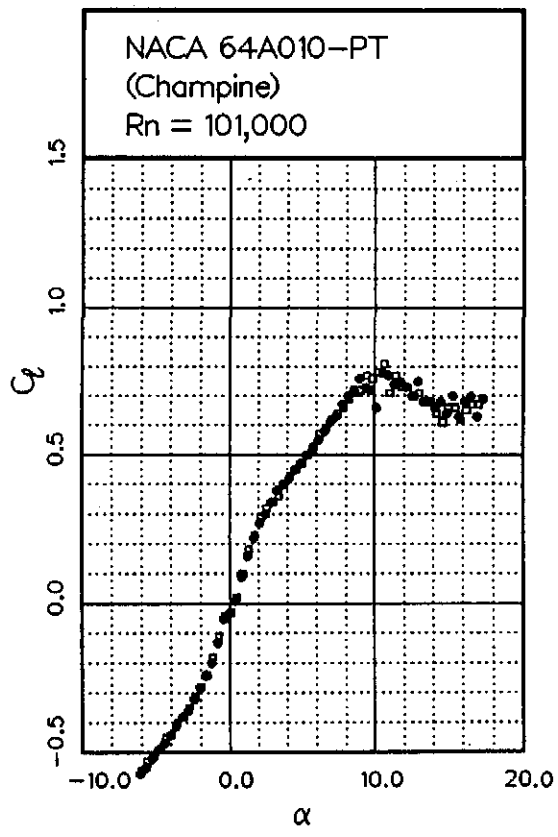
NACA 64A010–PT
(Champine)
Rn = 101,000
C_l
α
1.5
1.0
0.5
0.0
−0.5
−10.0
0.0
10.0
20.0

Fig. 12.66

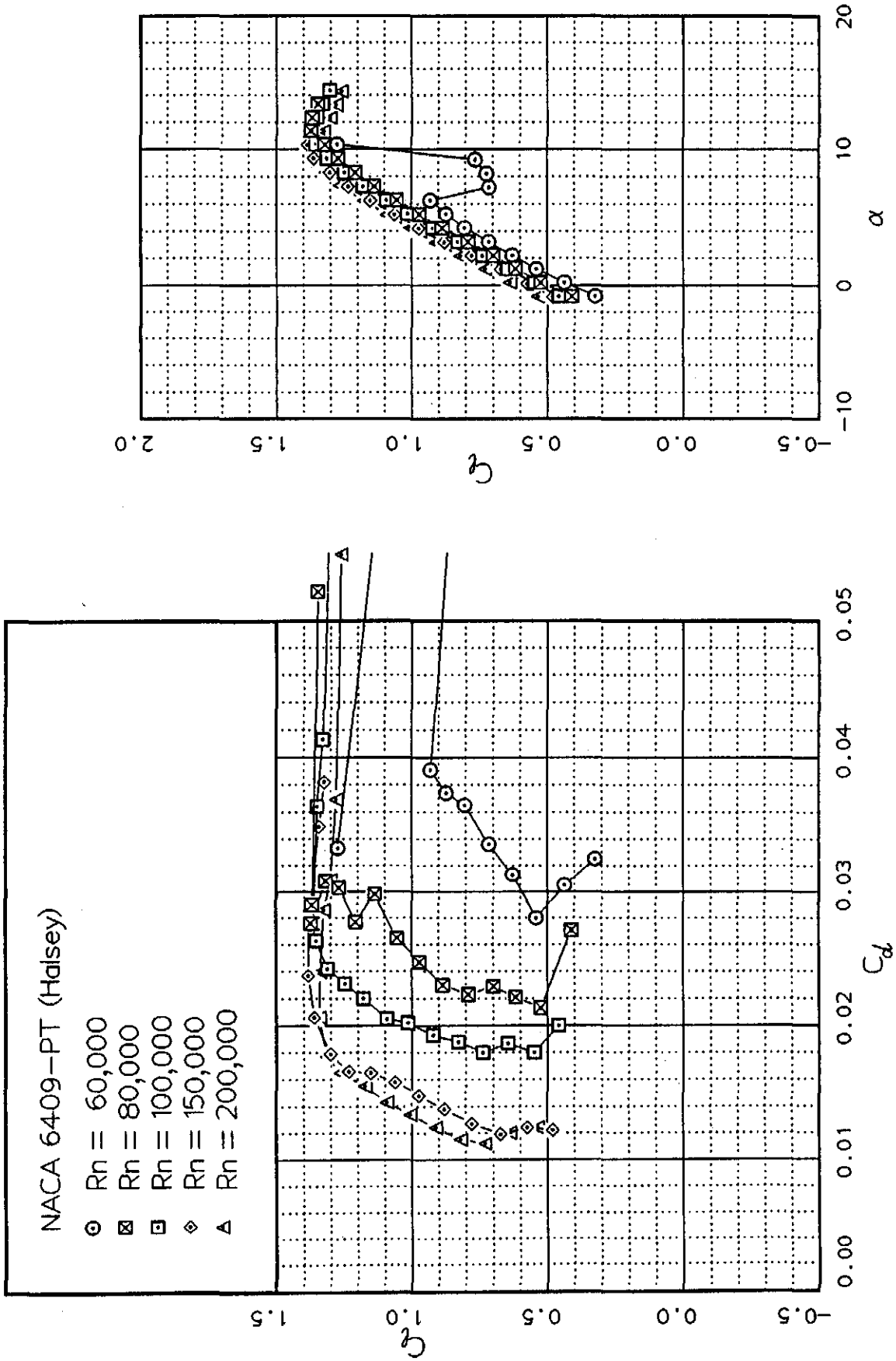
NACA 6409–PT (Halsey)
Rn = 60,000
Rn = 80,000
Rn = 100,000
Rn = 150,000
Rn = 200,000
α
C_d
C_l
20
10
0
−10
0.05
0.04
0.03
0.02
0.01
0.00
−0.5
0.0
0.5
1.0
1.5
2.0

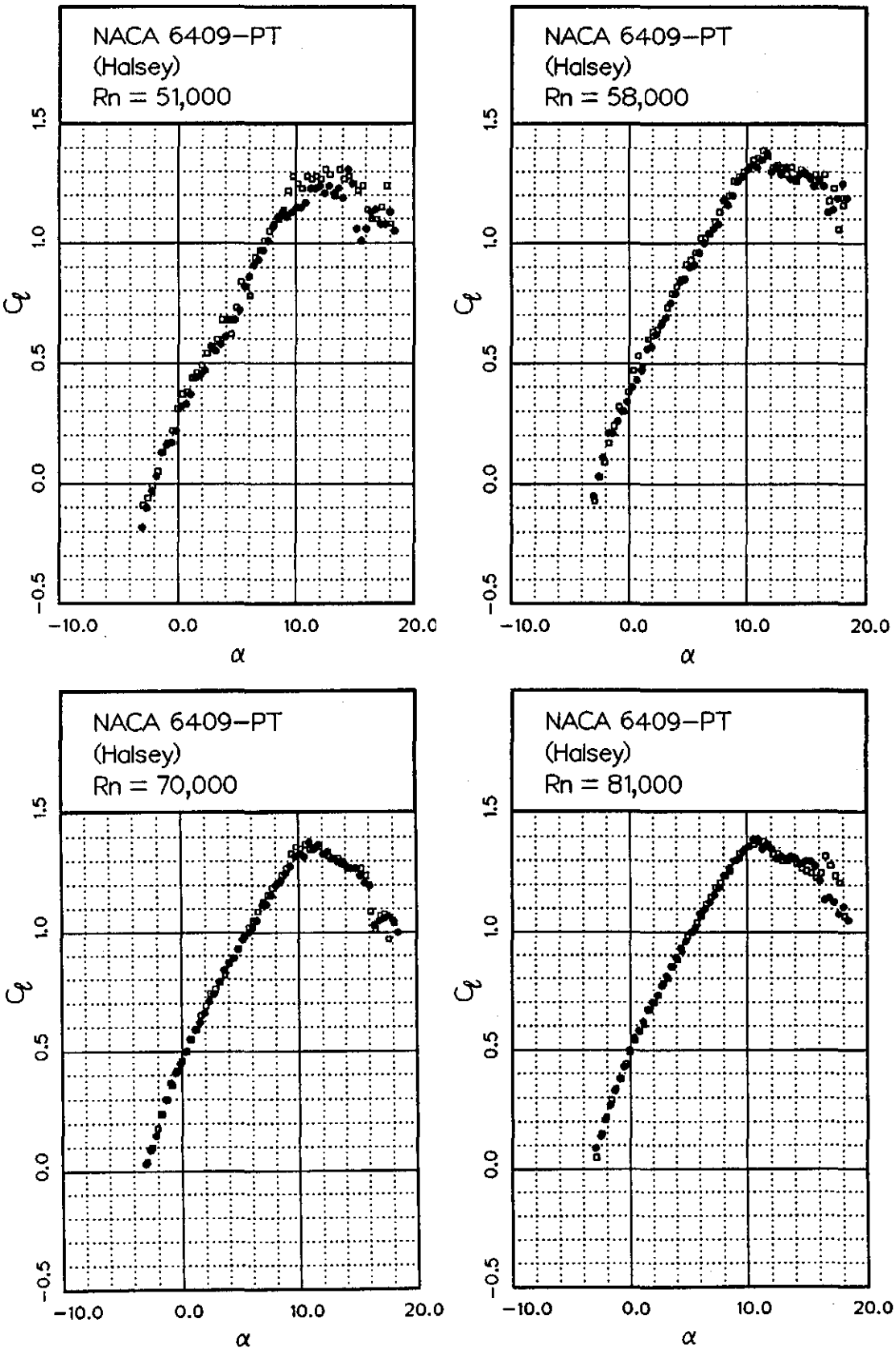
NACA 6409–PT
(Halsey)
Rn = 51,000
NACA 6409–PT
(Halsey)
Rn = 58,000
NACA 6409–PT
(Halsey)
Rn = 70,000
NACA 6409–PT
(Halsey)
Rn = 81,000
C_ℓ
α
1.5
1.0
0.5
0.0
−0.5
−10.0
0.0
10.0
20.0

Fig. 12.68

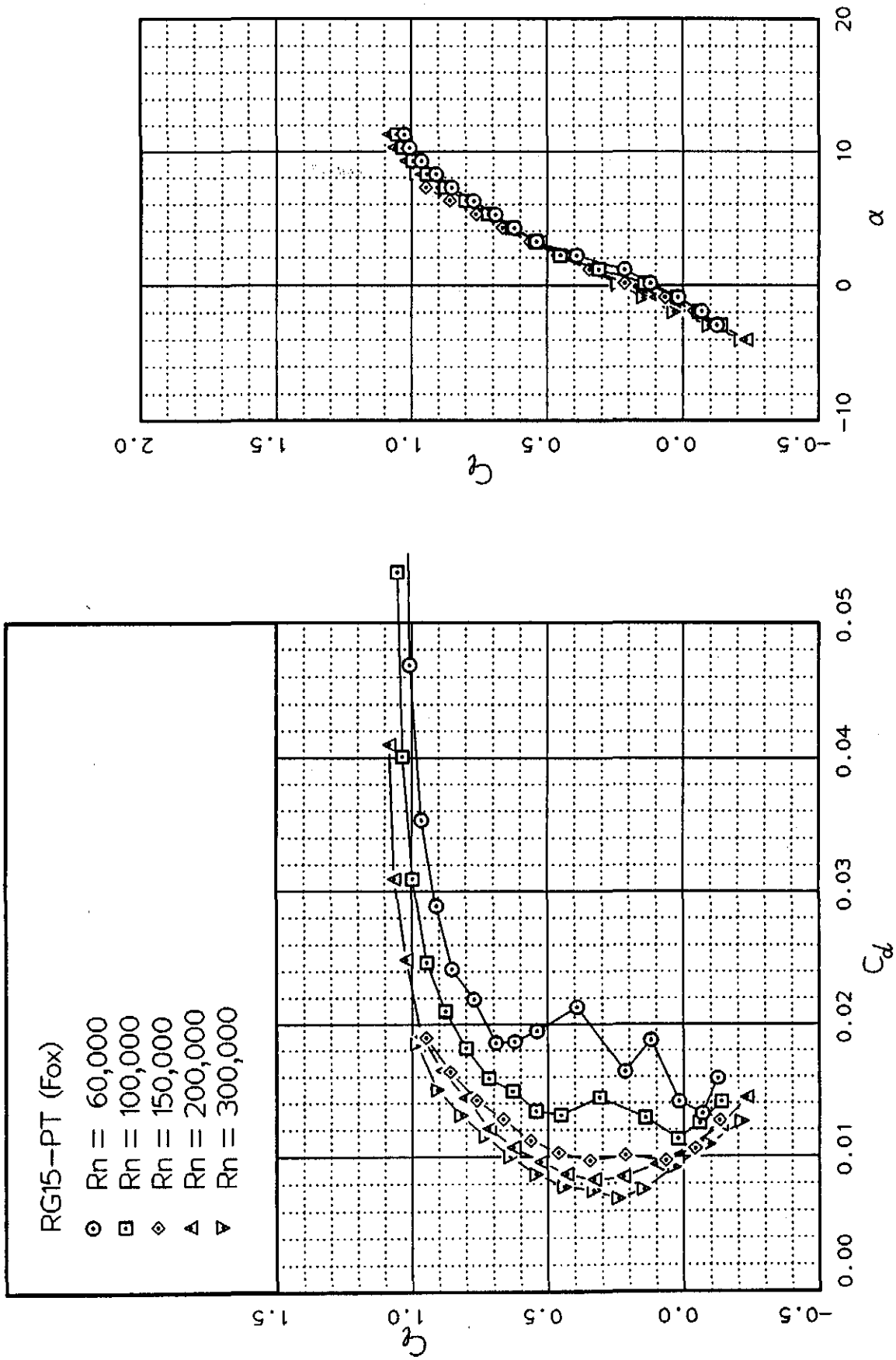
RG15–PT (Fox)
Rn = 60,000
Rn = 100,000
Rn = 150,000
Rn = 200,000
Rn = 300,000
0.00
0.01
0.02
0.03
0.04
0.05
C_d
−0.5
0.0
0.5
1.0
1.5
C_l
20
10
0
−10
α
−0.5
0.0
0.5
1.0
1.5
2.0
C_l

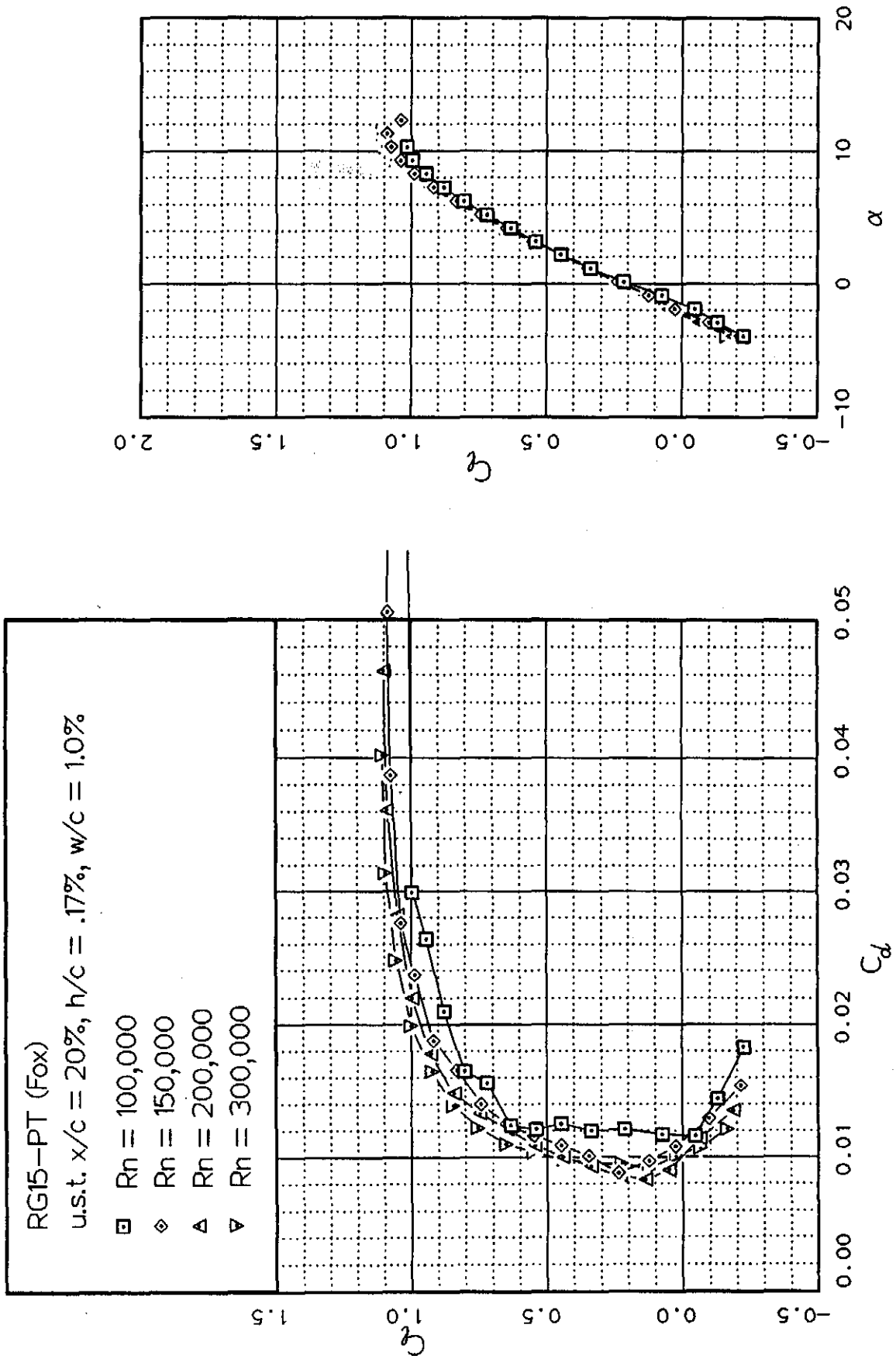
RG15–PT (Fox)
u.s.t. x/c = 20%, h/c = .17%, w/c = 1.0%
Rn = 100,000
Rn = 150,000
Rn = 200,000
Rn = 300,000
C_l
C_d
α

Fig. 12.70

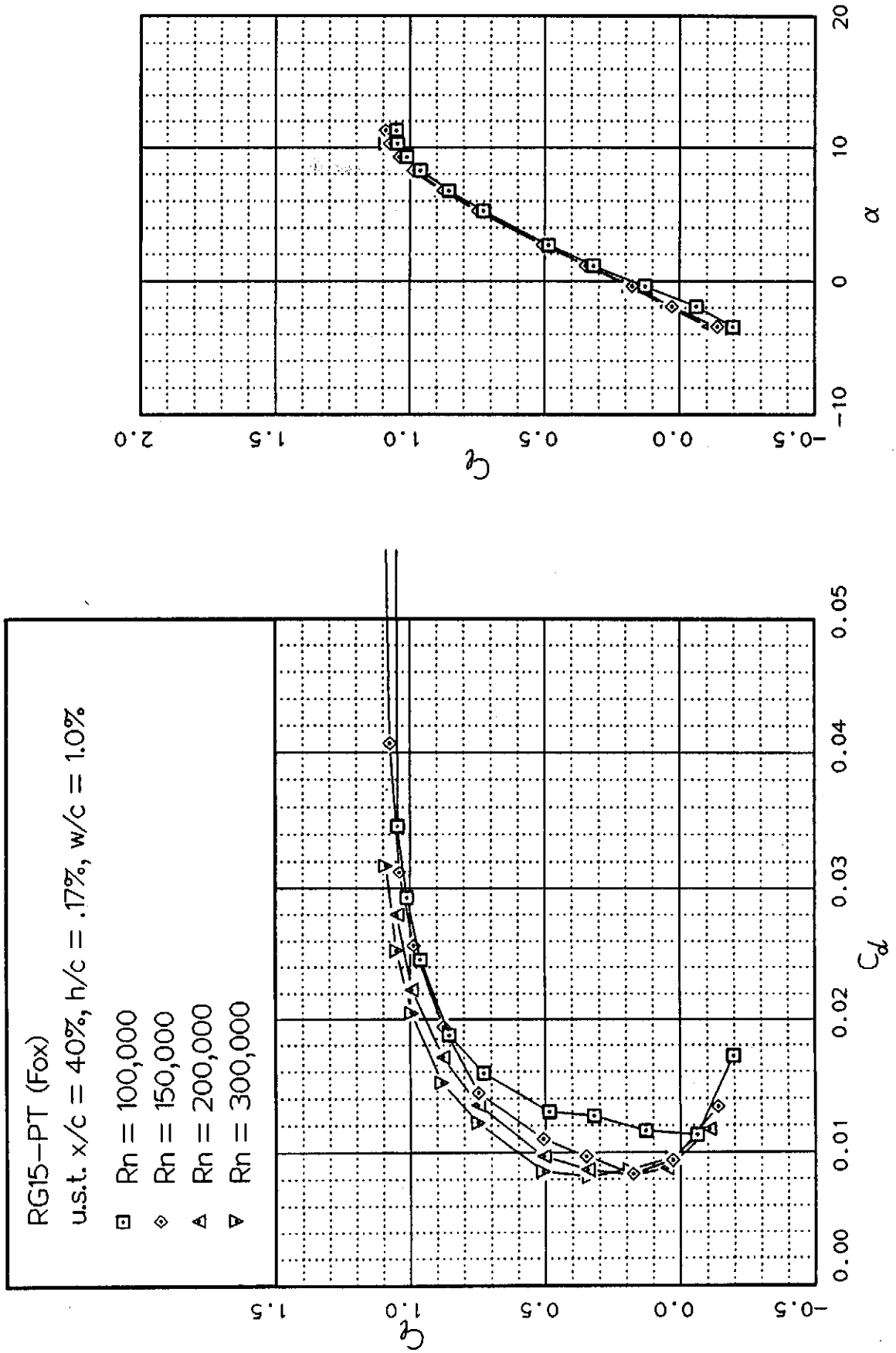
RG15–PT (Fox)
u.s.t. x/c = 40%, h/c = .17%, w/c = 1.0%
Rn = 100,000
Rn = 150,000
Rn = 200,000
Rn = 300,000
α
C_d
C_l
20
10
0
−10
0.05
0.04
0.03
0.02
0.01
0.00
−0.5
0.0
0.5
1.0
1.5
2.0

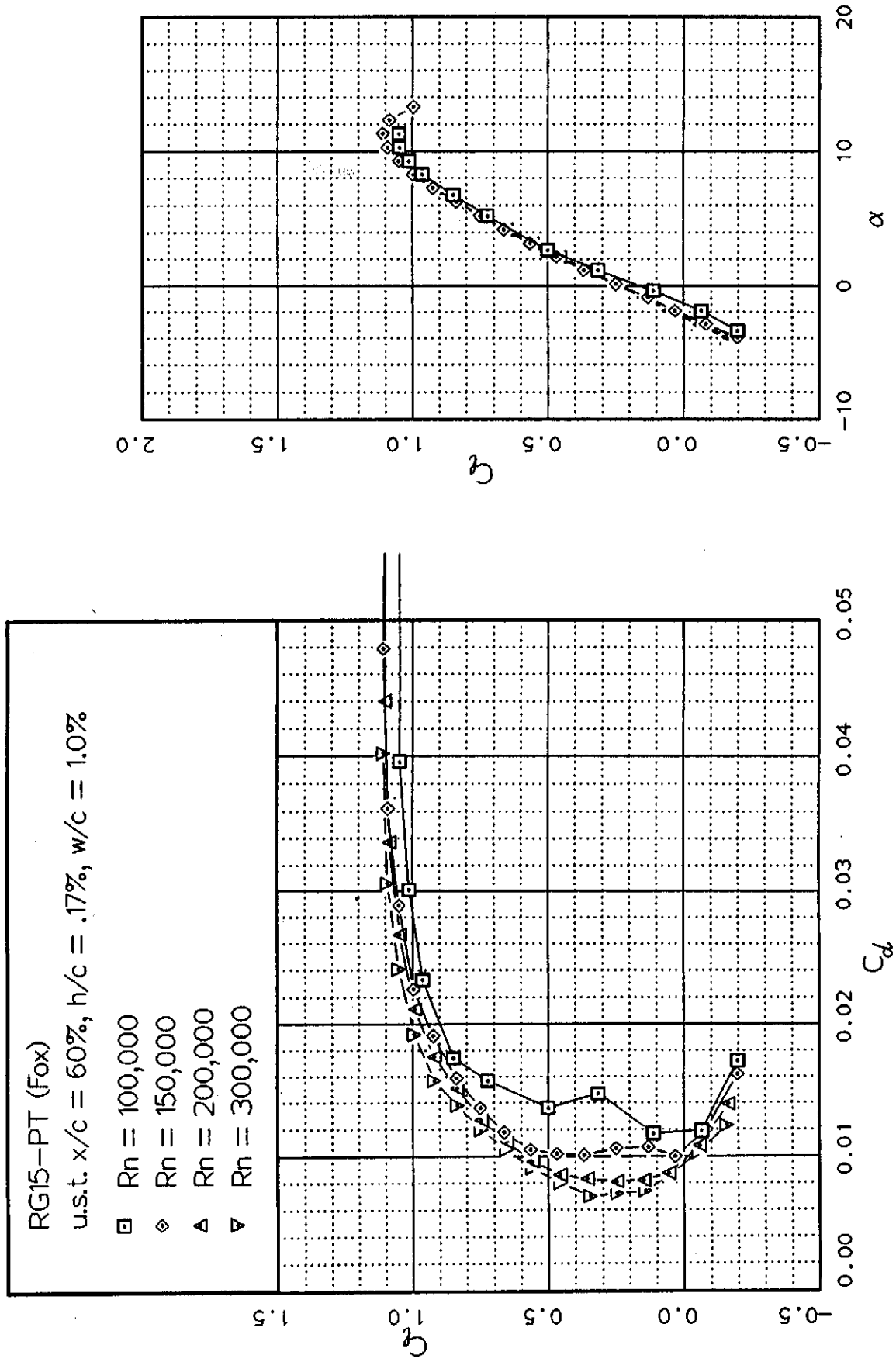
RG15–PT (Fox)
u.s.t. x/c = 60%, h/c = .17%, w/c = 1.0%
Rn = 100,000
Rn = 150,000
Rn = 200,000
Rn = 300,000
α
C_l
C_d
20
10
0
−10
−0.5
0.0
0.5
1.0
1.5
2.0
0.00
0.01
0.02
0.03
0.04
0.05

Fig. 12.72

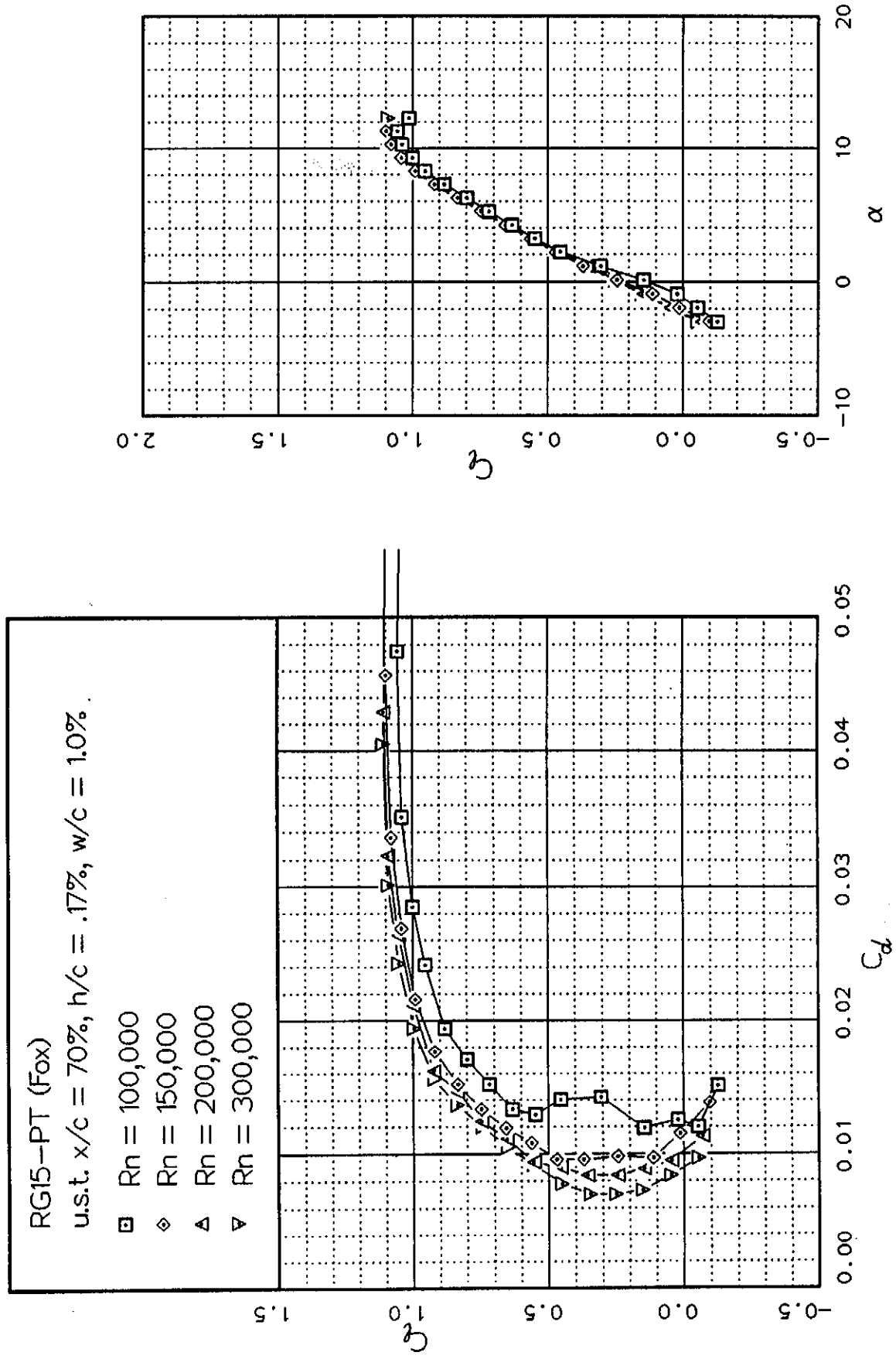
RG15–PT (Fox)
u.s.t. x/c = 70%, h/c = .17%, w/c = 1.0%
Rn = 100,000
Rn = 150,000
Rn = 200,000
Rn = 300,000
α
C_d
C_l
20
10
0
−10
0.05
0.04
0.03
0.02
0.01
0.00
−0.5
0.0
0.5
1.0
1.5
2.0

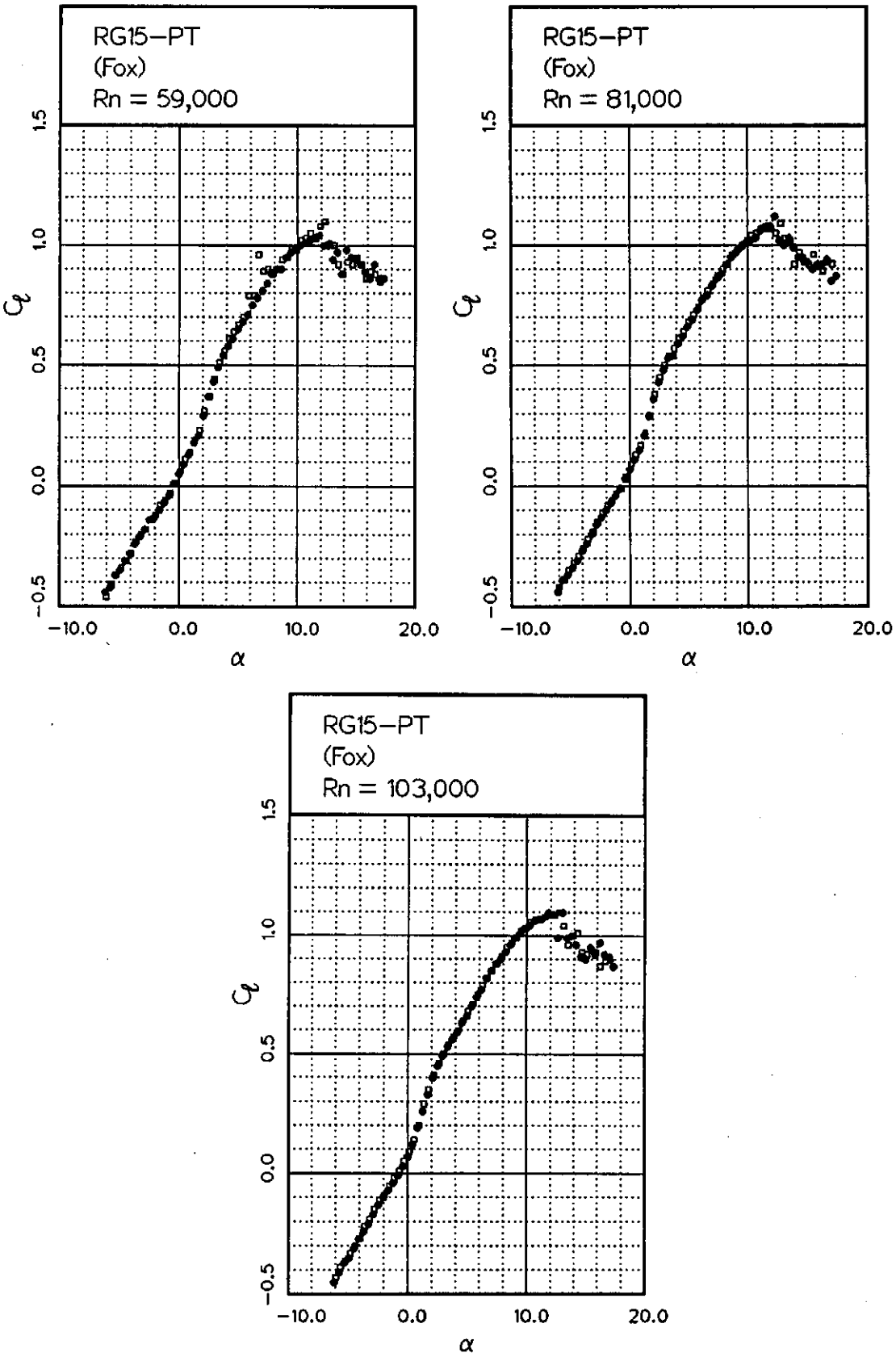
RG15–PT
(Fox)
Rn = 59,000
RG15–PT
(Fox)
Rn = 81,000
RG15–PT
(Fox)
Rn = 103,000
C_l
α
1.5
1.0
0.5
0.0
−0.5
−10.0
0.0
10.0
20.0

Fig. 12.74

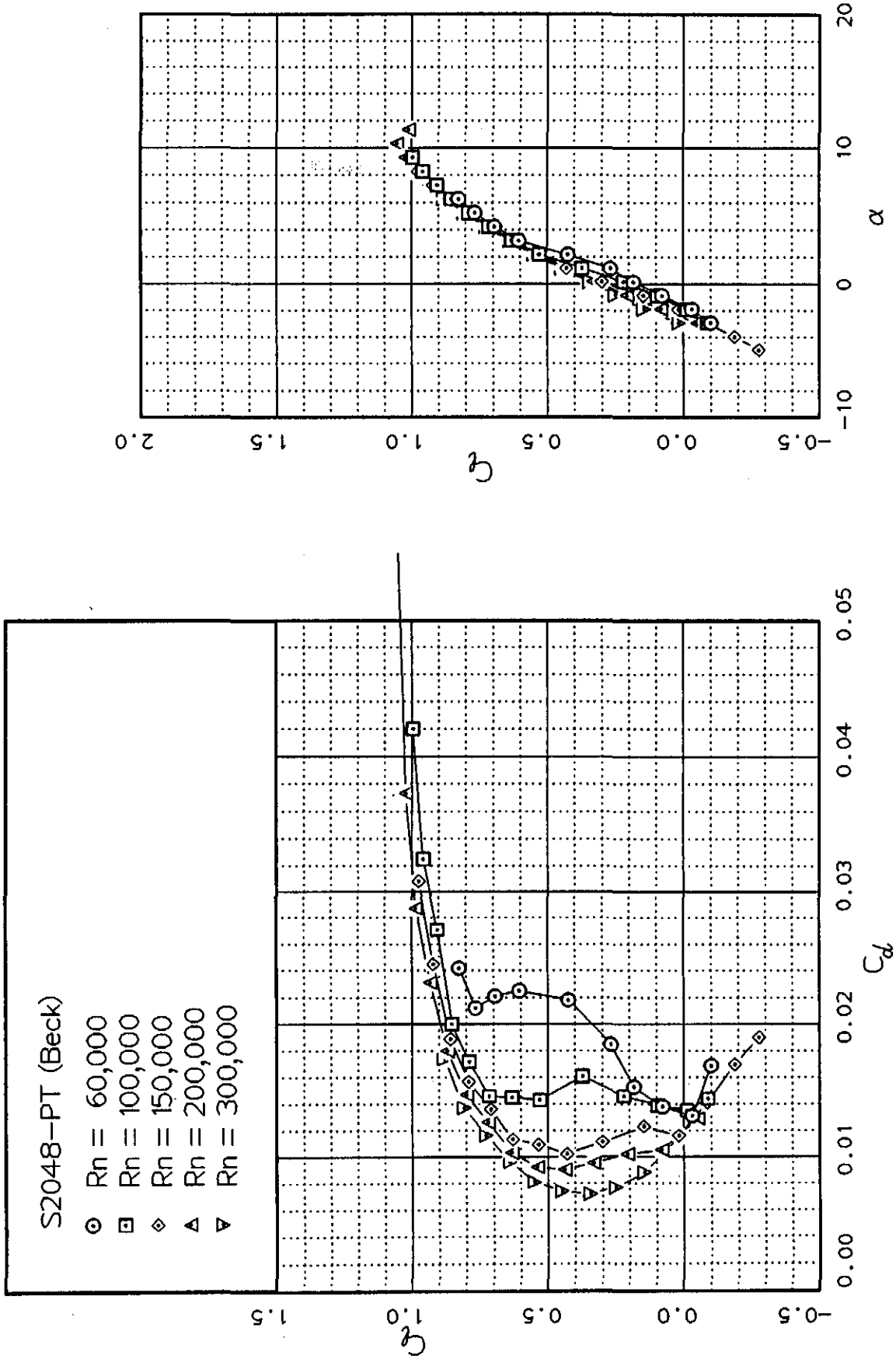
S2048–PT (Beck)
Rn = 60,000
Rn = 100,000
Rn = 150,000
Rn = 200,000
Rn = 300,000
α
C_l
C_d

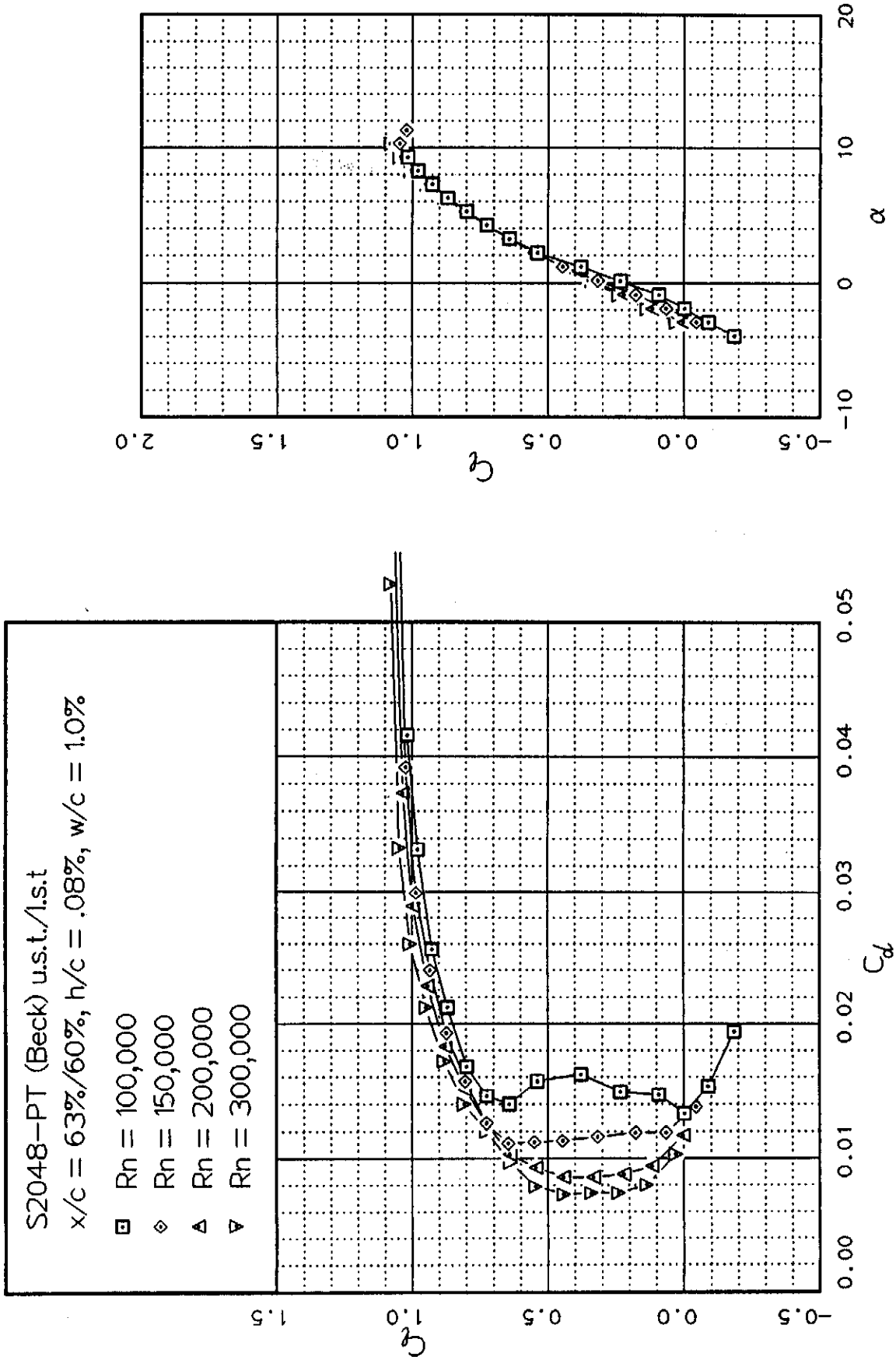
S2048–PT (Beck) u.s.t./l.s.t
x/c = 63%/60%, h/c = .08%, w/c = 1.0%
Rn = 100,000
Rn = 150,000
Rn = 200,000
Rn = 300,000
−0.5
0.0
0.5
1.0
1.5
2.0
c_l
−10
0
10
20
α
0.00
0.01
0.02
0.03
0.04
0.05
c_d

Fig. 12.76

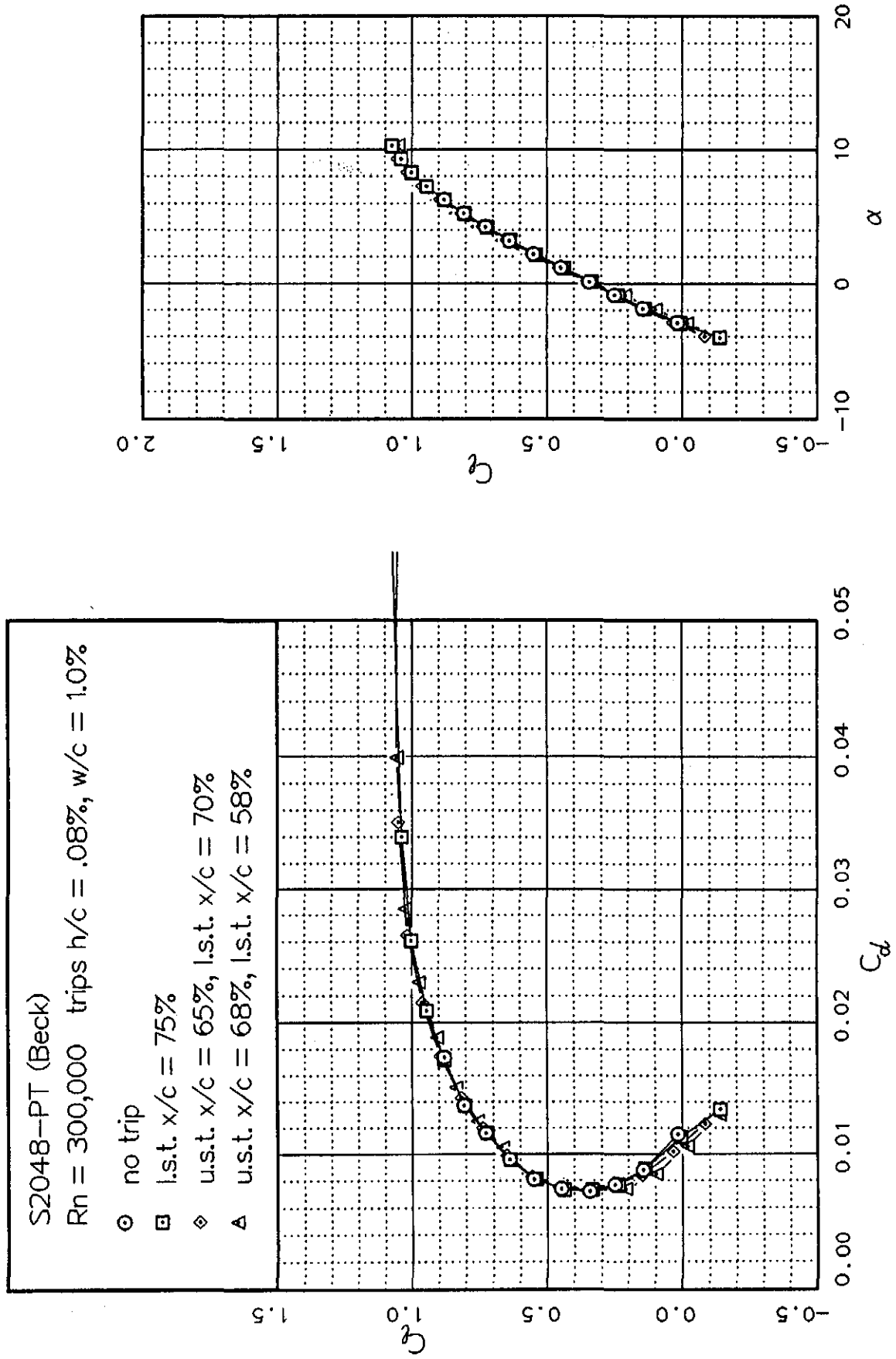
S2048–PT (Beck)
Rn = 300,000 trips h/c = .08%, w/c = 1.0%
no trip
l.s.t. x/c = 75%
u.s.t. x/c = 65%, l.s.t. x/c = 70%
u.s.t. x/c = 68%, l.s.t. x/c = 58%
−0.5
0.0
0.5
1.0
1.5
2.0
c_l
−10
0
10
20
α
0.00
0.01
0.02
0.03
0.04
0.05
c_d

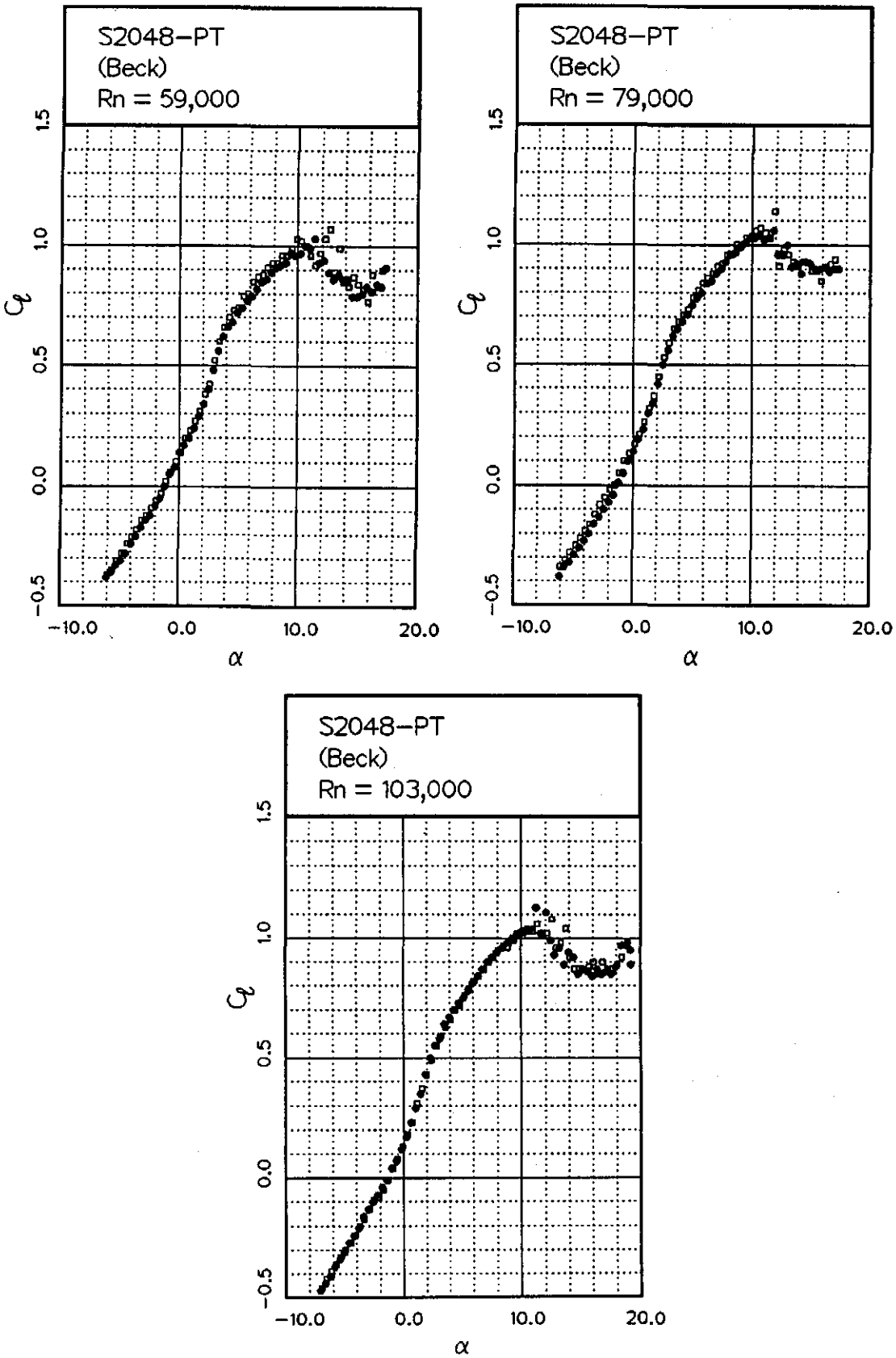
S2048–PT
(Beck)
Rn = 59,000
S2048–PT
(Beck)
Rn = 79,000
S2048–PT
(Beck)
Rn = 103,000
C_ℓ
α
1.5
1.0
0.5
0.0
−0.5
−10.0
0.0
10.0
20.0

Fig. 12.78

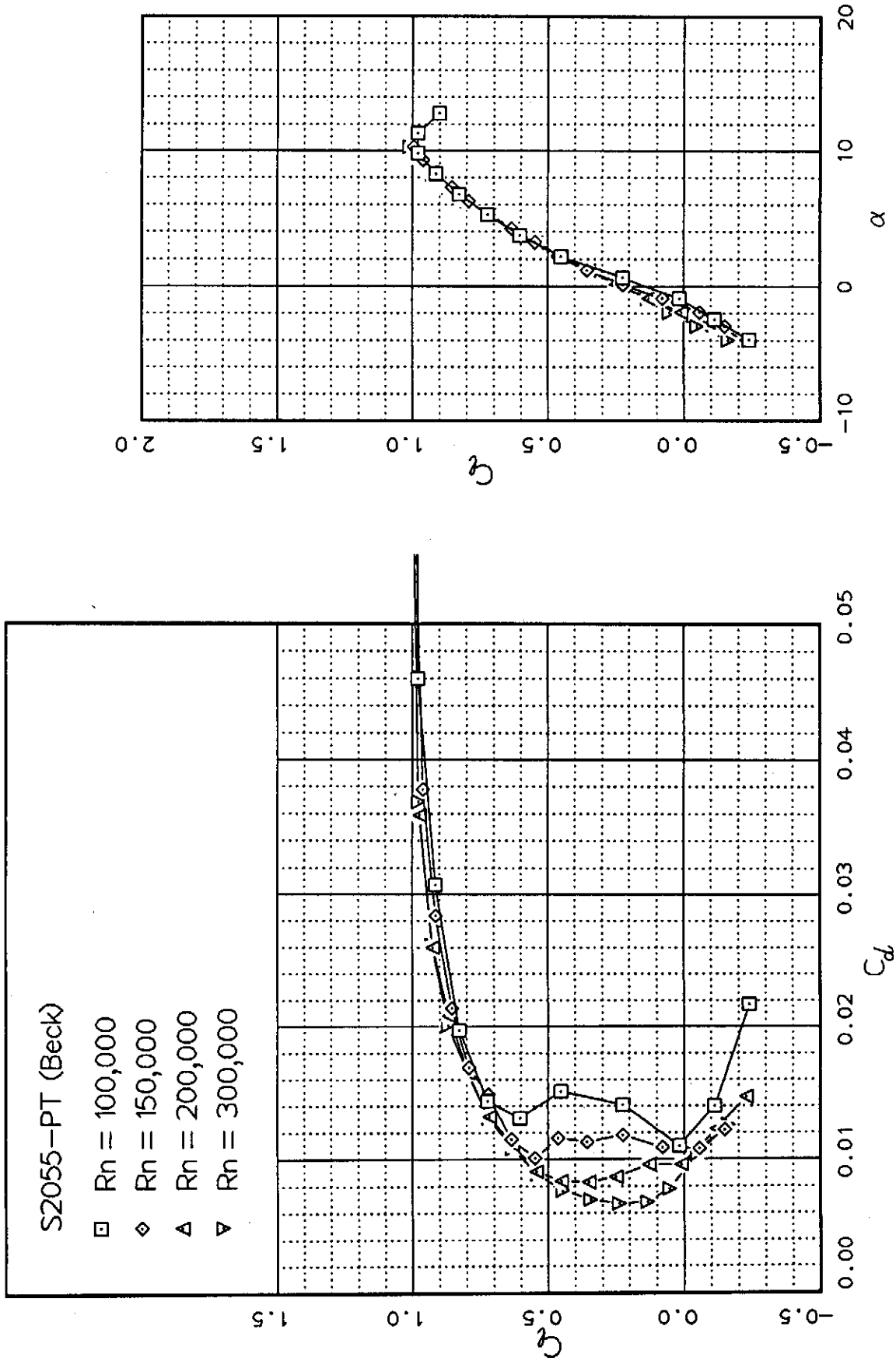
S2055-PT (Beck)
Rn = 100,000
Rn = 150,000
Rn = 200,000
Rn = 300,000
−0.5
0.0
0.5
1.0
1.5
2.0
−10
0
10
20
α
0.00
0.01
0.02
0.03
0.04
0.05
C_d
C_l

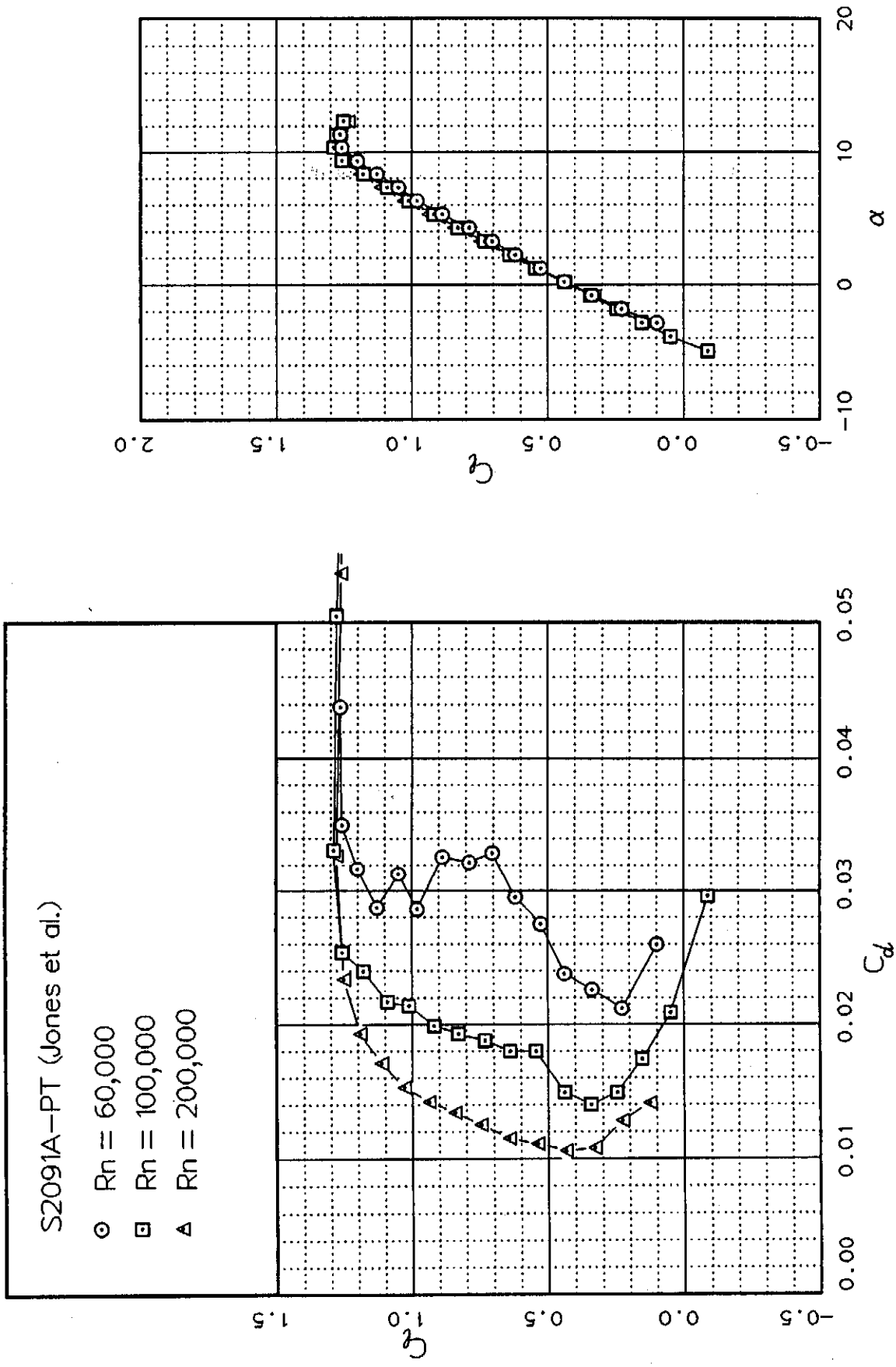
α
20
10
0
−10
−0.5
0.0
0.5
1.0
1.5
2.0
C_l
S2091A–PT (Jones et al.)
Rn = 60,000
Rn = 100,000
Rn = 200,000
C_d
0.00
0.01
0.02
0.03
0.04
0.05

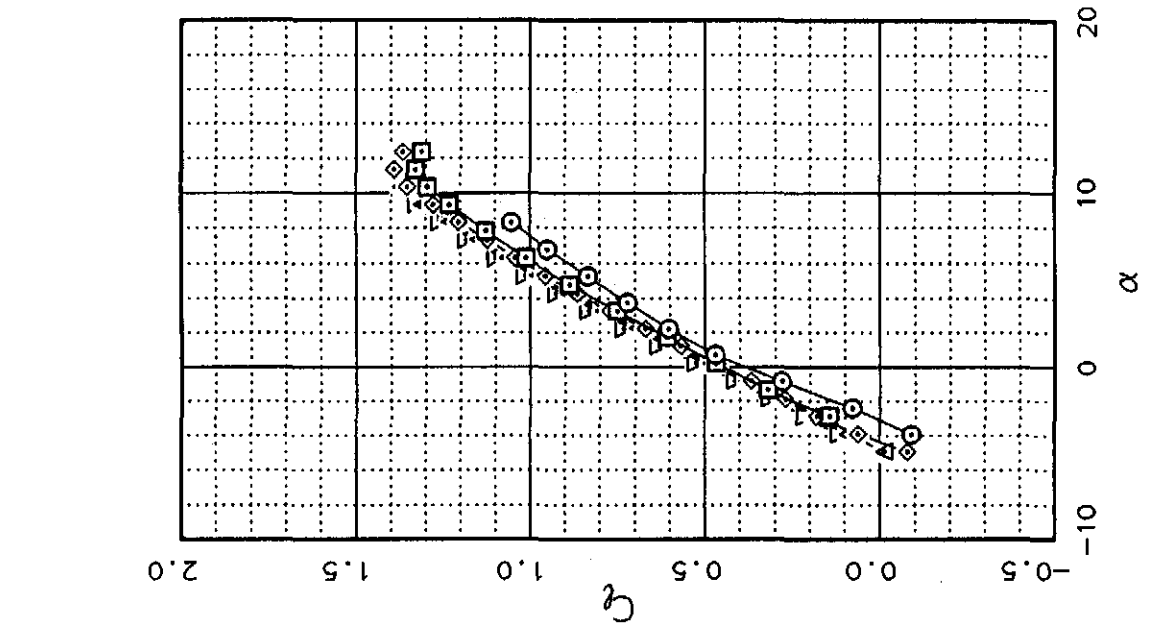
20
10
0
−10
α
−0.5
0.0
0.5
1.0
1.5
2.0
c_l

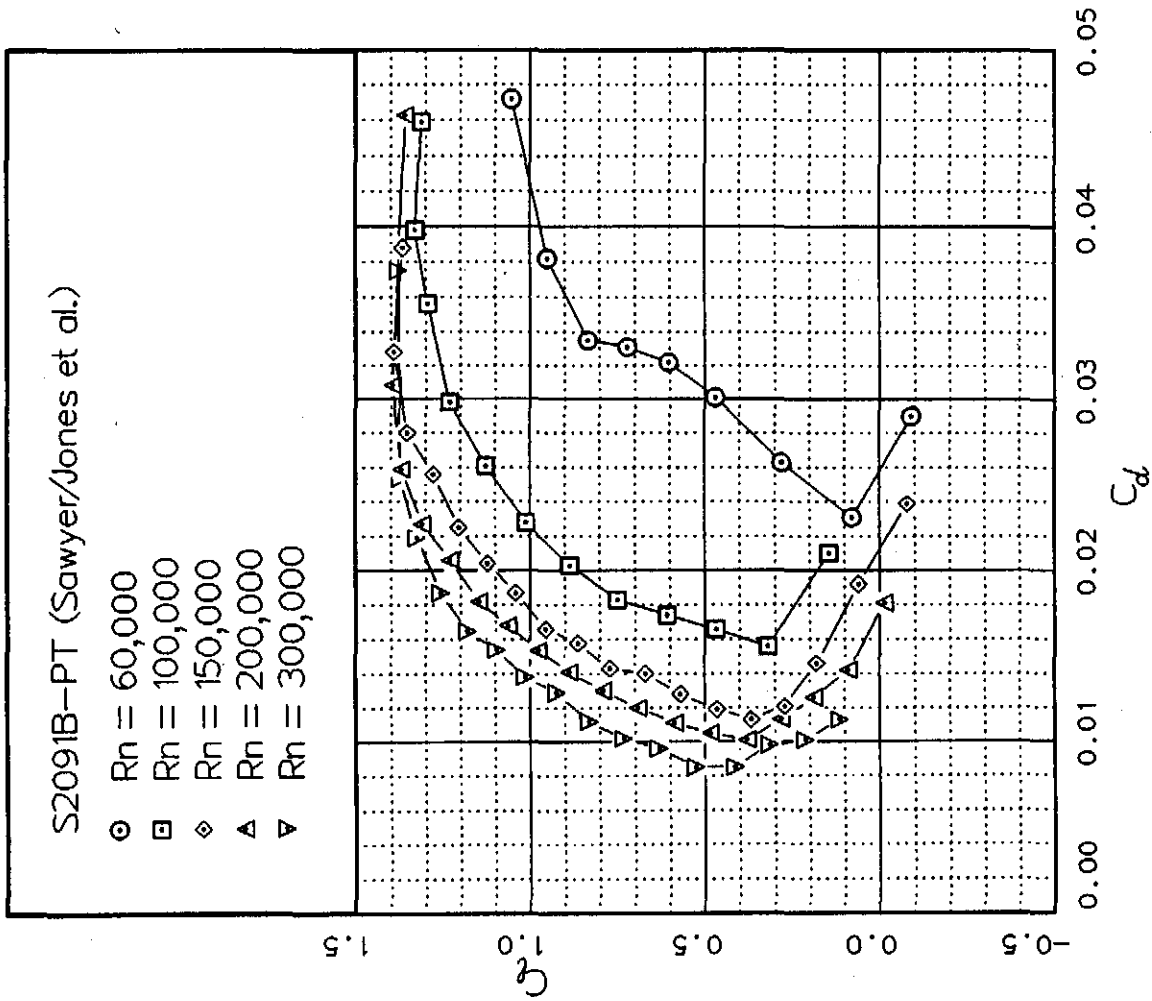
S2091B–PT (Sawyer/Jones et al.)
Rn = 60,000
Rn = 100,000
Rn = 150,000
Rn = 200,000
Rn = 300,000
0.05
0.04
0.03
0.02
0.01
0.00
C_d
−0.5
0.0
0.5
1.0
1.5
c_l

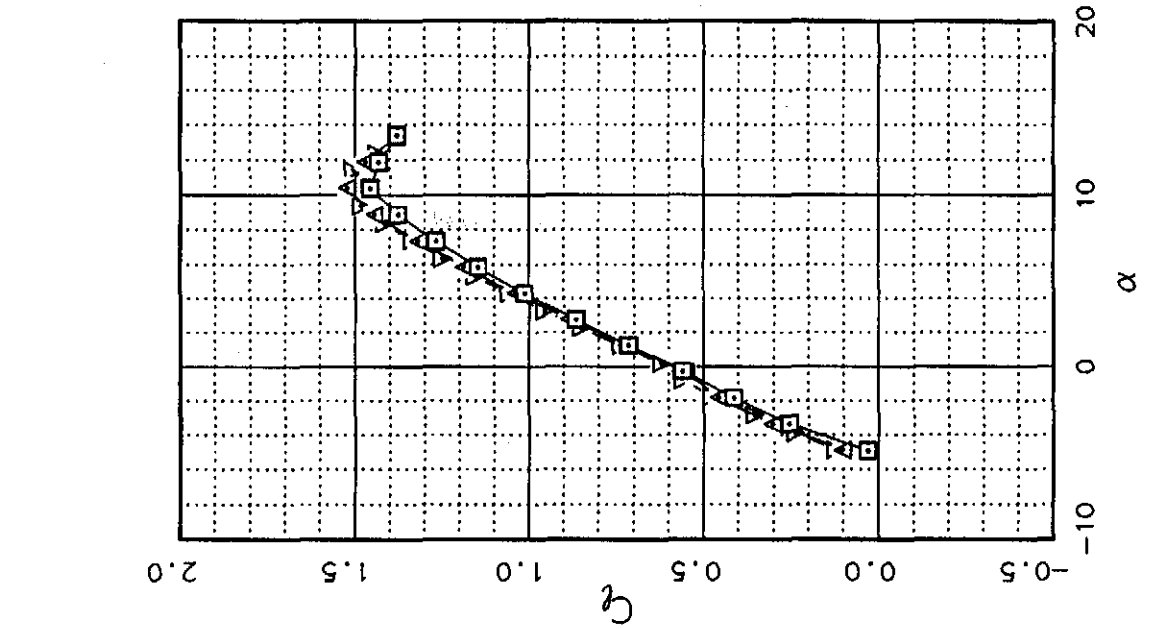
20
10
0
−10
α
−0.5
0.0
0.5
1.0
1.5
2.0
cl

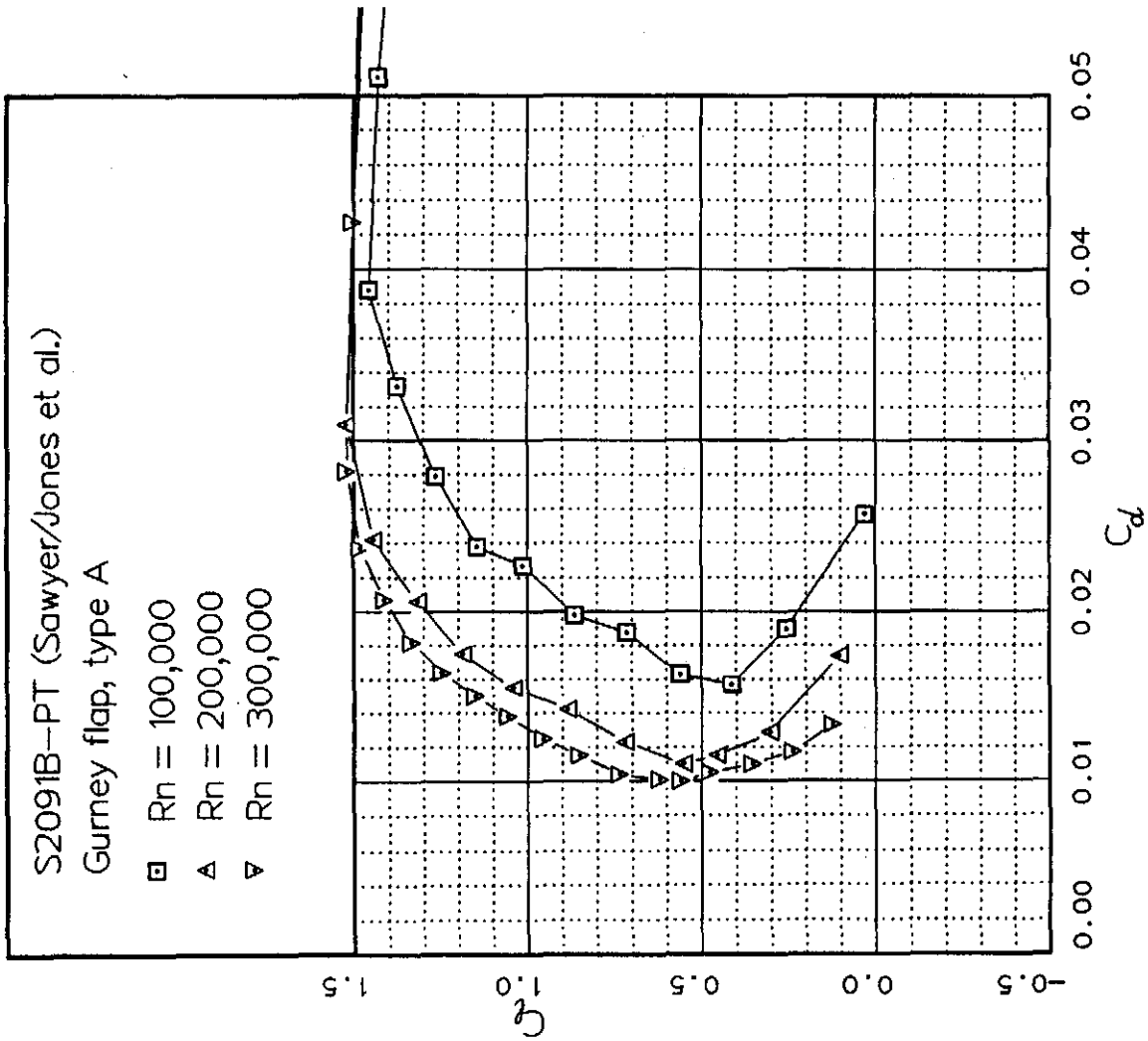
S2091B–PT (Sawyer/Jones et al.)
Gurney flap, type A
Rn = 100,000
Rn = 200,000
Rn = 300,000
0.05
0.04
0.03
0.02
0.01
0.00
cd
−0.5
0.0
0.5
1.0
1.5
cl

Fig. 12.82

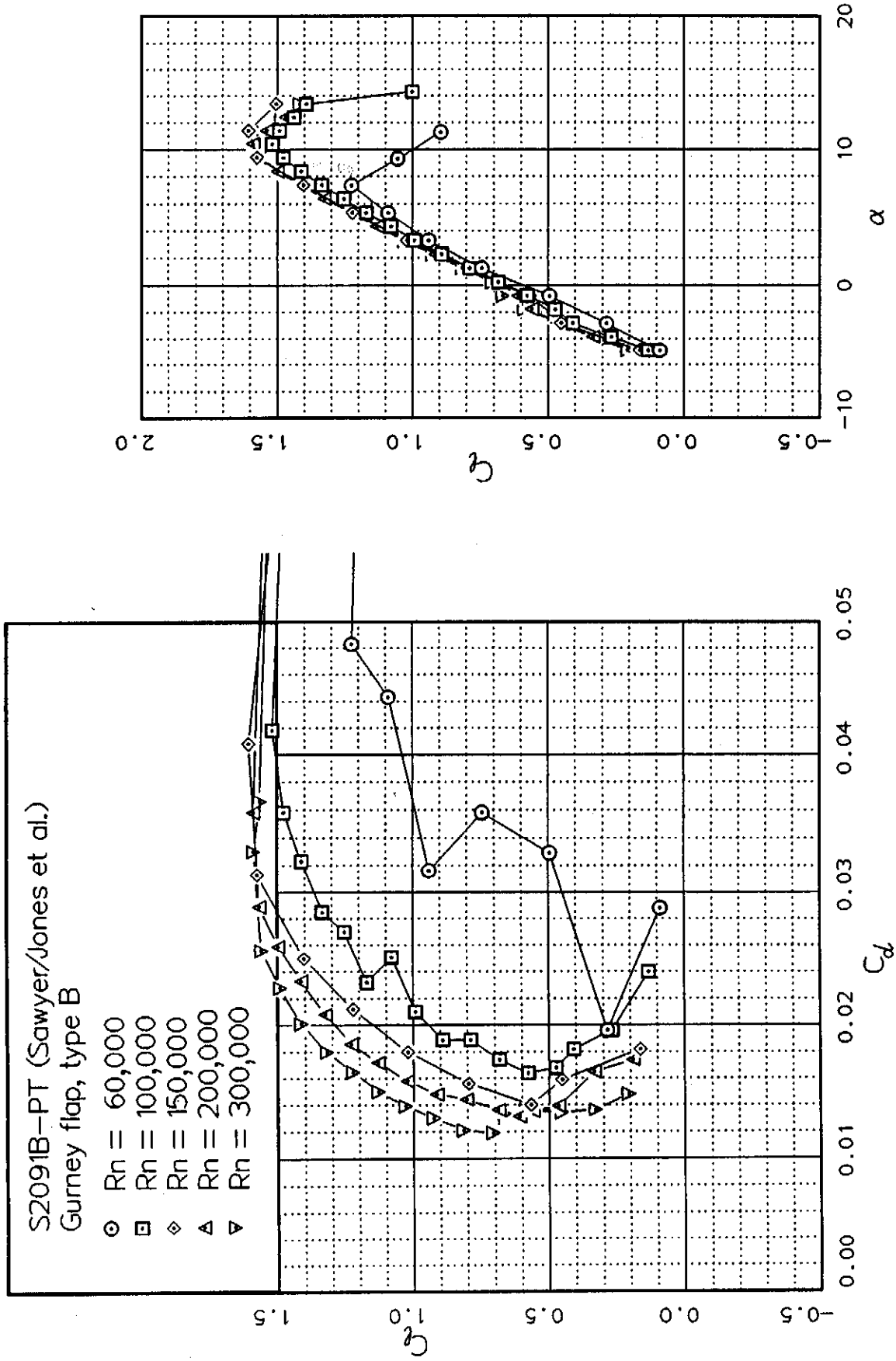
S2091B–PT (Sawyer/Jones et al.)
Gurney flap, type B
Rn = 60,000
Rn = 100,000
Rn = 150,000
Rn = 200,000
Rn = 300,000
α
C_l
C_d
20
10
0
−10
−0.5
0.0
0.5
1.0
1.5
2.0
0.00
0.01
0.02
0.03
0.04
0.05

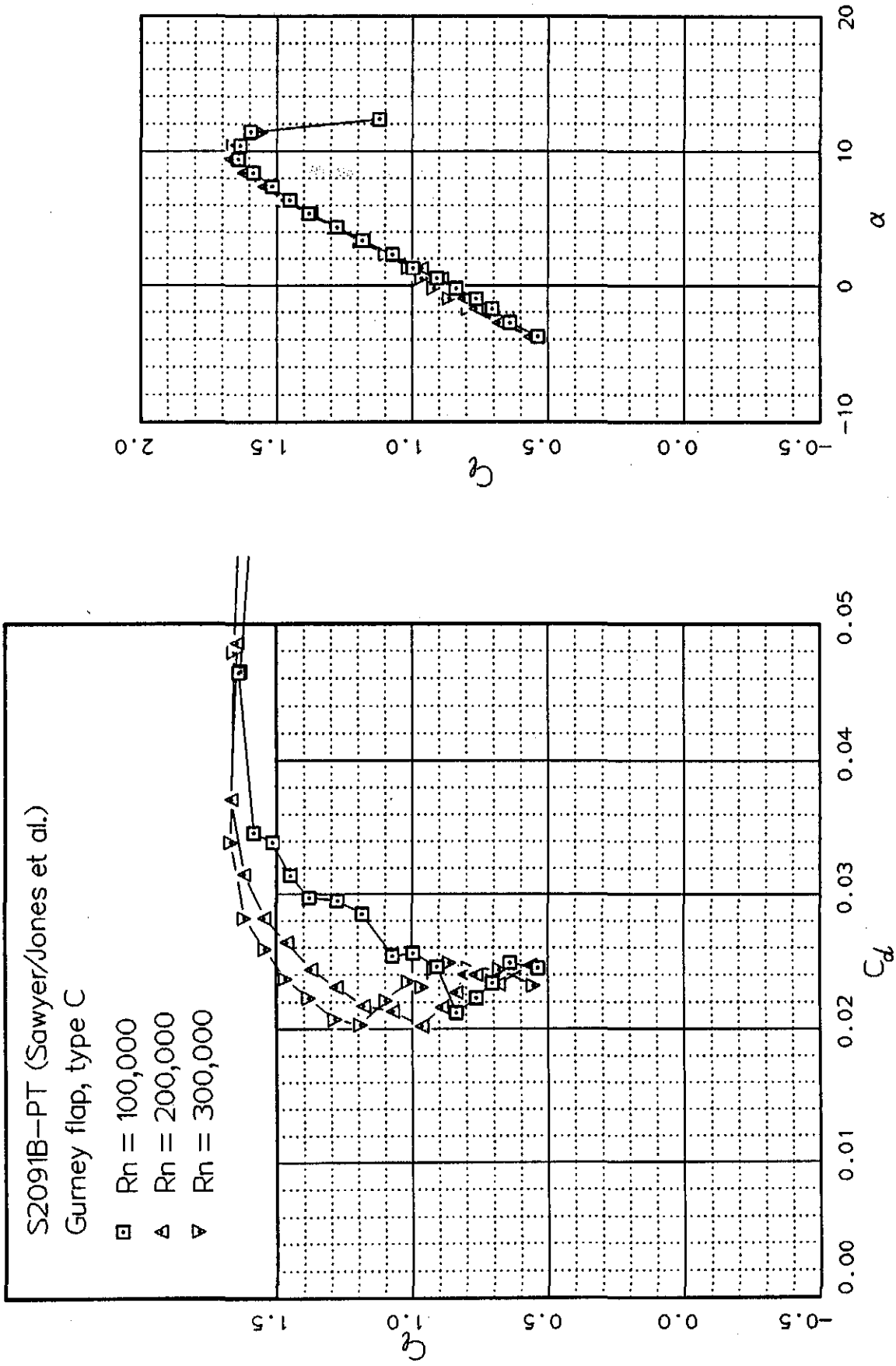
S2091B–PT (Sawyer/Jones et al.)
Gurney flap, type C
Rn = 100,000
Rn = 200,000
Rn = 300,000
α
C_d
C_l
20
10
0
−10
0.05
0.04
0.03
0.02
0.01
0.00
−0.5
0.0
0.5
1.0
1.5
2.0

Fig. 12.84

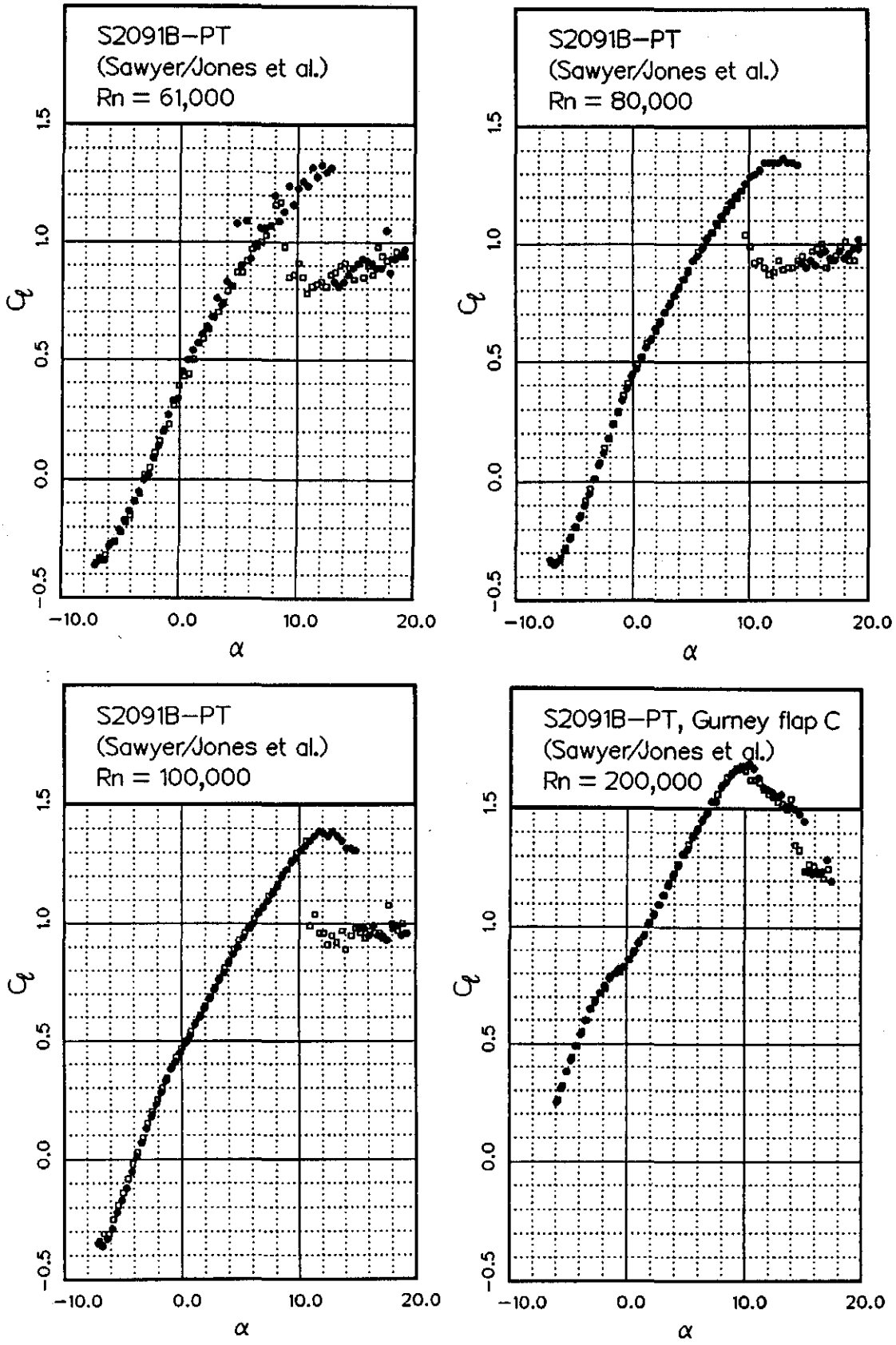
S2091B–PT
(Sawyer/Jones et al.)
Rn = 61,000
S2091B–PT
(Sawyer/Jones et al.)
Rn = 80,000
S2091B–PT
(Sawyer/Jones et al.)
Rn = 100,000
S2091B–PT, Gurney flap C
(Sawyer/Jones et al.)
Rn = 200,000
C_ℓ
α
1.5
1.0
0.5
0.0
−0.5
−10.0
0.0
10.0
20.0

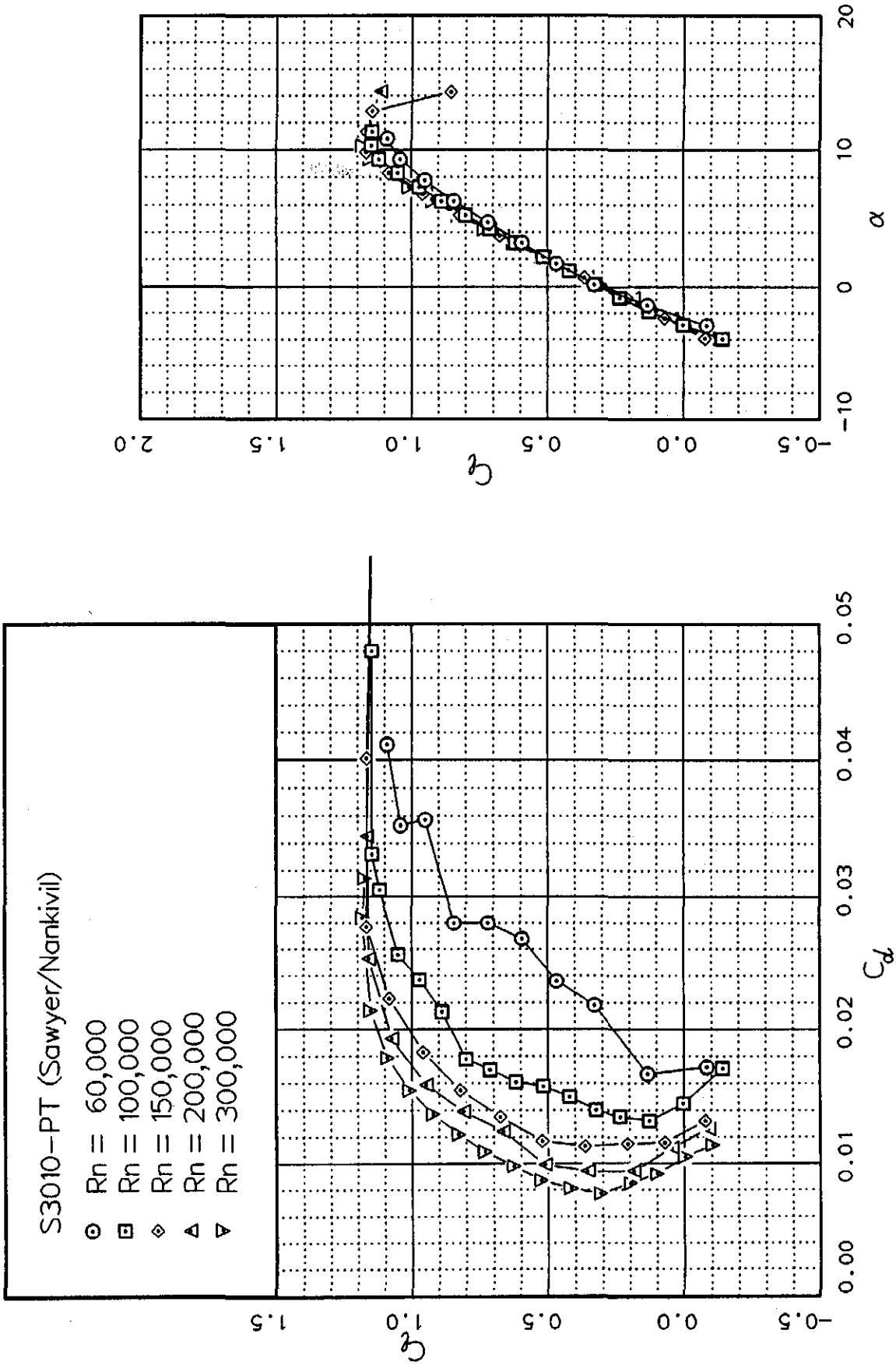
S3010-PT (Sawyer/Nankivil)
Rn = 60,000
Rn = 100,000
Rn = 150,000
Rn = 200,000
Rn = 300,000
C_l
C_d
α

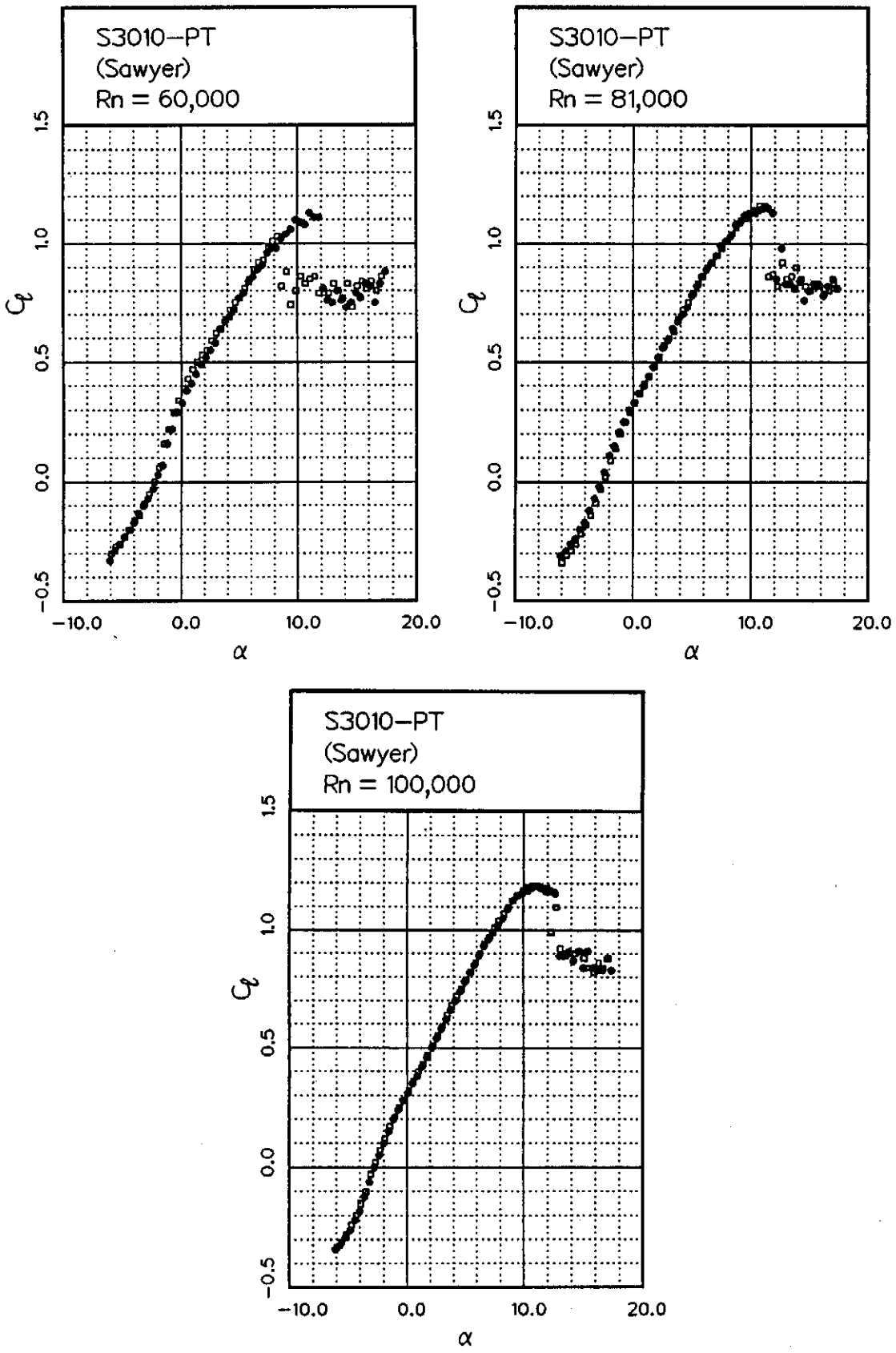
S3010–PT
(Sawyer)
Rn = 60,000
S3010–PT
(Sawyer)
Rn = 81,000
S3010–PT
(Sawyer)
Rn = 100,000
C_ℓ
α
1.5
1.0
0.5
0.0
−0.5
−10.0
0.0
10.0
20.0

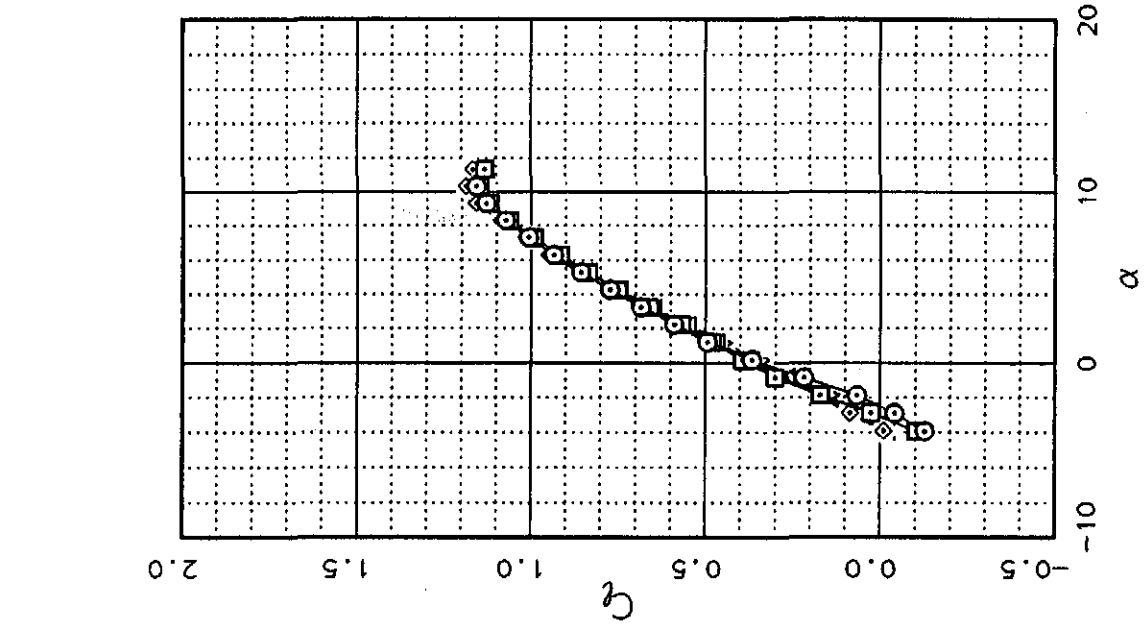
20
10
0
−10
α
−0.5
0.0
0.5
1.0
1.5
2.0
Cl

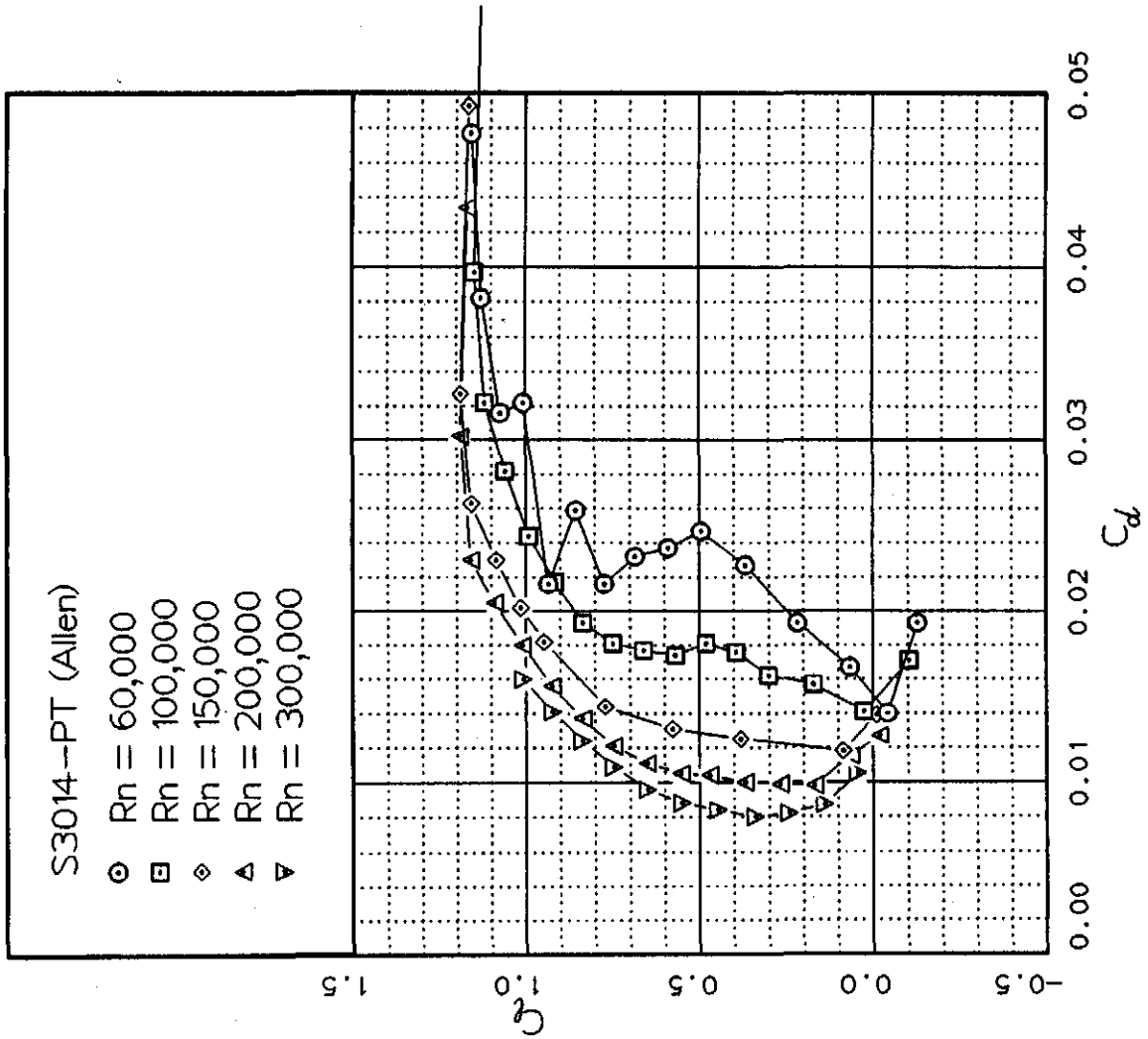
S3014–PT (Allen)
Rn = 60,000
Rn = 100,000
Rn = 150,000
Rn = 200,000
Rn = 300,000
0.05
0.04
0.03
0.02
0.01
0.00
Cd
−0.5
0.0
0.5
1.0
1.5
Cl

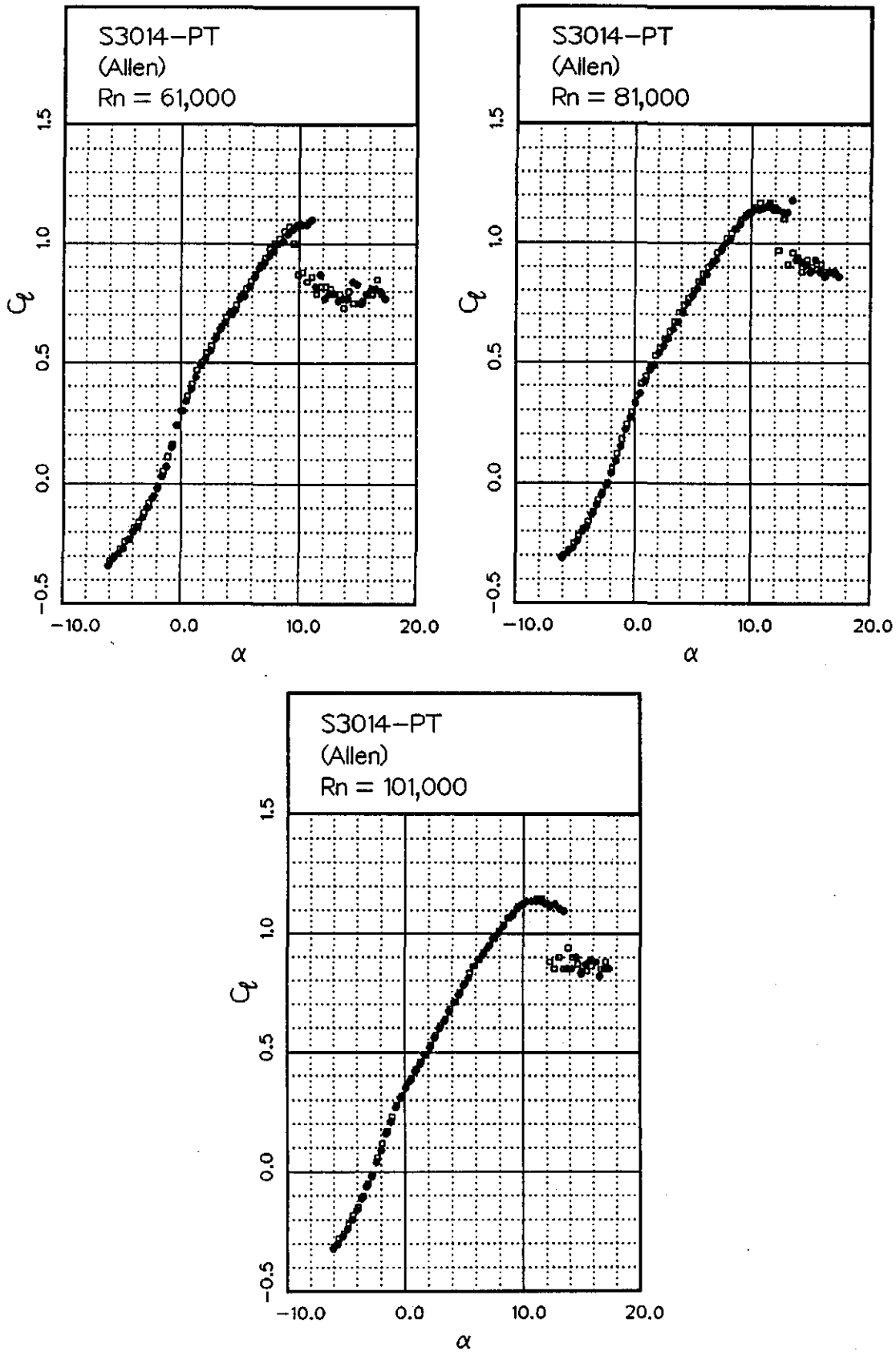
S3014–PT
(Allen)
Rn = 61,000
S3014–PT
(Allen)
Rn = 81,000
S3014–PT
(Allen)
Rn = 101,000
C_ℓ
α
1.5
1.0
0.5
0.0
−0.5
−10.0
0.0
10.0
20.0

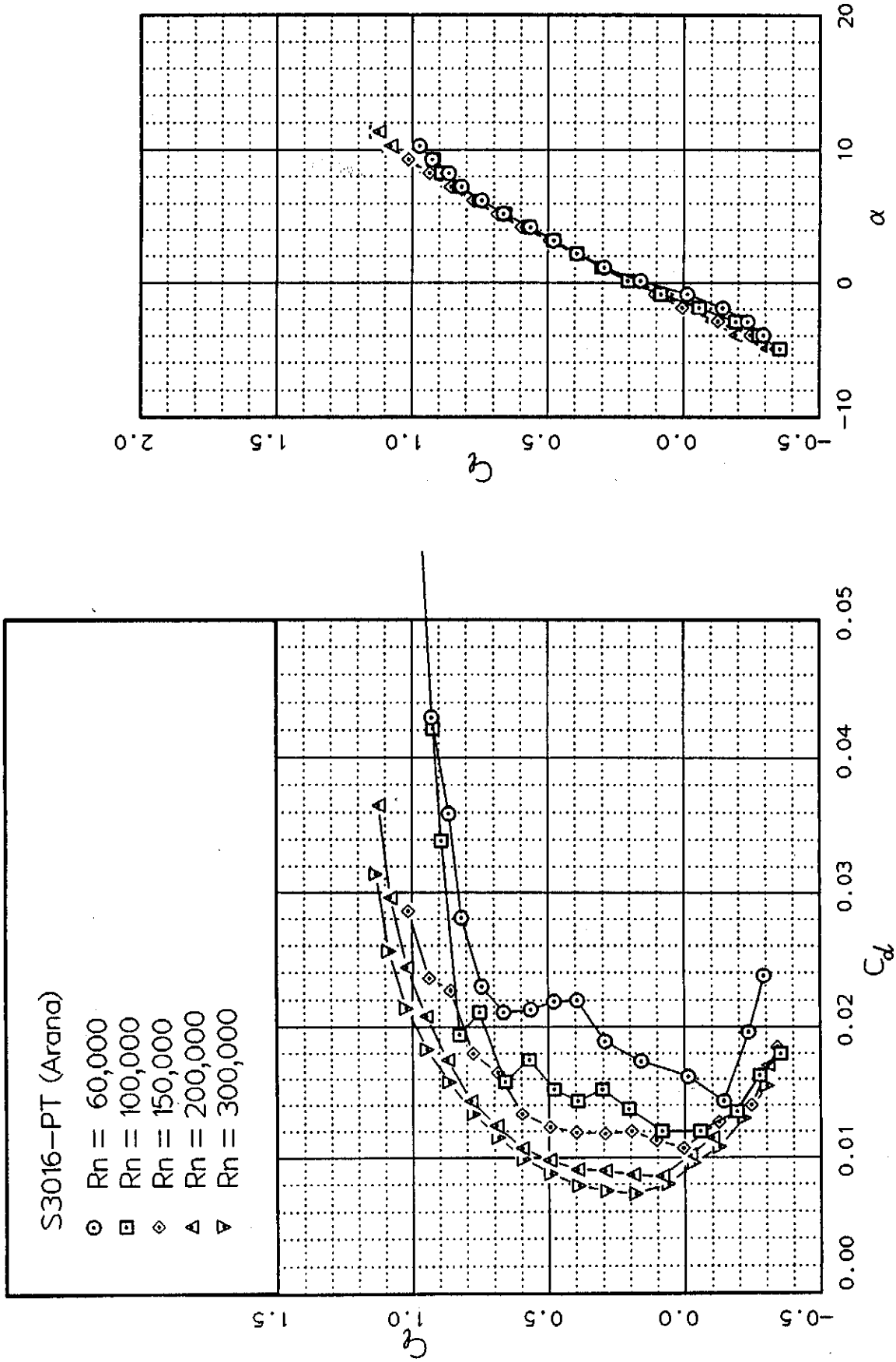
S3016–PT (Arana)
Rn = 60,000
Rn = 100,000
Rn = 150,000
Rn = 200,000
Rn = 300,000
C_l
C_d
α

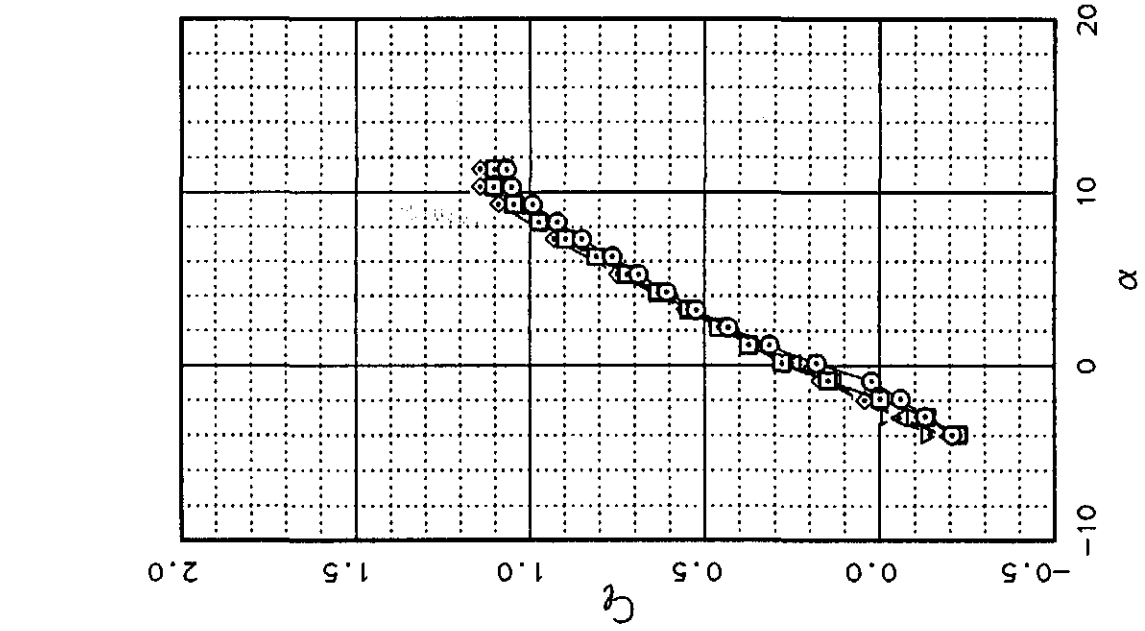
20
10
0
−10
α
−0.5
0.0
0.5
1.0
1.5
2.0
C_l

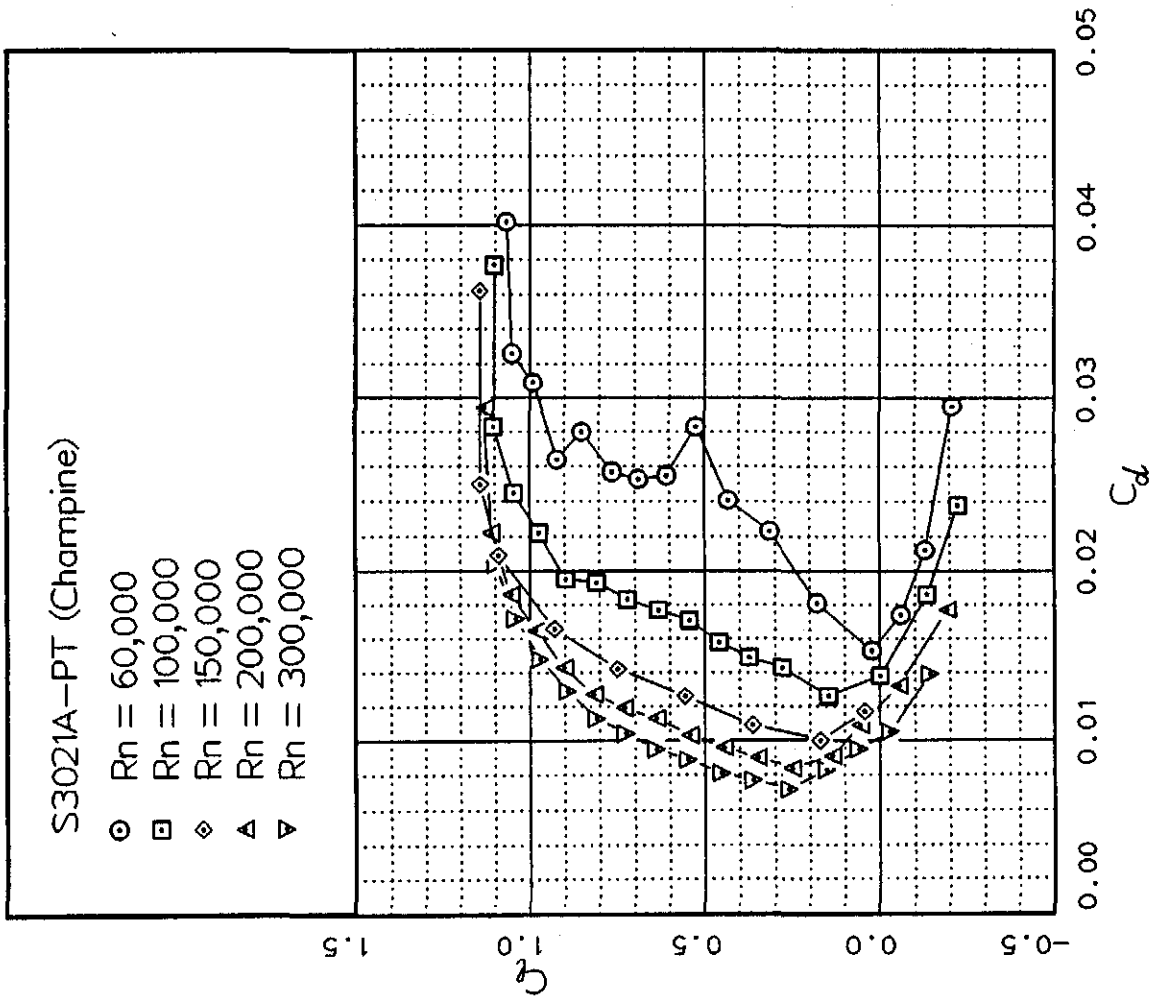
S3021A–PT (Champine)
Rn = 60,000
Rn = 100,000
Rn = 150,000
Rn = 200,000
Rn = 300,000
0.05
0.04
0.03
0.02
0.01
0.00
C_d
−0.5
0.0
0.5
1.0
1.5
C_l

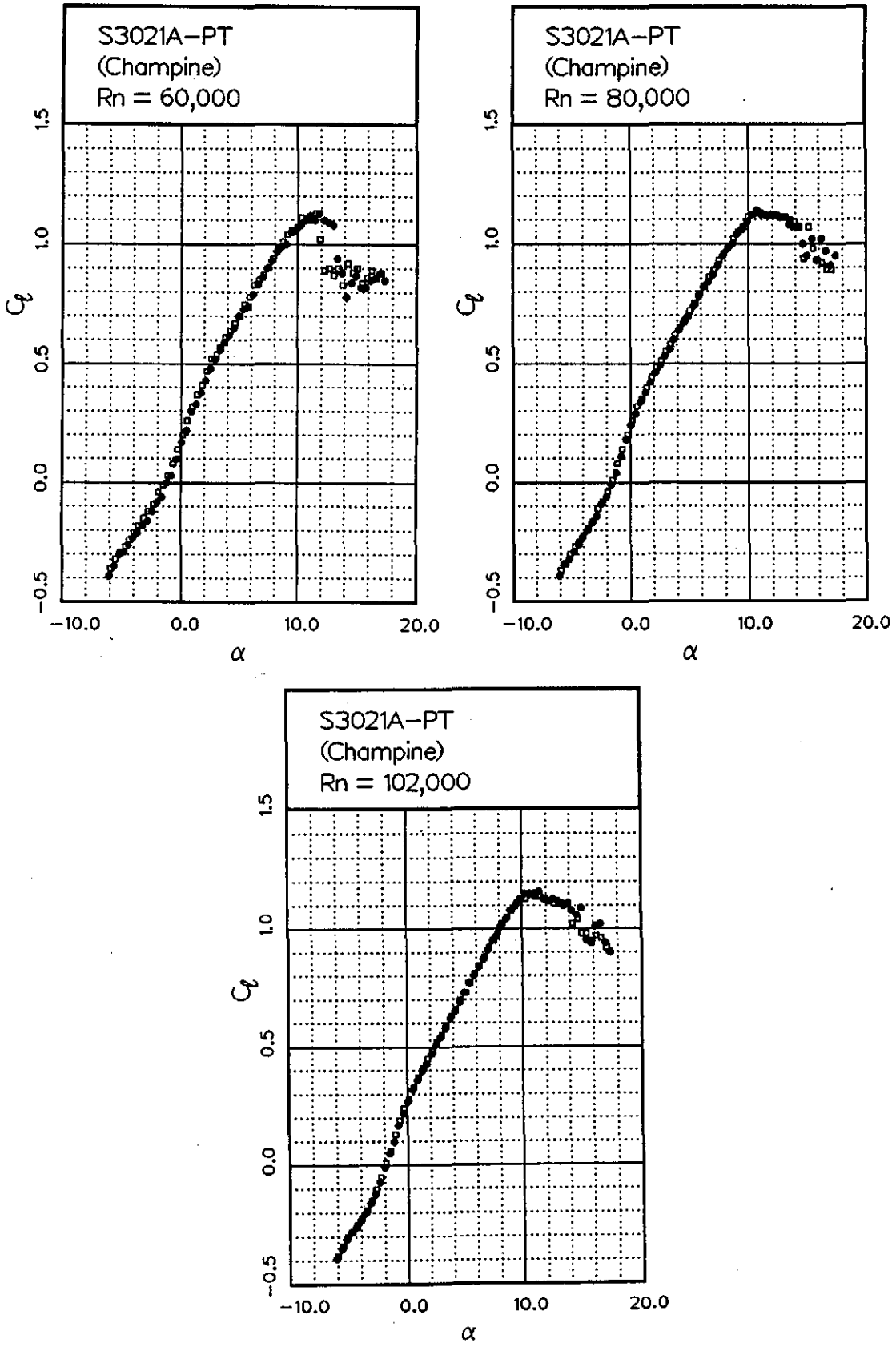
S3021A–PT
(Champine)
Rn = 60,000
S3021A–PT
(Champine)
Rn = 80,000
S3021A–PT
(Champine)
Rn = 102,000
C_ℓ
α
1.5
1.0
0.5
0.0
−0.5
−10.0
0.0
10.0
20.0

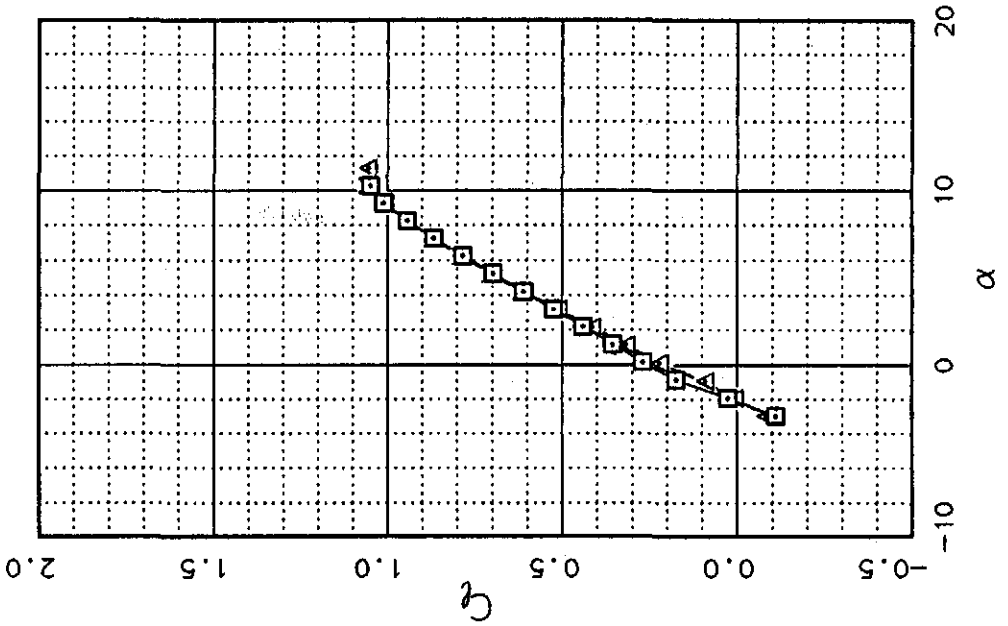
20
10
0
−10
α
−0.5
0.0
0.5
1.0
1.5
2.0
cl

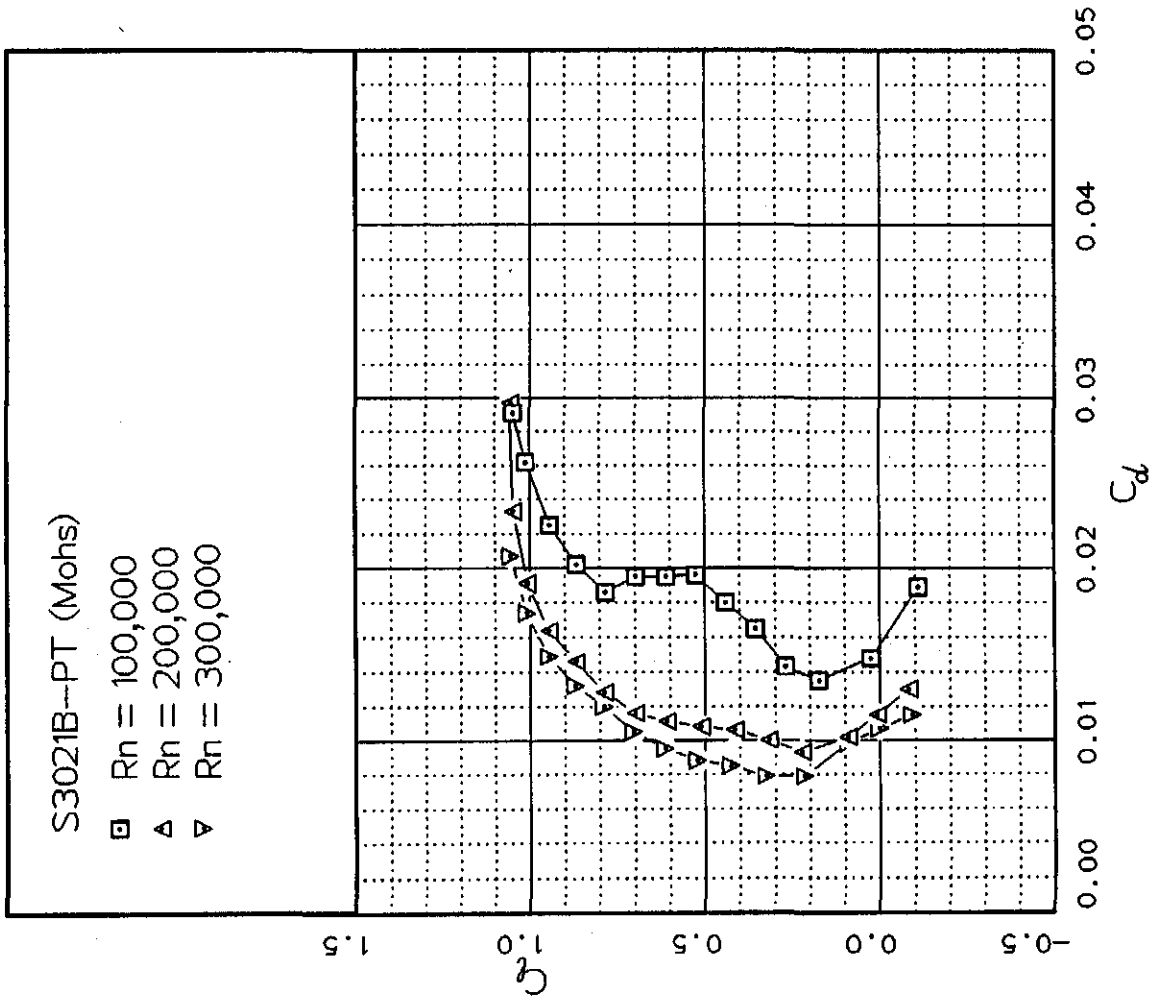
S3021B--PT (Mohs)
Rn = 100,000
Rn = 200,000
Rn = 300,000
0.05
0.04
0.03
0.02
0.01
0.00
Cd
−0.5
0.0
0.5
1.0
1.5
cl

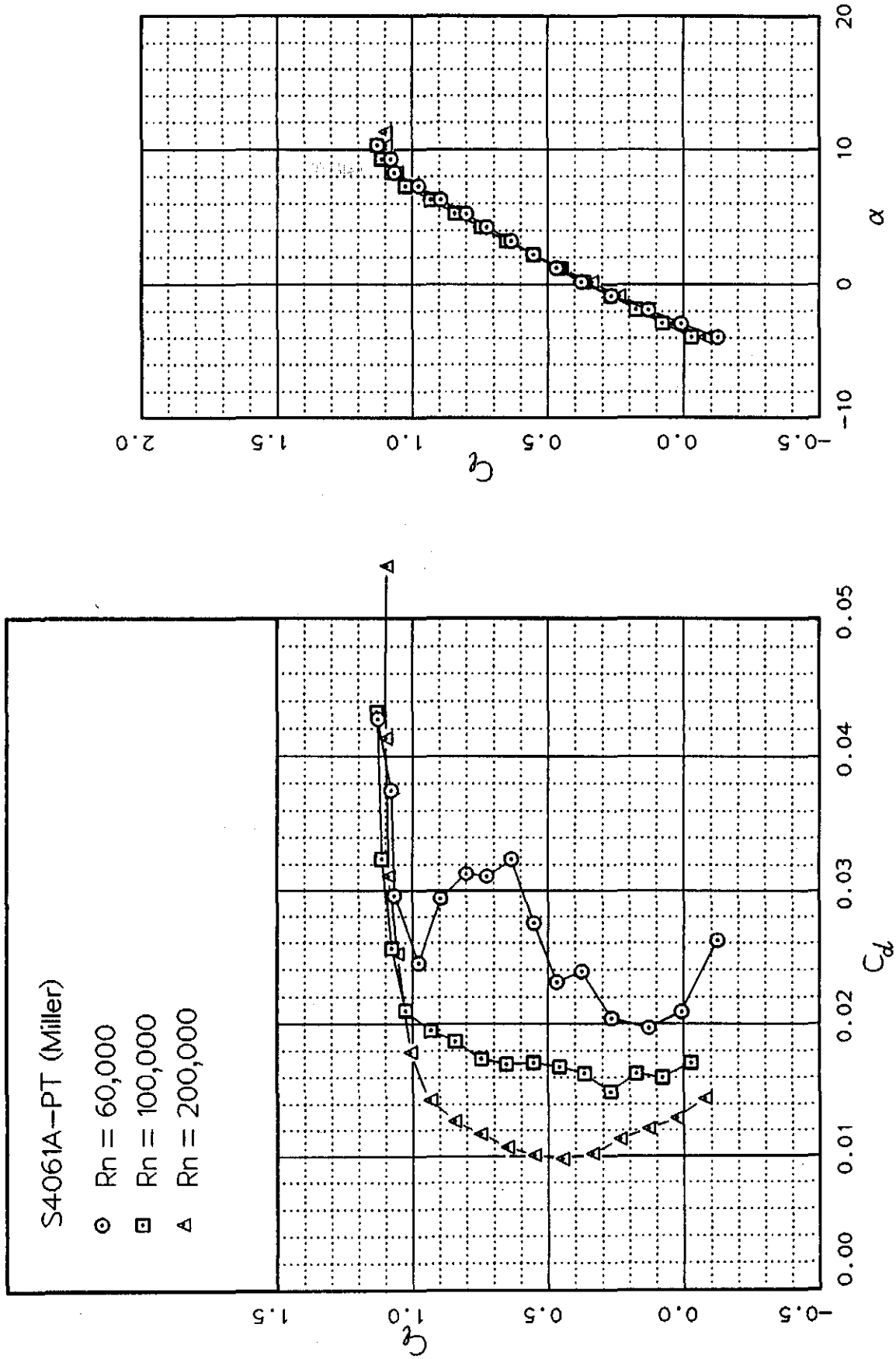
S4061A–PT (Miller)
Rn = 60,000
Rn = 100,000
Rn = 200,000
C_l
C_d
α
−0.5
0.0
0.5
1.0
1.5
2.0
0.00
0.01
0.02
0.03
0.04
0.05
−10
0
10
20

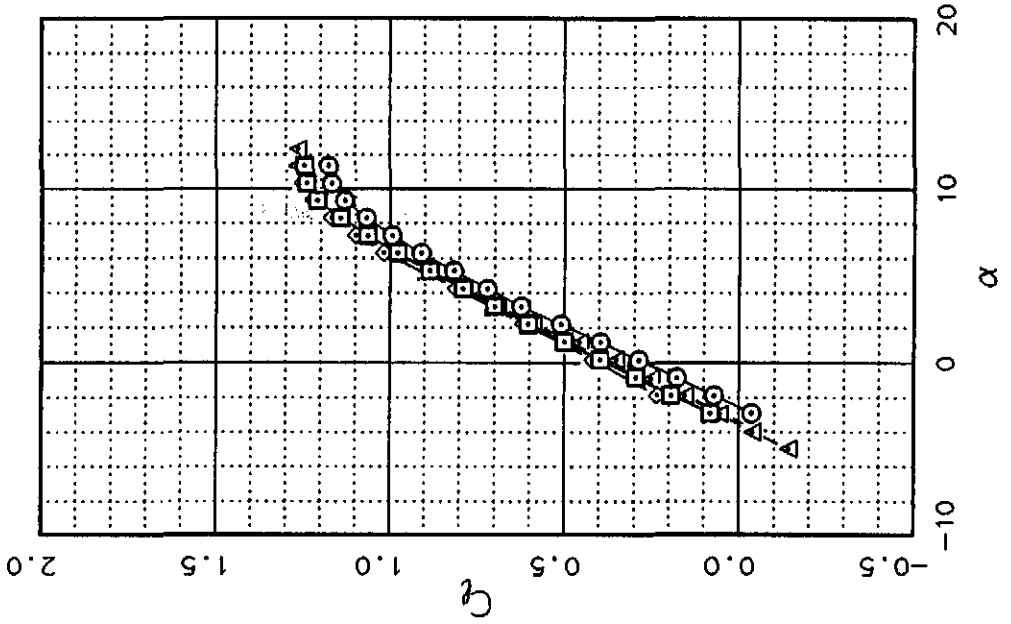
20
10
0
−10
α
−0.5
0.0
0.5
1.0
1.5
2.0
cl

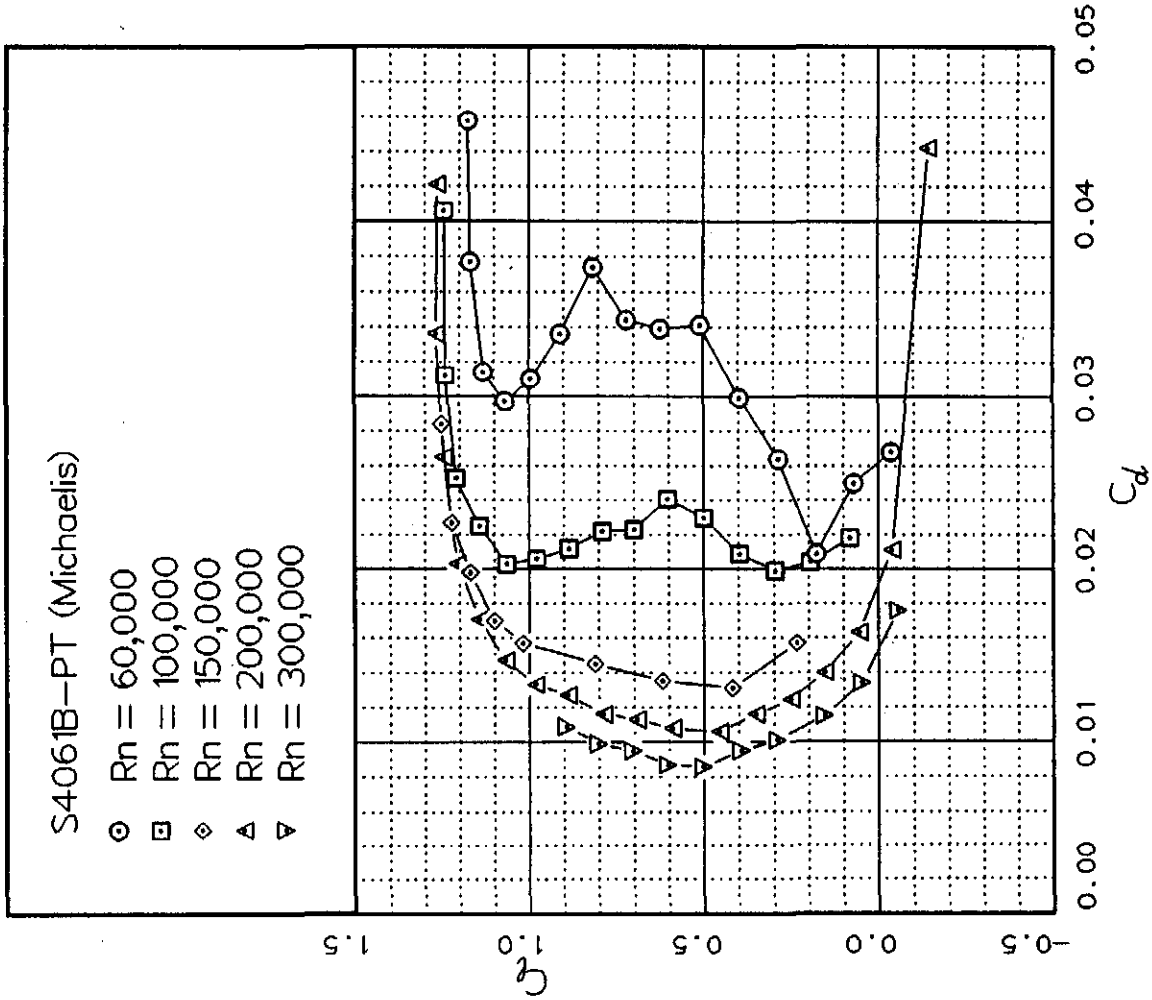
S4061B–PT (Michaelis)
Rn = 60,000
Rn = 100,000
Rn = 150,000
Rn = 200,000
Rn = 300,000
0.05
0.04
0.03
0.02
0.01
0.00
Cd
−0.5
0.0
0.5
1.0
1.5
cl

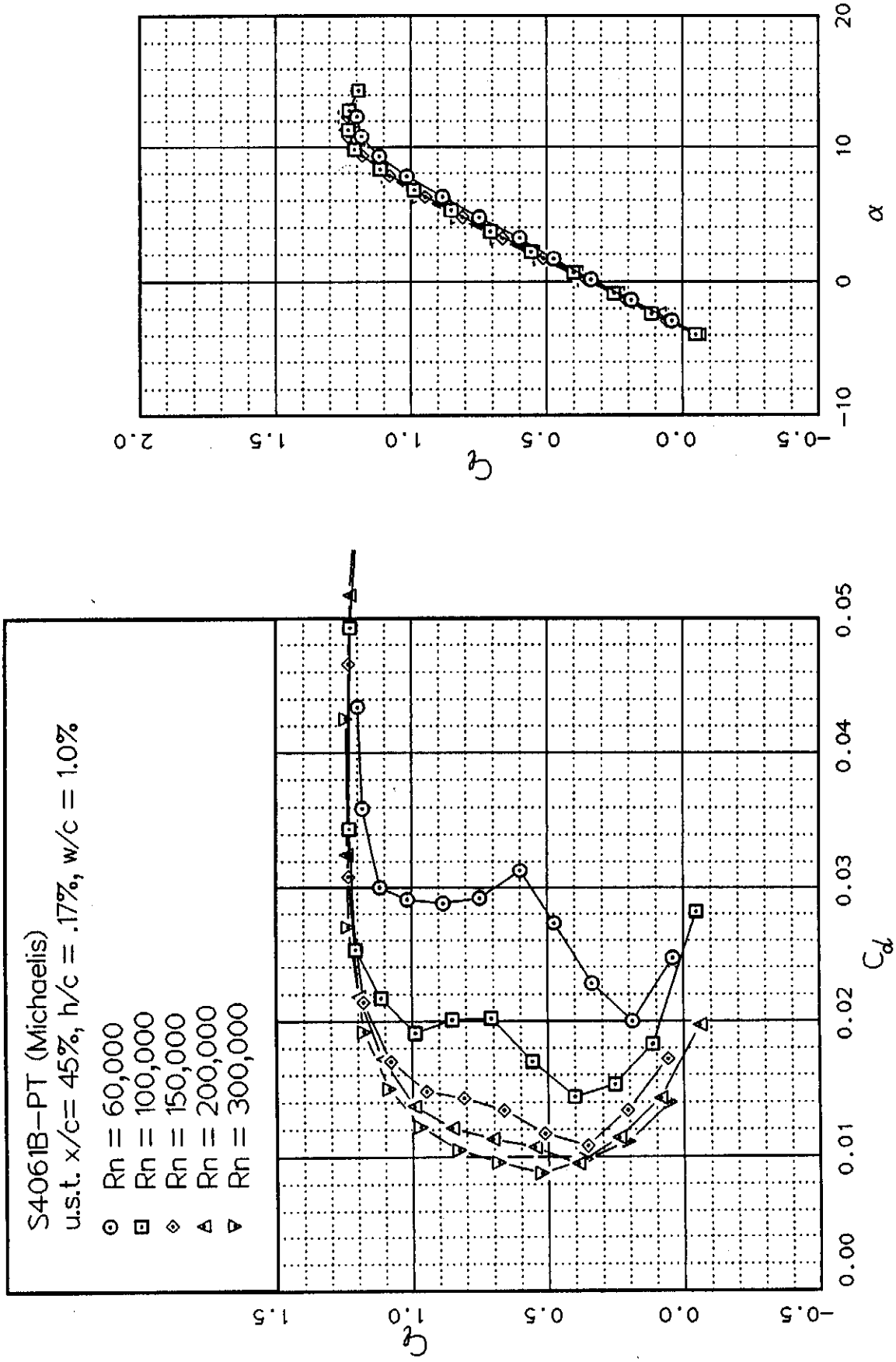
S4061B–PT (Michaelis)
u.s.t. x/c= 45%, h/c = .17%, w/c = 1.0%
Rn = 60,000
Rn = 100,000
Rn = 150,000
Rn = 200,000
Rn = 300,000
α
C_d
C_l
C_l

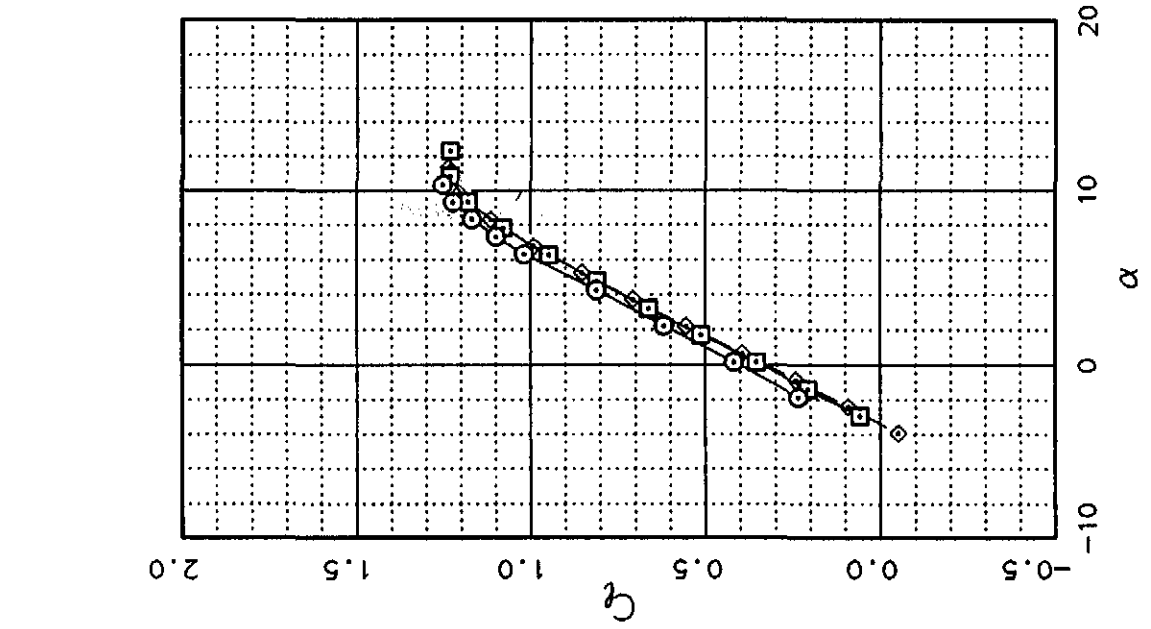
α
20
10
0
−10
−0.5
0.0
0.5
1.0
1.5
2.0
c_l

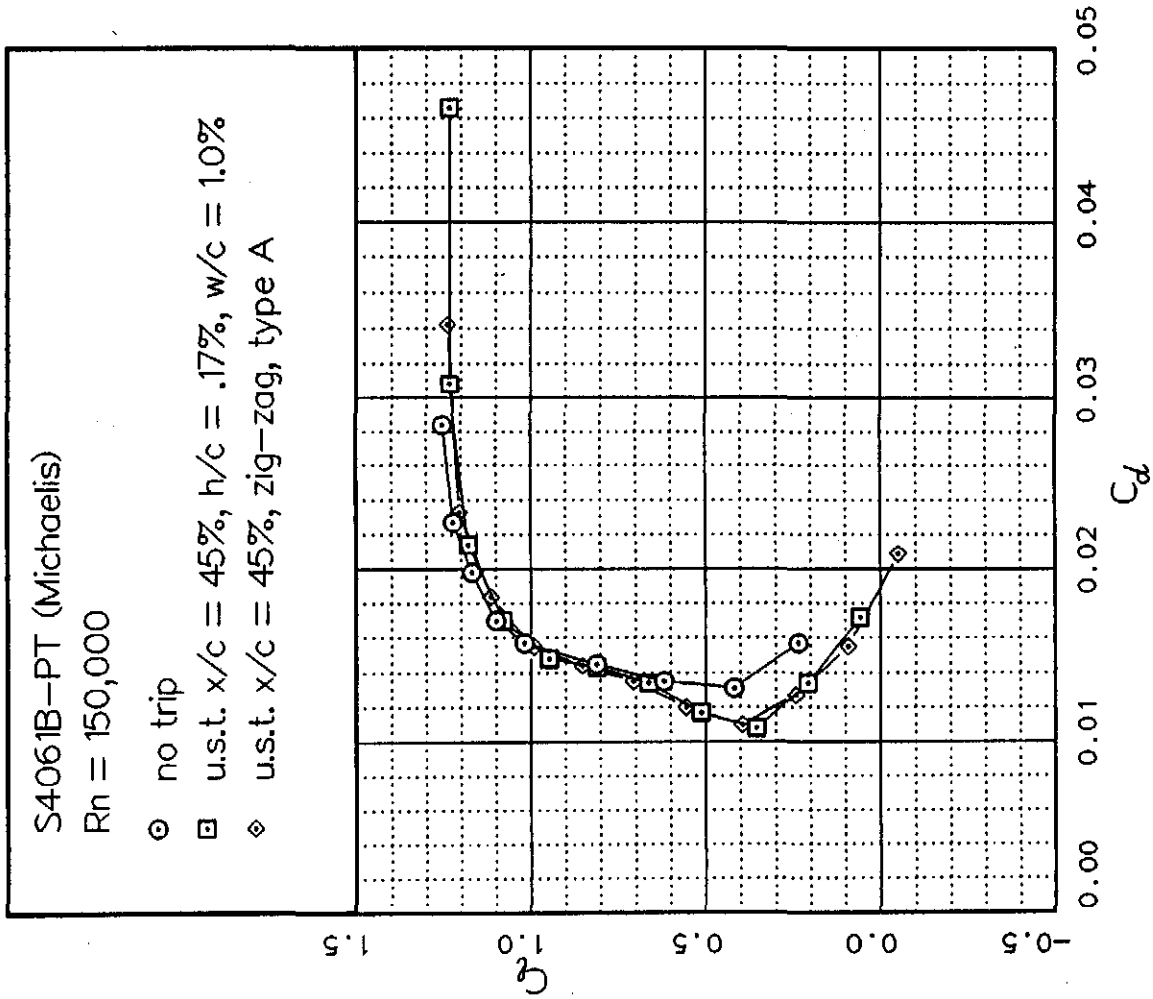
S4061B–PT (Michaelis)
Rn = 150,000
no trip
u.s.t. x/c = 45%, h/c = .17%, w/c = 1.0%
u.s.t. x/c = 45%, zig–zag, type A
c_l
−0.5
0.0
0.5
1.0
1.5
c_d
0.00
0.01
0.02
0.03
0.04
0.05

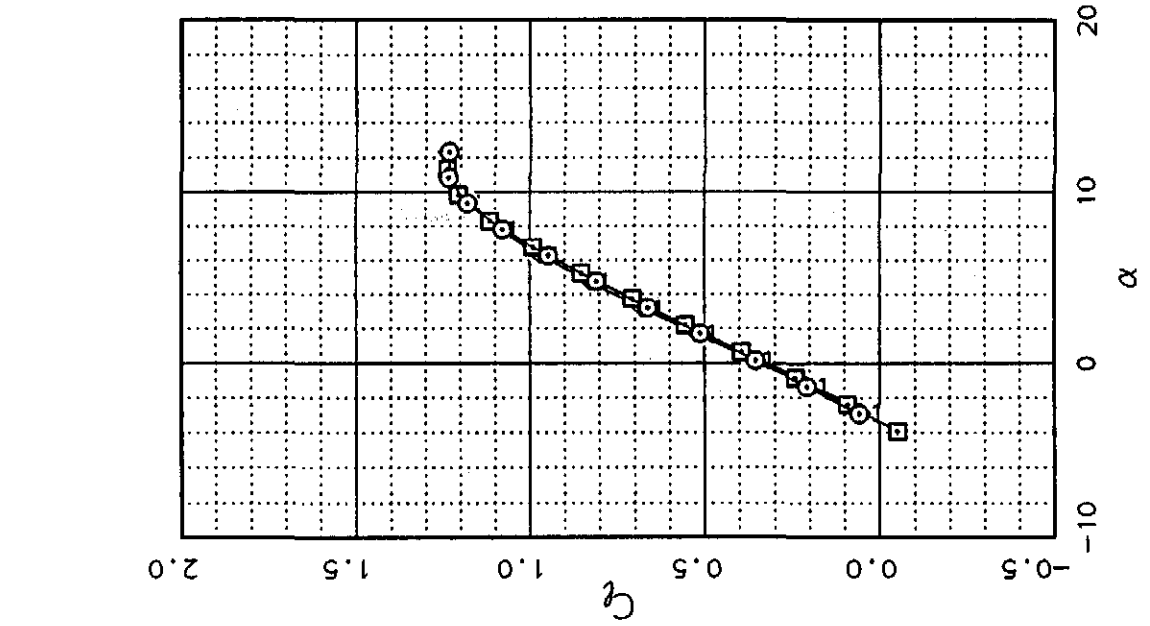
α
20
10
0
−10
−0.5
0.0
0.5
1.0
1.5
2.0
C_l

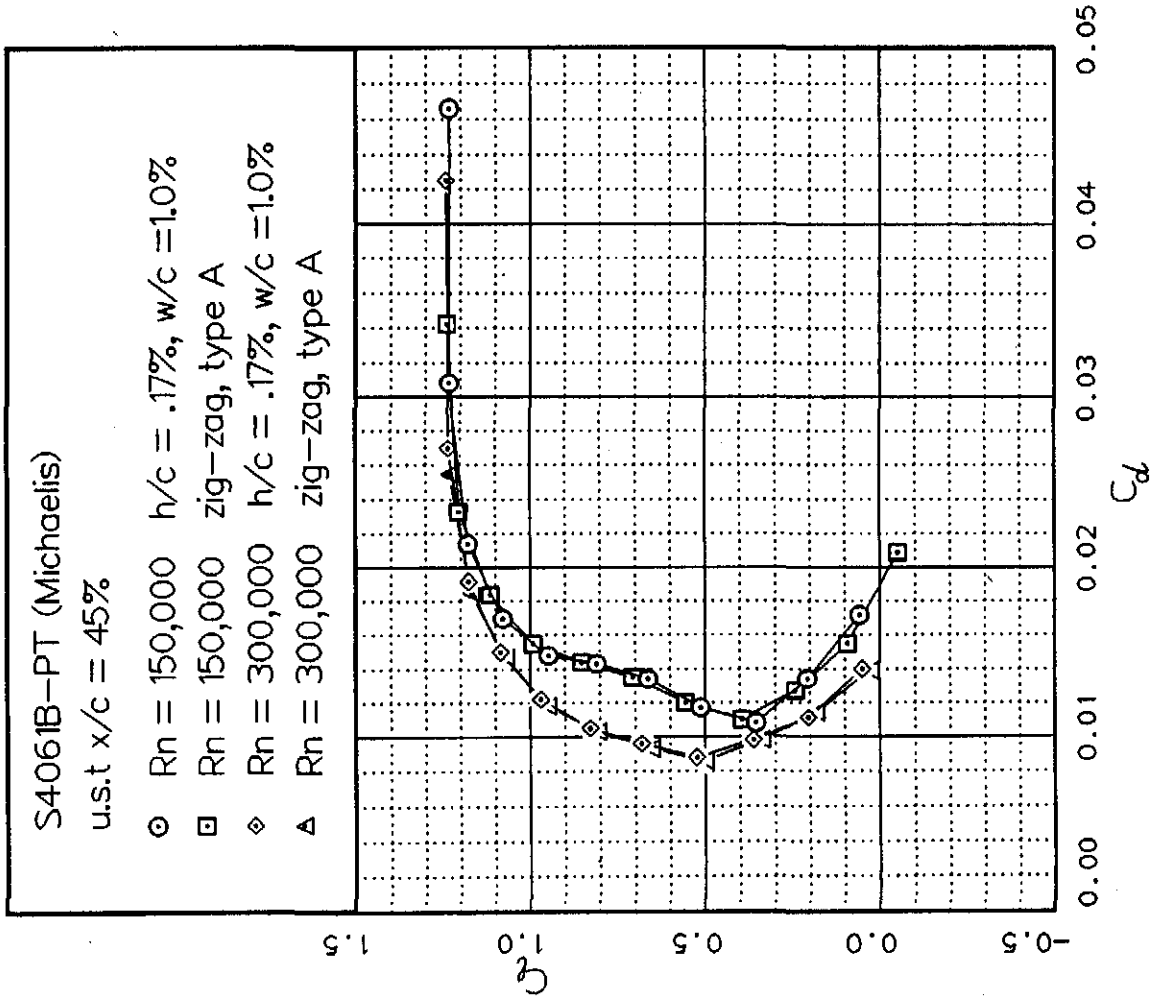
S4061B–PT (Michaelis)
u.s.t x/c = 45%
Rn = 150,000 h/c = .17%, w/c =1.0%
Rn = 150,000 zig–zag, type A
Rn = 300,000 h/c = .17%, w/c =1.0%
Rn = 300,000 zig–zag, type A
0.05
0.04
0.03
0.02
0.01
0.00
−0.5
0.0
0.5
1.0
1.5
C_d
C_l

Fig. 12.98

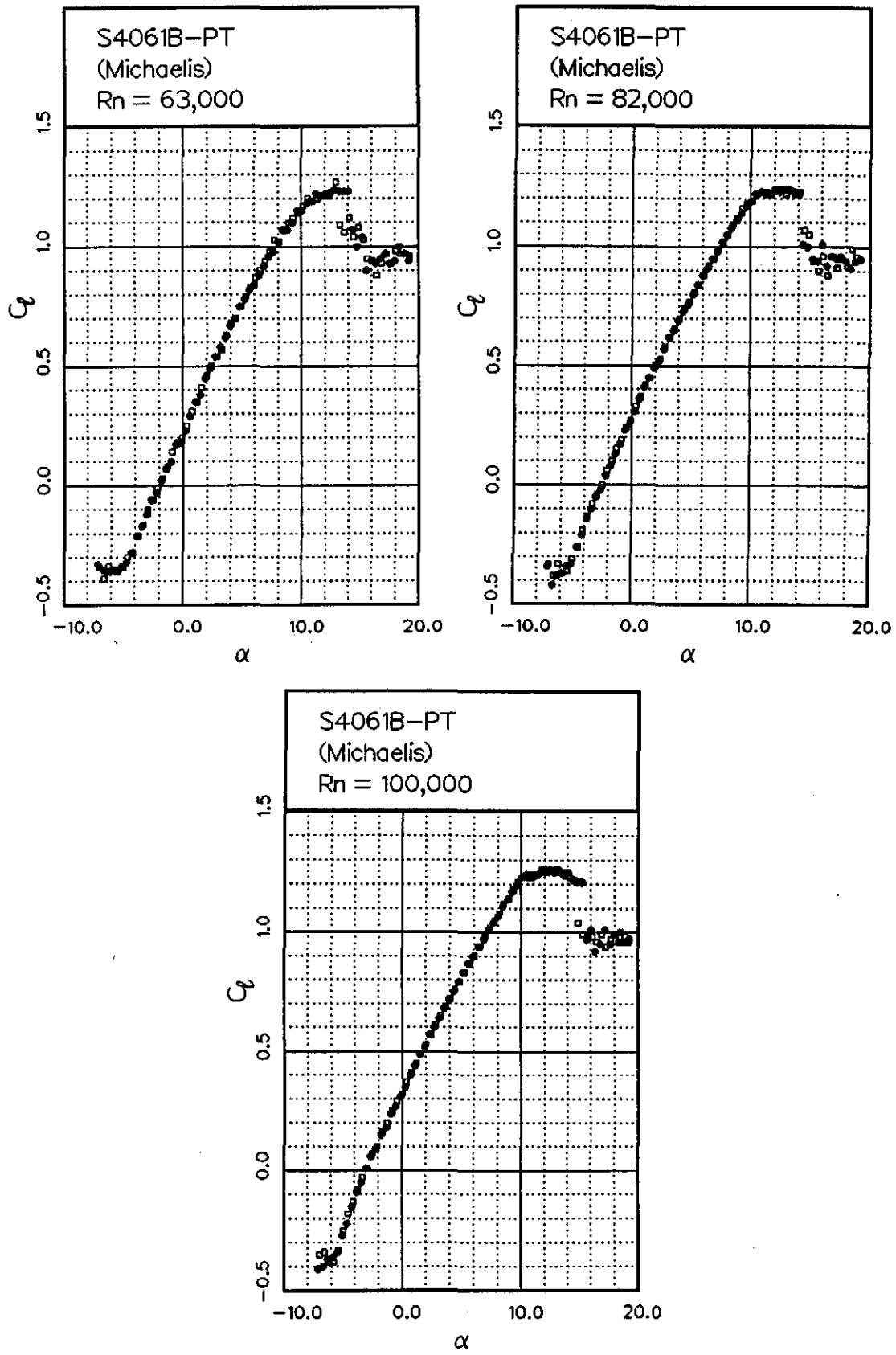
S4061B–PT
(Michaelis)
Rn = 63,000
S4061B–PT
(Michaelis)
Rn = 82,000
S4061B–PT
(Michaelis)
Rn = 100,000
C_ℓ
α
1.5
1.0
0.5
0.0
−0.5
−10.0
0.0
10.0
20.0

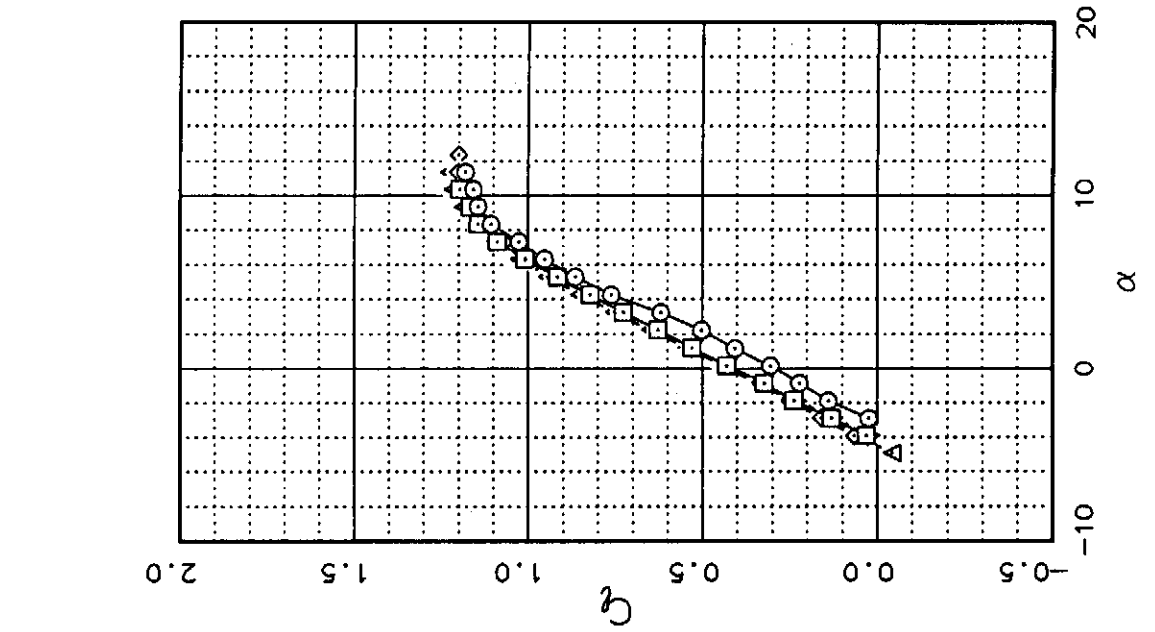
20
10
0
−10
α
−0.5
0.0
0.5
1.0
1.5
2.0
C_l

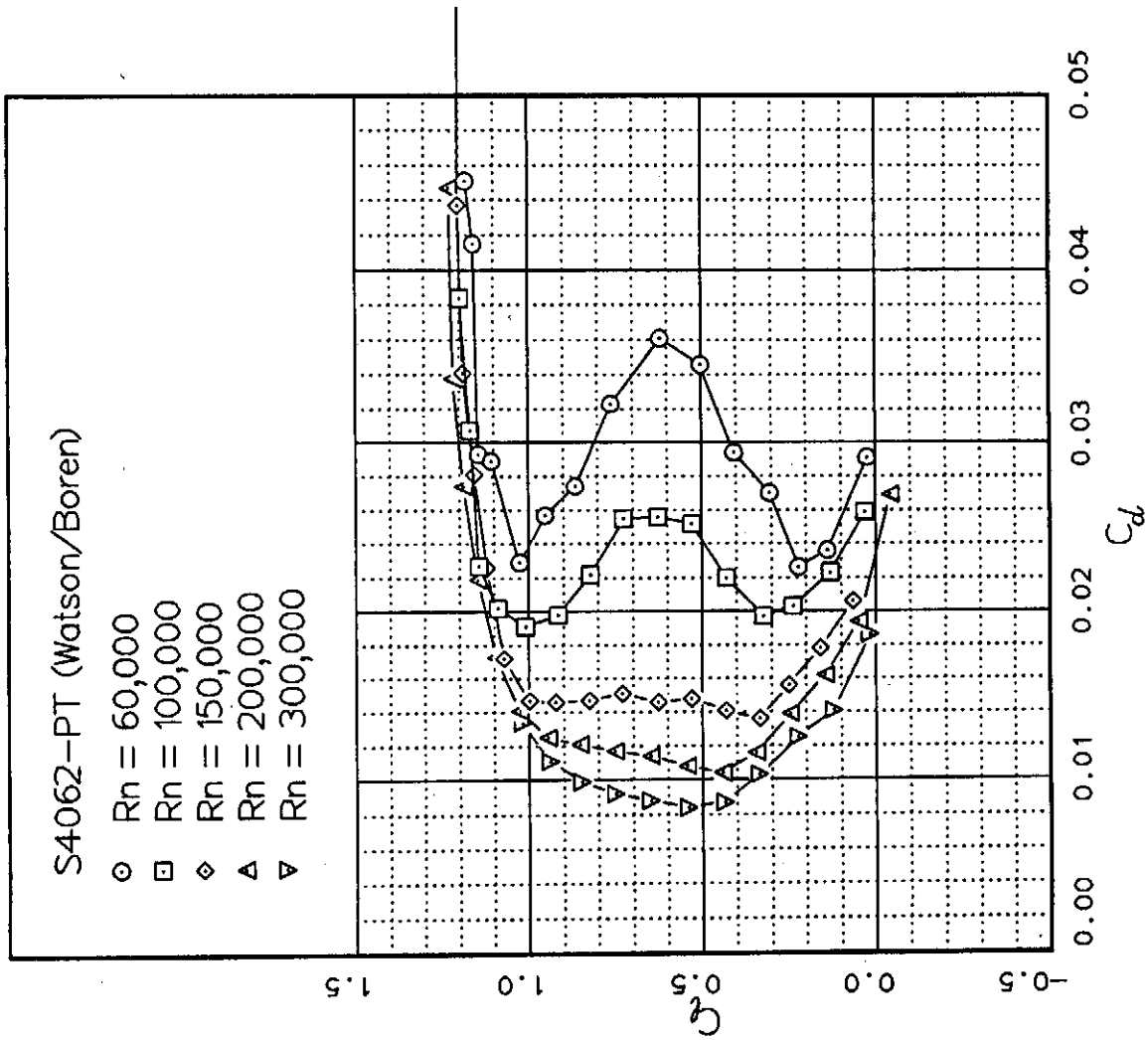
S4062-PT (Watson/Boren)
Rn = 60,000
Rn = 100,000
Rn = 150,000
Rn = 200,000
Rn = 300,000
0.05
0.04
0.03
0.02
0.01
0.00
C_d
−0.5
0.0
0.5
1.0
1.5
C_l

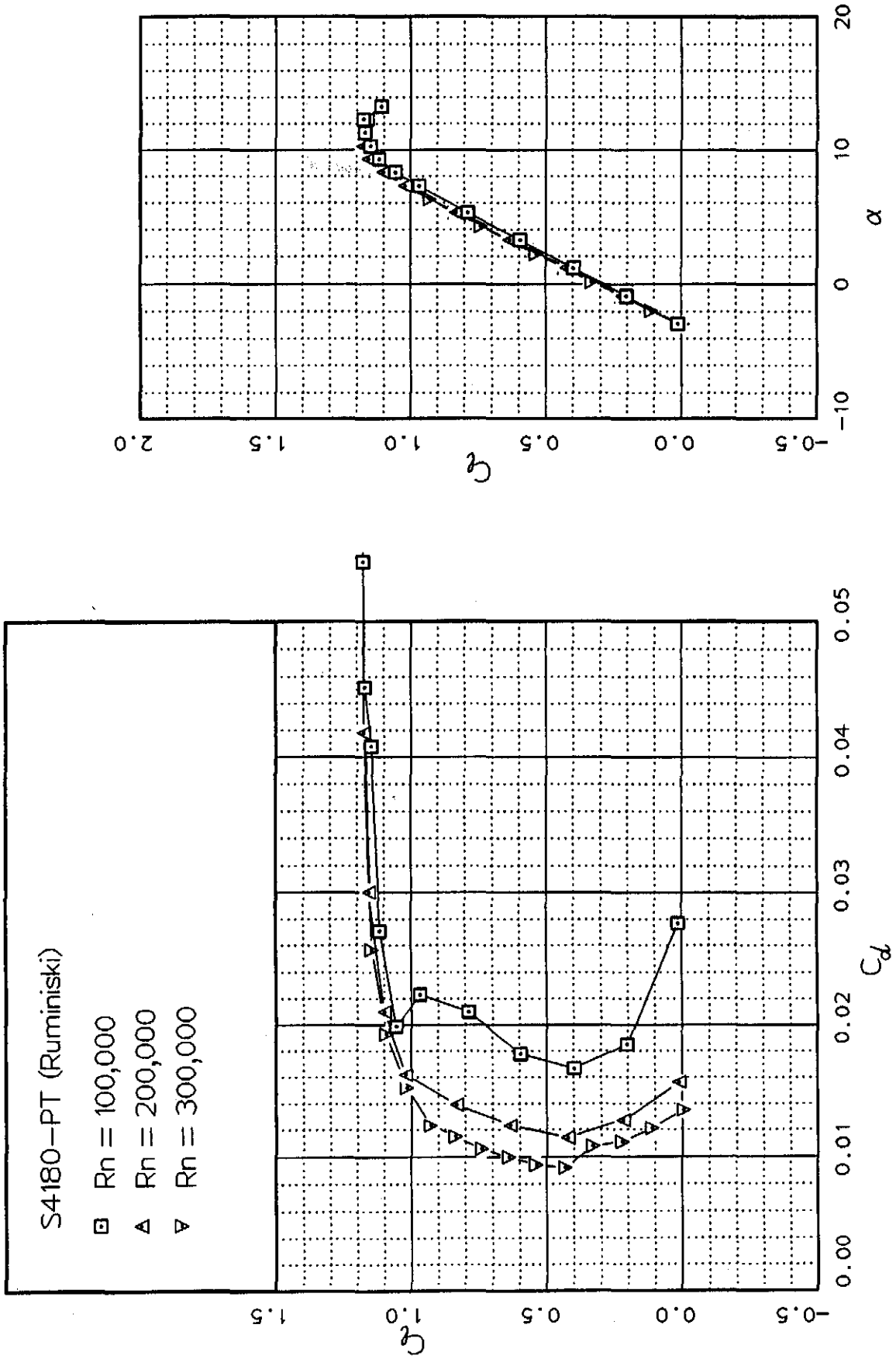
S4180–PT (Ruminiski)
Rn = 100,000
Rn = 200,000
Rn = 300,000
C_l
α
C_d
−0.5
0.0
0.5
1.0
1.5
2.0
−10
0
10
20
0.00
0.01
0.02
0.03
0.04
0.05

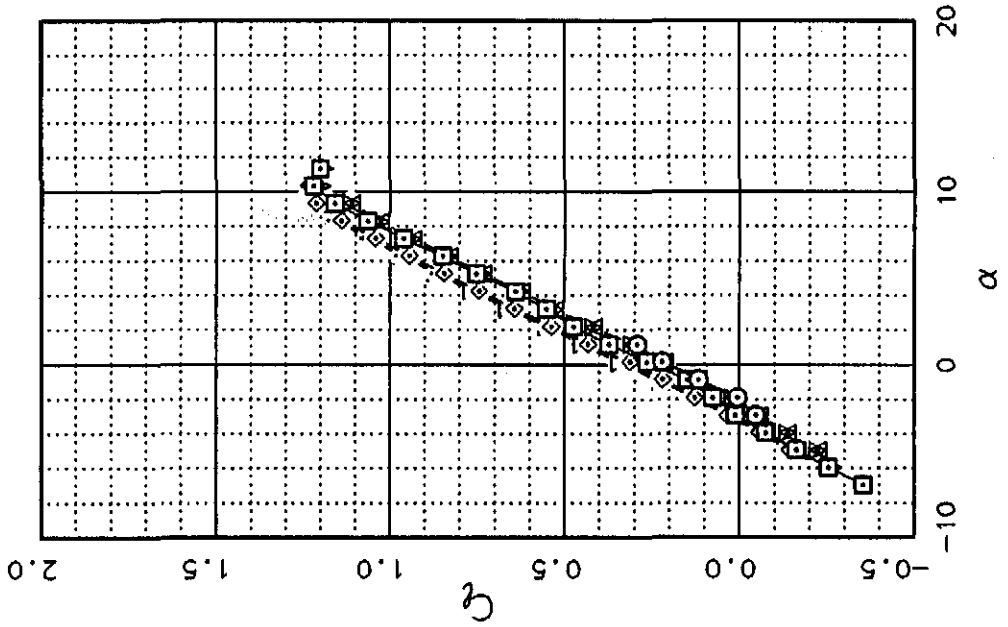
20
10
0
−10
α
−0.5
0.0
0.5
1.0
1.5
2.0
Cl

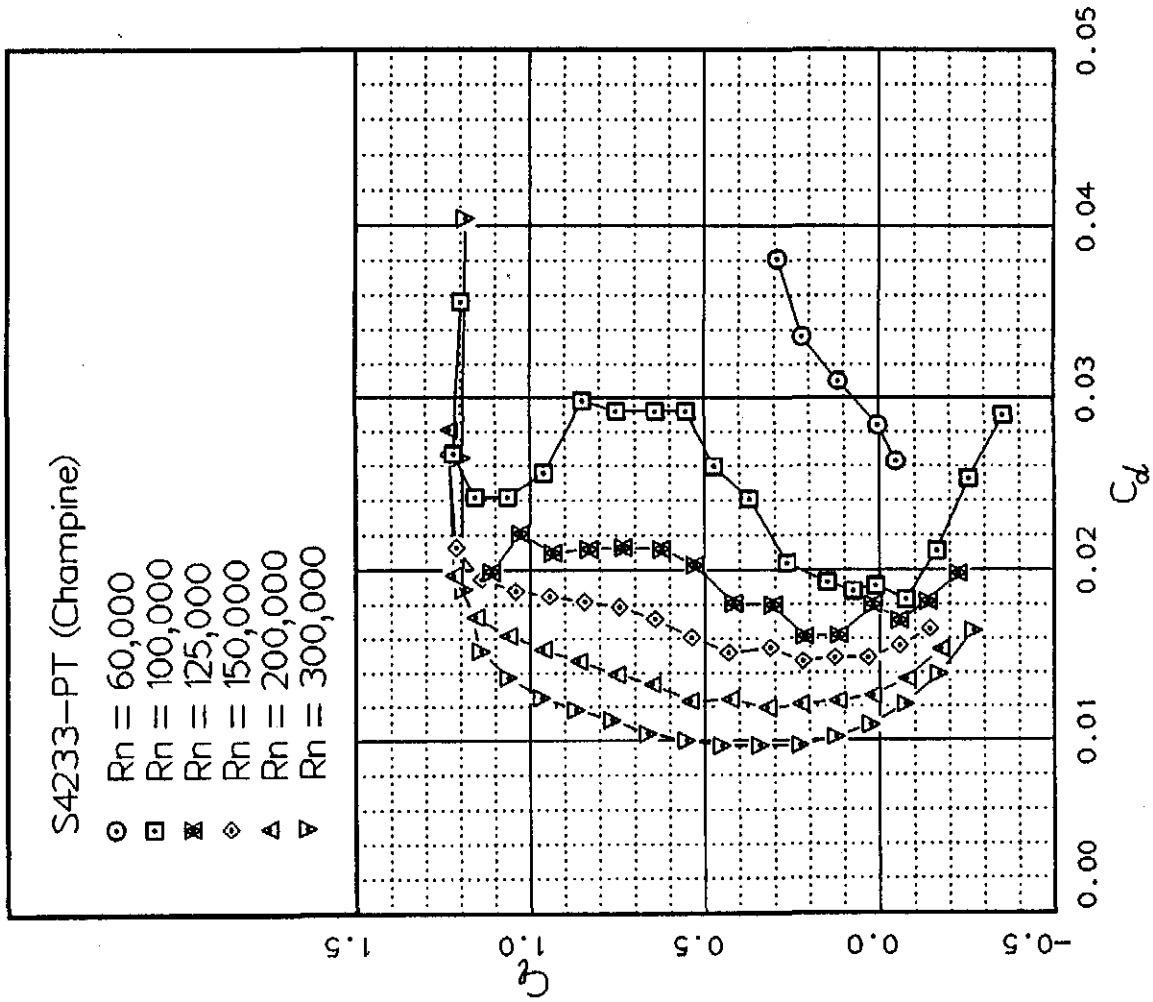
S4233-PT (Champine)
Rn = 60,000
Rn = 100,000
Rn = 125,000
Rn = 150,000
Rn = 200,000
Rn = 300,000
0.05
0.04
0.03
0.02
0.01
0.00
Cd
−0.5
0.0
0.5
1.0
1.5
Cl

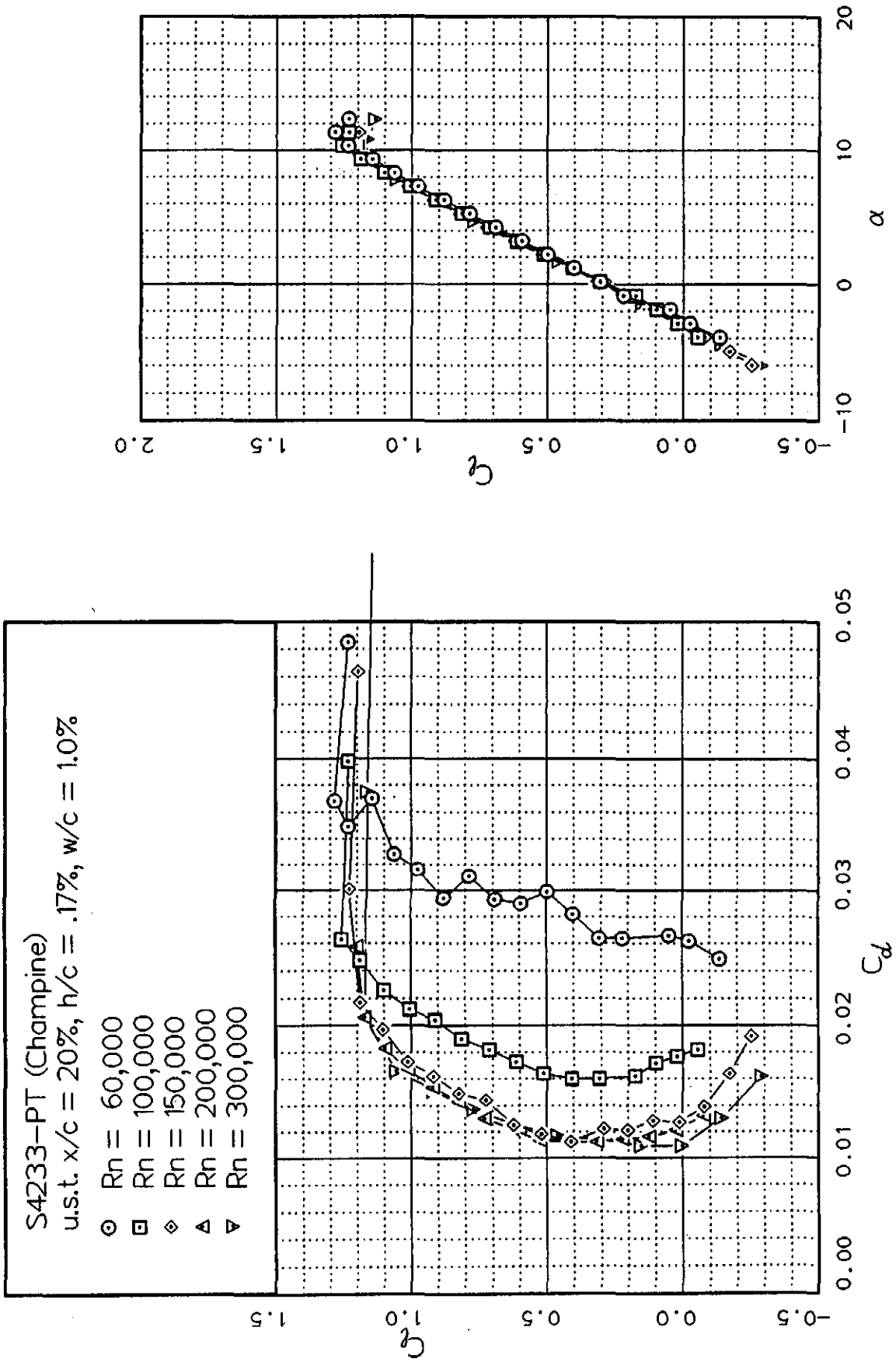
S4233-PT (Champine)
u.s.t. x/c = 20%, h/c = .17%, w/c = 1.0%
Rn = 60,000
Rn = 100,000
Rn = 150,000
Rn = 200,000
Rn = 300,000
C_l
C_d
α

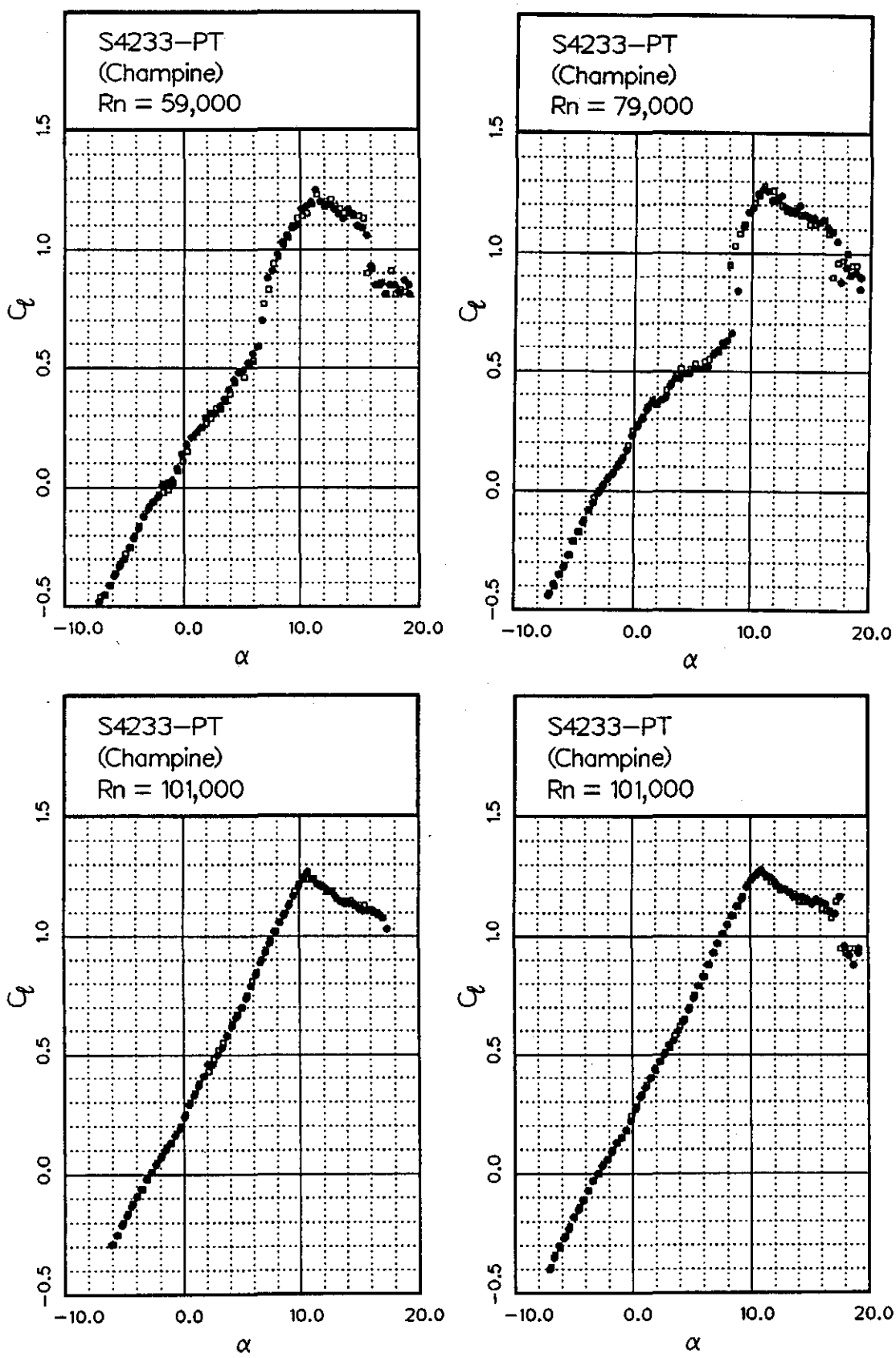
S4233–PT
(Champine)
Rn = 59,000
S4233–PT
(Champine)
Rn = 79,000
S4233–PT
(Champine)
Rn = 101,000
S4233–PT
(Champine)
Rn = 101,000
C_l
α
1.5
1.0
0.5
0.0
−0.5
−10.0
0.0
10.0
20.0

Fig. 12.104

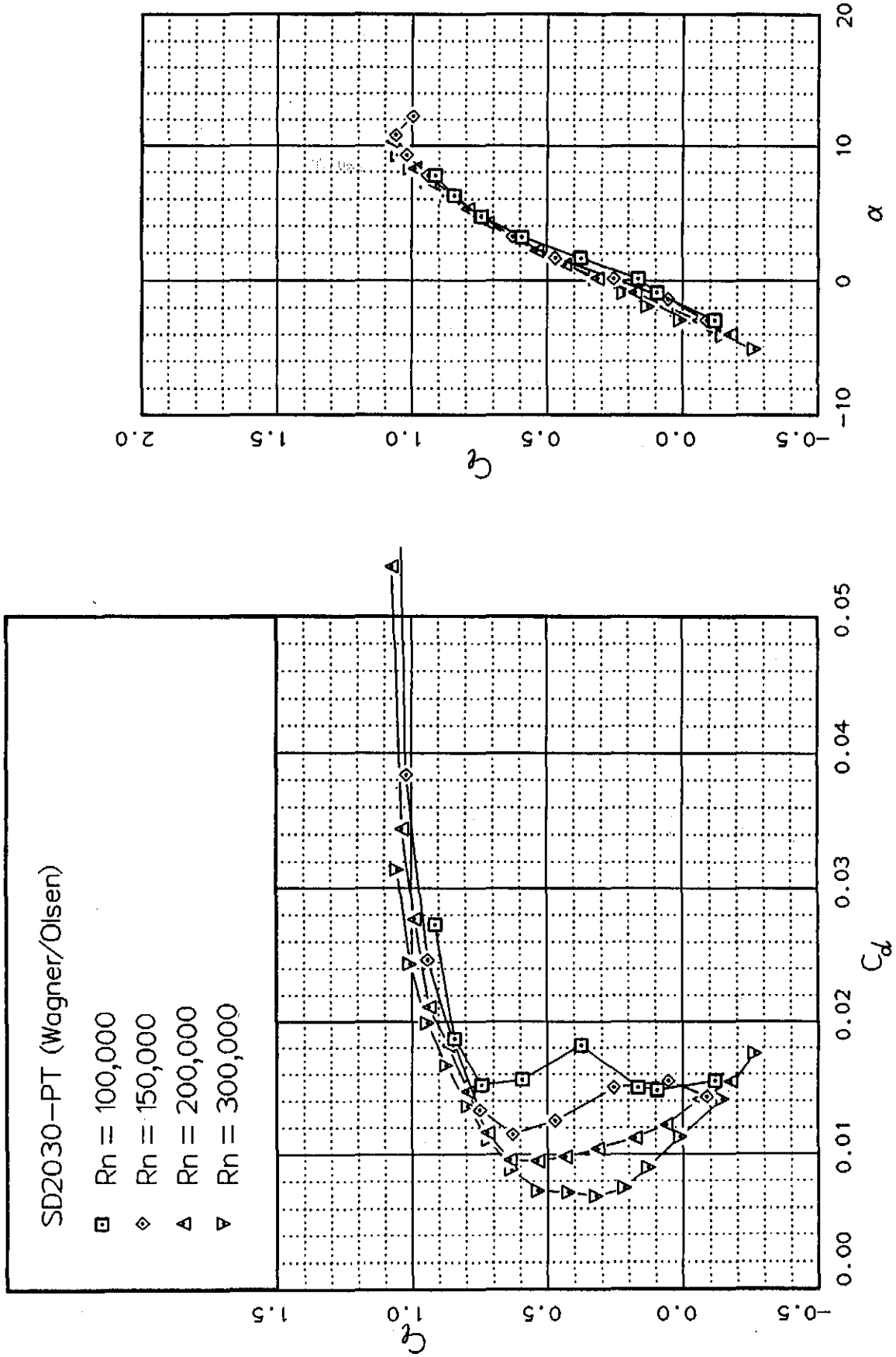
SD2030–PT (Wagner/Olsen)
Rn = 100,000
Rn = 150,000
Rn = 200,000
Rn = 300,000
−0.5
0.0
0.5
1.0
1.5
2.0
−10
0
10
20
α
0.00
0.01
0.02
0.03
0.04
0.05
C_d
C_l

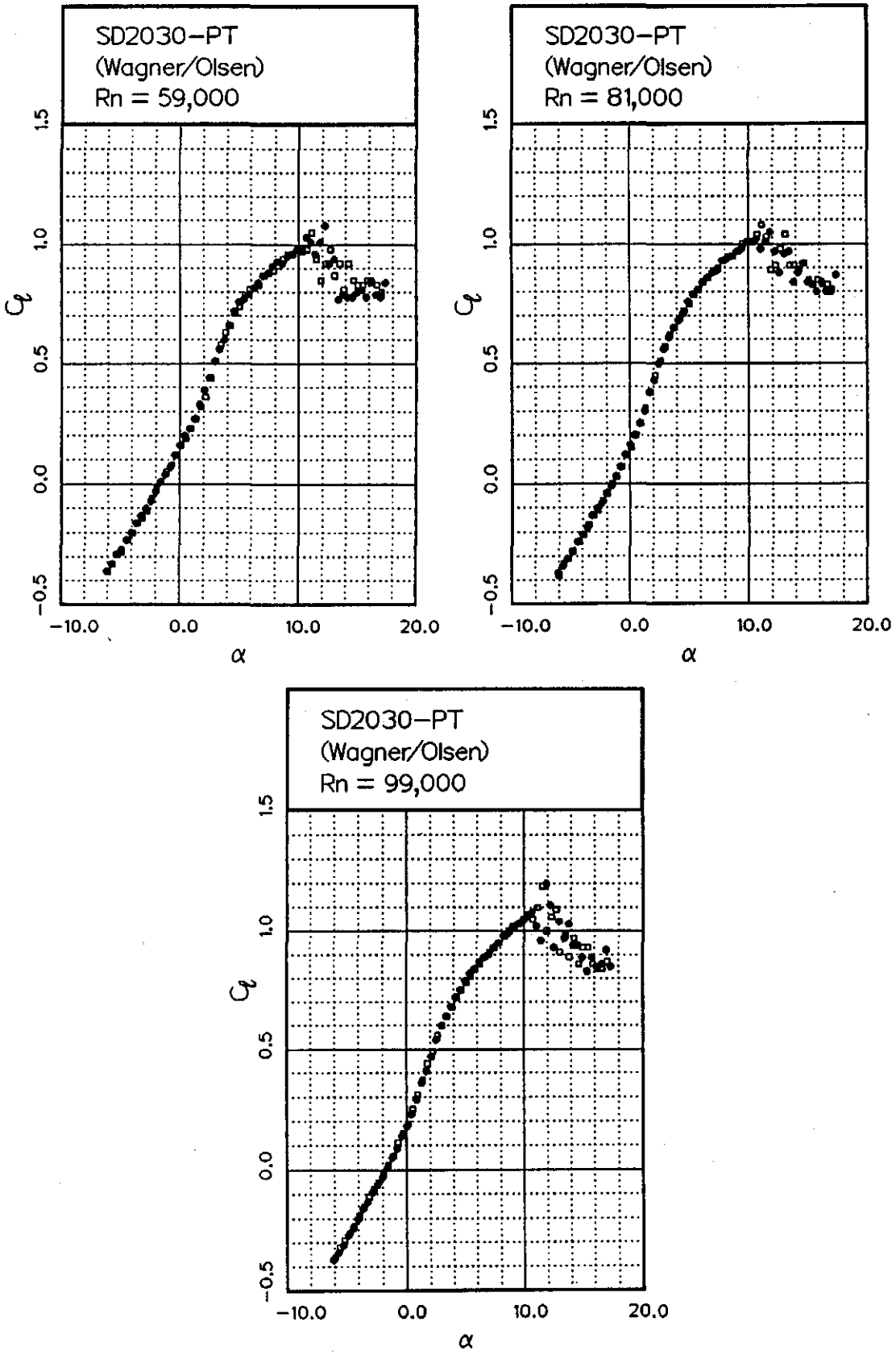
SD2030–PT
(Wagner/Olsen)
Rn = 59,000
SD2030–PT
(Wagner/Olsen)
Rn = 81,000
SD2030–PT
(Wagner/Olsen)
Rn = 99,000
C_l
α
1.5
1.0
0.5
0.0
−0.5
−10.0
0.0
10.0
20.0

Fig. 12.106

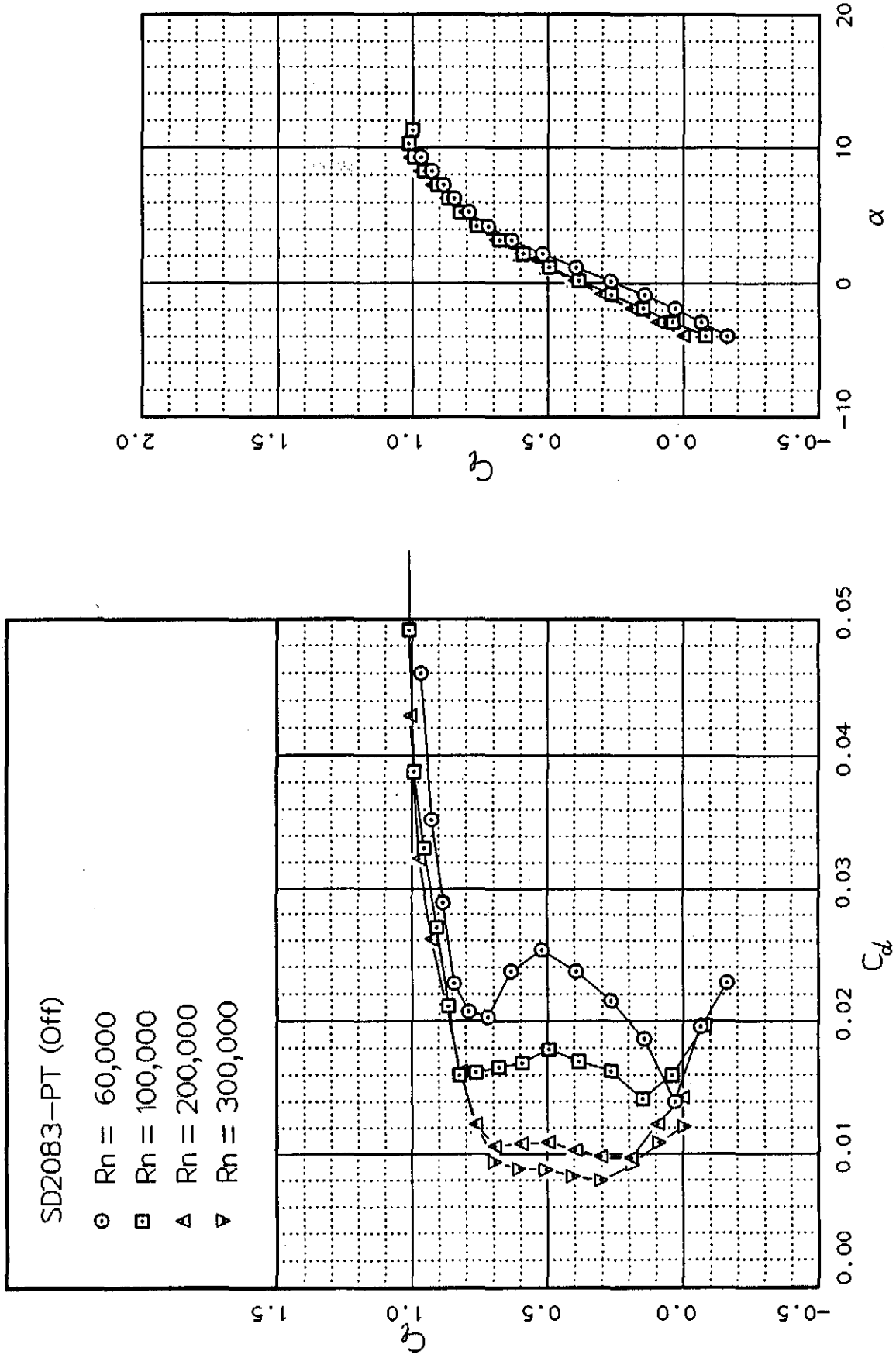
SD2083–PT (Off)
Rn = 60,000
Rn = 100,000
Rn = 200,000
Rn = 300,000
−0.5
0.0
0.5
1.0
1.5
2.0
−10
0
10
20
α
0.00
0.01
0.02
0.03
0.04
0.05
C_d
C_l

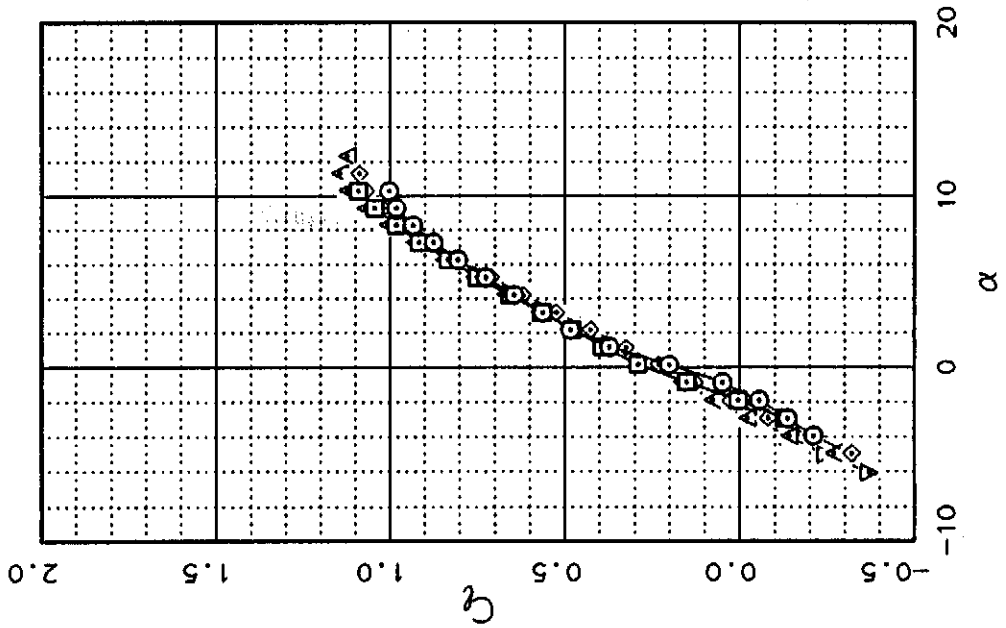
20
10
0
−10
α
−0.5
0.0
0.5
1.0
1.5
2.0
C_l

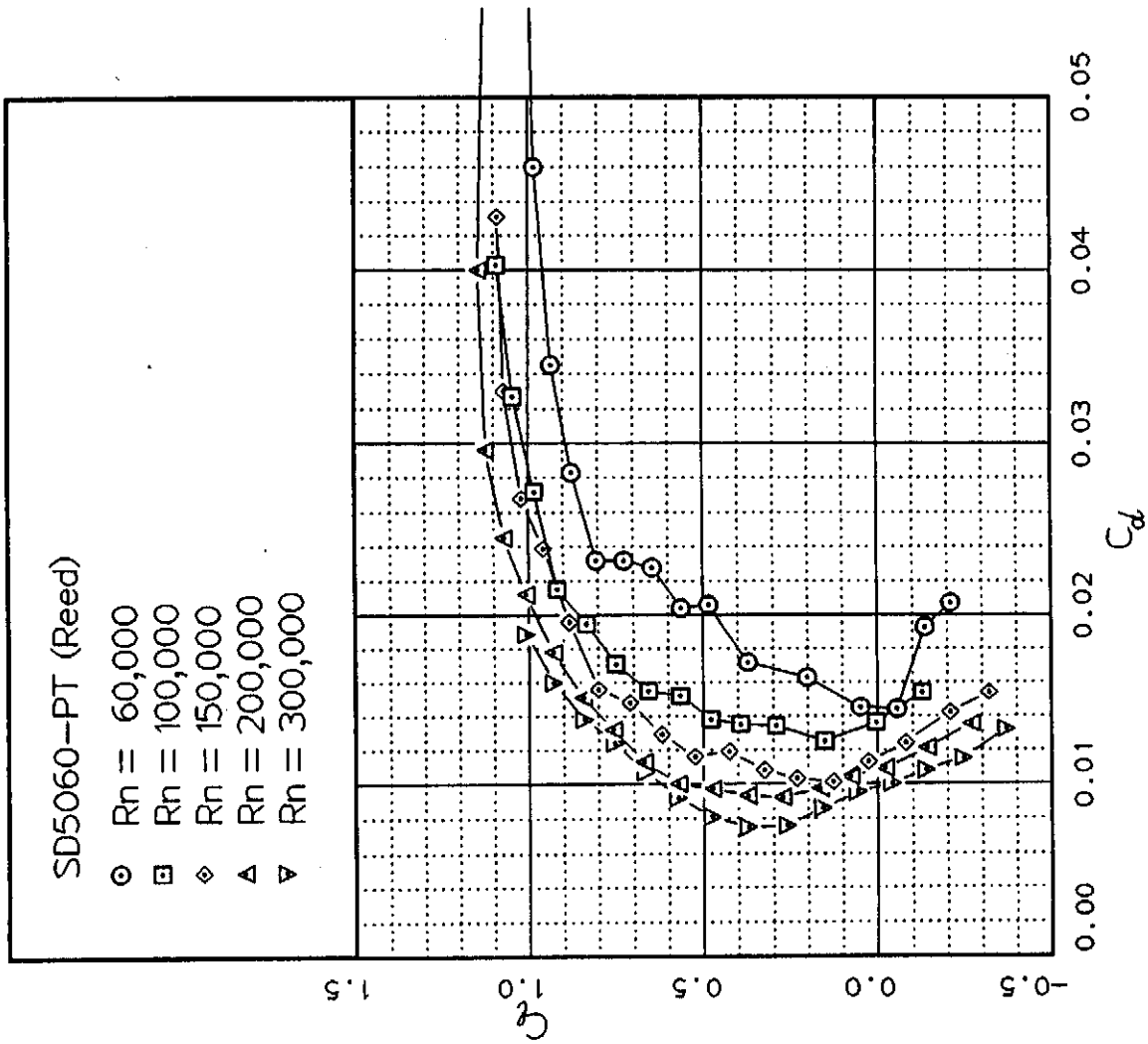
SD5060−PT (Reed)
Rn = 60,000
Rn = 100,000
Rn = 150,000
Rn = 200,000
Rn = 300,000
0.05
0.04
0.03
0.02
0.01
0.00
C_d
−0.5
0.0
0.5
1.0
1.5
C_l

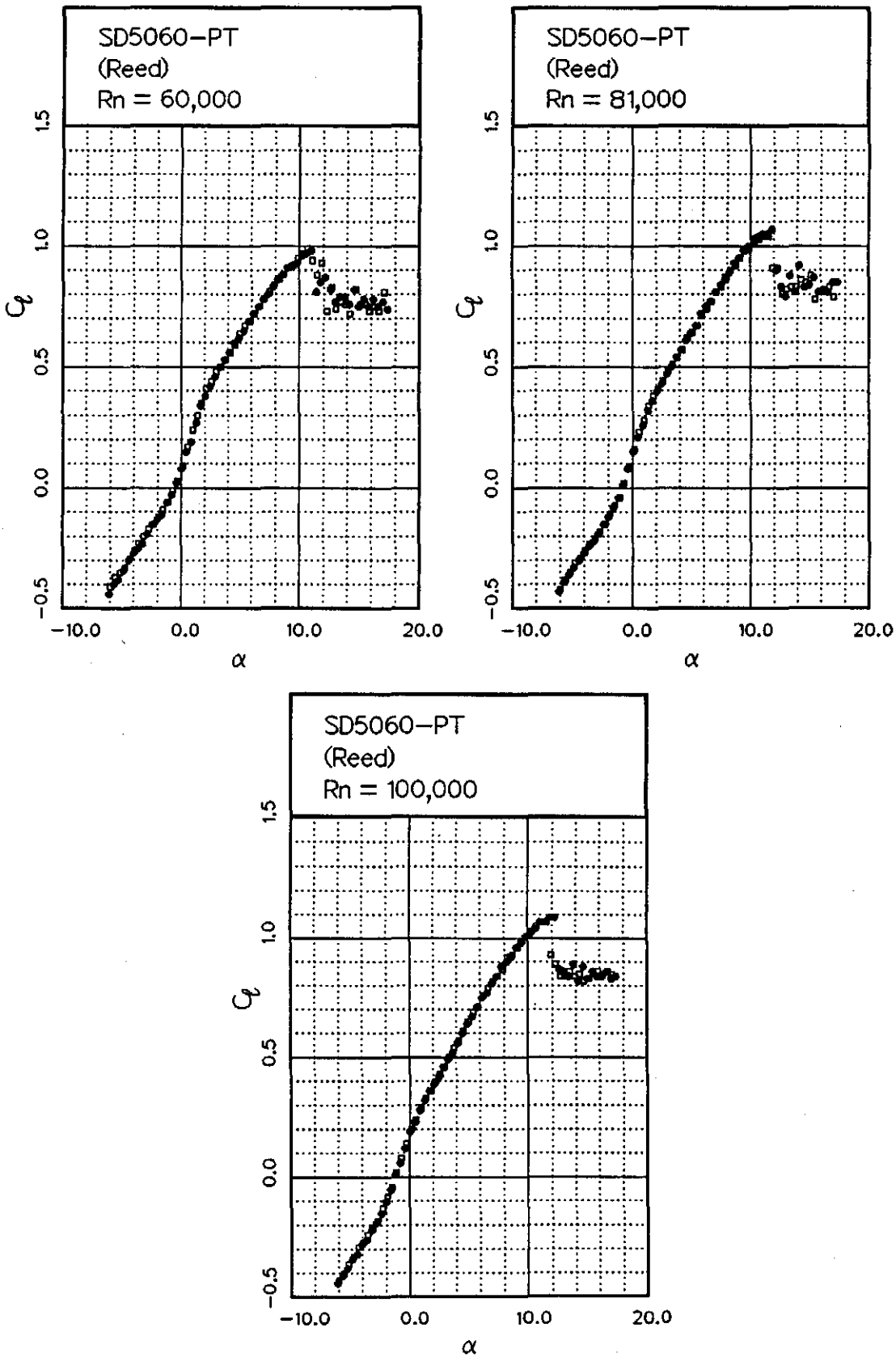
SD5060–PT
(Reed)
Rn = 60,000
SD5060–PT
(Reed)
Rn = 81,000
SD5060–PT
(Reed)
Rn = 100,000
C_ℓ
α
1.5
1.0
0.5
0.0
−0.5
−10.0
0.0
10.0
20.0

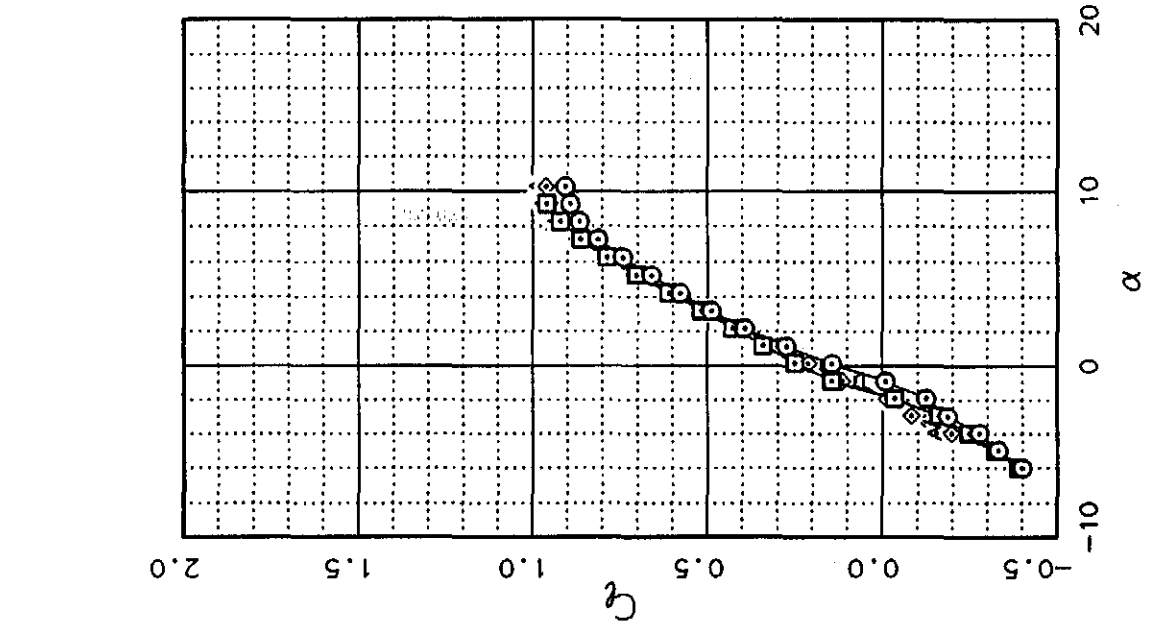
20
10
0
−10
α
−0.5
0.0
0.5
1.0
1.5
2.0
Cl

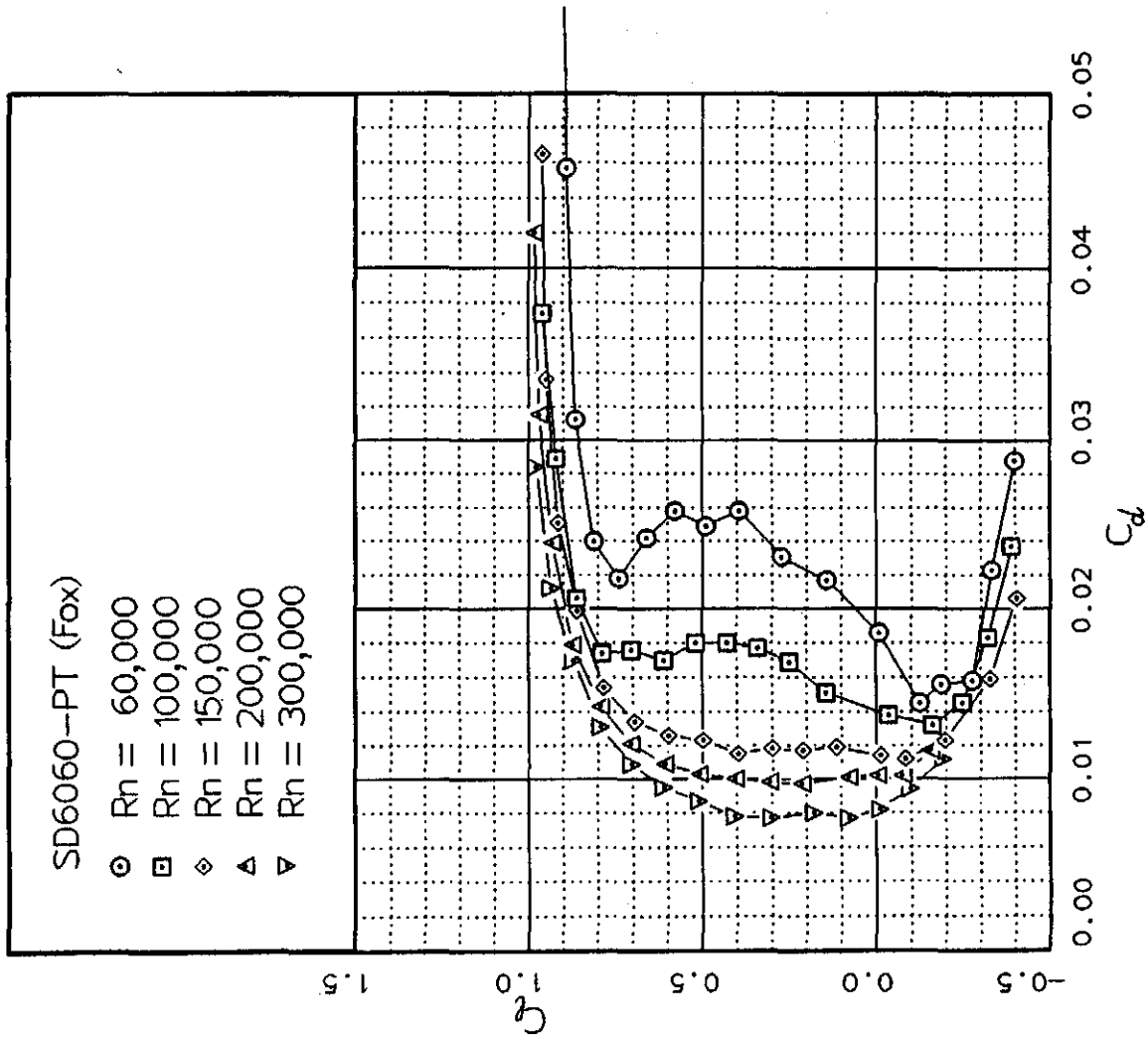
SD6060−PT (Fox)
Rn = 60,000
Rn = 100,000
Rn = 150,000
Rn = 200,000
Rn = 300,000
0.05
0.04
0.03
0.02
0.01
0.00
Cd
−0.5
0.0
0.5
1.0
1.5
Cl

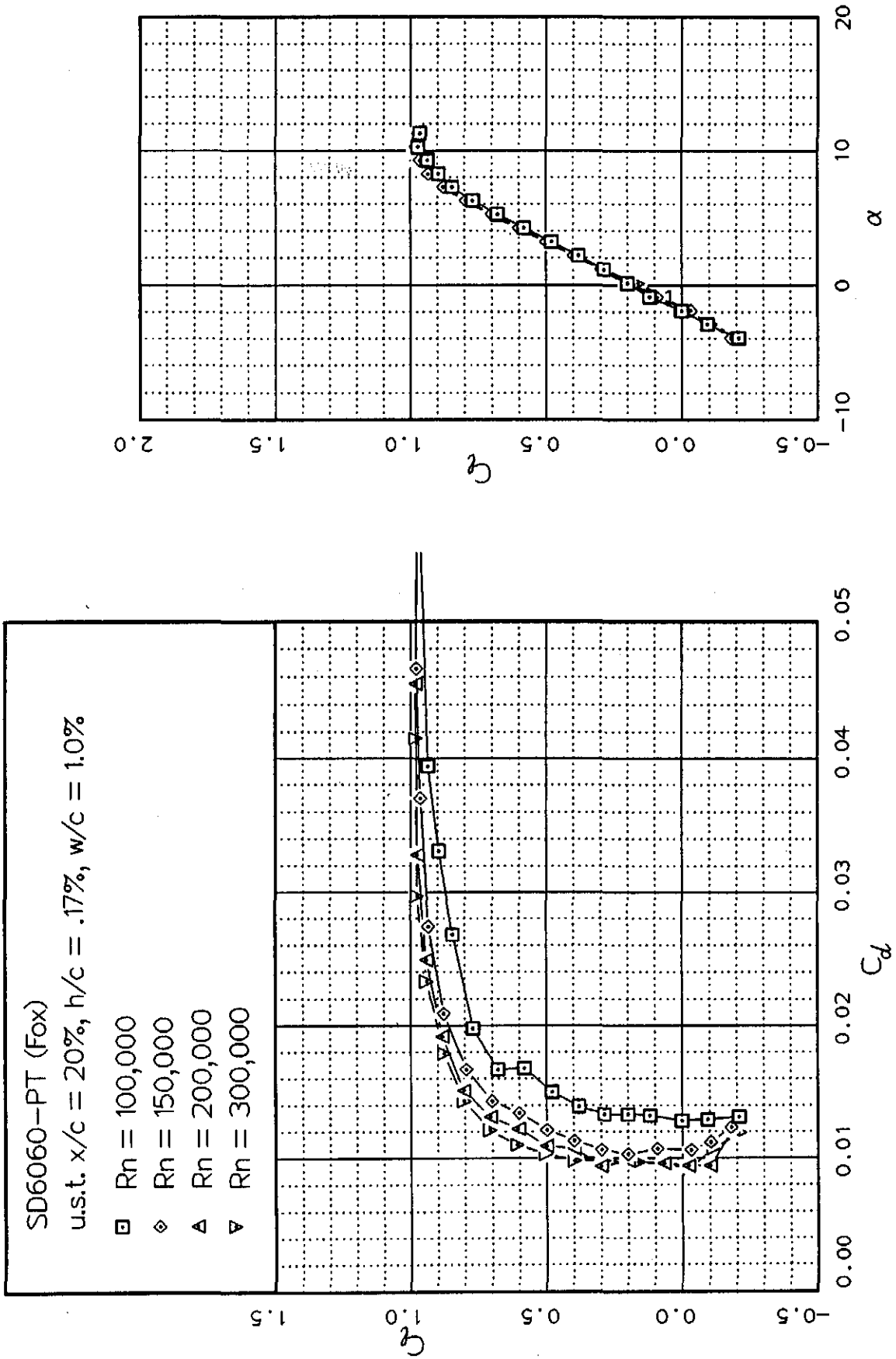
SD6060–PT (Fox)
u.s.t. x/c = 20%, h/c = .17%, w/c = 1.0%
Rn = 100,000
Rn = 150,000
Rn = 200,000
Rn = 300,000
−0.5
0.0
0.5
1.0
1.5
2.0
c_l
−10
0
10
20
α
0.00
0.01
0.02
0.03
0.04
0.05
c_d

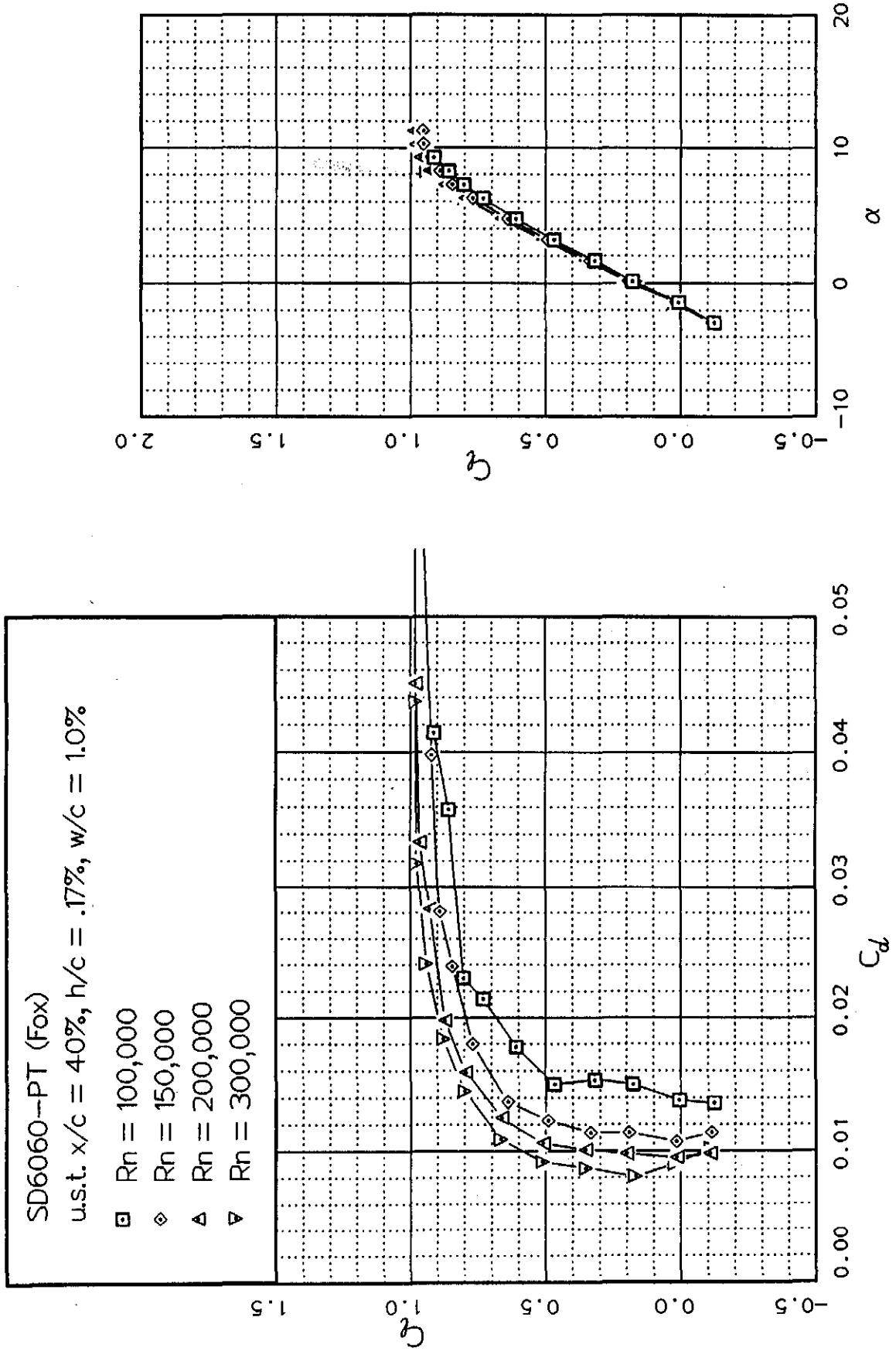
SD6060–PT (Fox)
u.s.t. x/c = 40%, h/c = .17%, w/c = 1.0%
Rn = 100,000
Rn = 150,000
Rn = 200,000
Rn = 300,000
0.05
0.04
0.03
0.02
0.01
0.00
C_d
1.5
1.0
0.5
0.0
−0.5
ℓ
20
10
0
−10
α
2.0
1.5
1.0
0.5
0.0
−0.5
ℓ

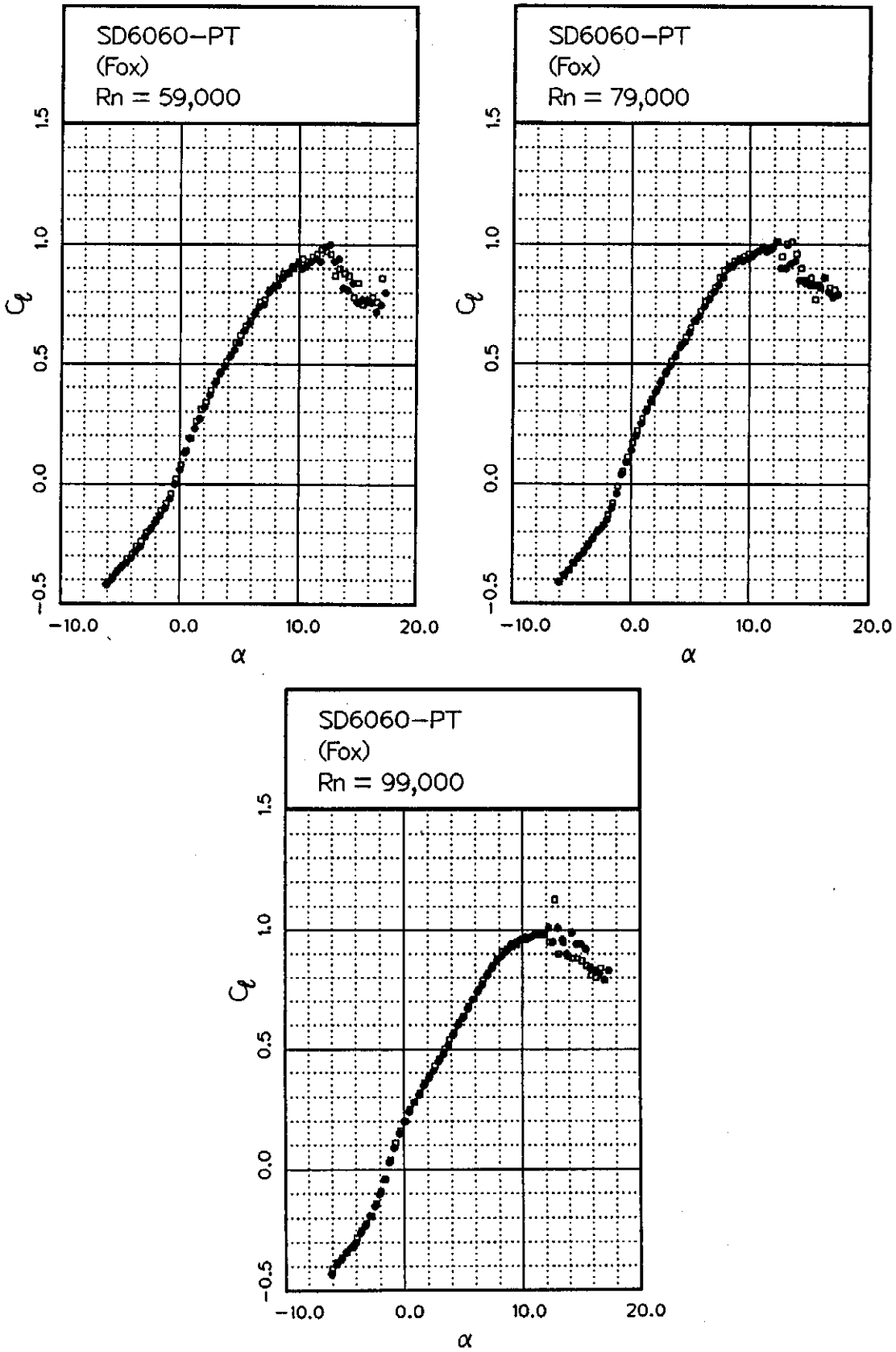
SD6060–PT
(Fox)
Rn = 59,000
SD6060–PT
(Fox)
Rn = 79,000
SD6060–PT
(Fox)
Rn = 99,000
C_ℓ
α
1.5
1.0
0.5
0.0
−0.5
−10.0
0.0
10.0
20.0

Fig. 12.113

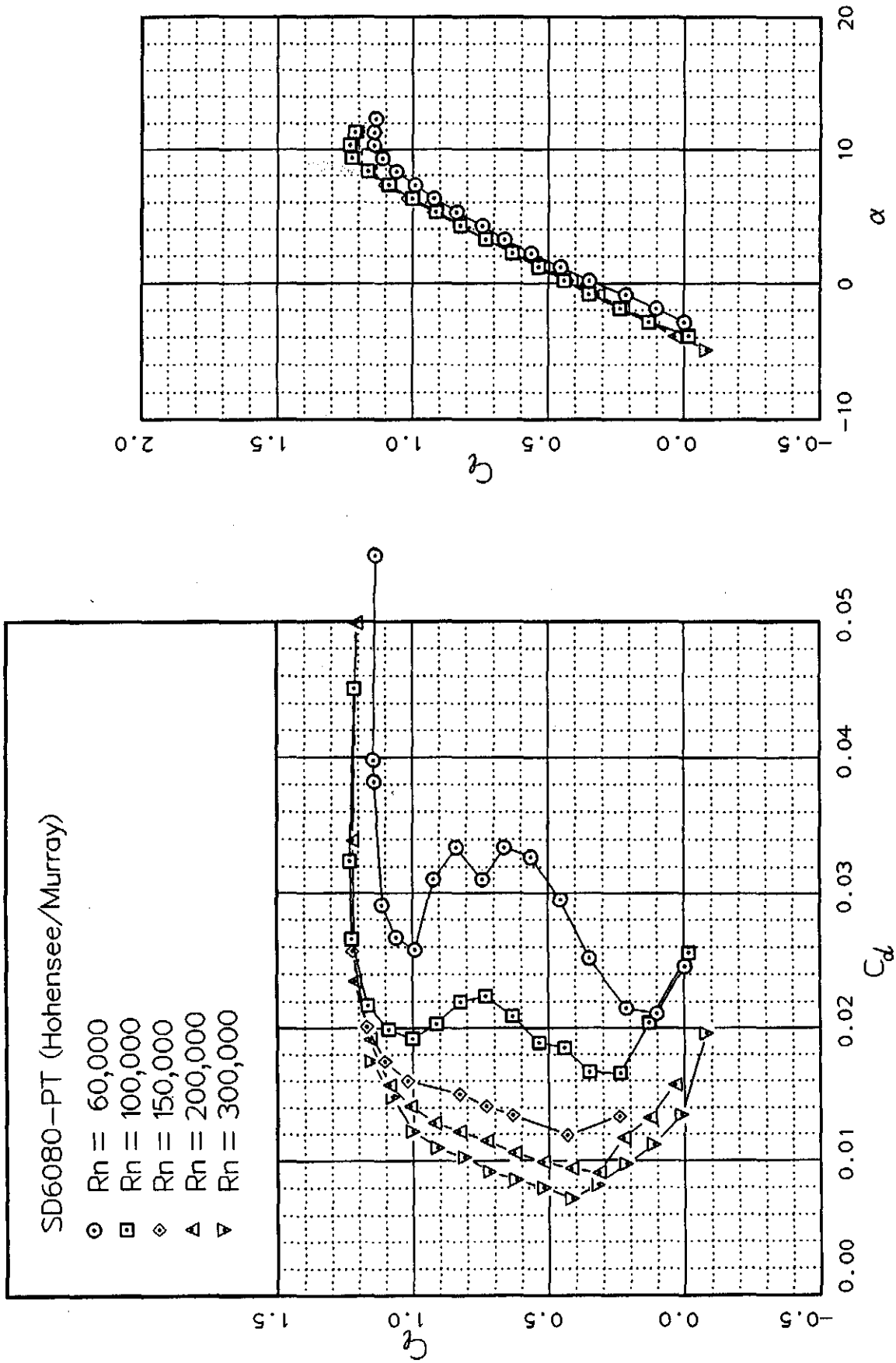
SD6080–PT (Hohensee/Murray)
Rn = 60,000
Rn = 100,000
Rn = 150,000
Rn = 200,000
Rn = 300,000
α
C_l
C_l

Fig. 12.114

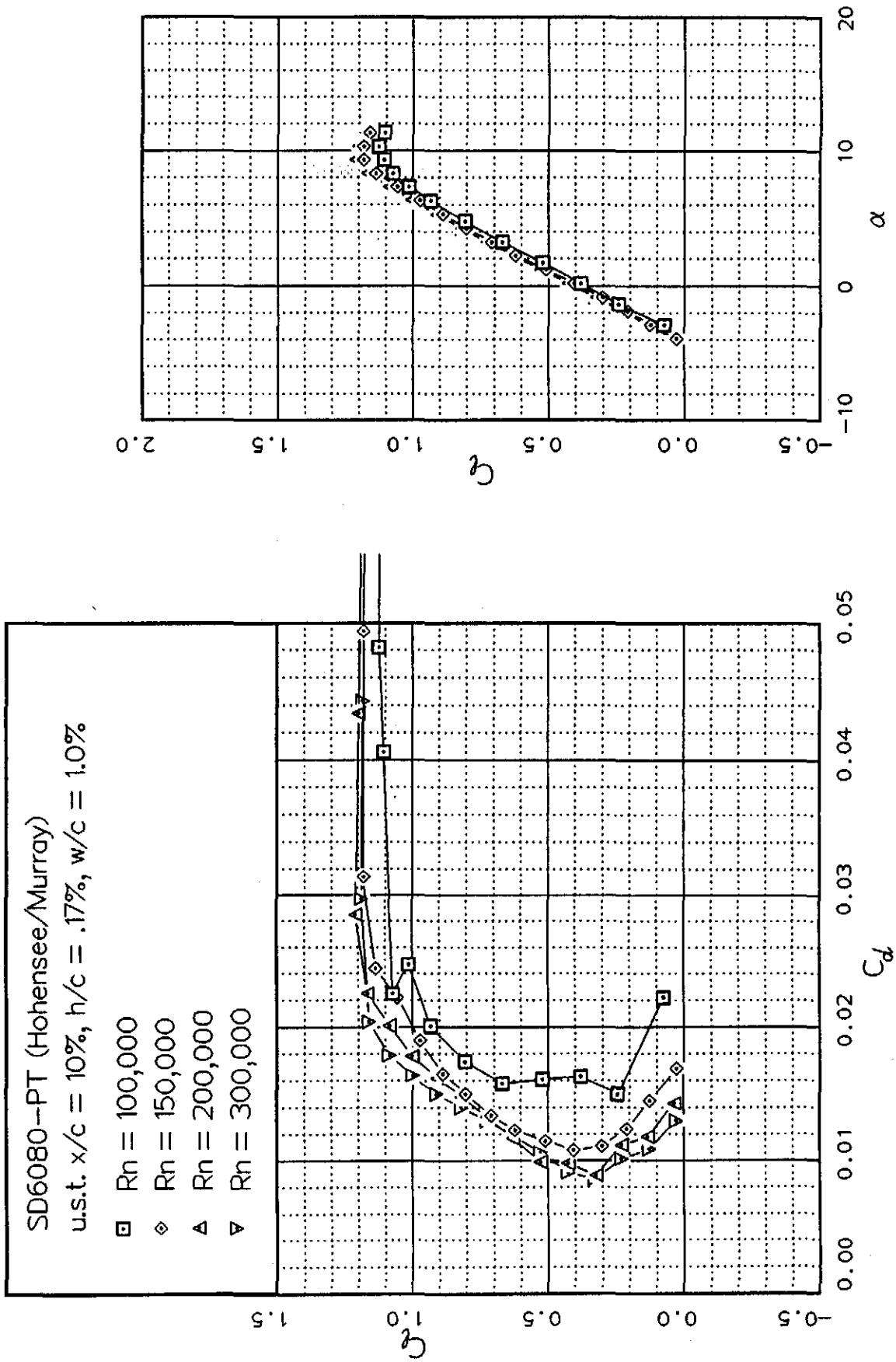
SD6080–PT (Hohensee/Murray)
u.s.t. x/c = 10%, h/c = .17%, w/c = 1.0%
Rn = 100,000
Rn = 150,000
Rn = 200,000
Rn = 300,000
α
C_d
C_l
20
10
0
−10
0.05
0.04
0.03
0.02
0.01
0.00
−0.5
0.0
0.5
1.0
1.5
2.0

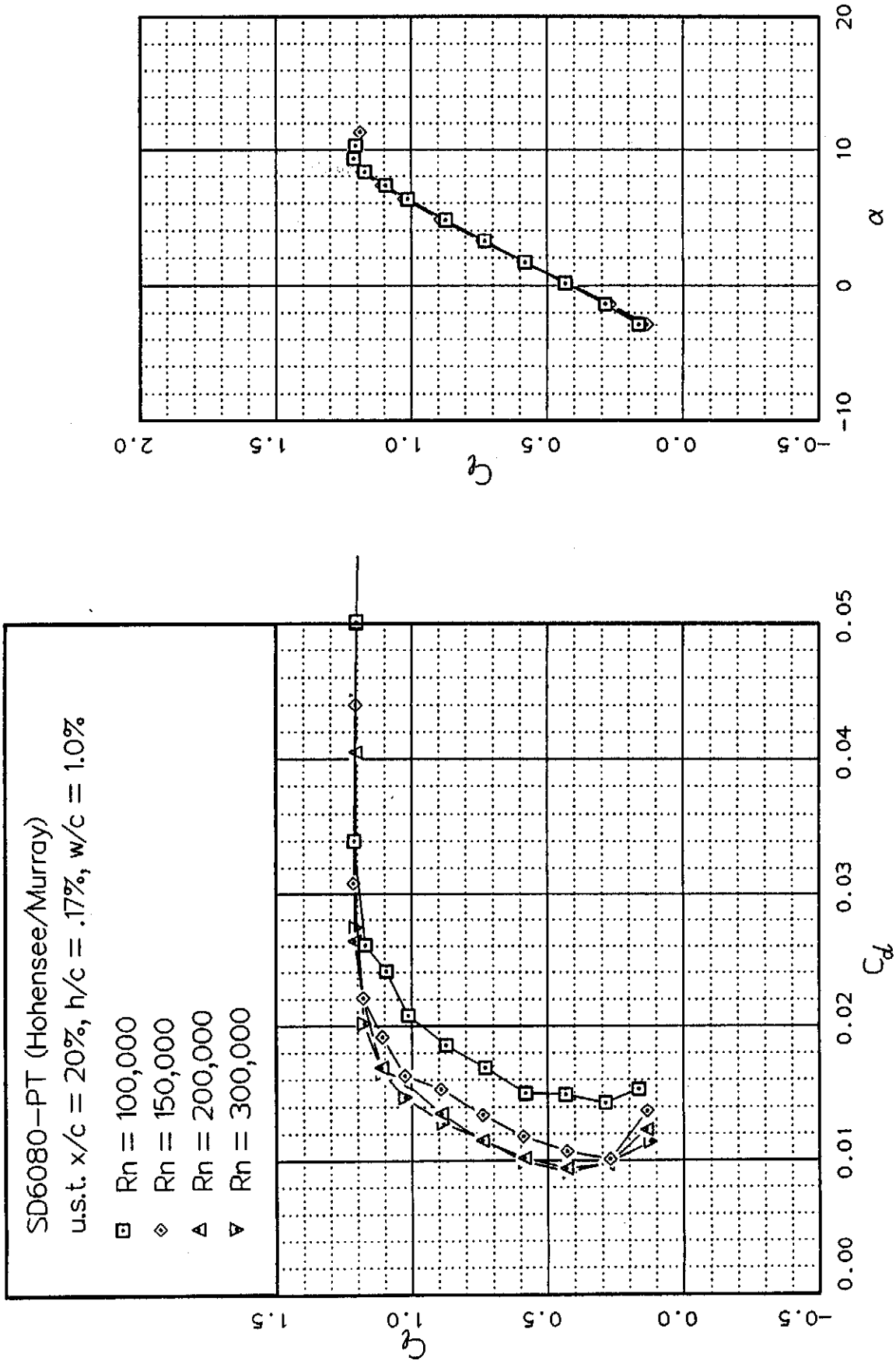
SD6080–PT (Hohensee/Murray)
u.s.t. x/c = 20%, h/c = .17%, w/c = 1.0%
Rn = 100,000
Rn = 150,000
Rn = 200,000
Rn = 300,000
α
C_d
C_l
20
10
0
−10
0.05
0.04
0.03
0.02
0.01
0.00
−0.5
0.0
0.5
1.0
1.5
2.0

Fig. 12.116

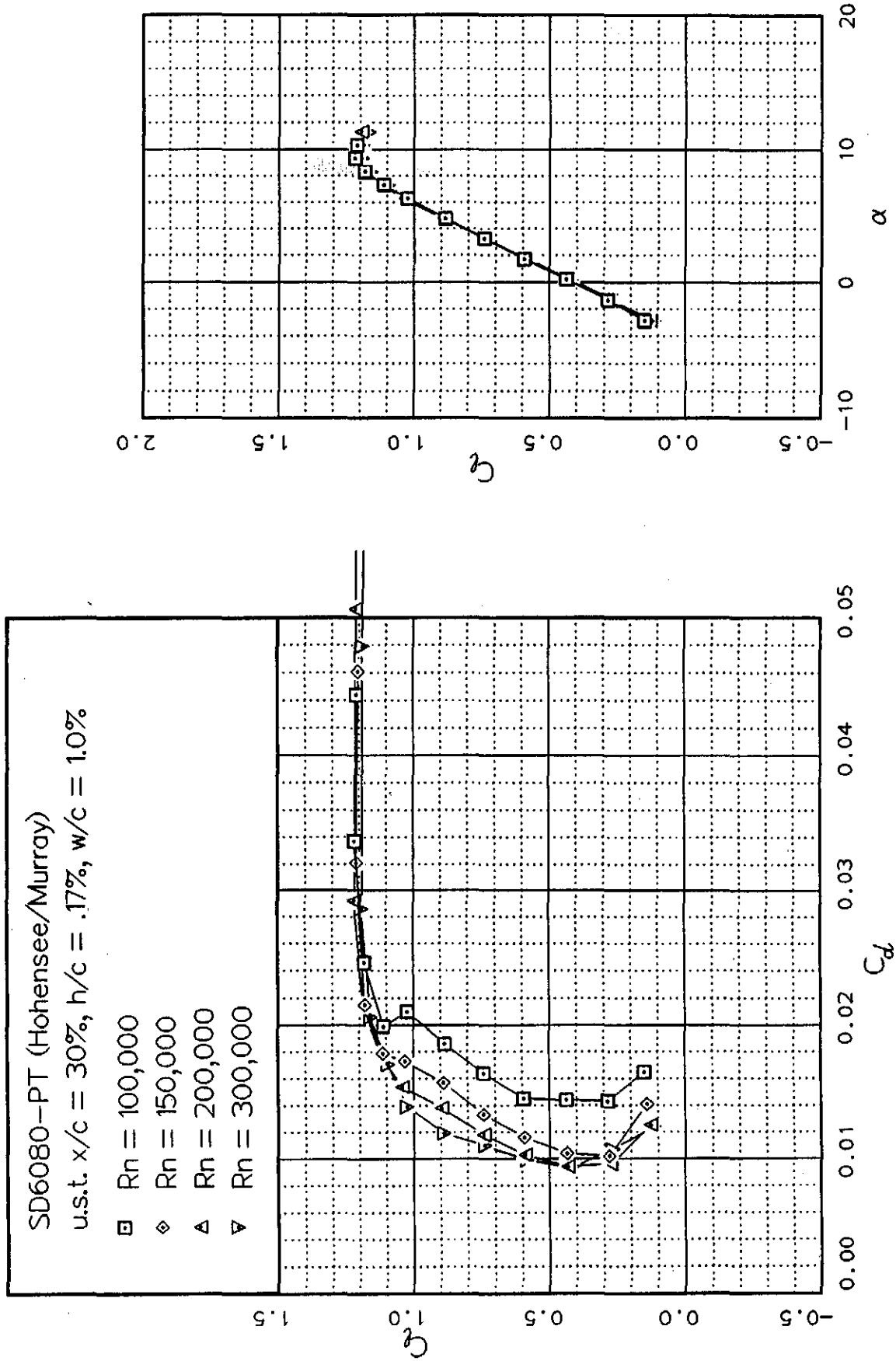
SD6080–PT (Hohensee/Murray)
u.s.t. x/c = 30%, h/c = .17%, w/c = 1.0%
Rn = 100,000
Rn = 150,000
Rn = 200,000
Rn = 300,000
−0.5
0.0
0.5
1.0
1.5
2.0
c_l
−10
0
10
20
α
0.00
0.01
0.02
0.03
0.04
0.05
c_d

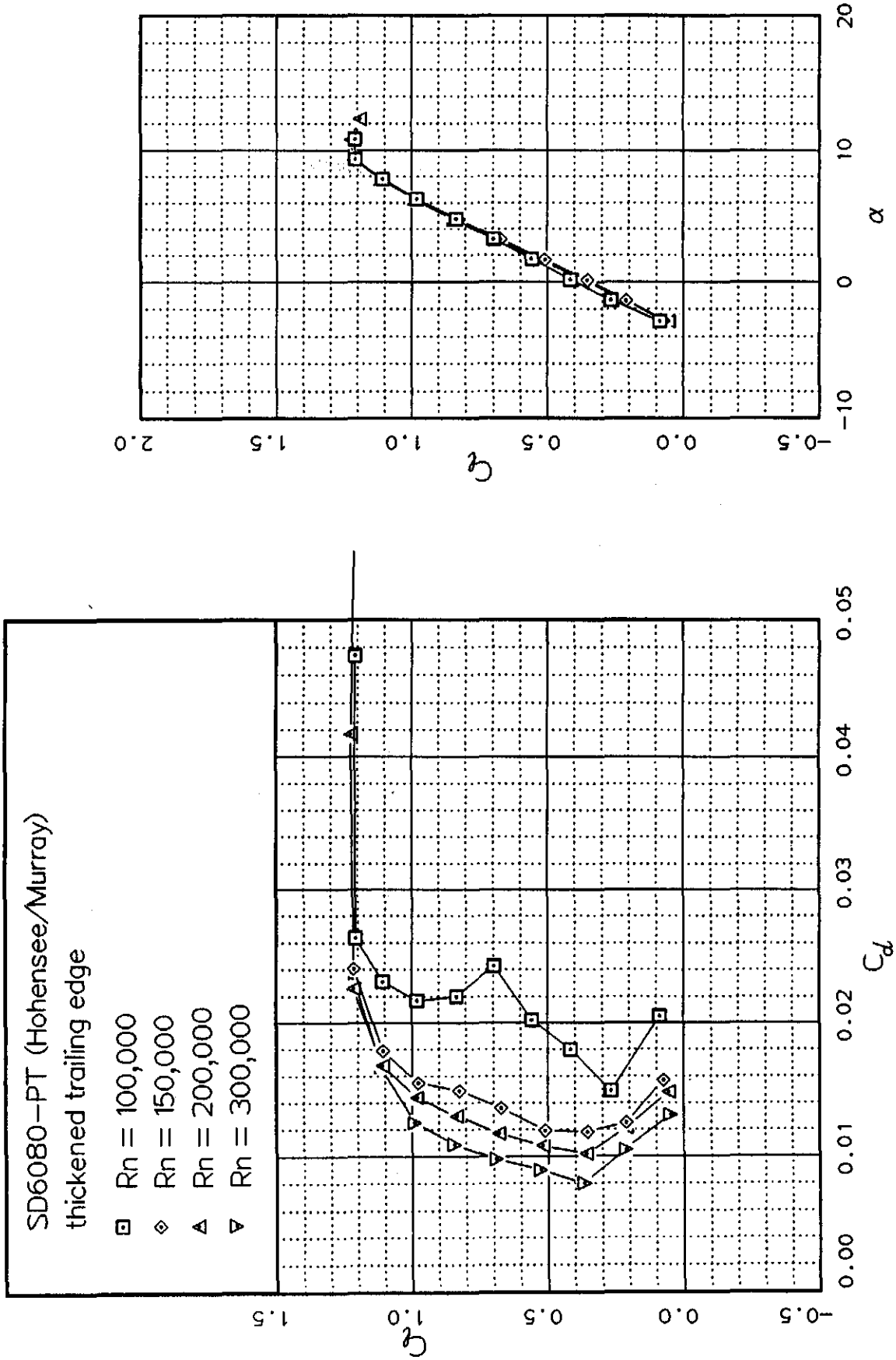
SD6080–PT (Hohensee/Murray)
thickened trailing edge
Rn = 100,000
Rn = 150,000
Rn = 200,000
Rn = 300,000
−0.5
0.0
0.5
1.0
1.5
2.0
cl
−10
0
10
20
α
0.00
0.01
0.02
0.03
0.04
0.05
cd

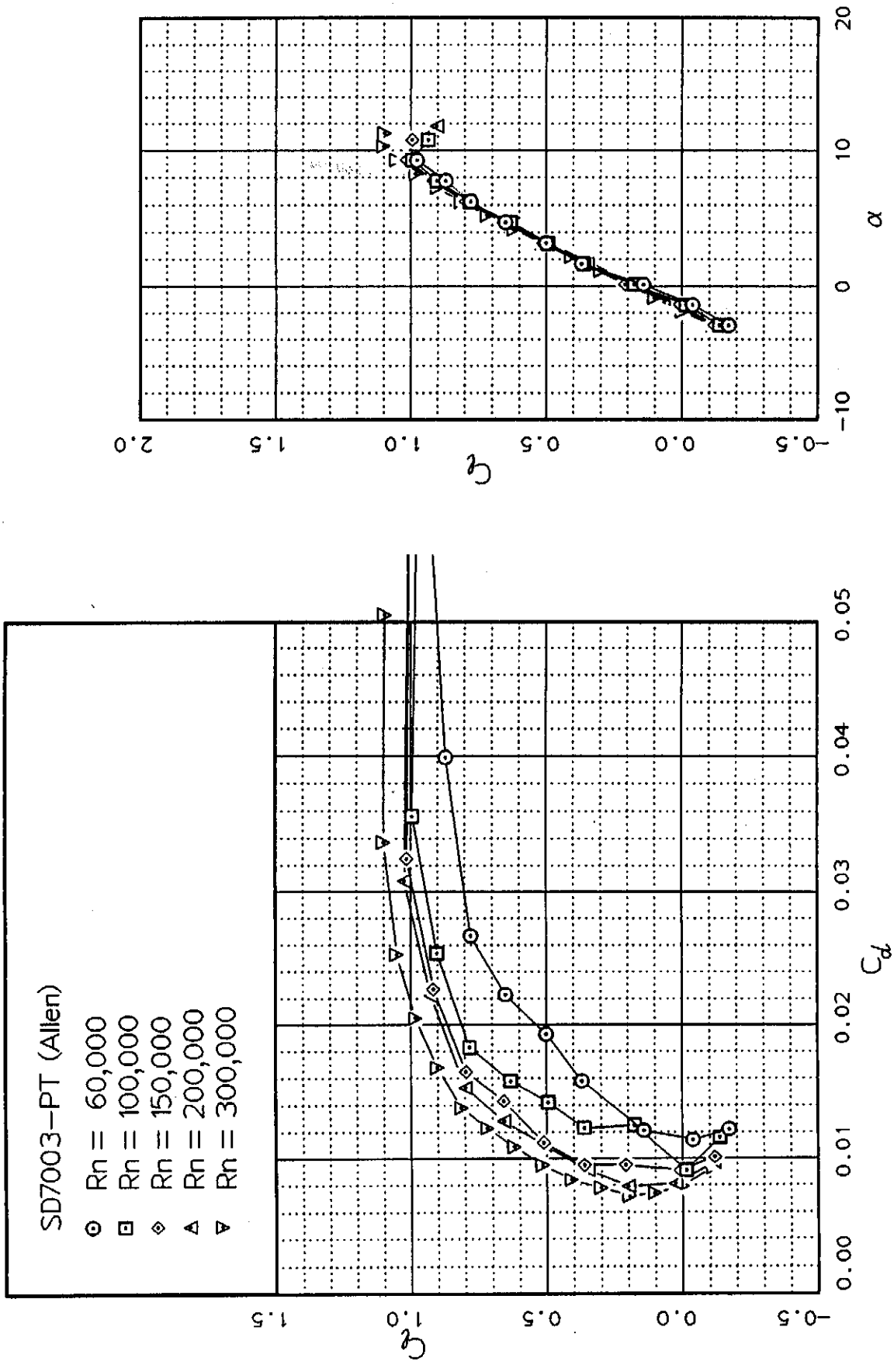
SD7003-PT (Allen)
Rn = 60,000
Rn = 100,000
Rn = 150,000
Rn = 200,000
Rn = 300,000
α
C_l
C_d

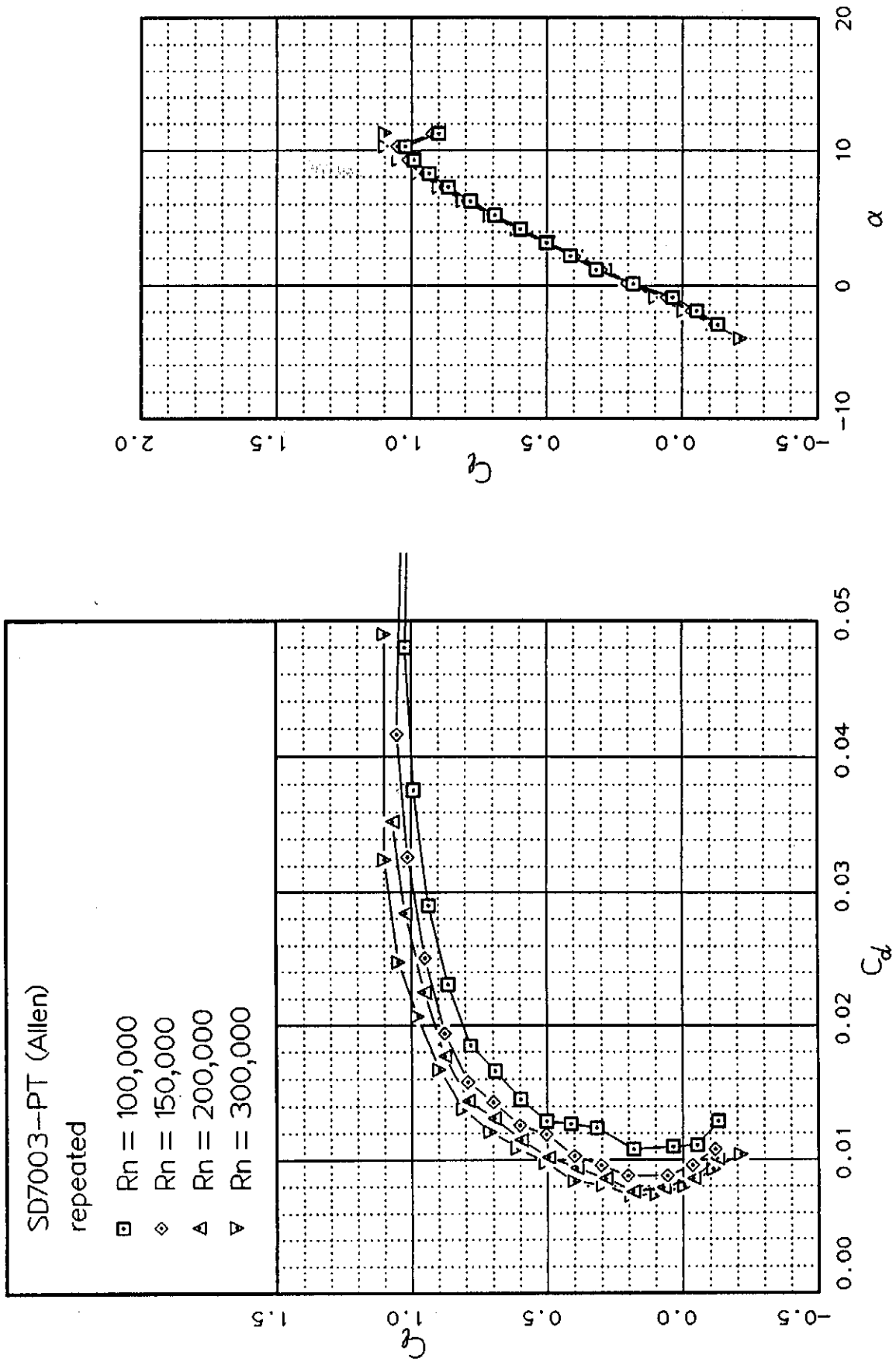
SD7003-PT (Allen)
repeated
Rn = 100,000
Rn = 150,000
Rn = 200,000
Rn = 300,000
-0.5
0.0
0.5
1.0
1.5
2.0
-10
0
10
20
α
0.00
0.01
0.02
0.03
0.04
0.05
C_d

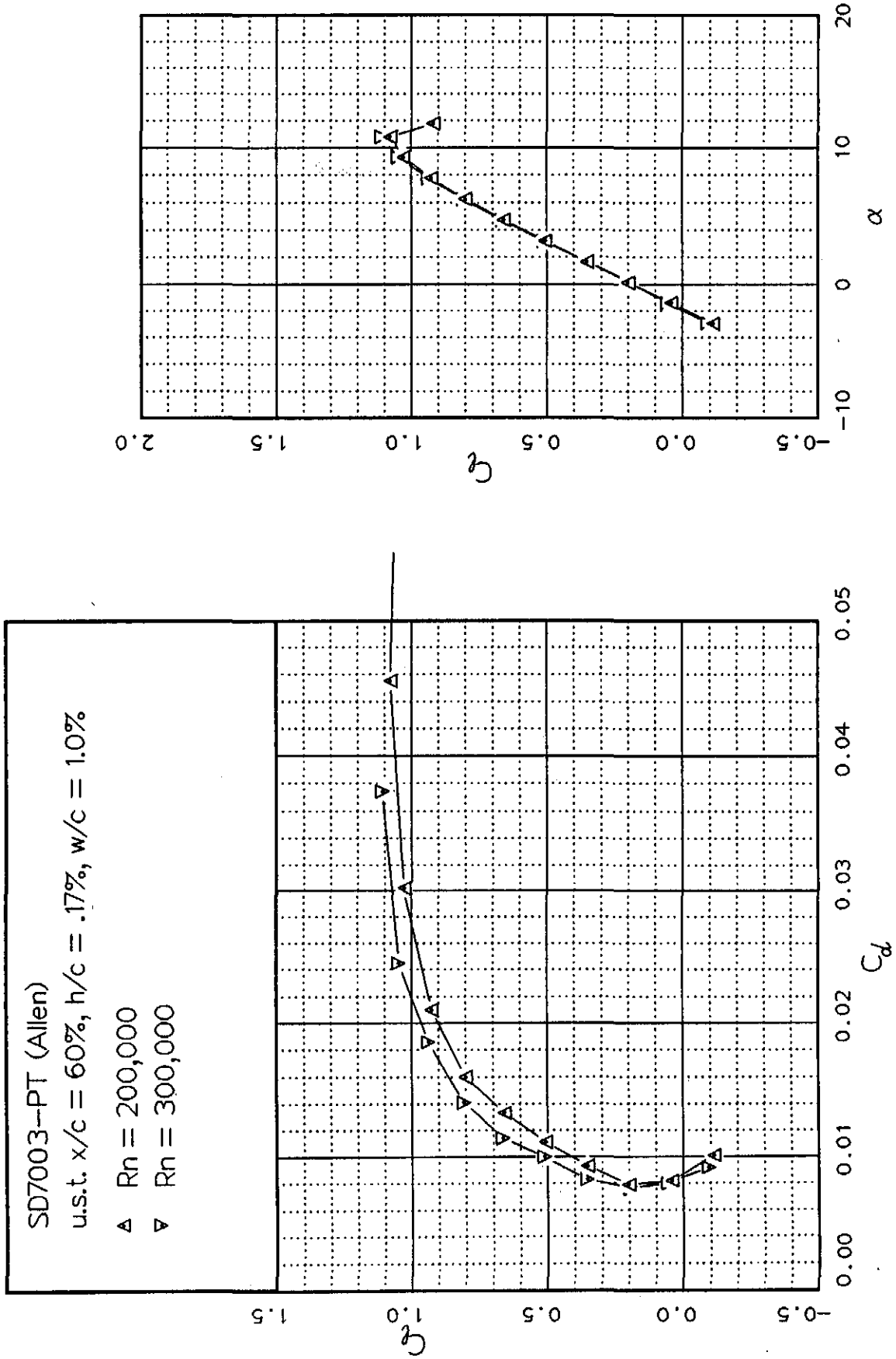
SD7003-PT (Allen)
u.s.t. x/c = 60%, h/c = .17%, w/c = 1.0%
Rn = 200,000
Rn = 300,000
α
C_l
C_d
20
10
0
−10
0.05
0.04
0.03
0.02
0.01
0.00
−0.5
0.0
0.5
1.0
1.5
2.0

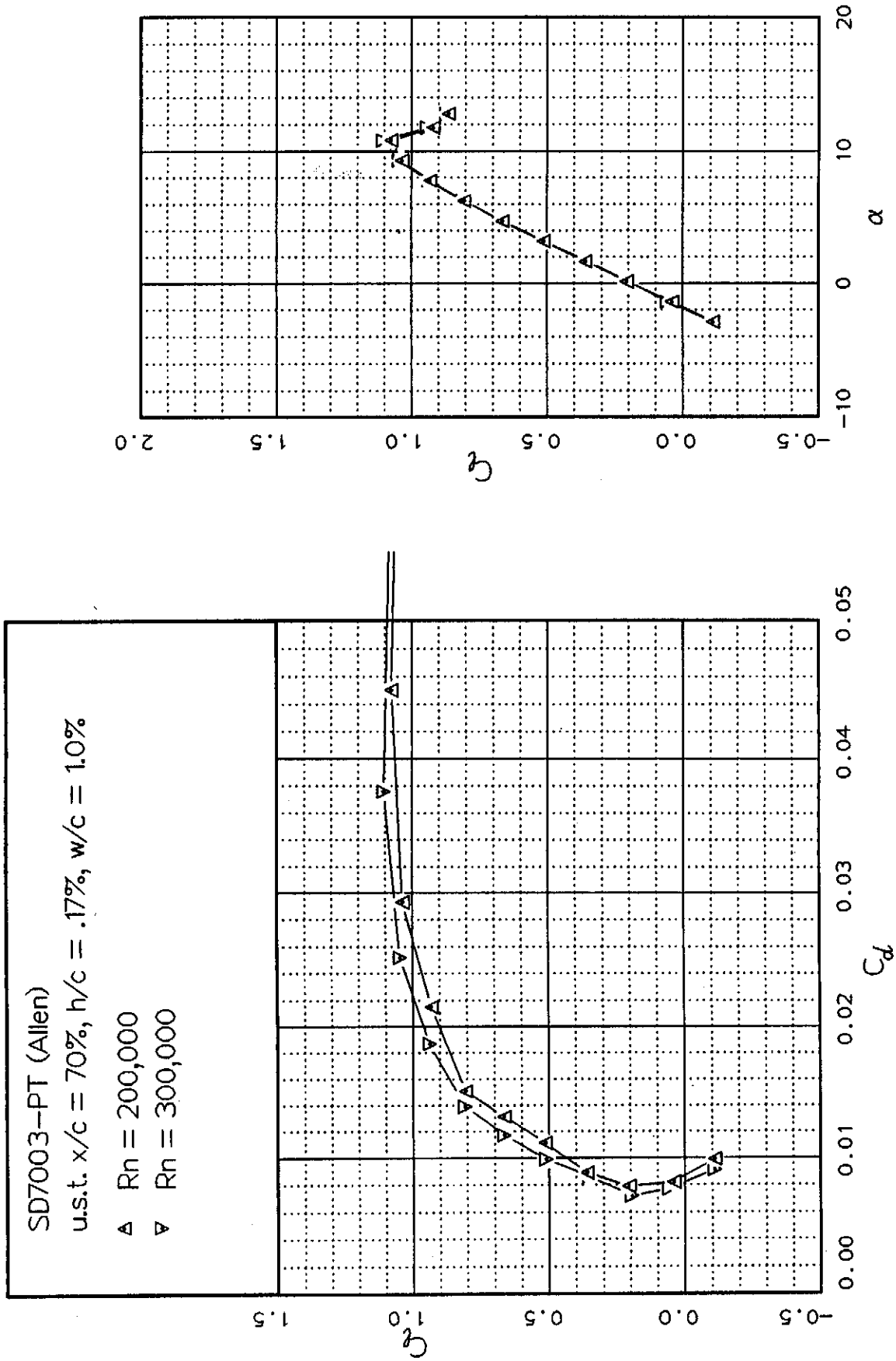
SD7003-PT (Allen)
u.s.t. x/c = 70%, h/c = .17%, w/c = 1.0%
Rn = 200,000
Rn = 300,000
C_l
C_d
α

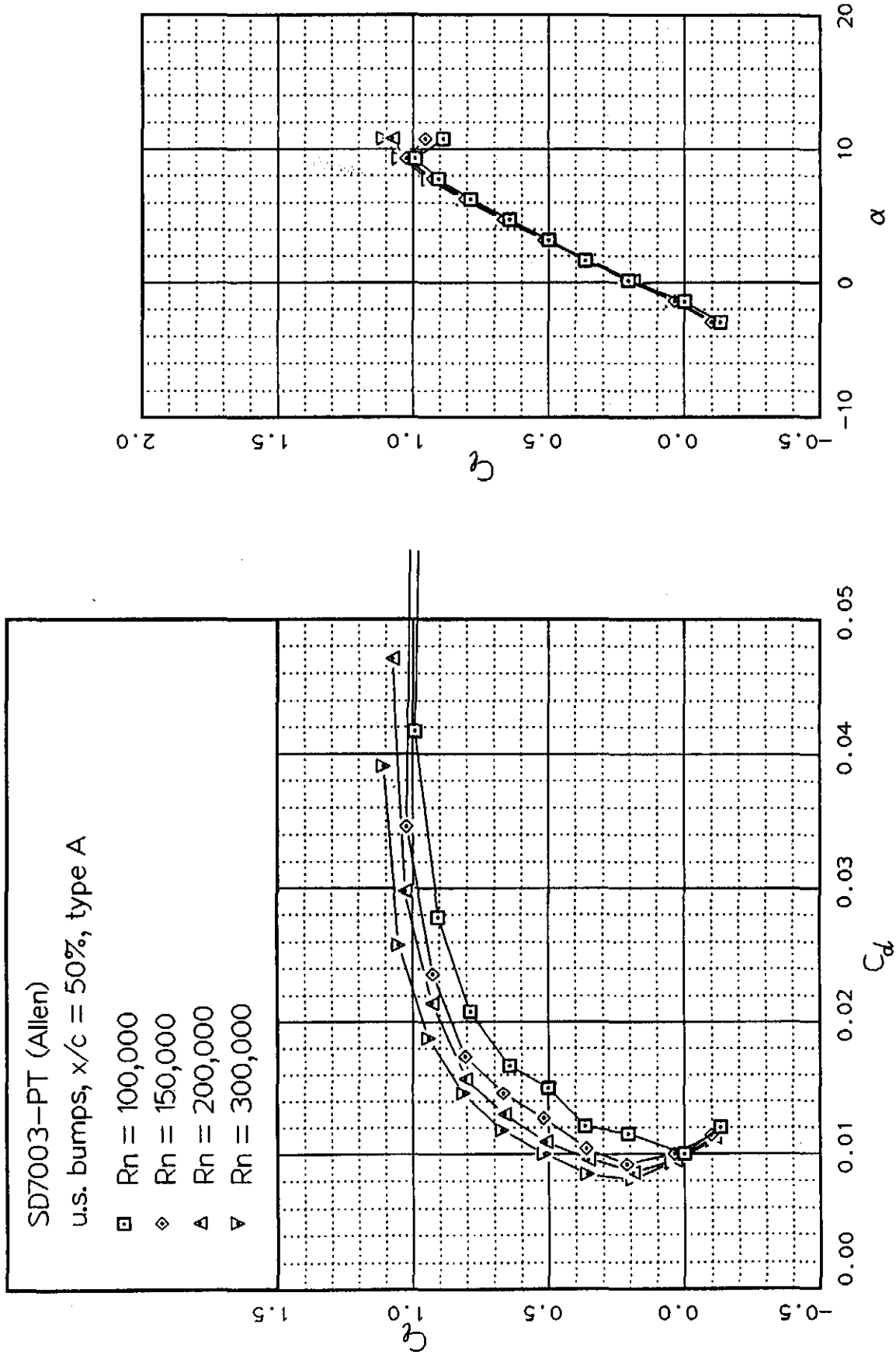
SD7003–PT (Allen)
u.s. bumps, x/c = 50%, type A
Rn = 100,000
Rn = 150,000
Rn = 200,000
Rn = 300,000
C_l
C_d
α

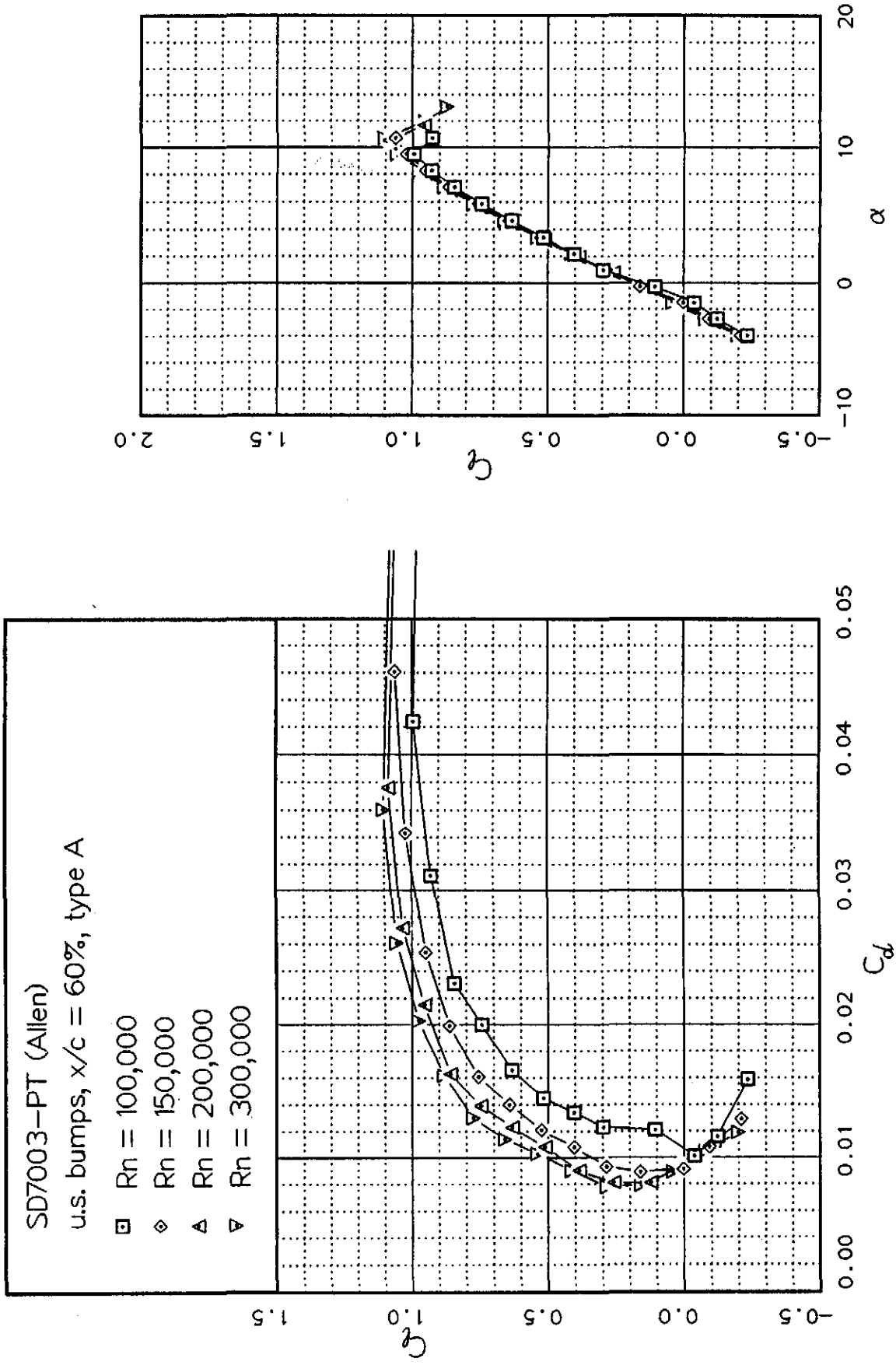
SD7003–PT (Allen)
u.s. bumps, x/c = 60%, type A
Rn = 100,000
Rn = 150,000
Rn = 200,000
Rn = 300,000
α
C_d
C_l
20
10
0
−10
0.05
0.04
0.03
0.02
0.01
0.00
−0.5
0.0
0.5
1.0
1.5
2.0

Fig. 12.124

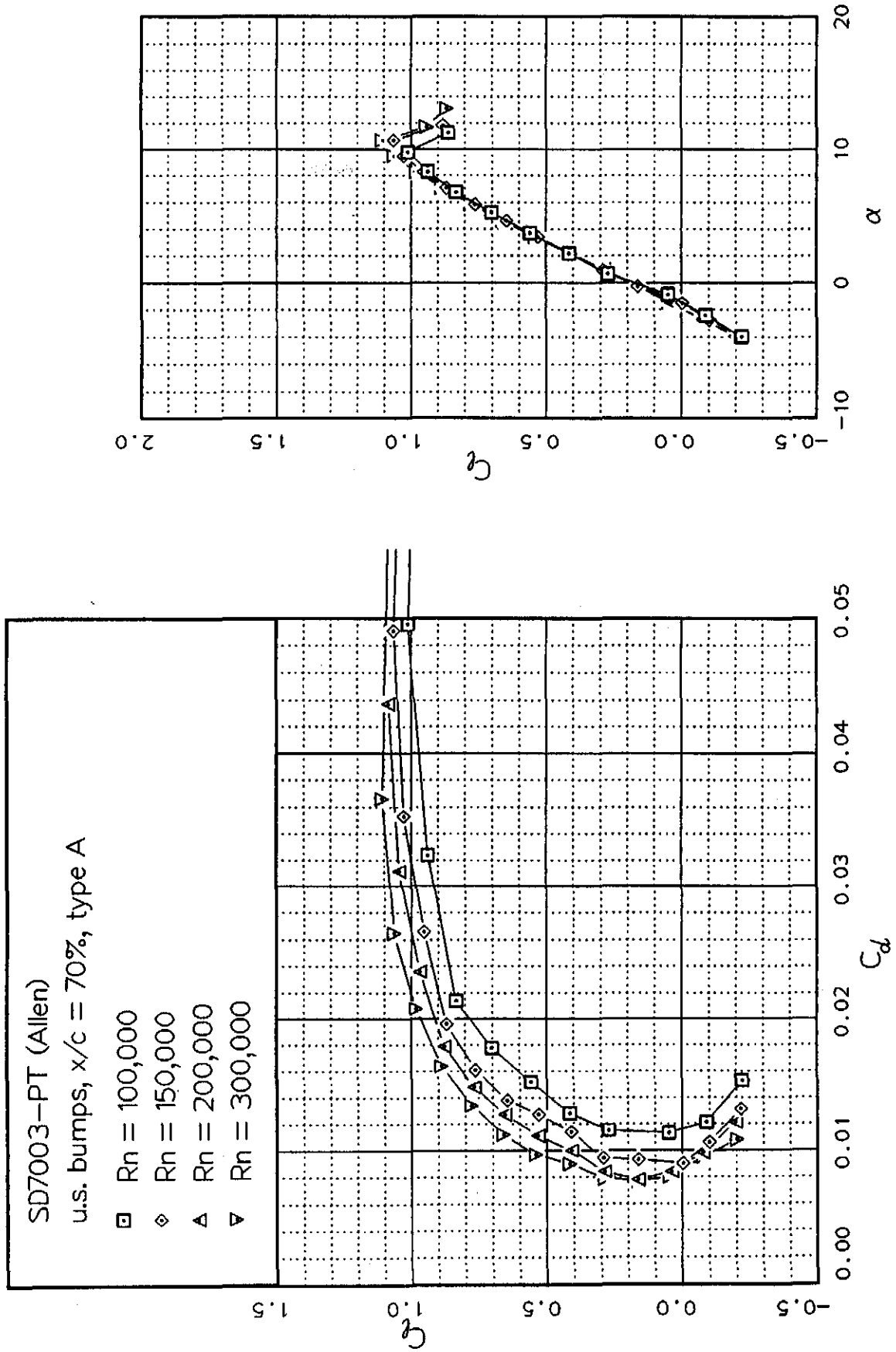
SD7003–PT (Allen)
u.s. bumps, x/c = 70%, type A
Rn = 100,000
Rn = 150,000
Rn = 200,000
Rn = 300,000
C_l
C_d
α

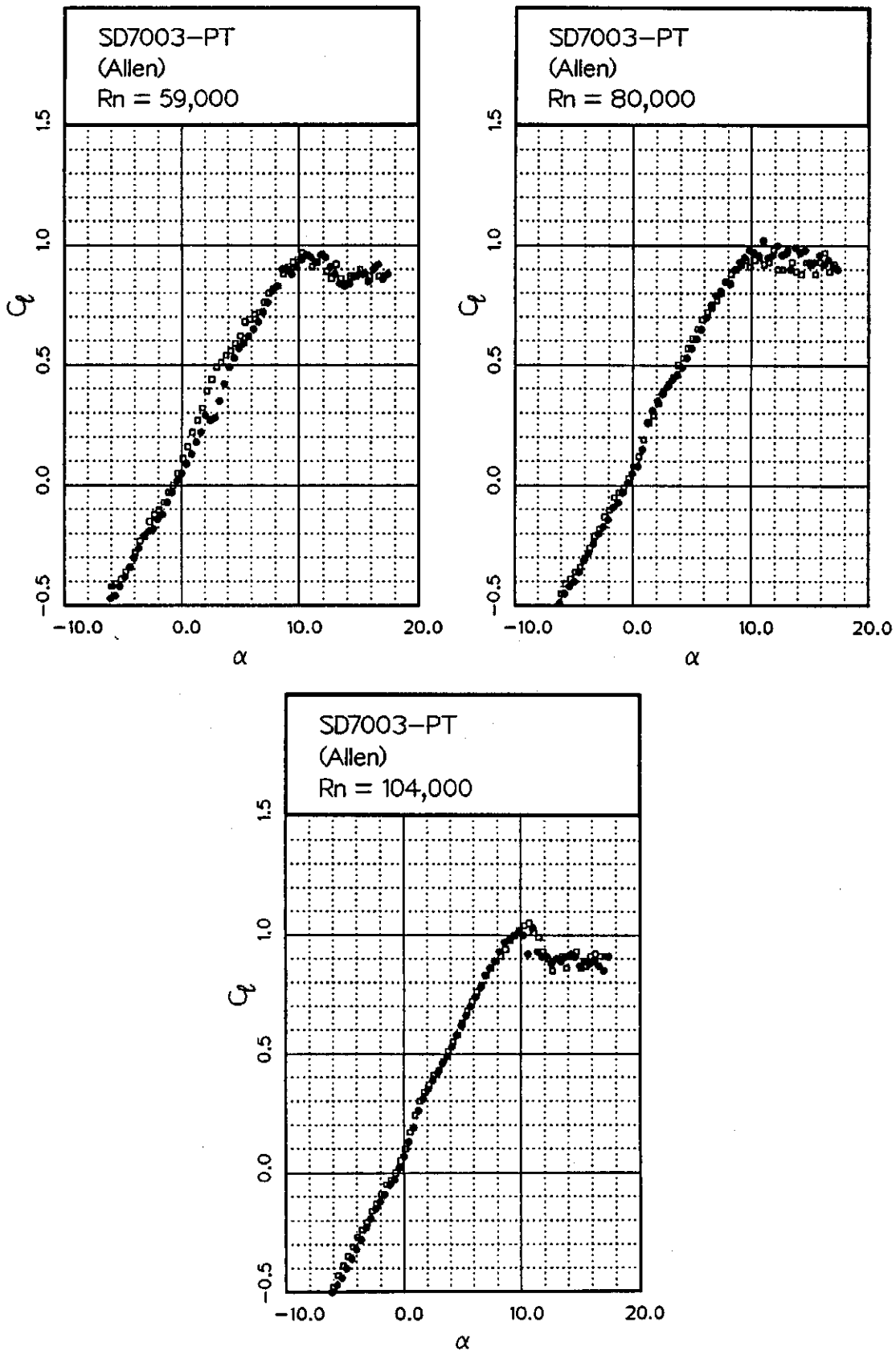
SD7003–PT
(Allen)
Rn = 59,000
SD7003–PT
(Allen)
Rn = 80,000
SD7003–PT
(Allen)
Rn = 104,000
C_ℓ
α
1.5
1.0
0.5
0.0
−0.5
−10.0
0.0
10.0
20.0

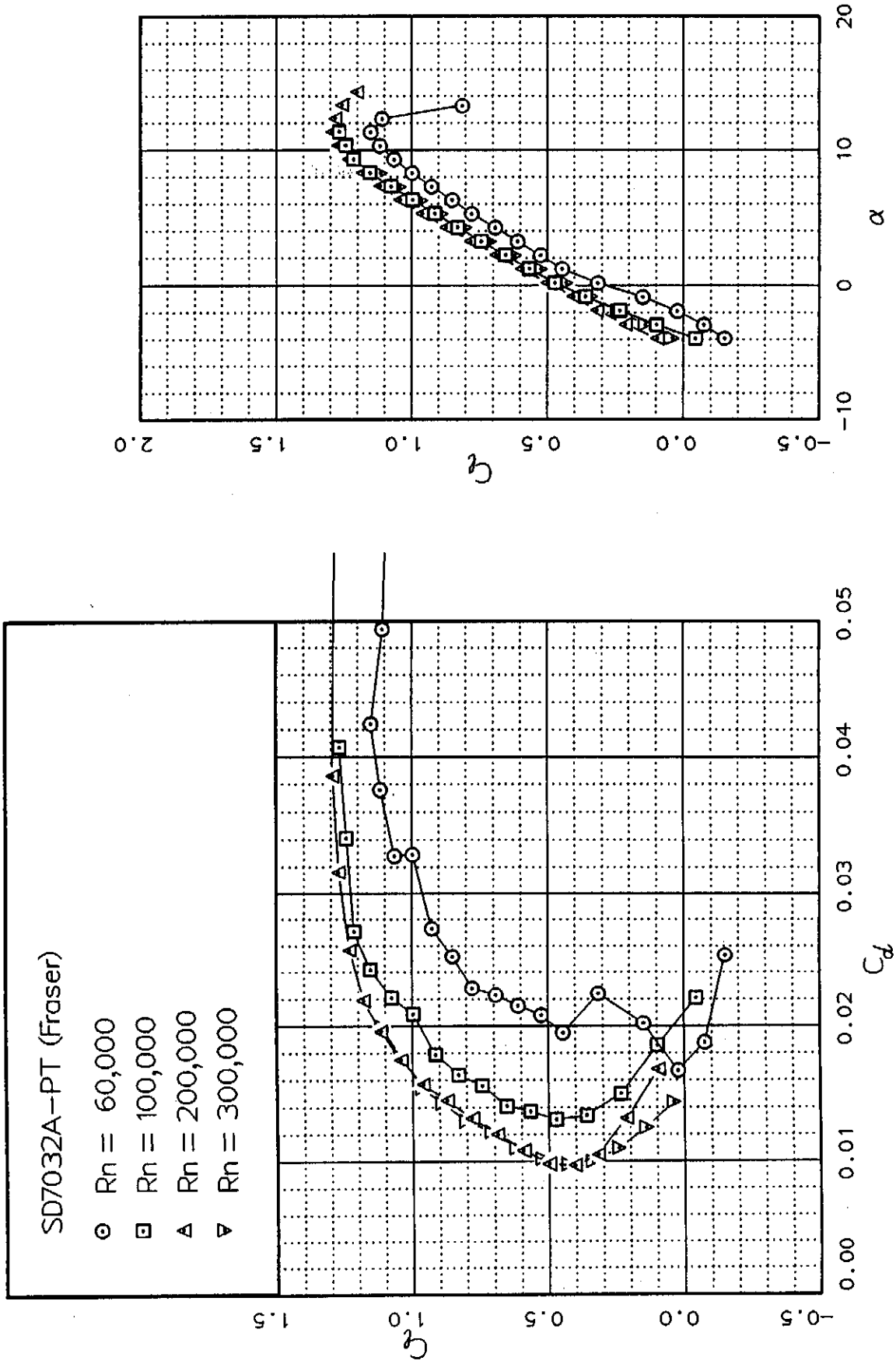
SD7032A-PT (Fraser)
Rn = 60,000
Rn = 100,000
Rn = 200,000
Rn = 300,000
−0.5
0.0
0.5
1.0
1.5
2.0
c_l
−10
0
10
20
α
0.00
0.01
0.02
0.03
0.04
0.05
c_d

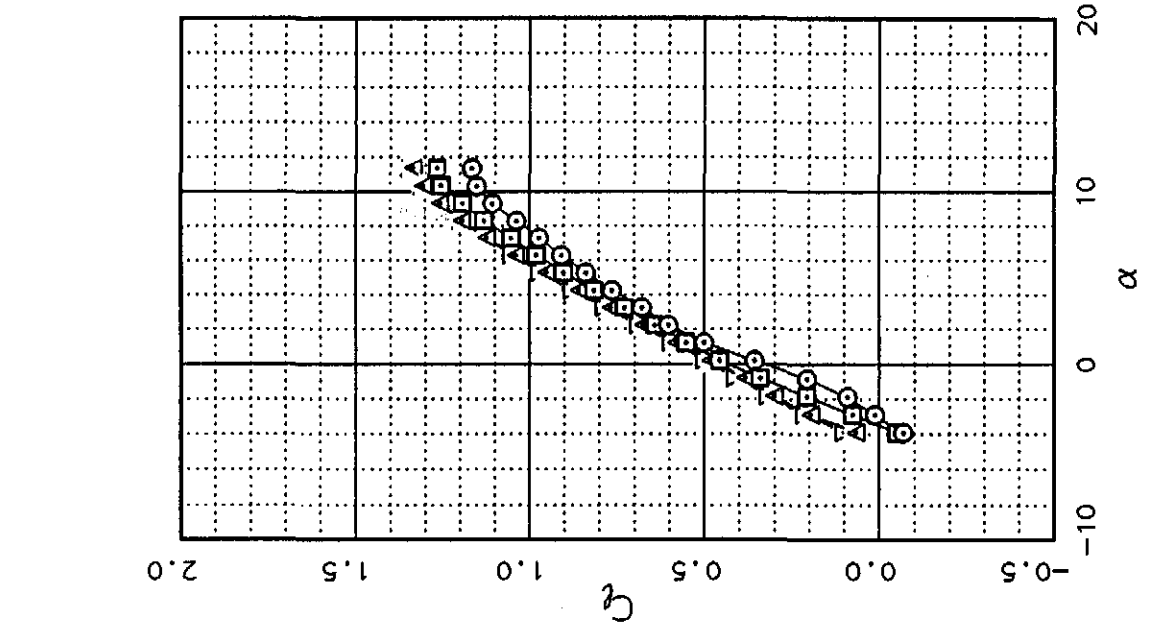
20
10
0
−10
α
−0.5
0.0
0.5
1.0
1.5
2.0
CL

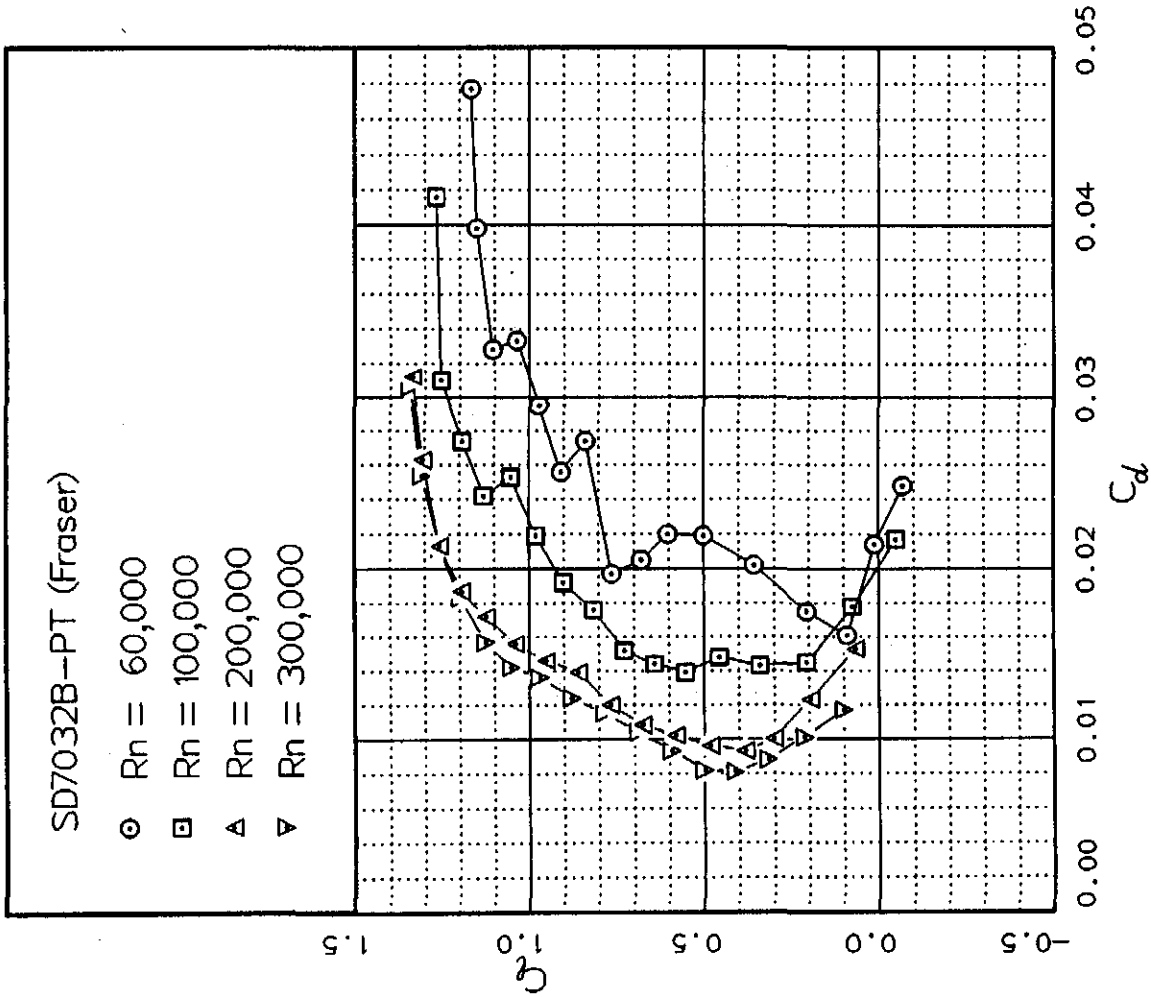
SD7032B–PT (Fraser)
Rn = 60,000
Rn = 100,000
Rn = 200,000
Rn = 300,000
0.05
0.04
0.03
0.02
0.01
0.00
Cd
−0.5
0.0
0.5
1.0
1.5
CL

Fig. 12.128

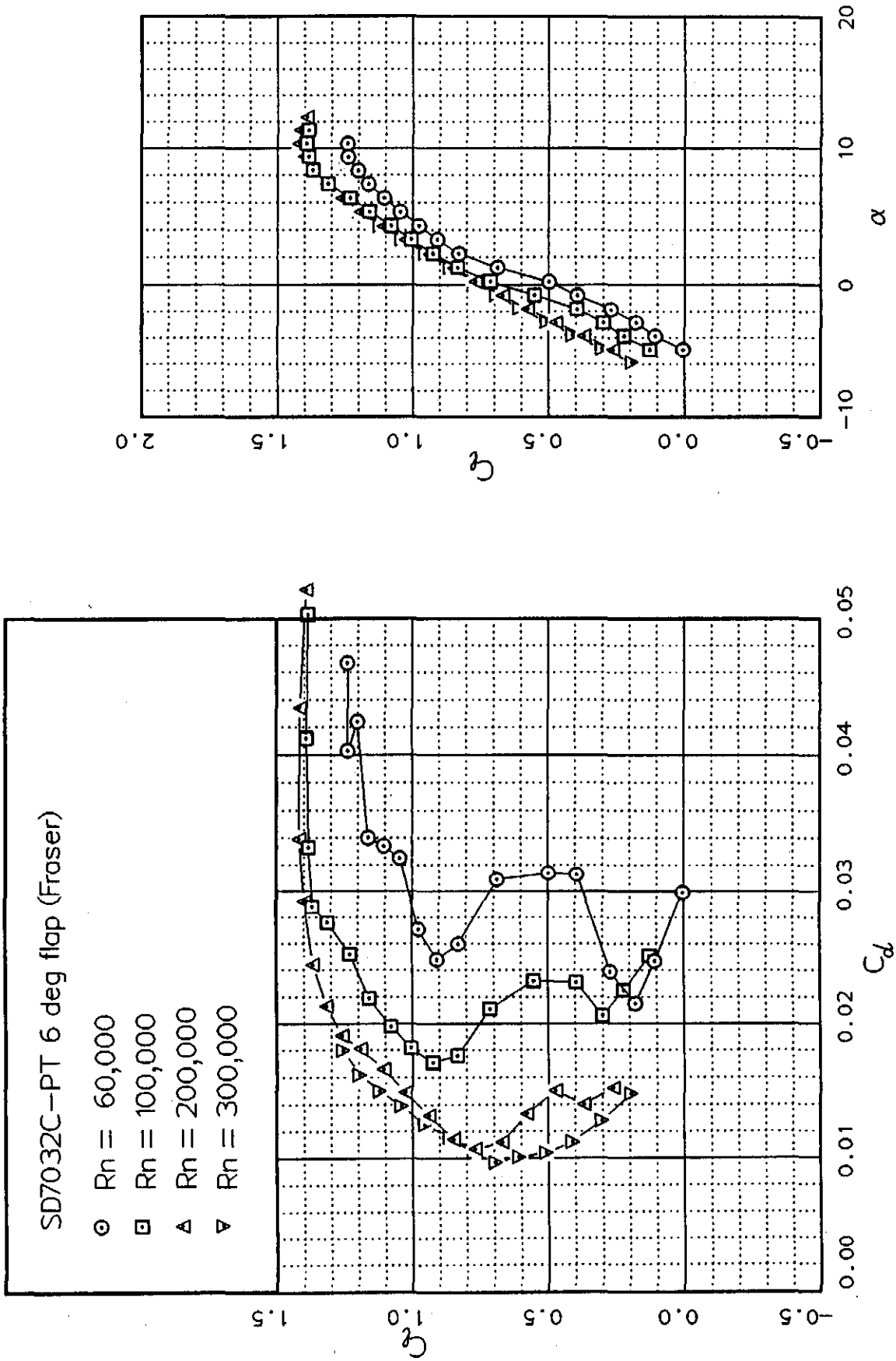
SD7032C–PT 6 deg flap (Fraser)
Rn = 60,000
Rn = 100,000
Rn = 200,000
Rn = 300,000
α
20
10
0
−10
−0.5
0.0
0.5
1.0
1.5
2.0
C_l
C_d
0.00
0.01
0.02
0.03
0.04
0.05

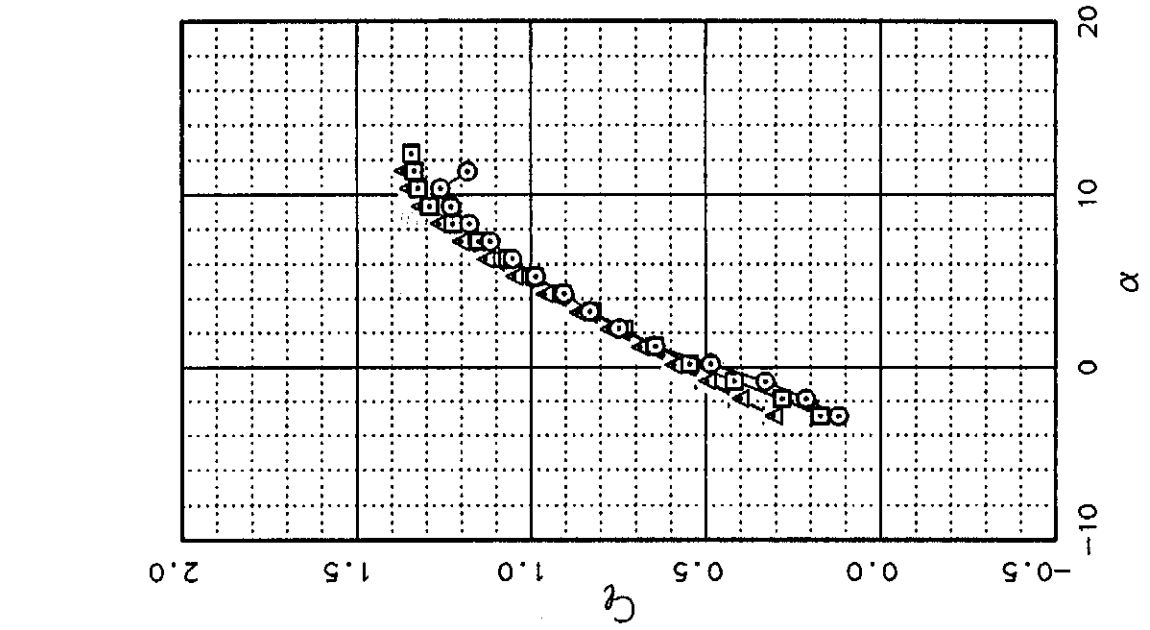
20
10
0
−10
α
−0.5
0.0
0.5
1.0
1.5
2.0
C_l

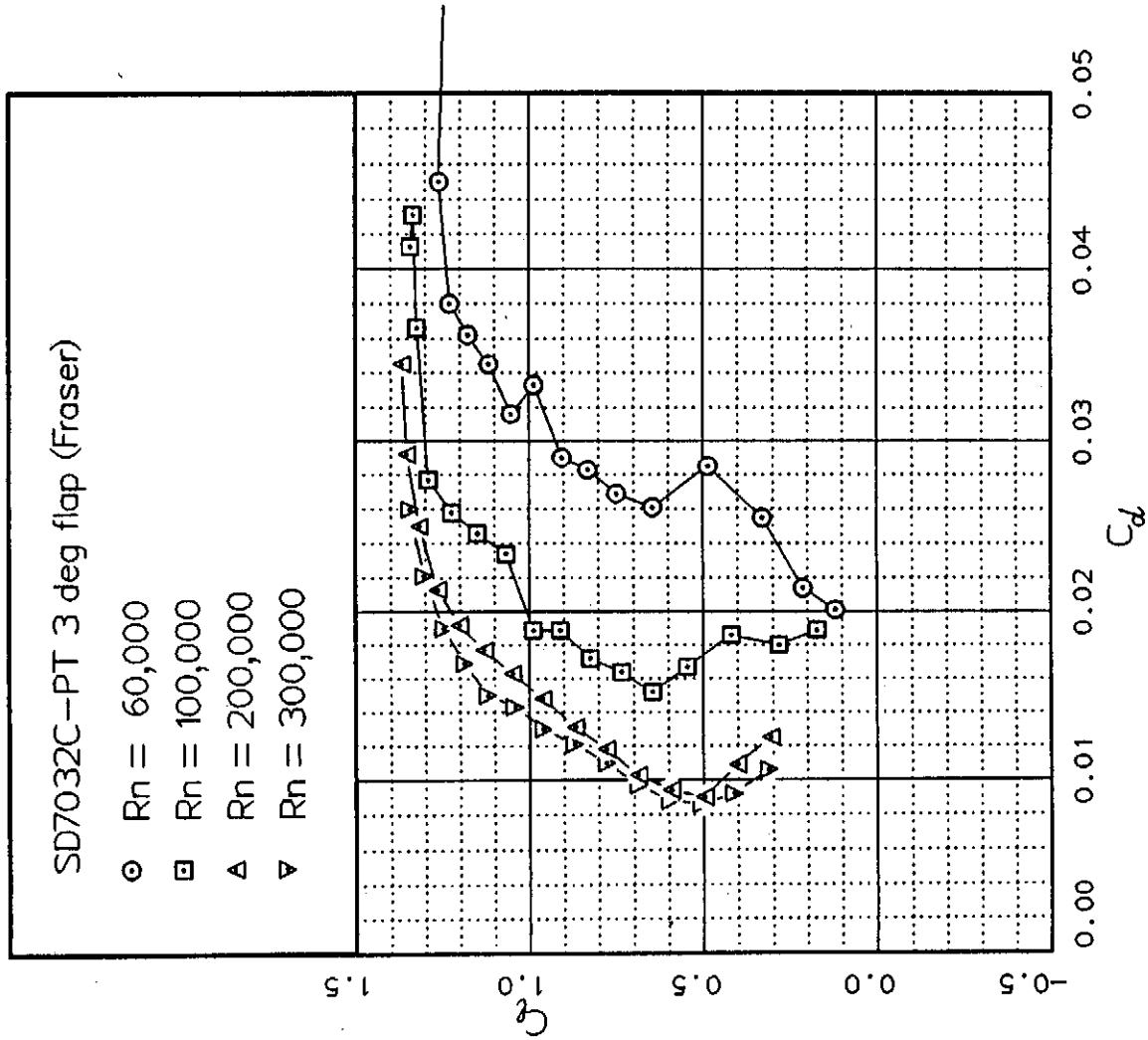
SD7032C−PT 3 deg flap (Fraser)
Rn = 60,000
Rn = 100,000
Rn = 200,000
Rn = 300,000
0.05
0.04
0.03
0.02
0.01
0.00
C_d
−0.5
0.0
0.5
1.0
1.5
C_l

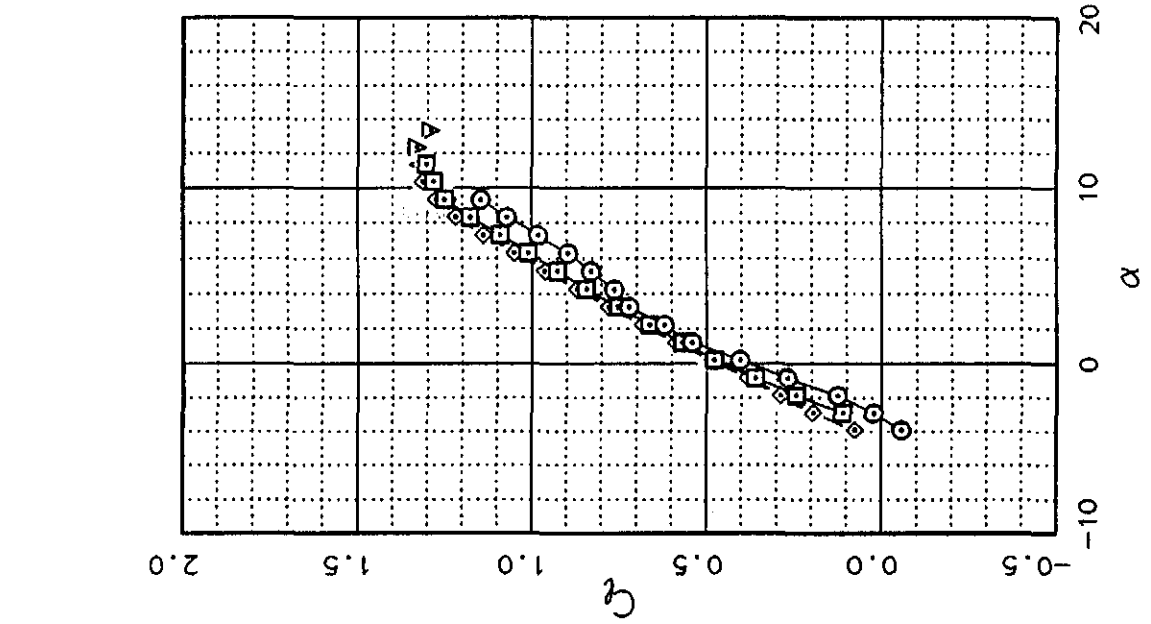
20
10
0
−10
α
−0.5
0.0
0.5
1.0
1.5
2.0
C_l

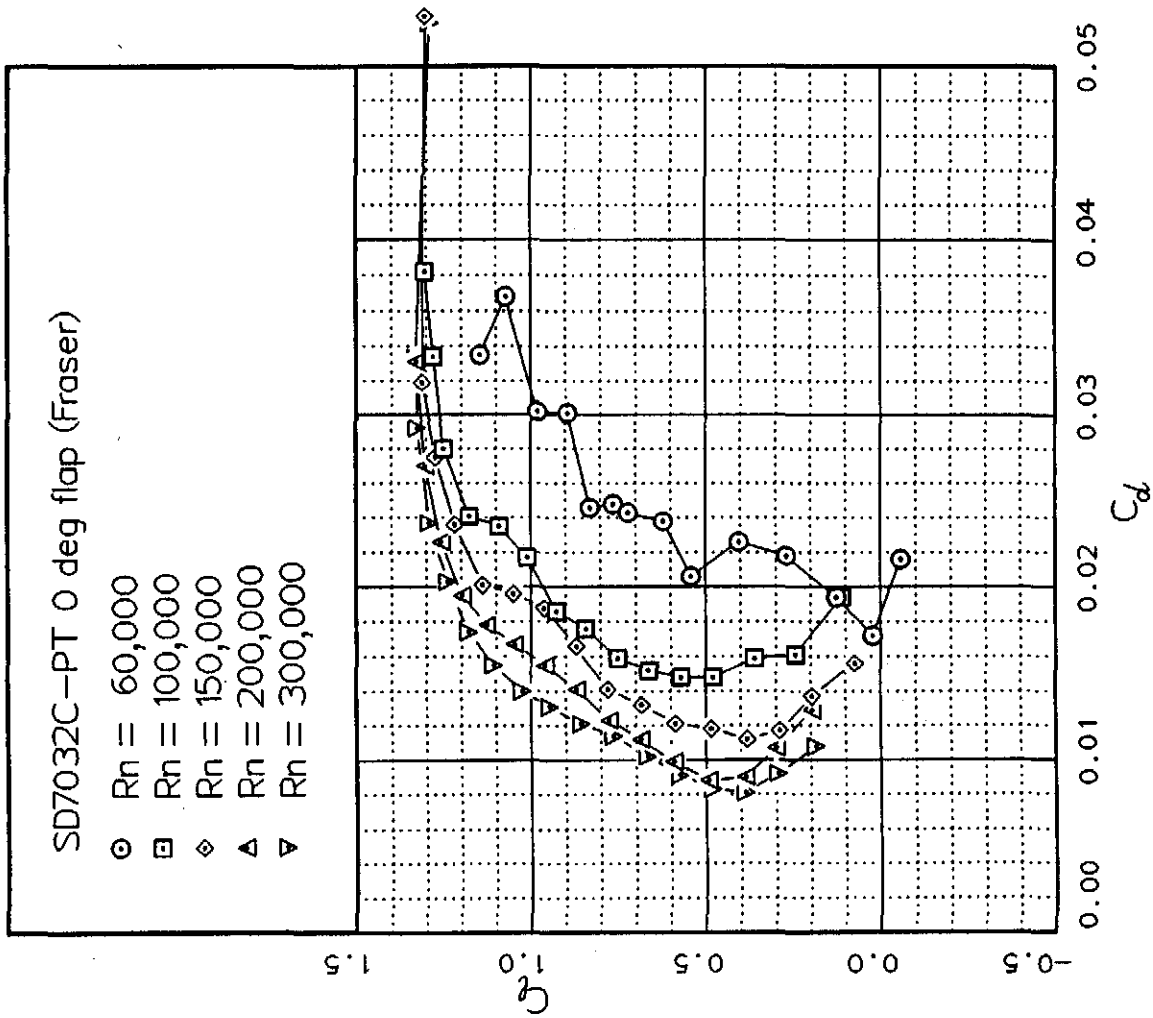
SD7032C−PT 0 deg flap (Fraser)
Rn = 60,000
Rn = 100,000
Rn = 150,000
Rn = 200,000
Rn = 300,000
0.05
0.04
0.03
0.02
0.01
0.00
C_d
−0.5
0.0
0.5
1.0
1.5
C_l

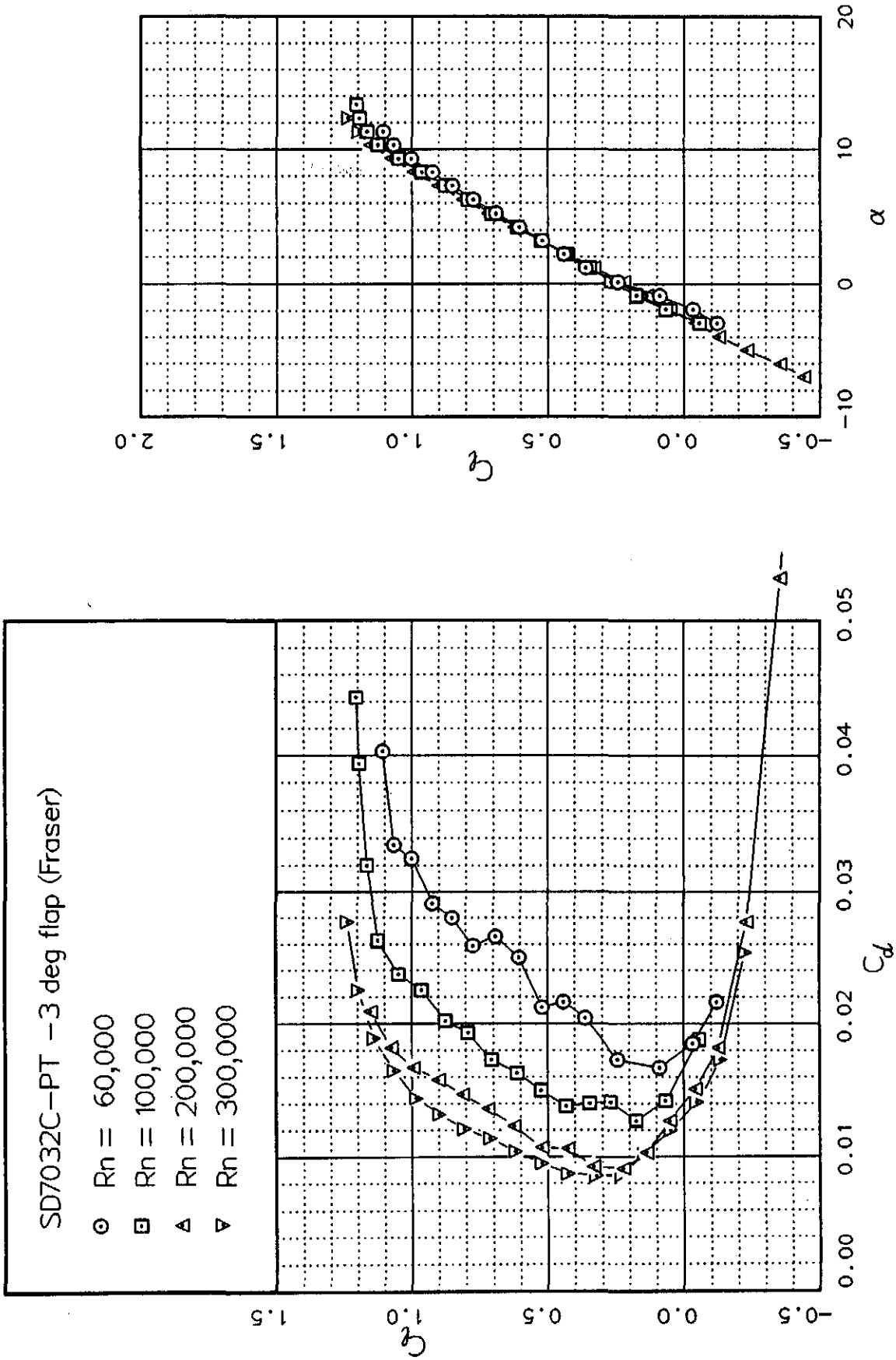
SD7032C–PT –3 deg flap (Fraser)
Rn = 60,000
Rn = 100,000
Rn = 200,000
Rn = 300,000
α
20
10
0
−10
−0.5
0.0
0.5
1.0
1.5
2.0
C_l
C_d
0.00
0.01
0.02
0.03
0.04
0.05

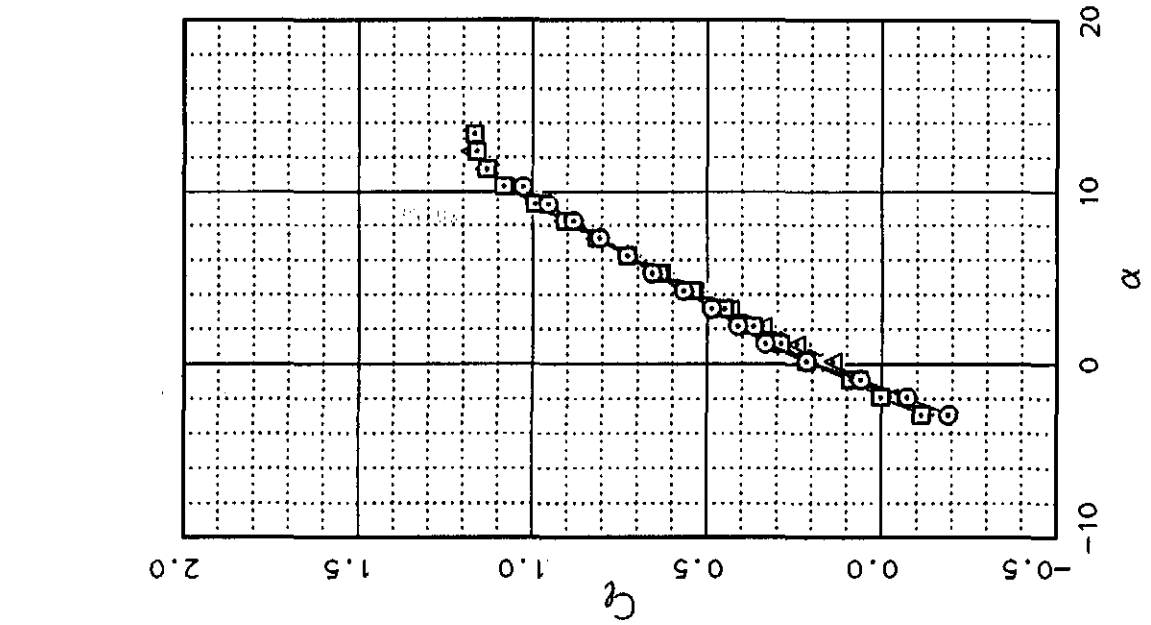
20
10
0
−10
α
−0.5
0.0
0.5
1.0
1.5
2.0
c_l

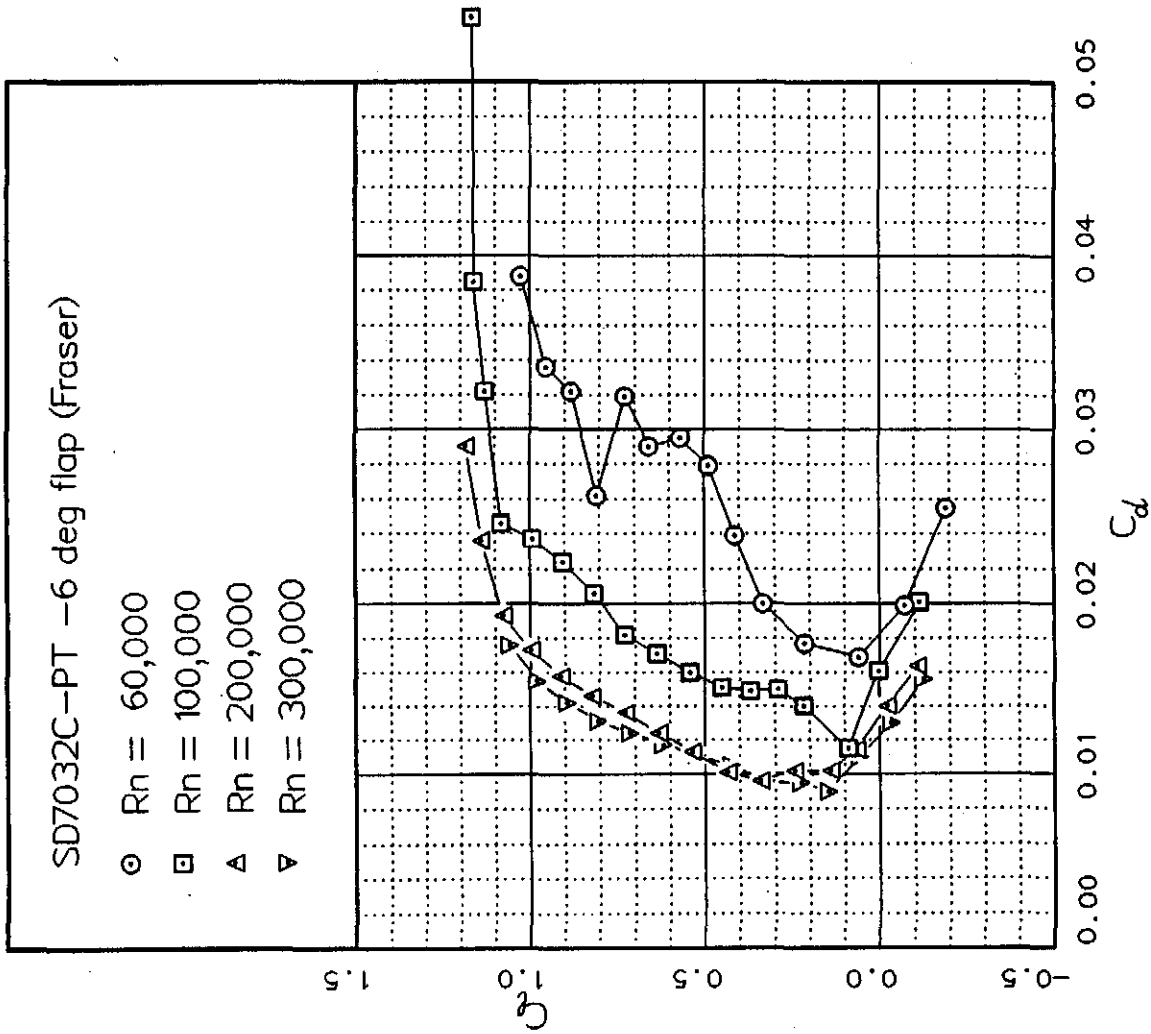
SD7032C−PT −6 deg flap (Fraser)
Rn = 60,000
Rn = 100,000
Rn = 200,000
Rn = 300,000
0.05
0.04
0.03
0.02
0.01
0.00
C_d
−0.5
0.0
0.5
1.0
1.5
c_l

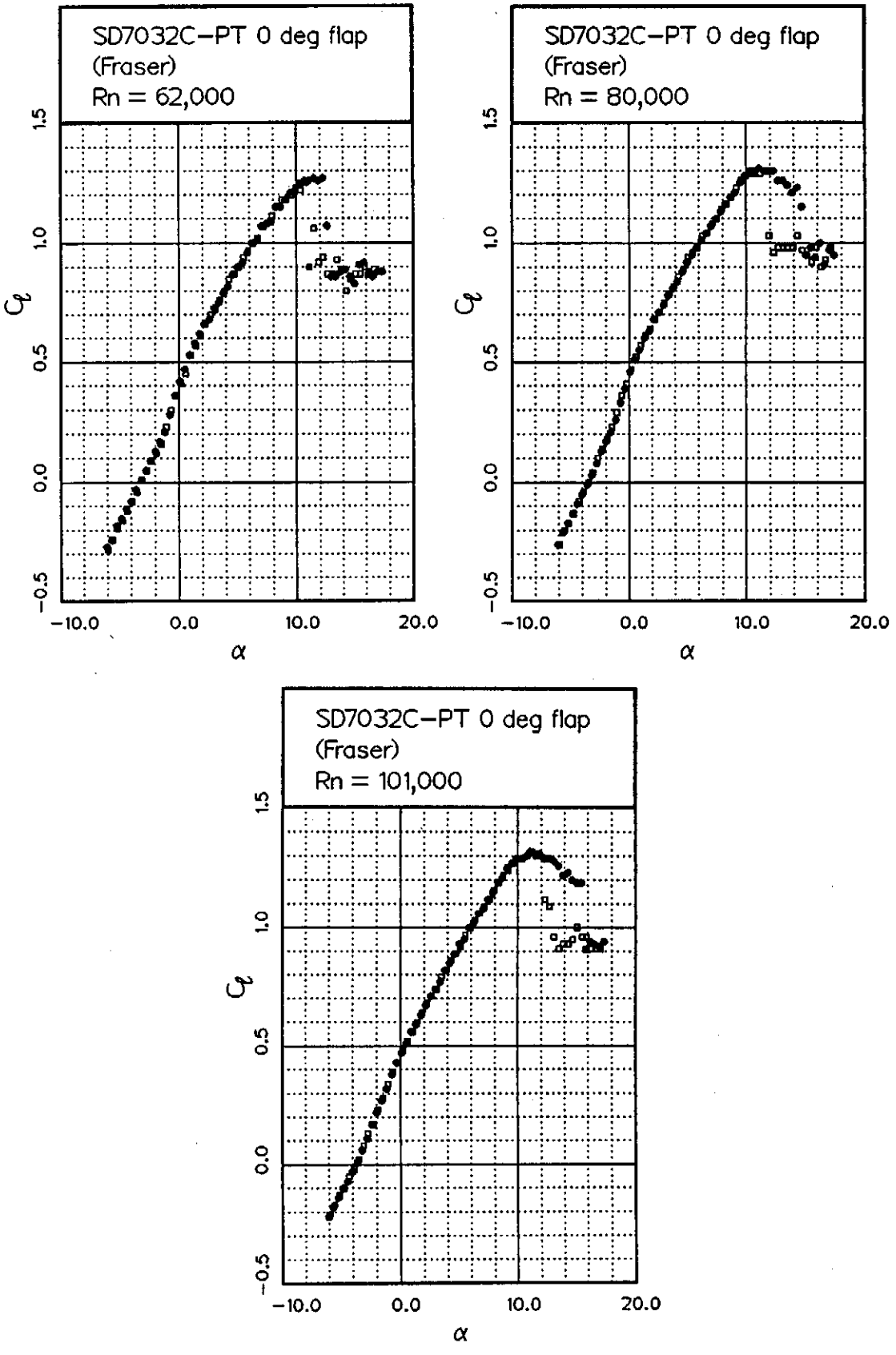
SD7032C–PT 0 deg flap
(Fraser)
Rn = 62,000
SD7032C–PT 0 deg flap
(Fraser)
Rn = 80,000
SD7032C–PT 0 deg flap
(Fraser)
Rn = 101,000
C_ℓ
α
1.5
1.0
0.5
0.0
−0.5
−10.0
0.0
10.0
20.0

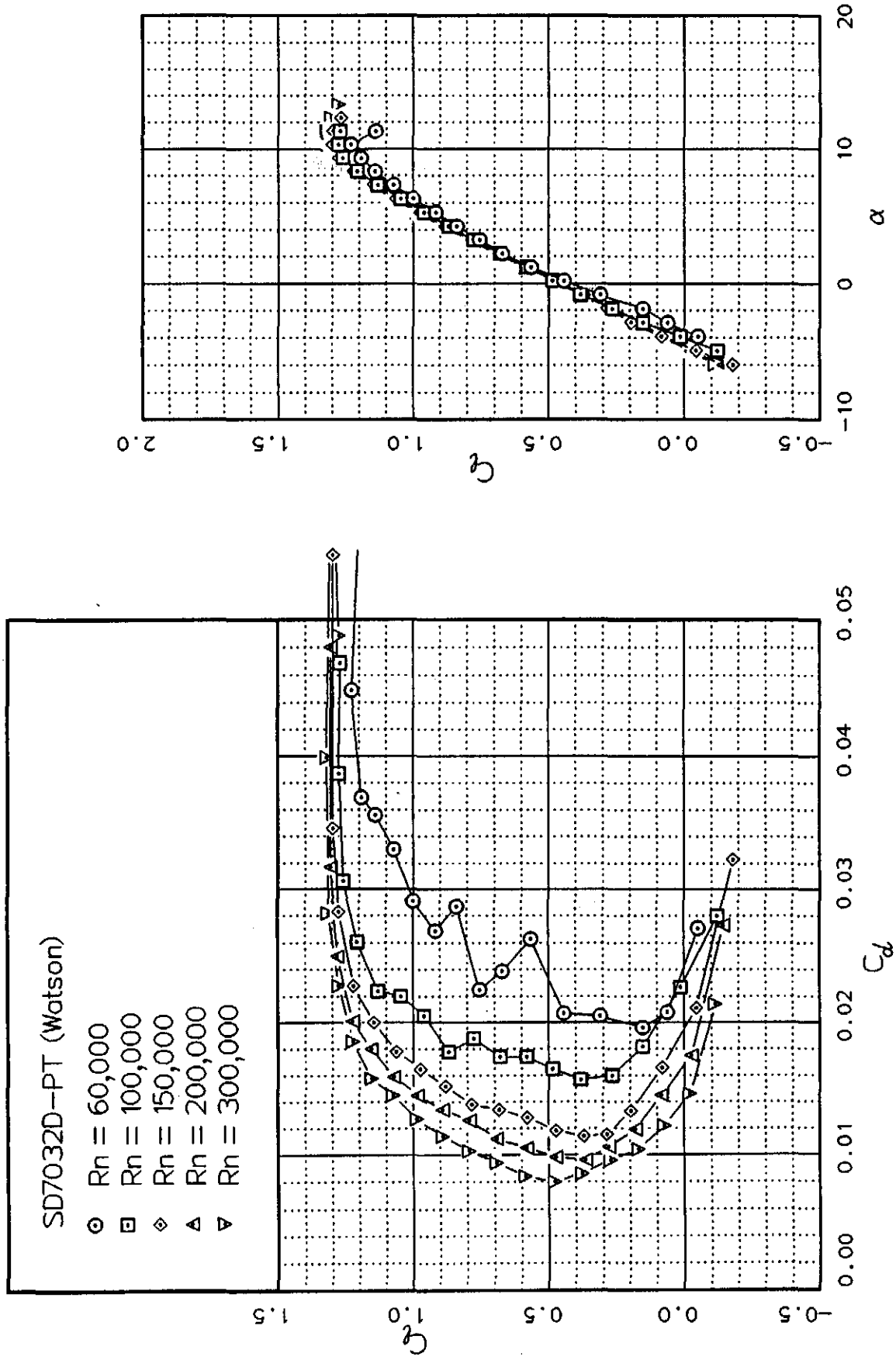
SD7032D–PT (Watson)
Rn = 60,000
Rn = 100,000
Rn = 150,000
Rn = 200,000
Rn = 300,000
−0.5
0.0
0.5
1.0
1.5
2.0
c_l
20
10
0
−10
α
0.05
0.04
0.03
0.02
0.01
0.00
c_d

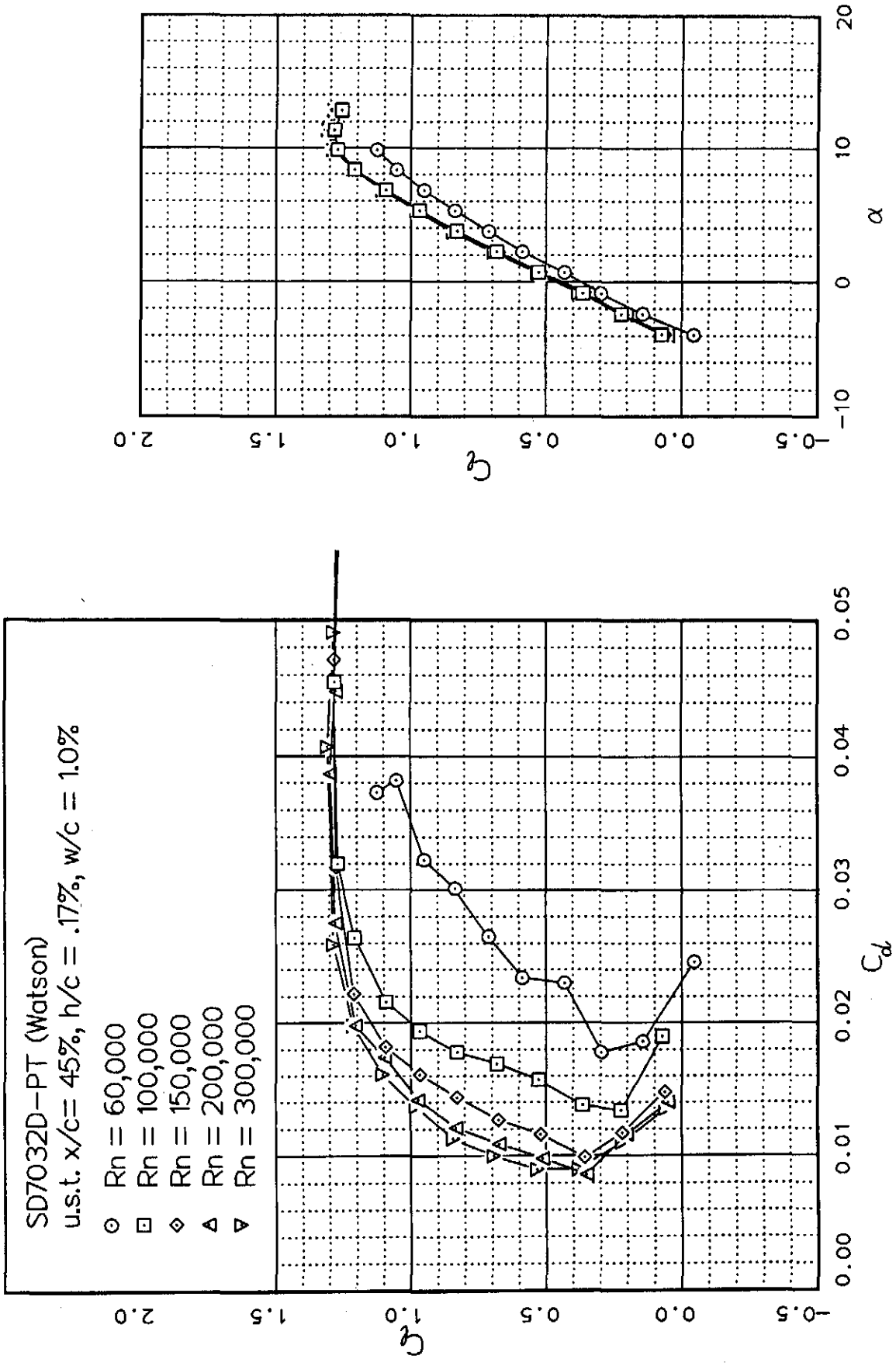
SD7032D–PT (Watson)
u.s.t. x/c= 45%, h/c = .17%, w/c = 1.0%
Rn = 60,000
Rn = 100,000
Rn = 150,000
Rn = 200,000
Rn = 300,000
−0.5
0.0
0.5
1.0
1.5
2.0
c_l
−10
0
10
20
α
0.00
0.01
0.02
0.03
0.04
0.05
c_d

Fig. 12.136

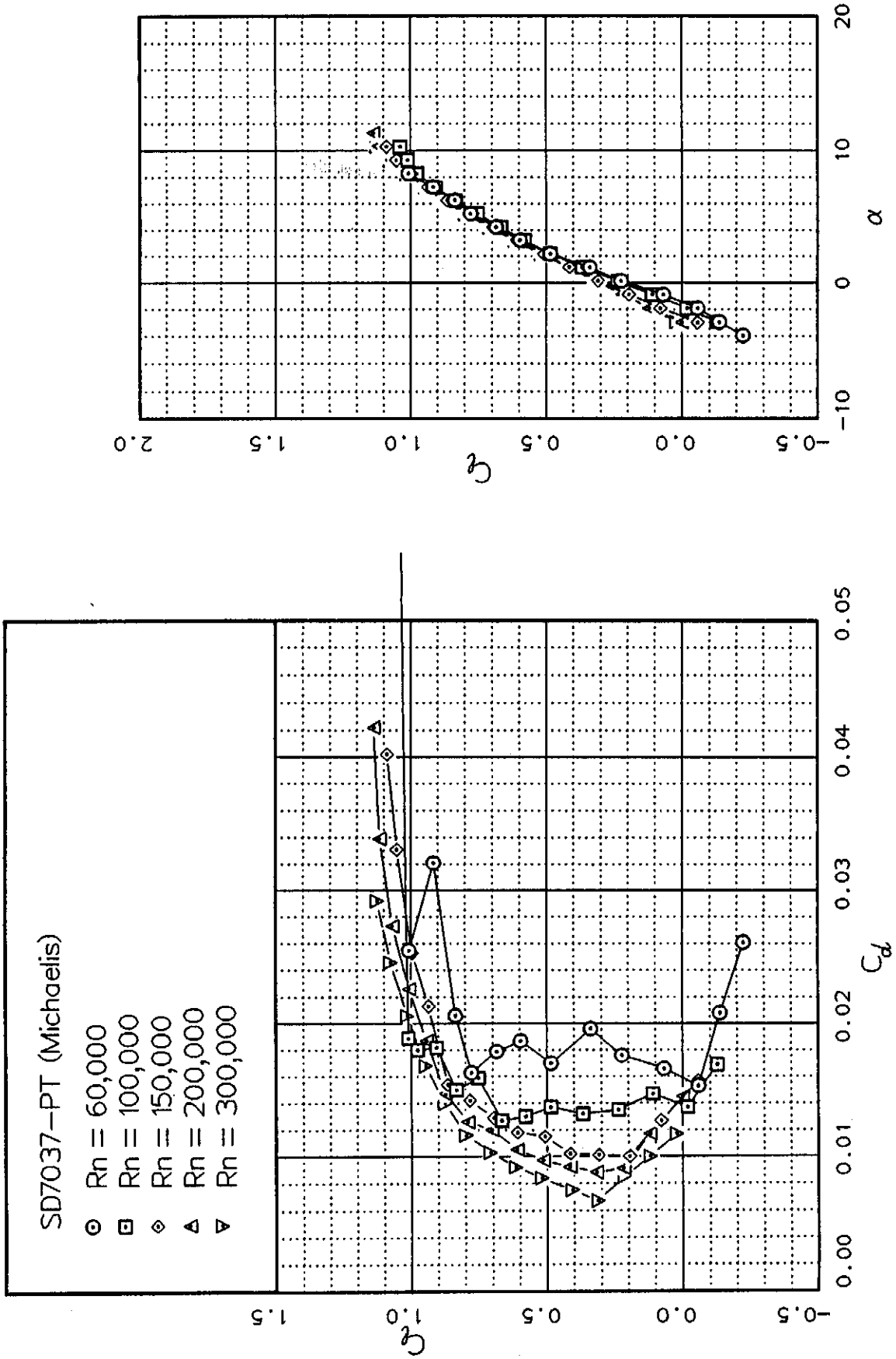
SD7037–PT (Michaelis)
Rn = 60,000
Rn = 100,000
Rn = 150,000
Rn = 200,000
Rn = 300,000
α
C_d
C_l
20
10
0
−10
0.05
0.04
0.03
0.02
0.01
0.00
−0.5
0.0
0.5
1.0
1.5
2.0

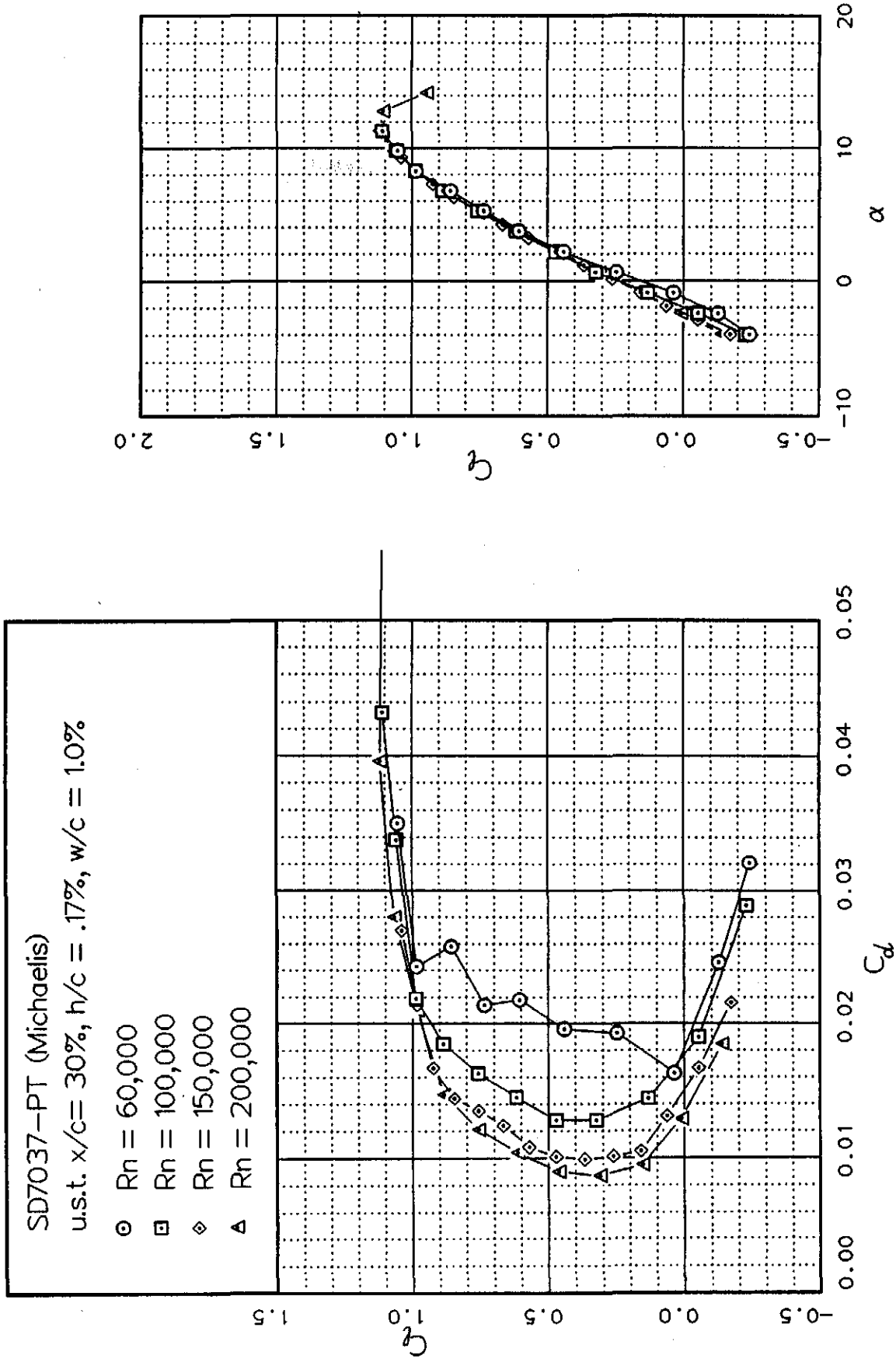
SD7037–PT (Michaelis)
u.s.t. x/c= 30%, h/c = .17%, w/c = 1.0%
Rn = 60,000
Rn = 100,000
Rn = 150,000
Rn = 200,000
−0.5
0.0
0.5
1.0
1.5
2.0
c_l
20
10
0
−10
α
0.00
0.01
0.02
0.03
0.04
0.05
c_d

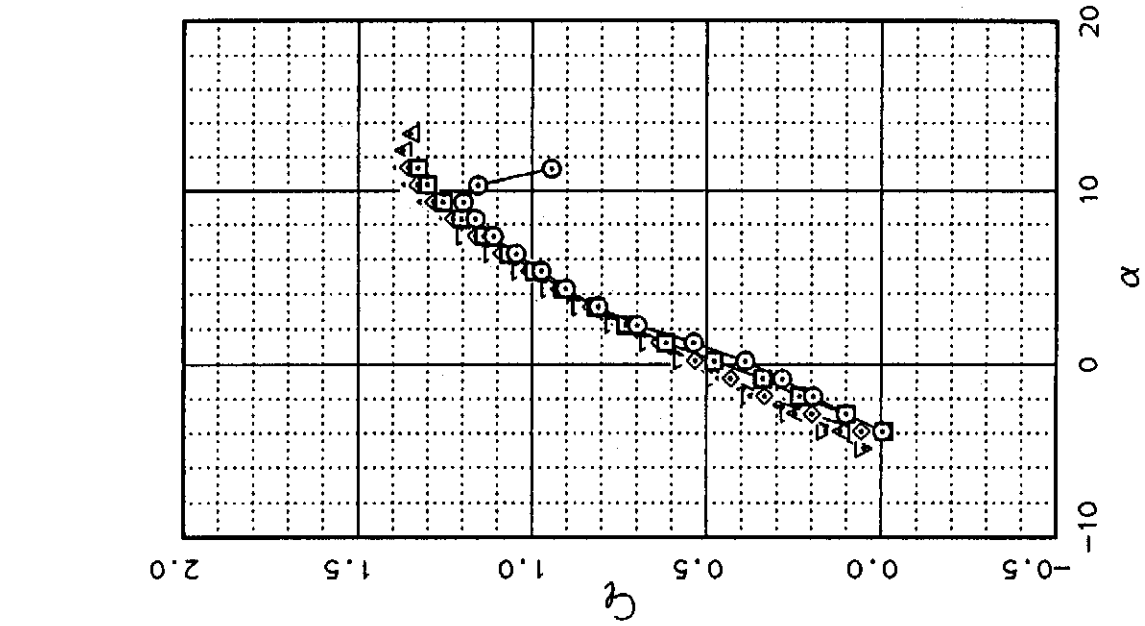
20
10
0
−10
α
−0.5
0.0
0.5
1.0
1.5
2.0
c_l

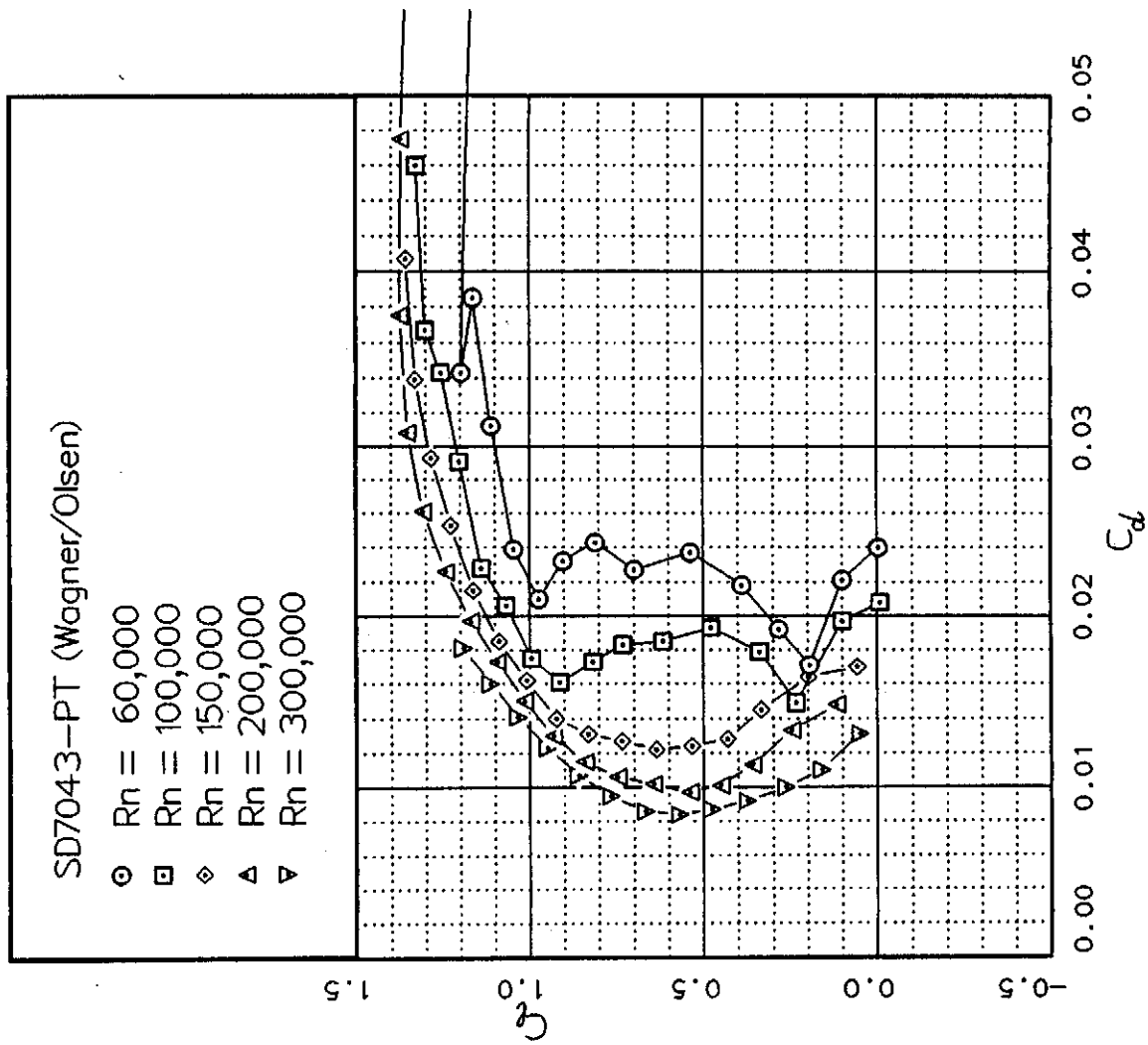
SD7043−PT (Wagner/Olsen)
Rn = 60,000
Rn = 100,000
Rn = 150,000
Rn = 200,000
Rn = 300,000
0.05
0.04
0.03
0.02
0.01
0.00
C_d
−0.5
0.0
0.5
1.0
1.5
c_l

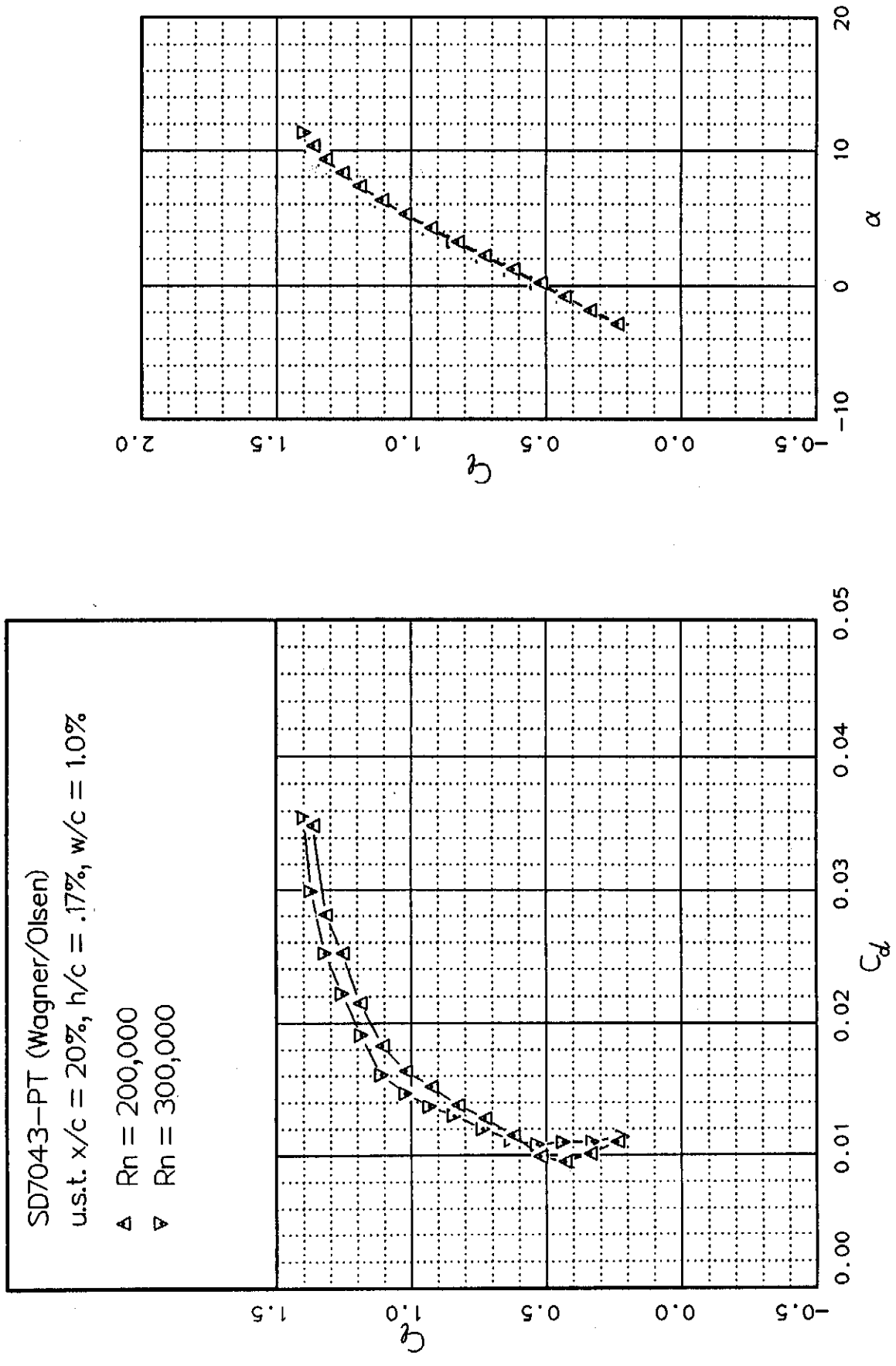
SD7043–PT (Wagner/Olsen)
u.s.t. x/c = 20%, h/c = .17%, w/c = 1.0%
Rn = 200,000
Rn = 300,000
C_l
C_d
α

Fig. 12.140

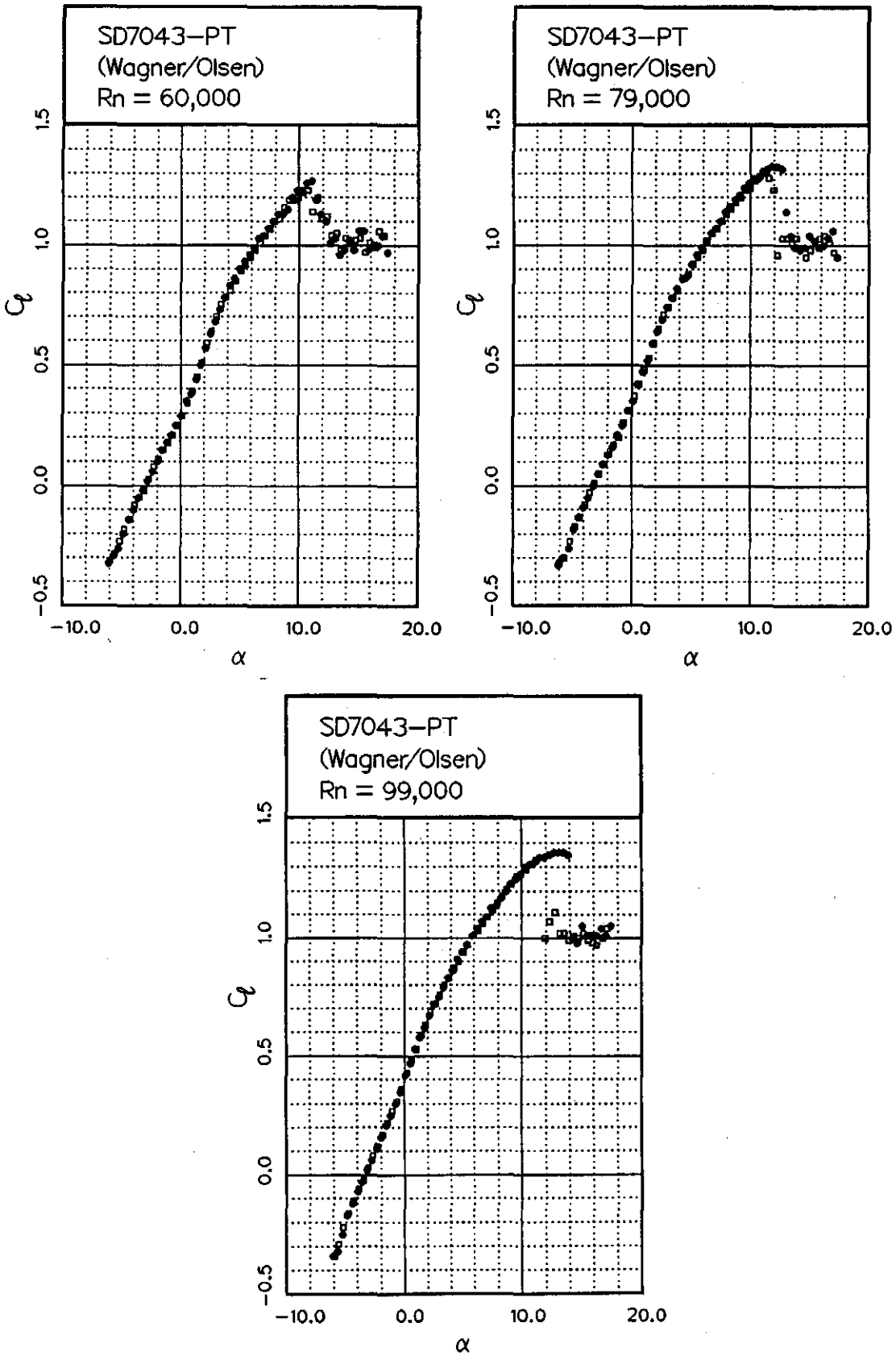
SD7043–PT
(Wagner/Olsen)
Rn = 60,000
SD7043–PT
(Wagner/Olsen)
Rn = 79,000
SD7043–PT
(Wagner/Olsen)
Rn = 99,000
c_ℓ
α
1.5
1.0
0.5
0.0
−0.5
−10.0
0.0
10.0
20.0

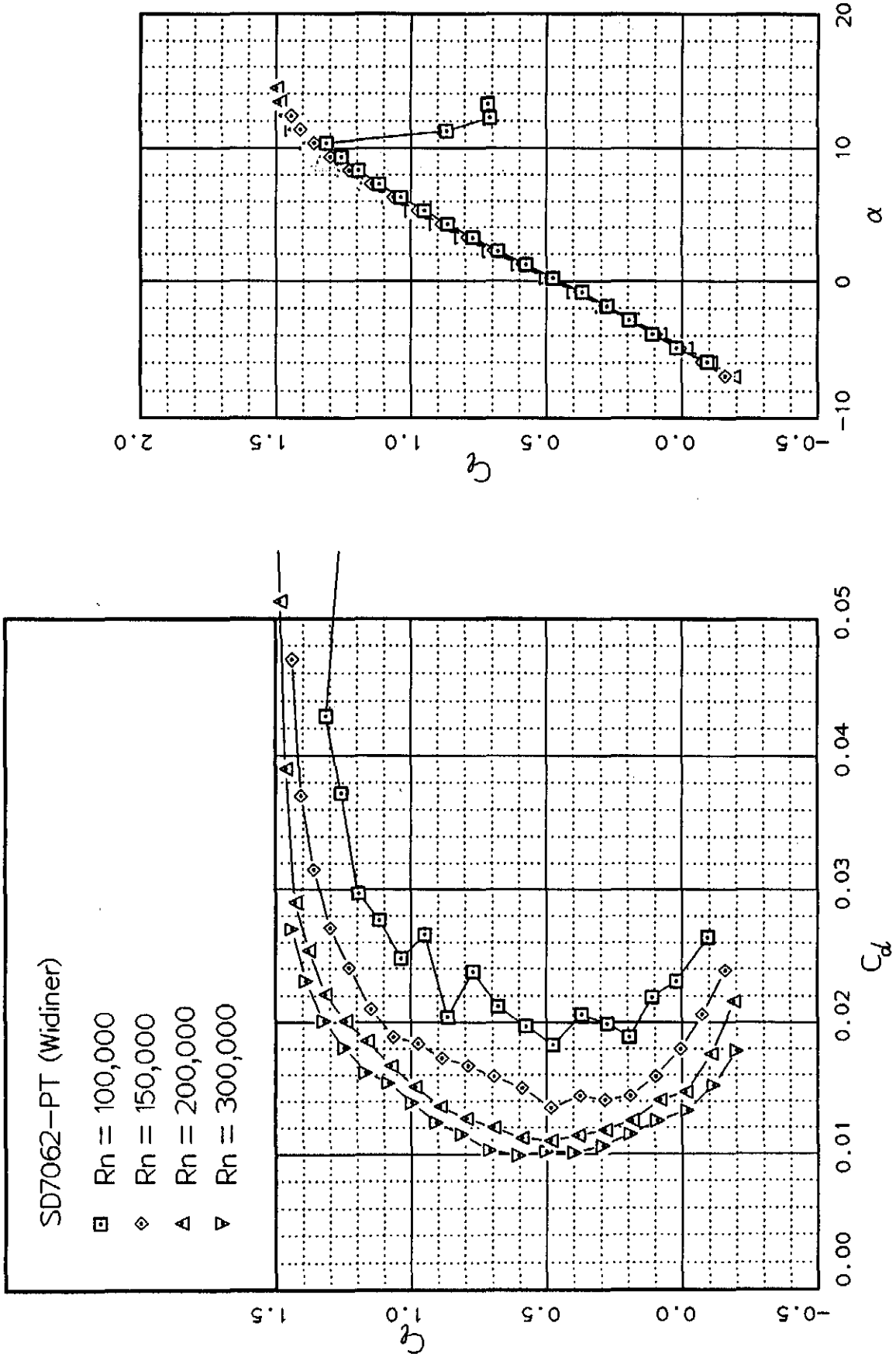
SD7062–PT (Widiner)
Rn = 100,000
Rn = 150,000
Rn = 200,000
Rn = 300,000
α
C_d
C_l
20
10
0
−10
0.05
0.04
0.03
0.02
0.01
0.00
−0.5
0.0
0.5
1.0
1.5
2.0

Fig. 12.142

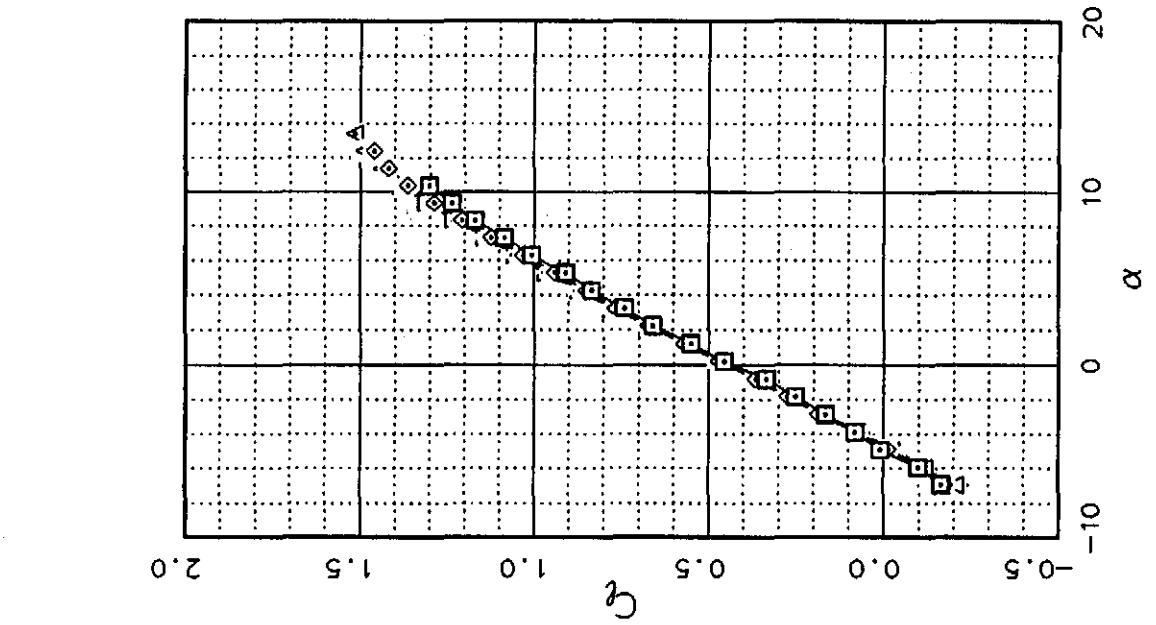
20
10
0
−10
α
−0.5
0.0
0.5
1.0
1.5
2.0
c_l

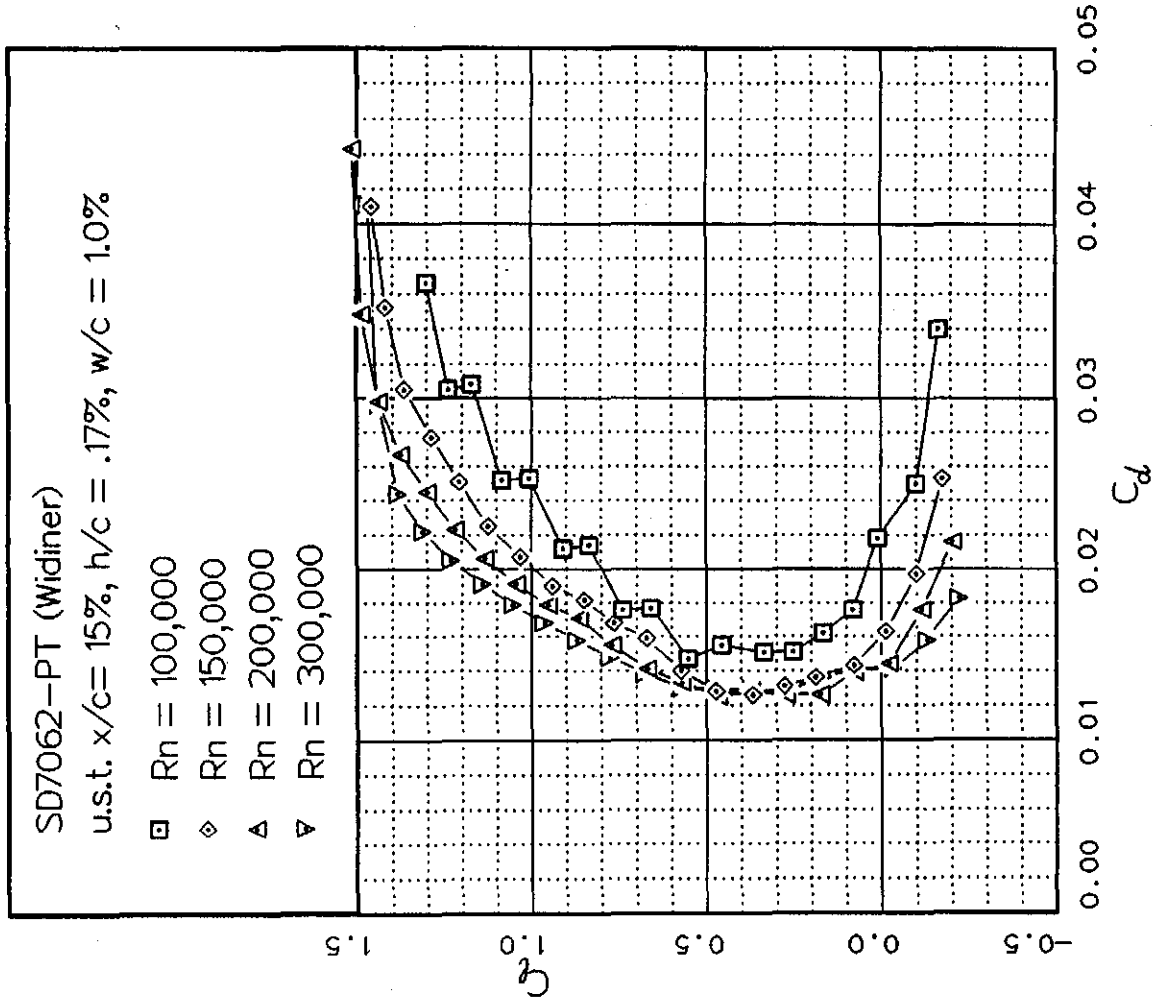
SD7062−PT (Widiner)
u.s.t. x/c= 15%, h/c = .17%, w/c = 1.0%
Rn = 100,000
Rn = 150,000
Rn = 200,000
Rn = 300,000
0.05
0.04
0.03
0.02
0.01
0.00
C_d
−0.5
0.0
0.5
1.0
1.5
c_l

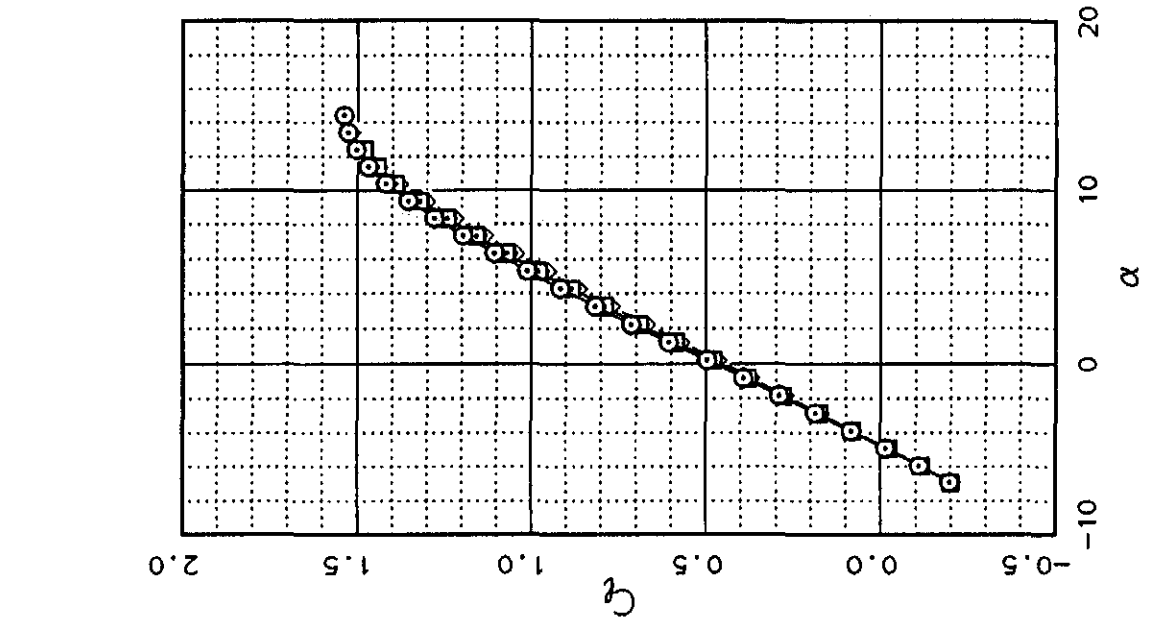
20
10
0
−10
α
−0.5
0.0
0.5
1.0
1.5
2.0
c_l

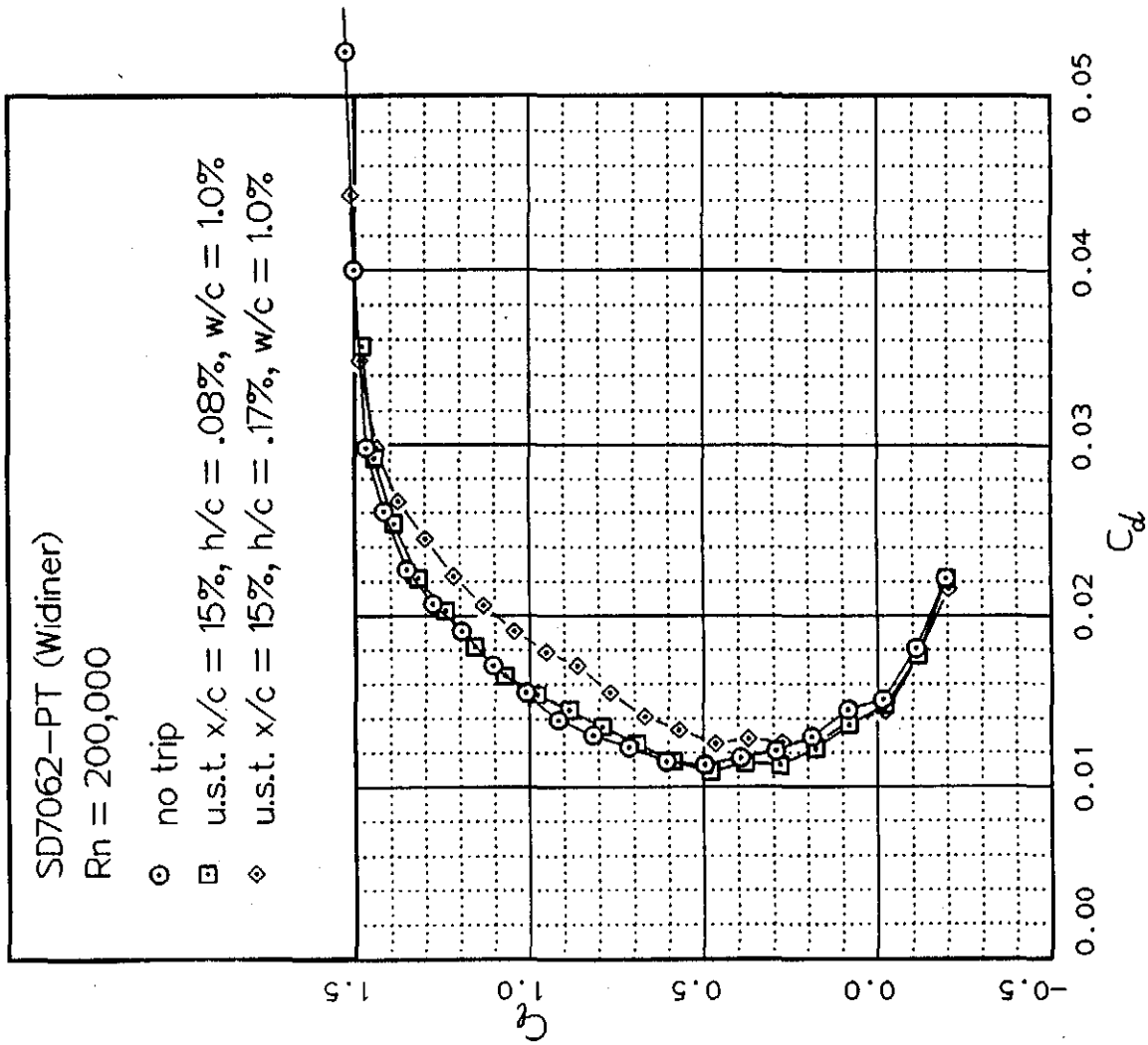
SD7062–PT (Widiner)
Rn = 200,000
⊙ no trip
⊡ u.s.t. x/c = 15%, h/c = .08%, w/c = 1.0%
◇ u.s.t. x/c = 15%, h/c = .17%, w/c = 1.0%
0.05
0.04
0.03
0.02
0.01
0.00
C_d
−0.5
0.0
0.5
1.0
1.5
c_l

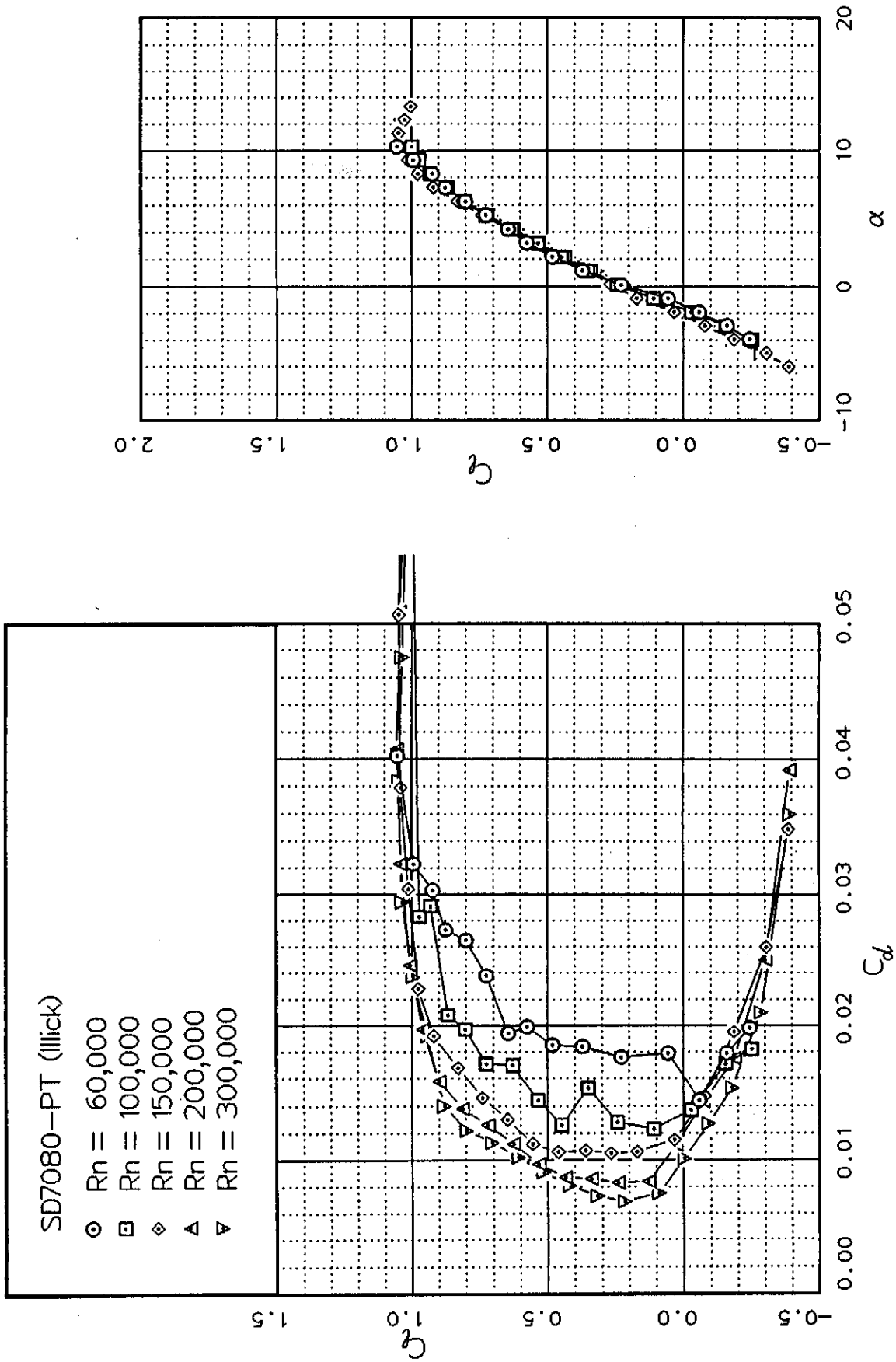
SD7080–PT (Illick)
Rn = 60,000
Rn = 100,000
Rn = 150,000
Rn = 200,000
Rn = 300,000
α
C_d
C_l
C_l
20
10
0
−10
0.05
0.04
0.03
0.02
0.01
0.00
−0.5
0.0
0.5
1.0
1.5
2.0

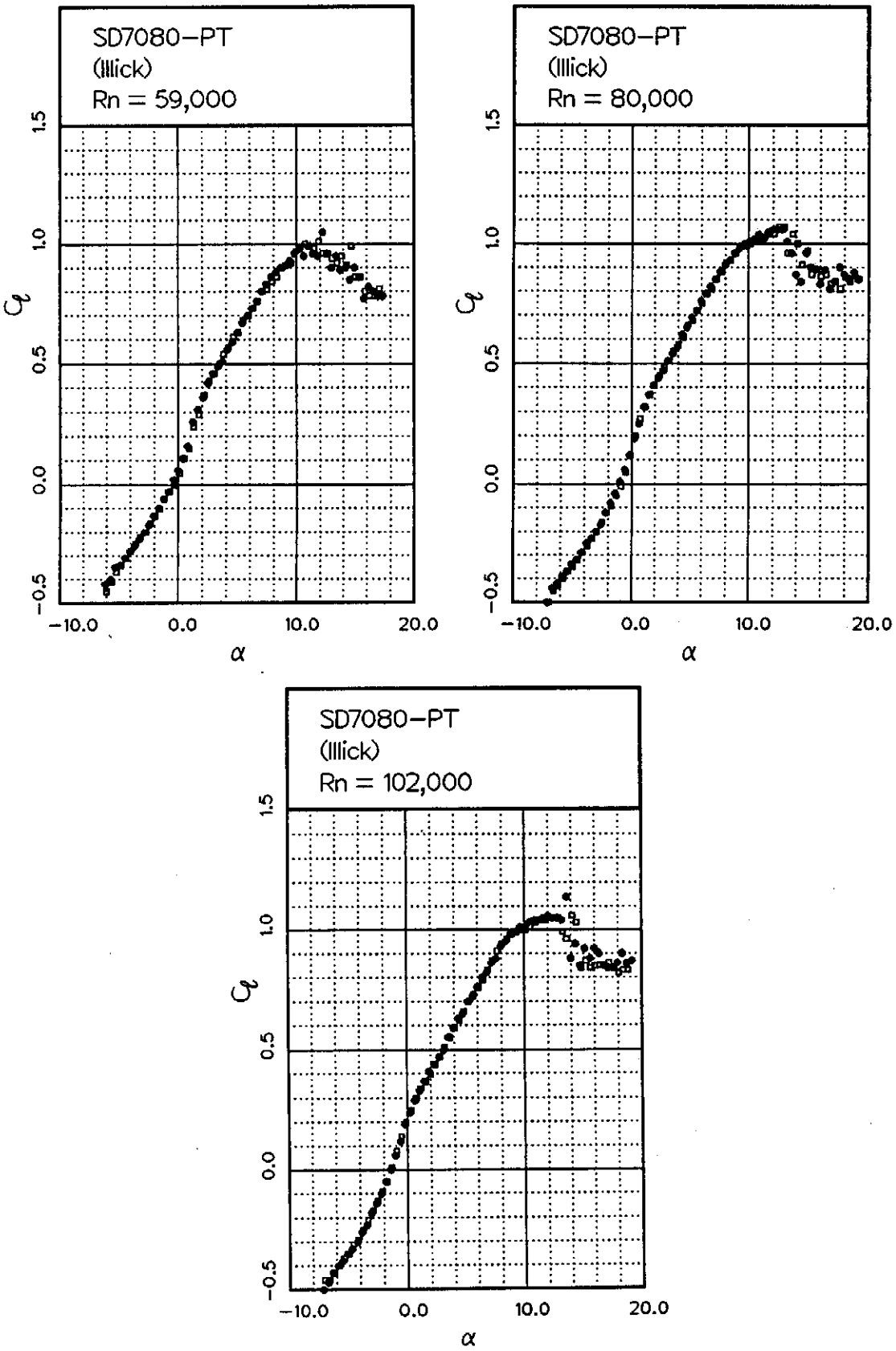
SD7080–PT
(Illick)
Rn = 59,000
SD7080–PT
(Illick)
Rn = 80,000
SD7080–PT
(Illick)
Rn = 102,000
C_ℓ
α
1.5
1.0
0.5
0.0
−0.5
−10.0
0.0
10.0
20.0

Fig. 12.146

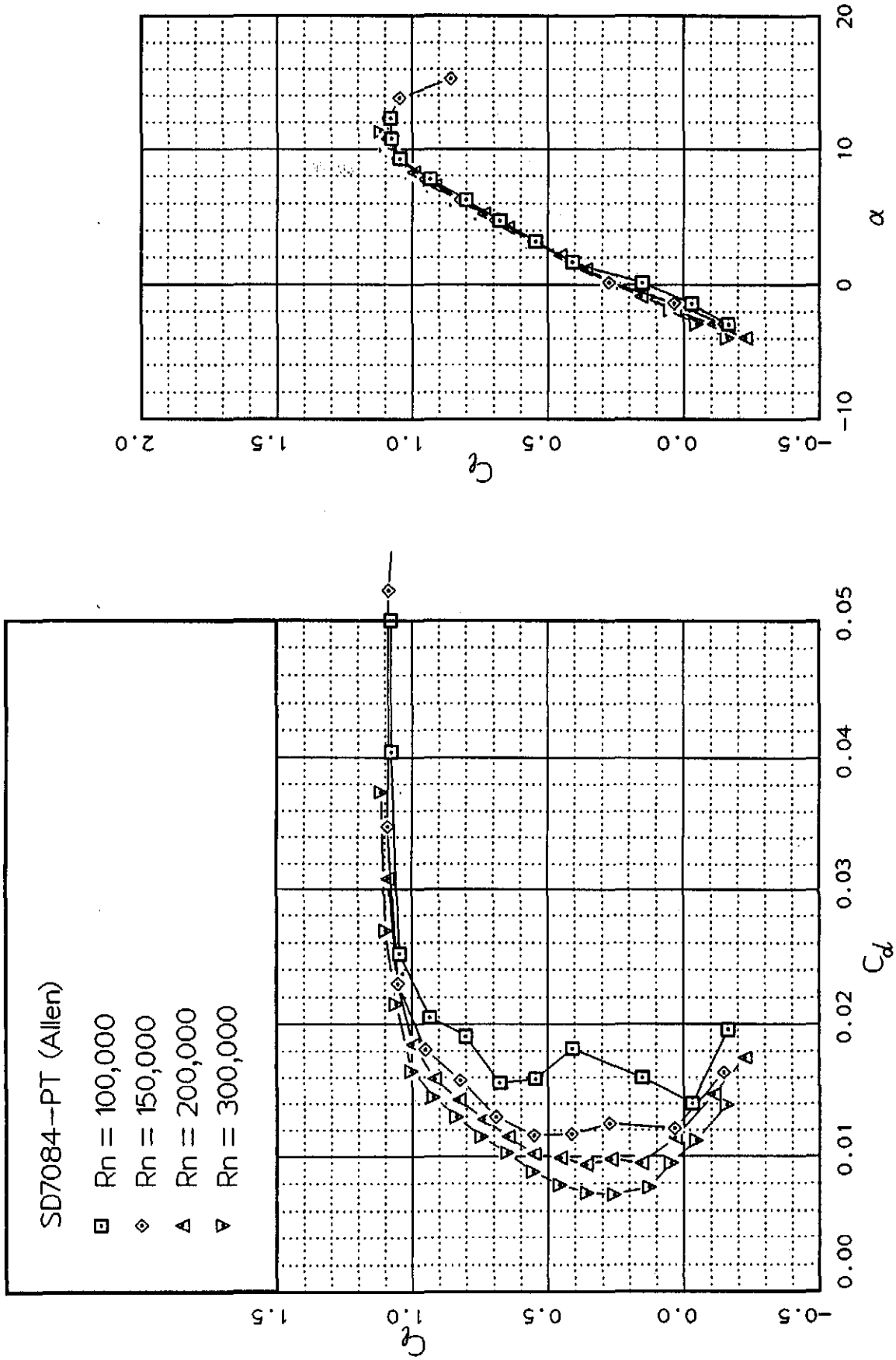
SD7084-PT (Allen)
Rn = 100,000
Rn = 150,000
Rn = 200,000
Rn = 300,000
C_l
C_d
α

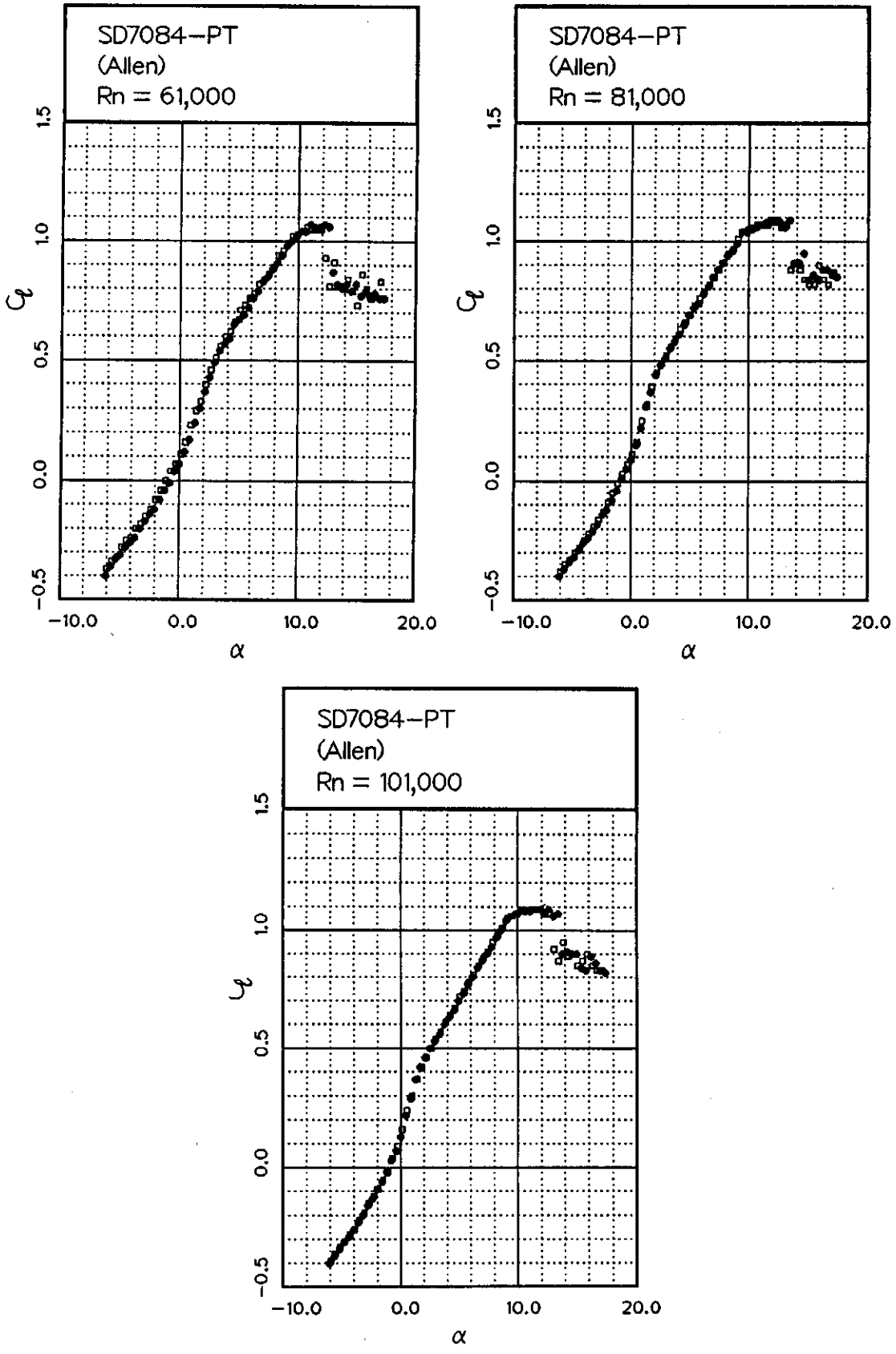
SD7084–PT
(Allen)
Rn = 61,000
SD7084–PT
(Allen)
Rn = 81,000
SD7084–PT
(Allen)
Rn = 101,000
C_l
α
1.5
1.0
0.5
0.0
−0.5
−10.0
0.0
10.0
20.0

Fig. 12.148

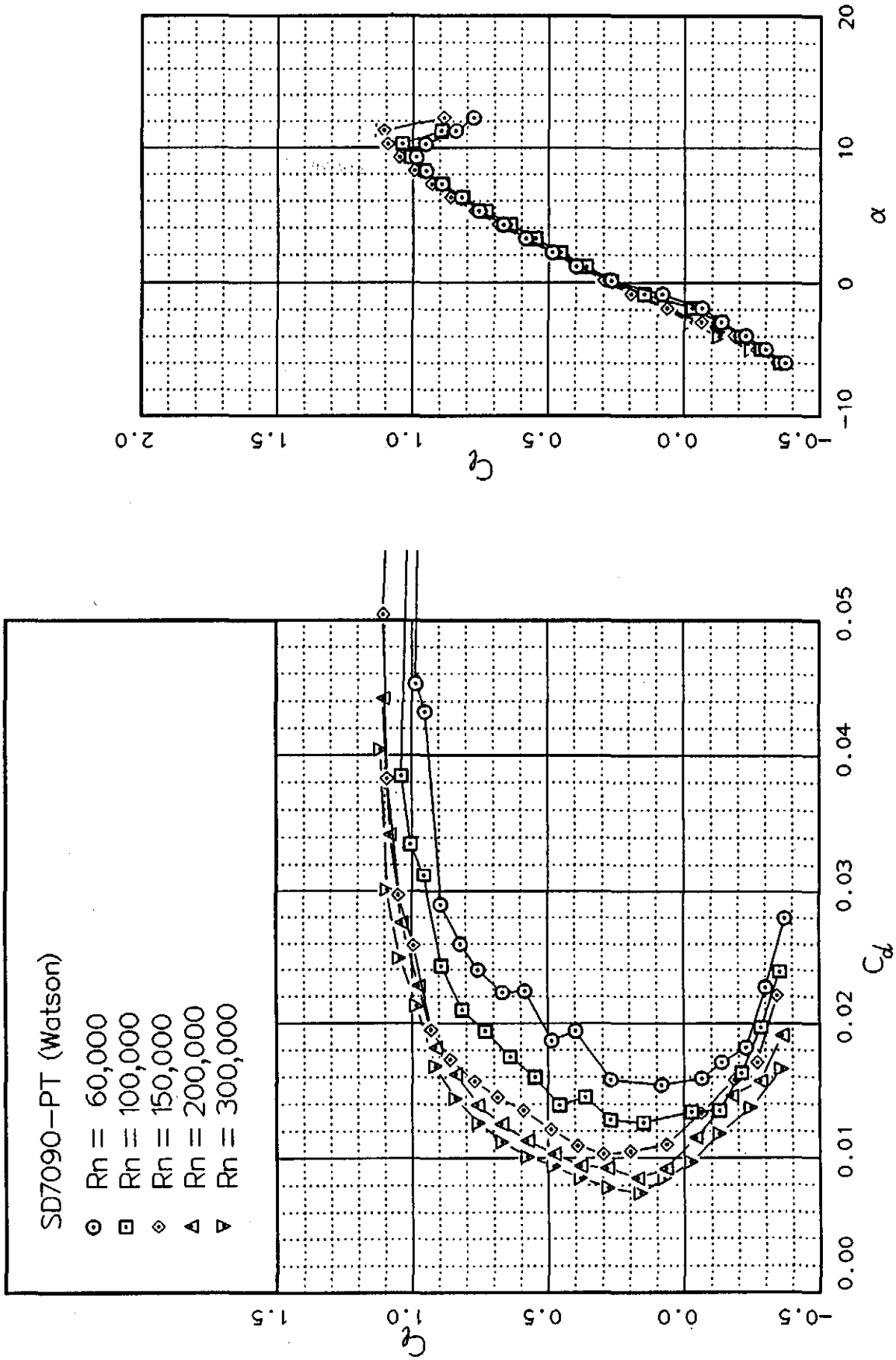
SD7090–PT (Watson)
Rn = 60,000
Rn = 100,000
Rn = 150,000
Rn = 200,000
Rn = 300,000
C_l
C_d
α

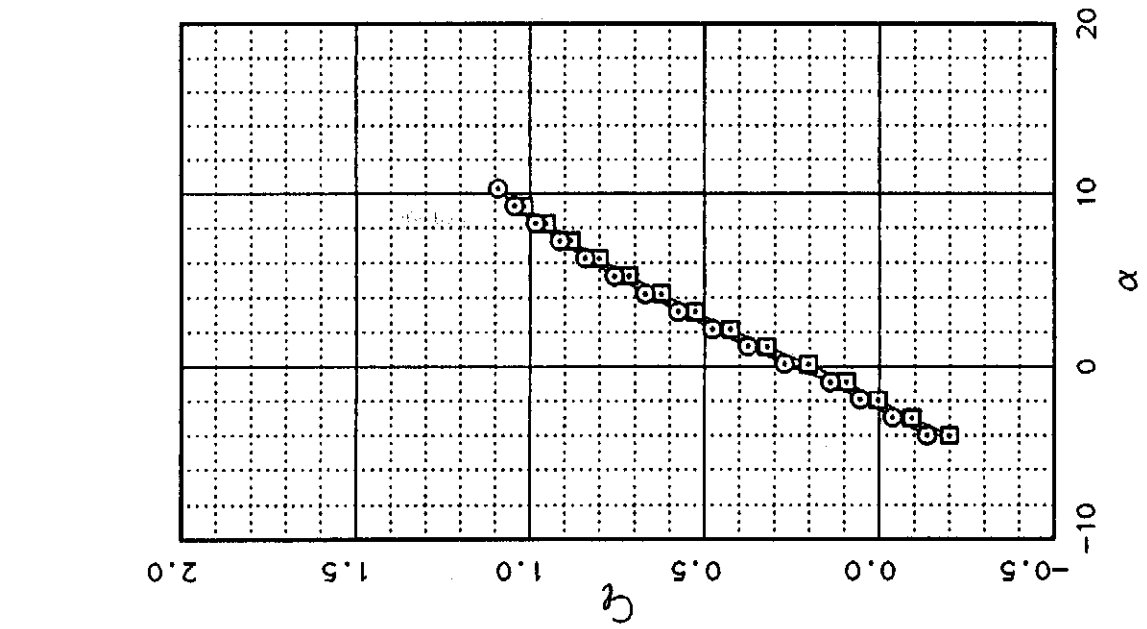
α
20
10
0
−10
−0.5
0.0
0.5
1.0
1.5
2.0
c_l

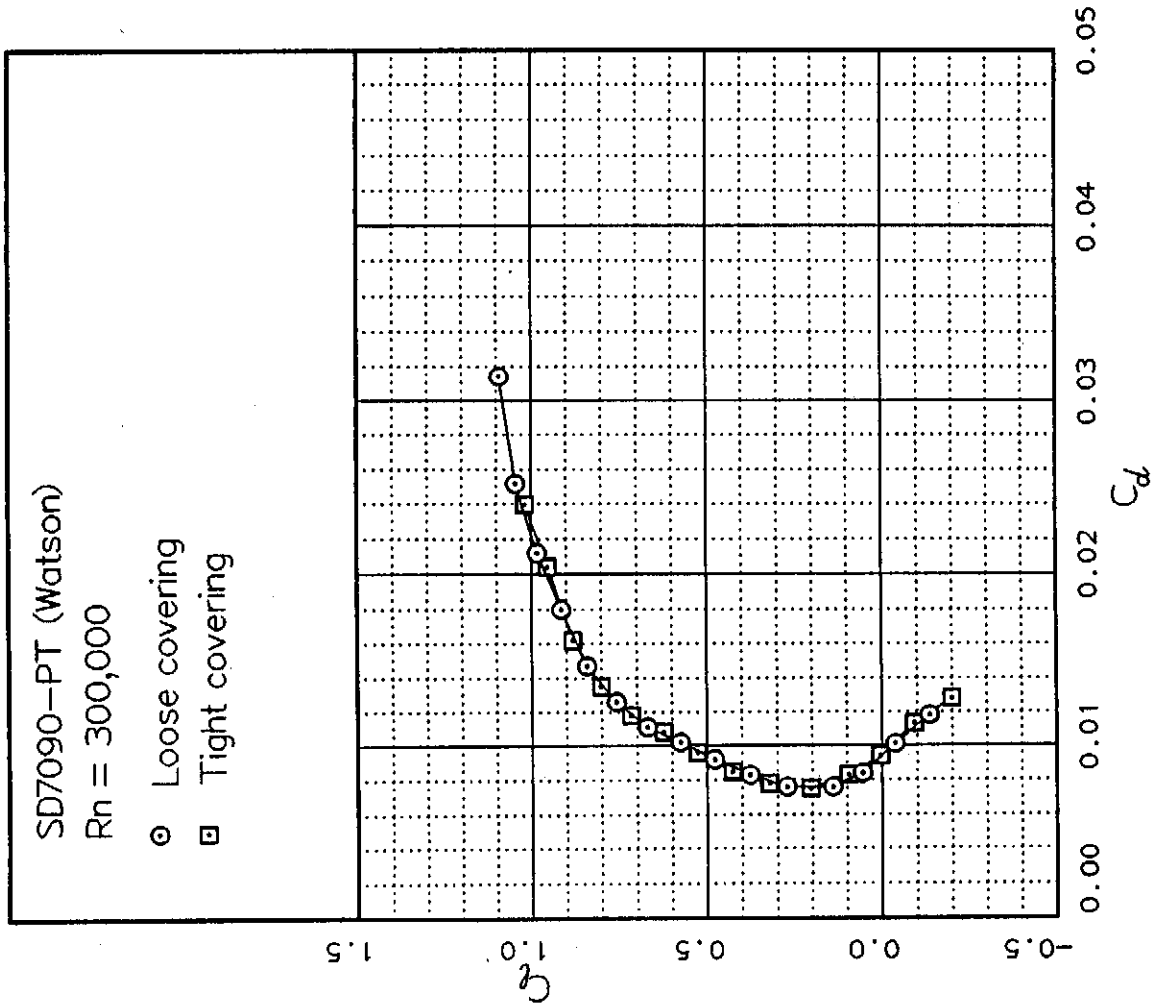
SD7090–PT (Watson)
Rn = 300,000
Loose covering
Tight covering
0.05
0.04
0.03
0.02
0.01
0.00
−0.5
0.0
0.5
1.0
1.5
c_d
c_l

Fig. 12.150

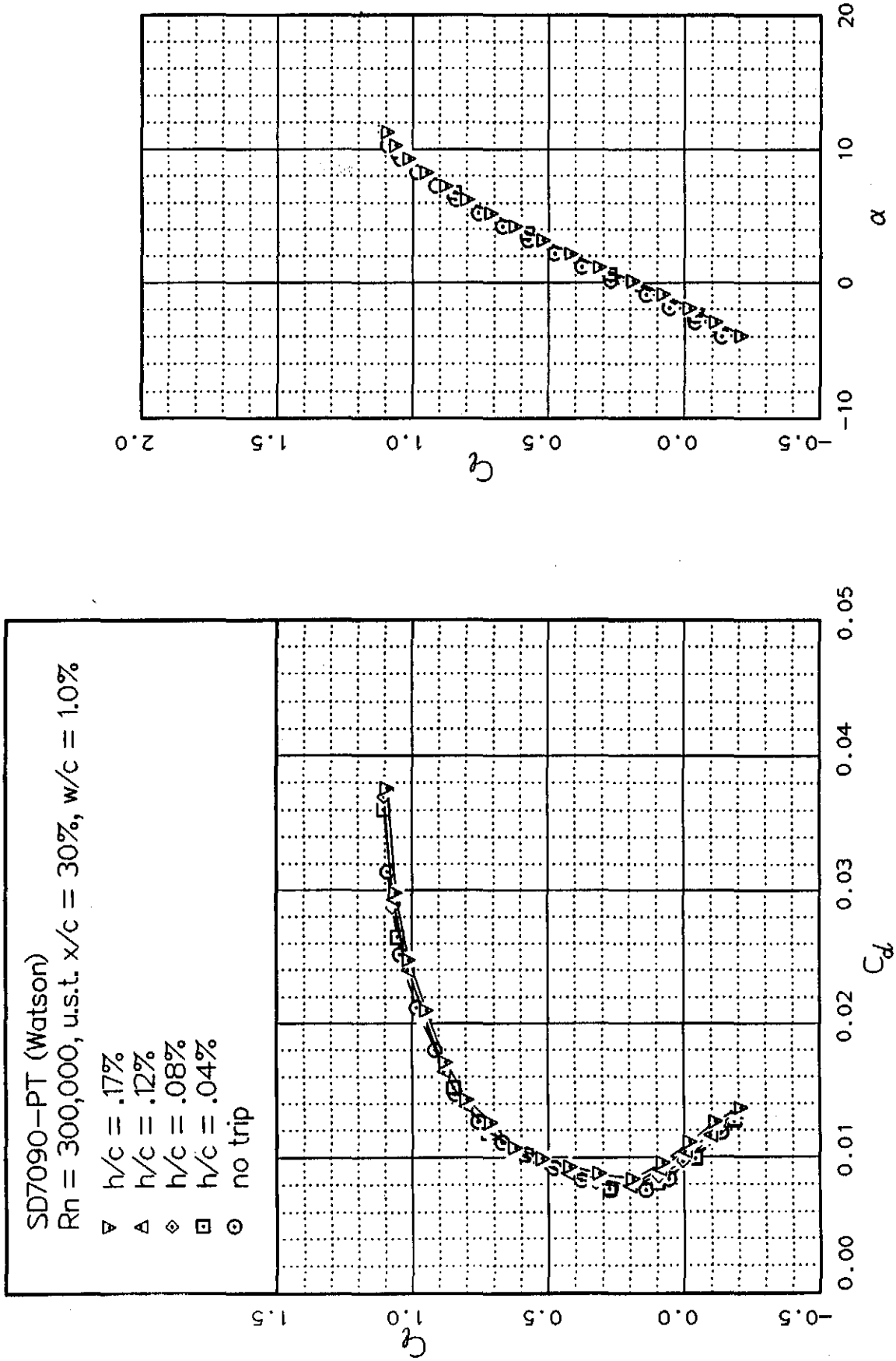
SD7090–PT (Watson)
Rn = 300,000, u.s.t. x/c = 30%, w/c = 1.0%
h/c = .17%
h/c = .12%
h/c = .08%
h/c = .04%
no trip
−0.5
0.0
0.5
1.0
1.5
2.0
c_l
0.00
0.01
0.02
0.03
0.04
0.05
c_d
−10
0
10
20
α

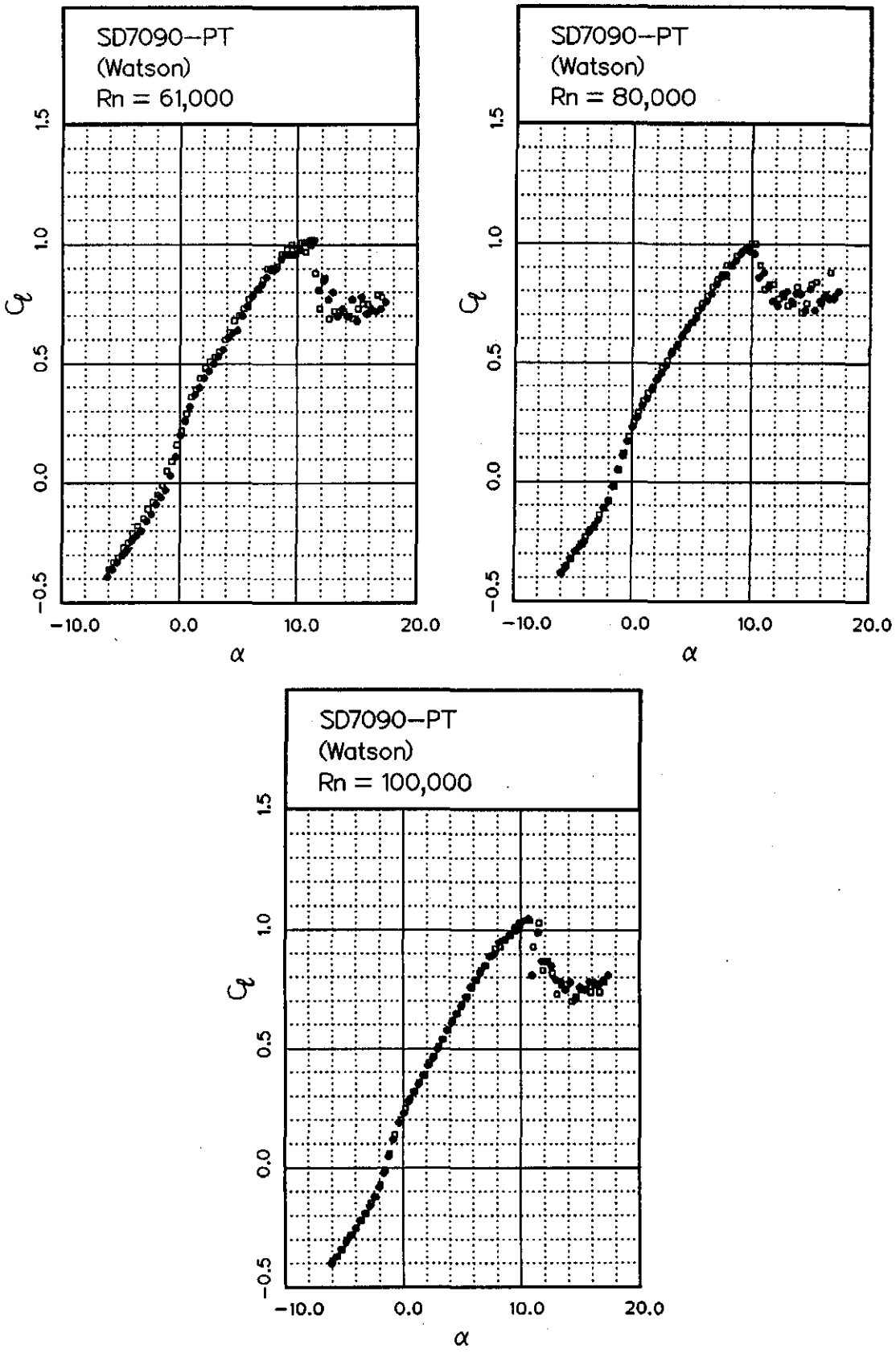
SD7090–PT
(Watson)
Rn = 61,000
SD7090–PT
(Watson)
Rn = 80,000
SD7090–PT
(Watson)
Rn = 100,000
C_l
α
1.5
1.0
0.5
0.0
−0.5
−10.0
0.0
10.0
20.0

Fig. 12.152

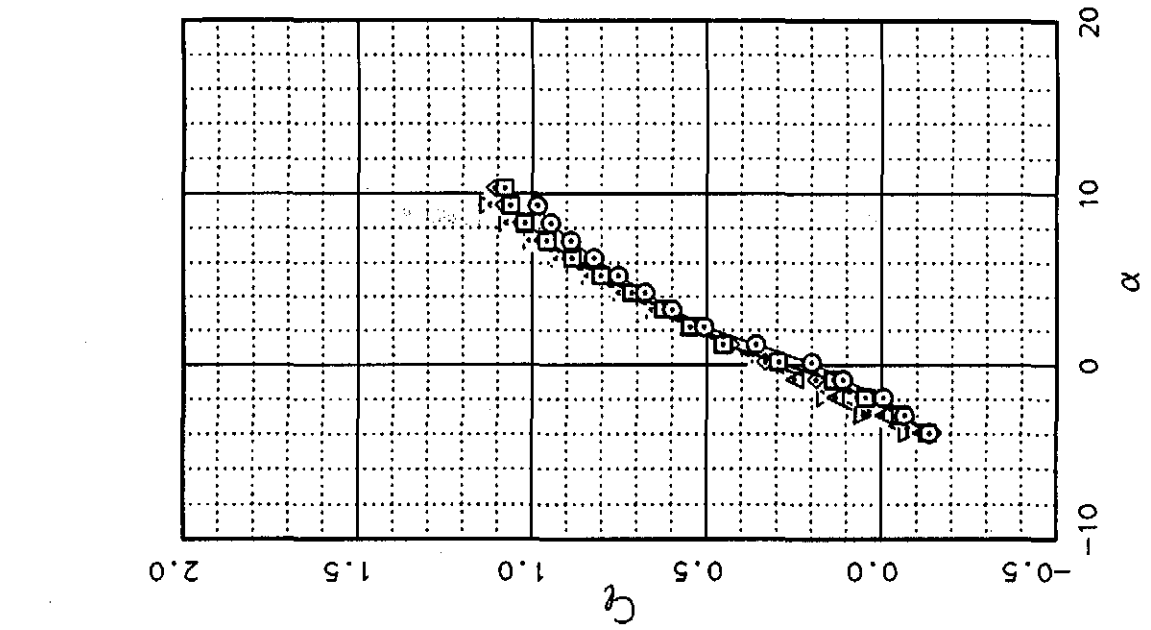
20
10
0
−10
α
−0.5
0.0
0.5
1.0
1.5
2.0
c_l

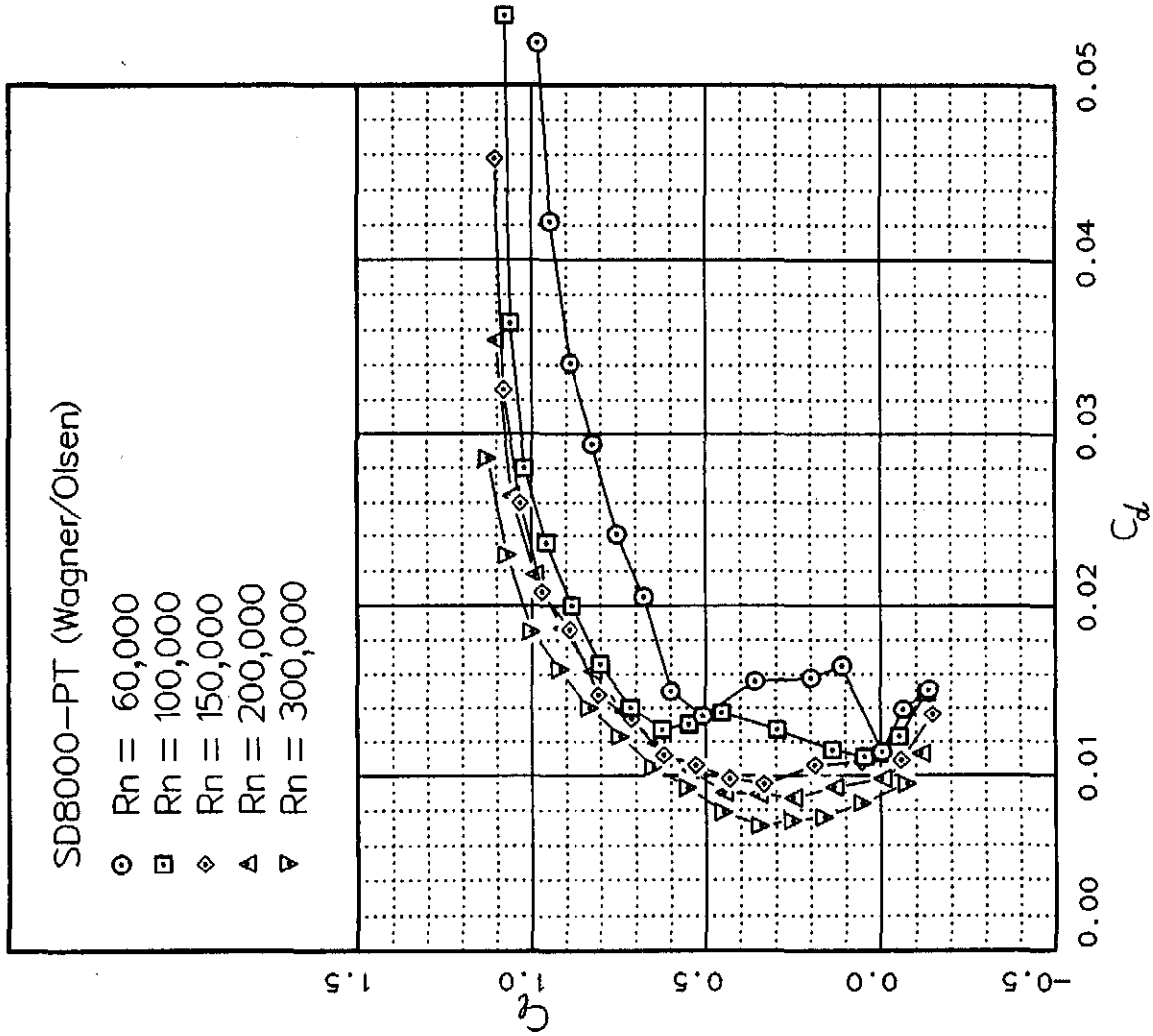
SD8000–PT (Wagner/Olsen)
Rn = 60,000
Rn = 100,000
Rn = 150,000
Rn = 200,000
Rn = 300,000
0.05
0.04
0.03
0.02
0.01
0.00
C_d
−0.5
0.0
0.5
1.0
1.5
c_l

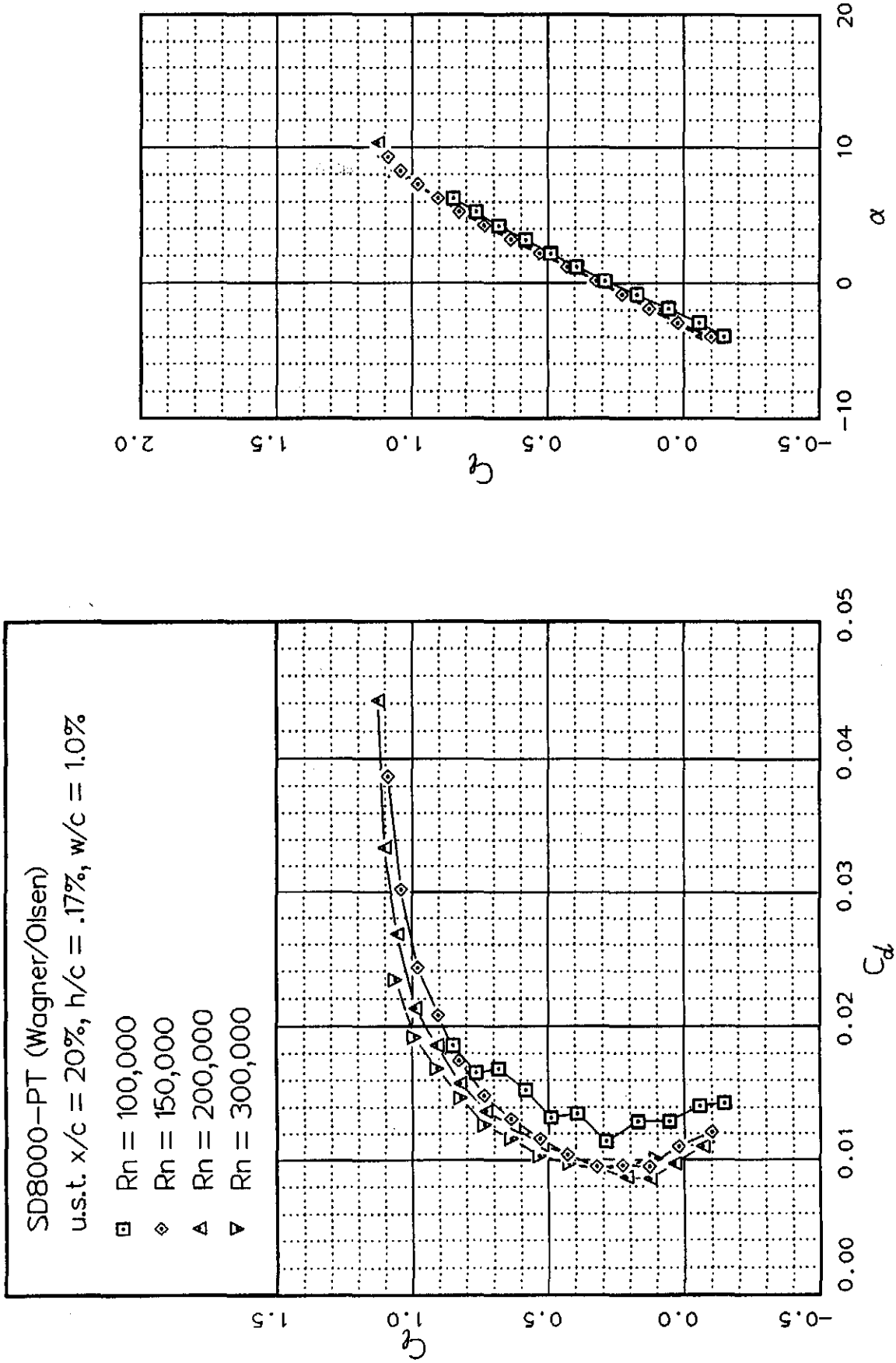
SD8000–PT (Wagner/Olsen)
u.s.t. x/c = 20%, h/c = .17%, w/c = 1.0%
Rn = 100,000
Rn = 150,000
Rn = 200,000
Rn = 300,000
−0.5
0.0
0.5
1.0
1.5
2.0
C_l
−10
0
10
20
α
0.00
0.01
0.02
0.03
0.04
0.05
C_d

Fig. 12.154

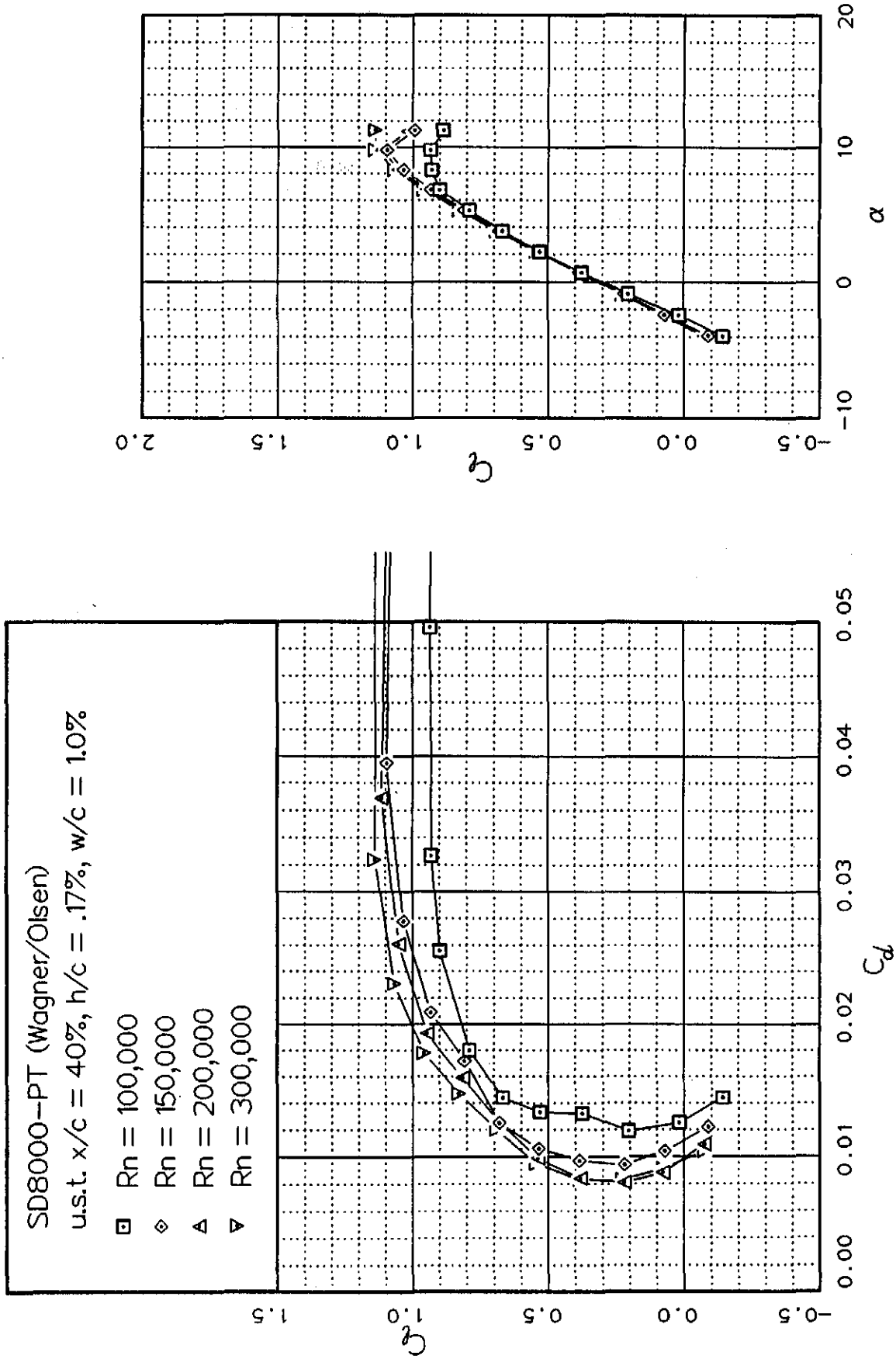
SD8000–PT (Wagner/Olsen)
u.s.t. x/c = 40%, h/c = .17%, w/c = 1.0%
Rn = 100,000
Rn = 150,000
Rn = 200,000
Rn = 300,000
α
C_d
C_l
20
10
0
−10
0.05
0.04
0.03
0.02
0.01
0.00
−0.5
0.0
0.5
1.0
1.5
2.0

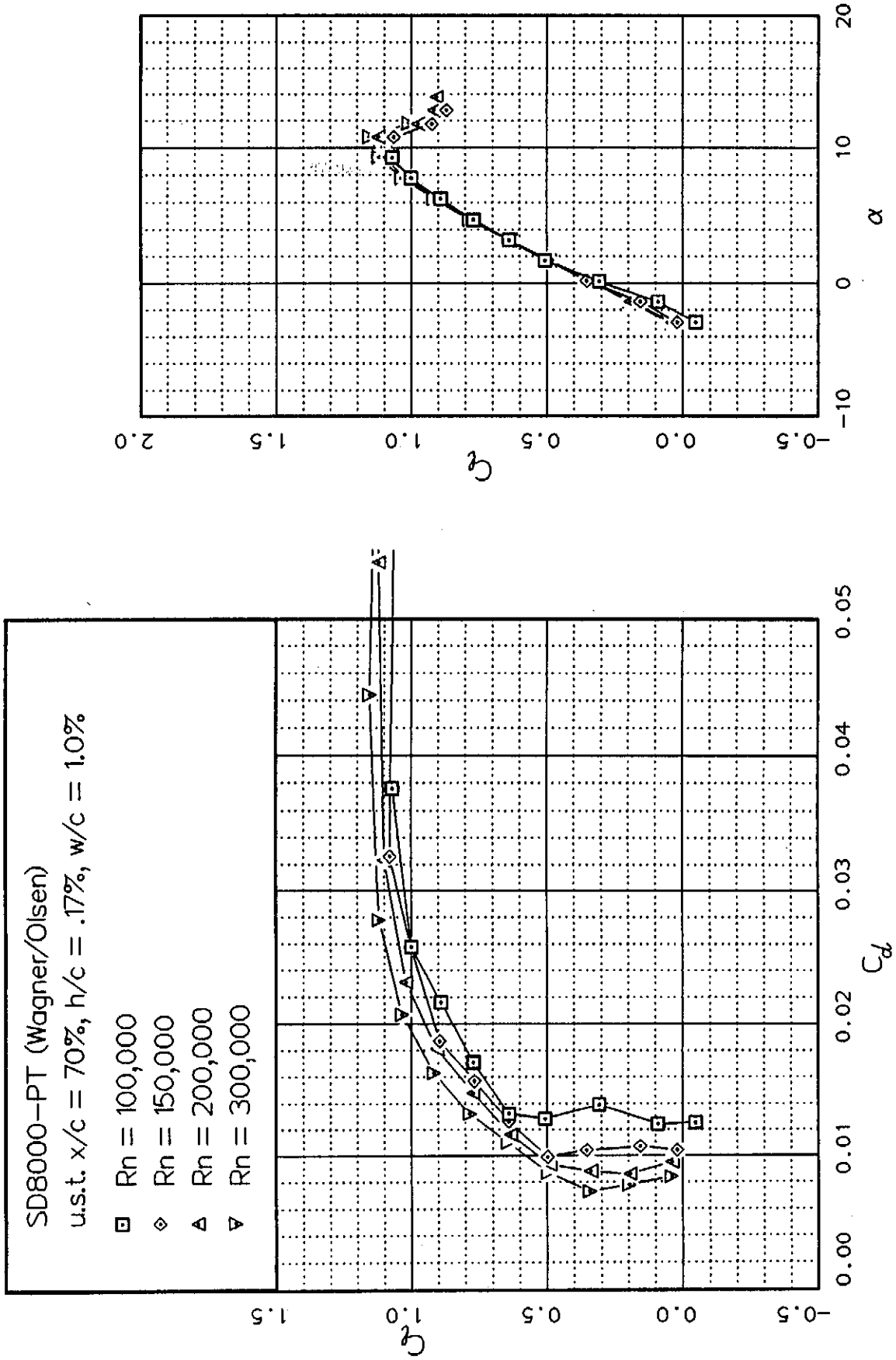
SD8000–PT (Wagner/Olsen)
u.s.t. x/c = 70%, h/c = .17%, w/c = 1.0%
Rn = 100,000
Rn = 150,000
Rn = 200,000
Rn = 300,000
−0.5
0.0
0.5
1.0
1.5
2.0
c_l
−10
0
10
20
α
0.00
0.01
0.02
0.03
0.04
0.05
c_d

Fig. 12.156

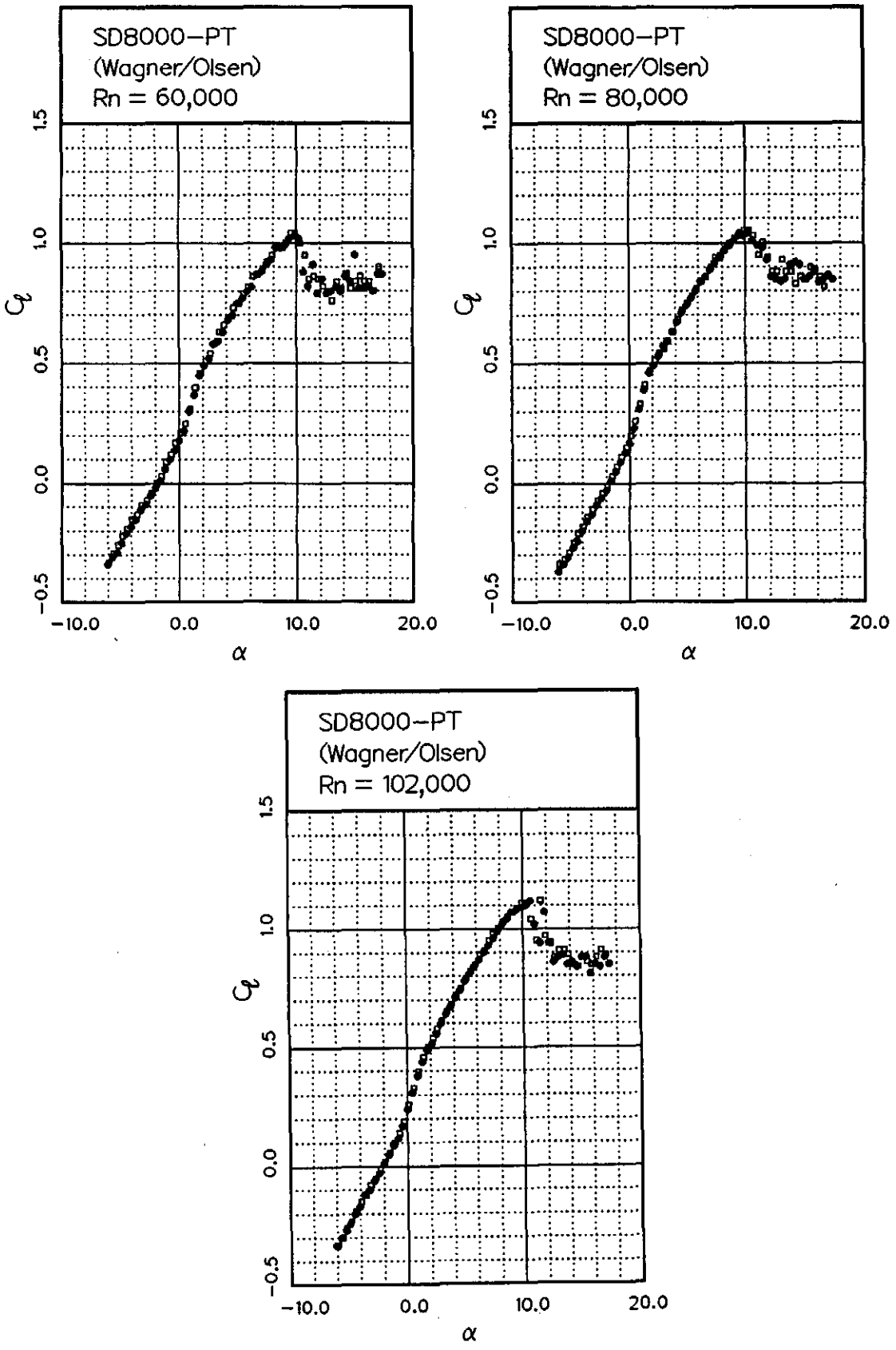
SD8000–PT
(Wagner/Olsen)
Rn = 60,000
SD8000–PT
(Wagner/Olsen)
Rn = 80,000
SD8000–PT
(Wagner/Olsen)
Rn = 102,000
c_ℓ
α
1.5
1.0
0.5
0.0
−0.5
−10.0
0.0
10.0
20.0

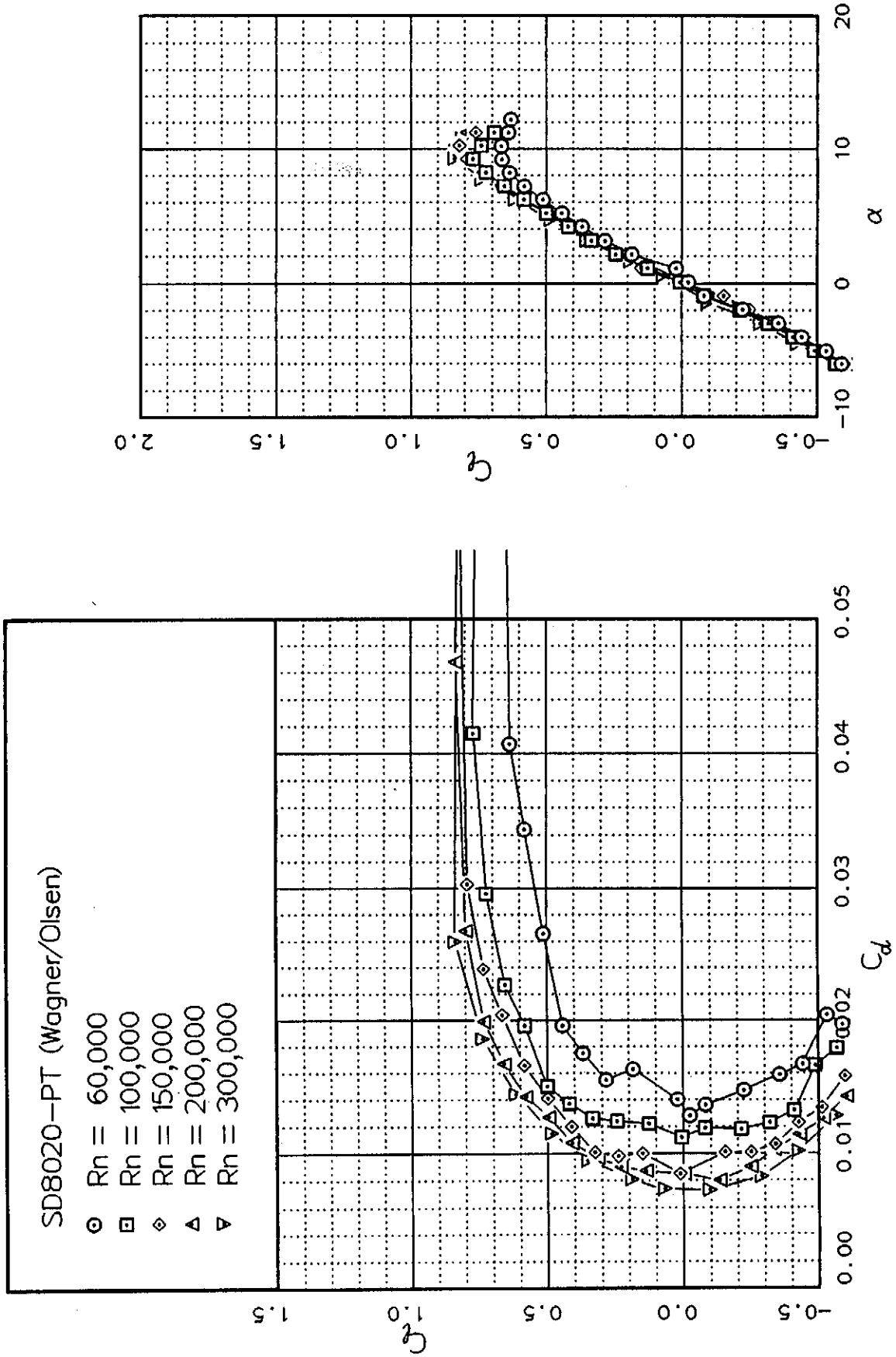
SD8020–PT (Wagner/Olsen)
Rn = 60,000
Rn = 100,000
Rn = 150,000
Rn = 200,000
Rn = 300,000
α
C_d
C_l
C_l

Fig. 12.158

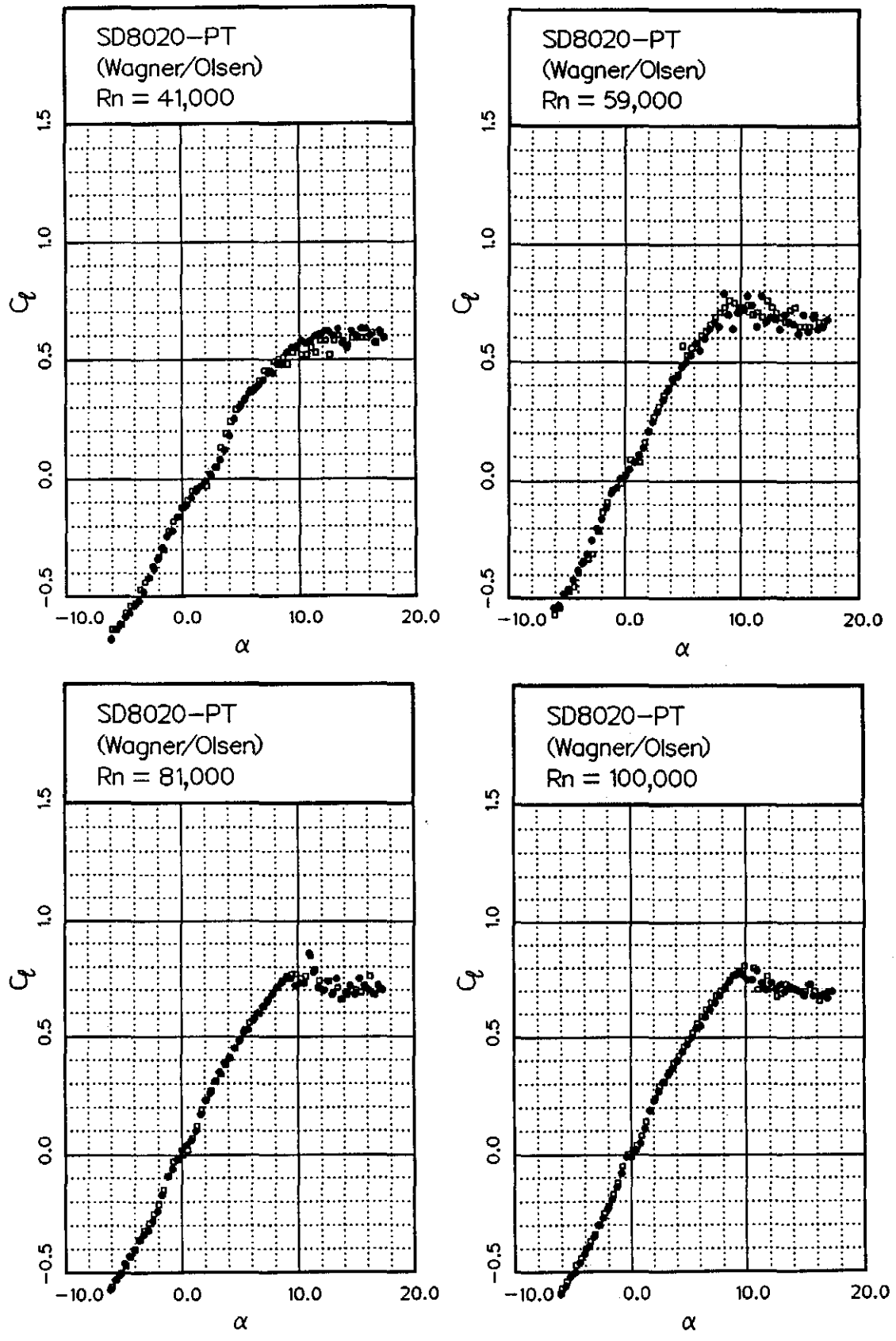
SD8020–PT
(Wagner/Olsen)
Rn = 41,000
SD8020–PT
(Wagner/Olsen)
Rn = 59,000
SD8020–PT
(Wagner/Olsen)
Rn = 81,000
SD8020–PT
(Wagner/Olsen)
Rn = 100,000
C_ℓ
α
1.5
1.0
0.5
0.0
−0.5
−10.0
0.0
10.0
20.0

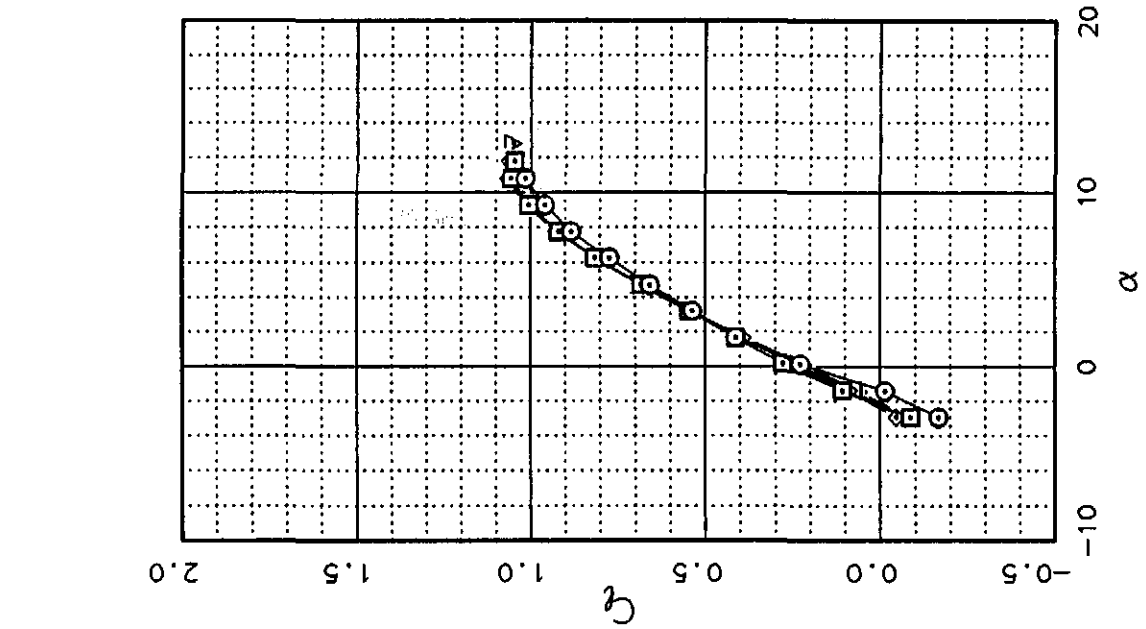
20
10
0
−10
α
−0.5
0.0
0.5
1.0
1.5
2.0
Cl

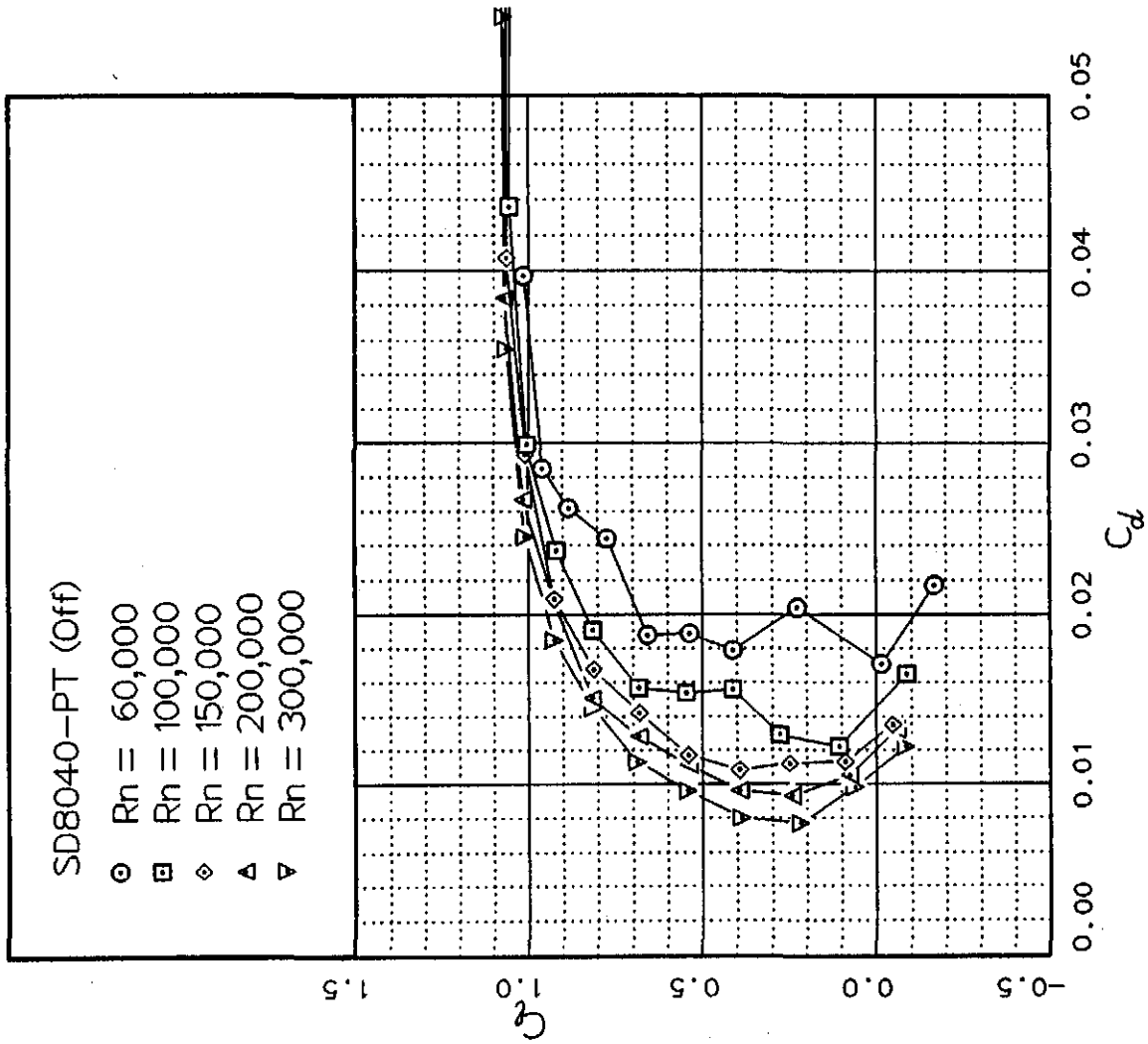
SD8040–PT (Off)
Rn = 60,000
Rn = 100,000
Rn = 150,000
Rn = 200,000
Rn = 300,000
0.05
0.04
0.03
0.02
0.01
0.00
Cd
−0.5
0.0
0.5
1.0
1.5
Cl

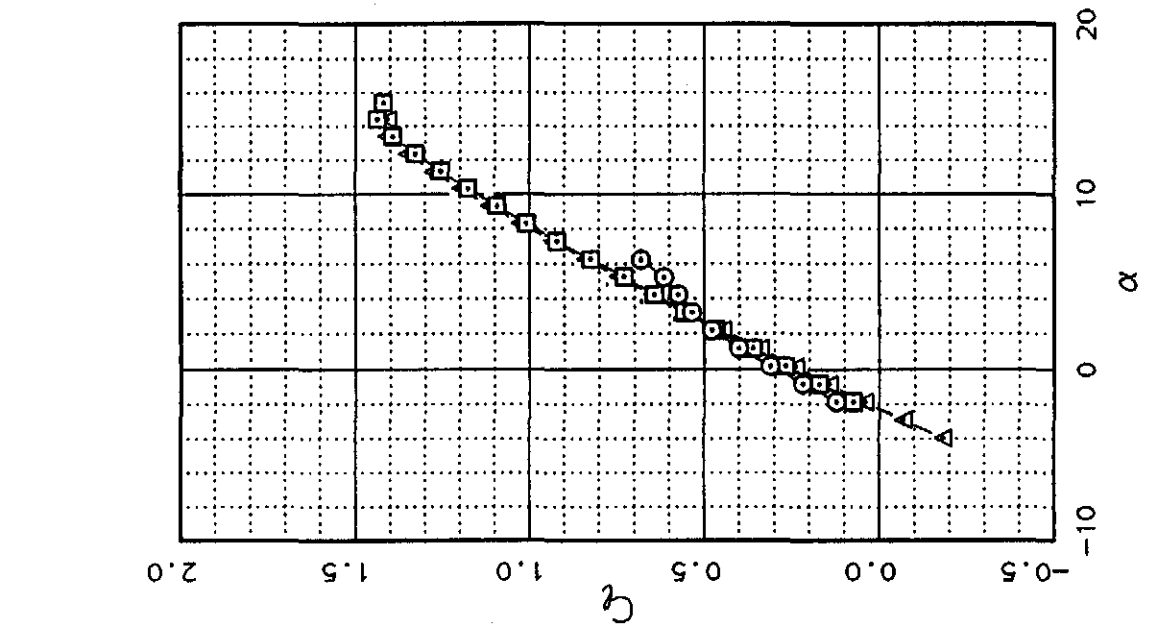
20
10
0
−10
α
−0.5
0.0
0.5
1.0
1.5
2.0
c_l

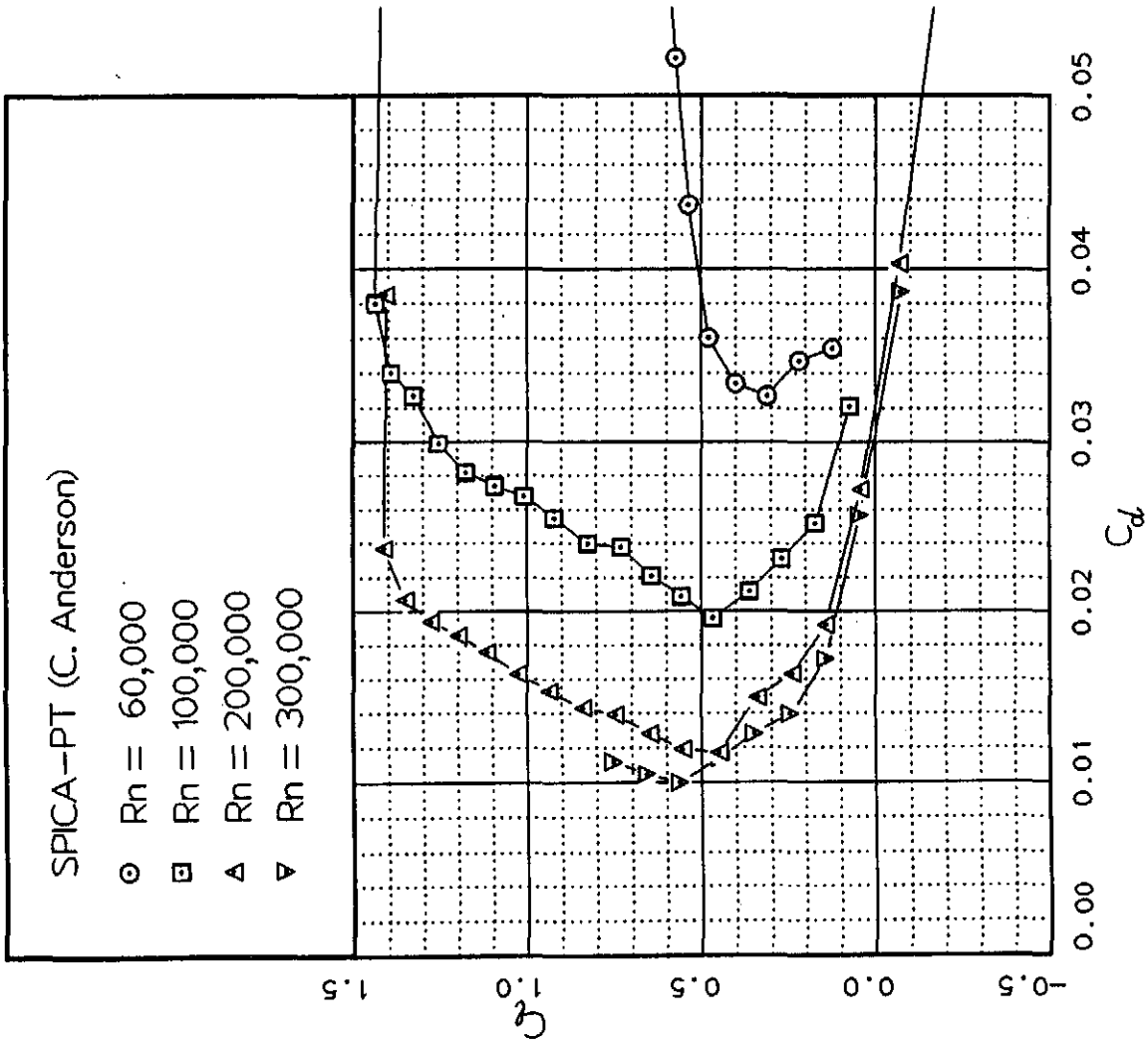
SPICA–PT (C. Anderson)
Rn = 60,000
Rn = 100,000
Rn = 200,000
Rn = 300,000
0.05
0.04
0.03
0.02
0.01
0.00
C_d
−0.5
0.0
0.5
1.0
1.5
c_l

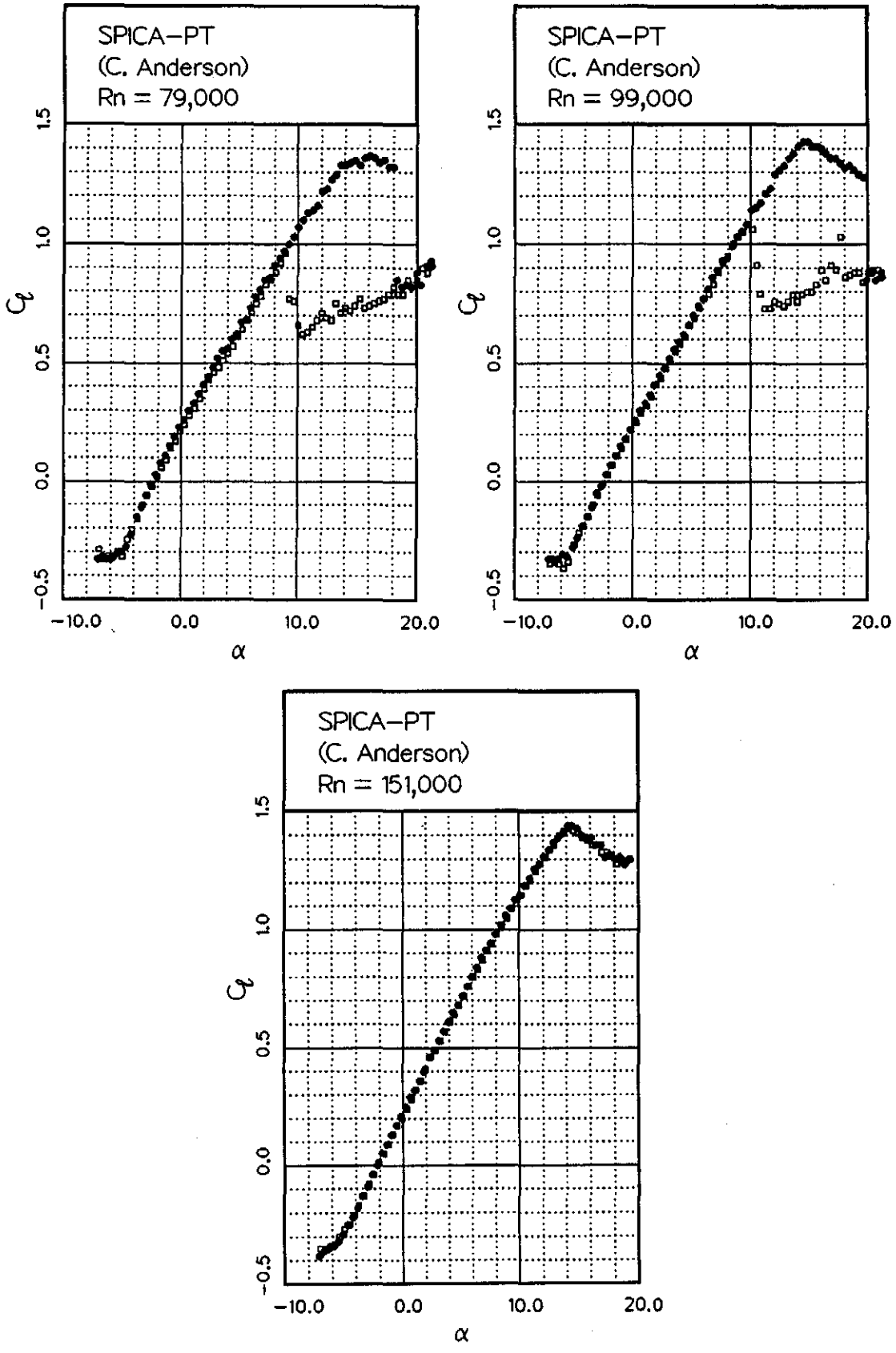
SPICA–PT
(C. Anderson)
Rn = 79,000
SPICA–PT
(C. Anderson)
Rn = 99,000
SPICA–PT
(C. Anderson)
Rn = 151,000
C_ℓ
α
1.5
1.0
0.5
0.0
−0.5
−10.0
0.0
10.0
20.0

Fig. 12.162

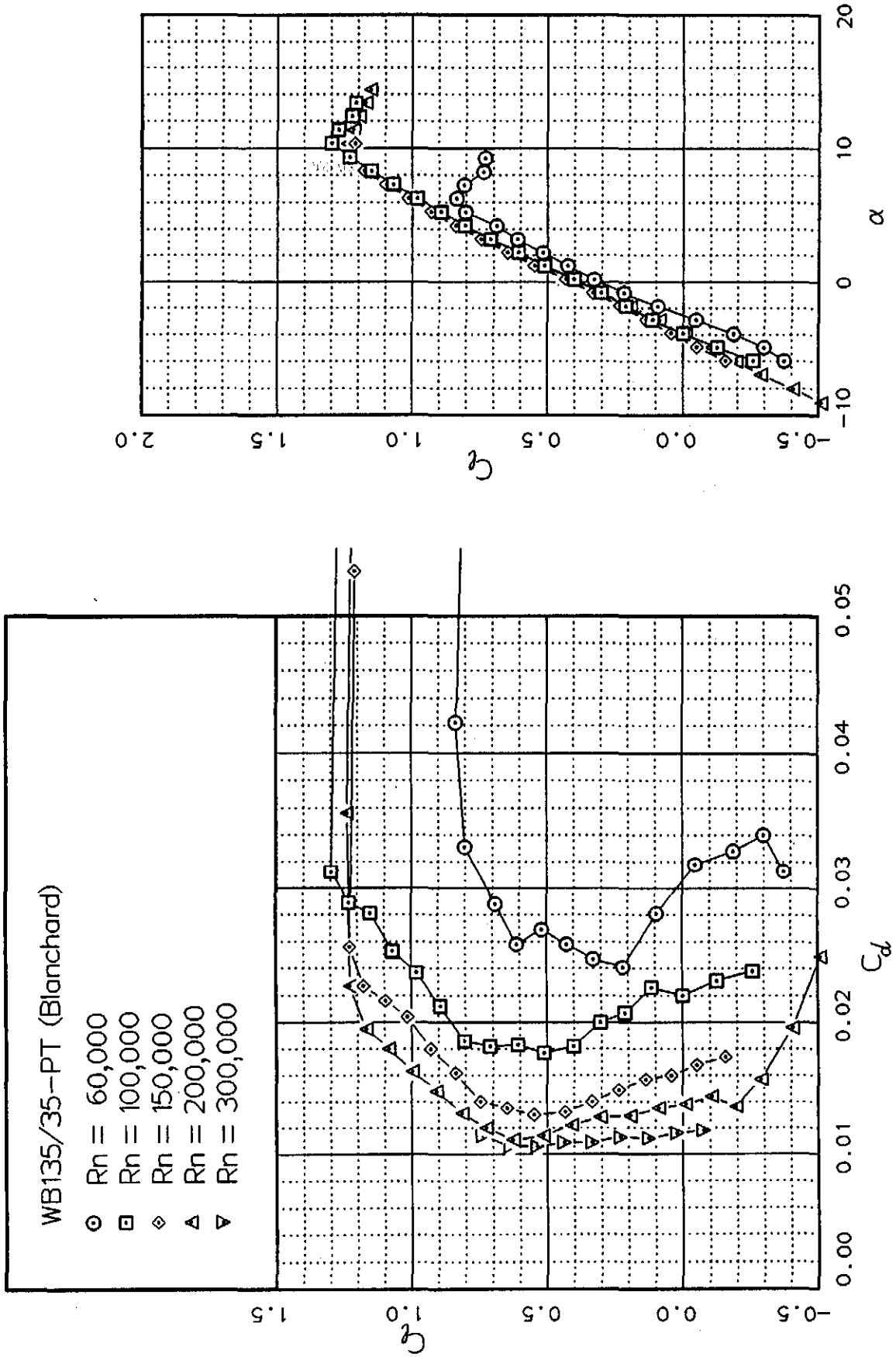
WB135/35-PT (Blanchard)
Rn = 60,000
Rn = 100,000
Rn = 150,000
Rn = 200,000
Rn = 300,000
α
C_d
C_l
C_l
20
10
0
−10
0.05
0.04
0.03
0.02
0.01
0.00
−0.5
0.0
0.5
1.0
1.5
2.0

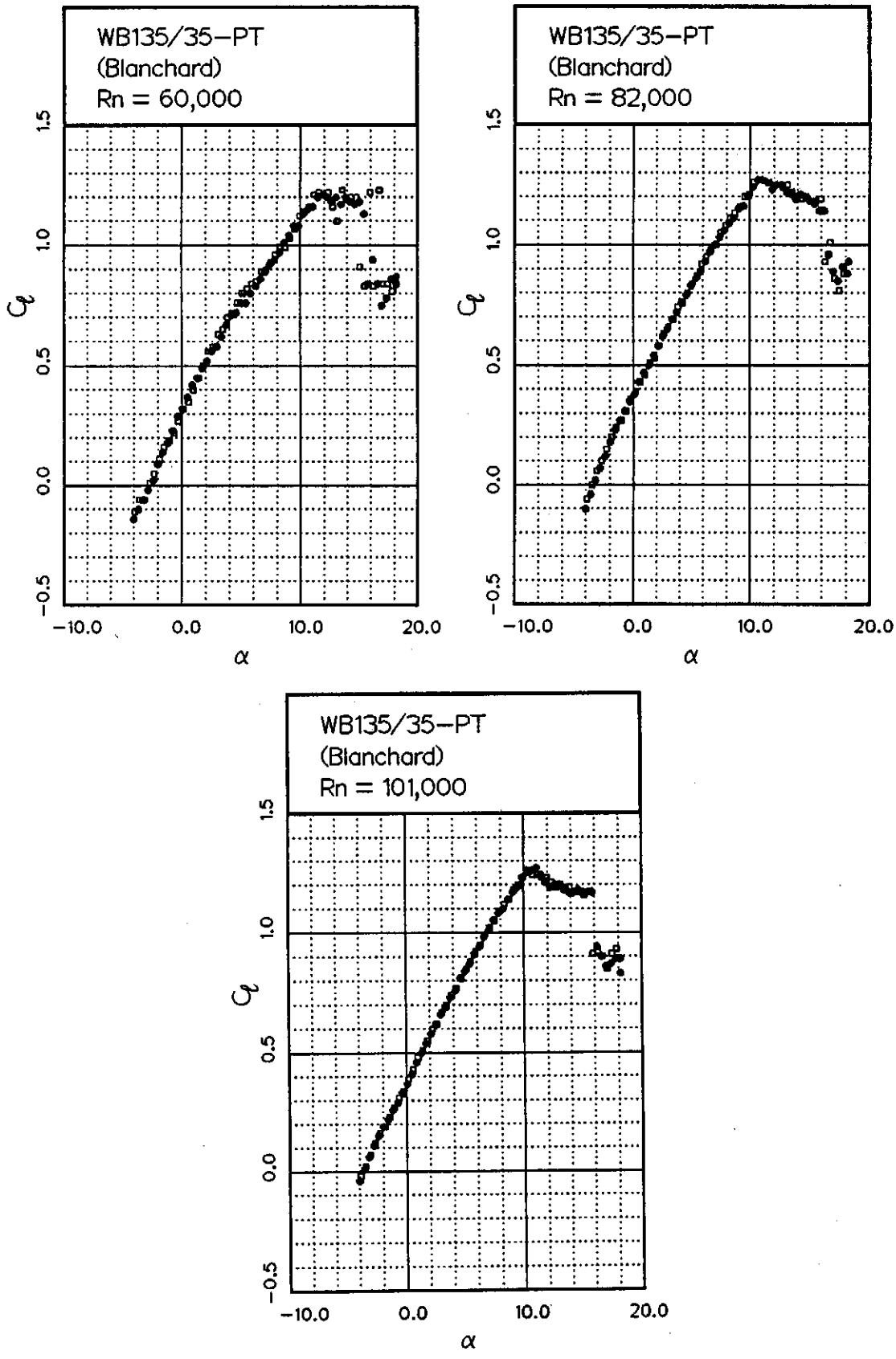
WB135/35–PT
(Blanchard)
Rn = 60,000
WB135/35–PT
(Blanchard)
Rn = 82,000
WB135/35–PT
(Blanchard)
Rn = 101,000
C_ℓ
α
1.5
1.0
0.5
0.0
−0.5
−10.0
0.0
10.0
20.0

Fig. 12.164

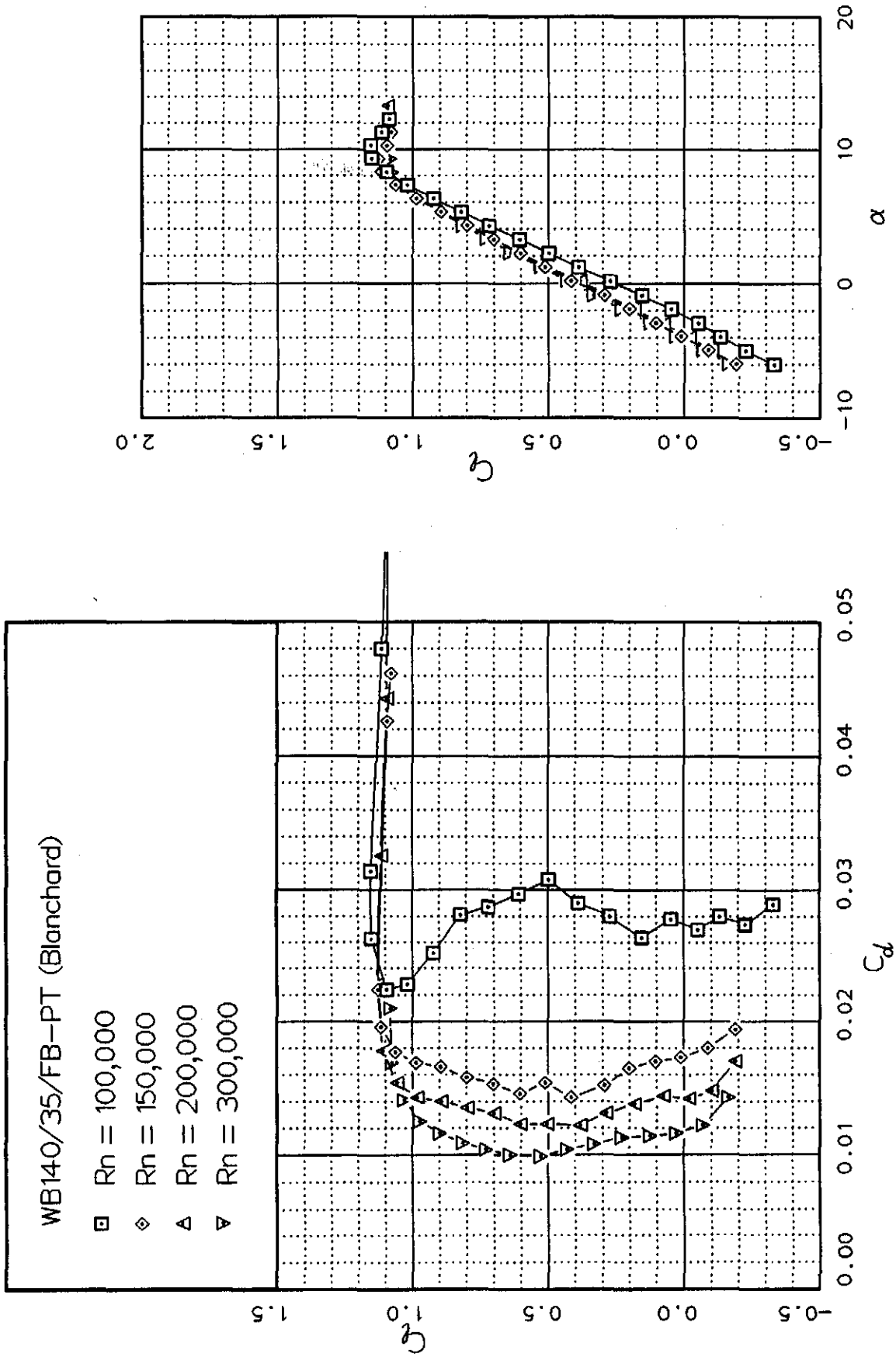
WB140/35/FB-PT (Blanchard)
Rn = 100,000
Rn = 150,000
Rn = 200,000
Rn = 300,000
c_l
c_d
α

AQUILA-PT

Fig. 12.1

$Rn = 59400.$

α	C_l	C_d
-1.86	0.261	0.0238
-0.83	0.352	0.0224
0.18	0.445	0.0213
1.20	0.525	0.0224
2.23	0.607	0.0298
3.23	0.686	0.0291
4.26	0.764	0.0354
5.27	0.839	0.0358
6.28	0.911	0.0404
7.30	0.989	0.0373
8.33	1.061	0.0383
9.34	1.120	0.0422
10.34	1.148	0.0507

$Rn = 101100.$

α	C_l	C_d
-1.86	0.251	0.0196
-0.84	0.340	0.0179
0.18	0.450	0.0152
1.21	0.538	0.0153
2.22	0.625	0.0166
3.24	0.726	0.0184
4.27	0.815	0.0197
5.28	0.899	0.0206
6.29	0.984	0.0215
7.33	1.069	0.0239
8.33	1.146	0.0251
9.35	1.215	0.0285
10.36	1.241	0.0359
11.36	1.280	0.0385
12.37	1.298	0.0471
13.37	1.295	0.0573

$Rn = 150500.$

α	C_l	C_d
1.19	0.537	0.0128
3.24	0.732	0.0154
5.28	0.916	0.0176
7.32	1.087	0.0214
8.34	1.159	0.0221
9.36	1.217	0.0245
11.37	1.292	0.0346

$Rn = 203900.$

α	C_l	C_d
-1.89	0.235	0.0162
-0.85	0.336	0.0141
0.17	0.439	0.0128
1.19	0.541	0.0113
2.22	0.641	0.0124
3.26	0.741	0.0130
4.26	0.833	0.0138
5.28	0.921	0.0150
6.31	1.006	0.0170
7.32	1.085	0.0182
8.34	1.156	0.0193
9.35	1.216	0.0222
10.37	1.268	0.0265
11.35	1.302	0.0314
12.37	1.312	0.0356
13.38	1.305	0.0475
14.36	1.292	0.0670

$Rn = 301100.$

α	C_l	C_d
-3.93	0.041	0.0254
-2.91	0.143	0.0187
-1.87	0.248	0.0143
-0.89	0.346	0.0122
0.14	0.448	0.0113
1.13	0.545	0.0091
2.18	0.646	0.0099
3.21	0.742	0.0111
4.23	0.834	0.0119
5.28	0.925	0.0131
6.30	1.010	0.0139
7.32	1.088	0.0152

CLARK-Y-PT

Fig. 12.3

$Rn = 61300.$

α	C_l	C_d
-3.95	-0.210	0.0282
-2.92	-0.100	0.0269
-1.90	0.006	0.0223
-0.88	0.113	0.0252
0.15	0.245	0.0278
1.18	0.365	0.0313
2.20	0.522	0.0324
3.24	0.646	0.0303
4.26	0.744	0.0284
5.28	0.836	0.0271
6.29	0.918	0.0266
7.32	1.005	0.0283
8.33	1.079	0.0305
9.34	1.152	0.0326
10.35	1.172	0.0332
11.34	1.172	0.0364

$Rn = 102600.$

α	C_l	C_d
-3.94	-0.137	0.0228
-2.92	0.002	0.0208
-1.87	0.137	0.0198
-0.85	0.287	0.0189
0.17	0.399	0.0192
1.20	0.501	0.0179
2.21	0.595	0.0184
3.25	0.691	0.0179
4.25	0.782	0.0186
5.28	0.876	0.0190
6.29	0.963	0.0209
7.32	1.043	0.0214
8.34	1.126	0.0225
9.36	1.198	0.0259
10.36	1.213	0.0299
11.35	1.210	0.0383

$Rn = 203800.$

α	C_l	C_d
-3.96	-0.011	0.0143
-2.90	0.086	0.0128
-1.91	0.176	0.0120
-0.85	0.272	0.0097
0.17	0.399	0.0098
1.19	0.496	0.0098
2.22	0.596	0.0104
3.24	0.691	0.0114
4.27	0.788	0.0124
5.28	0.874	0.0134
6.30	0.960	0.0151
7.31	1.041	0.0162
8.34	1.109	0.0187
9.34	1.147	0.0216
10.34	1.163	0.0271
11.35	1.168	0.0349
12.34	1.170	0.0427
13.36	1.166	0.0539
14.35	1.148	0.0724

$Rn = 301200.$

α	C_l	C_d
-4.93	-0.098	0.0136
-3.91	-0.007	0.0120
-2.90	0.088	0.0110
-1.87	0.188	0.0103
-0.86	0.283	0.0092
0.16	0.407	0.0084
1.20	0.510	0.0087
2.23	0.605	0.0095
3.24	0.699	0.0101
4.26	0.791	0.0112
5.29	0.882	0.0120

DAE51-PT

Fig. 12.5

$Rn = 60400.$

α	C_l	C_d
-2.91	0.041	0.0296
-1.89	0.157	0.0246
-0.87	0.299	0.0227
0.18	0.402	0.0256
1.20	0.481	0.0273
2.22	0.600	0.0281
3.24	0.711	0.0286
4.25	0.794	0.0279
5.29	0.896	0.0247
6.28	0.944	0.0238
7.31	1.015	0.0248
8.31	1.064	0.0399

$Rn = 101400.$

α	C_l	C_d
-2.90	0.116	0.0224
-1.87	0.233	0.0205
-0.84	0.346	0.0197
0.18	0.448	0.0175
1.22	0.546	0.0172
2.22	0.644	0.0190
3.25	0.742	0.0191
4.25	0.834	0.0196
5.29	0.922	0.0198
6.30	1.004	0.0191
7.33	1.065	0.0233
8.32	1.120	0.0311
9.33	1.145	0.0352
10.33	1.166	0.0390

$Rn = 153500.$

α	C_l	C_d
-2.87	0.240	0.0166
-1.84	0.337	0.0134
-0.82	0.426	0.0120
0.20	0.526	0.0115
1.20	0.627	0.0125
2.23	0.730	0.0130
3.27	0.829	0.0145
4.28	0.924	0.0152
5.31	1.014	0.0151
6.31	1.069	0.0194
7.32	1.104	0.0246
8.34	1.135	0.0313
9.35	1.161	0.0388
10.33	1.181	0.0500
11.34	1.191	0.0640

$Rn = 203200.$

α	C_l	C_d
-2.92	0.235	0.0140
-1.86	0.336	0.0121
-0.83	0.427	0.0090
0.17	0.529	0.0099
1.21	0.637	0.0099
2.23	0.740	0.0109
3.27	0.841	0.0119
4.26	0.934	0.0127
5.30	1.015	0.0141
6.31	1.064	0.0184
7.31	1.102	0.0239
8.33	1.138	0.0294
9.35	1.166	0.0372
10.33	1.184	0.0458
11.34	1.186	0.0651

$Rn = 310400.$

α	C_l	C_d
-2.88	0.232	0.0118
-1.84	0.340	0.0104
-0.82	0.438	0.0081
0.17	0.542	0.0078
1.22	0.648	0.0085
2.22	0.748	0.0091
3.26	0.844	0.0101
4.24	0.929	0.0108
5.18	0.991	0.0132
6.28	1.043	0.0181
7.31	1.092	0.0230
8.33	1.133	0.0272
9.34	1.159	0.0344
10.34	1.174	0.0474

DAE51-PT

Fig. 12.6

$Rn = 100100.$

α	C_l	C_d
-2.90	0.177	0.0218
-1.37	0.340	0.0164
0.18	0.490	0.0179
1.72	0.637	0.0188
3.26	0.778	0.0208
4.77	0.916	0.0209
6.31	1.047	0.0202
7.82	1.116	0.0268
9.34	1.157	0.0367

$Rn = 148600.$

α	C_l	C_d
-2.87	0.198	0.0180
-1.33	0.337	0.0134
0.17	0.481	0.0128

1.74	0.638	0.0136
3.25	0.787	0.0149
4.78	0.932	0.0157
6.31	1.045	0.0184
7.83	1.117	0.0275
9.34	1.167	0.0367
10.86	1.194	0.0502

$Rn = 197900.$

α	C_l	C_d
-2.89	0.185	0.0158
-1.34	0.339	0.0128
0.19	0.485	0.0109
1.73	0.646	0.0113
3.24	0.800	0.0124
4.80	0.947	0.0136
6.31	1.052	0.0189
7.82	1.129	0.0265
9.33	1.179	0.0362

$Rn = 301600.$

α	C_l	C_d
-2.88	0.175	0.0137
-1.36	0.336	0.0115
0.17	0.489	0.0087
1.71	0.652	0.0094
3.23	0.807	0.0103
4.78	0.947	0.0126
6.29	1.042	0.0188
7.81	1.123	0.0245
9.34	1.171	0.0350
10.85	1.186	0.0550
12.34	1.181	0.0757

DF101-PT

Fig. 12.8

$Rn = 58100.$

α	C_l	C_d
-4.99	-0.360	0.0240
-3.97	-0.293	0.0195
-2.95	-0.226	0.0174
-1.92	-0.112	0.0173
-0.89	0.035	0.0175
0.14	0.202	0.0211
1.17	0.354	0.0218
2.20	0.458	0.0221
3.21	0.541	0.0218
4.23	0.624	0.0245
5.24	0.701	0.0270
6.26	0.775	0.0262
7.28	0.842	0.0344
8.29	0.909	0.0358
9.31	0.970	0.0429
10.31	1.016	0.0463

$Rn = 101700.$

α	C_l	C_d
-6.00	-0.414	0.0214
-4.97	-0.351	0.0170
-3.97	-0.250	0.0174
-2.95	-0.124	0.0149
-1.91	0.012	0.0138
-0.87	0.187	0.0143
0.16	0.293	0.0152
1.17	0.375	0.0150
2.19	0.463	0.0144
3.21	0.551	0.0159
4.24	0.640	0.0157
5.25	0.721	0.0179
6.26	0.799	0.0184
7.28	0.875	0.0220
8.30	0.950	0.0268
9.32	1.022	0.0297
10.33	1.074	0.0321
11.33	1.093	0.0379
12.33	1.083	0.0500
13.29	0.841	0.1833

$Rn = 153700.$

α	C_l	C_d
-5.99	-0.417	0.0195
-4.97	-0.331	0.0155
-3.95	-0.194	0.0137
-2.93	-0.067	0.0127
-1.90	0.036	0.0110
-0.87	0.167	0.0108
0.16	0.283	0.0107
1.17	0.375	0.0110
2.19	0.469	0.0115
3.22	0.563	0.0118
4.23	0.648	0.0126
5.26	0.730	0.0144
6.27	0.814	0.0163
7.29	0.896	0.0182
8.31	0.974	0.0204
9.32	1.049	0.0217
10.33	1.110	0.0238
11.34	1.141	0.0273
12.34	1.131	0.0333
13.34	1.101	0.0420

$Rn = 201400.$

α	C_l	C_d
-5.99	-0.395	0.0152
-4.97	-0.265	0.0126
-3.93	-0.149	0.0102
-2.92	-0.050	0.0105
-1.89	0.040	0.0100
-0.88	0.135	0.0093
0.15	0.283	0.0092
1.18	0.379	0.0096
2.20	0.473	0.0103
3.22	0.564	0.0107
4.24	0.651	0.0123
5.25	0.737	0.0139
6.26	0.819	0.0152
7.29	0.900	0.0170
8.30	0.980	0.0188
9.32	1.055	0.0201
10.33	1.112	0.0228
11.34	1.143	0.0275
12.34	1.134	0.0335
13.31	1.106	0.0418
14.31	1.060	0.0603

$Rn = 305500.$

α	C_l	C_d
-6.00	-0.351	0.0145
-4.96	-0.238	0.0118
-3.94	-0.145	0.0106
-2.93	-0.055	0.0101
-1.90	0.037	0.0094
-0.88	0.132	0.0086
0.14	0.235	0.0078
1.17	0.380	0.0083
2.19	0.474	0.0089
3.21	0.562	0.0099
4.24	0.649	0.0110
5.25	0.731	0.0123
6.26	0.815	0.0136
7.29	0.896	0.0147
8.31	0.976	0.0162
9.31	1.048	0.0177
10.34	1.104	0.0201

DF102-PT

Fig. 12.9

$Rn = 59100.$

α	C_l	C_d
-3.98	-0.323	0.0214
-2.96	-0.245	0.0196
-1.93	-0.135	0.0204
-0.93	-0.022	0.0214
0.12	0.156	0.0227
1.15	0.338	0.0231
2.18	0.450	0.0219
3.19	0.505	0.0223
4.22	0.598	0.0195
5.23	0.679	0.0242
6.25	0.759	0.0322
7.27	0.826	0.0395
8.28	0.872	0.0456
9.27	0.882	0.0455
10.25	0.767	0.1178

$Rn = 100200.$

α	C_l	C_d
-3.97	-0.294	0.0178
-2.95	-0.181	0.0169
-1.92	-0.047	0.0155
-0.89	0.136	0.0131
0.13	0.260	0.0144
1.16	0.354	0.0146
2.18	0.440	0.0148
3.20	0.524	0.0149
4.23	0.613	0.0160
5.22	0.688	0.0177
6.26	0.766	0.0211
7.26	0.841	0.0242
8.28	0.908	0.0284
9.29	0.973	0.0307
10.32	1.027	0.0401
11.31	0.938	0.0826

$Rn = 149100.$

α	C_l	C_d
-3.95	-0.235	0.0156
-2.43	-0.053	0.0127
-0.89	0.115	0.0118
0.65	0.295	0.0119
2.17	0.435	0.0122
3.70	0.571	0.0128
5.24	0.691	0.0160
6.76	0.808	0.0193
8.29	0.923	0.0248
9.81	1.029	0.0294
11.32	1.126	0.0327
12.84	1.202	0.0393
14.35	1.214	0.0471

$Rn = 200900.$

α	C_l	C_d
-3.97	-0.193	0.0129
-2.96	-0.097	0.0114
-1.93	-0.008	0.0109
-0.91	0.079	0.0102
0.13	0.229	0.0095
1.16	0.338	0.0098
2.17	0.435	0.0105
3.19	0.526	0.0111
4.22	0.612	0.0132
5.23	0.695	0.0147
6.26	0.777	0.0165
7.27	0.855	0.0189
8.28	0.932	0.0209
9.31	1.008	0.0238
10.32	1.079	0.0260
11.34	1.144	0.0282
12.34	1.201	0.0316
13.35	1.237	0.0383
14.34	1.226	0.0547
15.33	1.176	0.0462

$Rn = 300900.$

α	C_l	C_d
-4.03	-0.197	0.0107
-2.97	-0.107	0.0105
-1.93	-0.018	0.0095
-0.91	0.076	0.0091
0.12	0.171	0.0083
1.12	0.325	0.0085
2.16	0.434	0.0091
3.18	0.525	0.0103
4.21	0.613	0.0120
5.24	0.699	0.0135
6.24	0.780	0.0148
7.27	0.861	0.0160
8.28	0.939	0.0176
9.31	1.016	0.0190
10.31	1.088	0.0208
11.34	1.154	0.0232
12.34	1.213	0.0260
13.35	1.243	0.0326
14.35	1.232	0.0488

DF103-PT

Fig. 12.10

$Rn = 62500.$

α	C_l	C_d
-2.98	-0.264	0.0184
-1.43	-0.121	0.0194
0.09	0.137	0.0205
1.66	0.306	0.0204
3.19	0.424	0.0203
4.71	0.556	0.0216
6.22	0.649	0.0206
7.77	0.786	0.0270
9.27	0.856	0.0267
10.77	0.888	0.0347

$Rn = 99700.$

α	C_l	C_d
-2.94	-0.156	0.0143
-1.41	0.064	0.0133

0.13	0.248	0.0140
1.66	0.381	0.0147
3.18	0.512	0.0161
4.73	0.645	0.0188
6.23	0.763	0.0196
7.76	0.863	0.0226
9.29	0.926	0.0293
10.79	0.961	0.0424
12.30	0.962	0.0547

$Rn = 148500.$

α	C_l	C_d
-2.94	-0.096	0.0130
-1.42	0.046	0.0119
0.13	0.234	0.0109
1.67	0.373	0.0122
3.21	0.515	0.0125
4.74	0.651	0.0147
6.23	0.771	0.0170
7.77	0.860	0.0198
9.27	0.924	0.0266
10.80	0.960	0.0374

$Rn = 203200.$

α	C_l	C_d
-2.95	-0.111	0.0118
-1.43	0.021	0.0102
0.14	0.218	0.0096
1.67	0.372	0.0100
3.18	0.516	0.0109
4.72	0.657	0.0127
6.26	0.775	0.0149
7.77	0.858	0.0183
9.27	0.923	0.0253
10.80	0.959	0.0358
12.28	0.965	0.0586

$Rn = 304800.$

α	C_l	C_d
-1.98	-0.030	0.0096
-0.44	0.109	0.0083
1.12	0.314	0.0082
2.69	0.477	0.0091
4.21	0.618	0.0102
5.74	0.740	0.0120
7.25	0.828	0.0158
8.78	0.906	0.0208
10.29	0.960	0.0285
11.79	0.991	0.0489
13.29	1.018	0.0894

E193-PT

Fig. 12.11

$Rn = 60200.$

α	C_l	C_d
-3.95	-0.202	0.0310
-2.93	-0.079	0.0236
-1.90	0.063	0.0196
-0.87	0.211	0.0172
0.16	0.324	0.0197
1.19	0.414	0.0242
2.20	0.501	0.0265
3.21	0.583	0.0292
4.23	0.629	0.0402
5.25	0.741	0.0415
6.29	0.868	0.0388
7.30	0.972	0.0334
8.33	1.062	0.0279
9.33	1.111	0.0282
10.34	1.121	0.0339
11.33	1.128	0.0470
12.34	1.126	0.0560
13.32	1.047	0.0539

$Rn = 97500.$

α	C_l	C_d
-3.95	-0.125	0.0197
-2.91	0.004	0.0168
-1.88	0.104	0.0138
-0.87	0.223	0.0134
0.14	0.317	0.0141
1.19	0.412	0.0161
2.20	0.506	0.0190
3.21	0.599	0.0210
4.23	0.687	0.0226
5.26	0.780	0.0234
6.28	0.876	0.0217
7.30	0.972	0.0222
8.33	1.063	0.0216
9.32	1.110	0.0231
10.34	1.119	0.0334
11.34	1.125	0.0402
12.34	1.121	0.0519

$Rn = 204200.$

α	C_l	C_d
-3.94	-0.106	0.0148
-2.95	-0.017	0.0129
-1.89	0.085	0.0123
-0.88	0.179	0.0106
0.15	0.298	0.0100
1.18	0.401	0.0107
2.19	0.505	0.0112
3.22	0.608	0.0122
4.24	0.706	0.0127
5.26	0.803	0.0134
6.28	0.898	0.0133
7.31	0.980	0.0147
8.31	1.040	0.0177
9.31	1.081	0.0221
10.33	1.103	0.0282
11.34	1.104	0.0326
12.33	1.100	0.0382

$Rn = 303100.$

α	C_l	C_d
-2.92	-0.006	0.0115
-1.89	0.097	0.0107
-0.88	0.198	0.0097
0.15	0.315	0.0085
1.16	0.416	0.0088
2.19	0.514	0.0092
3.20	0.616	0.0097
4.24	0.715	0.0107
5.25	0.811	0.0112

E193MOD-PT

Fig. 12.12

$Rn = 100300.$

α	C_l	C_d
-2.93	0.069	0.0192
-0.87	0.262	0.0180
0.15	0.364	0.0179
2.20	0.555	0.0206
4.24	0.745	0.0231
6.29	0.944	0.0228
7.32	1.045	0.0219
8.33	1.133	0.0209
9.35	1.210	0.0227
10.35	1.238	0.0232

$Rn = 149400.$

α	C_l	C_d
-2.89	0.090	0.0143
-0.85	0.277	0.0128
0.18	0.388	0.0131
2.22	0.594	0.0146
4.26	0.795	0.0157
6.30	0.985	0.0174
7.31	1.078	0.0178
8.34	1.164	0.0201
9.36	1.203	0.0260
10.34	1.219	0.0348

$Rn = 207900.$

α	C_l	C_d
-9.03	-0.410	0.1195
-8.00	-0.366	0.0932
-6.97	-0.264	0.0414
-5.97	-0.188	0.0194
-5.03	-0.111	0.0160
-3.94	-0.013	0.0137
-2.89	0.082	0.0122
-1.88	0.181	0.0115
-0.86	0.283	0.0102
0.15	0.392	0.0099
1.20	0.502	0.0101
2.20	0.606	0.0105
3.23	0.710	0.0120
4.26	0.811	0.0127
5.28	0.908	0.0135
6.31	1.003	0.0141
7.33	1.090	0.0158
8.33	1.155	0.0179
9.33	1.185	0.0231
10.34	1.205	0.0287
11.34	1.208	0.0338

$Rn = 307800.$

α	C_l	C_d
-2.91	0.090	0.0111
-1.89	0.192	0.0104
-0.89	0.295	0.0093
0.13	0.397	0.0084
1.17	0.514	0.0085
2.20	0.619	0.0092
3.24	0.720	0.0097
4.25	0.817	0.0107
5.28	0.914	0.0116
6.30	1.004	0.0127
7.31	1.081	0.0138
8.32	1.135	0.0166
9.34	1.164	0.0222
10.35	1.186	0.0270
11.34	1.199	0.0317
12.34	1.212	0.0312

E205A-PT

Fig. 12.13

$Rn = 59800.$

α	C_l	C_d
-3.96	-0.220	0.0241
-2.92	-0.101	0.0207
-1.90	0.080	0.0166
-0.85	0.207	0.0170
0.16	0.294	0.0208
1.17	0.373	0.0247
2.18	0.449	0.0277
3.21	0.524	0.0291
4.22	0.598	0.0340
5.24	0.665	0.0377
6.25	0.727	0.0430
7.28	0.830	0.0389
8.29	0.915	0.0323
9.31	0.987	0.0289
10.32	1.021	0.0289
11.32	1.034	0.0354

$Rn = 99500.$

α	C_l	C_d
-3.93	-0.144	0.0198
-2.92	-0.019	0.0156
-1.88	0.098	0.0139
-0.86	0.197	0.0144
0.16	0.289	0.0154
1.18	0.380	0.0177
2.20	0.468	0.0195
3.21	0.557	0.0210
4.23	0.645	0.0217
5.25	0.732	0.0228
6.27	0.821	0.0226
7.29	0.911	0.0225
8.32	0.993	0.0223
9.32	1.047	0.0242
10.33	1.074	0.0288
11.32	1.083	0.0333

$Rn = 150600.$

α	C_l	C_d
-1.90	0.048	0.0126
-0.86	0.180	0.0110
0.15	0.276	0.0114
1.16	0.372	0.0123
3.22	0.564	0.0149
5.25	0.750	0.0157
7.30	0.930	0.0173
8.31	0.996	0.0185
9.33	1.045	0.0220
10.33	1.076	0.0259
11.32	1.076	0.0281

$Rn = 202100.$

α	C_l	C_d
-4.98	-0.265	0.0195
-3.94	-0.161	0.0154
-2.92	-0.072	0.0129
-1.89	0.024	0.0116
-0.90	0.120	0.0108
0.15	0.258	0.0098
1.16	0.357	0.0106
2.19	0.455	0.0109
3.20	0.551	0.0119
4.24	0.650	0.0128

5.26	0.743	0.0131
6.27	0.838	0.0135
7.30	0.927	0.0143
8.30	0.995	0.0161
9.31	1.050	0.0192
10.32	1.088	0.0230
11.34	1.090	0.0256
12.31	1.081	0.0278

$Rn = 301800.$

α	C_l	C_d
-1.92	0.019	0.0109
-0.88	0.117	0.0101
0.14	0.244	0.0084
1.16	0.357	0.0091
2.19	0.457	0.0093
3.21	0.555	0.0099
4.22	0.652	0.0103
5.25	0.748	0.0112
6.27	0.840	0.0118
7.28	0.916	0.0133
8.31	0.979	0.0160

E205B-PT

Fig. 12.14

$Rn = 63600.$

α	C_l	C_d
-4.94	-0.193	0.0252
-3.94	-0.108	0.0186
-2.92	0.014	0.0152
-1.88	0.154	0.0126
-0.84	0.279	0.0185
0.16	0.372	0.0225
1.18	0.456	0.0248
2.21	0.532	0.0277
3.22	0.625	0.0336
4.24	0.718	0.0324
5.26	0.809	0.0300
6.28	0.882	0.0302
7.29	0.967	0.0287
8.32	1.031	0.0267
9.32	1.054	0.0280
10.33	1.061	0.0456

$Rn = 105200.$

α	C_l	C_d
-5.99	-0.282	0.0277
-4.95	-0.172	0.0200
-3.91	-0.041	0.0154
-2.89	0.082	0.0136
-1.87	0.194	0.0135
-0.85	0.294	0.0162
0.17	0.378	0.0171
1.19	0.464	0.0190
2.22	0.563	0.0195
3.23	0.651	0.0207
4.25	0.736	0.0205
5.28	0.817	0.0219
6.28	0.912	0.0210
7.31	1.005	0.0210
8.31	1.049	0.0258
9.31	1.059	0.0343

$Rn = 151100.$

α	C_l	C_d
-6.00	-0.261	0.0235
-4.94	-0.137	0.0181
-3.92	-0.018	0.0138
-2.89	0.070	0.0118
-1.88	0.160	0.0099
-0.87	0.268	0.0104
0.15	0.366	0.0117
1.19	0.468	0.0134
2.21	0.569	0.0148
3.22	0.662	0.0158
4.24	0.763	0.0166
5.27	0.861	0.0171
6.30	0.956	0.0175
7.30	1.027	0.0192
8.33	1.065	0.0275
9.33	1.082	0.0338
10.32	1.076	0.0584

$Rn = 206600.$

α	C_l	C_d
-4.95	-0.131	0.0149
-3.91	-0.031	0.0127
-2.91	0.061	0.0108
-1.88	0.149	0.0093
-0.87	0.258	0.0092
0.15	0.361	0.0098
1.19	0.467	0.0111
2.20	0.570	0.0120
3.24	0.675	0.0132
4.24	0.775	0.0136
5.28	0.875	0.0138
6.28	0.960	0.0145
7.31	1.024	0.0175
8.32	1.068	0.0242
9.32	1.091	0.0313
10.32	1.088	0.0439
11.31	1.081	0.0588

$Rn = 304300.$

α	C_l	C_d
-5.98	-0.221	0.0171
-4.95	-0.129	0.0136
-3.95	-0.040	0.0120
-2.92	0.051	0.0106
-1.90	0.156	0.0095
-0.86	0.255	0.0081
0.16	0.367	0.0082
1.19	0.473	0.0089
2.20	0.578	0.0094
3.24	0.684	0.0104
4.24	0.782	0.0110
5.28	0.877	0.0116
6.28	0.957	0.0134
7.30	1.017	0.0172
8.31	1.068	0.0222
9.33	1.099	0.0280
10.32	1.096	0.0463
11.31	1.083	0.0758
12.30	1.066	0.1016

E214A-PT

Fig. 12.16

$Rn = 101600.$

α	C_l	C_d
-7.00	-0.398	0.0727
-5.99	-0.364	0.0582
-4.97	-0.271	0.0369
-3.95	-0.126	0.0293
-2.91	0.006	0.0227
-1.88	0.136	0.0200
-0.86	0.260	0.0210
0.17	0.392	0.0212
1.20	0.523	0.0197
2.23	0.636	0.0198
3.25	0.734	0.0182
4.26	0.828	0.0200
5.28	0.917	0.0196
6.30	1.002	0.0209
7.33	1.094	0.0201
8.34	1.176	0.0227
9.35	1.230	0.0260
10.35	1.247	0.0382
11.37	1.255	0.0498
12.37	1.247	0.0665

$Rn = 146700.$

α	C_l	C_d
-4.95	-0.109	0.0263
-3.39	0.084	0.0180
-1.86	0.273	0.0139
-0.34	0.417	0.0120
1.20	0.566	0.0122
2.75	0.728	0.0130
4.27	0.882	0.0145
5.79	1.025	0.0172
7.33	1.163	0.0183
8.86	1.264	0.0221
10.37	1.305	0.0338
11.86	1.303	0.0547
13.36	1.267	0.0817

$Rn = 201800.$

α	C_l	C_d
-7.00	-0.350	0.0864
-6.02	-0.209	0.0481
-4.99	-0.060	0.0227
-3.94	0.070	0.0175
-2.88	0.193	0.0146
-1.89	0.301	0.0116
-0.84	0.407	0.0113
0.16	0.505	0.0108
1.16	0.600	0.0101
2.13	0.696	0.0108
3.24	0.806	0.0112
4.23	0.899	0.0115
5.29	0.997	0.0128
6.30	1.087	0.0141
7.30	1.169	0.0159
8.34	1.235	0.0178
9.36	1.278	0.0244
10.36	1.301	0.0302
11.37	1.305	0.0423
12.38	1.291	0.0674

$Rn = 299000.$

α	C_l	C_d
-4.93	-0.029	0.0177
-3.90	0.075	0.0133
-2.89	0.176	0.0118
-1.86	0.283	0.0106
-0.84	0.392	0.0090
0.19	0.496	0.0090
1.19	0.594	0.0086
2.23	0.692	0.0091
3.25	0.795	0.0101
4.26	0.893	0.0110
5.28	0.988	0.0123
6.30	1.076	0.0133
7.28	1.147	0.0151
8.31	1.209	0.0179
9.32	1.255	0.0233

E214B-PT

Fig. 12.17

$Rn = 59800.$

α	C_l	C_d
-5.98	-0.383	0.0763
-4.97	-0.243	0.0435
-3.94	-0.108	0.0327
-2.90	0.010	0.0274
-1.87	0.118	0.0235
-0.86	0.199	0.0247
0.16	0.327	0.0296
1.19	0.493	0.0308
2.22	0.567	0.0364
3.23	0.672	0.0407
4.27	0.844	0.0380
5.30	0.988	0.0345
6.33	1.101	0.0319
7.35	1.186	0.0289
8.37	1.257	0.0306
9.38	1.324	0.0310
10.39	1.344	0.0329
11.38	1.318	0.0388

$Rn = 99300.$

α	C_l	C_d
-5.97	-0.342	0.0694
-4.95	-0.182	0.0357
-3.93	-0.045	0.0276
-2.89	0.096	0.0216
-1.86	0.238	0.0216
-0.84	0.349	0.0226
0.19	0.473	0.0207
1.22	0.614	0.0207
2.25	0.733	0.0214
3.28	0.836	0.0208
4.30	0.935	0.0211
5.32	1.029	0.0211
6.33	1.118	0.0207
7.35	1.206	0.0206
8.37	1.281	0.0226
9.38	1.331	0.0266
10.39	1.335	0.0366
11.39	1.317	0.0461

$Rn = 202600.$

α	C_l	C_d
-5.96	-0.215	0.0421
-5.01	-0.083	0.0230
-3.90	0.072	0.0172
-2.88	0.219	0.0137
-1.86	0.342	0.0112
-0.84	0.444	0.0107
0.19	0.541	0.0105
1.20	0.622	0.0105
2.24	0.735	0.0108
3.26	0.836	0.0116

4.27	0.931	0.0122
5.29	1.026	0.0133
6.32	1.112	0.0143
7.34	1.178	0.0162
8.35	1.232	0.0204
9.36	1.271	0.0253
10.36	1.276	0.0335
11.37	1.270	0.0441

$Rn = 301800.$

α	C_l	C_d
-5.94	-0.067	0.0200
-4.89	0.057	0.0148
-3.87	0.172	0.0120
-2.85	0.286	0.0098
-1.82	0.392	0.0089
-0.80	0.492	0.0087
0.21	0.590	0.0089
1.23	0.683	0.0095
2.24	0.779	0.0098

E214C-PT

Fig. 12.18

$Rn = 102700.$

α	C_l	C_d
-0.82	0.450	0.0269
0.71	0.670	0.0235
2.29	0.878	0.0202
3.81	1.022	0.0193
5.33	1.147	0.0213
6.87	1.262	0.0209
8.38	1.328	0.0268
9.87	1.317	0.0385

$Rn = 151100.$

α	C_l	C_d
-0.80	0.586	0.0188
0.74	0.763	0.0144
2.27	0.916	0.0135
3.82	1.060	0.0153
5.34	1.195	0.0166
6.87	1.293	0.0191
8.39	1.347	0.0252
9.87	1.338	0.0400
11.38	1.316	0.0559
12.88	1.281	0.0797

$Rn = 200800.$

α	C_l	C_d
-0.79	0.627	0.0142
0.75	0.788	0.0115
2.27	0.925	0.0121
3.79	1.070	0.0136
5.31	1.197	0.0153
6.87	1.285	0.0187
8.35	1.340	0.0250
9.88	1.342	0.0373
11.36	1.324	0.0548

$Rn = 301000.$

α	C_l	C_d
-0.78	0.643	0.0096
0.77	0.789	0.0105
2.28	0.931	0.0115
3.82	1.067	0.0123
5.34	1.187	0.0142
6.82	1.266	0.0184
8.29	1.324	0.0241
9.88	1.345	0.0344
11.35	1.332	0.0518
12.86	1.295	0.0777

E214C-PT

Fig. 12.19

$Rn = 59700.$

α	C_l	C_d
-3.92	-0.103	0.0260
-2.91	0.002	0.0251
-1.89	0.086	0.0210
-0.87	0.194	0.0233
0.16	0.321	0.0294
1.19	0.460	0.0326
2.20	0.516	0.0354
3.23	0.623	0.0370
4.27	0.774	0.0369
5.29	0.899	0.0344
6.30	0.985	0.0316
7.33	1.075	0.0296
8.35	1.150	0.0271
9.36	1.217	0.0288
10.36	1.239	0.0335
11.37	1.246	0.0421
12.37	1.241	0.0569
13.36	1.232	0.0598
14.35	1.132	0.1175

$Rn = 100600.$

α	C_l	C_d
-3.93	-0.084	0.0256
-2.89	0.062	0.0202
-1.86	0.200	0.0208
-0.84	0.321	0.0208
0.18	0.433	0.0211
1.22	0.553	0.0204
2.23	0.668	0.0195
3.24	0.779	0.0190
4.28	0.878	0.0199
5.30	0.966	0.0203
6.31	1.044	0.0213
7.34	1.131	0.0207
8.35	1.194	0.0214
9.36	1.262	0.0233
10.38	1.287	0.0305
11.37	1.286	0.0407
12.36	1.280	0.0485
13.36	1.271	0.0561
14.37	1.248	0.0783

$Rn = 151300.$

α	C_l	C_d
-4.95	-0.125	0.0278
-3.92	0.002	0.0232
-2.90	0.134	0.0194
-1.88	0.289	0.0158
-0.85	0.416	0.0148
0.19	0.506	0.0128
1.21	0.598	0.0123
2.23	0.711	0.0125
3.26	0.804	0.0143
4.28	0.899	0.0145
5.31	1.008	0.0153
6.32	1.093	0.0157
7.33	1.172	0.0167
8.36	1.228	0.0200
9.36	1.271	0.0233
10.37	1.287	0.0307

$Rn = 201700.$

α	C_l	C_d
-4.99	-0.105	0.0257
-4.01	0.011	0.0204
-2.97	0.171	0.0156
-1.91	0.310	0.0123
-0.91	0.415	0.0109
0.12	0.515	0.0105
1.17	0.607	0.0103
2.17	0.705	0.0107
3.21	0.809	0.0117
4.26	0.908	0.0122
5.28	1.003	0.0133
6.30	1.089	0.0146
7.32	1.160	0.0156
8.35	1.217	0.0189
9.36	1.258	0.0241
10.37	1.272	0.0327

$Rn = 302800.$

α	C_l	C_d
-4.93	-0.008	0.0170
-3.89	0.114	0.0133
-2.86	0.230	0.0100
-1.84	0.337	0.0086
-0.82	0.440	0.0084
0.21	0.538	0.0089
1.23	0.634	0.0094
2.24	0.729	0.0096
3.27	0.829	0.0103
4.27	0.921	0.0112
5.28	1.011	0.0118
6.31	1.095	0.0127
7.30	1.160	0.0154
8.27	1.220	0.0184
9.27	1.261	0.0228

E214C-PT

Fig. 12.20

$Rn = 104200.$

α	C_l	C_d
-3.95	-0.196	0.0269
-2.93	-0.042	0.0198
-1.88	0.106	0.0162
-0.85	0.236	0.0147
0.17	0.345	0.0155
1.20	0.457	0.0157
2.20	0.565	0.0173
3.25	0.672	0.0187
4.25	0.771	0.0183
5.27	0.876	0.0206
6.30	0.978	0.0210
7.31	1.077	0.0193
8.35	1.166	0.0207
9.36	1.237	0.0220
10.35	1.267	0.0315

$Rn = 149900.$

α	C_l	C_d
-2.89	0.050	0.0172
-0.84	0.278	0.0113
0.19	0.362	0.0115
1.18	0.462	0.0120
3.23	0.666	0.0141
5.28	0.866	0.0150
7.32	1.056	0.0164
9.36	1.195	0.0212
10.37	1.230	0.0281
11.36	1.230	0.0388
12.36	1.218	0.0545
13.36	1.210	0.0691

$Rn = 198400.$

α	C_l	C_d
-6.01	-0.336	0.0561
-4.97	-0.202	0.0275
-3.95	-0.064	0.0189
-2.93	0.064	0.0145
-1.89	0.179	0.0109
-0.89	0.276	0.0106
0.15	0.369	0.0103
1.17	0.463	0.0103
2.20	0.573	0.0111
3.22	0.678	0.0117
4.25	0.781	0.0120
5.28	0.880	0.0129
6.29	0.975	0.0140
7.32	1.060	0.0149
8.34	1.131	0.0171
9.35	1.190	0.0203
10.36	1.223	0.0272

$Rn = 303400.$

α	C_l	C_d
-5.99	-0.285	0.0480
-4.96	-0.152	0.0186
-3.91	-0.029	0.0134
-2.89	0.083	0.0112
-1.85	0.188	0.0097
-0.85	0.291	0.0094
0.17	0.392	0.0091
1.19	0.489	0.0092
2.21	0.588	0.0091
3.24	0.692	0.0097
4.24	0.790	0.0102

E214C-PT

Fig. 12.21

$Rn = 100600.$

α	C_l	C_d
-3.98	-0.283	0.0317
-2.44	-0.082	0.0221
-0.90	0.105	0.0146
0.64	0.273	0.0155
2.17	0.426	0.0185
3.70	0.566	0.0214
5.25	0.701	0.0216
6.78	0.844	0.0215
8.30	0.987	0.0205
9.82	1.115	0.0208
11.34	1.178	0.0296
12.84	1.155	0.0481

$Rn = 149400.$

α	C_l	C_d
-3.99	-0.242	0.0283

-2.43	-0.036	0.0163
-0.89	0.125	0.0121
0.63	0.248	0.0119
2.17	0.406	0.0131
3.70	0.564	0.0146
5.22	0.718	0.0145
6.78	0.869	0.0154
8.29	1.012	0.0162
9.83	1.125	0.0192
11.34	1.183	0.0304
12.84	1.164	0.0481

$Rn = 196500.$

α	C_l	C_d
-3.96	-0.206	0.0231
-2.44	-0.024	0.0139
-0.94	0.120	0.0113
0.60	0.252	0.0113
2.18	0.414	0.0115
3.71	0.576	0.0115
5.23	0.733	0.0124
6.78	0.890	0.0138
8.29	1.025	0.0147
9.83	1.134	0.0186
11.35	1.189	0.0296
12.84	1.171	0.0495

$Rn = 302500.$

α	C_l	C_d
-3.97	-0.184	0.0170
-2.48	-0.037	0.0128
-0.90	0.119	0.0105
0.62	0.271	0.0095
2.15	0.415	0.0090
3.68	0.578	0.0095
5.20	0.737	0.0103
6.76	0.888	0.0114
8.30	1.016	0.0134
9.82	1.124	0.0179
11.34	1.183	0.0264

E214C-PT

Fig. 12.22

$Rn = 97600.$

α	C_l	C_d
-3.93	-0.114	0.0291
-2.41	0.103	0.0217
-0.85	0.308	0.0160
0.69	0.456	0.0135
2.21	0.612	0.0140
3.75	0.765	0.0167
5.28	0.907	0.0180
6.81	1.044	0.0184
8.34	1.161	0.0222
9.86	1.260	0.0261
11.34	1.248	0.0309
12.85	1.203	0.0555

$Rn = 150200.$

α	C_l	C_d
-3.93	-0.060	0.0227
-2.38	0.144	0.0142
-0.85	0.313	0.0115
0.69	0.451	0.0111
2.21	0.609	0.0114
3.75	0.766	0.0134
5.29	0.911	0.0142
6.80	1.046	0.0156
8.34	1.167	0.0177
9.86	1.246	0.0228
11.37	1.261	0.0317

$Rn = 199200.$

α	C_l	C_d
-3.96	-0.009	0.0180
-2.42	0.166	0.0118
-0.86	0.325	0.0105
0.65	0.463	0.0102
2.20	0.614	0.0109
3.72	0.773	0.0120
5.27	0.920	0.0139
6.81	1.058	0.0155
8.33	1.179	0.0180
9.86	1.251	0.0263
11.36	1.256	0.0351
12.85	1.232	0.0494

$Rn = 298800.$

α	C_l	C_d
-3.91	0.025	0.0139
-2.39	0.172	0.0117
-0.86	0.330	0.0110
0.68	0.484	0.0108
2.20	0.626	0.0112
3.70	0.774	0.0124
5.24	0.923	0.0133
6.78	1.062	0.0151
8.32	1.184	0.0178
9.84	1.243	0.0257
11.36	1.254	0.0400

E374A-PT

Fig. 12.24

$Rn = 58900.$

α	C_l	C_d
-6.00	-0.410	0.0303
-4.97	-0.355	0.0257
-3.94	-0.268	0.0194
-2.95	-0.175	0.0180
-1.92	-0.041	0.0197
-0.89	0.098	0.0243
0.13	0.198	0.0269
1.16	0.310	0.0308
2.17	0.412	0.0309
3.20	0.546	0.0317
4.24	0.649	0.0377
5.25	0.751	0.0386
6.28	0.843	0.0315
7.29	0.929	0.0303
8.31	0.979	0.0302
9.30	0.994	0.0437
10.31	1.006	0.0625
11.31	1.023	0.0770

$Rn = 97800.$

α	C_l	C_d
-5.99	-0.386	0.0298
-4.98	-0.321	0.0237
-3.94	-0.196	0.0183
-2.94	-0.083	0.0138
-1.90	0.081	0.0164
-0.86	0.218	0.0185
0.17	0.303	0.0202
1.18	0.392	0.0226
2.19	0.483	0.0236
3.21	0.576	0.0257
4.24	0.671	0.0233
5.25	0.764	0.0216
6.27	0.863	0.0203
7.30	0.953	0.0189
8.31	0.993	0.0238
9.31	1.010	0.0345

$Rn = 151800.$

α	C_l	C_d
-6.01	-0.397	0.0264
-4.97	-0.274	0.0205
-3.94	-0.134	0.0145
-2.92	-0.034	0.0120
-1.92	0.036	0.0118
-0.88	0.166	0.0122
0.14	0.278	0.0120
1.16	0.368	0.0125
2.20	0.467	0.0132
3.20	0.563	0.0141
4.22	0.660	0.0145
5.26	0.759	0.0148
6.28	0.853	0.0148
7.28	0.924	0.0173
8.29	0.965	0.0223
9.31	0.993	0.0316
10.30	1.013	0.0404
11.31	1.020	0.0507
12.31	1.012	0.0690
13.30	1.014	0.1385

$Rn = 201300.$

α	C_l	C_d
-6.00	-0.356	0.0220
-4.96	-0.220	0.0159
-3.93	-0.120	0.0127
-2.92	-0.037	0.0111
-1.90	0.038	0.0102
-0.90	0.136	0.0096
0.16	0.275	0.0100
1.18	0.370	0.0104
2.19	0.469	0.0110
3.22	0.573	0.0115
4.23	0.673	0.0120
5.25	0.773	0.0126
6.27	0.855	0.0137
7.29	0.912	0.0182
8.29	0.954	0.0233
9.29	0.984	0.0302
10.30	0.999	0.0401
11.31	1.000	0.0492

$Rn = 300400.$

α	C_l	C_d
-6.01	-0.322	0.0186
-4.98	-0.225	0.0141
-3.99	-0.144	0.0114
-2.95	-0.052	0.0101
-2.00	0.033	0.0084
-0.94	0.127	0.0082
0.10	0.243	0.0080
1.14	0.371	0.0085
2.17	0.473	0.0088
3.20	0.579	0.0092
4.24	0.681	0.0098
5.26	0.776	0.0107
6.27	0.852	0.0128
7.28	0.910	0.0170

E374B-PT

Fig. 12.25

$Rn = 59200.$

α	C_l	C_d
-6.00	-0.400	0.0343
-4.98	-0.350	0.0275
-3.96	-0.290	0.0196
-2.94	-0.184	0.0185
-1.92	-0.096	0.0188
-0.90	0.034	0.0222
0.13	0.174	0.0271
1.15	0.271	0.0285
2.18	0.364	0.0320
3.19	0.433	0.0374
4.21	0.545	0.0404
5.25	0.703	0.0366
6.27	0.817	0.0311
7.29	0.906	0.0267
8.30	0.957	0.0263
9.30	0.973	0.0384
10.30	1.006	0.0498

$Rn = 97300.$

α	C_l	C_d
-5.98	-0.403	0.0278
-4.98	-0.327	0.0223
-3.95	-0.217	0.0173
-2.93	-0.093	0.0146
-1.89	0.081	0.0162
-0.87	0.190	0.0191
0.14	0.276	0.0207
1.17	0.360	0.0239
2.18	0.446	0.0261
3.21	0.532	0.0285
4.23	0.632	0.0269
5.24	0.733	0.0220
6.27	0.824	0.0203
7.30	0.917	0.0195
8.30	0.934	0.0292
9.30	0.963	0.0339
10.32	0.996	0.0436

$Rn = 151000.$

α	C_l	C_d
-4.98	-0.279	0.0186
-3.93	-0.146	0.0141
-2.91	-0.055	0.0112
-1.90	0.022	0.0117
-0.87	0.190	0.0118
0.16	0.285	0.0127
1.17	0.369	0.0140
2.20	0.457	0.0140
3.21	0.549	0.0150
4.24	0.645	0.0149
5.26	0.742	0.0144
6.27	0.835	0.0150
7.29	0.893	0.0190
8.30	0.927	0.0258
9.31	0.962	0.0328
10.31	0.988	0.0426

11.31	0.997	0.0509
12.31	0.995	0.0684

$Rn = 201600.$

α	C_l	C_d
-6.00	-0.365	0.0204
-4.97	-0.229	0.0153
-3.94	-0.136	0.0125
-2.94	-0.061	0.0108
-1.90	0.019	0.0097
-0.88	0.118	0.0105
0.15	0.272	0.0108
1.17	0.366	0.0115
2.19	0.455	0.0119
3.21	0.551	0.0124
4.24	0.646	0.0124
5.25	0.744	0.0124
6.28	0.829	0.0141
7.28	0.881	0.0196
8.30	0.923	0.0248
9.30	0.958	0.0319
10.30	0.980	0.0405
11.31	0.984	0.0564
12.33	1.015	0.0793

$Rn = 308600.$

α	C_l	C_d
-5.98	-0.334	0.0171
-4.96	-0.237	0.0136
-3.94	-0.157	0.0112
-2.93	-0.069	0.0100
-1.91	0.018	0.0085
-0.88	0.100	0.0085
0.14	0.218	0.0088
1.17	0.358	0.0090
2.19	0.453	0.0092
3.21	0.548	0.0097
4.23	0.645	0.0099
5.26	0.738	0.0105
6.27	0.813	0.0133
7.28	0.867	0.0180
8.29	0.916	0.0227
9.30	0.957	0.0285
10.30	0.978	0.0371
11.31	0.984	0.0492
12.32	1.047	0.0878
13.12	0.981	0.1619
14.23	0.928	0.2177

E374B-PT

Fig. 12.26

$Rn = 100800.$

α	C_l	C_d
-2.93	-0.094	0.0125
-1.39	0.124	0.0118
0.14	0.271	0.0148
1.67	0.405	0.0213
3.19	0.519	0.0241
4.72	0.651	0.0200
6.27	0.802	0.0193
7.77	0.888	0.0231
9.29	0.932	0.0339
10.81	0.969	0.0443
11.81	0.970	0.0641

$Rn = 153400.$

α	C_l	C_d
-3.95	-0.181	0.0155
-2.94	-0.093	0.0123
-1.92	-0.005	0.0112
-0.87	0.162	0.0118
0.14	0.265	0.0115
1.16	0.357	0.0119
2.19	0.456	0.0123
3.22	0.557	0.0148
4.23	0.649	0.0147
5.26	0.742	0.0144
6.26	0.831	0.0149
7.29	0.886	0.0202
8.29	0.919	0.0264
9.30	0.953	0.0338
10.29	0.975	0.0435

$Rn = 202400.$

α	C_l	C_d
-2.93	-0.090	0.0118
-1.43	0.038	0.0101
0.16	0.259	0.0106
1.67	0.394	0.0106
3.20	0.539	0.0110
4.72	0.688	0.0121
6.25	0.823	0.0143
7.79	0.896	0.0227
9.29	0.949	0.0324
10.81	0.975	0.0485
11.82	0.983	0.0607

$Rn = 305000.$

α	C_l	C_d
-2.94	-0.088	0.0112
-1.41	0.045	0.0091
0.12	0.220	0.0091
1.66	0.399	0.0094
3.20	0.541	0.0097
4.72	0.689	0.0100
6.26	0.813	0.0144
7.77	0.893	0.0211
9.30	0.952	0.0297
10.79	0.975	0.0440
11.81	0.995	0.0540

E374B-PT

Fig. 12.27

$Rn = 103600.$

α	C_l	C_d
-2.94	-0.058	0.0131
-1.37	0.139	0.0123
0.14	0.268	0.0123
1.66	0.394	0.0136
3.22	0.535	0.0142
4.72	0.675	0.0153
6.27	0.814	0.0164
7.77	0.902	0.0193
9.29	0.938	0.0300
10.80	0.974	0.0434

$Rn = 151300.$

α	C_l	C_d
-2.93	-0.069	0.0106
-1.41	0.094	0.0113
0.15	0.273	0.0105
1.67	0.408	0.0115
3.19	0.550	0.0121
4.75	0.691	0.0134
6.27	0.822	0.0154
7.78	0.899	0.0246
9.29	0.947	0.0363
10.80	0.972	0.0539
11.80	0.979	0.0668
12.79	0.970	0.1307

$Rn = 200700.$

α	C_l	C_d
-2.94	-0.069	0.0107
-1.41	0.062	0.0093
0.14	0.272	0.0101
1.68	0.411	0.0102
3.20	0.549	0.0112
4.74	0.690	0.0128
6.26	0.820	0.0153
7.78	0.907	0.0248
9.29	0.961	0.0331
10.81	0.981	0.0496
11.81	0.992	0.0609

$Rn = 304200.$

α	C_l	C_d
-2.93	-0.079	0.0102
-1.91	0.008	0.0087
-0.90	0.089	0.0089
0.14	0.222	0.0093
1.16	0.349	0.0098
2.18	0.438	0.0106
3.20	0.531	0.0109
4.22	0.629	0.0117
5.25	0.726	0.0127
6.26	0.813	0.0149
7.27	0.873	0.0195
8.29	0.920	0.0246
9.31	0.953	0.0317

E374B-PT

Fig. 12.28

$Rn = 100600.$

α	C_l	C_d
-3.97	-0.276	0.0196
-2.43	-0.088	0.0148
-0.89	0.146	0.0176
0.64	0.284	0.0206
2.18	0.409	0.0236
3.71	0.547	0.0233
5.22	0.681	0.0198
6.77	0.815	0.0180
8.29	0.897	0.0230
9.80	0.948	0.0354
11.31	0.975	0.0538

$Rn = 149400.$

α	C_l	C_d
-3.96	-0.193	0.0161
-2.42	-0.043	0.0125
-0.89	0.120	0.0120
0.65	0.291	0.0130
2.17	0.418	0.0140
3.71	0.557	0.0143
5.23	0.699	0.0142
6.76	0.822	0.0161
8.29	0.904	0.0233
9.80	0.964	0.0348
11.30	0.987	0.0539

$Rn = 196300.$

α	C_l	C_d
-3.96	-0.168	0.0134
-2.42	-0.048	0.0102
-0.89	0.079	0.0101
0.66	0.287	0.0112
2.17	0.421	0.0118
3.70	0.562	0.0122
5.23	0.707	0.0126
6.76	0.822	0.0160
8.30	0.914	0.0224
9.80	0.975	0.0327
11.30	0.996	0.0506
12.81	1.013	0.1085

$Rn = 300000.$

α	C_l	C_d
-3.96	-0.198	0.0122
-2.44	-0.065	0.0095
-0.91	0.064	0.0079
0.64	0.251	0.0089
2.16	0.417	0.0094
3.72	0.562	0.0097
5.25	0.699	0.0110
6.76	0.813	0.0150
8.29	0.914	0.0205
9.80	0.980	0.0305
11.31	1.009	0.0466
12.80	1.031	0.0997
14.29	0.970	0.1964

E374C-PT

Fig. 12.29

$Rn = 147300.$

α	C_l	C_d
-3.94	-0.149	0.0143
-2.41	-0.045	0.0124
-0.89	0.142	0.0133
0.65	0.270	0.0141
2.16	0.409	0.0153
3.69	0.555	0.0156
5.24	0.703	0.0152
6.78	0.844	0.0162
8.28	0.919	0.0260
9.81	0.973	0.0370
11.30	0.991	0.0564
12.79	0.982	0.1210

$Rn = 200700.$

α	C_l	C_d
-3.96	-0.188	0.0139
-2.42	-0.065	0.0106
-0.90	0.071	0.0102
0.64	0.252	0.0113
2.18	0.403	0.0121
3.70	0.557	0.0129
5.23	0.708	0.0125
6.78	0.847	0.0155
8.30	0.929	0.0245
9.80	0.983	0.0351
11.30	0.996	0.0520
12.75	1.003	0.1213

$Rn = 300300.$

α	C_l	C_d
-3.95	-0.212	0.0120
-2.43	-0.070	0.0097
-0.88	0.057	0.0086
0.63	0.241	0.0091
2.17	0.396	0.0095
3.71	0.558	0.0104
5.25	0.711	0.0108
6.77	0.842	0.0154
8.29	0.932	0.0224
9.81	0.986	0.0322
11.32	0.999	0.0483

E387A-PT

Fig. 12.31

$Rn = 59700.$

α	C_l	C_d
-3.95	-0.211	0.0382
-2.95	-0.125	0.0268
-1.91	0.006	0.0210
-0.89	0.133	0.0204
0.14	0.286	0.0223
1.17	0.390	0.0262
2.20	0.487	0.0288
3.23	0.589	0.0303
4.25	0.690	0.0325
5.27	0.782	0.0324
6.28	0.873	0.0306
7.31	0.973	0.0288
8.32	1.060	0.0258
9.35	1.133	0.0280
10.34	1.150	0.0368
11.34	1.142	0.0586

$Rn = 99800.$

α	C_l	C_d
-3.95	-0.169	0.0286
-2.93	-0.030	0.0204
-1.89	0.115	0.0150
-0.87	0.220	0.0135
0.16	0.322	0.0141
1.18	0.415	0.0158
2.20	0.510	0.0188
3.22	0.601	0.0199
4.24	0.692	0.0217
5.26	0.783	0.0210
6.28	0.881	0.0202
7.31	0.979	0.0194
8.33	1.064	0.0204
9.33	1.110	0.0252
10.34	1.122	0.0367
11.35	1.134	0.0479

$Rn = 149600.$

α	C_l	C_d
-1.89	0.133	0.0120
0.16	0.322	0.0113
2.20	0.523	0.0132
3.23	0.623	0.0143
4.24	0.720	0.0153
6.29	0.913	0.0158
7.31	1.005	0.0155
8.33	1.070	0.0195
9.35	1.109	0.0273

$Rn = 199800.$

α	C_l	C_d
-3.95	-0.097	0.0187
-2.93	-0.004	0.0141
-1.88	0.092	0.0120
-0.87	0.188	0.0102
0.15	0.291	0.0093
1.18	0.397	0.0101
2.20	0.503	0.0107
3.22	0.605	0.0115
4.24	0.705	0.0119
5.26	0.805	0.0125
6.29	0.905	0.0128
7.31	0.994	0.0145
8.32	1.058	0.0181
9.34	1.106	0.0246
10.34	1.131	0.0322
11.34	1.126	0.0475

$Rn = 303100.$

α	C_l	C_d
-3.91	-0.094	0.0166
-2.92	0.003	0.0125
-1.89	0.103	0.0106
-0.90	0.202	0.0093
0.14	0.302	0.0080
1.18	0.417	0.0085
2.21	0.521	0.0091
3.23	0.624	0.0093
4.25	0.722	0.0098
5.27	0.823	0.0105
6.29	0.914	0.0114
7.31	0.991	0.0138
8.32	1.053	0.0176
9.34	1.103	0.0233
10.33	1.129	0.0296
11.34	1.123	0.0449

E387A-PT

Fig. 12.32

$Rn = 99500.$

α	C_l	C_d
-3.95	-0.152	0.0274
-2.90	-0.005	0.0193
-1.87	0.127	0.0146
-0.88	0.221	0.0146
0.16	0.318	0.0154
1.18	0.413	0.0175
2.19	0.506	0.0183
3.21	0.599	0.0218
4.22	0.683	0.0221
5.25	0.780	0.0224
6.27	0.876	0.0217
7.29	0.973	0.0196
8.32	1.059	0.0203
9.32	1.106	0.0256
10.32	1.120	0.0345

$Rn = 149600.$

α	C_l	C_d
-2.90	0.025	0.0147
-1.88	0.114	0.0130
-0.89	0.195	0.0107
0.14	0.298	0.0114
1.16	0.398	0.0123
2.18	0.501	0.0133
3.21	0.601	0.0145
4.24	0.702	0.0153
5.26	0.800	0.0153
6.27	0.894	0.0159
7.30	0.988	0.0154
8.31	1.058	0.0186
9.34	1.104	0.0249

$Rn = 202000.$

α	C_l	C_d
-3.94	-0.096	0.0179
-2.94	-0.005	0.0138
-1.90	0.089	0.0118
-0.88	0.183	0.0092
0.16	0.285	0.0088
1.18	0.389	0.0102
2.20	0.493	0.0107
3.21	0.595	0.0116
4.24	0.695	0.0121
5.26	0.794	0.0130
6.27	0.893	0.0130
7.29	0.980	0.0140
8.30	1.044	0.0185
9.33	1.092	0.0245
10.33	1.120	0.0322
11.33	1.120	0.0434

$Rn = 302200.$

α	C_l	C_d
-3.94	-0.110	0.0164
-2.97	-0.018	0.0128
-1.91	0.082	0.0105
-0.89	0.183	0.0096
0.15	0.284	0.0082
1.18	0.396	0.0085
2.20	0.501	0.0088
3.22	0.605	0.0097
4.24	0.708	0.0100
5.27	0.810	0.0107
6.29	0.905	0.0111
7.30	0.985	0.0137
8.32	1.050	0.0175
9.33	1.102	0.0231
10.34	1.131	0.0309

E387A-PT

Fig. 12.33

$Rn = 101500.$

α	C_l	C_d
-2.90	0.015	0.0173
-1.39	0.147	0.0120
0.16	0.297	0.0118
1.68	0.445	0.0139
3.21	0.595	0.0151
4.75	0.742	0.0165
6.28	0.887	0.0176
7.30	0.977	0.0196
8.31	1.059	0.0204
9.33	1.096	0.0266
10.34	1.102	0.0378
11.32	1.103	0.0535

$Rn = 153000.$

α	C_l	C_d
-2.91	0.000	0.0152
-1.38	0.139	0.0113
0.15	0.288	0.0101
1.67	0.443	0.0112
3.23	0.599	0.0122
4.76	0.749	0.0135
6.27	0.893	0.0143
7.30	0.982	0.0168
8.32	1.059	0.0191
9.33	1.098	0.0265
10.34	1.115	0.0362
11.33	1.110	0.0484

$Rn = 200400.$

α	C_l	C_d
-3.92	-0.092	0.0177
-2.91	-0.001	0.0138
-1.89	0.095	0.0119
-0.88	0.188	0.0102
0.16	0.292	0.0092
1.18	0.397	0.0094
2.20	0.500	0.0104
3.22	0.602	0.0109
4.24	0.702	0.0120
5.27	0.800	0.0123
6.29	0.896	0.0136
7.31	0.984	0.0157
8.33	1.055	0.0196
9.33	1.100	0.0260
10.35	1.121	0.0349

$Rn = 311800.$

α	C_l	C_d
-3.95	-0.110	0.0173
-2.95	-0.018	0.0134
-1.94	0.081	0.0114
-0.91	0.182	0.0100
0.13	0.282	0.0083
1.17	0.394	0.0089
2.19	0.496	0.0093
3.22	0.599	0.0103
4.24	0.699	0.0111
5.26	0.797	0.0116
6.28	0.891	0.0131
7.31	0.979	0.0146
8.31	1.042	0.0187
9.32	1.093	0.0240
10.34	1.114	0.0324
11.32	1.109	0.0495
12.32	1.100	0.0678

E387A-PT

Fig. 12.34

$Rn = 101000.$

α	C_l	C_d
-3.94	-0.111	0.0268
-2.91	0.030	0.0174
-1.88	0.126	0.0162
-0.87	0.216	0.0128
0.16	0.328	0.0117
1.17	0.420	0.0119
2.19	0.519	0.0136
3.23	0.617	0.0134
4.23	0.710	0.0146
5.26	0.812	0.0172
6.29	0.909	0.0180

7.30	1.003	0.0207
8.32	1.082	0.0195
9.33	1.131	0.0263
10.34	1.160	0.0335
11.34	1.169	0.0442
12.35	1.158	0.0505
13.34	1.144	0.0525
14.34	1.175	0.0600

$Rn = 153700.$

α	C_l	C_d
-3.91	-0.084	0.0213
-2.92	-0.009	0.0159
-1.90	0.086	0.0149
-0.88	0.185	0.0123
0.15	0.285	0.0116
1.17	0.401	0.0112
2.18	0.500	0.0107
3.22	0.602	0.0114
4.23	0.706	0.0116
5.26	0.800	0.0133
6.28	0.893	0.0121
7.28	0.982	0.0147
8.31	1.048	0.0165
9.33	1.107	0.0222
10.34	1.134	0.0290
11.34	1.132	0.0402
12.34	1.123	0.0397
13.35	1.111	0.0358
14.33	1.116	0.4500

$Rn = 201300.$

α	C_l	C_d
-3.96	-0.079	0.0187
-2.93	0.016	0.0144
-1.89	0.111	0.0121
-0.86	0.207	0.0113
0.16	0.299	0.0091
1.17	0.405	0.0096
2.19	0.507	0.0106
3.21	0.604	0.0103
4.23	0.702	0.0114
5.25	0.795	0.0120
6.27	0.888	0.0133
7.30	0.969	0.0165
8.31	1.036	0.0195
9.32	1.093	0.0243
10.34	1.120	0.0303
11.34	1.117	0.0388
12.32	1.109	0.0426

$Rn = 301300.$

α	C_l	C_d
-3.98	-0.089	0.0160
-2.97	0.001	0.0127
-1.91	0.100	0.0110
-0.90	0.197	0.0103
0.13	0.296	0.0080
1.16	0.399	0.0083
2.19	0.502	0.0087
3.21	0.601	0.0090
4.24	0.699	0.0101
5.26	0.793	0.0103
6.27	0.881	0.0112
7.30	0.959	0.0143
8.31	1.028	0.0175
9.33	1.086	0.0225
10.33	1.116	0.0285
11.33	1.115	0.0416
12.33	1.105	0.0487
13.33	1.088	0.0682
14.32	1.069	0.0798

E387B-PT

Fig. 12.36

$Rn = 97000.$

α	C_l	C_d
-3.91	-0.029	0.0177
-2.90	0.076	0.0163
-1.86	0.180	0.0153
-0.85	0.282	0.0148
0.18	0.379	0.0168
1.20	0.469	0.0178
2.22	0.567	0.0181
3.24	0.667	0.0182
4.25	0.766	0.0189
5.28	0.859	0.0197
6.30	0.952	0.0207
7.32	1.041	0.0199
8.34	1.101	0.0256
9.35	1.134	0.0307

$Rn = 202600.$

α	C_l	C_d
-3.92	-0.057	0.0147
-2.91	0.040	0.0131
-1.88	0.142	0.0126
-0.85	0.246	0.0122
0.17	0.349	0.0105
1.19	0.457	0.0107
2.21	0.560	0.0106
3.24	0.662	0.0110
4.25	0.759	0.0121
5.26	0.852	0.0133
6.29	0.939	0.0143
7.30	1.006	0.0175
8.32	1.055	0.0246
9.33	1.086	0.0316
10.32	1.098	0.0425
11.32	1.100	0.0550

Flat Plate-PT

Fig. 12.37

$Rn = 100100.$

α	C_l	C_d
-3.99	-0.383	0.0335
-2.96	-0.274	0.0238
-1.95	-0.186	0.0181
-0.91	-0.077	0.0152
0.10	0.017	0.0143
1.13	0.127	0.0170
2.14	0.216	0.0180
3.16	0.324	0.0263
4.19	0.417	0.0365
5.20	0.517	0.0544
6.24	0.614	0.0723
7.24	0.674	0.0921

$Rn = 199700.$

α	C_l	C_d
-3.98	-0.379	0.0290
-2.97	-0.280	0.0204
-1.95	-0.184	0.0150
-0.92	-0.082	0.0144
0.10	0.014	0.0143
1.12	0.109	0.0135
2.15	0.211	0.0171
3.16	0.307	0.0243
4.18	0.404	0.0348
5.20	0.506	0.0494
6.23	0.609	0.0705

$Rn = 300400.$

α	C_l	C_d
-3.99	-0.374	0.0301
-2.97	-0.275	0.0207
-1.94	-0.178	0.0139
-0.93	-0.078	0.0138
0.10	0.015	0.0131
1.12	0.110	0.0143
2.15	0.211	0.0158
3.16	0.310	0.0232
4.19	0.407	0.0342
5.21	0.508	0.0491
6.22	0.606	0.0691
7.25	0.685	0.0959

FX60-100

Fig. 12.39

$Rn = 59600.$

α	C_l	C_d
-3.94	-0.148	0.0268
-2.42	-0.052	0.0209
-0.90	0.065	0.0185
0.65	0.225	0.0194
2.18	0.461	0.0232
3.73	0.635	0.0250
5.24	0.769	0.0228
6.78	0.889	0.0227
8.31	1.007	0.0216
9.83	1.100	0.0335
11.34	1.151	0.0445

$Rn = 99400.$

α	C_l	C_d
-4.98	-0.286	0.0314
-3.94	-0.200	0.0231
-2.91	-0.104	0.0188
-1.91	0.008	0.0162
-0.89	0.138	0.0166
0.16	0.282	0.0166
1.18	0.415	0.0161
2.21	0.522	0.0160
3.23	0.622	0.0163
4.24	0.713	0.0164
5.27	0.804	0.0166
6.28	0.897	0.0170
7.31	0.983	0.0187
8.32	1.062	0.0223
9.34	1.135	0.0246
10.35	1.192	0.0309
11.36	1.219	0.0402

$Rn = 152300.$

α	C_l	C_d
-3.95	-0.175	0.0203
-2.93	-0.050	0.0183
-1.90	0.100	0.0153
-0.87	0.224	0.0135
0.16	0.337	0.0137
1.17	0.430	0.0128
2.19	0.520	0.0119
3.23	0.621	0.0118
4.25	0.722	0.0120
5.26	0.814	0.0134
6.29	0.902	0.0148
7.31	0.989	0.0171
8.32	1.067	0.0201
9.33	1.134	0.0248
10.34	1.177	0.0304
11.35	1.189	0.0420
12.35	1.169	0.0513

$Rn = 203400.$

α	C_l	C_d
-5.00	-0.295	0.0287
-3.95	-0.186	0.0193
-2.92	-0.054	0.0149
-1.90	0.087	0.0114
-0.89	0.206	0.0105
0.16	0.310	0.0108
1.17	0.412	0.0104
2.21	0.512	0.0104
3.21	0.606	0.0101
4.23	0.701	0.0105
5.26	0.796	0.0116
6.28	0.886	0.0136
7.30	0.973	0.0158
8.31	1.052	0.0185
9.33	1.120	0.0233
10.34	1.168	0.0299
11.36	1.190	0.0393

$Rn = 298800.$

α	C_l	C_d
-2.92	0.012	0.0123
-1.88	0.128	0.0104
-0.86	0.236	0.0093
0.17	0.340	0.0093
1.18	0.441	0.0093
2.21	0.541	0.0095
3.21	0.635	0.0097
4.22	0.721	0.0098
5.26	0.812	0.0112
6.27	0.900	0.0129
7.28	0.982	0.0148

FX63-137A-PT

Fig. 12.40

$Rn = 200100.$

α	C_l	C_d
-6.92	-0.021	0.0360
-5.89	0.085	0.0201
-4.88	0.186	0.0172
-3.85	0.292	0.0149
-2.83	0.403	0.0142
-1.80	0.515	0.0142
-0.79	0.610	0.0149
0.24	0.724	0.0156
1.27	0.829	0.0159
2.30	0.931	0.0167
3.32	1.031	0.0163

4.33	1.122	0.0163
5.36	1.210	0.0166
6.38	1.299	0.0175
7.39	1.385	0.0185
8.41	1.460	0.0198
9.42	1.525	0.0219
10.43	1.573	0.0254
11.44	1.599	0.0298
12.44	1.607	0.0368

$Rn = 299500.$

α	C_l	C_d
-6.91	-0.028	0.0248
-5.89	0.088	0.0165
-4.88	0.191	0.0144
-3.85	0.301	0.0128
-2.83	0.412	0.0123
-1.79	0.527	0.0116
-0.77	0.635	0.0121
0.23	0.736	0.0122
1.24	0.838	0.0123
2.23	0.935	0.0125
3.20	1.024	0.0130
4.28	1.125	0.0136
5.34	1.220	0.0144
6.37	1.300	0.0155
7.39	1.379	0.0165
8.40	1.452	0.0183
9.41	1.512	0.0205
10.43	1.552	0.0240
11.44	1.571	0.0295

FX63-137B-PT

Fig. 12.41

$Rn = 100800.$

α	C_l	C_d
-3.87	0.210	0.0308
-2.85	0.345	0.0279
-1.82	0.473	0.0276
-0.79	0.581	0.0287
0.22	0.684	0.0265
1.26	0.778	0.0260
2.27	0.870	0.0271
3.30	0.974	0.0263
4.32	1.074	0.0249
5.34	1.174	0.0234
6.36	1.277	0.0262
7.39	1.373	0.0259
8.40	1.459	0.0274
9.42	1.532	0.0291
10.42	1.560	0.0353
11.44	1.597	0.0522

$Rn = 155600.$

α	C_l	C_d
-6.93	-0.092	0.0463
-5.90	0.056	0.0233
-4.89	0.164	0.0196
-3.86	0.273	0.0175
-2.83	0.390	0.0162
-1.81	0.499	0.0157
-0.79	0.604	0.0166
0.25	0.707	0.0172
1.26	0.811	0.0182
2.29	0.912	0.0184
3.30	1.008	0.0186
4.32	1.100	0.0183
5.35	1.196	0.0193
6.36	1.290	0.0202
7.38	1.379	0.0219
8.40	1.462	0.0235
9.42	1.532	0.0249
10.42	1.587	0.0275
11.43	1.615	0.0326

$Rn = 200700.$

α	C_l	C_d
-5.90	0.083	0.0186
-4.88	0.186	0.0160
-3.86	0.291	0.0148
-2.85	0.399	0.0143
-1.79	0.520	0.0140
-0.79	0.626	0.0147
0.25	0.733	0.0150
1.28	0.842	0.0158
2.30	0.946	0.0158
3.30	1.046	0.0161
4.33	1.140	0.0164
5.35	1.229	0.0164
6.36	1.320	0.0183
7.38	1.407	0.0199
8.42	1.486	0.0215
9.43	1.551	0.0247
10.44	1.597	0.0272
11.44	1.613	0.0364
12.44	1.616	0.0504
13.44	1.623	0.0519

$Rn = 308600.$

α	C_l	C_d
-6.94	-0.049	0.0329
-5.92	0.080	0.0160
-4.89	0.190	0.0137
-3.84	0.304	0.0124
-2.83	0.420	0.0118
-1.79	0.538	0.0119
-0.79	0.647	0.0120
0.24	0.754	0.0122
1.28	0.862	0.0129
2.28	0.964	0.0130
3.31	1.062	0.0134
4.33	1.156	0.0139
5.36	1.247	0.0146
6.37	1.333	0.0148
7.39	1.411	0.0162
8.42	1.491	0.0185
9.42	1.539	0.0210
10.43	1.575	0.0260
11.43	1.589	0.0313
12.43	1.592	0.0443

HQ2/9A-PT

Fig. 12.42

$Rn = 62000.$

α	C_l	C_d
-2.95	-0.189	0.0155
-1.94	-0.119	0.0143
-0.92	-0.042	0.0141
0.10	0.080	0.0154
1.13	0.207	0.0175
2.17	0.379	0.0212
3.20	0.530	0.0190
4.22	0.609	0.0188
5.24	0.675	0.0220
6.26	0.769	0.0281
7.28	0.833	0.0238
8.28	0.887	0.0320
9.30	0.936	0.0476

$Rn = 98300.$

α	C_l	C_d
-3.96	-0.219	0.0204
-2.94	-0.139	0.0172
-1.92	-0.051	0.0122
-0.91	0.037	0.0116
0.14	0.165	0.0140
1.16	0.321	0.0152
2.19	0.464	0.0144
3.20	0.556	0.0144
4.23	0.649	0.0149
5.25	0.735	0.0153
6.26	0.815	0.0183
7.28	0.878	0.0225
8.29	0.934	0.0282
9.30	0.982	0.0359
10.31	1.008	0.0500
11.31	0.979	0.1163

$Rn = 149000.$

α	C_l	C_d
-3.96	-0.213	0.0170
-2.94	-0.123	0.0148
-1.92	-0.017	0.0128
-0.88	0.121	0.0113
0.14	0.251	0.0106
1.18	0.366	0.0113
2.20	0.459	0.0107
3.21	0.558	0.0110
4.23	0.652	0.0117
5.26	0.738	0.0131
6.27	0.815	0.0162
7.28	0.890	0.0208
8.30	0.955	0.0241
9.31	1.004	0.0323
10.32	1.037	0.0395

$Rn = 208700.$

α	C_l	C_d
-3.96	-0.222	0.0155
-2.93	-0.106	0.0134
-1.90	0.031	0.0108
-0.88	0.158	0.0091
0.15	0.250	0.0088
1.17	0.347	0.0083
2.19	0.452	0.0086
3.21	0.553	0.0092
4.23	0.646	0.0104
5.25	0.737	0.0124
6.27	0.819	0.0150
7.30	0.898	0.0184
8.30	0.965	0.0221
9.32	1.015	0.0281
10.32	1.046	0.0371
11.31	1.029	0.0967

$Rn = 303400.$

α	C_l	C_d
-3.96	-0.177	0.0137
-2.94	-0.049	0.0109
-1.91	0.061	0.0084
-0.88	0.154	0.0072
0.14	0.250	0.0075
1.18	0.348	0.0072
2.19	0.457	0.0075
3.21	0.564	0.0084
4.24	0.657	0.0101
5.25	0.742	0.0125
6.27	0.826	0.0145
7.28	0.907	0.0171
8.31	0.981	0.0203
9.31	1.038	0.0249
10.33	1.076	0.0324
11.32	1.079	0.0437

HQ2/9A-PT

Fig. 12.43

$Rn = 98200.$

α	C_l	C_d
-3.95	-0.236	0.0205
-2.95	-0.155	0.0166
-1.93	-0.045	0.0131
-0.88	0.084	0.0144
0.14	0.226	0.0136
1.15	0.338	0.0133
2.19	0.439	0.0134
3.19	0.542	0.0139
4.23	0.647	0.0156
5.25	0.742	0.0154
6.26	0.826	0.0192
7.27	0.886	0.0243
8.30	0.945	0.0307
9.30	0.992	0.0386
10.31	1.022	0.0532
11.30	1.001	0.1139

$Rn = 151600.$

α	C_l	C_d
-3.97	-0.209	0.0163
-2.94	-0.089	0.0139
-1.93	0.029	0.0107
-0.90	0.129	0.0101
0.13	0.227	0.0092
1.15	0.339	0.0098
2.18	0.443	0.0100
3.21	0.544	0.0106
4.22	0.642	0.0125
5.24	0.734	0.0143
6.26	0.821	0.0168
7.29	0.893	0.0214
8.31	0.959	0.0253
9.31	1.010	0.0332

$Rn = 202100.$

α	C_l	C_d
-3.96	-0.171	0.0150
-2.94	-0.056	0.0125
-1.93	0.046	0.0094
-0.91	0.135	0.0088
0.10	0.227	0.0089
1.15	0.331	0.0088
2.17	0.436	0.0095
3.19	0.538	0.0109
4.20	0.637	0.0122

5.24	0.734	0.0136
6.27	0.824	0.0164
7.29	0.902	0.0198
8.31	0.970	0.0231
9.31	1.020	0.0293
10.32	1.051	0.0378
11.30	1.054	0.0783

$Rn = 311700.$

α	C_l	C_d
-3.96	-0.163	0.0128
-2.97	-0.071	0.0116
-2.06	0.014	0.0111
-0.95	0.119	0.0098
0.10	0.221	0.0097
1.15	0.323	0.0093
2.15	0.432	0.0096
3.20	0.545	0.0106
4.20	0.644	0.0116
5.25	0.744	0.0129
6.25	0.825	0.0154
7.28	0.906	0.0176
8.30	0.981	0.0208
9.31	1.038	0.0256
10.32	1.073	0.0329
11.32	1.073	0.0432
12.43	1.017	0.1496

HQ2/9A-PT

Fig. 12.44

$Rn = 101600.$

α	C_l	C_d
-3.46	-0.185	0.0177
-1.92	-0.006	0.0116
-0.38	0.148	0.0136
1.15	0.331	0.0134
2.70	0.492	0.0147
5.23	0.722	0.0164
6.78	0.842	0.0222
8.30	0.933	0.0299
9.30	0.978	0.0434
10.30	1.003	0.0541

$Rn = 153300.$

α	C_l	C_d
-3.45	-0.129	0.0145
-1.91	0.040	0.0099
-0.37	0.179	0.0088
1.16	0.344	0.0093
2.69	0.499	0.0104
5.25	0.739	0.0138
6.77	0.858	0.0184
8.29	0.953	0.0260
9.31	1.004	0.0317
10.32	1.035	0.0425
11.31	1.025	0.1019

$Rn = 205300.$

α	C_l	C_d
-3.46	-0.108	0.0132
-1.90	0.043	0.0092
-0.39	0.182	0.0090
1.16	0.334	0.0085
2.68	0.496	0.0098
5.24	0.733	0.0132
6.77	0.858	0.0174
8.29	0.966	0.0228
9.32	1.018	0.0287
10.31	1.049	0.0382
11.31	1.042	0.0903

$Rn = 305200.$

α	C_l	C_d
-3.46	-0.116	0.0127
-1.97	0.023	0.0105
-0.43	0.180	0.0084
1.15	0.332	0.0081
2.69	0.500	0.0085
5.24	0.740	0.0130
6.77	0.866	0.0162
8.29	0.975	0.0201
9.31	1.033	0.0252
10.32	1.069	0.0324
11.31	1.070	0.0429

HQ2/9A-PT

Fig. 12.45

$Rn = 151600.$

α	C_l	C_d
-3.96	-0.224	0.0174
-2.98	-0.135	0.0150
-1.91	-0.022	0.0121
-0.90	0.122	0.0102
0.13	0.254	0.0112
1.15	0.362	0.0108
2.18	0.461	0.0107
3.17	0.558	0.0115
4.22	0.658	0.0112
5.24	0.747	0.0134
6.24	0.823	0.0173
7.29	0.900	0.0200
8.29	0.965	0.0241
9.30	1.013	0.0311
10.31	1.047	0.0404
11.31	1.037	0.0917

$Rn = 200000.$

α	C_l	C_d
-3.98	-0.215	0.0157
-2.97	-0.106	0.0138
-1.96	0.027	0.0112
-0.91	0.162	0.0098
0.10	0.262	0.0096
1.15	0.361	0.0095
2.15	0.460	0.0091
3.19	0.561	0.0093
4.19	0.654	0.0105
5.23	0.744	0.0130
6.26	0.829	0.0157
7.27	0.908	0.0191
8.28	0.979	0.0221
9.30	1.031	0.0283
10.32	1.064	0.0372

$Rn = 308100.$

α	C_l	C_d
-4.07	-0.185	0.0135
-3.01	-0.056	0.0116
-2.01	0.054	0.0093
-0.95	0.158	0.0074
0.03	0.250	0.0076
1.05	0.357	0.0078
2.13	0.471	0.0081
3.17	0.576	0.0091
4.21	0.670	0.0107
5.24	0.756	0.0129
6.25	0.837	0.0147
7.27	0.917	0.0168
8.30	0.991	0.0201
9.30	1.047	0.0242
10.33	1.084	0.0320

HQ2/9B-PT

Fig. 12.47

$Rn = 60800.$

α	C_l	C_d
-2.94	-0.146	0.0197
-1.43	-0.026	0.0156
0.10	0.116	0.0155
1.65	0.329	0.0179
3.19	0.539	0.0195
4.74	0.663	0.0188
6.26	0.781	0.0228
7.77	0.863	0.0282
9.30	0.928	0.0422
10.80	0.962	0.0751

$Rn = 100100.$

α	C_l	C_d
-2.94	-0.143	0.0189
-1.42	-0.014	0.0134
0.13	0.149	0.0150
1.66	0.382	0.0161
3.20	0.559	0.0149
4.75	0.690	0.0148
6.26	0.825	0.0160
7.77	0.904	0.0249
9.31	0.980	0.0386
10.79	0.999	0.0707
12.30	0.935	0.1433
13.77	0.849	0.1783

$Rn = 152000.$

α	C_l	C_d
-2.94	-0.149	0.0151
-1.39	0.025	0.0124
0.12	0.231	0.0103
1.67	0.393	0.0107
3.20	0.538	0.0116
4.73	0.680	0.0116
6.26	0.802	0.0153
7.78	0.902	0.0214
9.29	0.973	0.0314
10.80	1.020	0.0508
12.30	0.979	0.1425
13.76	0.888	0.2090

$Rn = 202400.$

α	C_l	C_d
-3.97	-0.218	0.0158
-2.46	-0.051	0.0128
-0.90	0.151	0.0102
0.63	0.295	0.0086
2.18	0.452	0.0092
3.71	0.603	0.0097
5.25	0.739	0.0119
6.75	0.855	0.0166
8.29	0.950	0.0242
9.79	1.014	0.0350

$Rn = 303500.$

α	C_l	C_d
-4.01	-0.201	0.0132
-2.49	-0.012	0.0102
-0.95	0.142	0.0077
0.62	0.287	0.0074
2.15	0.445	0.0075
3.70	0.604	0.0086
5.22	0.739	0.0117
6.76	0.864	0.0155
8.30	0.968	0.0218
9.81	1.037	0.0307
11.31	1.053	0.0736
12.73	1.011	0.1481

HQ2/9B-PT

Fig. 12.48

$Rn = 58900.$

α	C_l	C_d
-2.97	-0.140	0.0201
-1.43	-0.018	0.0136
0.13	0.172	0.0145
1.66	0.374	0.0196
3.22	0.564	0.0214
4.74	0.698	0.0239
6.27	0.806	0.0240
7.77	0.881	0.0270
9.30	0.929	0.0546
10.81	0.959	0.0751

$Rn = 100800.$

α	C_l	C_d
-2.94	-0.132	0.0163
-1.42	0.049	0.0125
0.13	0.217	0.0133
1.66	0.391	0.0124
3.21	0.549	0.0148
4.73	0.683	0.0151
6.24	0.801	0.0176
7.78	0.894	0.0249
9.28	0.960	0.0370
10.81	1.008	0.0581
12.30	0.952	0.1444
13.78	0.840	0.1970

$Rn = 149300.$

α	C_l	C_d
-2.93	-0.070	0.0136
-1.41	0.080	0.0102
0.11	0.226	0.0091
1.68	0.397	0.0109
3.19	0.550	0.0116
4.74	0.694	0.0123
6.26	0.814	0.0176
7.79	0.913	0.0236
9.30	0.980	0.0362
10.82	1.027	0.0677
12.31	0.974	0.1588

$Rn = 204700.$

α	C_l	C_d
-2.96	-0.080	0.0124
-1.41	0.068	0.0088
0.13	0.210	0.0078

1.66	0.376	0.0082
3.18	0.534	0.0089
4.73	0.683	0.0108
6.25	0.802	0.0153
7.77	0.907	0.0206
9.31	0.983	0.0286
10.81	1.033	0.0471
12.30	1.004	0.1300
13.81	0.936	0.1999

$Rn = 299200.$

α	C_l	C_d
-2.92	-0.072	0.0114
-1.43	0.078	0.0088
0.12	0.227	0.0081
1.65	0.385	0.0078
3.19	0.548	0.0084
4.74	0.692	0.0111
6.27	0.820	0.0152
7.79	0.930	0.0202
9.31	1.009	0.0288
10.81	1.052	0.0531
12.23	1.010	0.1387
13.78	0.946	0.1930

HQ2/9B-PT

Fig. 12.49

$Rn = 59000.$

α	C_l	C_d
-2.96	-0.173	0.0185
-1.42	0.007	0.0149
0.13	0.169	0.0163
1.66	0.354	0.0169
3.20	0.525	0.0201
4.72	0.645	0.0175
6.24	0.764	0.0227
7.78	0.854	0.0265
9.28	0.916	0.0396
10.80	0.947	0.0731

$Rn = 100200.$

α	C_l	C_d
-2.95	-0.130	0.0158
-1.42	0.032	0.0134
0.11	0.193	0.0119
1.66	0.348	0.0132
3.20	0.492	0.0139
4.72	0.632	0.0151
6.25	0.767	0.0181
7.77	0.851	0.0267
9.28	0.911	0.0407
10.79	0.952	0.0750
12.29	0.870	0.1908
13.76	0.769	0.2198

$Rn = 200100.$

α	C_l	C_d
-2.94	-0.071	0.0128
-1.40	0.072	0.0102
0.12	0.215	0.0094
1.66	0.378	0.0096
3.19	0.540	0.0107
4.74	0.691	0.0115
6.26	0.814	0.0159
7.78	0.915	0.0218
9.31	0.989	0.0323
10.82	1.036	0.0564

$Rn = 302500.$

α	C_l	C_d
-2.96	-0.080	0.0121
-1.44	0.072	0.0096
0.13	0.226	0.0086
1.67	0.385	0.0081
3.19	0.549	0.0090
4.73	0.700	0.0108
6.26	0.822	0.0149
7.78	0.933	0.0196
9.31	1.010	0.0276
10.82	1.051	0.0519
12.19	1.011	0.1333

HQ2/9B-PT

Fig. 12.50

$Rn = 202400.$

α	C_l	C_d
-3.97	-0.218	0.0158
-2.46	-0.051	0.0128
-0.90	0.151	0.0102
0.63	0.295	0.0086
2.18	0.452	0.0092
3.71	0.603	0.0097
5.25	0.739	0.0119
6.75	0.855	0.0166
8.29	0.950	0.0242
9.79	1.014	0.0350

$Rn = 199700.$

α	C_l	C_d
-2.93	-0.078	0.0135
-0.92	0.107	0.0096
1.16	0.315	0.0093
3.20	0.526	0.0103
5.22	0.723	0.0122
7.28	0.880	0.0189
9.29	0.983	0.0312

$Rn = 200100.$

α	C_l	C_d
-2.94	-0.071	0.0128
-1.40	0.072	0.0102
0.12	0.215	0.0094
1.66	0.378	0.0096
3.19	0.540	0.0107
4.74	0.691	0.0115
6.26	0.814	0.0159
7.78	0.915	0.0218
9.31	0.989	0.0323
10.82	1.036	0.0564

$Rn = 204700.$

α	C_l	C_d
-2.96	-0.080	0.0124
-1.41	0.068	0.0088
0.13	0.210	0.0078
1.66	0.376	0.0082
3.18	0.534	0.0089
4.73	0.683	0.0108
6.25	0.802	0.0153
7.77	0.907	0.0206
9.31	0.983	0.0286
10.81	1.033	0.0471
12.30	1.004	0.1300
13.81	0.936	0.1999

J5012-PT

Fig. 12.52

$Rn = 56500.$

α	C_l	C_d
-6.04	-0.596	0.0242
-5.03	-0.510	0.0206
-4.01	-0.447	0.0218
-2.99	-0.380	0.0222
-1.97	-0.201	0.0218
-0.92	-0.002	0.0224
0.09	0.008	0.0175
1.11	0.112	0.0204
2.16	0.340	0.0203
3.20	0.449	0.0223
4.21	0.529	0.0194
5.24	0.631	0.0215
6.25	0.689	0.0251
7.26	0.742	0.0285
8.27	0.802	0.0406
9.27	0.842	0.0494

$Rn = 97800.$

α	C_l	C_d
-6.01	-0.550	0.0187
-5.00	-0.485	0.0164
-4.00	-0.407	0.0159
-2.97	-0.342	0.0160
-1.96	-0.264	0.0156
-0.93	-0.124	0.0185
0.09	0.039	0.0165
1.14	0.230	0.0160
2.17	0.352	0.0151
3.19	0.423	0.0147
4.19	0.494	0.0152
5.22	0.568	0.0170
6.22	0.629	0.0225
7.24	0.693	0.0275
8.26	0.760	0.0344
9.26	0.811	0.0455

$Rn = 151300.$

α	C_l	C_d
-6.05	-0.548	0.0163
-5.02	-0.483	0.0140
-3.99	-0.411	0.0126
-2.98	-0.329	0.0120
-1.95	-0.210	0.0122
-0.93	-0.079	0.0126
0.10	0.031	0.0131
1.12	0.152	0.0125
2.15	0.292	0.0123
3.17	0.391	0.0120
4.18	0.458	0.0131
5.20	0.518	0.0147
6.22	0.587	0.0191
7.24	0.654	0.0225
8.25	0.717	0.0282
9.27	0.776	0.0327
10.27	0.793	0.0579

$Rn = 201900.$

α	C_l	C_d
-6.04	-0.551	0.0161
-5.01	-0.480	0.0134
-3.98	-0.401	0.0116
-2.97	-0.289	0.0113
-1.97	-0.160	0.0113
-0.93	-0.048	0.0107
0.09	0.043	0.0101
1.11	0.122	0.0096
2.13	0.235	0.0100
3.16	0.365	0.0105
4.19	0.464	0.0119
5.21	0.528	0.0141
6.22	0.599	0.0174
7.23	0.670	0.0212
8.26	0.738	0.0250
9.26	0.791	0.0326
10.26	0.824	0.0597

$Rn = 303100.$

α	C_l	C_d
-6.04	-0.545	0.0140
-5.01	-0.455	0.0129
-4.02	-0.345	0.0115
-2.97	-0.224	0.0094
-1.93	-0.115	0.0086
-0.92	-0.027	0.0080
0.09	0.054	0.0082
1.12	0.144	0.0082
2.13	0.240	0.0084
3.16	0.339	0.0091
4.18	0.442	0.0107
5.20	0.530	0.0131
6.22	0.605	0.0158
7.23	0.678	0.0191
8.25	0.745	0.0231
9.26	0.800	0.0287
10.28	0.843	0.0537

MB253515-PT

Fig. 12.53

$Rn = 60100.$

α	C_l	C_d
-7.02	-0.531	0.0437
-6.02	-0.451	0.0374
-4.98	-0.354	0.0308
-3.96	-0.260	0.0263
-2.94	-0.190	0.0324
-1.91	0.002	0.0321
-0.90	0.076	0.0327
0.12	0.112	0.0366
1.14	0.194	0.0398
2.15	0.231	0.0446
3.16	0.285	0.0522
4.18	0.354	0.0637

$Rn = 99500.$

α	C_l	C_d
-6.48	-0.368	0.0283
-5.66	-0.286	0.0248
-4.86	-0.222	0.0226
-4.04	-0.165	0.0215
-3.23	-0.092	0.0222
-2.42	-0.038	0.0234
-1.58	0.072	0.0262
-0.76	0.226	0.0298
0.06	0.331	0.0280

0.87	0.369	0.0297
1.68	0.391	0.0313
2.49	0.446	0.0329
3.30	0.500	0.0356
4.13	0.595	0.0333
4.94	0.694	0.0321
5.77	0.788	0.0280
6.58	0.860	0.0254
7.38	0.926	0.0228
8.21	0.991	0.0224
9.02	1.051	0.0218
9.82	1.040	0.0278
10.61	1.002	0.0459
11.41	0.978	0.0433

$Rn = 126700.$

α	C_l	C_d
-2.91	-0.029	0.0193
-1.90	0.050	0.0199
-0.87	0.181	0.0218
0.17	0.353	0.0228
1.19	0.476	0.0211
2.20	0.549	0.0208
3.23	0.621	0.0216
4.23	0.704	0.0216
5.26	0.789	0.0228
6.27	0.870	0.0201
7.29	0.952	0.0218
8.32	1.033	0.0202
9.31	1.028	0.0273
10.32	0.998	0.0325

$Rn = 149700.$

α	C_l	C_d
-5.95	-0.237	0.0206
-4.97	-0.175	0.0177
-3.94	-0.127	0.0156
-2.92	-0.047	0.0157
-1.91	0.033	0.0167
-0.88	0.120	0.0173
0.16	0.268	0.0180
1.18	0.434	0.0179
2.21	0.546	0.0180
3.23	0.624	0.0182
4.24	0.705	0.0183
5.26	0.789	0.0180
6.28	0.870	0.0180
7.29	0.949	0.0185
8.32	1.034	0.0193
9.32	1.032	0.0258
10.31	0.998	0.0423

$Rn = 177600.$

α	C_l	C_d
-2.91	-0.027	0.0136
-1.90	0.053	0.0141
-0.88	0.141	0.0150
0.14	0.266	0.0160
1.19	0.427	0.0151
2.20	0.563	0.0151
3.23	0.650	0.0153
4.24	0.730	0.0150
5.26	0.811	0.0158
6.29	0.890	0.0159
7.30	0.970	0.0165
8.30	1.011	0.0201
9.30	0.994	0.0332
10.30	0.971	0.0448
11.30	0.961	0.0522

$Rn = 200100.$

α	C_l	C_d
-6.99	-0.309	0.0211
-5.98	-0.240	0.0180
-4.97	-0.170	0.0161
-3.95	-0.111	0.0133
-2.91	-0.034	0.0127
-1.90	0.053	0.0129
-0.88	0.139	0.0134
0.14	0.238	0.0138
1.17	0.370	0.0143
2.21	0.543	0.0144
3.24	0.642	0.0148
4.25	0.720	0.0147
5.26	0.800	0.0149
6.28	0.880	0.0151
7.30	0.961	0.0162
8.32	1.013	0.0177
9.31	0.998	0.0252
10.30	0.964	0.0378
11.30	0.952	0.0443

$Rn = 250100.$

α	C_l	C_d
-2.93	-0.034	0.0110
-1.89	0.059	0.0109
-0.87	0.152	0.0113
0.13	0.247	0.0114
1.17	0.367	0.0116
2.20	0.522	0.0130
3.22	0.658	0.0121
4.25	0.748	0.0126
5.28	0.829	0.0127
6.28	0.907	0.0137
7.30	0.976	0.0145
8.29	1.001	0.0187
9.29	0.982	0.0324
10.29	0.968	0.0391

$Rn = 301600.$

α	C_l	C_d
-7.09	-0.348	0.0191
-6.05	-0.272	0.0167
-5.03	-0.193	0.0144
-3.96	-0.118	0.0118
-2.97	-0.044	0.0103
-1.92	0.047	0.0105
-0.88	0.146	0.0101
0.13	0.241	0.0100
1.17	0.341	0.0103
2.18	0.465	0.0108
3.22	0.610	0.0112
4.24	0.722	0.0111
5.26	0.801	0.0116
6.28	0.878	0.0125
7.30	0.947	0.0138
8.30	0.976	0.0176
9.30	0.958	0.0270
10.30	0.943	0.0371

MB253515-PT

Fig. 12.54

$Rn = 59600.$

α	C_l	C_d
-2.92	-0.053	0.0238
-1.88	0.166	0.0254
-0.83	0.348	0.0250
0.17	0.396	0.0251
1.20	0.444	0.0259
2.21	0.517	0.0267
3.23	0.587	0.0273
4.24	0.671	0.0270
5.27	0.761	0.0272
6.28	0.849	0.0291
7.29	0.920	0.0311
8.24	0.613	0.0965

$Rn = 101300.$

α	C_l	C_d
-4.95	-0.200	0.0189
-3.93	-0.134	0.0146
-2.92	-0.070	0.0161
-1.90	0.008	0.0174
-0.87	0.181	0.0178
0.17	0.354	0.0168
1.19	0.463	0.0168
2.21	0.541	0.0169
3.24	0.615	0.0172
4.24	0.697	0.0179
5.26	0.778	0.0180
6.28	0.863	0.0197
7.30	0.939	0.0210
8.32	1.015	0.0235
9.33	1.090	0.0254
10.33	1.051	0.0288
11.31	1.004	0.0390
12.31	0.991	0.0464

$Rn = 203600.$

α	C_l	C_d
-2.91	-0.060	0.0115
-1.90	0.029	0.0117
-0.89	0.115	0.0121
0.14	0.213	0.0119
1.18	0.346	0.0128
2.21	0.517	0.0135
3.23	0.611	0.0141
4.24	0.675	0.0147
5.25	0.749	0.0154
6.28	0.830	0.0168
7.30	0.914	0.0181
8.31	0.988	0.0196
9.32	1.010	0.0266
10.31	0.974	0.0414
11.31	0.959	0.0506
12.31	0.955	0.0586
13.31	0.955	0.0714
14.31	0.952	0.0881

$Rn = 306300.$

α	C_l	C_d
-2.93	-0.066	0.0108
-1.90	0.018	0.0108
-0.89	0.109	0.0114
0.14	0.202	0.0118
1.15	0.298	0.0122
2.19	0.437	0.0129
3.22	0.582	0.0135
4.24	0.668	0.0135
5.26	0.736	0.0143
6.27	0.816	0.0149
7.29	0.899	0.0159
8.30	0.972	0.0178

M06-13-128-PT

Fig. 12.56

$Rn = 201600.$

α	C_l	C_d
-3.93	0.007	0.0342
-2.91	0.107	0.0303
-1.88	0.206	0.0307
-0.86	0.303	0.0344
0.17	0.388	0.0414
1.18	0.463	0.0492
2.22	0.558	0.0518
3.22	0.666	0.0497
4.26	0.782	0.0410
5.28	0.894	0.0344
6.28	1.002	0.0300
7.32	1.113	0.0266
8.34	1.220	0.0240
9.36	1.326	0.0212
10.38	1.430	0.0194
11.38	1.460	0.0336

$Rn = 232000.$

α	C_l	C_d
-4.98	-0.157	0.0534
-3.92	-0.043	0.0378
-2.93	0.060	0.0284
-1.89	0.162	0.0261
-0.85	0.265	0.0251
0.16	0.366	0.0251
1.18	0.462	0.0271
2.20	0.562	0.0298
3.22	0.663	0.0302
4.25	0.766	0.0276
5.28	0.871	0.0251
6.30	0.975	0.0235
7.32	1.078	0.0218
8.35	1.183	0.0201
9.36	1.283	0.0179
10.37	1.364	0.0176
11.37	1.364	0.0395
12.39	1.326	0.0629
13.36	1.291	0.0501

$Rn = 254600.$

α	C_l	C_d
-3.92	0.000	0.0306
-2.90	0.103	0.0253
-1.88	0.202	0.0226
-0.85	0.304	0.0219
0.16	0.407	0.0209
1.18	0.510	0.0213
2.21	0.611	0.0224
3.25	0.716	0.0228
4.25	0.817	0.0227
5.28	0.922	0.0214
6.30	1.028	0.0183
7.32	1.131	0.0175

8.35	1.231	0.0178
9.37	1.325	0.0172
10.38	1.366	0.0234
11.37	1.364	0.0463
12.37	1.325	0.0732

$Rn = 302900.$

α	C_l	C_d
-3.92	-0.001	0.0305
-2.90	0.104	0.0228
-1.89	0.205	0.0201
-0.86	0.313	0.0183
0.15	0.417	0.0168
1.19	0.523	0.0163
2.22	0.626	0.0174
3.25	0.729	0.0170
4.27	0.830	0.0169
5.30	0.933	0.0165
6.30	1.031	0.0159
7.32	1.132	0.0149
8.34	1.232	0.0153
9.37	1.321	0.0155
10.38	1.352	0.0239
11.35	1.331	0.0579
12.35	1.297	0.0705

M06-13-128-PT

Fig. 12.57

$Rn = 200900.$

α	C_l	C_d
-2.90	0.100	0.0213
-1.90	0.198	0.0184
-0.84	0.303	0.0162
0.16	0.405	0.0143
1.19	0.507	0.0141
2.22	0.611	0.0149
3.23	0.709	0.0156
4.25	0.808	0.0161
5.28	0.906	0.0172
6.29	0.998	0.0178
7.32	1.091	0.0189
8.34	1.178	0.0205
9.35	1.268	0.0223
10.38	1.348	0.0233
11.38	1.359	0.0433
12.37	1.326	0.0502

$Rn = 251600.$

α	C_l	C_d
-2.91	0.105	0.0209
-1.88	0.204	0.0174
-0.86	0.306	0.0155
0.18	0.412	0.0133
1.20	0.516	0.0130
2.21	0.618	0.0136
3.25	0.720	0.0140
4.25	0.816	0.0149
5.29	0.914	0.0157
6.29	1.009	0.0162
7.32	1.103	0.0175
8.34	1.194	0.0185
9.34	1.281	0.0198
10.37	1.351	0.0205
11.36	1.332	0.0499
12.36	1.293	0.0570

$Rn = 307400.$

α	C_l	C_d
-2.90	0.092	0.0207
-1.91	0.193	0.0167
-0.88	0.298	0.0148
0.17	0.410	0.0126
1.17	0.510	0.0124
2.21	0.617	0.0128
3.22	0.717	0.0135
4.25	0.816	0.0141
5.28	0.913	0.0146
6.29	1.006	0.0158
7.33	1.100	0.0163
8.33	1.190	0.0175
9.36	1.283	0.0185
10.37	1.332	0.0234
11.34	1.309	0.0358
12.33	1.267	0.0465
13.32	1.222	0.0558

M06-13-128-PT

Fig. 12.58

$Rn = 199500.$

α	C_l	C_d
-3.93	0.007	0.0348
-2.91	0.109	0.0309
-1.88	0.210	0.0313
-0.86	0.309	0.0350
0.17	0.396	0.0422
1.18	0.473	0.0501
2.22	0.569	0.0528
3.22	0.679	0.0506
4.26	0.798	0.0418
5.28	0.913	0.0351
6.29	1.022	0.0306
7.33	1.136	0.0271
8.35	1.245	0.0244
9.37	1.354	0.0216
10.38	1.430	0.0194
11.38	1.460	0.0336

$Rn = 203600.$

α	C_l	C_d
-3.91	0.011	0.0277
-2.89	0.113	0.0216
-1.86	0.216	0.0184
-0.84	0.319	0.0156
0.17	0.422	0.0135
1.20	0.529	0.0132
2.22	0.632	0.0138
3.24	0.733	0.0142
4.26	0.835	0.0150
5.29	0.934	0.0156
6.31	1.031	0.0165
7.34	1.127	0.0176
8.36	1.222	0.0187
9.36	1.314	0.0189
10.39	1.380	0.0200
11.37	1.357	0.0511
12.39	1.317	0.0725

$Rn = 204100.$

α	C_l	C_d
-3.92	0.000	0.0288
-2.90	0.104	0.0230
-1.86	0.206	0.0195
-0.85	0.308	0.0175
0.16	0.410	0.0148
1.18	0.512	0.0155
2.21	0.616	0.0166
3.23	0.719	0.0165
4.26	0.816	0.0179
5.28	0.916	0.0189
6.31	1.016	0.0201
7.33	1.112	0.0215
8.35	1.211	0.0215
9.37	1.307	0.0202
10.38	1.368	0.0194
11.37	1.378	0.0328

$Rn = 203600.$

α	C_l	C_d
-3.91	0.008	0.0283
-2.90	0.108	0.0228
-1.87	0.211	0.0196
-0.85	0.313	0.0170
0.17	0.417	0.0140
1.19	0.522	0.0138
2.21	0.627	0.0140
3.24	0.731	0.0142
4.27	0.832	0.0148
5.28	0.929	0.0152
6.31	1.027	0.0162
7.33	1.122	0.0171
8.35	1.215	0.0175
9.36	1.305	0.0192
10.38	1.370	0.0194
11.37	1.356	0.0462
12.36	1.315	0.0694

$Rn = 200900.$

α	C_l	C_d
-2.90	0.100	0.0213
-1.90	0.198	0.0184
-0.84	0.303	0.0162
0.16	0.405	0.0143
1.19	0.507	0.0141
2.22	0.611	0.0149
3.23	0.709	0.0156
4.25	0.808	0.0161
5.28	0.906	0.0172
6.29	0.998	0.0178
7.32	1.091	0.0189
8.34	1.178	0.0205
9.35	1.268	0.0223
10.38	1.348	0.0233
11.38	1.359	0.0433
12.37	1.326	0.0502

NACA 0009-PT

Fig. 12.60

$Rn = 59700.$

α	C_l	C_d
-6.02	-0.504	0.0267
-5.03	-0.448	0.0181
-3.99	-0.381	0.0160
-3.00	-0.293	0.0142
-1.95	-0.141	0.0159
-0.92	-0.044	0.0118
0.09	-0.007	0.0119
1.10	0.057	0.0152
2.13	0.217	0.0156
3.15	0.354	0.0163
4.19	0.438	0.0179
5.19	0.508	0.0192
6.22	0.580	0.0238
7.23	0.646	0.0337
8.23	0.694	0.0438
9.26	0.727	0.1067
10.25	0.704	0.1493

$Rn = 100300.$

α	C_l	C_d
-6.03	-0.540	0.0241
-5.00	-0.460	0.0192
-3.98	-0.388	0.0148
-2.98	-0.311	0.0125
-1.96	-0.195	0.0122
-0.91	-0.041	0.0106
0.09	-0.004	0.0096
1.11	0.119	0.0106
2.15	0.257	0.0117
3.15	0.353	0.0118
4.19	0.440	0.0138
5.21	0.523	0.0175
6.21	0.596	0.0217
7.23	0.669	0.0264
8.24	0.727	0.0394

$Rn = 150600.$

α	C_l	C_d
-6.04	-0.545	0.0225
-5.03	-0.465	0.0183
-4.00	-0.381	0.0150
-2.99	-0.309	0.0113
-1.96	-0.224	0.0094
-0.94	-0.068	0.0084
0.07	0.036	0.0087
1.11	0.170	0.0099
2.15	0.261	0.0097
3.16	0.347	0.0109
4.18	0.435	0.0129
5.21	0.521	0.0149
6.21	0.601	0.0185
7.24	0.673	0.0245
8.24	0.735	0.0339
9.25	0.772	0.0718

$Rn = 199000.$

α	C_l	C_d
-6.04	-0.544	0.0216
-5.01	-0.462	0.0171
-4.00	-0.377	0.0145
-2.99	-0.303	0.0111
-2.01	-0.224	0.0089
-0.94	-0.090	0.0085
0.10	0.060	0.0081
1.10	0.167	0.0083
2.13	0.253	0.0084
3.15	0.346	0.0100
4.19	0.439	0.0118
5.19	0.526	0.0143
6.23	0.611	0.0180
7.24	0.684	0.0228
8.24	0.748	0.0309
9.25	0.787	0.0629

$Rn = 302900.$

α	C_l	C_d
-6.05	-0.560	0.0202
-5.04	-0.475	0.0156
-3.98	-0.385	0.0131
-2.98	-0.294	0.0109
-1.95	-0.184	0.0084
-0.99	-0.090	0.0073
0.08	0.014	0.0068
1.10	0.127	0.0068
2.14	0.244	0.0080
3.17	0.345	0.0092
4.19	0.439	0.0114
5.21	0.528	0.0129
6.22	0.613	0.0159
7.23	0.686	0.0199
8.25	0.753	0.0279
9.27	0.792	0.0575

NACA 2.5411-PT

Fig. 12.62

$Rn = 58200.$

α	C_l	C_d
-1.95	-0.140	0.0190
-0.92	-0.026	0.0180
0.11	0.130	0.0203
1.14	0.253	0.0200
2.18	0.370	0.0222
3.21	0.486	0.0207
4.21	0.580	0.0233
5.23	0.652	0.0247
6.24	0.725	0.0265
7.26	0.811	0.0252
8.28	0.874	0.0314
9.29	0.934	0.0376
10.30	0.978	0.0486
11.30	0.996	0.0643

$Rn = 101500.$

α	C_l	C_d
-3.96	-0.273	0.0213
-2.96	-0.168	0.0175
-1.92	-0.030	0.0153
-0.88	0.118	0.0136
0.15	0.240	0.0133
1.16	0.328	0.0137
2.17	0.411	0.0139
3.20	0.503	0.0140
4.22	0.596	0.0156
5.24	0.683	0.0163
6.26	0.763	0.0185
7.27	0.821	0.0230
8.28	0.873	0.0277
9.30	0.926	0.0339
10.30	0.973	0.0431

$Rn = 200600.$

α	C_l	C_d
-3.96	-0.180	0.0142
-2.94	-0.066	0.0110
-1.91	0.029	0.0114
-0.88	0.113	0.0099
0.13	0.239	0.0088
1.17	0.339	0.0093
2.19	0.438	0.0101
3.21	0.537	0.0112
4.23	0.631	0.0121
5.24	0.715	0.0136
6.26	0.785	0.0168
7.28	0.851	0.0210
8.29	0.914	0.0242
9.30	0.970	0.0293
10.31	1.015	0.0370
11.32	1.044	0.0479

$Rn = 303300.$

α	C_l	C_d
-3.94	-0.155	0.0125
-2.94	-0.067	0.0110
-1.91	0.027	0.0099
-0.90	0.119	0.0093
0.12	0.206	0.0080
1.17	0.344	0.0084
2.18	0.441	0.0088
3.21	0.537	0.0095
4.22	0.625	0.0107
5.24	0.703	0.0126

NACA 64A010-PT

Fig. 12.64

$Rn = 62800.$

α	C_l	C_d
-5.01	-0.484	0.0154
-4.00	-0.404	0.0152
-2.97	-0.330	0.0146
-1.95	-0.190	0.0179
-0.91	-0.030	0.0174
-0.40	-0.013	0.0191
0.08	-0.007	0.0135
0.60	-0.005	0.0135
1.10	0.018	0.0149
1.62	0.088	0.0189
2.14	0.206	0.0181
3.15	0.333	0.0162
4.18	0.413	0.0170
5.20	0.471	0.0227
6.20	0.525	0.0296
7.22	0.572	0.0415

$Rn = 104200.$

α	C_l	C_d
-5.01	-0.465	0.0143
-3.99	-0.398	0.0129
-2.98	-0.327	0.0124
-1.96	-0.240	0.0124
-0.93	-0.089	0.0127
0.09	0.012	0.0121
1.15	0.191	0.0133
2.16	0.301	0.0130
3.16	0.368	0.0127
4.19	0.434	0.0131
5.20	0.493	0.0203
6.22	0.559	0.0262
7.23	0.621	0.0334
8.25	0.676	0.0494

$Rn = 150200.$

α	C_l	C_d
-6.02	-0.565	0.0181
-4.52	-0.465	0.0123
-3.00	-0.347	0.0110
-1.47	-0.223	0.0103
0.07	0.002	0.0104
1.63	0.227	0.0108
3.16	0.362	0.0102
4.70	0.468	0.0154
6.21	0.574	0.0217
7.74	0.673	0.0366

$Rn = 203300.$

α	C_l	C_d
-5.01	-0.454	0.0129
-4.00	-0.383	0.0100
-2.97	-0.299	0.0096
-1.95	-0.184	0.0098
-0.91	-0.048	0.0092
0.11	0.053	0.0093
1.13	0.155	0.0091
2.15	0.291	0.0094
3.18	0.384	0.0099
4.20	0.450	0.0131
5.21	0.526	0.0166
6.23	0.601	0.0201
7.24	0.665	0.0272
8.26	0.724	0.0523

$Rn = 301000.$

α	C_l	C_d
-5.02	-0.463	0.0120
-4.04	-0.385	0.0100
-2.98	-0.266	0.0083
-1.95	-0.140	0.0075
-0.91	-0.040	0.0073
0.11	0.049	0.0075
1.13	0.140	0.0075
2.15	0.244	0.0081
3.17	0.365	0.0104
4.19	0.448	0.0122
5.20	0.527	0.0146
6.23	0.602	0.0177
7.25	0.670	0.0235

NACA 6409-PT

Fig. 12.66

$Rn = 61400.$

α	C_l	C_d
-0.83	0.325	0.0325
0.19	0.438	0.0305
1.19	0.541	0.0280
2.22	0.629	0.0313
3.23	0.716	0.0336
4.26	0.805	0.0365
5.26	0.873	0.0374
6.28	0.931	0.0391
7.24	0.714	0.0958
8.24	0.723	0.1167
9.25	0.765	0.1196
10.36	1.274	0.0333

$Rn = 79400.$

α	C_l	C_d
-0.84	0.411	0.0271
0.18	0.525	0.0213
1.21	0.618	0.0221
2.21	0.700	0.0229
3.24	0.792	0.0223
4.25	0.887	0.0230
5.26	0.972	0.0247
6.28	1.055	0.0265
7.32	1.138	0.0298
8.32	1.207	0.0277
9.35	1.271	0.0303
10.35	1.320	0.0308
11.36	1.373	0.0276
12.36	1.369	0.0290
13.35	1.347	0.0521

$Rn = 102600.$

α	C_l	C_d
-0.84	0.459	0.0200
0.14	0.549	0.0180
1.18	0.646	0.0187
2.20	0.739	0.0180
3.23	0.829	0.0188
4.24	0.922	0.0193
5.27	1.015	0.0202
6.29	1.093	0.0205
7.32	1.179	0.0220
8.31	1.248	0.0231
9.34	1.312	0.0242
10.37	1.353	0.0263
11.35	1.366	0.0276
12.36	1.350	0.0364
13.36	1.329	0.0413
14.36	1.303	0.0571

$Rn = 147300.$

α	C_l	C_d
-0.90	0.481	0.0122
0.10	0.575	0.0124
1.18	0.673	0.0119
2.20	0.779	0.0127
3.19	0.880	0.0138
4.23	0.974	0.0148
5.23	1.063	0.0158
6.26	1.153	0.0165
7.28	1.234	0.0166
8.31	1.301	0.0179
9.35	1.361	0.0206
10.33	1.383	0.0237
11.33	1.383	0.0276
12.35	1.343	0.0349
13.34	1.324	0.0382

$Rn = 200100.$

α	C_l	C_d
-0.87	0.536	0.0124
0.18	0.639	0.0120
1.20	0.730	0.0112
2.18	0.821	0.0115
3.17	0.912	0.0124
4.21	1.006	0.0134
5.20	1.092	0.0143
6.22	1.175	0.0155
7.38	1.265	0.0165
8.32	1.315	0.0177
9.31	1.342	0.0206
10.33	1.339	0.0240
11.33	1.325	0.0286
12.33	1.301	0.0309
13.29	1.280	0.0369
14.29	1.260	0.0549

RG15-PT

Fig. 12.68

$Rn = 59600.$

α	C_l	C_d
-2.93	-0.125	0.0159
-1.92	-0.069	0.0132
-0.91	0.017	0.0141
0.12	0.120	0.0188
1.14	0.215	0.0164
2.18	0.392	0.0213
3.21	0.540	0.0195
4.23	0.622	0.0187
5.23	0.691	0.0186
6.25	0.772	0.0219
7.28	0.853	0.0242
8.29	0.911	0.0289
9.30	0.965	0.0353
10.32	1.009	0.0469
11.33	1.026	0.0693

$Rn = 99600.$

α	C_l	C_d
-2.93	-0.139	0.0141
-1.93	-0.059	0.0125
-0.91	0.021	0.0113
0.13	0.141	0.0129
1.16	0.310	0.0144
2.19	0.452	0.0131
3.21	0.544	0.0134
4.23	0.630	0.0149
5.25	0.718	0.0159
6.27	0.801	0.0182
7.28	0.877	0.0210
8.29	0.946	0.0247
9.31	0.997	0.0309
10.32	1.035	0.0401
11.33	1.055	0.0536

$Rn = 146100.$

α	C_l	C_d
-2.92	-0.133	0.0127
-1.90	-0.043	0.0106
-0.90	0.065	0.0097
0.13	0.214	0.0101
1.16	0.345	0.0097
2.19	0.461	0.0103
3.21	0.564	0.0112
4.24	0.665	0.0128
5.26	0.763	0.0142
6.28	0.860	0.0164
7.30	0.949	0.0190

$Rn = 200900.$

α	C_l	C_d
-4.00	-0.232	0.0144
-2.96	-0.139	0.0123
-1.92	-0.027	0.0108
-0.91	0.098	0.0094
0.12	0.221	0.0085
1.15	0.329	0.0083
2.19	0.430	0.0087
3.19	0.526	0.0096
4.22	0.627	0.0107
5.25	0.716	0.0121
6.26	0.804	0.0144
7.28	0.890	0.0165
8.30	0.965	0.0191
9.31	1.022	0.0249
10.33	1.065	0.0309
11.33	1.084	0.0410

$Rn = 302600.$

α	C_l	C_d
-3.99	-0.215	0.0126
-2.97	-0.095	0.0109
-1.97	0.034	0.0092
-0.93	0.146	0.0076
0.05	0.239	0.0069
1.09	0.331	0.0075
2.17	0.440	0.0078
3.20	0.543	0.0087
4.23	0.639	0.0100
5.24	0.730	0.0115
6.27	0.820	0.0131
7.29	0.907	0.0150
8.30	0.981	0.0185

RG15-PT

Fig. 12.69

$Rn = 102300.$

α	C_l	C_d
-3.96	-0.227	0.0183
-2.94	-0.130	0.0144
-1.93	-0.046	0.0116
-0.90	0.076	0.0117
0.12	0.214	0.0121
1.16	0.338	0.0120
2.19	0.447	0.0125
3.20	0.541	0.0121
4.24	0.633	0.0124
5.24	0.721	0.0156
6.25	0.804	0.0165
7.27	0.879	0.0210
8.30	0.945	0.0264
9.31	0.997	0.0299
10.31	1.017	0.0625

$Rn = 151600.$

α	C_l	C_d
-3.97	-0.216	0.0154
-2.94	-0.099	0.0129
-1.91	0.027	0.0108
-0.89	0.124	0.0097
0.13	0.237	0.0088
1.17	0.347	0.0101
2.19	0.449	0.0109
3.21	0.549	0.0116
4.23	0.648	0.0125
5.24	0.743	0.0140
6.27	0.833	0.0166
7.28	0.917	0.0188
8.31	0.989	0.0237
9.30	1.040	0.0276
10.33	1.076	0.0387
11.32	1.089	0.0505
12.30	1.038	0.1342

$Rn = 201200.$

α	C_l	C_d
-3.97	-0.188	0.0135
-2.93	-0.062	0.0114
-1.92	0.050	0.0090
-0.90	0.137	0.0083
0.14	0.229	0.0086
1.15	0.338	0.0093
2.17	0.442	0.0100
3.20	0.546	0.0109
4.22	0.647	0.0121
5.24	0.747	0.0133
6.26	0.843	0.0148
7.29	0.929	0.0178
8.29	0.998	0.0220
9.32	1.053	0.0282
10.32	1.089	0.0361
11.32	1.103	0.0463

$Rn = 313500.$

α	C_l	C_d
-3.97	-0.164	0.0121
-2.96	-0.065	0.0107
-1.96	0.025	0.0101
-0.94	0.125	0.0091
0.11	0.225	0.0095
1.15	0.330	0.0096
2.17	0.440	0.0098
3.19	0.549	0.0104
4.22	0.652	0.0110
5.26	0.754	0.0122
6.27	0.845	0.0139
7.28	0.924	0.0165
8.31	1.000	0.0199
9.32	1.057	0.0248
10.31	1.096	0.0314
11.31	1.107	0.0402

RG15-PT

Fig. 12.70

$Rn = 101700.$

α	C_l	C_d
-3.45	-0.198	0.0172
-1.92	-0.062	0.0113
-0.39	0.128	0.0116
1.15	0.320	0.0127
2.69	0.486	0.0130
5.26	0.728	0.0159
6.78	0.856	0.0188
8.29	0.962	0.0246
9.31	1.012	0.0293
10.32	1.047	0.0346
11.32	1.051	0.0744

$Rn = 151900.$

α	C_l	C_d
-3.44	-0.140	0.0134
-1.92	0.028	0.0094
-0.38	0.175	0.0084
1.16	0.349	0.0097
2.70	0.508	0.0110
5.26	0.748	0.0144
6.78	0.877	0.0194
8.30	0.987	0.0257
9.31	1.040	0.0312
10.32	1.075	0.0407
11.33	1.091	0.0559

$Rn = 202700.$

α	C_l	C_d
-3.43	-0.107	0.0117
-1.93	0.049	0.0088
-0.38	0.180	0.0083
1.17	0.343	0.0087
2.70	0.506	0.0097
5.26	0.749	0.0135
6.78	0.879	0.0171
8.29	0.995	0.0223
9.32	1.049	0.0280

$Rn = 305100.$

α	C_l	C_d
-3.49	-0.114	0.0120
-2.00	0.032	0.0096
-0.39	0.189	0.0087
1.13	0.340	0.0082
2.70	0.509	0.0086
5.25	0.750	0.0122
6.79	0.884	0.0152
8.30	0.995	0.0205
9.31	1.051	0.0253
10.32	1.090	0.0317

RG15-PT

Fig. 12.71

$Rn = 101000.$

α	C_l	C_d
-3.45	-0.198	0.0172
-1.93	-0.065	0.0119
-0.38	0.112	0.0117
1.16	0.316	0.0147
2.69	0.500	0.0136
5.24	0.723	0.0157
6.77	0.850	0.0174
8.30	0.964	0.0233
9.31	1.013	0.0301
10.32	1.048	0.0396
11.32	1.050	0.0779

$Rn = 152800.$

α	C_l	C_d
-3.95	-0.198	0.0162
-2.93	-0.082	0.0120
-1.92	0.032	0.0100
-0.91	0.131	0.0107
0.12	0.249	0.0106
1.16	0.368	0.0101
2.18	0.469	0.0102
3.21	0.566	0.0105
4.23	0.663	0.0118
5.24	0.751	0.0136
6.27	0.839	0.0159
7.29	0.925	0.0191
8.30	0.998	0.0226
9.31	1.051	0.0289
10.32	1.092	0.0362
11.33	1.110	0.0479
12.32	1.086	0.1002
13.29	0.997	0.1993

$Rn = 202300.$

α	C_l	C_d
-3.95	-0.164	0.0139
-2.97	-0.058	0.0108
-1.91	0.055	0.0087
-0.92	0.148	0.0082
0.12	0.248	0.0081

1.15	0.357	0.0083
2.16	0.457	0.0086
3.19	0.558	0.0096
4.22	0.654	0.0111
5.25	0.747	0.0127
6.26	0.836	0.0151
7.29	0.922	0.0175
8.29	0.994	0.0211
9.32	1.049	0.0267
10.32	1.087	0.0337
11.33	1.105	0.0440
12.19	1.089	0.0944

$Rn = 307600.$

α	C_l	C_d
-4.02	-0.158	0.0123
-2.96	-0.052	0.0103
-1.97	0.047	0.0086
-0.98	0.142	0.0074
0.11	0.247	0.0072
1.10	0.345	0.0070
2.16	0.457	0.0080
3.18	0.559	0.0091
4.21	0.655	0.0105
5.25	0.749	0.0120
6.27	0.836	0.0138
7.28	0.921	0.0157
8.30	0.995	0.0192
9.32	1.053	0.0241
10.32	1.094	0.0306
11.32	1.109	0.0402

RG15-PT

Fig. 12.72

$Rn = 101000.$

α	C_l	C_d
-2.96	-0.128	0.0151
-1.93	-0.054	0.0120
-0.92	0.021	0.0125
0.11	0.145	0.0119
1.15	0.304	0.0142
2.19	0.454	0.0140
3.20	0.548	0.0129
4.21	0.633	0.0133
5.23	0.718	0.0152
6.25	0.800	0.0171
7.28	0.883	0.0194
8.29	0.954	0.0242
9.30	1.001	0.0285
10.31	1.040	0.0351
11.31	1.057	0.0475
12.30	1.014	0.1151

$Rn = 153300.$

α	C_l	C_d
-2.93	-0.097	0.0138
-1.93	0.013	0.0115
-0.91	0.112	0.0097
0.12	0.243	0.0098
1.14	0.370	0.0096
2.17	0.470	0.0096
3.17	0.563	0.0108
4.20	0.657	0.0119
5.25	0.748	0.0133
6.26	0.834	0.0152
7.28	0.919	0.0177
8.30	0.991	0.0216
9.30	1.042	0.0269
10.32	1.080	0.0336
11.33	1.099	0.0457

$Rn = 201300.$

α	C_l	C_d
-2.97	-0.071	0.0113
-1.93	0.044	0.0095
-0.91	0.146	0.0089
0.10	0.245	0.0084
1.15	0.357	0.0084
2.15	0.454	0.0090
3.19	0.555	0.0094
4.23	0.653	0.0111
5.24	0.747	0.0124
6.24	0.836	0.0146
7.27	0.923	0.0162
8.30	0.998	0.0211
9.32	1.053	0.0264
10.34	1.092	0.0323
11.33	1.108	0.0429

$Rn = 300600.$

α	C_l	C_d
-2.97	-0.055	0.0097
-1.97	0.047	0.0084
-0.94	0.152	0.0073
0.12	0.249	0.0070
1.12	0.346	0.0070
2.15	0.451	0.0078
3.19	0.555	0.0092
4.20	0.650	0.0105
5.25	0.745	0.0120
6.26	0.836	0.0136
7.28	0.922	0.0156
8.30	0.996	0.0194
9.31	1.053	0.0243
10.32	1.091	0.0301
11.31	1.108	0.0405
12.30	1.092	0.0882

S2048-PT

Fig. 12.74

$Rn = 58800.$

α	C_l	C_d
-2.93	-0.101	0.0169
-1.91	-0.031	0.0131
-0.89	0.078	0.0138
0.13	0.183	0.0153
1.16	0.268	0.0185
2.19	0.425	0.0218
3.22	0.605	0.0225
4.24	0.695	0.0221
5.26	0.767	0.0212
6.27	0.827	0.0242

$Rn = 99500.$

α	C_l	C_d
-2.93	-0.089	0.0144
-1.92	-0.012	0.0135
-0.89	0.096	0.0139
0.15	0.220	0.0146
1.18	0.373	0.0161
2.20	0.530	0.0143
3.23	0.632	0.0145
4.24	0.716	0.0146
5.26	0.790	0.0172
6.27	0.854	0.0200
7.29	0.906	0.0271
8.29	0.959	0.0325
9.31	0.996	0.0420

$Rn = 154000.$

α	C_l	C_d
-4.97	-0.277	0.0190
-3.97	-0.188	0.0170
-2.93	-0.086	0.0141
-1.92	0.018	0.0116
-0.88	0.147	0.0123
0.14	0.300	0.0111
1.17	0.430	0.0102
2.20	0.535	0.0109
3.23	0.630	0.0113
4.23	0.711	0.0136
5.26	0.792	0.0157
6.27	0.859	0.0189
7.29	0.922	0.0245
8.30	0.976	0.0308

$Rn = 200900.$

α	C_l	C_d
-2.94	-0.051	0.0129
-1.89	0.082	0.0105
-0.87	0.207	0.0102
0.16	0.332	0.0095
1.18	0.439	0.0090
2.20	0.540	0.0092
3.22	0.634	0.0103
4.24	0.720	0.0126
5.26	0.800	0.0147
6.28	0.870	0.0180
7.30	0.934	0.0231
8.30	0.986	0.0287
9.32	1.023	0.0373
10.33	1.054	0.0583
11.35	1.013	0.1328

$Rn = 302800.$

α	C_l	C_d
-2.94	0.017	0.0115
-1.89	0.145	0.0088
-0.88	0.250	0.0077
0.10	0.344	0.0072
1.16	0.449	0.0074
2.18	0.550	0.0081
3.19	0.640	0.0096
4.24	0.728	0.0116
5.26	0.808	0.0137
6.28	0.881	0.0174

S2048-PT

Fig. 12.75

$Rn = 102200.$

α	C_l	C_d
-3.95	-0.185	0.0194
-2.93	-0.090	0.0153
-1.91	-0.002	0.0133
-0.89	0.092	0.0147
0.13	0.233	0.0149
1.17	0.379	0.0162
2.20	0.539	0.0157
3.23	0.642	0.0140
4.25	0.725	0.0146
5.26	0.800	0.0168
6.27	0.870	0.0212
7.30	0.927	0.0256
8.30	0.980	0.0332
9.31	1.018	0.0416

$Rn = 148800.$

α	C_l	C_d
-2.92	-0.045	0.0138
-1.91	0.065	0.0119
-0.89	0.177	0.0119
0.17	0.317	0.0116
1.18	0.446	0.0113
2.20	0.550	0.0112
3.22	0.646	0.0111
4.24	0.726	0.0126
5.26	0.805	0.0157
6.27	0.874	0.0193
7.29	0.934	0.0240
8.31	0.986	0.0299
9.31	1.025	0.0392
10.33	1.048	0.0566
11.30	1.023	0.1301

$Rn = 198700.$

α	C_l	C_d
-2.92	0.003	0.0117
-1.92	0.116	0.0094
-0.87	0.220	0.0088
0.15	0.333	0.0086
1.17	0.443	0.0086
2.19	0.545	0.0093
3.23	0.641	0.0103
4.24	0.724	0.0125
5.25	0.806	0.0151
6.28	0.879	0.0183
7.29	0.943	0.0228
8.31	0.998	0.0289
9.31	1.035	0.0373
10.32	1.066	0.0567

$Rn = 300800.$

α	C_l	C_d
-2.94	0.029	0.0103
-1.93	0.136	0.0080
-0.92	0.240	0.0074
0.13	0.341	0.0074
1.14	0.442	0.0073
2.19	0.546	0.0079
3.21	0.638	0.0097
4.24	0.727	0.0120
5.26	0.809	0.0140
6.26	0.883	0.0172
7.29	0.950	0.0212
8.31	1.008	0.0260
9.30	1.048	0.0333
10.31	1.079	0.0527

S2048-PT

Fig. 12.76

$Rn = 302800.$

α	C_l	C_d
-2.94	0.017	0.0115

-1.89	0.145	0.0088
-0.88	0.250	0.0077
0.10	0.344	0.0072
1.16	0.449	0.0074
2.18	0.550	0.0081
3.19	0.640	0.0096
4.24	0.728	0.0116
5.26	0.808	0.0137
6.28	0.881	0.0174

$Rn = 303900.$

α	C_l	C_d
-4.07	-0.140	0.0134
-2.99	0.006	0.0113
-1.90	0.137	0.0089
-0.92	0.237	0.0077
0.10	0.335	0.0073
1.13	0.437	0.0073
2.16	0.541	0.0081
3.21	0.636	0.0096
4.21	0.722	0.0116
5.24	0.805	0.0137
6.25	0.880	0.0172
7.27	0.946	0.0209
8.31	1.002	0.0261
9.32	1.040	0.0340
10.30	1.074	0.0558

$Rn = 301300.$

α	C_l	C_d
-3.96	-0.084	0.0123
-2.94	0.034	0.0102
-1.90	0.149	0.0084
-0.87	0.253	0.0078
0.14	0.351	0.0073
1.19	0.456	0.0075
2.20	0.558	0.0083
3.22	0.650	0.0099
4.25	0.738	0.0120
5.25	0.818	0.0143
6.29	0.895	0.0175
7.29	0.962	0.0215
8.31	1.017	0.0265
9.32	1.053	0.0351

$Rn = 306300.$

α	C_l	C_d
-4.00	-0.136	0.0130
-2.97	-0.019	0.0106
-1.94	0.098	0.0085
-0.89	0.210	0.0074
0.11	0.349	0.0073
1.16	0.464	0.0077
2.17	0.572	0.0085
3.21	0.667	0.0105
4.25	0.758	0.0125
5.27	0.839	0.0151
6.26	0.908	0.0189
7.30	0.974	0.0230
8.30	1.025	0.0285
9.29	1.059	0.0399
10.36	1.050	0.0968

S2055-PT

Fig. 12.78

$Rn = 103100.$

α	C_l	C_d
-3.95	-0.239	0.0217
-2.44	-0.113	0.0140
-0.90	0.016	0.0110
0.63	0.225	0.0141
2.18	0.453	0.0151
3.72	0.604	0.0131
5.25	0.722	0.0144
6.78	0.827	0.0197
8.29	0.914	0.0307
9.80	0.980	0.0460
11.31	0.980	0.1021
12.80	0.901	0.1804

$Rn = 152700.$

α	C_l	C_d
-2.95	-0.150	0.0122
-1.91	-0.057	0.0108
-0.88	0.079	0.0109
0.12	0.225	0.0118
1.16	0.357	0.0113
2.19	0.464	0.0116
3.22	0.548	0.0101
4.22	0.635	0.0115
5.24	0.720	0.0149
6.26	0.792	0.0169
7.28	0.856	0.0214
8.28	0.914	0.0284
9.31	0.962	0.0378
10.30	0.997	0.0646

$Rn = 202000.$

α	C_l	C_d
-3.96	-0.229	0.0147
-2.95	-0.120	0.0123
-1.90	0.009	0.0096
-0.89	0.128	0.0096
0.14	0.249	0.0087
1.16	0.350	0.0083
2.19	0.450	0.0084
3.20	0.543	0.0091
4.21	0.630	0.0111
5.24	0.716	0.0132
6.26	0.795	0.0165
7.27	0.865	0.0208
8.29	0.925	0.0260
9.31	0.974	0.0359

$Rn = 304800.$

α	C_l	C_d
-3.96	-0.162	0.0126
-2.94	-0.048	0.0104
-1.92	0.053	0.0078
-0.88	0.134	0.0068
0.13	0.238	0.0067
1.16	0.344	0.0070
2.18	0.447	0.0077
3.20	0.540	0.0089
4.22	0.632	0.0108
5.25	0.719	0.0131
6.26	0.798	0.0166
7.28	0.869	0.0201
8.28	0.928	0.0262
9.31	0.979	0.0369
10.30	1.011	0.0764

S2091A-PT

Fig. 12.79

$Rn = 60800.$

α	C_l	C_d
-2.89	0.099	0.0260
-1.85	0.228	0.0212
-0.83	0.338	0.0226
0.19	0.439	0.0238
1.21	0.526	0.0275
2.23	0.619	0.0295
3.25	0.704	0.0329
4.27	0.789	0.0322
5.29	0.888	0.0326
6.31	0.981	0.0286
7.32	1.050	0.0313
8.35	1.129	0.0287
9.35	1.201	0.0317
10.37	1.259	0.0350
11.37	1.265	0.0438

$Rn = 99200.$

α	C_l	C_d
-4.95	-0.088	0.0296
-3.89	0.049	0.0209
-2.87	0.154	0.0174
-1.85	0.246	0.0149
-0.83	0.343	0.0140
0.18	0.440	0.0149
1.21	0.545	0.0180
2.23	0.640	0.0180
3.26	0.732	0.0188
4.27	0.830	0.0193
5.29	0.919	0.0199
6.31	1.012	0.0214
7.33	1.091	0.0217
8.35	1.179	0.0240
9.37	1.258	0.0254
10.37	1.289	0.0331
11.37	1.279	0.0504
12.37	1.252	0.0683

$Rn = 201500.$

α	C_l	C_d
-2.87	0.126	0.0141
-1.88	0.227	0.0128
-0.84	0.329	0.0108
0.18	0.435	0.0106
1.21	0.540	0.0111
2.23	0.645	0.0115
3.25	0.747	0.0125
4.27	0.844	0.0134
5.29	0.939	0.0142
6.31	1.030	0.0153
7.33	1.114	0.0171
8.35	1.192	0.0193
9.36	1.252	0.0234
10.36	1.278	0.0327
11.36	1.262	0.0535
12.36	1.235	0.0767

S2091B-PT

Fig. 12.80

$Rn = 60400.$

α	C_l	C_d
-3.93	-0.091	0.0290
-2.40	0.079	0.0231
-0.85	0.280	0.0263
0.70	0.471	0.0301
2.23	0.604	0.0322
3.74	0.722	0.0331
5.27	0.835	0.0335
6.80	0.951	0.0382
8.33	1.054	0.0472

$Rn = 101300.$

α	C_l	C_d
-2.87	0.145	0.0210
-1.35	0.321	0.0156
0.19	0.469	0.0166
1.73	0.609	0.0174
3.26	0.751	0.0183
4.79	0.887	0.0203
6.31	1.012	0.0228
7.84	1.127	0.0261
9.35	1.232	0.0298
10.37	1.294	0.0356
11.37	1.330	0.0398
12.38	1.312	0.0459

$Rn = 149300.$

α	C_l	C_d
-4.93	-0.079	0.0239
-3.90	0.061	0.0192
-2.87	0.180	0.0146
-1.86	0.272	0.0121
-0.83	0.368	0.0113
0.17	0.466	0.0119
1.22	0.570	0.0128
2.24	0.670	0.0140
3.26	0.771	0.0143
4.28	0.865	0.0158
5.30	0.957	0.0166
6.32	1.043	0.0187
7.34	1.123	0.0204
8.35	1.205	0.0225
9.36	1.278	0.0256
10.38	1.352	0.0280
11.38	1.392	0.0328
12.38	1.366	0.0388

$Rn = 198400.$

α	C_l	C_d
-4.90	-0.013	0.0181
-3.91	0.090	0.0142
-2.87	0.188	0.0126
-1.84	0.282	0.0113
-0.84	0.380	0.0101
0.19	0.485	0.0105
1.22	0.588	0.0111
2.25	0.692	0.0120
3.25	0.791	0.0130
4.28	0.888	0.0141
5.31	0.979	0.0154
6.31	1.065	0.0168
7.34	1.148	0.0182
8.36	1.230	0.0206

9.38	1.310	0.0227
10.38	1.370	0.0259
11.40	1.395	0.0308
12.39	1.360	0.0463

$Rn = 303900.$

α	C_l	C_d
-3.91	0.115	0.0113
-2.88	0.213	0.0101
-1.85	0.316	0.0098
-0.83	0.414	0.0085
0.21	0.526	0.0085
1.23	0.632	0.0096
2.24	0.733	0.0102
3.28	0.832	0.0112
4.29	0.925	0.0129
5.31	1.014	0.0138
6.32	1.099	0.0154
7.34	1.182	0.0165
8.35	1.258	0.0187
9.38	1.325	0.0219
10.38	1.373	0.0254
11.38	1.378	0.0375

S2091B-PT

Fig. 12.81

$Rn = 99600.$

α	C_l	C_d
-4.93	0.031	0.0257
-3.35	0.256	0.0190
-1.84	0.413	0.0157
-0.29	0.560	0.0163
1.24	0.715	0.0188
2.76	0.866	0.0198
4.30	1.013	0.0227
5.84	1.145	0.0238
7.36	1.266	0.0279
8.90	1.376	0.0332
10.40	1.456	0.0388
11.90	1.430	0.0510
13.40	1.378	0.0628

$Rn = 200000.$

α	C_l	C_d
-4.90	0.104	0.0174
-3.35	0.304	0.0128
-1.84	0.457	0.0115
-0.30	0.552	0.0110
1.24	0.721	0.0123
2.77	0.886	0.0142
4.31	1.040	0.0155
5.85	1.187	0.0175
7.37	1.318	0.0206
8.90	1.444	0.0242
10.42	1.522	0.0309
11.90	1.468	0.0604
13.39	1.379	0.1139

$Rn = 298500.$

α	C_l	C_d
-4.89	0.124	0.0133
-3.90	0.238	0.0117
-2.84	0.354	0.0110
-1.80	0.476	0.0105
-0.82	0.559	0.0100
0.18	0.620	0.0101
1.20	0.736	0.0104
2.26	0.851	0.0115
3.26	0.956	0.0125
4.30	1.058	0.0138
5.31	1.153	0.0150
6.34	1.247	0.0164
7.38	1.334	0.0182
8.38	1.414	0.0207
9.39	1.482	0.0237
10.42	1.523	0.0282
11.42	1.504	0.0427
12.38	1.437	0.0861

S2091B-PT

Fig. 12.82

$Rn = 59200.$

α	C_l	C_d
-4.91	0.088	0.0288
-2.85	0.285	0.0196
-0.81	0.495	0.0329
1.25	0.744	0.0358
3.29	0.940	0.0316
5.33	1.090	0.0443
7.36	1.225	0.0483
9.34	1.055	0.1727
11.30	0.896	0.2234

$Rn = 100400.$

α	C_l	C_d
-4.90	0.131	0.0240
-3.87	0.267	0.0196
-2.82	0.409	0.0182
-1.81	0.474	0.0168
-0.78	0.577	0.0164
0.23	0.683	0.0174
1.26	0.789	0.0189
2.29	0.892	0.0189
3.31	0.992	0.0210
4.33	1.079	0.0251
5.34	1.171	0.0232
6.36	1.253	0.0270
7.38	1.335	0.0285
8.40	1.411	0.0323
9.41	1.477	0.0358
10.43	1.518	0.0418
11.42	1.491	0.0553
12.40	1.438	0.0787
13.40	1.392	0.1052
14.31	1.001	0.2596

$Rn = 146200.$

α	C_l	C_d
-4.89	0.163	0.0182
-2.82	0.452	0.0159
-0.79	0.567	0.0140
1.26	0.797	0.0156
3.31	1.021	0.0180
5.35	1.222	0.0212
7.38	1.403	0.0250
9.44	1.574	0.0313
11.43	1.606	0.0408
13.41	1.503	0.0609

$Rn = 199700.$

α	C_l	C_d
-4.88	0.190	0.0174
-3.86	0.334	0.0165
-2.81	0.465	0.0139
-1.79	0.560	0.0135
-0.79	0.609	0.0131
0.23	0.688	0.0136
1.26	0.805	0.0144
2.27	0.915	0.0148
3.30	1.023	0.0158
4.34	1.131	0.0172
5.35	1.230	0.0186
6.38	1.325	0.0208
7.39	1.414	0.0233
8.40	1.498	0.0259
9.43	1.567	0.0289
10.44	1.589	0.0358
11.42	1.538	0.0657
12.42	1.467	0.1061

$Rn = 306400.$

α	C_l	C_d
-4.88	0.206	0.0148
-3.86	0.330	0.0136
-2.82	0.454	0.0134
-1.79	0.587	0.0136
-0.79	0.666	0.0133
0.22	0.707	0.0119
1.26	0.816	0.0121
2.27	0.926	0.0130
3.27	1.030	0.0139
4.29	1.130	0.0150
5.32	1.224	0.0165
6.34	1.320	0.0180
7.39	1.414	0.0201
8.38	1.492	0.0228
9.42	1.560	0.0256
10.41	1.588	0.0330
11.42	1.565	0.0366
12.38	1.483	0.0967
13.38	1.416	0.1330

S2091B-PT

Fig. 12.83

$Rn = 99800.$

α	C_l	C_d
-3.78	0.537	0.0245
-2.77	0.640	0.0249
-1.76	0.705	0.0234
-1.01	0.764	0.0223
-0.23	0.838	0.0212
0.54	0.909	0.0246
1.29	0.997	0.0256
2.32	1.073	0.0254
3.36	1.184	0.0285
4.36	1.277	0.0295
5.39	1.381	0.0297
6.40	1.451	0.0314
7.42	1.516	0.0339
8.43	1.586	0.0346
9.44	1.640	0.0464
10.44	1.632	0.0465
11.44	1.597	0.0565
12.35	1.122	0.2719

$Rn = 199300.$

α	C_l	C_d
-3.80	0.565	0.0247
-2.78	0.681	0.0233
-1.75	0.765	0.0240
-1.00	0.808	0.0240
-0.24	0.839	0.0227
0.51	0.892	0.0216
1.28	0.965	0.0202
2.31	1.072	0.0213
3.35	1.180	0.0217
4.37	1.280	0.0231
5.38	1.373	0.0244
6.40	1.462	0.0264
7.41	1.545	0.0282
8.43	1.621	0.0315
9.45	1.669	0.0371
10.45	1.645	0.0486

$Rn = 302700.$

α	C_l	C_d
-3.80	0.553	0.0232
-2.79	0.680	0.0244
-1.74	0.793	0.0245
-0.98	0.863	0.0249
-0.22	0.921	0.0244
0.52	0.966	0.0231
1.31	1.014	0.0235
2.32	1.099	0.0221
3.32	1.191	0.0203
4.33	1.286	0.0207
5.36	1.382	0.0223
6.37	1.468	0.0237
7.33	1.543	0.0259
8.39	1.619	0.0282
9.42	1.670	0.0339
10.42	1.657	0.0479
11.42	1.558	0.0988

S3010-PT

Fig. 12.85

$Rn = 60900.$

α	C_l	C_d
-2.96	-0.084	0.0172
-1.41	0.133	0.0167
0.14	0.329	0.0218
1.69	0.468	0.0236
3.23	0.594	0.0268
4.73	0.719	0.0280
6.28	0.844	0.0280
7.79	0.951	0.0357
9.32	1.042	0.0353
10.82	1.091	0.0411

$Rn = 100500.$

α	C_l	C_d
-3.95	-0.142	0.0171
-2.90	0.003	0.0145
-1.89	0.128	0.0132
-0.86	0.235	0.0135
0.15	0.324	0.0140
1.17	0.421	0.0150
2.19	0.517	0.0158
3.22	0.618	0.0161
4.24	0.713	0.0170
5.25	0.801	0.0178
6.27	0.890	0.0213

7.30	0.972	0.0237
8.32	1.051	0.0256
9.32	1.120	0.0305
10.34	1.148	0.0332
11.34	1.148	0.0480

$Rn = 147400.$

α	C_l	C_d
-3.92	-0.078	0.0132
-2.40	0.071	0.0116
-0.87	0.208	0.0115
0.66	0.365	0.0113
2.18	0.522	0.0117
3.73	0.676	0.0135
5.26	0.822	0.0155
6.81	0.959	0.0183
8.31	1.084	0.0223
9.85	1.167	0.0277
11.34	1.167	0.0401
12.85	1.147	0.0601
14.28	0.857	0.2484

$Rn = 203900.$

α	C_l	C_d
-3.92	-0.090	0.0126
-2.41	0.045	0.0112
-0.88	0.185	0.0094
0.67	0.356	0.0094
2.20	0.512	0.0099
3.71	0.664	0.0124
5.25	0.811	0.0139
6.78	0.948	0.0159
8.31	1.075	0.0193
9.85	1.159	0.0253
11.34	1.166	0.0345
12.84	1.147	0.0564
14.32	1.116	0.0738

$Rn = 301000.$

α	C_l	C_d
-3.98	-0.105	0.0114
-2.94	-0.004	0.0105
-1.91	0.099	0.0092
-0.92	0.197	0.0085
0.14	0.307	0.0077
1.14	0.416	0.0081
2.18	0.525	0.0087
3.19	0.626	0.0098
4.24	0.732	0.0109
5.25	0.829	0.0122
6.28	0.923	0.0137
7.29	1.010	0.0155
8.32	1.091	0.0179
9.34	1.153	0.0214
10.34	1.182	0.0284
11.33	1.175	0.0314

S3014-PT

Fig. 12.87

$Rn = 62000.$

α	C_l	C_d
-3.93	-0.128	0.0193
-2.92	-0.042	0.0140
-1.89	0.066	0.0167
-0.86	0.217	0.0193
0.17	0.367	0.0227
1.21	0.495	0.0247
2.23	0.590	0.0237
3.25	0.685	0.0232
4.27	0.774	0.0216
5.28	0.857	0.0259
6.29	0.935	0.0216
7.32	1.007	0.0322
8.33	1.073	0.0316
9.34	1.129	0.0382
10.35	1.158	0.0477

$Rn = 99900.$

α	C_l	C_d
-3.93	-0.104	0.0171
-2.89	0.026	0.0141
-1.87	0.171	0.0157
-0.84	0.301	0.0162
0.17	0.394	0.0176
1.20	0.481	0.0181
2.23	0.569	0.0174
3.24	0.661	0.0177
4.26	0.750	0.0181
5.28	0.836	0.0193
6.30	0.916	0.0217
7.31	0.992	0.0244
8.32	1.061	0.0282
9.34	1.118	0.0322
10.35	1.148	0.0397
11.35	1.132	0.0566

$Rn = 151500.$

α	C_l	C_d
-3.91	-0.011	0.0139
-2.88	0.086	0.0118
0.17	0.381	0.0125
2.22	0.577	0.0131
4.27	0.772	0.0144
6.30	0.948	0.0182
7.31	1.015	0.0202
8.33	1.086	0.0230
9.34	1.158	0.0263
10.35	1.188	0.0327
11.34	1.166	0.0493

$Rn = 200800.$

α	C_l	C_d
-3.92	-0.019	0.0127
-2.90	0.065	0.0115
-1.88	0.168	0.0098
-0.85	0.268	0.0099
0.17	0.369	0.0100
1.19	0.470	0.0104
2.21	0.554	0.0105
3.24	0.651	0.0111
4.26	0.747	0.0121
5.27	0.837	0.0137
6.30	0.925	0.0156
7.31	1.011	0.0180
8.34	1.091	0.0205
9.35	1.160	0.0230
10.36	1.189	0.0302
11.36	1.169	0.0434

$Rn = 303700.$

α	C_l	C_d
-2.89	0.044	0.0105
-1.88	0.138	0.0087
-0.99	0.242	0.0082
0.17	0.340	0.0080
1.19	0.447	0.0084
2.22	0.551	0.0088
3.23	0.650	0.0096
4.26	0.747	0.0109
5.28	0.837	0.0124
6.29	0.923	0.0141
7.31	1.008	0.0160

S3016-PT

Fig. 12.89

$Rn = 59100.$

α	C_l	C_d
-3.98	-0.293	0.0238
-2.96	-0.235	0.0196
-1.94	-0.144	0.0143
-0.90	-0.013	0.0162
0.13	0.159	0.0174
1.15	0.293	0.0189
2.19	0.394	0.0220
3.20	0.479	0.0219
4.21	0.565	0.0213
5.24	0.665	0.0211
6.25	0.745	0.0230
7.27	0.819	0.0281
8.28	0.866	0.0359
9.30	0.928	0.0429
10.31	0.974	0.0601

$Rn = 103300.$

α	C_l	C_d
-4.99	-0.354	0.0180
-3.98	-0.277	0.0163
-2.96	-0.192	0.0135
-1.92	-0.057	0.0120
-0.90	0.084	0.0120
0.13	0.205	0.0137
1.15	0.303	0.0152
2.19	0.393	0.0143
3.19	0.480	0.0152
4.22	0.571	0.0175
5.24	0.660	0.0158
6.24	0.753	0.0211
7.27	0.828	0.0194
8.28	0.893	0.0339
9.29	0.923	0.0421

$Rn = 152700.$

α	C_l	C_d
-4.99	-0.341	0.0185
-3.96	-0.245	0.0140
-2.94	-0.126	0.0127
-1.91	0.005	0.0107
-0.89	0.105	0.0113
0.14	0.196	0.0120
1.15	0.294	0.0118
2.17	0.399	0.0119
3.20	0.496	0.0123
4.21	0.598	0.0133
5.23	0.687	0.0165
6.25	0.777	0.0180
7.27	0.859	0.0227
8.29	0.938	0.0236
9.32	1.015	0.0286

$Rn = 208900.$

α	C_l	C_d
-4.96	-0.306	0.0171
-3.96	-0.190	0.0137
-2.93	-0.102	0.0115
-1.93	-0.020	0.0102
-0.90	0.083	0.0086
0.14	0.191	0.0087
1.15	0.293	0.0090
2.18	0.396	0.0091
3.19	0.498	0.0098
4.22	0.598	0.0107
5.24	0.693	0.0124
6.27	0.786	0.0143
7.27	0.872	0.0175
8.31	0.950	0.0208
9.31	1.021	0.0244
10.32	1.081	0.0296
11.34	1.124	0.0365

$Rn = 304800.$

α	C_l	C_d
-4.99	-0.303	0.0155
-3.98	-0.219	0.0130
-2.95	-0.127	0.0108
-1.92	-0.033	0.0096
-0.90	0.060	0.0080
0.11	0.180	0.0073
1.16	0.286	0.0075
2.17	0.390	0.0079
3.20	0.493	0.0088
4.22	0.592	0.0099
5.23	0.686	0.0115
6.25	0.777	0.0133
7.28	0.866	0.0158
8.30	0.947	0.0183
9.32	1.023	0.0214
10.33	1.086	0.0256
11.33	1.134	0.0314

S3021A-PT

Fig. 12.90

$Rn = 58800.$

α	C_l	C_d
-3.96	-0.207	0.0295
-2.94	-0.130	0.0212
-1.92	-0.060	0.0174
-0.90	0.023	0.0153
0.13	0.179	0.0181
1.16	0.314	0.0223
2.18	0.432	0.0241
3.20	0.524	0.0283
4.22	0.608	0.0255
5.25	0.689	0.0253
6.26	0.764	0.0257
7.28	0.851	0.0280
8.29	0.922	0.0264
9.31	0.992	0.0309
10.32	1.052	0.0326
11.33	1.069	0.0402

$Rn = 99500.$

α	C_l	C_d
-3.95	-0.224	0.0238
-2.95	-0.135	0.0186

-1.92	-0.001	0.0138
-0.87	0.147	0.0126
0.15	0.279	0.0143
1.17	0.374	0.0149
2.18	0.460	0.0158
3.21	0.545	0.0171
4.21	0.633	0.0177
5.25	0.722	0.0183
6.27	0.810	0.0193
7.29	0.898	0.0195
8.30	0.975	0.0222
9.32	1.046	0.0245
10.33	1.104	0.0283
11.34	1.104	0.0377

$Rn = 149300.$

α	C_l	C_d
-2.00	0.043	0.0117
-0.88	0.170	0.0100
1.16	0.364	0.0109
3.22	0.557	0.0126
5.26	0.750	0.0142
7.29	0.931	0.0166
9.34	1.090	0.0209
10.35	1.142	0.0250
11.34	1.145	0.0362

$Rn = 200600.$

α	C_l	C_d
-4.03	-0.193	0.0177
-2.99	-0.056	0.0132
-1.90	0.056	0.0109
-0.93	0.135	0.0091
0.15	0.250	0.0084
1.18	0.348	0.0090
2.19	0.445	0.0096
3.21	0.542	0.0103
4.24	0.639	0.0113
5.25	0.730	0.0119
6.27	0.818	0.0127
7.29	0.903	0.0143
8.31	0.984	0.0165
9.32	1.055	0.0186
10.34	1.111	0.0222
11.33	1.131	0.0294

$Rn = 303700.$

α	C_l	C_d
-3.94	-0.144	0.0139
-2.92	-0.029	0.0105
-1.95	0.059	0.0095
-0.92	0.152	0.0083
0.12	0.259	0.0072
1.17	0.362	0.0077
2.17	0.452	0.0081
3.21	0.548	0.0089
4.23	0.639	0.0095
5.26	0.726	0.0104
6.27	0.810	0.0113
7.29	0.893	0.0129
8.31	0.972	0.0148
9.33	1.042	0.0172
10.34	1.099	0.0204

S3021B-PT

Fig. 12.92

$Rn = 99300.$

α	C_l	C_d
-2.96	-0.110	0.0189
-1.93	0.026	0.0148
-0.87	0.174	0.0135
0.15	0.270	0.0143
1.16	0.356	0.0165
2.19	0.441	0.0180
3.21	0.526	0.0196
4.22	0.611	0.0195
5.25	0.698	0.0195
6.26	0.785	0.0186
7.28	0.868	0.0202
8.29	0.944	0.0225
9.31	1.012	0.0262
10.31	1.048	0.0291

$Rn = 201300.$

α	C_l	C_d
-2.97	-0.082	0.0130
-1.93	0.008	0.0115
-0.94	0.091	0.0102
0.11	0.222	0.0093
1.14	0.318	0.0100
2.17	0.415	0.0106
3.19	0.512	0.0108
4.22	0.609	0.0111
5.24	0.700	0.0116
6.27	0.788	0.0128
7.27	0.869	0.0146
8.29	0.946	0.0164
9.30	1.007	0.0191
10.30	1.048	0.0233
11.31	1.057	0.0297

$Rn = 304800.$

α	C_l	C_d
-2.99	-0.092	0.0115
-1.96	0.001	0.0107
-0.98	0.092	0.0098
0.05	0.215	0.0079
1.08	0.326	0.0079
2.14	0.426	0.0085
3.19	0.523	0.0088
4.20	0.615	0.0095
5.23	0.705	0.0105
6.25	0.790	0.0120
7.27	0.872	0.0132
8.28	0.947	0.0149
9.30	1.010	0.0174
10.31	1.056	0.0207

S4061A-PT

Fig. 12.93

$Rn = 60400.$

α	C_l	C_d
-3.94	-0.124	0.0262
-2.92	0.008	0.0209
-1.90	0.128	0.0197
-0.87	0.266	0.0204
0.17	0.376	0.0239
1.20	0.468	0.0231
2.20	0.553	0.0275
3.22	0.635	0.0324
4.26	0.725	0.0311
5.26	0.801	0.0313
6.29	0.896	0.0294
7.31	0.978	0.0245
8.32	1.067	0.0296
9.33	1.080	0.0375
10.35	1.130	0.0427

$Rn = 99800.$

α	C_l	C_d
-3.92	-0.027	0.0171
-2.89	0.078	0.0160
-1.87	0.174	0.0163
-0.86	0.269	0.0149
0.17	0.366	0.0163
1.19	0.458	0.0168
2.21	0.554	0.0171
3.24	0.653	0.0170
4.25	0.746	0.0174
5.28	0.843	0.0187
6.28	0.933	0.0195
7.31	1.026	0.0210
8.32	1.078	0.0256
9.33	1.114	0.0324
10.34	1.132	0.0432

$Rn = 200400.$

α	C_l	C_d
-3.95	-0.076	0.0144
-2.93	0.027	0.0129
-1.89	0.131	0.0121
-0.86	0.236	0.0113
0.16	0.338	0.0102
1.18	0.448	0.0098
2.19	0.552	0.0101
3.22	0.652	0.0107
4.26	0.751	0.0117
5.27	0.846	0.0127
6.30	0.937	0.0143
7.30	1.008	0.0179
8.32	1.057	0.0252
9.33	1.089	0.0311
10.34	1.100	0.0413
11.33	1.098	0.0539

S4061B-PT

Fig. 12.94

$Rn = 60200.$

α	C_l	C_d
-2.91	-0.036	0.0268
-1.89	0.071	0.0250
-0.88	0.177	0.0209
0.15	0.287	0.0264
1.18	0.397	0.0299
2.20	0.510	0.0341
3.23	0.624	0.0339
4.24	0.721	0.0344
5.27	0.817	0.0374
6.28	0.911	0.0336
7.31	0.995	0.0310
8.33	1.069	0.0297
9.34	1.131	0.0314
10.33	1.169	0.0377
11.36	1.176	0.0458

$Rn = 100000.$

α	C_l	C_d
-2.90	0.082	0.0218
-1.87	0.194	0.0204
-0.84	0.296	0.0199
0.18	0.398	0.0209
1.20	0.500	0.0230
2.22	0.604	0.0241
3.24	0.700	0.0223
4.26	0.791	0.0222
5.28	0.886	0.0212
6.31	0.979	0.0206
7.31	1.065	0.0203
8.33	1.143	0.0225
9.34	1.210	0.0253
10.35	1.240	0.0312
11.37	1.245	0.0406

$Rn = 150800.$

α	C_l	C_d
-1.87	0.234	0.0157
0.16	0.419	0.0131
2.23	0.619	0.0135
4.25	0.812	0.0145
6.31	1.019	0.0157
7.33	1.100	0.0170
8.34	1.169	0.0198
9.34	1.223	0.0227
10.36	1.253	0.0284

$Rn = 198900.$

α	C_l	C_d
-4.97	-0.142	0.0442
-3.99	-0.039	0.0211
-2.95	0.055	0.0163
-1.91	0.154	0.0140
-0.91	0.252	0.0124
0.16	0.352	0.0116
1.16	0.457	0.0106
2.21	0.591	0.0108
3.24	0.692	0.0113
4.24	0.789	0.0116
5.28	0.890	0.0127
6.30	0.983	0.0133
7.32	1.069	0.0147
8.34	1.144	0.0171
9.35	1.207	0.0203
10.35	1.247	0.0265
11.36	1.267	0.0336
12.36	1.264	0.0421

$Rn = 300300.$

α	C_l	C_d
-3.92	-0.056	0.0176
-2.91	0.048	0.0134
-1.87	0.155	0.0115
-0.85	0.291	0.0101
0.18	0.393	0.0095
1.20	0.502	0.0086
2.21	0.603	0.0087
3.22	0.703	0.0095
4.25	0.803	0.0099
5.24	0.895	0.0109

S4061B-PT

Fig. 12.95

$Rn = 60900.$

α	C_l	C_d
-2.92	0.039	0.0247
-1.38	0.188	0.0200
0.15	0.337	0.0228
1.68	0.475	0.0273
3.23	0.600	0.0313
4.74	0.749	0.0292
6.27	0.884	0.0288
7.80	1.016	0.0291
9.32	1.117	0.0300
10.85	1.182	0.0359
12.36	1.199	0.0434

$Rn = 100700.$

α	C_l	C_d
-3.94	-0.048	0.0282
-2.39	0.114	0.0183
-0.87	0.253	0.0153
0.68	0.402	0.0144
2.20	0.558	0.0170
3.71	0.708	0.0202
5.27	0.852	0.0201
6.78	0.989	0.0191
8.32	1.114	0.0217
9.84	1.208	0.0253
11.36	1.231	0.0344
12.84	1.227	0.0493
14.35	1.193	0.0603

$Rn = 150200.$

α	C_l	C_d
-2.93	0.058	0.0172
-1.39	0.207	0.0134
0.15	0.355	0.0108
1.71	0.513	0.0117
3.21	0.663	0.0134
4.77	0.810	0.0143
6.27	0.948	0.0148
7.83	1.079	0.0170
9.35	1.179	0.0214
10.85	1.233	0.0308
12.33	1.233	0.0466

$Rn = 200500.$

α	C_l	C_d
-3.94	-0.060	0.0197
-2.41	0.086	0.0143
-0.86	0.239	0.0114
0.66	0.391	0.0095
2.20	0.550	0.0107
3.72	0.706	0.0113
5.28	0.855	0.0121
6.79	0.993	0.0137
8.33	1.109	0.0172
9.84	1.197	0.0218
11.34	1.241	0.0325
12.85	1.229	0.0516
14.35	1.197	0.0624

$Rn = 299700.$

α	C_l	C_d
-2.90	0.050	0.0140
-1.39	0.204	0.0111
0.14	0.362	0.0098
1.69	0.524	0.0088
3.22	0.682	0.0096
4.74	0.829	0.0105
6.28	0.970	0.0122
7.80	1.085	0.0150
9.34	1.178	0.0192
10.86	1.235	0.0270
12.34	1.243	0.0425

S4061B-PT

Fig. 12.96

$Rn = 150800.$

α	C_l	C_d
-1.87	0.234	0.0157
0.16	0.419	0.0131
2.23	0.619	0.0135
4.25	0.812	0.0145
6.31	1.019	0.0157
7.33	1.100	0.0170
8.34	1.169	0.0198
9.34	1.223	0.0227
10.36	1.253	0.0284

$Rn = 150200.$

α	C_l	C_d
-2.93	0.058	0.0172
-1.39	0.207	0.0134
0.15	0.355	0.0108
1.71	0.513	0.0117
3.21	0.663	0.0134
4.77	0.810	0.0143
6.27	0.948	0.0148
7.83	1.079	0.0170
9.35	1.179	0.0214
10.85	1.233	0.0308
12.33	1.233	0.0466

$Rn = 151000.$

α	C_l	C_d
-3.93	-0.051	0.0209
-2.39	0.092	0.0155
-0.88	0.241	0.0127
0.65	0.395	0.0110
2.21	0.556	0.0120
3.74	0.707	0.0135
5.25	0.853	0.0144
6.79	0.992	0.0155
8.32	1.115	0.0184
9.85	1.205	0.0233
11.34	1.239	0.0342

S4061B-PT

Fig. 12.97

$Rn = 150200.$

α	C_l	C_d
-2.93	0.058	0.0172
-1.39	0.207	0.0134
0.15	0.355	0.0108
1.71	0.513	0.0117
3.21	0.663	0.0134
4.77	0.810	0.0143
6.27	0.948	0.0148
7.83	1.079	0.0170
9.35	1.179	0.0214
10.85	1.233	0.0308
12.33	1.233	0.0466

$Rn = 151000.$

α	C_l	C_d
-3.93	-0.051	0.0209
-2.39	0.092	0.0155
-0.88	0.241	0.0127
0.65	0.395	0.0110
2.21	0.556	0.0120
3.74	0.707	0.0135
5.25	0.853	0.0144
6.79	0.992	0.0155
8.32	1.115	0.0184
9.85	1.205	0.0233
11.34	1.239	0.0342

$Rn = 299700.$

α	C_l	C_d
-2.90	0.050	0.0140
-1.39	0.204	0.0111
0.14	0.362	0.0098
1.69	0.524	0.0088
3.22	0.682	0.0096
4.74	0.829	0.0105
6.28	0.970	0.0122
7.80	1.085	0.0150
9.34	1.178	0.0192
10.86	1.235	0.0270
12.34	1.243	0.0425

$Rn = 301300.$

α	C_l	C_d
-2.91	0.029	0.0139
-1.38	0.183	0.0114
0.13	0.340	0.0098
1.67	0.501	0.0086
3.17	0.654	0.0093
4.73	0.807	0.0103
6.28	0.950	0.0118
7.80	1.071	0.0147
9.32	1.170	0.0185
10.84	1.232	0.0255

S4062-PT

Fig. 12.99

$Rn = 59300.$

α	C_l	C_d
-2.90	0.024	0.0291
-1.88	0.139	0.0236
-0.86	0.222	0.0226
0.16	0.305	0.0270
1.17	0.407	0.0294
2.21	0.502	0.0346
3.23	0.619	0.0361
4.26	0.761	0.0323
5.29	0.865	0.0274
6.30	0.953	0.0257
7.32	1.027	0.0229
8.33	1.107	0.0289
9.35	1.145	0.0293
10.35	1.158	0.0415
11.35	1.181	0.0451

$Rn = 98900.$

α	C_l	C_d
-3.90	0.031	0.0259
-2.89	0.131	0.0223
-1.86	0.238	0.0203
-0.84	0.324	0.0197
0.18	0.430	0.0220
1.21	0.529	0.0252
2.23	0.627	0.0256
3.25	0.726	0.0255
4.27	0.822	0.0222
5.29	0.916	0.0198
6.31	1.009	0.0191
7.33	1.090	0.0202
8.34	1.144	0.0227
9.34	1.168	0.0307
10.36	1.197	0.0384

$Rn = 150200.$

α	C_l	C_d
-3.92	0.066	0.0206
-2.88	0.159	0.0178
-1.84	0.251	0.0156
-0.82	0.335	0.0136
0.18	0.432	0.0141
1.19	0.531	0.0148
2.22	0.627	0.0146
3.25	0.731	0.0151
4.27	0.826	0.0147
5.29	0.923	0.0146
6.31	0.999	0.0147
7.32	1.072	0.0172
8.34	1.122	0.0226
9.34	1.157	0.0281
10.35	1.189	0.0341
11.36	1.203	0.0437
12.35	1.201	0.0621

$Rn = 201600.$

α	C_l	C_d
-4.93	-0.042	0.0269
-3.95	0.049	0.0194
-2.90	0.146	0.0162
-1.86	0.246	0.0139
-0.85	0.345	0.0116
0.19	0.442	0.0104
1.21	0.545	0.0108
2.23	0.650	0.0114
3.26	0.753	0.0117
4.28	0.853	0.0121
5.30	0.945	0.0125
6.31	1.026	0.0141
7.33	1.095	0.0173
8.34	1.147	0.0219
9.35	1.189	0.0274
10.36	1.217	0.0338
11.36	1.229	0.0447

$Rn = 304900.$

α	C_l	C_d
-3.91	0.016	0.0186
-2.88	0.121	0.0141
-1.86	0.225	0.0125
-0.86	0.337	0.0103
0.17	0.436	0.0087
1.19	0.541	0.0084
2.23	0.650	0.0088
3.25	0.751	0.0092
4.26	0.848	0.0099

5.29	0.939	0.0111
6.31	1.019	0.0134

S4180-PT

Fig. 12.100

$Rn = 106400.$

α	C_l	C_d
-2.91	0.013	0.0277
-0.88	0.202	0.0185
1.16	0.398	0.0167
3.23	0.596	0.0178
5.26	0.789	0.0210
7.29	0.968	0.0223
8.32	1.056	0.0199
9.33	1.116	0.0271
10.33	1.148	0.0408
11.34	1.171	0.0452
12.35	1.176	0.0543
13.32	1.110	0.1460

$Rn = 201800.$

α	C_l	C_d
-2.92	0.011	0.0156
-0.86	0.217	0.0127
1.18	0.423	0.0114
3.23	0.635	0.0123
5.27	0.833	0.0139
7.30	1.021	0.0162
8.32	1.100	0.0210
9.33	1.156	0.0300
10.32	1.175	0.0418
11.34	1.175	0.0647
12.35	1.162	0.0975

$Rn = 304700.$

α	C_l	C_d
-2.95	-0.005	0.0135
-1.93	0.111	0.0121
-0.87	0.221	0.0111
0.14	0.331	0.0108
1.17	0.431	0.0092
2.19	0.538	0.0094
3.20	0.639	0.0100
4.24	0.741	0.0106
5.26	0.838	0.0115
6.28	0.929	0.0123
7.30	1.017	0.0152
8.32	1.093	0.0193
9.32	1.146	0.0257
10.32	1.170	0.0418

S4233-PT

Fig. 12.101

$Rn = 60300.$

α	C_l	C_d
-2.92	-0.047	0.0263
-1.90	0.005	0.0284
-0.88	0.116	0.0310
0.15	0.220	0.0336
1.16	0.292	0.0381

$Rn = 101300.$

α	C_l	C_d
-6.97	-0.354	0.0290
-5.97	-0.255	0.0253
-4.94	-0.163	0.0211
-3.94	-0.075	0.0183
-2.91	0.011	0.0191
-1.90	0.076	0.0188
-0.89	0.149	0.0193
0.15	0.265	0.0204
1.17	0.373	0.0241
2.19	0.474	0.0260
3.22	0.552	0.0292
4.23	0.640	0.0292
5.25	0.752	0.0292
6.28	0.849	0.0298
7.30	0.962	0.0256
8.33	1.065	0.0242
9.34	1.159	0.0242
10.35	1.221	0.0267
11.35	1.199	0.0356

$Rn = 127300.$

α	C_l	C_d
-4.97	-0.224	0.0198
-3.95	-0.138	0.0182
-2.92	-0.057	0.0171
-1.90	0.019	0.0180
-0.87	0.117	0.0162
0.13	0.214	0.0162
1.16	0.306	0.0180
2.18	0.418	0.0181
3.20	0.528	0.0203
4.23	0.624	0.0212
5.25	0.734	0.0213
6.27	0.832	0.0212
7.28	0.935	0.0210
8.30	1.028	0.0221
9.33	1.111	0.0199

$Rn = 150200.$

α	C_l	C_d
-4.94	-0.144	0.0166
-3.92	-0.057	0.0156
-2.91	0.033	0.0149
-1.89	0.128	0.0149
-0.86	0.219	0.0147
0.16	0.313	0.0155
1.18	0.433	0.0152
2.20	0.538	0.0161
3.24	0.643	0.0172
4.25	0.745	0.0179
5.28	0.845	0.0182
6.30	0.945	0.0185
7.32	1.042	0.0188
8.35	1.140	0.0195
9.35	1.213	0.0213
10.37	1.234	0.0267

$Rn = 200200.$

α	C_l	C_d
-5.05	-0.174	0.0154
-3.99	-0.077	0.0136
-2.97	0.020	0.0126
-1.94	0.120	0.0123
-0.90	0.225	0.0121
0.13	0.321	0.0119
1.15	0.428	0.0124
2.18	0.542	0.0123
3.22	0.651	0.0133
4.24	0.754	0.0139
5.27	0.862	0.0147
6.30	0.964	0.0154
7.31	1.064	0.0162
8.34	1.158	0.0173
9.36	1.220	0.0197
10.36	1.234	0.0281

$Rn = 305100.$

α	C_l	C_d
-5.97	-0.269	0.0165
-4.95	-0.170	0.0139
-3.98	-0.074	0.0121
-2.98	0.025	0.0109
-1.98	0.124	0.0102
-0.98	0.226	0.0097
0.11	0.342	0.0097
1.17	0.451	0.0097
2.17	0.552	0.0100
3.23	0.663	0.0104
4.25	0.766	0.0112
5.27	0.869	0.0118
6.29	0.967	0.0125
7.32	1.062	0.0137
8.34	1.142	0.0153
9.34	1.191	0.0189
10.35	1.196	0.0265
11.35	1.186	0.0404

S4233-PT

Fig. 12.102

$Rn = 60200.$

α	C_l	C_d
-3.94	-0.136	0.0249
-2.92	-0.024	0.0262
-1.89	0.049	0.0266
-0.86	0.220	0.0264
0.15	0.306	0.0264
1.18	0.403	0.0282
2.20	0.500	0.0299
3.23	0.595	0.0290
4.24	0.691	0.0293
5.27	0.787	0.0311
6.28	0.881	0.0294
7.30	0.977	0.0316
8.32	1.064	0.0328
9.35	1.145	0.0370
10.36	1.234	0.0349
11.37	1.284	0.0368
12.36	1.234	0.0485

$Rn = 101700.$

α	C_l	C_d
-3.93	-0.055	0.0182
-2.91	0.021	0.0177
-1.88	0.099	0.0172
-0.87	0.175	0.0162
0.17	0.308	0.0160
1.18	0.409	0.0160
2.21	0.513	0.0164
3.22	0.613	0.0173
4.25	0.713	0.0182
5.27	0.815	0.0190
6.30	0.912	0.0204
7.31	1.006	0.0212
8.34	1.101	0.0226
9.35	1.189	0.0248
10.37	1.257	0.0263
11.36	1.233	0.0398

$Rn = 152100.$

α	C_l	C_d
-5.98	-0.253	0.0192
-4.97	-0.172	0.0164
-3.92	-0.080	0.0139
-2.92	0.011	0.0127
-1.88	0.108	0.0128
-0.88	0.201	0.0121
0.14	0.290	0.0122
1.17	0.411	0.0112
2.20	0.520	0.0118
3.20	0.622	0.0125
4.23	0.724	0.0144
5.26	0.824	0.0149
6.27	0.920	0.0162
7.30	1.014	0.0173
8.32	1.105	0.0197
9.35	1.189	0.0217
10.34	1.229	0.0301
11.36	1.197	0.0464

$Rn = 202200.$

α	C_l	C_d
-3.93	-0.076	0.0132
-2.92	0.024	0.0121
-1.88	0.124	0.0116
-0.87	0.222	0.0114
0.16	0.318	0.0112
1.18	0.415	0.0112
2.21	0.526	0.0113
3.23	0.629	0.0122
4.25	0.730	0.0130
5.27	0.826	0.0143
6.30	0.921	0.0154
7.31	1.013	0.0167
8.33	1.098	0.0183
9.35	1.173	0.0206
10.36	1.202	0.0258

$Rn = 298900.$

α	C_l	C_d
-6.00	-0.289	0.0162
-4.43	-0.144	0.0130
-2.92	0.002	0.0109
-1.41	0.152	0.0109
0.16	0.313	0.0114
1.68	0.460	0.0117
3.21	0.616	0.0125
4.77	0.770	0.0137
6.29	0.917	0.0151
7.82	1.056	0.0166
9.34	1.170	0.0205
10.84	1.162	0.0375
12.33	1.137	0.0629

SD2030-PT

Fig. 12.104

$Rn = 101000.$

α	C_l	C_d
-2.94	-0.119	0.0155
-0.91	0.094	0.0148

0.11	0.165	0.0150
1.66	0.376	0.0182
3.19	0.593	0.0156
4.72	0.743	0.0152
6.27	0.844	0.0187
7.76	0.914	0.0273

$Rn = 150200.$

α	C_l	C_d
-2.94	-0.089	0.0143
-1.39	0.053	0.0155
0.13	0.255	0.0150
1.66	0.471	0.0125
3.23	0.628	0.0115
4.74	0.749	0.0133
6.26	0.849	0.0186
7.78	0.942	0.0247
9.32	1.021	0.0384
10.81	1.062	0.0780
12.27	0.996	0.1826

$Rn = 198100.$

α	C_l	C_d
-3.96	-0.176	0.0154
-2.94	-0.061	0.0141
-1.93	0.060	0.0122
-0.90	0.176	0.0112
0.14	0.315	0.0104
1.18	0.436	0.0098
2.20	0.538	0.0095
3.23	0.640	0.0096
4.23	0.721	0.0116
5.25	0.794	0.0147
6.27	0.867	0.0182
7.28	0.936	0.0211
8.30	0.991	0.0277
9.30	1.036	0.0344
10.31	1.074	0.0536

$Rn = 303800.$

α	C_l	C_d
-5.08	-0.265	0.0176
-4.07	-0.146	0.0141
-2.91	0.009	0.0113
-1.92	0.129	0.0090
-0.95	0.217	0.0075
0.11	0.322	0.0069
1.07	0.424	0.0072
2.16	0.536	0.0073
3.20	0.635	0.0089
4.22	0.718	0.0111
5.24	0.795	0.0136
6.26	0.874	0.0167
7.28	0.945	0.0199
8.30	1.007	0.0244
9.30	1.053	0.0314

SD2083-PT

Fig. 12.106

$Rn = 63300.$

α	C_l	C_d
-3.95	-0.161	0.0229
-2.92	-0.066	0.0196
-1.90	0.030	0.0140
-0.88	0.142	0.0187
0.15	0.267	0.0215
1.18	0.395	0.0237
2.21	0.521	0.0253
3.23	0.635	0.0237
4.25	0.721	0.0203
5.27	0.792	0.0207
6.28	0.846	0.0228
7.29	0.885	0.0289
8.30	0.928	0.0352
9.31	0.968	0.0460

$Rn = 101200.$

α	C_l	C_d
-3.93	-0.081	0.0197
-2.90	0.040	0.0160
-1.88	0.148	0.0142
-0.85	0.265	0.0163
0.17	0.385	0.0170
1.20	0.494	0.0179
2.22	0.593	0.0169
3.24	0.679	0.0166
4.26	0.764	0.0162
5.27	0.825	0.0160
6.28	0.867	0.0211
7.29	0.908	0.0270
8.30	0.956	0.0331
9.31	0.993	0.0388
10.32	1.013	0.0492
11.29	1.002	0.0893

$Rn = 200900.$

α	C_l	C_d
-3.91	0.003	0.0143
-2.90	0.095	0.0123
-1.87	0.191	0.0097
-0.83	0.303	0.0098
0.17	0.400	0.0103
1.20	0.499	0.0109
2.23	0.599	0.0108
3.24	0.694	0.0106
4.26	0.767	0.0123
5.27	0.821	0.0163
6.29	0.876	0.0212
7.29	0.929	0.0261
8.31	0.974	0.0323
9.31	1.010	0.0429

$Rn = 300700.$

α	C_l	C_d
-3.92	-0.006	0.0121
-2.90	0.088	0.0109
-1.89	0.184	0.0092
-0.85	0.302	0.0080
0.18	0.405	0.0083
1.19	0.505	0.0088
2.21	0.603	0.0089
3.24	0.693	0.0094
4.24	0.761	0.0121
5.27	0.821	0.0162

SD5060-PT

Fig. 12.107

$Rn = 60000.$

α	C_l	C_d
-3.95	-0.211	0.0207
-2.94	-0.137	0.0193
-1.92	-0.056	0.0144
-0.90	0.049	0.0145
0.14	0.201	0.0163
1.18	0.372	0.0172
2.18	0.484	0.0206
3.20	0.563	0.0204
4.23	0.645	0.0228
5.25	0.726	0.0232
6.26	0.806	0.0232
7.29	0.876	0.0283
8.30	0.935	0.0345
9.31	0.983	0.0460
10.31	1.004	0.0627

$Rn = 99800.$

α	C_l	C_d
-2.94	-0.128	0.0154
-1.91	0.004	0.0136
-0.87	0.151	0.0125
0.15	0.291	0.0134
1.19	0.393	0.0135
2.20	0.479	0.0138
3.21	0.566	0.0152
4.23	0.658	0.0155
5.25	0.751	0.0171
6.27	0.835	0.0195
7.29	0.918	0.0215
8.31	0.983	0.0272
9.32	1.045	0.0327
10.32	1.092	0.0403

$Rn = 150400.$

α	C_l	C_d
-4.98	-0.320	0.0154
-3.96	-0.209	0.0142
-2.92	-0.081	0.0124
-1.92	0.026	0.0113
-0.89	0.127	0.0101
0.15	0.231	0.0103
1.15	0.325	0.0108
2.19	0.426	0.0119
3.20	0.524	0.0116
4.23	0.619	0.0129
5.25	0.711	0.0148
6.27	0.801	0.0156
7.28	0.884	0.0196
8.30	0.958	0.0239
9.32	1.021	0.0268
10.32	1.071	0.0330
11.33	1.089	0.0431

$Rn = 202500.$

α	C_l	C_d
-4.96	-0.269	0.0135
-3.95	-0.142	0.0121
-2.91	-0.022	0.0109
-1.90	0.077	0.0104
-0.88	0.165	0.0097
0.15	0.273	0.0092
1.17	0.373	0.0093
2.20	0.474	0.0097
3.22	0.572	0.0100
4.24	0.670	0.0113
5.26	0.758	0.0132
6.27	0.845	0.0151
7.30	0.931	0.0178
8.31	1.008	0.0212
9.32	1.072	0.0245
10.34	1.123	0.0296
11.34	1.145	0.0400
12.34	1.124	0.0605

$Rn = 304100.$

α	C_l	C_d
-6.07	-0.371	0.0132
-5.05	-0.247	0.0115
-4.01	-0.140	0.0108
-2.98	-0.042	0.0100
-1.93	0.057	0.0095
-0.91	0.157	0.0086
0.13	0.259	0.0076
1.16	0.371	0.0075
2.19	0.475	0.0081
3.22	0.572	0.0092
4.23	0.666	0.0107
5.25	0.755	0.0124
6.26	0.841	0.0138
7.30	0.929	0.0160
8.30	1.007	0.0189

SD6060-PT

Fig. 12.109

$Rn = 59100.$

α	C_l	C_d
-6.00	-0.399	0.0288
-4.97	-0.331	0.0223
-3.96	-0.277	0.0158
-2.96	-0.187	0.0156
-1.93	-0.125	0.0145
-0.93	-0.009	0.0186
0.12	0.143	0.0217
1.15	0.273	0.0231
2.17	0.395	0.0258
3.19	0.490	0.0249
4.21	0.579	0.0258
5.23	0.661	0.0242
6.25	0.742	0.0218
7.26	0.813	0.0240
8.28	0.866	0.0312
9.28	0.892	0.0457
10.28	0.906	0.0662

$Rn = 100600.$

α	C_l	C_d
-5.98	-0.388	0.0237
-4.99	-0.322	0.0183
-3.96	-0.248	0.0145
-2.95	-0.161	0.0132
-1.92	-0.035	0.0138
-0.89	0.144	0.0151
0.16	0.249	0.0169
1.17	0.341	0.0177
2.19	0.429	0.0180
3.21	0.519	0.0180
4.22	0.611	0.0170
5.25	0.704	0.0176
6.26	0.788	0.0174
7.27	0.863	0.0206
8.29	0.921	0.0289
9.30	0.960	0.0374

$Rn = 155700.$

α	C_l	C_d
-5.99	-0.403	0.0206

-4.97	-0.328	0.0159
-3.95	-0.197	0.0123
-2.93	-0.083	0.0112
-1.91	-0.012	0.0114
-0.89	0.115	0.0119
0.13	0.211	0.0117
1.15	0.300	0.0118
2.18	0.398	0.0115
3.21	0.499	0.0123
4.23	0.598	0.0126
5.24	0.695	0.0134
6.27	0.784	0.0154
7.27	0.860	0.0199
8.28	0.916	0.0251
9.31	0.950	0.0336
10.29	0.961	0.0465

$Rn = 199700.$

α	C_l	C_d
-3.97	-0.154	0.0117
-2.93	-0.076	0.0102
-1.92	-0.006	0.0102
-0.90	0.078	0.0101
0.15	0.213	0.0097
1.16	0.305	0.0098
2.18	0.404	0.0100
3.20	0.507	0.0103
4.22	0.609	0.0109
5.25	0.707	0.0121
6.26	0.794	0.0143
7.28	0.873	0.0179
8.30	0.934	0.0239
9.31	0.971	0.0315
10.31	0.985	0.0420

$Rn = 307400.$

α	C_l	C_d
-3.99	-0.191	0.0112
-2.96	-0.099	0.0094
-1.94	-0.012	0.0082
-0.91	0.078	0.0077
0.12	0.177	0.0080
1.15	0.302	0.0077
2.18	0.407	0.0078
3.20	0.510	0.0087
4.22	0.610	0.0095
5.24	0.705	0.0109
6.27	0.794	0.0131
7.28	0.871	0.0170
8.29	0.937	0.0212
9.30	0.978	0.0284

SD6060-PT

Fig. 12.110

$Rn = 100900.$

α	C_l	C_d
-3.96	-0.209	0.0131
-2.93	-0.094	0.0129
-1.93	0.001	0.0128
-0.89	0.119	0.0132
0.12	0.200	0.0133
1.15	0.287	0.0133
2.17	0.381	0.0139
3.20	0.480	0.0150
4.22	0.582	0.0168
5.24	0.679	0.0167
6.25	0.771	0.0198
7.28	0.846	0.0268
8.29	0.897	0.0331
9.30	0.937	0.0394
10.30	0.972	0.0611
11.30	0.967	0.0957

$Rn = 154200.$

α	C_l	C_d
-3.96	-0.180	0.0123
-2.94	-0.105	0.0112
-1.91	-0.033	0.0106
-0.91	0.092	0.0107
0.14	0.200	0.0103
1.15	0.297	0.0106
2.18	0.399	0.0113
3.19	0.499	0.0121
4.22	0.601	0.0134
5.24	0.701	0.0143
6.26	0.796	0.0167
7.28	0.879	0.0209
8.28	0.935	0.0274
9.30	0.965	0.0370
10.30	0.980	0.0466
11.30	0.975	0.0653

$Rn = 205500.$

α	C_l	C_d
-3.96	-0.186	0.0121
-2.94	-0.102	0.0094
-1.91	-0.023	0.0094
-0.89	0.067	0.0096
0.11	0.200	0.0098
1.15	0.299	0.0094
2.16	0.398	0.0107
3.19	0.501	0.0109
4.22	0.605	0.0122
5.24	0.707	0.0131
6.26	0.805	0.0151
7.28	0.884	0.0192
8.30	0.944	0.0249
9.29	0.977	0.0328
10.30	0.983	0.0455
11.30	0.975	0.0669

$Rn = 313800.$

α	C_l	C_d
-3.98	-0.212	0.0119
-2.93	-0.113	0.0107
-1.92	-0.026	0.0092
-0.90	0.062	0.0095
0.12	0.161	0.0097
1.16	0.288	0.0098
2.17	0.397	0.0098
3.21	0.504	0.0103
4.22	0.608	0.0110
5.23	0.709	0.0121
6.26	0.804	0.0143
7.27	0.877	0.0179
8.29	0.942	0.0233
9.29	0.978	0.0297
10.30	0.981	0.0415

SD6060-PT

Fig. 12.111

$Rn = 103200.$

α	C_l	C_d
-2.94	-0.123	0.0136
-1.42	0.006	0.0138
0.13	0.177	0.0150
1.66	0.317	0.0153
3.19	0.468	0.0150
4.73	0.609	0.0178
6.24	0.731	0.0214
7.26	0.804	0.0230
8.28	0.859	0.0358
9.28	0.915	0.0414

$Rn = 152000.$

α	C_l	C_d
-2.94	-0.114	0.0114
-1.41	0.016	0.0107
0.14	0.191	0.0114
1.66	0.334	0.0114
3.20	0.491	0.0123
4.74	0.640	0.0137
6.25	0.770	0.0180
7.27	0.846	0.0239
8.28	0.892	0.0281
9.30	0.923	0.0398
10.30	0.954	0.0564
11.29	0.954	0.1261

$Rn = 200900.$

α	C_l	C_d
-2.94	-0.108	0.0098
-1.41	0.015	0.0095
0.13	0.200	0.0098
1.67	0.353	0.0101
3.20	0.510	0.0106
4.74	0.663	0.0125
6.27	0.797	0.0159
7.27	0.873	0.0198
8.30	0.930	0.0283
9.29	0.965	0.0334
10.30	0.981	0.0450
11.31	0.987	0.0711

$Rn = 309100.$

α	C_l	C_d
-2.94	-0.110	0.0102
-1.41	0.022	0.0090
0.12	0.167	0.0081
1.67	0.352	0.0087
3.21	0.512	0.0092
4.75	0.667	0.0109
6.26	0.801	0.0145
7.28	0.879	0.0184
8.30	0.942	0.0241
9.31	0.977	0.0318
10.30	0.983	0.0437

SD6080-PT

Fig. 12.113

$Rn = 59400.$

α	C_l	C_d
-2.90	-0.001	0.0246
-1.89	0.101	0.0211
-0.88	0.213	0.0215
0.17	0.350	0.0252
1.19	0.455	0.0295
2.21	0.563	0.0327
3.24	0.661	0.0334
4.26	0.742	0.0310
5.27	0.838	0.0334
6.29	0.923	0.0310
7.30	0.992	0.0258
8.32	1.061	0.0267
9.33	1.112	0.0291
10.34	1.142	0.0382
11.33	1.144	0.0398
12.35	1.137	0.0548

$Rn = 100400.$

α	C_l	C_d
-3.90	-0.017	0.0256
-2.89	0.130	0.0204
-1.88	0.235	0.0166
-0.83	0.349	0.0167
0.18	0.443	0.0185
1.21	0.536	0.0189
2.23	0.633	0.0209
3.25	0.731	0.0224
4.27	0.824	0.0220
5.29	0.914	0.0203
6.30	1.003	0.0192
7.33	1.090	0.0199
8.35	1.166	0.0217
9.37	1.225	0.0266
10.36	1.232	0.0324
11.35	1.215	0.0451

$Rn = 149700.$

α	C_l	C_d
-1.89	0.240	0.0133
0.18	0.431	0.0119
2.23	0.634	0.0134
3.24	0.731	0.0141
4.27	0.829	0.0150
6.30	1.020	0.0160
7.32	1.103	0.0175
8.34	1.171	0.0201
9.35	1.223	0.0257

$Rn = 200500.$

α	C_l	C_d
-3.94	0.036	0.0157
-2.88	0.129	0.0132
-1.88	0.224	0.0117
-0.84	0.315	0.0091
0.13	0.417	0.0094
1.17	0.521	0.0099
2.21	0.627	0.0106
3.23	0.729	0.0115
4.26	0.829	0.0122
5.27	0.923	0.0128
6.31	1.011	0.0141
7.32	1.087	0.0157
8.35	1.160	0.0192
9.35	1.213	0.0235
10.34	1.221	0.0339
11.34	1.208	0.0499

$Rn = 301100.$

α	C_l	C_d
-4.93	-0.081	0.0196

-3.94	0.011	0.0134
-2.91	0.113	0.0112
-1.91	0.214	0.0097
-0.87	0.320	0.0082
0.13	0.416	0.0072
1.16	0.519	0.0080
2.16	0.621	0.0086
3.16	0.719	0.0092
4.13	0.811	0.0103
5.19	0.910	0.0110
6.27	1.003	0.0122
7.26	1.077	0.0148
8.31	1.152	0.0175

SD6080-PT

Fig. 12.114

$Rn = 100100.$

α	C_l	C_d
-2.90	0.075	0.0222
-1.35	0.243	0.0150
0.17	0.381	0.0163
1.71	0.522	0.0161
3.24	0.670	0.0158
4.78	0.807	0.0174
6.29	0.934	0.0201
7.31	1.014	0.0247
8.32	1.073	0.0225
9.34	1.106	0.0406
10.32	1.125	0.0482
11.34	1.105	0.1122

$Rn = 151900.$

α	C_l	C_d
-3.92	0.028	0.0169
-2.88	0.125	0.0145
-1.87	0.210	0.0124
-0.85	0.302	0.0111
0.17	0.406	0.0108
1.20	0.510	0.0115
2.23	0.622	0.0123
3.23	0.709	0.0134
4.26	0.803	0.0150
5.29	0.889	0.0165
6.29	0.973	0.0190
7.32	1.057	0.0222
8.32	1.136	0.0244
9.35	1.181	0.0314
10.33	1.181	0.0494
11.35	1.161	0.0795

$Rn = 199400.$

α	C_l	C_d
-3.92	0.036	0.0143
-2.89	0.133	0.0118
-1.87	0.230	0.0112
-0.85	0.323	0.0089
0.17	0.426	0.0098
1.19	0.527	0.0099
2.23	0.629	0.0117
3.24	0.724	0.0133
4.27	0.818	0.0148
5.28	0.910	0.0162
6.32	1.003	0.0178
7.32	1.085	0.0201
8.35	1.166	0.0225
9.35	1.210	0.0285
10.36	1.199	0.0434
11.36	1.174	0.0825

$Rn = 308500.$

α	C_l	C_d
-3.92	0.028	0.0130
-2.90	0.127	0.0109
-1.88	0.230	0.0101
-0.87	0.329	0.0086
0.17	0.427	0.0091
1.21	0.528	0.0106
2.21	0.627	0.0119
3.22	0.725	0.0130
4.24	0.820	0.0140
5.27	0.911	0.0150
6.28	1.000	0.0164
7.32	1.086	0.0179
8.34	1.161	0.0204
9.34	1.188	0.0297
10.34	1.186	0.0443

SD6080-PT

Fig. 12.115

$Rn = 100500.$

α	C_l	C_d
-2.88	0.164	0.0153
-1.37	0.287	0.0143
0.16	0.434	0.0149
1.70	0.582	0.0150
3.25	0.730	0.0169
4.77	0.874	0.0186
6.30	1.013	0.0208
7.32	1.095	0.0241
8.35	1.172	0.0261
9.34	1.212	0.0340
10.34	1.205	0.0501

$Rn = 153800.$

α	C_l	C_d
-2.88	0.133	0.0137
-1.36	0.270	0.0101
0.18	0.429	0.0107
1.72	0.590	0.0118
3.24	0.739	0.0134
4.79	0.893	0.0153
6.29	1.026	0.0163
7.32	1.109	0.0192
8.34	1.180	0.0221
9.35	1.215	0.0308
10.35	1.208	0.0440
11.36	1.189	0.0718

$Rn = 204800.$

α	C_l	C_d
-2.89	0.136	0.0123
-1.37	0.280	0.0097
0.17	0.431	0.0094
1.69	0.586	0.0102
3.24	0.741	0.0115
4.78	0.891	0.0135
6.30	1.026	0.0158
7.32	1.113	0.0169
8.35	1.182	0.0221
9.35	1.212	0.0264
10.34	1.208	0.0405

$Rn = 304200.$

α	C_l	C_d
-2.91	0.121	0.0114
-1.39	0.279	0.0098
0.14	0.421	0.0091
1.70	0.583	0.0099
3.23	0.739	0.0116
4.76	0.885	0.0128
6.31	1.024	0.0147
7.31	1.110	0.0165
8.34	1.176	0.0202
9.34	1.207	0.0274
10.35	1.204	0.0443

SD6080-PT

Fig. 12.116

$Rn = 99100.$

α	C_l	C_d
-2.88	0.150	0.0165
-1.36	0.285	0.0143
0.19	0.438	0.0144
1.72	0.595	0.0145
3.25	0.742	0.0164
4.77	0.885	0.0186
6.30	1.024	0.0210
7.33	1.112	0.0199
8.34	1.182	0.0246
9.35	1.218	0.0337
10.35	1.210	0.0444

$Rn = 149300.$

α	C_l	C_d
-2.88	0.140	0.0141
-1.36	0.280	0.0102
0.19	0.437	0.0104
1.72	0.593	0.0116
3.24	0.743	0.0133
4.77	0.890	0.0157
6.31	1.032	0.0173
7.33	1.113	0.0179
8.34	1.180	0.0215
9.34	1.211	0.0321
10.34	1.203	0.0461

$Rn = 197800.$

α	C_l	C_d
-2.88	0.127	0.0125
-1.38	0.274	0.0096
0.18	0.431	0.0094
1.72	0.591	0.0103
3.25	0.743	0.0118
4.78	0.897	0.0138
6.31	1.042	0.0154
7.32	1.121	0.0177
8.33	1.188	0.0215
9.35	1.219	0.0292
10.34	1.213	0.0506
11.35	1.197	0.0709

$Rn = 300300.$

α	C_l	C_d
-2.89	0.114	0.0124
-1.39	0.267	0.0107
0.16	0.419	0.0093
1.70	0.581	0.0099
3.24	0.739	0.0110
4.78	0.889	0.0119
6.30	1.025	0.0139
7.32	1.095	0.0171
8.33	1.160	0.0206
9.34	1.190	0.0286
10.34	1.188	0.0479
11.32	1.169	0.0775

SD6080-PT

Fig. 12.117

$Rn = 98100.$

α	C_l	C_d
-2.90	0.087	0.0205
-1.35	0.267	0.0149
0.17	0.417	0.0180
1.72	0.558	0.0202
3.24	0.698	0.0243
4.77	0.835	0.0220
6.30	0.981	0.0217
7.82	1.108	0.0231
9.36	1.209	0.0264
10.85	1.210	0.0474

$Rn = 151700.$

α	C_l	C_d
-2.90	0.074	0.0157
-1.39	0.211	0.0125
0.12	0.354	0.0118
1.67	0.510	0.0119
3.23	0.672	0.0136
4.74	0.826	0.0149
6.27	0.977	0.0155
7.81	1.108	0.0179
9.33	1.215	0.0241

$Rn = 200000.$

α	C_l	C_d
-2.93	0.056	0.0148
-1.38	0.212	0.0121
0.16	0.358	0.0102
1.69	0.521	0.0108
3.23	0.680	0.0117
4.75	0.835	0.0130
6.28	0.983	0.0144
7.79	1.110	0.0168
9.35	1.216	0.0226
10.86	1.225	0.0417
12.35	1.190	0.0860

$Rn = 299800.$

α	C_l	C_d
-2.98	0.048	0.0131
-1.40	0.214	0.0105
0.14	0.367	0.0080
1.64	0.528	0.0090
3.19	0.691	0.0098
4.71	0.844	0.0109
6.28	0.990	0.0125
7.80	1.116	0.0167
9.32	1.210	0.0230

SD7003-PT

Fig. 12.118

$Rn = 60300.$

α	C_l	C_d

-2.95	-0.172	0.0122
-1.41	-0.039	0.0114
0.12	0.142	0.0121
1.67	0.370	0.0158
3.20	0.501	0.0193
4.73	0.651	0.0223
6.26	0.779	0.0267
7.78	0.871	0.0399
9.30	0.978	0.0736

$Rn = 102000.$

α	C_l	C_d
-2.93	-0.138	0.0116
-1.41	-0.014	0.0091
0.13	0.176	0.0125
1.67	0.362	0.0123
3.20	0.494	0.0142
4.73	0.632	0.0158
6.26	0.784	0.0183
7.78	0.904	0.0254
9.31	0.995	0.0356
10.81	0.936	0.1200

$Rn = 151800.$

α	C_l	C_d
-2.93	-0.119	0.0101
-1.40	0.008	0.0091
0.13	0.209	0.0095
1.67	0.362	0.0095
3.19	0.511	0.0112
4.73	0.658	0.0143
6.26	0.797	0.0165
7.79	0.917	0.0227
9.31	1.015	0.0325
10.82	0.995	0.0949

$Rn = 200800.$

α	C_l	C_d
-2.92	-0.115	0.0097
-1.40	0.026	0.0081
0.14	0.199	0.0079
1.66	0.350	0.0091
3.20	0.507	0.0110
4.74	0.657	0.0128
6.28	0.799	0.0153
7.80	0.926	0.0222
9.31	1.024	0.0308
10.83	0.982	0.1169
11.82	0.905	0.1858

$Rn = 300300.$

α	C_l	C_d
-2.94	-0.112	0.0093
-1.91	0.000	0.0079
-0.90	0.103	0.0074
0.14	0.196	0.0072
1.15	0.301	0.0078
2.18	0.409	0.0084
3.20	0.516	0.0095
4.23	0.620	0.0109
5.25	0.719	0.0123
6.26	0.814	0.0138
7.28	0.903	0.0168
8.31	0.983	0.0205
9.32	1.053	0.0253
10.34	1.101	0.0337
11.32	1.098	0.0505

SD7003-PT

Fig. 12.119

$Rn = 99600.$

α	C_l	C_d
-2.94	-0.131	0.0129
-1.91	-0.053	0.0111
-0.90	0.036	0.0110
0.13	0.181	0.0108
1.16	0.318	0.0124
2.19	0.413	0.0127
3.19	0.502	0.0129
4.21	0.598	0.0145
5.23	0.692	0.0166
6.25	0.783	0.0185
7.28	0.865	0.0231
8.29	0.936	0.0290
9.30	0.992	0.0376
10.32	1.024	0.0480
11.29	0.901	0.1563

$Rn = 153300.$

α	C_l	C_d
-2.93	-0.119	0.0108
-1.92	-0.035	0.0096
-0.89	0.058	0.0088
0.14	0.203	0.0088
1.15	0.302	0.0096
2.17	0.400	0.0103
3.20	0.504	0.0119
4.21	0.601	0.0126
5.24	0.699	0.0143
6.26	0.793	0.0158
7.28	0.878	0.0194
8.30	0.950	0.0251
9.31	1.013	0.0327
10.32	1.054	0.0416
11.28	0.925	0.1646

$Rn = 201500.$

α	C_l	C_d
-2.93	-0.126	0.0101
-1.92	-0.038	0.0086
-0.91	0.072	0.0079
0.12	0.184	0.0076
1.14	0.286	0.0086
2.18	0.392	0.0094
3.21	0.496	0.0102
4.22	0.596	0.0115
5.24	0.696	0.0131
6.27	0.791	0.0144
7.28	0.878	0.0177
8.30	0.953	0.0225
9.31	1.022	0.0284
10.33	1.070	0.0353

$Rn = 303700.$

α	C_l	C_d
-3.98	-0.214	0.0104
-2.92	-0.112	0.0093
-1.92	-0.005	0.0080
-0.91	0.099	0.0074
0.12	0.191	0.0073
1.16	0.296	0.0081
2.17	0.402	0.0084
3.19	0.507	0.0098
4.21	0.611	0.0109
5.23	0.711	0.0121
6.27	0.809	0.0138
7.29	0.899	0.0167
8.31	0.978	0.0207
9.32	1.049	0.0248
10.34	1.099	0.0325
11.33	1.100	0.0490

SD7003-PT

Fig. 12.120

$Rn = 199500.$

α	C_l	C_d
-2.96	-0.113	0.0101
-1.40	0.042	0.0082
0.12	0.201	0.0079
1.66	0.353	0.0093
3.20	0.507	0.0111
4.74	0.659	0.0133
6.25	0.801	0.0160
7.79	0.927	0.0210
9.32	1.029	0.0302
10.82	1.078	0.0455
11.80	0.921	0.1899

$Rn = 301600.$

α	C_l	C_d
-2.92	-0.094	0.0092
-1.41	0.055	0.0080
0.13	0.195	0.0076
1.66	0.354	0.0083
3.19	0.511	0.0100
4.73	0.664	0.0114
6.25	0.808	0.0141
7.80	0.939	0.0186
9.31	1.048	0.0245
10.82	1.108	0.0374

SD7003-PT

Fig. 12.121

$Rn = 201200.$

α	C_l	C_d
-2.94	-0.111	0.0099
-1.41	0.040	0.0082
0.12	0.206	0.0079
1.66	0.359	0.0089
3.19	0.513	0.0111
4.72	0.664	0.0131
6.25	0.806	0.0151
7.79	0.933	0.0215
9.31	1.036	0.0293
10.83	1.077	0.0450
11.78	0.921	0.1799
12.80	0.864	0.2182

$Rn = 298000.$

α	C_l	C_d
-2.94	-0.110	0.0091
-1.40	0.057	0.0077
0.11	0.195	0.0072
1.67	0.353	0.0086
3.19	0.511	0.0099
4.73	0.664	0.0117
6.27	0.809	0.0139
7.80	0.939	0.0187
9.31	1.047	0.0252
10.83	1.106	0.0376
11.79	0.942	0.1814
12.79	0.874	0.2202

SD7003-PT

Fig. 12.122

$Rn = 101700.$

α	C_l	C_d
-2.95	-0.133	0.0120
-1.42	0.000	0.0100
0.14	0.207	0.0115
1.66	0.366	0.0121
3.19	0.501	0.0150
4.74	0.645	0.0167
6.26	0.789	0.0208
7.79	0.906	0.0278
9.31	0.992	0.0417
10.79	0.888	0.1601

$Rn = 150600.$

α	C_l	C_d
-2.94	-0.099	0.0114
-1.40	0.037	0.0100
0.14	0.212	0.0092
1.67	0.362	0.0104
3.19	0.518	0.0127
4.74	0.666	0.0146
6.27	0.808	0.0174
7.78	0.926	0.0236
9.32	1.024	0.0346
10.79	0.954	0.1398

$Rn = 205000.$

α	C_l	C_d
-2.95	-0.109	0.0112
-1.40	0.034	0.0095
0.15	0.189	0.0086
1.66	0.354	0.0096
3.18	0.510	0.0109
4.74	0.662	0.0130
6.27	0.805	0.0157
7.79	0.929	0.0214
9.31	1.030	0.0298
10.82	1.076	0.0471

$Rn = 300500.$

α	C_l	C_d
-2.94	-0.103	0.0110
-1.40	0.046	0.0093
0.12	0.192	0.0081
1.66	0.358	0.0085
3.20	0.517	0.0100
4.74	0.672	0.0118
6.27	0.816	0.0146
7.78	0.943	0.0188
9.32	1.052	0.0258
10.82	1.108	0.0391

SD7003-PT

Fig. 12.123

$Rn = 99700.$

α	C_l	C_d
-3.96	-0.234	0.0159

-2.73	-0.123	0.0116
-1.53	-0.038	0.0101
-0.30	0.106	0.0121
0.96	0.297	0.0123
2.17	0.404	0.0134
3.40	0.517	0.0145
4.63	0.633	0.0166
5.85	0.744	0.0200
7.07	0.845	0.0231
8.29	0.929	0.0311
9.50	0.995	0.0424
10.71	0.928	0.1357

$Rn = 151800.$

α	C_l	C_d
-3.96	-0.210	0.0129
-2.73	-0.093	0.0108
-1.51	0.002	0.0091
-0.28	0.161	0.0089
0.94	0.286	0.0093
2.17	0.404	0.0108
3.40	0.525	0.0121
4.63	0.642	0.0140
5.85	0.756	0.0161
7.08	0.863	0.0199
8.29	0.951	0.0254
9.51	1.023	0.0343
10.73	1.064	0.0461

$Rn = 202300.$

α	C_l	C_d
-2.96	-0.109	0.0112
-1.72	0.010	0.0094
-0.49	0.122	0.0081
0.74	0.259	0.0081
1.97	0.386	0.0090
3.21	0.512	0.0108
4.43	0.632	0.0123
5.64	0.747	0.0139
6.87	0.859	0.0163
8.09	0.955	0.0215
9.32	1.035	0.0272
10.52	1.087	0.0376
11.67	0.956	0.1591

$Rn = 300700.$

α	C_l	C_d
-3.95	-0.199	0.0119
-2.74	-0.079	0.0105
-1.52	0.041	0.0089
-0.29	0.157	0.0079
0.94	0.284	0.0078
2.18	0.414	0.0090
3.40	0.538	0.0103
4.64	0.659	0.0114
5.86	0.775	0.0130
7.07	0.882	0.0162
8.30	0.977	0.0203
9.52	1.057	0.0261
10.73	1.105	0.0360
11.98	0.952	0.1724
13.07	0.872	0.2246

SD7003-PT

Fig. 12.124

$Rn = 100600.$

α	C_l	C_d
-3.96	-0.222	0.0153
-2.43	-0.090	0.0121
-0.89	0.049	0.0113
0.65	0.271	0.0115
2.18	0.415	0.0128
3.71	0.559	0.0152
5.25	0.702	0.0178
6.78	0.834	0.0214
8.30	0.939	0.0324
9.81	1.013	0.0496
11.30	0.863	0.1808

$Rn = 150200.$

α	C_l	C_d
-3.96	-0.217	0.0131
-2.73	-0.101	0.0106
-1.52	-0.003	0.0090
-0.28	0.161	0.0093
0.95	0.291	0.0094
2.18	0.410	0.0114
3.41	0.530	0.0127
4.63	0.647	0.0138
5.86	0.763	0.0161
7.09	0.869	0.0196
8.29	0.954	0.0266
9.51	1.028	0.0353
10.72	1.066	0.0491
11.87	0.881	0.1911

$Rn = 201400.$

α	C_l	C_d
-3.94	-0.197	0.0121
-2.74	-0.078	0.0098
-1.51	0.039	0.0084
-0.29	0.163	0.0078
0.96	0.286	0.0084
2.18	0.409	0.0100
3.39	0.533	0.0111
4.64	0.655	0.0127
5.86	0.769	0.0148
7.08	0.878	0.0179
8.30	0.969	0.0236
9.51	1.045	0.0311
10.72	1.087	0.0437

$Rn = 301600.$

α	C_l	C_d
-3.97	-0.202	0.0108
-2.73	-0.078	0.0095
-1.49	0.046	0.0080
-0.27	0.162	0.0077
0.94	0.286	0.0079
2.18	0.415	0.0090
3.40	0.541	0.0097
4.63	0.661	0.0112
5.86	0.779	0.0134
7.09	0.888	0.0164
8.30	0.983	0.0208
9.53	1.065	0.0265
10.73	1.109	0.0366
11.74	0.942	0.1817
13.11	0.868	0.2264

SD7032A-PT

Fig. 12.126

$Rn = 64200.$

α	C_l	C_d
-3.93	-0.152	0.0253
-2.92	-0.076	0.0188
-1.91	0.022	0.0167
-0.87	0.149	0.0202
0.16	0.315	0.0224
1.19	0.446	0.0195
2.21	0.525	0.0208
3.22	0.610	0.0215
4.24	0.692	0.0223
5.26	0.779	0.0228
6.28	0.851	0.0252
7.29	0.927	0.0273
8.31	0.998	0.0329
9.33	1.065	0.0328
10.34	1.117	0.0376
11.34	1.151	0.0424
12.33	1.109	0.0494
13.28	0.813	0.2163

$Rn = 104600.$

α	C_l	C_d
-3.93	-0.045	0.0221
-2.90	0.098	0.0186
-1.86	0.233	0.0150
-0.83	0.360	0.0134
0.19	0.472	0.0131
1.22	0.567	0.0137
2.24	0.654	0.0141
3.25	0.744	0.0156
4.27	0.831	0.0164
5.29	0.915	0.0179
6.31	0.997	0.0209
7.32	1.076	0.0221
8.35	1.154	0.0242
9.36	1.214	0.0271
10.37	1.243	0.0341
11.38	1.267	0.0407

$Rn = 200100.$

α	C_l	C_d
-3.92	0.095	0.0168
-2.88	0.213	0.0132
-1.85	0.319	0.0105
-0.84	0.404	0.0097
0.19	0.499	0.0098
1.20	0.594	0.0108
2.24	0.689	0.0120
3.25	0.782	0.0132
4.28	0.873	0.0145
5.29	0.961	0.0157
6.32	1.043	0.0175
7.34	1.116	0.0196
8.34	1.180	0.0219
9.35	1.232	0.0257
10.37	1.272	0.0316
11.37	1.293	0.0386
12.36	1.282	0.0635
13.36	1.256	0.0588
14.31	1.201	0.0966

$Rn = 301700.$

α	C_l	C_d
-3.91	0.039	0.0144
-2.89	0.140	0.0125
-1.87	0.242	0.0110
-0.84	0.340	0.0100
0.18	0.431	0.0098
1.20	0.524	0.0102
2.21	0.620	0.0110
3.23	0.712	0.0122
4.25	0.804	0.0130
5.27	0.891	0.0143
6.26	0.965	0.0154
7.29	1.045	0.0178
8.31	1.115	0.0200

SD7032B-PT

Fig. 12.127

$Rn = 61200.$

α	C_l	C_d
-3.92	-0.069	0.0248
-2.90	0.012	0.0214
-1.89	0.091	0.0161
-0.87	0.206	0.0175
0.17	0.357	0.0202
1.20	0.501	0.0219
2.23	0.603	0.0220
3.25	0.679	0.0205
4.26	0.764	0.0197
5.27	0.839	0.0274
6.29	0.909	0.0256
7.31	0.973	0.0295
8.31	1.037	0.0333
9.33	1.106	0.0328
10.34	1.151	0.0398
11.35	1.167	0.0477

$Rn = 101300.$

α	C_l	C_d
-3.92	-0.050	0.0217
-2.89	0.076	0.0178
-1.86	0.207	0.0145
-0.84	0.341	0.0143
0.19	0.457	0.0148
1.21	0.553	0.0139
2.23	0.642	0.0144
3.25	0.729	0.0152
4.26	0.816	0.0176
5.28	0.903	0.0192
6.30	0.981	0.0219
7.32	1.053	0.0253
8.34	1.131	0.0242
9.35	1.192	0.0274
10.37	1.254	0.0310
11.37	1.267	0.0416

$Rn = 203400.$

α	C_l	C_d
-3.91	0.067	0.0153
-2.88	0.196	0.0123
-1.85	0.301	0.0100
-0.83	0.383	0.0093
0.19	0.483	0.0096
1.21	0.582	0.0102
2.24	0.675	0.0108
3.24	0.768	0.0120
4.27	0.860	0.0139

5.30	0.952	0.0146
6.31	1.040	0.0156
7.34	1.124	0.0172
8.34	1.194	0.0187
9.35	1.257	0.0213
10.37	1.305	0.0263
11.38	1.337	0.0312

$Rn = 305400.$

α	C_l	C_d
-3.88	0.100	0.0117
-2.87	0.213	0.0101
-1.85	0.318	0.0088
-0.83	0.413	0.0081
0.19	0.499	0.0082
1.22	0.594	0.0093
2.22	0.689	0.0104
3.26	0.786	0.0115
4.26	0.879	0.0124
5.30	0.970	0.0136
6.30	1.052	0.0142
7.31	1.125	0.0157
8.34	1.199	0.0183
9.34	1.257	0.0212
10.36	1.309	0.0254
11.37	1.344	0.0306

SD7032C-PT

Fig. 12.128

$Rn = 59400.$

α	C_l	C_d
-4.92	0.005	0.0299
-3.89	0.107	0.0247
-2.86	0.179	0.0215
-1.86	0.271	0.0239
-0.82	0.395	0.0313
0.20	0.499	0.0314
1.25	0.688	0.0309
2.27	0.830	0.0260
3.29	0.909	0.0248
4.30	0.977	0.0271
5.31	1.046	0.0325
6.32	1.105	0.0334
7.35	1.163	0.0340
8.35	1.201	0.0424
9.36	1.238	0.0403
10.36	1.240	0.0467

$Rn = 100500.$

α	C_l	C_d
-4.91	0.127	0.0251
-3.88	0.221	0.0225
-2.86	0.300	0.0206
-1.84	0.397	0.0231
-0.79	0.553	0.0232
0.23	0.715	0.0211
1.26	0.835	0.0176
2.28	0.926	0.0171
3.31	1.006	0.0182
4.31	1.080	0.0198
5.33	1.160	0.0219
6.34	1.230	0.0252
7.38	1.312	0.0276
8.39	1.368	0.0288
9.38	1.383	0.0333
10.39	1.391	0.0412
11.39	1.385	0.0503

$Rn = 200500.$

α	C_l	C_d
-4.90	0.263	0.0152
-3.88	0.369	0.0140
-2.86	0.473	0.0150
-1.82	0.579	0.0133
-0.83	0.670	0.0112
0.22	0.770	0.0107
1.21	0.850	0.0114
2.23	0.939	0.0132
3.26	1.027	0.0149
4.24	1.108	0.0166
5.31	1.192	0.0181
6.31	1.261	0.0191
7.34	1.317	0.0213
8.38	1.367	0.0244
9.39	1.399	0.0292
10.37	1.418	0.0339
11.38	1.416	0.0434
12.37	1.392	0.0521

$Rn = 302500.$

α	C_l	C_d
-5.86	0.193	0.0148
-4.84	0.303	0.0128
-3.82	0.411	0.0112
-2.82	0.508	0.0104
-1.78	0.608	0.0101
-0.78	0.695	0.0097
0.23	0.775	0.0104
1.27	0.863	0.0116
2.29	0.955	0.0125
3.31	1.041	0.0139
4.31	1.123	0.0150
5.35	1.197	0.0162
6.32	1.257	0.0180

SD7032C-PT

Fig. 12.129

$Rn = 60100.$

α	C_l	C_d
-2.89	0.120	0.0201
-1.87	0.213	0.0214
-0.86	0.330	0.0255
0.18	0.486	0.0285
1.22	0.645	0.0261
2.26	0.749	0.0269
3.26	0.832	0.0283
4.30	0.906	0.0290
5.30	0.987	0.0333
6.32	1.053	0.0316
7.33	1.117	0.0345
8.35	1.177	0.0362
9.35	1.229	0.0380
10.37	1.260	0.0450
11.35	1.182	0.1061

$Rn = 101400.$

α	C_l	C_d
-2.88	0.172	0.0189
-1.87	0.282	0.0180
-0.84	0.419	0.0186
0.17	0.546	0.0167
1.23	0.646	0.0152
2.24	0.735	0.0164
3.26	0.825	0.0172
4.30	0.911	0.0189
5.29	0.989	0.0189
6.31	1.067	0.0234
7.33	1.149	0.0246
8.34	1.224	0.0258
9.36	1.291	0.0277
10.38	1.324	0.0366
11.38	1.335	0.0431
12.37	1.343	0.0413

$Rn = 202700.$

α	C_l	C_d
-2.90	0.307	0.0125
-1.87	0.402	0.0109
-0.84	0.497	0.0090
0.12	0.592	0.0094
1.17	0.688	0.0103
2.20	0.779	0.0118
3.21	0.868	0.0131
4.28	0.962	0.0148
5.30	1.048	0.0163
6.30	1.131	0.0177
7.31	1.201	0.0192
8.35	1.265	0.0213
9.35	1.317	0.0250
10.38	1.353	0.0292
11.39	1.368	0.0345

$Rn = 303200.$

α	C_l	C_d
-2.85	0.313	0.0106
-1.84	0.412	0.0092
-0.81	0.506	0.0086
0.22	0.596	0.0088
1.23	0.686	0.0097
2.26	0.779	0.0110
3.27	0.871	0.0121
4.29	0.961	0.0130
5.27	1.042	0.0143
6.30	1.120	0.0150
7.28	1.188	0.0169
8.27	1.247	0.0190
9.34	1.304	0.0221
10.33	1.344	0.0260

SD7032C-PT

Fig. 12.130

$Rn = 62200.$

α	C_l	C_d
-3.92	-0.058	0.0216
-2.92	0.023	0.0172
-1.88	0.126	0.0194
-0.85	0.269	0.0218
0.18	0.405	0.0226
1.20	0.542	0.0206
2.22	0.621	0.0238
3.25	0.722	0.0243
4.25	0.764	0.0248
5.27	0.831	0.0246
6.28	0.896	0.0301
7.30	0.982	0.0302
8.32	1.072	0.0368
9.33	1.146	0.0335

$Rn = 102100.$

α	C_l	C_d
-2.89	0.111	0.0194
-1.85	0.244	0.0161
-0.84	0.362	0.0159
0.19	0.479	0.0148
1.22	0.570	0.0148
2.24	0.663	0.0152
3.26	0.753	0.0159
4.27	0.844	0.0176
5.30	0.927	0.0186
6.31	1.011	0.0217
7.33	1.091	0.0235
8.34	1.177	0.0241
9.36	1.250	0.0280
10.38	1.281	0.0334
11.38	1.304	0.0382

$Rn = 151200.$

α	C_l	C_d
-3.91	0.075	0.0156
-2.88	0.196	0.0137
-1.86	0.290	0.0117
-0.85	0.383	0.0112
0.18	0.485	0.0118
1.20	0.588	0.0121
2.23	0.684	0.0132
3.24	0.780	0.0141
4.27	0.871	0.0166
5.30	0.963	0.0188
6.31	1.051	0.0196
7.32	1.139	0.0201
8.35	1.218	0.0236
9.36	1.274	0.0275
10.37	1.312	0.0319
11.37	1.305	0.0528

$Rn = 200300.$

α	C_l	C_d
-2.89	0.196	0.0129
-1.85	0.300	0.0107
-0.83	0.387	0.0090
0.20	0.493	0.0088
1.23	0.592	0.0099
2.24	0.686	0.0112
3.26	0.777	0.0123
4.28	0.869	0.0141
5.30	0.959	0.0155
6.32	1.048	0.0167
7.33	1.127	0.0178
8.35	1.197	0.0195
9.36	1.258	0.0226
10.38	1.303	0.0270
11.37	1.328	0.0331

$Rn = 302000.$

α	C_l	C_d
-2.87	0.185	0.0108
-1.84	0.294	0.0092
-0.85	0.387	0.0081
0.20	0.482	0.0083
1.20	0.575	0.0091
2.22	0.668	0.0102
3.25	0.764	0.0114
4.26	0.857	0.0121
5.28	0.947	0.0131

6.30	1.025	0.0140
7.33	1.108	0.0155
8.33	1.179	0.0174
9.34	1.239	0.0203
10.36	1.292	0.0237
11.38	1.325	0.0292
12.37	1.330	0.0333
13.35	1.291	0.0524

SD7032C-PT

Fig. 12.131

$Rn = 62600.$

α	C_l	C_d
-2.94	-0.122	0.0216
-1.92	-0.033	0.0185
-0.91	0.089	0.0167
0.13	0.243	0.0173
1.17	0.362	0.0204
2.20	0.442	0.0216
3.21	0.521	0.0212
4.22	0.605	0.0250
5.24	0.691	0.0266
6.25	0.774	0.0259
7.28	0.851	0.0280
8.30	0.924	0.0291
9.31	1.002	0.0325
10.33	1.067	0.0335
11.34	1.108	0.0403

$Rn = 101500.$

α	C_l	C_d
-2.93	-0.056	0.0188
-1.91	0.067	0.0142
-0.88	0.175	0.0127
0.15	0.269	0.0141
1.17	0.347	0.0140
2.19	0.433	0.0138
3.21	0.525	0.0150
4.22	0.613	0.0163
5.24	0.707	0.0173
6.26	0.794	0.0193
7.29	0.877	0.0202
8.30	0.964	0.0225
9.31	1.049	0.0237
10.34	1.125	0.0263
11.35	1.167	0.0320
12.34	1.195	0.0394
13.36	1.206	0.0443

$Rn = 200800.$

α	C_l	C_d
-7.01	-0.441	0.0772
-6.02	-0.352	0.0531
-4.96	-0.231	0.0277
-3.96	-0.128	0.0182
-2.93	-0.042	0.0151
-1.91	0.052	0.0127
-0.89	0.137	0.0103
0.13	0.223	0.0091
1.17	0.333	0.0093
2.17	0.427	0.0106
3.20	0.523	0.0107
4.22	0.624	0.0123
5.25	0.720	0.0136
6.26	0.813	0.0147
7.28	0.904	0.0158
8.31	0.995	0.0167
9.33	1.077	0.0182
10.34	1.153	0.0209

$Rn = 301600.$

α	C_l	C_d
-4.98	-0.226	0.0254
-3.97	-0.135	0.0173
-2.95	-0.048	0.0141
-1.91	0.049	0.0120
-0.90	0.147	0.0102
0.12	0.230	0.0086
1.13	0.323	0.0086
2.18	0.426	0.0087
3.20	0.523	0.0095
4.22	0.619	0.0104
5.22	0.713	0.0114
6.25	0.808	0.0121
7.28	0.900	0.0132
8.29	0.984	0.0144
9.32	1.067	0.0165
10.34	1.140	0.0189
11.33	1.198	0.0225
12.35	1.237	0.0277

SD7032C-PT

Fig. 12.132

$Rn = 59900.$

α	C_l	C_d
-2.94	-0.191	0.0255
-1.92	-0.072	0.0199
-0.90	0.061	0.0169
0.14	0.215	0.0177
1.16	0.334	0.0200
2.18	0.413	0.0239
3.20	0.488	0.0279
4.22	0.568	0.0295
5.24	0.658	0.0290
6.25	0.729	0.0319
7.27	0.808	0.0262
8.29	0.883	0.0322
9.30	0.955	0.0336
10.32	1.027	0.0388

$Rn = 102000.$

α	C_l	C_d
-2.93	-0.114	0.0201
-1.91	0.004	0.0161
-0.90	0.090	0.0115
0.15	0.216	0.0140
1.16	0.290	0.0150
2.17	0.369	0.0149
3.18	0.451	0.0151
4.22	0.544	0.0160
5.23	0.638	0.0171
6.26	0.730	0.0182
7.28	0.817	0.0206
8.29	0.906	0.0224
9.30	0.993	0.0237
10.34	1.083	0.0246
11.33	1.131	0.0322
12.35	1.162	0.0385
13.35	1.168	0.0536

$Rn = 201500.$

α	C_l	C_d
-2.94	-0.110	0.0164
-1.91	-0.022	0.0140
-0.90	0.068	0.0114
0.13	0.141	0.0102
1.14	0.243	0.0102
2.17	0.342	0.0096
3.18	0.436	0.0101
4.21	0.536	0.0113
5.23	0.632	0.0124
6.25	0.728	0.0136
7.27	0.823	0.0146
8.29	0.915	0.0158
9.31	0.999	0.0173
10.33	1.078	0.0193
11.34	1.140	0.0236
12.34	1.183	0.0290

$Rn = 300700.$

α	C_l	C_d
-2.94	-0.127	0.0156
-1.91	-0.034	0.0130
-0.91	0.058	0.0110
0.12	0.147	0.0090
1.13	0.225	0.0095
2.17	0.326	0.0096
3.19	0.425	0.0105
4.20	0.524	0.0111
5.22	0.620	0.0117
6.24	0.714	0.0124
7.27	0.806	0.0131
8.28	0.894	0.0142
9.30	0.980	0.0155
10.31	1.060	0.0176

SD7032D-PT

Fig. 12.134

$Rn = 59200.$

α	C_l	C_d
-3.92	-0.052	0.0271
-2.91	0.062	0.0208
-1.89	0.153	0.0196
-0.85	0.310	0.0205
0.19	0.444	0.0207
1.20	0.565	0.0263
2.23	0.671	0.0239
3.26	0.755	0.0225
4.26	0.839	0.0287
5.29	0.917	0.0269
6.31	1.000	0.0291
7.32	1.073	0.0330
8.33	1.141	0.0356
9.33	1.192	0.0369
10.36	1.229	0.0449
11.34	1.140	0.0845

$Rn = 99800.$

α	C_l	C_d
-4.96	-0.123	0.0280
-3.91	0.013	0.0227
-2.89	0.153	0.0182
-1.89	0.266	0.0160
-0.85	0.383	0.0157
0.20	0.486	0.0165
1.21	0.581	0.0174
2.23	0.680	0.0174
3.25	0.777	0.0188
4.26	0.869	0.0178
5.28	0.961	0.0205
6.30	1.046	0.0220
7.31	1.131	0.0224
8.34	1.207	0.0261
9.35	1.260	0.0306
10.35	1.275	0.0387
11.35	1.271	0.0469

$Rn = 147800.$

α	C_l	C_d
-5.97	-0.180	0.0323
-4.93	-0.045	0.0211
-3.90	0.082	0.0166
-2.87	0.196	0.0133
-1.87	0.285	0.0115
-0.86	0.370	0.0114
0.16	0.473	0.0118
1.20	0.579	0.0128
2.23	0.683	0.0134
3.24	0.784	0.0138
4.27	0.882	0.0152
5.28	0.975	0.0165
6.30	1.063	0.0178
7.34	1.146	0.0200
8.34	1.221	0.0228
9.34	1.275	0.0283
10.35	1.298	0.0346
11.37	1.297	0.0547
12.34	1.268	0.0576

$Rn = 199100.$

α	C_l	C_d
-6.00	-0.145	0.0273
-4.98	-0.025	0.0175
-3.89	0.083	0.0145
-2.89	0.180	0.0119
-1.87	0.278	0.0106
-0.88	0.364	0.0096
0.18	0.474	0.0098
1.20	0.581	0.0105
2.23	0.691	0.0112
3.24	0.793	0.0126
4.27	0.891	0.0134
5.28	0.984	0.0145
6.30	1.073	0.0159
7.33	1.156	0.0180
8.32	1.225	0.0201
9.35	1.281	0.0250
10.35	1.307	0.0317
11.37	1.307	0.0480

$Rn = 302600.$

α	C_l	C_d
-5.94	-0.115	0.0214
-4.95	-0.021	0.0146
-3.92	0.073	0.0122
-2.90	0.168	0.0104
-1.90	0.272	0.0096
-0.88	0.377	0.0086
0.17	0.478	0.0080
1.17	0.586	0.0084
2.20	0.692	0.0094
3.21	0.794	0.0103

4.24	0.891	0.0114
5.29	0.988	0.0127
6.28	1.074	0.0145
7.30	1.155	0.0158
8.35	1.224	0.0186
9.33	1.276	0.0228
10.35	1.313	0.0282
11.36	1.321	0.0399
12.35	1.303	0.0643
13.33	1.275	0.0489

SD7032D-PT

Fig. 12.135

$Rn = 60500.$

α	C_l	C_d
-3.94	-0.046	0.0246
-2.37	0.144	0.0186
-0.84	0.297	0.0178
0.68	0.433	0.0230
2.23	0.588	0.0234
3.73	0.712	0.0265
5.27	0.837	0.0301
6.79	0.951	0.0323
8.31	1.053	0.0382
9.83	1.125	0.0373

$Rn = 100700.$

α	C_l	C_d
-3.89	0.072	0.0190
-2.38	0.223	0.0134
-0.83	0.365	0.0138
0.71	0.528	0.0157
2.23	0.683	0.0169
3.77	0.829	0.0178
5.29	0.968	0.0194
6.81	1.093	0.0216
8.35	1.208	0.0264
9.86	1.271	0.0320
11.37	1.284	0.0455
12.85	1.259	0.0609

$Rn = 151500.$

α	C_l	C_d
-3.91	0.061	0.0148
-2.38	0.219	0.0117
-0.83	0.358	0.0099
0.70	0.521	0.0116
2.21	0.676	0.0127
3.74	0.828	0.0144
5.28	0.968	0.0161
6.80	1.095	0.0182
8.35	1.212	0.0222
9.84	1.278	0.0317
11.34	1.286	0.0471
12.85	1.259	0.0689

$Rn = 201200.$

α	C_l	C_d
-3.96	0.049	0.0140
-2.42	0.204	0.0116
-0.85	0.352	0.0086
0.65	0.513	0.0098
2.19	0.674	0.0109
3.77	0.833	0.0121
5.29	0.972	0.0142
6.81	1.098	0.0174
8.32	1.206	0.0198
9.86	1.279	0.0275
11.35	1.299	0.0387
12.85	1.279	0.0448

$Rn = 302000.$

α	C_l	C_d
-3.93	0.059	0.0135
-2.37	0.219	0.0110
-0.83	0.380	0.0090
0.67	0.533	0.0090
2.19	0.694	0.0100
3.70	0.844	0.0113
5.24	0.981	0.0137
6.78	1.106	0.0161
8.33	1.214	0.0198
9.83	1.287	0.0259
11.36	1.308	0.0407
12.82	1.287	0.0491

SD7037-PT

Fig. 12.136

$Rn = 62600.$

α	C_l	C_d
-3.95	-0.225	0.0261
-2.95	-0.138	0.0208
-1.92	-0.058	0.0153
-0.90	0.068	0.0166
0.13	0.223	0.0176
1.16	0.339	0.0196
2.19	0.485	0.0170
3.22	0.597	0.0187
4.24	0.685	0.0179
5.26	0.779	0.0163
6.27	0.837	0.0206
7.29	0.917	0.0321
8.31	1.008	0.0255

$Rn = 103900.$

α	C_l	C_d
-2.95	-0.128	0.0169
-1.93	-0.019	0.0137
-0.90	0.109	0.0147
0.14	0.236	0.0135
1.16	0.368	0.0132
2.19	0.486	0.0137
3.22	0.579	0.0130
4.23	0.667	0.0127
5.26	0.753	0.0159
6.26	0.834	0.0150
7.27	0.907	0.0182
8.30	0.977	0.0180
9.31	1.011	0.0189
10.30	1.039	0.0567

$Rn = 153400.$

α	C_l	C_d
-2.98	-0.058	0.0157
-1.92	0.079	0.0127
-0.89	0.195	0.0100
0.14	0.309	0.0101
1.17	0.415	0.0102
2.17	0.508	0.0115
3.23	0.609	0.0118
4.22	0.696	0.0129
5.24	0.784	0.0142
6.26	0.866	0.0154
7.28	0.936	0.0213
8.30	0.997	0.0253
9.30	1.053	0.0331
10.32	1.089	0.0402

$Rn = 204200.$

α	C_l	C_d
-2.97	-0.001	0.0145
-1.91	0.120	0.0117
-0.89	0.217	0.0091
0.13	0.318	0.0088
1.16	0.416	0.0092
2.18	0.514	0.0097
3.22	0.611	0.0105
4.23	0.703	0.0120
5.26	0.792	0.0126
6.26	0.874	0.0147
7.28	0.944	0.0187
8.28	1.008	0.0226
9.31	1.069	0.0273
10.35	1.117	0.0339
11.32	1.138	0.0422

$Rn = 302900.$

α	C_l	C_d
-2.96	0.021	0.0117
-1.93	0.119	0.0100
-0.93	0.214	0.0085
0.09	0.313	0.0067
1.01	0.406	0.0075
2.16	0.519	0.0084
3.18	0.615	0.0092
4.20	0.708	0.0103
5.23	0.798	0.0116
6.25	0.876	0.0140
7.27	0.947	0.0168
8.28	1.015	0.0206
9.30	1.076	0.0246
10.32	1.126	0.0292

SD7037-PT

Fig. 12.137

$Rn = 57500.$

α	C_l	C_d
-3.98	-0.243	0.0321
-2.45	-0.127	0.0246
-0.92	0.037	0.0163
0.64	0.247	0.0193
2.18	0.441	0.0196
3.72	0.606	0.0218
5.25	0.735	0.0214
6.78	0.858	0.0258
8.28	0.986	0.0243
9.81	1.054	0.0350

$Rn = 98700.$

α	C_l	C_d
-3.98	-0.228	0.0289
-2.43	-0.054	0.0190
-0.91	0.132	0.0144
0.65	0.324	0.0128
2.18	0.471	0.0128
3.72	0.618	0.0145
5.26	0.758	0.0163
6.77	0.887	0.0185
8.29	0.988	0.0219
9.83	1.059	0.0338
11.32	1.110	0.0432

$Rn = 149600.$

α	C_l	C_d
-3.96	-0.173	0.0216
-2.92	-0.054	0.0167
-1.89	0.063	0.0131
-0.88	0.159	0.0105
0.13	0.261	0.0101
1.15	0.367	0.0099
2.18	0.472	0.0101
3.21	0.571	0.0108
4.22	0.666	0.0124
5.24	0.757	0.0135
6.27	0.846	0.0144
7.28	0.924	0.0167
8.30	0.983	0.0214
9.31	1.041	0.0270

$Rn = 199800.$

α	C_l	C_d
-3.95	-0.139	0.0185
-2.42	0.010	0.0129
-0.91	0.153	0.0095
0.64	0.310	0.0087
2.18	0.462	0.0090
3.72	0.613	0.0104
5.25	0.757	0.0121
6.78	0.885	0.0147
8.30	0.982	0.0210
9.82	1.068	0.0280
11.32	1.119	0.0396
12.84	1.105	0.0736
14.22	0.945	0.2166

SD7043-PT

Fig. 12.138

$Rn = 61600.$

α	C_l	C_d
-3.90	-0.004	0.0240
-2.89	0.100	0.0221
-1.87	0.194	0.0171
-0.86	0.283	0.0192
0.17	0.389	0.0218
1.22	0.537	0.0237
2.24	0.699	0.0227
3.27	0.811	0.0243
4.29	0.904	0.0232
5.30	0.974	0.0210
6.31	1.046	0.0239
7.33	1.111	0.0312
8.35	1.163	0.0385
9.35	1.198	0.0343
10.34	1.156	0.0685
11.31	0.945	0.1752

$Rn = 103800.$

α	C_l	C_d
-3.91	-0.008	0.0208
-2.90	0.100	0.0197
-1.87	0.233	0.0149
-0.85	0.339	0.0179
0.18	0.479	0.0193
1.22	0.617	0.0185

2.25	0.732	0.0183
3.27	0.818	0.0173
4.28	0.914	0.0161
5.30	0.995	0.0175
6.30	1.068	0.0206
7.33	1.139	0.0228
8.34	1.203	0.0291
9.35	1.256	0.0343
10.37	1.301	0.0367
11.36	1.328	0.0460

$Rn = 154900.$

α	C_l	C_d
-3.89	0.057	0.0170
-2.88	0.198	0.0164
-1.85	0.334	0.0145
-0.83	0.431	0.0128
0.20	0.534	0.0124
1.22	0.636	0.0122
2.25	0.735	0.0127
3.27	0.832	0.0131
4.29	0.924	0.0140
5.31	1.009	0.0162
6.33	1.089	0.0185
7.34	1.163	0.0215
8.35	1.227	0.0253
9.37	1.284	0.0293
10.37	1.331	0.0339
11.38	1.357	0.0407

$Rn = 204000.$

α	C_l	C_d
-3.88	0.117	0.0148
-2.86	0.246	0.0133
-1.84	0.359	0.0113
-0.83	0.451	0.0101
0.20	0.539	0.0097
1.23	0.644	0.0102
2.26	0.748	0.0106
3.28	0.843	0.0115
4.28	0.932	0.0130
5.31	1.015	0.0150
6.32	1.094	0.0173
7.35	1.170	0.0197
8.36	1.242	0.0226
9.37	1.307	0.0261
10.38	1.353	0.0308
11.38	1.375	0.0375
12.38	1.372	0.0475
13.39	1.350	0.0645

$Rn = 303400.$

α	C_l	C_d
-4.90	0.049	0.0131
-3.87	0.159	0.0110
-2.86	0.262	0.0100
-1.82	0.374	0.0092
-0.82	0.476	0.0087
0.21	0.569	0.0084
1.23	0.667	0.0086
2.25	0.767	0.0095
3.26	0.859	0.0107
4.29	0.949	0.0123
5.30	1.034	0.0141
6.32	1.113	0.0160
7.33	1.191	0.0181

SD7043-PT

Fig. 12.139

$Rn = 202900.$

α	C_l	C_d
-2.88	0.237	0.0110
-1.87	0.337	0.0101
-0.84	0.431	0.0095
0.20	0.522	0.0099
1.22	0.623	0.0115
2.23	0.727	0.0128
3.24	0.827	0.0138
4.27	0.927	0.0152
5.30	1.022	0.0164
6.30	1.108	0.0183
7.34	1.191	0.0215
8.34	1.255	0.0252
9.35	1.317	0.0281
10.37	1.364	0.0349

$Rn = 303700.$

α	C_l	C_d
-2.88	0.219	0.0114
-1.84	0.330	0.0110
-0.82	0.437	0.0110
0.19	0.533	0.0108
1.20	0.631	0.0111
2.20	0.735	0.0120
3.26	0.841	0.0130
4.23	0.933	0.0137
5.25	1.022	0.0147
6.26	1.111	0.0161
7.32	1.187	0.0191
8.33	1.257	0.0222
9.34	1.321	0.0252
10.36	1.371	0.0299
11.37	1.397	0.0355

SD7062-PT

Fig. 12.141

$Rn = 102600.$

α	C_l	C_d
-5.93	-0.094	0.0264
-4.91	0.020	0.0231
-3.90	0.109	0.0219
-2.86	0.195	0.0189
-1.85	0.277	0.0199
-0.83	0.369	0.0206
0.20	0.477	0.0183
1.22	0.577	0.0197
2.24	0.678	0.0212
3.26	0.771	0.0238
4.27	0.864	0.0204
5.30	0.950	0.0266
6.32	1.037	0.0248
7.33	1.118	0.0277
8.35	1.195	0.0297
9.37	1.259	0.0372
10.38	1.314	0.0429
11.28	0.870	0.1586
12.26	0.708	0.2118
13.26	0.716	0.2228

$Rn = 149700.$

α	C_l	C_d
-6.94	-0.160	0.0239
-5.92	-0.075	0.0206
-4.91	0.006	0.0180
-3.90	0.097	0.0159
-2.87	0.190	0.0144
-1.85	0.284	0.0141
-0.83	0.376	0.0144
0.20	0.483	0.0135
1.23	0.590	0.0150
2.25	0.694	0.0159
3.25	0.790	0.0167
4.28	0.886	0.0173
5.31	0.975	0.0184
6.33	1.066	0.0189
7.33	1.147	0.0210
8.35	1.229	0.0241
9.37	1.300	0.0271
10.38	1.359	0.0315
11.40	1.408	0.0370
12.40	1.441	0.0470

$Rn = 210500.$

α	C_l	C_d
-6.94	-0.192	0.0216
-5.95	-0.107	0.0176
-4.91	-0.014	0.0147
-3.90	0.081	0.0141
-2.86	0.183	0.0125
-1.85	0.284	0.0118
-0.84	0.383	0.0114
0.20	0.483	0.0110
1.22	0.590	0.0112
2.24	0.695	0.0120
3.26	0.795	0.0127
4.29	0.892	0.0136
5.30	0.985	0.0151
6.33	1.075	0.0167
7.35	1.164	0.0186
8.36	1.243	0.0201
9.38	1.316	0.0221
10.40	1.379	0.0254
11.40	1.430	0.0290
12.41	1.464	0.0390
13.41	1.485	0.0512
14.42	1.497	0.0588

$Rn = 305800.$

α	C_l	C_d
-7.00	-0.201	0.0179
-6.00	-0.117	0.0152
-4.98	-0.020	0.0133
-3.90	0.090	0.0125
-2.92	0.188	0.0115
-1.87	0.293	0.0106
-0.82	0.398	0.0101
0.21	0.502	0.0102
1.22	0.605	0.0099
2.25	0.712	0.0103
3.27	0.812	0.0115
4.28	0.906	0.0124
5.31	0.997	0.0139
6.31	1.084	0.0154
7.33	1.168	0.0162
8.37	1.249	0.0181
9.38	1.323	0.0201
10.39	1.388	0.0231
11.40	1.442	0.0270

SD7062-PT

Fig. 12.142

$Rn = 100800.$

α	C_l	C_d
-6.95	-0.165	0.0340
-5.93	-0.100	0.0250
-4.91	0.010	0.0218
-3.89	0.082	0.0176
-2.88	0.166	0.0162
-1.84	0.252	0.0151
-0.83	0.336	0.0151
0.18	0.457	0.0155
1.22	0.552	0.0147
2.23	0.659	0.0177
3.25	0.740	0.0176
4.28	0.835	0.0214
5.28	0.909	0.0212
6.30	1.007	0.0253
7.33	1.086	0.0252
8.34	1.171	0.0308
9.35	1.237	0.0305
10.37	1.302	0.0366

$Rn = 151700.$

α	C_l	C_d
-6.95	-0.175	0.0253
-5.93	-0.099	0.0197
-4.89	-0.013	0.0163
-3.91	0.078	0.0143
-2.86	0.187	0.0136
-1.84	0.276	0.0131
-0.83	0.367	0.0126
0.20	0.472	0.0128
1.21	0.572	0.0140
2.24	0.671	0.0159
3.26	0.765	0.0168
4.26	0.850	0.0182
5.30	0.941	0.0190
6.31	1.032	0.0207
7.34	1.124	0.0225
8.35	1.208	0.0251
9.37	1.288	0.0277
10.39	1.364	0.0305
11.40	1.419	0.0352
12.41	1.458	0.0410

$Rn = 204500.$

α	C_l	C_d
-6.97	-0.204	0.0216
-5.94	-0.115	0.0176
-4.92	-0.023	0.0144
-3.88	0.076	0.0139
-2.88	0.173	0.0126
-1.85	0.272	0.0126
-0.83	0.371	0.0128
0.19	0.465	0.0125
1.21	0.570	0.0133
2.23	0.668	0.0141
3.25	0.770	0.0155
4.27	0.864	0.0171
5.29	0.953	0.0179
6.31	1.045	0.0191
7.34	1.133	0.0206
8.35	1.218	0.0223
9.36	1.299	0.0245
10.39	1.376	0.0267

11.40	1.439	0.0298
12.41	1.488	0.0348
13.41	1.515	0.0443

$Rn = 302700.$

α	C_l	C_d
-6.98	-0.222	0.0183
-5.98	-0.131	0.0158
-4.93	-0.034	0.0141
-3.91	0.064	0.0141
-2.88	0.167	0.0136
-1.86	0.268	0.0128
-0.84	0.372	0.0129
0.19	0.470	0.0129
1.22	0.570	0.0130
2.24	0.677	0.0138
3.24	0.776	0.0148
4.28	0.871	0.0158
5.29	0.964	0.0168
6.32	1.055	0.0179
7.33	1.143	0.0191
8.36	1.231	0.0205
9.38	1.311	0.0222
10.37	1.384	0.0244
11.39	1.440	0.0296
12.41	1.470	0.0411

SD7062-PT

Fig. 12.143

$Rn = 207600.$

α	C_l	C_d
-6.94	-0.197	0.0222
-5.95	-0.110	0.0181
-4.91	-0.014	0.0151
-3.90	0.084	0.0145
-2.86	0.188	0.0129
-1.85	0.292	0.0121
-0.84	0.394	0.0117
0.20	0.497	0.0113
1.22	0.607	0.0115
2.24	0.714	0.0123
3.27	0.817	0.0130
4.29	0.917	0.0139
5.31	1.012	0.0155
6.34	1.106	0.0171
7.36	1.196	0.0191
8.37	1.278	0.0207
9.39	1.353	0.0227
10.41	1.417	0.0261
11.41	1.470	0.0298
12.42	1.504	0.0400
13.42	1.527	0.0525
14.43	1.538	0.0602

$Rn = 204900.$

α	C_l	C_d
-6.95	-0.200	0.0222
-5.96	-0.116	0.0177
-4.93	-0.022	0.0148
-3.89	0.081	0.0136
-2.88	0.177	0.0122
-1.86	0.280	0.0113
-0.85	0.381	0.0114
0.20	0.480	0.0109
1.21	0.587	0.0115
2.23	0.691	0.0125
3.26	0.790	0.0135
4.28	0.885	0.0145
5.29	0.980	0.0154
6.32	1.072	0.0165
7.33	1.158	0.0182
8.36	1.242	0.0203
9.37	1.320	0.0222
10.39	1.389	0.0254
11.40	1.444	0.0292
12.42	1.481	0.0356

$Rn = 204500.$

α	C_l	C_d
-6.97	-0.204	0.0216
-5.94	-0.115	0.0176
-4.92	-0.023	0.0144
-3.88	0.076	0.0139
-2.88	0.173	0.0126
-1.85	0.272	0.0126
-0.83	0.371	0.0128
0.19	0.465	0.0125
1.21	0.570	0.0133
2.23	0.668	0.0141
3.25	0.770	0.0155
4.27	0.864	0.0171
5.29	0.953	0.0179
6.31	1.045	0.0191
7.34	1.133	0.0206
8.35	1.218	0.0223
9.36	1.299	0.0245
10.39	1.376	0.0267
11.40	1.439	0.0298
12.41	1.488	0.0348
13.41	1.515	0.0443

SD7080-PT

Fig. 12.144

$Rn = 62600.$

α	C_l	C_d
-3.95	-0.244	0.0198
-2.94	-0.160	0.0179
-1.93	-0.058	0.0144
-0.91	0.056	0.0179
0.11	0.228	0.0176
1.17	0.371	0.0184
2.20	0.482	0.0185
3.22	0.576	0.0199
4.22	0.645	0.0194
5.25	0.726	0.0238
6.26	0.801	0.0265
7.27	0.876	0.0273
8.29	0.924	0.0303
9.31	0.994	0.0323
10.31	1.054	0.0402

$Rn = 103500.$

α	C_l	C_d
-3.98	-0.252	0.0182
-2.95	-0.156	0.0171
-1.92	-0.029	0.0137
-0.90	0.109	0.0123
0.14	0.243	0.0128
1.16	0.351	0.0153
2.18	0.448	0.0126
3.20	0.535	0.0144
4.22	0.629	0.0170
5.25	0.726	0.0171
6.26	0.803	0.0197
7.28	0.868	0.0208
8.30	0.932	0.0291
9.31	0.973	0.0283
10.31	0.999	0.0628

$Rn = 149800.$

α	C_l	C_d
-6.00	-0.388	0.0349
-4.98	-0.305	0.0260
-3.95	-0.186	0.0195
-2.94	-0.079	0.0147
-1.91	0.034	0.0115
-0.89	0.171	0.0106
0.15	0.267	0.0105
1.17	0.361	0.0107
2.20	0.461	0.0106
3.21	0.555	0.0112
4.24	0.648	0.0130
5.25	0.740	0.0146
6.27	0.830	0.0168
7.28	0.920	0.0192
8.30	0.977	0.0228
9.31	1.013	0.0304
10.32	1.041	0.0379
11.32	1.049	0.0506
12.32	1.026	0.0691
13.33	1.004	0.1087

$Rn = 205700.$

α	C_l	C_d
-6.00	-0.391	0.0392
-4.98	-0.300	0.0250
-3.96	-0.187	0.0175
-2.93	-0.074	0.0143
-1.91	0.028	0.0111
-0.88	0.129	0.0084
0.14	0.240	0.0083
1.17	0.340	0.0086
2.18	0.435	0.0087
3.21	0.533	0.0097
4.24	0.625	0.0112
5.25	0.721	0.0126
6.27	0.813	0.0138
7.29	0.900	0.0158
8.30	0.961	0.0197
9.31	1.007	0.0246
10.31	1.042	0.0323
11.32	1.056	0.0407
12.32	1.044	0.0508
13.31	1.007	0.0744

$Rn = 301800.$

α	C_l	C_d
-6.02	-0.393	0.0360
-4.99	-0.285	0.0210
-3.96	-0.180	0.0153
-2.97	-0.092	0.0127
-1.93	-0.003	0.0101
-0.90	0.090	0.0075
0.13	0.216	0.0069
1.14	0.317	0.0073
2.18	0.420	0.0081
3.21	0.516	0.0091
4.22	0.608	0.0102
5.24	0.705	0.0113
6.26	0.799	0.0122
7.28	0.881	0.0140
8.30	0.944	0.0192
9.31	0.997	0.0237
10.31	1.036	0.0294
11.32	1.048	0.0384
12.31	1.036	0.0475
13.30	1.009	0.0673

SD7084-PT

Fig. 12.146

$Rn = 100900.$

α	C_l	C_d
-2.95	-0.164	0.0196
-1.42	-0.031	0.0140
0.12	0.151	0.0160
1.68	0.409	0.0182
3.20	0.545	0.0159
4.73	0.677	0.0156
6.26	0.802	0.0191
7.79	0.935	0.0205
9.31	1.047	0.0252
10.82	1.078	0.0404
12.34	1.079	0.0500

$Rn = 152400.$

α	C_l	C_d
-2.94	-0.149	0.0164
-1.40	0.034	0.0121
0.15	0.274	0.0125
1.68	0.413	0.0117
3.19	0.552	0.0116
4.74	0.692	0.0130
6.26	0.822	0.0158
7.78	0.951	0.0181
9.31	1.053	0.0230
10.82	1.091	0.0348
12.33	1.088	0.0521
13.82	1.046	0.0634
15.27	0.857	0.2306

$Rn = 197500.$

α	C_l	C_d
-3.95	-0.226	0.0175
-2.96	-0.111	0.0147
-1.91	0.032	0.0114
-0.89	0.155	0.0095
0.14	0.268	0.0098
1.17	0.359	0.0094
2.17	0.454	0.0099
3.21	0.552	0.0102
4.24	0.647	0.0115
5.23	0.737	0.0128
6.27	0.829	0.0143
7.28	0.917	0.0159
8.30	0.997	0.0185
9.31	1.058	0.0233
10.32	1.089	0.0308

$Rn = 303000.$

α	C_l	C_d
-3.97	-0.159	0.0139
-2.94	-0.046	0.0112
-1.92	0.046	0.0095

-0.91	0.126	0.0077
0.13	0.256	0.0072
1.16	0.357	0.0073
2.18	0.457	0.0079
3.20	0.556	0.0089
4.22	0.651	0.0103
5.25	0.746	0.0115
6.27	0.838	0.0130
7.28	0.923	0.0145
8.31	1.002	0.0165
9.32	1.059	0.0215
10.32	1.099	0.0269
11.33	1.116	0.0374

SD7090-PT

Fig. 12.148

$Rn = 59600.$

α	C_l	C_d
-5.98	-0.373	0.0280
-4.96	-0.301	0.0227
-3.95	-0.228	0.0182
-2.93	-0.138	0.0171
-1.91	-0.064	0.0159
-0.88	0.082	0.0154
0.15	0.270	0.0158
1.18	0.399	0.0194
2.20	0.487	0.0187
3.22	0.585	0.0224
4.24	0.667	0.0223
5.26	0.757	0.0240
6.27	0.821	0.0260
7.28	0.893	0.0290
8.29	0.951	0.0432
9.31	0.987	0.0453
10.31	0.953	0.0911
11.29	0.842	0.1435
12.28	0.778	0.1960

$Rn = 99100.$

α	C_l	C_d
-5.98	-0.354	0.0239
-4.96	-0.283	0.0197
-3.95	-0.211	0.0163
-2.94	-0.132	0.0135
-1.91	-0.029	0.0134
-0.88	0.148	0.0126
0.15	0.270	0.0128
1.17	0.362	0.0145
2.19	0.457	0.0139
3.22	0.549	0.0160
4.23	0.640	0.0175
5.24	0.731	0.0194
6.27	0.816	0.0210
7.29	0.892	0.0243
8.30	0.957	0.0312
9.32	1.007	0.0335
10.32	1.039	0.0385
11.30	0.895	0.1565

$Rn = 149000.$

α	C_l	C_d
-5.97	-0.343	0.0221
-4.96	-0.269	0.0171
-3.94	-0.185	0.0158
-2.93	-0.064	0.0133
-1.91	0.064	0.0110
-0.87	0.197	0.0105
0.15	0.297	0.0103
1.18	0.392	0.0109
2.19	0.489	0.0121
3.22	0.590	0.0135
4.24	0.685	0.0145
5.26	0.772	0.0157
6.27	0.861	0.0173
7.28	0.931	0.0195
8.31	0.994	0.0259
9.32	1.049	0.0297
10.32	1.092	0.0383
11.33	1.106	0.0504
12.29	0.887	0.1747

$Rn = 199100.$

α	C_l	C_d
-6.00	-0.361	0.0191
-4.96	-0.280	0.0157
-3.95	-0.178	0.0146
-2.92	-0.044	0.0115
-1.90	0.067	0.0092
-0.88	0.171	0.0085
0.16	0.284	0.0093
1.16	0.381	0.0094
2.20	0.478	0.0103
3.22	0.577	0.0113
4.24	0.671	0.0125
5.26	0.759	0.0139
6.28	0.841	0.0162
7.29	0.915	0.0182
8.30	0.977	0.0228
9.31	1.037	0.0276
10.34	1.083	0.0342
11.33	1.107	0.0442

$Rn = 298600.$

α	C_l	C_d
-6.02	-0.359	0.0166
-4.99	-0.247	0.0137
-4.02	-0.130	0.0118
-2.98	-0.025	0.0097
-1.91	0.072	0.0085
-0.88	0.161	0.0074
0.13	0.280	0.0078
1.16	0.381	0.0085
2.20	0.480	0.0094
3.21	0.576	0.0101
4.23	0.669	0.0112
5.25	0.756	0.0126
6.27	0.840	0.0144
7.28	0.916	0.0168
8.31	0.984	0.0213
9.32	1.046	0.0249
10.33	1.094	0.0301
11.33	1.116	0.0404

SD7090-PT

Fig. 12.149

$Rn = 304000.$

α	C_l	C_d
-4.00	-0.136	0.0118
-2.96	-0.038	0.0101
-1.91	0.055	0.0084
-0.92	0.140	0.0076
0.15	0.272	0.0076
1.17	0.377	0.0083
2.18	0.478	0.0092
3.20	0.576	0.0102
4.22	0.670	0.0111
5.24	0.758	0.0126
6.26	0.842	0.0147
7.27	0.915	0.0180
8.29	0.984	0.0212
9.30	1.045	0.0252
10.32	1.092	0.0314

$Rn = 298400.$

α	C_l	C_d
-4.01	-0.200	0.0128
-2.99	-0.093	0.0113
-1.95	0.004	0.0094
-0.90	0.095	0.0083
0.12	0.203	0.0075
1.15	0.322	0.0078
2.17	0.427	0.0085
3.20	0.527	0.0096
4.23	0.624	0.0108
5.25	0.717	0.0118
6.25	0.802	0.0135
7.28	0.883	0.0162
8.29	0.954	0.0204
9.29	1.018	0.0240

SD7090-PT

Fig. 12.150

$Rn = 302500.$

α	C_l	C_d
-4.00	-0.210	0.0136
-2.95	-0.116	0.0126
-1.94	-0.021	0.0111
-0.88	0.076	0.0096
0.11	0.187	0.0084
1.15	0.310	0.0088
2.17	0.418	0.0093
3.19	0.519	0.0099
4.23	0.621	0.0107
5.23	0.711	0.0125
6.26	0.798	0.0143
7.27	0.876	0.0171
8.29	0.948	0.0210
9.31	1.012	0.0248
10.31	1.061	0.0298
11.32	1.090	0.0376

$Rn = 305900.$

α	C_l	C_d
-3.98	-0.191	0.0133
-2.95	-0.096	0.0116
-1.94	-0.004	0.0104
-0.91	0.090	0.0091
0.11	0.201	0.0079
1.13	0.321	0.0085
2.18	0.429	0.0088
3.20	0.530	0.0096
4.21	0.627	0.0106
5.24	0.721	0.0121
6.25	0.804	0.0138
7.27	0.884	0.0164
8.30	0.954	0.0207
9.31	1.017	0.0240
10.31	1.069	0.0293

$Rn = 304600.$

α	C_l	C_d
-3.98	-0.184	0.0130
-2.97	-0.092	0.0113
-1.92	0.003	0.0097
-0.92	0.093	0.0086
0.13	0.206	0.0078
1.15	0.326	0.0081
2.17	0.429	0.0086
3.20	0.530	0.0096
4.21	0.627	0.0104
5.23	0.718	0.0120
6.26	0.805	0.0138
7.26	0.884	0.0163
8.30	0.957	0.0205
9.31	1.019	0.0243
10.31	1.072	0.0287
11.31	1.103	0.0370

$Rn = 300000.$

α	C_l	C_d
-3.98	-0.186	0.0127
-2.47	-0.043	0.0099
-0.91	0.097	0.0081
0.65	0.274	0.0077
2.18	0.432	0.0087
3.70	0.580	0.0102
5.24	0.722	0.0118
6.77	0.848	0.0152
8.30	0.960	0.0207
9.82	1.054	0.0265
11.33	1.105	0.0360

$Rn = 304000.$

α	C_l	C_d
-4.00	-0.136	0.0118
-2.96	-0.038	0.0101
-1.91	0.055	0.0084
-0.92	0.140	0.0076
0.15	0.272	0.0076
1.17	0.377	0.0083
2.18	0.478	0.0092
3.20	0.576	0.0102
4.22	0.670	0.0111
5.24	0.758	0.0126
6.26	0.842	0.0147
7.27	0.915	0.0180
8.29	0.984	0.0212
9.30	1.045	0.0252
10.32	1.092	0.0314

SD8000-PT

Fig. 12.152

$Rn = 62500.$

α	C_l	C_d
-3.94	-0.138	0.0151
-2.93	-0.065	0.0139
-1.91	-0.004	0.0114
-0.88	0.111	0.0165
0.13	0.200	0.0158
1.17	0.360	0.0156
2.20	0.508	0.0135

3.23	0.599	0.0150
4.24	0.677	0.0205
5.26	0.753	0.0241
6.28	0.823	0.0294
7.28	0.889	0.0341
8.30	0.946	0.0422
9.31	0.984	0.0523

$Rn = 102500.$

α	C_l	C_d
-3.93	-0.133	0.0149
-2.91	-0.053	0.0123
-1.91	0.046	0.0111
-0.88	0.138	0.0115
0.15	0.296	0.0127
1.17	0.454	0.0137
2.21	0.548	0.0130
3.23	0.624	0.0127
4.24	0.715	0.0140
5.26	0.803	0.0166
6.28	0.885	0.0200
7.30	0.958	0.0236
8.31	1.021	0.0280
9.32	1.062	0.0364
10.34	1.078	0.0539

$Rn = 154500.$

α	C_l	C_d
-3.93	-0.149	0.0136
-2.94	-0.058	0.0109
-1.90	0.054	0.0108
-0.86	0.188	0.0106
0.16	0.334	0.0095
1.18	0.432	0.0098
2.21	0.529	0.0106
3.22	0.620	0.0112
4.25	0.712	0.0133
5.27	0.806	0.0148
6.28	0.892	0.0186
7.30	0.971	0.0208
8.32	1.033	0.0260
9.33	1.082	0.0326
10.34	1.107	0.0458

$Rn = 200000.$

α	C_l	C_d
-3.92	-0.115	0.0113
-2.91	-0.004	0.0098
-1.89	0.133	0.0093
-0.85	0.250	0.0087
0.17	0.350	0.0089
1.18	0.448	0.0090
2.21	0.546	0.0103
3.23	0.642	0.0119
4.26	0.737	0.0138
5.27	0.826	0.0162
6.28	0.915	0.0187
7.30	0.992	0.0218
8.32	1.058	0.0264
9.33	1.105	0.0354

$Rn = 302300.$

α	C_l	C_d
-3.94	-0.076	0.0095
-2.91	0.053	0.0084
-1.88	0.160	0.0076
-0.85	0.251	0.0074
0.15	0.344	0.0071
1.18	0.450	0.0079
2.20	0.552	0.0093
3.23	0.650	0.0105
4.25	0.744	0.0123
5.26	0.833	0.0140
6.29	0.920	0.0163
7.30	1.001	0.0185
8.31	1.070	0.0229
9.34	1.126	0.0286

SD8000-PT

Fig. 12.153

$Rn = 104900.$

α	C_l	C_d
-3.93	-0.147	0.0143
-2.93	-0.057	0.0141
-1.89	0.055	0.0129
-0.87	0.171	0.0129
0.13	0.289	0.0114
1.17	0.394	0.0135
2.18	0.491	0.0132
3.21	0.583	0.0153
4.23	0.682	0.0169
5.26	0.765	0.0166
6.26	0.849	0.0186

$Rn = 153800.$

α	C_l	C_d
-3.96	-0.100	0.0121
-2.94	0.022	0.0110
-1.90	0.127	0.0095
-0.87	0.226	0.0096
0.15	0.322	0.0095
1.18	0.429	0.0104
2.20	0.532	0.0116
3.23	0.638	0.0131
4.25	0.736	0.0149
5.26	0.828	0.0175
6.27	0.906	0.0208
7.30	0.980	0.0243
8.31	1.043	0.0302
9.33	1.089	0.0387

$Rn = 206500.$

α	C_l	C_d
-3.92	-0.066	0.0110
-2.93	0.036	0.0097
-1.89	0.126	0.0086
-0.87	0.213	0.0087
0.14	0.318	0.0094
1.17	0.424	0.0104
2.18	0.525	0.0111
3.21	0.629	0.0125
4.25	0.730	0.0137
5.25	0.824	0.0158
6.27	0.909	0.0186
7.30	0.990	0.0213
8.32	1.056	0.0268
9.33	1.104	0.0334
10.34	1.127	0.0442

$Rn = 311100.$

α	C_l	C_d
-3.98	-0.085	0.0113
-2.97	0.013	0.0109
-1.94	0.104	0.0101
-0.93	0.211	0.0096
0.12	0.313	0.0093
1.15	0.424	0.0097
2.16	0.532	0.0103
3.21	0.638	0.0116
4.23	0.736	0.0126
5.26	0.823	0.0147
6.27	0.909	0.0169
7.30	0.992	0.0192
8.31	1.063	0.0234

SD8000-PT

Fig. 12.154

$Rn = 99900.$

α	C_l	C_d
-3.94	-0.142	0.0144
-2.42	0.018	0.0125
-0.87	0.204	0.0119
0.67	0.376	0.0132
2.18	0.531	0.0133
3.72	0.669	0.0144
5.25	0.791	0.0180
6.76	0.901	0.0256
8.29	0.931	0.0327
9.78	0.936	0.0496
11.30	0.888	0.1782

$Rn = 152200.$

α	C_l	C_d
-3.91	-0.088	0.0122
-2.40	0.071	0.0104
-0.87	0.219	0.0094
0.68	0.386	0.0097
2.19	0.536	0.0106
3.72	0.681	0.0125
5.24	0.809	0.0172
6.79	0.934	0.0209
8.31	1.035	0.0278
9.81	1.097	0.0395
11.28	0.995	0.1512

$Rn = 202100.$

α	C_l	C_d
-3.94	-0.074	0.0109
-2.43	0.078	0.0088
-0.86	0.220	0.0081
0.66	0.382	0.0084
2.21	0.540	0.0099
3.73	0.685	0.0126
5.25	0.818	0.0159
6.79	0.948	0.0193
8.31	1.053	0.0261
9.81	1.116	0.0369
11.24	1.021	0.1473

$Rn = 301300.$

α	C_l	C_d
-3.96	-0.074	0.0104
-2.42	0.076	0.0091
-0.88	0.227	0.0083
0.66	0.385	0.0083
2.20	0.546	0.0095
3.73	0.692	0.0120
5.25	0.829	0.0147
6.78	0.959	0.0178
8.31	1.069	0.0231
9.84	1.140	0.0324
11.33	1.140	0.0586

SD8000-PT

Fig. 12.155

$Rn = 101300.$

α	C_l	C_d
-2.93	-0.048	0.0125
-1.40	0.091	0.0124
0.13	0.308	0.0139
1.69	0.507	0.0128
3.23	0.640	0.0132
4.74	0.771	0.0171
6.28	0.892	0.0216
7.80	1.001	0.0258
9.32	1.071	0.0376

$Rn = 150500.$

α	C_l	C_d
-2.93	0.020	0.0104
-1.38	0.156	0.0107
0.16	0.354	0.0104
1.69	0.498	0.0099
3.22	0.641	0.0126
4.75	0.768	0.0157
6.26	0.896	0.0187
7.80	1.003	0.0258
9.32	1.080	0.0326
10.81	1.065	0.0600
11.76	0.924	0.2143
12.79	0.870	0.2198

$Rn = 200800.$

α	C_l	C_d
-2.95	0.039	0.0095
-1.37	0.193	0.0086
0.16	0.339	0.0088
1.69	0.490	0.0093
3.21	0.634	0.0116
4.74	0.773	0.0148
6.26	0.905	0.0181
7.80	1.021	0.0231
9.33	1.101	0.0323
10.82	1.122	0.0541
11.75	0.975	0.2004
12.79	0.916	0.2233
13.78	0.907	0.2499

$Rn = 306100.$

α	C_l	C_d
-2.99	0.041	0.0084
-1.39	0.197	0.0078
0.16	0.342	0.0073
1.69	0.497	0.0087
3.21	0.643	0.0110
4.75	0.785	0.0132
6.28	0.917	0.0163
7.81	1.035	0.0207
9.32	1.121	0.0278
10.83	1.155	0.0444
11.81	1.009	0.1990

SD8020-PT

Fig. 12.157

$Rn = 59800.$

α	C_l	C_d
-6.03	-0.590	0.0197
-5.05	-0.533	0.0204
-4.01	-0.442	0.0167
-2.98	-0.356	0.0159
-1.96	-0.224	0.0147
-0.94	-0.082	0.0136
0.08	-0.024	0.0128
1.09	0.021	0.0140
2.14	0.184	0.0163
3.14	0.284	0.0155
4.17	0.369	0.0175
5.18	0.443	0.0196
6.20	0.513	0.0266
7.21	0.582	0.0344
8.22	0.636	0.0407
9.23	0.664	0.0825
10.24	0.666	0.1373
11.23	0.640	0.1627
12.23	0.631	0.1579

$Rn = 100500.$

α	C_l	C_d
-6.05	-0.569	0.0179
-5.02	-0.489	0.0166
-4.01	-0.410	0.0132
-2.98	-0.319	0.0123
-1.96	-0.214	0.0118
-0.94	-0.080	0.0119
0.09	0.006	0.0112
1.10	0.126	0.0122
2.13	0.244	0.0124
3.15	0.334	0.0126
4.18	0.420	0.0137
5.19	0.501	0.0150
6.22	0.583	0.0196
7.23	0.655	0.0227
8.24	0.723	0.0296
9.26	0.771	0.0415
10.26	0.740	0.1224
11.24	0.692	0.1609

$Rn = 151200.$

α	C_l	C_d
-6.06	-0.599	0.0158
-5.02	-0.513	0.0134
-4.01	-0.426	0.0123
-2.99	-0.340	0.0107
-1.96	-0.250	0.0101
-0.94	-0.155	0.0101
0.09	0.011	0.0085
1.11	0.150	0.0100
2.12	0.239	0.0098
3.15	0.326	0.0101
4.16	0.412	0.0120
5.20	0.499	0.0141
6.22	0.585	0.0166
7.24	0.666	0.0204
8.25	0.734	0.0239
9.27	0.793	0.0303
10.27	0.821	0.0575
11.25	0.761	0.1469

$Rn = 201100.$

α	C_l	C_d
-6.07	-0.605	0.0142
-5.02	-0.518	0.0126
-4.00	-0.428	0.0114
-2.99	-0.335	0.0103
-1.98	-0.249	0.0090
-0.93	-0.134	0.0080
0.09	-0.003	0.0085
1.12	0.137	0.0087
2.12	0.229	0.0090
3.16	0.317	0.0097
4.19	0.410	0.0108
5.20	0.496	0.0127
6.21	0.579	0.0142
7.23	0.660	0.0167
8.24	0.734	0.0199
9.27	0.799	0.0268
10.28	0.837	0.0468
11.25	0.793	0.1304

$Rn = 306700.$

α	C_l	C_d
-6.03	-0.566	0.0128
-4.51	-0.426	0.0102
-2.99	-0.289	0.0083
-1.42	-0.098	0.0073
0.61	0.068	0.0074
0.61	0.067	0.0073
1.63	0.188	0.0081
3.16	0.352	0.0095
4.69	0.485	0.0115
6.21	0.616	0.0144
7.75	0.738	0.0186
9.28	0.839	0.0260
10.79	0.809	0.1359

SD8040-PT

Fig. 12.159

$Rn = 62100.$

α	C_l	C_d
-2.95	-0.167	0.0217
-1.42	-0.014	0.0171
0.13	0.227	0.0204
1.66	0.413	0.0179
3.21	0.537	0.0189
4.72	0.658	0.0188
6.26	0.774	0.0244
7.77	0.884	0.0262
9.29	0.959	0.0285
10.81	1.015	0.0397

$Rn = 102300.$

α	C_l	C_d
-2.93	-0.087	0.0165
-1.40	0.107	0.0122
0.15	0.278	0.0129
1.67	0.413	0.0156
3.19	0.547	0.0154
4.73	0.684	0.0157
6.27	0.816	0.0191
7.78	0.920	0.0237
9.30	1.006	0.0299
10.82	1.056	0.0436
11.81	1.048	0.0679

$Rn = 150300.$

α	C_l	C_d
-2.93	-0.047	0.0135
-1.40	0.090	0.0113
0.13	0.249	0.0112
1.66	0.394	0.0108
3.21	0.541	0.0117
4.73	0.682	0.0142
6.25	0.813	0.0168
7.79	0.926	0.0209
9.30	1.008	0.0293
10.81	1.064	0.0407
11.81	1.063	0.0629

$Rn = 204900.$

α	C_l	C_d
-2.96	-0.058	0.0132
-1.39	0.077	0.0105
0.14	0.242	0.0093
1.67	0.394	0.0096
3.19	0.539	0.0111
4.73	0.684	0.0128
6.26	0.817	0.0151
7.79	0.929	0.0208
9.28	1.015	0.0267
10.81	1.071	0.0384
11.82	1.077	0.0584

$Rn = 301800.$

α	C_l	C_d
-2.96	-0.085	0.0122
-1.44	0.062	0.0098
0.12	0.218	0.0077
1.63	0.388	0.0080
3.19	0.542	0.0096
4.74	0.688	0.0113
6.26	0.815	0.0145
7.78	0.926	0.0185
9.29	1.011	0.0245
10.81	1.065	0.0355
11.80	1.071	0.0545
12.81	1.052	0.0923

SPICA-PT

Fig. 12.160

$Rn = 59900.$

α	C_l	C_d
-1.87	0.123	0.0354
-0.85	0.219	0.0347
0.16	0.312	0.0327
1.18	0.402	0.0334
2.20	0.479	0.0360
3.21	0.536	0.0437
4.22	0.575	0.0521
5.23	0.615	0.0626
6.24	0.681	0.0729

$Rn = 99600.$

α	C_l	C_d
-1.88	0.075	0.0321
-0.87	0.172	0.0252
0.16	0.269	0.0231
1.18	0.362	0.0212
2.20	0.468	0.0196
3.22	0.558	0.0209
4.23	0.643	0.0221
5.26	0.730	0.0238
6.27	0.825	0.0240
7.30	0.922	0.0255
8.32	1.009	0.0268
9.34	1.093	0.0274
10.35	1.176	0.0282
11.38	1.256	0.0299
12.39	1.329	0.0327
13.39	1.393	0.0340
14.41	1.437	0.0380
15.40	1.419	0.0593

$Rn = 202300.$

α	C_l	C_d
-3.96	-0.183	0.0577
-2.91	-0.069	0.0403
-1.89	0.042	0.0272
-0.88	0.143	0.0192
0.15	0.241	0.0163
1.17	0.341	0.0149
2.19	0.450	0.0117
3.22	0.555	0.0119
4.23	0.649	0.0128
5.26	0.747	0.0139
6.27	0.840	0.0143
7.30	0.936	0.0153
8.32	1.028	0.0163
9.34	1.117	0.0176
10.35	1.199	0.0186
11.37	1.278	0.0194
12.39	1.352	0.0207
13.40	1.412	0.0237
14.41	1.407	0.0385

$Rn = 301500.$

α	C_l	C_d
-2.98	-0.073	0.0387
-1.90	0.044	0.0257
-0.90	0.143	0.0172
0.15	0.245	0.0139
1.16	0.349	0.0128
2.18	0.448	0.0114
3.22	0.564	0.0100
4.23	0.658	0.0105
5.26	0.754	0.0112

WB135/35-PT

Fig. 12.162

$Rn = 61300.$

α	C_l	C_d
-5.97	-0.373	0.0313
-4.96	-0.299	0.0340
-3.95	-0.187	0.0328
-2.91	-0.047	0.0318
-1.88	0.094	0.0281
-0.85	0.219	0.0241
0.16	0.329	0.0247
1.19	0.426	0.0258
2.20	0.518	0.0269
3.22	0.611	0.0258
4.24	0.689	0.0288
5.27	0.803	0.0331
6.28	0.836	0.0422
7.27	0.808	0.0619
8.25	0.736	0.1121

9.27	0.730	0.1316

$Rn = 100500.$

α	C_l	C_d
-5.96	-0.259	0.0238
-4.95	-0.127	0.0231
-3.91	-0.001	0.0220
-2.89	0.114	0.0226
-1.87	0.212	0.0207
-0.84	0.303	0.0200
0.17	0.403	0.0182
1.21	0.512	0.0177
2.23	0.608	0.0183
3.24	0.711	0.0182
4.27	0.805	0.0186
5.29	0.894	0.0212
6.30	0.982	0.0237
7.33	1.070	0.0253
8.34	1.151	0.0281
9.36	1.231	0.0289
10.39	1.298	0.0312
11.37	1.274	0.0576
12.37	1.224	0.0687
13.35	1.210	0.0772

$Rn = 155700.$

α	C_l	C_d
-5.95	-0.157	0.0174
-4.92	-0.051	0.0168
-3.89	0.043	0.0160
-2.89	0.137	0.0157
-1.86	0.235	0.0149
-0.85	0.334	0.0140
0.19	0.434	0.0132
1.21	0.549	0.0130
2.22	0.648	0.0135
3.24	0.746	0.0140
4.27	0.839	0.0162
5.29	0.930	0.0180
6.31	1.016	0.0204
7.33	1.097	0.0216
8.35	1.178	0.0227
9.34	1.228	0.0256
10.36	1.211	0.0533

$Rn = 204000.$

α	C_l	C_d
-9.07	-0.510	0.0249
-8.06	-0.406	0.0196
-6.99	-0.287	0.0157
-6.00	-0.196	0.0136
-4.97	-0.107	0.0144
-3.95	-0.012	0.0138
-2.93	0.088	0.0135
-1.89	0.193	0.0129
-0.85	0.305	0.0128
0.17	0.410	0.0122
1.20	0.514	0.0114
2.23	0.627	0.0111
3.24	0.725	0.0120
4.26	0.814	0.0131
5.28	0.908	0.0148
6.30	0.999	0.0163
7.32	1.085	0.0180
8.34	1.168	0.0195
9.35	1.228	0.0227
10.36	1.239	0.0356
11.35	1.219	0.0623
12.35	1.198	0.0807
13.35	1.175	0.1035
14.34	1.155	0.1266

$Rn = 302700.$

α	C_l	C_d
-4.94	-0.078	0.0118
-3.91	0.021	0.0116
-2.88	0.125	0.0112
-1.87	0.230	0.0113
-0.85	0.335	0.0109
0.18	0.438	0.0109
1.18	0.536	0.0106
2.19	0.636	0.0106
3.22	0.738	0.0114

WB140/35/FB-PT

Fig. 12.164

$Rn = 98500.$

α	C_l	C_d
-6.01	-0.330	0.0289
-4.97	-0.226	0.0274
-3.94	-0.133	0.0280
-2.94	-0.052	0.0270
-1.89	0.047	0.0278
-0.88	0.154	0.0264
0.15	0.271	0.0280
1.18	0.388	0.0290
2.20	0.499	0.0308
3.22	0.607	0.0297
4.24	0.719	0.0287
5.26	0.822	0.0281
6.29	0.923	0.0252
7.31	1.020	0.0228
8.32	1.096	0.0224
9.34	1.152	0.0263
10.34	1.155	0.0314
11.32	1.114	0.0480
12.31	1.089	0.0625

$Rn = 153900.$

α	C_l	C_d
-5.97	-0.190	0.0194
-4.92	-0.088	0.0180
-3.90	0.011	0.0173
-2.91	0.104	0.0170
-1.87	0.201	0.0165
-0.85	0.293	0.0152
0.17	0.416	0.0143
1.19	0.511	0.0154
2.21	0.604	0.0146
3.24	0.702	0.0153
4.26	0.800	0.0158
5.28	0.896	0.0166
6.29	0.987	0.0169
7.33	1.063	0.0177
8.33	1.116	0.0196
9.32	1.128	0.0224
10.32	1.095	0.0426
11.32	1.079	0.0462

$Rn = 200500.$

α	C_l	C_d
-6.02	-0.189	0.0170
-4.95	-0.102	0.0148
-3.97	-0.019	0.0142
-2.98	0.076	0.0144
-1.91	0.182	0.0138
-0.85	0.287	0.0131
0.17	0.383	0.0122
1.18	0.505	0.0123
2.20	0.603	0.0123
3.22	0.700	0.0131
4.24	0.799	0.0135
5.28	0.895	0.0140
6.28	0.984	0.0143
7.31	1.057	0.0154
8.34	1.110	0.0178
9.33	1.132	0.0228
10.34	1.117	0.0326
11.32	1.095	0.0443
12.34	1.093	0.0551
13.33	1.094	0.0653

$Rn = 307600.$

α	C_l	C_d
-5.95	-0.163	0.0143
-4.94	-0.069	0.0122
-3.90	0.029	0.0116
-2.90	0.125	0.0114
-1.88	0.228	0.0113
-0.85	0.332	0.0108
0.18	0.429	0.0104
1.19	0.526	0.0099
2.23	0.638	0.0100
3.23	0.728	0.0104
4.24	0.816	0.0109
5.27	0.900	0.0116
6.26	0.973	0.0125
7.23	1.031	0.0141
8.29	1.076	0.0169
9.30	1.083	0.0210